**MONASH UNIVERSITY**
THESIS ACCEPTED IN SATISFACTION OF THE
REQUIREMENTS FOR THE DEGREE OF
DOCTOR OF PHILOSOPHY
ON..... 2 November 2001 .....
..... [redacted] ...
for Sec. Research Graduate School Committee

RE: Mc

## Errata

**Chapter 1**
p. 1 last line: "highlights" for "highlight"
p. 3, para. 4 : "of recent developments in VSA is beyond the scope of this project, it is" for "of recent VSA developments is beyond the scope of this project it is"
p.6, para 4: "heat in the range" for "heat of the range"
p.9, para 1: "NaX is maximum" for "NaX is a maximum"
p.10, para 3, line 6: delete "also"
p.10, para 4, line 1: "scale" for "scaled"
p. 10, para 4, line 5: "(full-scale) bed" for "(full-scale bed)
p.13, para 2, line 7: "link" for "linking"

**Chapter 2**
p.14, para 3, line 8: "140-130 kPa (abs)" for "1.4-1.3 bar (abs)"
p.14, para 3, line 9: "40-30 kPa (abs)" for "0.4-0.3 bar (abs)"
p.16, para 1, line 7: "are invaluable tools" for "are an invaluable tool"
p.19, para 1, line 5: "of the pressure" for "of pressure"
p.19, para 2, line 6: "The energy balance also includes" for "The energy balance is also developed to include"
p.19, para 3, line 1: "The energy balance also includes" for "The energy balance is also developed to include"
p.22, last para, line 2: "1988" for "1990"
p. 24, para 2, line 5: delete "more"
p.25, last para: "characterises" for "characterise"
p.32, para 1, line 6: "this is an established" for "this is established"
p.37, para 3, line 3: "the whole bed" for "the whole"
p.41, para 1, line 1: "expected, in" for "expected, with"
p.41, para 3, line 1: "Nodes" for "Node"
p.42, para 2, line 1: "which the nodes" for "which nodes"
p.43, para 1, line 3: "continues," for "continues"
p.43, last para, line 5: "demonstrates that there" for "demonstrates there"
p.44, last para, line 1: "In Figure 2-11," for "Where"
p.45, para 1, line 2: "prelayer," for "prelayer"
p.49, last para, line 6: "however," for "however ,"
p.54, para 1, line 1: "In Figure 2-17 C-C Depress is the Cocurrent Depressuration Step and L. Purge is the Low Pressure Purge step." for "where C-C Depress (Co-current depressurisation), and L. Purge (Low Pressure Purge)."
p.60, para 1, line 2: "prelayer can be developed" for "prelayer."
p.60, para 3, line 1: "In Figure 2-19, the" for "The"
p.60, para 3, line 2: delete paragraph break between para 3 and para 4.
p.60, para 4, line 1: delete "Where"
p.62, para 1, line 2: "as the end of the" for "as the end of the end of"
p.65, para 2, line 3: "Figures" for "Figure"
p.65, caption Figure 2-22: "Axially" for "Axial"
p.66, caption Figure 2-23: "Axially" for "Axial"
p.68, para 2, line 2: "2-58" for "2-59"
p.70, para 1, line 3: "there is still significant CPU time in" for "there is still a significant time computationally in"
p.77, para 1, line 4: "adsorptive" for "adsorptive,"
p.78, last para, line 3: "Moreover," for "Moreover"
p.85, para 3, line 3: "previously," for "previously"
p.86, last para, line 1: "where P', y', and T'" for "where P',y', and T'"
p.94, para 2, line 4: "This numerical approach implemented in MINSA was" for "This numerical approach used MINSA, but was"

**Chapter 3**

p.99, para 2, line 7: "Furthermore, the" for "Furthermore the"
p.101, para 3, line 5: "and in the industrial column the ratio" for "and the industrial column ratio"
p.106, para 1, line 9: "are more robust," for "are a more robust design,"
p.107, para 2, line 3: "The approximate values for the overall heat transfer co-efficients are polyurethane (0.3 $W/m^2 K$), PVC (1.1 $W/m^2K$) and metal (3.9 $W/m^2 K$)." for "The approximate values are polyurethane (0.3), PVC (1.1) and metal (3.9)."
p.111, para 1, line 6: "The product line has a small differential pressure type flowmeter, while the flows in the feed" for "The product line is a small differential pressure type flowmeter, while the feed"
p.111, para 1, line 8: "flow is verified with" for "flow was verified with"
p.111, para 1, line 9: "flowmeter is required" for "flowmeter was required"
p.111, para 3, line 6: "This figure is confirmed" for "This figure was confirmed"
p.111, para 4, line 1: "the feed gas was passed" for "the feed gas is passed"
p.112, para 2, line 1: "items is" for "items in"
p.113, para 1, line 1: "Two-bed six-step" for "Two bed six step"
p.113, below Table 3-1: "two-bed six-step" for "two bed six step"
p.113, caption Figure 3-7: "Figure 3-7 – Symmetric One Bed Representation of the Two Bed Cycle" for "Figure 3-7 – Symmetric One Bed Representation of Two Bed Cycle"
p.114, para 1, line 1: "Two-bed eight-step" for "Two bed eight step"
p.114, para 2, line 1: "One-bed five-step" for "One bed five step"
p.114, para 2, line 11: "one-bed" for "one bed"
p.114, para 1, line 2, Delete "The total cycle time varied between 60-70 seconds." Replace with "The total cycle was either 60 or 70 seconds."
p.115, para 1, line 1: "it requires a" for "they require a"
p.116, para 1, line 1: "typical of a VSA" for "typical of VSA"
p.116, para 2, line 2: "feed heater" for "feed heat"
p.116, para 3, line 3: "Appendix" for "Appendices"
p.117, Table 3-4, "" for " "
p.117, para 3, line 1: "Some parameters for dual" for "Some dual"
p.118, para 1, line 1: "PLC (Programmable Logic Controller)" for "PLC"
p.119, para 2, line 1: "for all PuAA400NaX and PuAANaXVSA6 experimental runs," for "for experimental runs PuAA400NaX# and PuAANaXVSA6#,"
p.119, para 2, line 6: "flows, the response of the flowmeters was slightly non-linear." for "flows there was a slightly non-linear response of the flowmeters."
p.119, para 2, line 7: "significant in terms of" for "significant terms in"
p.119, last line, "are" for "is"
p.120, para 1, line 5: "thermocouples by" for "thermocouples"
p.120, para 1, line 6: "adsorbent could" for "adsorbent can"

**Chapter 4**

p.122, para 3, line 4: "BPL carbon." for "BPL to separate air and helium."
p.123, para 2, line 6: "like in the" for "like the"
p.123, para 1, line 5: "." for "!"
p.127, para 1, line 5: "data are noted" for "data is noted"
p.127, Table 4-1: "Collins work predict" for "Collins work predicts"
p.139, para 1, line 2: "Likewise, Table 4-8 highlights that the" for "Likewise Table 4-8 highlights the"
p.139, para 2, line 4: "2000c" for "2000"
p.142, para 2, line 5: "i.e.," for "i.e."
p.146 second last line: "purity" for "purities"
p.148, last line: "significantly affects the shape of the" for "significantly shapes the"
p.149, third last line: "valve Cv," for "valve Cv"
p.154, para 1, line 1: "similar. However, the" for "similar, however the"
p.170, para 2, line 2: "2000c" for "2000
p.170, second last line: "profile. When the same cycle is run with MINSA and" for "profile when the same cycle is run with MINSA, and"
p.173, para 1, line 1: "Furthermore," for "Furthermore"

RE: M

p.176, last para, line 6: "that the average cyclic temperature swing between feed and purge was the same" for "that, the average cyclic temperature swing between feed and purge, was the same used"
p.177, last para,, line 2: "depression is" for "depression, is"
p.180, last para, line 1: "AA25LSX1" for "AALSX25"
p.194, first para, line 3: "In fact, it" for "In fact it"
p.197, para 1, line 2: "separate issue" for "aside"
p.220, last para, line 6: "Furthermore," for "Furthermore"

**Chapter 5**
p.225, para 2, line 1: "an air feed is used," for "air feed,"
p.225, para 3, line 1: "in more conventional units" for "in more units"
p.226, para 2, line 4: "plots of (1/BSF) and AFM as a function of temperature, where" for "plot (1/BSF) and AFM where"
p.241, para 4, line 2: "In practice, there" for "In practice there"
p.253, para 3, line 2: "apparent that" for "apparent the"

**Chapter 6**
p.262, para 1, line 1: "This study has addressed" for "This study has undertaken"
p.262, para 6, line 2: "can capture with reasonable accuracy" for "can reasonably accurately capture"
p.263, para 1, line 1: "The project has involved the design, construction, commissioning and operation of a" for "The project has designed, constructed, commissioned , and operated a"

**Appendices and Bibliography**
A2-1, para 4, line 4: "respective" for "respect"

**General change**
"However," for "However"

## Addendum

p. 16, para 3: delete the last two sentences
p.18, add to end of page: "However, for the purposes of this study, generally a constant mass transfer coefficient was used."
p.36, below Figure 2-5: add " (Taken from Lou et.al., 1999)
p.37, para 2, line 2: delete "-helium"
p.37, caption to Figure 2-6: delete "-Helium"
p.37, last line: delete "helium-air"
p.38: delete Figure 2-6a, and delete "The arrows indicate that the relative convective fluxes are measured at the wall entering the node."
p. 51: add caption, "Figure 2-15 – Temperature Swing Over Adsorption Step"
p. 52: add caption, "Figure 2-16 – Temperature Swing Over Desorption Step"
p.66, end of para 2: add "These represent the minimum temperatures for the cycle for different axially positioned thermocouples."
p.94, add the following footnote: "I acknowledge the important work in this area undertaken by Bob Thorogood and Roger Whitley.at Air Products and Chemicals, Inc."
p.109, para 3: add to the end of para, "It should be noted that the axial conductivity of the wall was ignored in these simulations. This can be an important effect in dissipating the temperature profile."
p.109: delete last sentence on page
p.117, para 3, line 2: "In other cases single site multicomponent Langmuir" for "In other cases, single site Langmuir"
p.228, para 1, line 2: "240 K" for "200 K"
p.274, last reference: "Chemeca 98, Port Douglas, 28th-30th September, 1998" for "Chemeca 98, Port Douglas"
p.275, first reference: "Texas, 1st-5th November 1999c" for "Texas,1999c"
p.275, second reference: "Newcastle, 27th-29th September, 1999a" for "Newcastle, 1999a"
p.275, third reference: "Texas, 1st-5th November 1999c" for "Texas,1999c"

# Thermal Profiles in Oxygen Vacuum Swing Adsorption (VSA) - Modelling, Observations and Optimisation

by

Simon J. Wilson

Bachelor of Science (Monash)

Bachelor of Engineering (Hons.) (Monash)

Master of Arts (Hons.) (Wollongong)

A thesis submitted in fulfillment of the requirements for the degree of Doctorate of Philosophy

Department of Chemical Engineering

Monash University

April 2001

# Declaration

To the best of my knowledge and belief this thesis contains no material that has been accepted for the award of any other degree or diploma in any University, and contains no material previously published or written by another person, except where due reference is given in the text.

Simon J. Wilson
Department of Chemical Engineering
Monash University
April 2001

# Acknowledgements

There are many people I would like to thank for assisting me during the course of this project. Oxygen VSA (even at a laboratory scale) proved not to be a simple unit operation for academic investigation. The technical staff in the Department of Chemical Engineering provided valuable advice and ongoing assistance in the wide range of tasks. Particularly thanks to Gil Atkin, Peter Froud, Ron Graham, Roy Harrip, John Barnard, and Paul Beardsley.

Thanks are also due to Greg Gondecki and Dr Doug Dee for providing advice (when not commercially confidential) based on their extensive experience with oxygen VSA at Air Product and Chemicals Inc. (APCI) and tolerating the steep learning curve I went through. I would also like to thank APCI, the DETYA (for an Australian Postgraduate Award) and the Department of Chemical Engineering for financial support.

I would also like to thank my fellow members of the Monash University Adsorption Research Group (Dr Paul Webley, Shannon Todd, Chris Beh, and Dr Ming He). Together much progress has been made establishing adsorption research at Monash University. Thanks to Chris Beh for the help working together developing and refining the oxygen VSA unit. Particular thanks also go to my supervisor, Dr Paul Webley for providing intellectual and financial support, and rekindling my interest in scientific enquiry. Of course these people bear no responsibility for the remaining faults with this thesis.

Personal thanks go to Lizi Sironic for being a good friend at Monash. Thanks are also due to my father, Robin, who has been always supportive of my career decisions, even when unconventional. Thanks also to my mother, Ruth, for being a willing and available grandparent. This made the completion of this thesis possible. Most of all I would like to thank my family (Susan, Jack and Owen) for their love and support, and simply putting up with me.

# Abstract

Adsorptive separations are a broad and growing field of chemical engineering that has enjoyed significant attention over the last decade. This thesis offers a small contribution to this field. It aims to investigate the surprising and sometimes severe axial temperature profiles that arise in oxygen Vacuum Swing Adsorption (VSA) - the so-called 'cold spot'. These thermal profiles are of significant academic and industrial interest and it is hoped that the work undertaken will be of interest to both communities.

This study develops a number of models and techniques (qualitative, simple, perturbation and numerical) to explain and predict the Cyclic Steady State (CSS) temperature profiles in oxygen VSA. At the core of these approaches is the understanding that the temperature profile is simply the result of the interaction between convected heat and the cyclic temperature swings associated with adsorption and desorption.

An approach is also developed to predict the depth of water penetration at CSS in an oxygen VSA adsorption bed. This ensemble of modelling approaches is applied to analyse experimental results from a laboratory scale oxygen VSA unit. The laboratory scale unit is developed to mimic the thermal performance of an industrial unit. Success in this regard was mixed.

The experimental investigation identifies a range of key process parameters that shape the CSS temperature profile. These experimental results compare well with the numerical simulations with MINSA, our in-house adsorption simulator. The simpler models also capture some of the key features of the CSS temperature profiles.

The study also addresses the sometimes confusing issue of how temperature profiles affect oxygen VSA separation performance. A performance criterion is developed based on cost that incorporates both oxygen recovery and Bed Sizing Factor (BSF). Using this performance criterion, a number of thermal optimisation strategies can be evaluated.

# Table of Contents

## Nomenclature

$A_{(1-6)}$ = Functions for full scale MSA

$A_b$, A = Cross sectional area of the bed ($m^2$)

$A_t$ = Total cross sectional area of the bed and adsorption column wall ($m^2$)

$A_W$ = Cross sectional area of the wall ($m^2$)

$C_{pad}$, $C_{ad}$ = Adsorbate heat capacity, (J/mol K)

$\overline{C}_{ad}$ = Average heat capacity of adsorbate) (J/kg K)

$\overline{C}_{pg}$ = Average heat capacity of gas (J/mol K)

$C_{pg}$ = Heat capacity of gas (J/mol K)

$C_{ps}$, $C_s$= Adsorbent heat capacity (J/kg K)

$C_{pw}$ = Wall heat capacity of gas (J/ kg K)

$C_{sp}$, $C_{sm}$ = Specific heat capacity of prelayer and mass respectively (J/kg K)

$C_{spost}$ = Heat capacity of inert (post layer) at the end of the bed (kJ/kg K)

D = Diameter of adsorption bed (m)

$D_{e,i}$ = Effective diffusion co-efficient for component i ($m^2$/sec)

$D_{K,i}$ = Knudsen diffusion coefficient for component i ($m^2$/sec)

$D_{m,i}$ = Multicomponent molecular diffusion co-efficient ( $m^2$/sec)

$D_0$ = Outer bed diameter of adsorption bed (includes wall diameter) (m)

$d_p$ = Adsorbent pellet diameter (m)

E = Enthalpy deviation flux used in simple energy balance (mol K)

$E_Z$ = Axial dispersion co-efficient ($m^2$/sec)

f, w, pr = Instantaneous molar flows used in simple energy balances (mol/sec)

F, W, Pr = Totalised molar flows used in simple energy balances (mol)

G = Function relating $\Delta H$ to the temperature minimum (K mol/ J)

$H_g$ = Gas enthalpy (J/mol)

$h_i^*$ = Enthalpy of pure i at $T_{ref}$ (J/mol)

$h_i^0$ = Enthalpy of pure i at T (J/mol)

$H_{N2}$ = Characteristic heat generation for nitrogen adsorption (Dimensionless)

$h_0$ = Outside heat transfer coefficient (J/$m^2$ sec K)

$H_{O2}$ = Characteristic heat generation for oxygen adsorption (Dimensionless)

$h_{wi}$ = Inside heat transfer coefficient (J/$m^2$ sec K)

$h_{wo}$ = Overall heat transfer coefficient (J/$m^2$ sec K)

ir= Nominal interest rate (%)

k = Ratio of heat capacities for air (Cp/Cv)

$k_b$ = Thermal conductivity of adsorption bed (W/m K)

$k_{er}$ = Effective radial conductivity (W/m K)

$k_g$ = Thermal conductivity of gas (W/m K)

$k_i$ = Mass transfer parameter in LDF model for component i, ($sec^{-1}$)

$k_{wz}$, $k_w$= Axial conductivity of wall (W/m K)

L = Bed length (m)

$m_1$, $m_2$, $b_{i,o}$,$d_{i,o}$, $Q_{i1}$, $Q_{i2}$ = Dual-site Langmuir parameters for multicomponent adsorption of nitrogen and oxygen

$m^d_1$, $m^d_2$, $m^d_3$ = Mass of cells 1, 2 and 3 respectively in Section 2.5 (kg)

$m_p$, $m_m$ = Mass of prelayer and main layer respectively used in energy balances (kg)

$m_{post}$ = Mass of the inert (post-layer) at the end of the bed (kg)

$m_{w1}$, $m_{w2}$, $b_{wo}$, $d_{wo}$, $Q_{w1}$, $Q_{w2}$ = Dual- site Langmuir parameters for water on NaX.

$M_{wg}$, $M_{w,i}$ = Molecular weight of gas and component i (g/mol)

$Mw_{O2}$, $Mw_{N2}$ = Molecular weight of oxygen and nitrogen respectively

$n_f$, $n_e$, = Adsorbent loading at end of feed and evacuation conditions respectively (mol/kg)

$n_i$ = Loading of component i, (mol/kg)

$n^i_{eq}$, $n_i^*$ = Equilibrium loading of component i, (mol/kg)

$n_{N2}$, $n_{02}$, $n_w$ = Adsorbent loading of nitrogen, oxygen, and water respectively (mol/kg)

$n_{w,ad}$ , $n_{w,de}$ = Water loading at end of adsorption and desorption steps (mol/kg)

P, p = Total pressure (bar abs)

$P_{atm}$ = Atmospheric pressure (bas abs.)

Pe = Axial Peclet number (Dimensionless)

$P_f$ = Total pressure at the end of the feed step (bar abs)

$P_{high}$ = High bed pressure at end of feed step (bar abs)

$p_i$ = Partial pressure of component i,(bar abs)

$P_{low}$ = Low bed pressure at end of evacuation or purge step (bar abs)

$P_w$ = Partial pressure of water (bar abs)

$q_{N2}$, $q_{O2}$ or $\Delta H_{N2}$, $\Delta H_{O2}$ =Heat of adsorption for nitrogen and oxygen (J/mol K)

Q, $Q_{loss}$ = Heat exchange with the system (J/m3)

R = Universal gas constant, $83.144x10^{-6}$ ($m^3$ bar/mol K)

Re = Reynolds number (Dimensionless)

Rec= Oxygen recovery (Dimensionless or %)

$r_p$ = Adsorbent pellet radius (m)

S= Selectivity of adsorbent with respect to nitrogen ($S= WC_{N2} / WC_{O2}$)

T = Temperature (K)

t = Temporal co-ordinate (sec)

$T^*(n)$ = Perturbation expansion of temperature in dimensionless form (Dimensionless)

$T_0$, $T_1$ = Short time scale temperature, long time scale temperature respectively (K)

$T_1^d$, $T_2^d$, $T_3^d$ = Dynamic temperature of inert 1, inert 2 and adsorbing cell 3 respectively (K)

$\overline{T}_2$ = Average temperature of cold spot (Simple energy balance) (K)

$T_{amb}$ = Ambient temperature (K)

$T_f$ = Feed Temperature (K)

$T_f$, $T_2$, $T_{3(main)}$, $T_4$ and $T_p$ = Temperatures of streams in simple energy balance (K)

$T_i$ = Initial bed temperature (K)

$T_{n,wall}$ = Temperature at wall for discretised element (K)

$T_{node}$ = Temperature of node in discretised element (K)

$t_o$ = Characteristic time (sec)

$T_p$ = Temperature of product gas (Simple energy balance) (K)

$T_{ref}$ = Reference temperature (K)

u = Superficial velocity (m/s)

U = Total internal energy of System (J)

$U_{ad}$ = Internal energy of adsorbate (J)

$U_g$ = Internal energy of gas (J)

$U_s$ = Internal energy of solid (J)

$u_o$ = Characteristic superficial velocity (m/sec)

v = Interstitial velocity (m/sec)

$V_{e,inlet}$ = Instantaneous volumetric flowrate into vacuum blower at inlet conditions ($m^3$/sec)

$V_f$ = Instantaneous volumetric flowrate of feed gas ($m^3$/sec)

$V_{f,\ inlet}$ = Instantaneous volumetric flowrate into feed blower at inlet conditions ($m^3$/sec)

W = Work done by the system ($J/m^3$)

$w_c$, $w_t$ = Velocity of thermal and composition waves respectively (m/sec)

$WC_{N2}$, $WC_{O2}$ = Working capacity of adsorbent with respect to nitrogen and oxygen (mol/kg adsorbent)

X = Scale of plant (TPDc)

y, $y_{N2}$ = Mole fraction of nitrogen (heavier component) (Dimensionless)

$y_i$ = Mole fraction of component i in gas phase (Dimensionless)

$y_{O2,f}$ = Mole fraction of oxygen in feed gas (Dimensionless)

$y_{O2,pr}$ = Mole fraction of oxygen in product gas (Dimensionless)

$y_w$ = Mole fraction of water in gas (Dimensionless)

$z$ = Spatial co-ordinate (m)

$z_w$ = Length of penetration of water loaded zone (m)

**Greek**

$\Delta n_{N2}$, $\Delta n_{O2}$ = Characteristic swing in nitrogen loading (mol/kg)

$\Delta T$ = Characteristic swing in temperature over a cycle (K)

$\Delta T_{main}$ = Average temperature swing of main layer over cycle (K)

$\Delta T_{post}$ = Temperature swing in the inert (post-layer) at the end of the bed (K)

$\Delta T_{prelayer}$ = Average temperature swing of prelayer over cycle (K)

$\alpha$= Characteristic quantity of cocurrent desorption (Dimensionless)

$\alpha_{N2,ad}$ = Selectivity of adsorbent for nitrogen at adsorption conditions (Dimensionless)

$\alpha_{N2,de}$ = Selectivity of adsorbent for nitrogen at desorption conditions (Dimensionless)

$\alpha_p$ = Pellet tortuosity (Dimensionless)

$\alpha_w$ = Two dimensional wall film heat transfer co-efficient. (W/m$^2$ K)

$\varepsilon$ = Dimensionless ratio of thermal capacitance of gas to solid (Dimensionless)

$\varepsilon_b$ = Bed interparticle voidage (Dimensionless)

$\varepsilon_p$ = Pellet voidage (Dimensionless)

$\varepsilon_t$ = Total bed voidage (Dimensionless)

$\phi_1$, $\phi_2$ = Ratio of gas capacitance to solid capacitance (sec$^{-1}$)

$\phi_s$ = Sphericity (Dimensionless)

$\eta_f$ = Feed blower efficiency (Dimensionless)

$\eta_v$ = Vacuum blower efficiency (Dimensionless)

$\varphi^*(0)$ = Constant of integration in MSA equation (Dimensionless)

$\kappa$ = K-B function

$\mu_g$ = Viscosity of gas (Pa.sec)

$\nu$ = Adjustable parameter to linearize the bed resistance term to account for the effect of the radial temperature distribution.

$\rho_b$ = Bulk adsorbent density (kg/ m$^3$)

$\rho_g$ = Gas density (kg/m$^3$) or (mol/ m$^3$)

$\rho_{go}$ = Characteristic gas density at 1 bar and 298 K. (mol/m$^3$)

$\rho_w$ = Wall density (kg/ m$^3$)

$\tau$ *= Slow timescale in perturbation analysis (sec)

$\tau_{ad}$ = Adsorption time (sec)

$\tau_c$ = Total cycle time (sec)

$\tau_{de}$ = Desorption time (sec)

$\tau_e$ = Evacuation time (sec)

$\tau_f$ = Feed time (sec)

$\omega = y\tau_{ad}/\tau_{de}$ (Dimensionless)

$\psi = \Delta H/C_{pg}$ (K)

$\gamma$ = Constant of integration in first order MSA equation

$\eta$ = Functional form for dynamic MSA

$\Phi$ = Surface potential

**Subscripts and Superscripts**

(*) = Variable in dimensionless form

(^)= Specific quantity

(') = Periodic function in the short time scale

($_{ad}$) = Adsorption

($^{adi,v}$) = Adiabaticity and voidage included determination of working capacity

($^{d}$) = Dynamic temperature defined in Section 2-5.

($_{de}$) = Desorption

($_{e}$) = Evacuation

($_{f}$) = Feed

($_{pr}$) = Product

**Abbreviations**

ACCB = Accumulated Convective Cycle Balance (J/m$^2$ K)

ADSIM - Adsorption Simulator (Commercial Product of Aspentech)

AFM – Adsorption Figure of Merit

APCI - Air Products and Chemicals Inc.

BSF – Bed Sizing Factor

BSF= Bed Sizing Factor (kg adsorbent/TPDc)

CCB = Convective Cycle Balance (J/m$^2$ K)

Cost ost $ per kg adsorbent

CSS - Cyclic Steady State

LDF - Linear Driving Force

MINSA - Monash Integrated Numerical Simulator of Adsorption

MSA - Multiple Scale Analysis

MTZ - Mass Transfer Zone

MUARG - Monash University Adsorption Research Group

NPC = Net Present Cost ($)

ODE - Ordinary Differential Equation

PDE - Partial Differential Equation

PE - Pressure Equalisation

PSA - Pressure Swing Adsorption

RCF = Relative Convective Flux ($W/m^2$ K)

RPSA - Rapid Pressure Swing Adsorption

SVR – Solvent Vapor Recovery

TPDc – Tonnes of Oxygen Per Day Contained

VSA - Vacuum Swing Adsorption

## List of Figures

## List of Tables

## List of Publications and Conference Papers

Wilson, S., Beh, C., Webley, P., Todd, R., The Effects of a Readily Adsorbed Trace Component (Water) in A Bulk Separation PSA Process: The Case of Oxygen VSA (Accepted Industrial & Engineering Chemistry Research, 2001)

Wilson, S., Todd, R., and Webley, P., Damping Thermal Swings in Oxygen Vacuum Swing Adsorption (VSA), 6th World Congress of Chemical Engineering, Melbourne, Australia 23-27 September 2001 (submitted)

Wilson, S., and Webley, P., "A Technique for Accelerated Convergence of Cyclic Steady State in Oxygen VSA Simulations", AICHE Annual Meeting 1999, Dallas, Texas

Wilson, S., and Webley, P., "Laboratory Scale Oxygen VSA and Thermal Behaviour: How Close to Industrial Scale?", AICHE Annual Meeting 1999, Dallas, Texas

Wilson, S., and Webley, P., "Thermal Effects in Oxygen Vacuum Swing Adsorption - An Accelerated Approximate Solution", Chemeca 99, Newcastle

Wilson, S., Webley, P., and He, J.,, "Thermal Effects in Oxygen Vacuum Swing Adsorption", Chemeca 98, Port Douglas

Beh, C., Wilson, S., Webley, P., He, J., "The Control of the Vacuum Swing Adsorption Process for Air Separation", Proceedings of the Second Pacific Basin Conference on Adsorption Science and Technology, Brisbane, Australia, May 14-18 2000, (World Scientific, Singapore, 2000)

Todd, R., Beh. C., Wilson, S., and Webley, P., Simplified Modelling of Pressure Drive Flow in Pressure Swing Adsorption, Melbourne Graduate Fluids Conference 2001, Monash University, Melbourne, Australia

Webley, P., Beh., C., He, J, Wilson, S., and Todd, S., "Numerical Simulation and Experimental Validation of Multiple Layer Non-Isothermal, Bulk Gas Separation", Proceedings of the Second Pacific Basin Conference on Adsorption Science and Technology, Brisbane, Australia, May 14-18 2000 (World Scientific, Singapore, 2000)

Webley, P., He, J., Todd, R., Wilson, S., and Beh, C., "Rapid Numerical Simulation and Control for PSA/VSA. II Cycle Simulation" (Submitted Industrial & Engineering Chemistry Research, 2000)

He, J., Webley, P., and Wilson, S., Optimisation of PSA Systems - Comparison of Equilibrium and Non-Equilibrium Models, Chemeca 98 , Port Douglas

Webley, P., He, J., Wilson, S, and Hu, E., "Optimization of PSA Systems for Air Separation", Fundamentals of Adsorption 6, 24-28 May 1998, Elsevier

## Background to this Project

The project was proposed by Dr Paul Webley to Air Products and Chemicals Inc. (APCI), and undertaken in the Department of Chemical Engineering at Monash University. The project was initially funded in February 1997. This project was the starting point, for the Monash University Adsorption Research Group led by Dr Paul Webley, and the first gas adsorption project at Monash University. As a consequence, the project involved the establishment of considerable research infrastructure - numerical simulators (ADSIM and MINSA), a laboratory scale VSA unit, accumulating and characterising a range of adsorbents, Micromeritics ASAP2010, apparatus for sieve regeneration after water contamination. This proved a time consuming and difficult task, despite the occasional technical advice from Greg Gondecki and Dr Doug Dee (APCI) by email. The Monash University Adsorption Research Group has subsequently expanded to include new personnel, projects and equipment. A Rapid PSA unit has been built and a new simulator developed that incorporates a pellet model. A study of oxygen VSA control is also underway using the VSA unit.

# Chapter One
# Thermal Profiles in Oxygen VSA - The Context and Issues

Over a short period oxygen VSA has grown to occupy a substantial niche in the production of industrial oxygen. In order to expand its application commercially, oxygen VSA has undergone sustained innovation. However one ongoing hurdle to the development of oxygen VSA has been the design uncertainty and performance alteration often associated with the severe axial cyclic steady state (CSS) temperature profiles that characterise this process technology. The temperature profiles also impact on some of the directions of oxygen VSA development. This chapter reviews some current developments in oxygen VSA technology and also details industrial and academic commentary on the so-called 'cold spot' in oxygen VSA. The review indicates there is a need for improved understanding of the thermal profiles as an important step for further innovation of oxygen VSA. This chapter also highlights one ongoing complication of the analysis of the thermal profiles in oxygen VSA. The thermal profiles evident in industrial scale oxygen VSA are not pronounced in typical laboratory VSA units due to heat exchange with the environment. This denies researchers the opportunity to apply laboratory scale tools to investigate this phenomenon and has also complicated scale up.

## 1.1 PSA[1] & VSA - The Background

Over the last thirty years, there has been a vast amount of industrial and academic intellectual effort and capital expended in the field of pressure swing adsorption, and the field is continuing to grow at a significant rate. This growth is reflected in the number of patents, journal articles, and the wide range of commercial applications of PSA (Sircar, 1996, p.49). Numerous excellent reviews of the field already exist and there is little benefit to be gained by restating these works (Ruthven et.al., 1994, Ruthven, 1984, Yang, 1987, Suzuki, 1990, Basmadjian, 1997, Kumar, 1996, Ruthven, 2000).

Instead this review will be limited to the key issues that underpin this research project. A useful starting point in this regard is to examine the recent history of industrial oxygen production through adsorption. This provides some general framework for understanding the key drivers that are shaping the evolution and commercial application of oxygen VSA, and more importantly highlight the reasons for undertaking this research project.

[1] A note on terminology. In the commercial world of gas adsorption, there is often distinction made between PSA, VPSA and VSA oxygen separation processes. The difference in these processes is whether the desorption step is to atmospheric or sub-atmospheric pressures.

## 1.2 Oxygen VSA and Competing Technologies

Oxygen is an industrial commodity used in a wide range of applications including wastewater treatment, metallurgical processes, pulp and paper and glass melting. This oxygen can be supplied principally by two competing process technologies - cryogenics and adsorption. Other alternative technologies exist such as the Moltox process, and (ceramic) membranes, however as yet, none of these processes has a strong commercial presence and they will be excluded from discussion here (Michael, 1997). This situation may change in the near future with the rapid growth of membrane technology, and its wider market penetration (Koros and Mahajan, 2001).

The competition between cryogenics and adsorption has produced intense rivalry to capture a larger share of the industrial oxygen market. Currently each process technology has a number of advantages and disadvantages over its competition. The traditional cryogenic production of oxygen offers economies of scale for the production of oxygen over 100 tpdc (tonne per day contained). The unit power consumption of cryogenic plants decreases as more efficient compressors are employed and process integration opportunities are exploited. In addition, above 90 tpdc, two parallel VSA plants are required and the cost is essentially two times a single plant, whereas with cryogenic plants the cost multiplier is 1.5 for doubling the plant size (Watson et.al., 1996 ).

Another distinct advantage of cryogenic plants is the ability to produce very high purity oxygen. Current adsorption systems for oxygen production are used to produce lower oxygen concentrations, typically 90-95% oxygen. However if these lower purities are acceptable, adsorption systems offer significantly lower capital costs than cryogenic plants for a wide range of product flows. Also, more recently attention is being paid to argon/oxygen separation in order to achieve 99+% purity by adsorption (Kanybin et.al.,1995).

Within the realm of adsorption technology for the industrial production of oxygen, there are essentially two competing processes - pressure swing adsorption (PSA) and vacuum swing adsorption (VSA). The essential difference between these two processes is that PSA operates at higher pressures (3-6 bar gauge) and is vented to atmospheric pressure on the desorption step. By contrast VSA operates slightly above atmospheric pressure, and the desorption step occurs at sub-atmospheric pressure, under vacuum. Currently, PSA technology is favoured

for the production of small quantities of oxygen (less than 5 tpdc). The distinct advantage of oxygen PSA over VSA is the lower capital cost, and the product oxygen is at elevated pressure and does not require an oxygen compressor after the process.

The main advantage of oxygen VSA over PSA for product flows greater than 5 tpdc is lower power costs, since VSA is more energy efficient. With the higher operating pressures of PSA, there is a greater amount of oxygen co-adsorption, and the selectivity of the molecular sieve is reduced. In effect the oxygen recovery for PSA is lower than for VSA. Also in the case of PSA, the entire air feed undergoes compression, whereas only the waste gas is evacuated in the case of VSA. As a result, more work is done on the entire feed stream in PSA (Kumar, 1996, p. 877-878). In addition, recent developments have seen a blurring of PSA and VSA whereby some emerging processes contain elements of both traditional PSA and VSA.

It is evident from the preceding descriptions of competing technologies, that there are significant competitive pressures to further develop these technologies and capture a larger slice of the industrial oxygen market. Moreover, as innovations drive the costs of industrial oxygen lower, it is clear new markets for oxygen will be found. The next section highlights some current directions of innovation in oxygen VSA, and points to the connection between these developments and thermal profiles in oxygen VSA.

### 1.2.1 Innovations in Oxygen VSA Technology and Thermal Implications

In contrast to cryogenic oxygen production, VSA can be considered a less mature technology, and as a result offers considerable scope for innovation and improvement (Campbell et.al., 1993). While a thorough review of recent VSA developments is beyond the scope of this project it is worthwhile to note a few of the recent innovations in oxygen VSA and the interaction between these developments and thermal profiles. The important point here is to demonstrate the centrality of how thermal issues impinge on several of the current directions of innovation of oxygen VSA.

One of the principal directions for the improvement of oxygen VSA has been the development of new molecular sieves. The resulting LiX and LiLSX molecular sieves offer improved nitrogen loading and selectivity than earlier generations of the molecular sieves (CaX and NaX) resulting in lower power costs and significantly smaller quantities of molecular sieve required (Kumar, 1996). One significant implication is that the increased loading and associated heat of adsorption can potentially lead to more severe CSS axial

temperature profiles. This can affect separation performance. This issue is explored at length through this thesis.

Another area of sieve development relates to sieves mounted on structured packing (such as monoliths). One of the significant energy losses associated with adsorptive separations is the pressure drop through the adsorbent bed. Potentially, structured packing offers much lower pressure drop with little resistance to mass transfer and a large adsorption surface area. (Li et.al., 1998). In addition, if the substrate for the adsorbent has a high thermal conductivity, thermal profiles could be dissipated by its utilisation (Calis et.al., 1995). Potentially this could lead to better molecular sieve utilisation.

Cycle development has also been a significant area of oxygen VSA process improvement (Kumar, 1996). New cycles have been developed, with steps such as co-current depressurisation, and feed repressurisation, which have both contributed to improvements in VSA performance. These steps can achieve marked reductions in power, and improve oxygen recovery. Efforts to reduce total cycle time are another current direction of cycle development. This achieves better adsorbent productivity and hence reduced capital costs. One manifestation of this direction to faster cycles is the development of one bed-one valve Rapid V/PSA (RV/PSA) where there is no purge or bed-to-bed connection. It is expected that such fast one bed cycles would not produce severe CSS temperature profiles. This issue is explored in this project. Much faster cycles (300 cycles/min) are also reported in recent patents by QuestAir Technologies with rotary pulsar VSA (Keefer et.al., 2000). The much smaller size associated with this revolutionary process technology will dramatically mitigate any CSS temperature profile.

The direction of new bed design can also impinge on the effect of thermal profiles in oxygen VSA. Radial beds have achieved some commercial prominence through Air Liquide's three-bed design (Poteau, et.al., 1993). The suggested advantages of radial beds are the elimination of fluidisation problems and better velocity profiles through the bed. One disadvantage of radial beds is higher construction costs.

In addition to these innovations and their thermal implications, some other suggested developments have been sought to improve oxygen VSA performance by modifying the thermal profiles (Rege and Yang, 1997, Notaro et.al., 1997, Gaffney et.al., 1993, Ackley

et.al., 2000). These strategies of 'thermal management' are explored in depth in Chapter Five.

These examples of current developments of oxygen VSA illustrate two points. Firstly, oxygen VSA is a fertile area of industrial research. Secondly, many areas of innovation require an understanding of thermal profiles in oxygen VSA, and 'thermal management' itself is a current area of oxygen VSA innovation. It is hoped that these brief examples highlight the industrial relevance of this project.

## 1.3 The 'Cold Spot' in Oxygen VSA- What is it?

Having introduced the industrial relevance of thermal profiles in oxygen VSA, it is timely to turn to the substantive business of this research project - thermal profiles in oxygen VSA. At the core of this research project is the need to develop a detailed understanding of the severe axial CSS thermal profiles in bulk gas separations such as oxygen VSA.

This physical phenomenon has been the source of much mystery and confusion in the academic and industrial communities (Ruthven et.al., 1994).This effect was first uncovered by Collins (1976) in a seminal patent, and is displayed in Figure 1.1.

> "Contrary to the prior art teachings of uniform adsorbent bed temperature during pressure swing air separation, it has been unexpectedly discovered that these thermally isolated beds experience a sharply depressed temperature zone in the adsorption bed inlet end ....." (Collins, 1976)

**Figure 1-1 – Axial CSS Temperature Profile (Collins, 1976)**

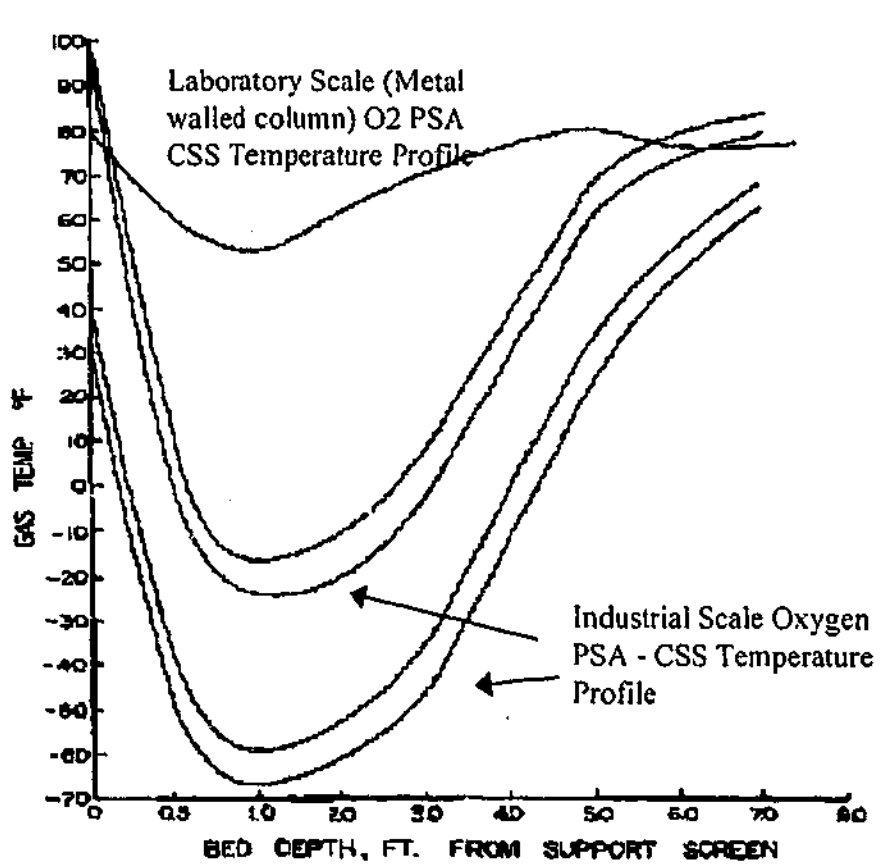


The essence of the problem is simple. It well known and understood that the adsorption of gas (nitrogen or oxygen) on to available sites in a zeolitic material releases heat of the range of 10-30 kJ/mol. The theoretical basis of this energy release has been thoroughly studied. As

a result it is expected that over a VSA cycle there will be a temperature swing associated with the adsorption and desorption steps. This temperature swing is observed, but in the case of some bulk gas separations, such as oxygen VSA, there is also a severe axial temperature profile as displayed in Figure 1.1. The magnitude of the profile far exceeds the 5-10 $^{o}$C temperature swing expected between adsorption and desorption steps. What underlying physical processes cause such a pronounced cyclic steady state temperature depression?

Curiously, Figure 1.1 is featured prominently in PSA literature as the object of much interest but little explanation (Ruthven et.al., 1994, 1984, Yang, 1987, Wankat, 1990). However, Collins himself made an important first step to detailing the mechanisms that give rise to the severe temperature profile.

> "It is believed that the inlet end temperature depression is most severe in those systems which experience an inadvertent heat regenerative step at such end. Such heat-regenerative step serves to cyclically receive and store the chilling effect of desorption during the counterflow periods of the process and to cyclically return the chilling effect to the bed during forward flow periods of the air separation process. When raw air which has not been pretreated is employed as the feed, a water-loaded zone develops in this region and essentially no oxygen-nitrogen separation occurs therein." (Collins, p.4, 1977)

A recent review of the history of oxygen VSA by Kumar offers some further explanation (Kumar, 1996). Kumar briefly indicates that the 'cold spot' results from differences in adsorptive characteristics, loading and heat of adsorption, of the different layers of adsorbent used in the bed (Kumar, 1996, p.890).

The brief explanations developed by Collins and Kumar are consistent with the models developed in this thesis. However, some researchers have offered accounts that are far less plausible. For example, Wankat offers the view that "the thermal wave of adsorption passes out of the column during the feed step, but stays in the column during the purge step because of the reduced gas density during purge. The result is a steady state temperature well below ambient." (Wankat, 1990, p.427) This is incorrect because, as will be demonstrated in this study, no such temperature depression is observed in a single layer adsorption bed with a dry air feed. Moreover a temperature depression could be caused by swinging the partial pressure in an adsorption column and keeping the total pressure (and hence gas density) the same. Likewise, Stegmaier speculated that water adsorption might directly cause the temperature depression (Stegmaier, 1996). However as shall be demonstrated in the course of this project, the effect of water is indirect.

Other researchers have witnessed the 'cold spot' but failed to grasp its significance. For example, Ishida and Takeuchi (1987) performed one of the earliest numerical simulations of a two layered oxygen PSA process. However they failed to appreciate the 'cold spot' phenomena and as a result they only simulated 60 cycles. This is very early in the evolution of the temperature profile, and the 'cold spot' will only appear as a slight dip. However Ishida and Takeuchi's paper is an important contribution to modelling bulk gas separation, and their ability to undertake non-isothermal cyclic numerical simulation for the required thousands of cycles was severely hampered by the slow CPU speed (8 Mhz).

These partial explanations, correct and otherwise, are offered to demonstrate that more work needs to be done to understand, explain and predict the thermal profiles in oxygen VSA under different process conditions. It is apparent that the industrial gas companies have through harsh experience acquired a detailed knowledge of the 'cold spot' in-house, but this is largely confidential. Within the open literature, there is not yet a detailed and complete explanation. This thesis undertakes this work in depth in Chapter Two.

While explanations of the 'cold spot' in oxygen VSA have been sparse and incomplete, some important research has been undertaken addressing issues of non-isothermality and temperature profiles in PSA adsorptive separation ($H_2/CH_4$ - Yang and Doong, 1985, $C_4H_{10}$/Air - Liu, et.al., 1998b, $H_2O$/Air -Lou, et.al., 1999, $H_2O$/Air - Lou, et.al., 1998, and $H_2/CO_2/CH_4/CO$ - Park, et.al., 1998, He/Air – Mahle et.al., 1996). While these systems do not display a 'cold spot', the mechanism that causes these profiles is still relevant to explanations of the 'cold spot' in oxygen PSA/VSA.

It is important to stress the 'cold spot' has been more than an unexpected curiosity to industrial gas companies. The separation performance of the oxygen VSA can be significantly affected by the severe axial temperature profile. This has seen a diversity of patents to both mitigate and exploit the 'cold spot'. Figure 1.2 highlights that the sieve productivity of the adsorbent NaX is a strong function of temperature for a specified partial pressure window. It is this non-linearity that can impact severely and unexpectedly on oxygen VSA performance.

**Figure 1-2**

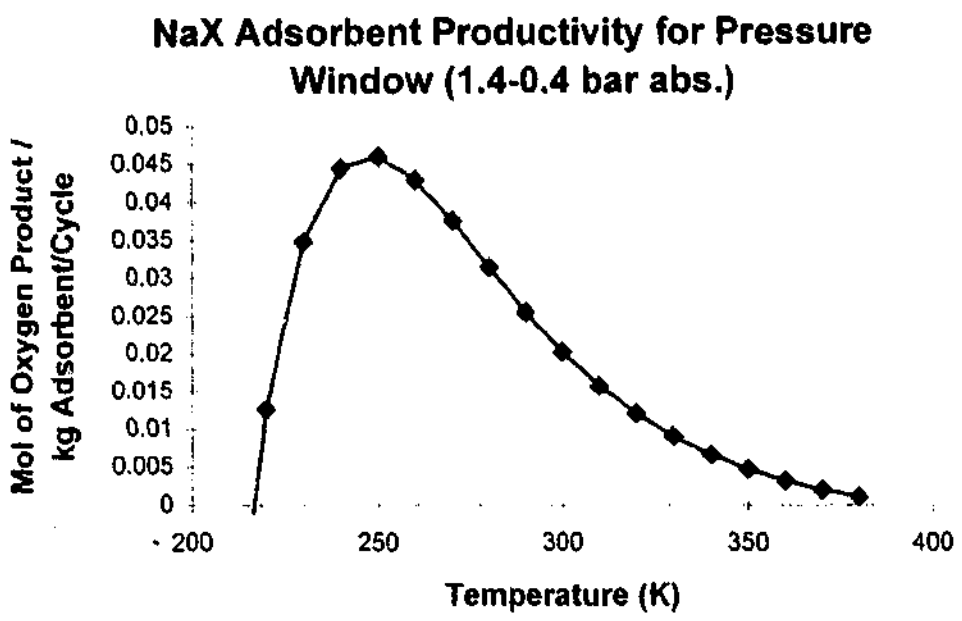


The productivity of NaX is a maximum at 250 K, but is reduced dramatically at temperatures below 240 K. At higher temperatures the productivity falls away gradually. The derivation of Figure 1.2, and the challenge of thermal optimisation strategies are taken up in Chapter Five.

## 1.4 Scale-Up Issues

One additional hurdle in the development of industrial oxygen VSA has been the absence of the 'cold spot' in laboratory scale columns. Collins (1976) first noted this point 25 years ago.

> "The temperature depression herein before described does not occur in adsorbent beds less than 12 inches effective diameter. In smaller beds, there is sufficient heat leak to the adsorbent such that the atmospheric heat moderates the depression and the process is not truly adiabatic." (Collins, 1976)

This is evident in the diagram of the axial temperature profiles in Figure 1.1, where the profile with the slightest temperature dip occurs in a small diameter metal walled (laboratory scale) column. This situation is problematic in two regards. Firstly, it has made investigating the 'cold spot' difficult because it is not evident using laboratory scale tools. Secondly, the absence or minimisation of the temperature depression in a laboratory scale column makes scaling up industrial plants an uncertain process. These two issues are central to this thesis, and form a substantial part of the work.

There is a large difference in the thermal behaviour of a 100 mm internal diameter metal walled laboratory column compared with a 2-3 metre diameter industrial column. As Collins suggests, in the case of the small laboratory column there is significant heat exchange with the environment, whereas in the case of the industrial column the thermal behaviour is much closer to adiabatic. Also the thermal capacitance and conductivity of the wall in a typical laboratory scale column can also play a role in shaping the cyclic steady state axial temperature profile. This raises an obvious question: "Can a novel laboratory scaled column be built with thermal characteristics that more closely mimic an industrial scale adsorption bed?" This question is addressed in Chapter Three.

It is also important to realise that achieving significant thermal profiles in a laboratory scaled column would be of more than explanatory value. The substantial difference in axial thermal profiles between laboratory and industrial columns can lead to very different efficiency in oxygen separation and overall VSA performance. For example, one patent suggests that there can be approximately a 20% reduction in performance in the industrial (full-scale bed) compared with a typical metal walled laboratory unit (Watson, et.al., 1996). This makes scale up of laboratory results a difficult process and can lead to commercial failures.

As will be demonstrated elsewhere in this thesis, it is not necessarily the case that the performance of an industrial VSA unit is always worse than a laboratory VSA unit. The critical point here is the differences in the thermal performance can give rise to differences in overall performance, and this makes scale up difficult. Circumstances under which the 'cold spot' can aid separation efficiency are also revealed in Chapter Five.

## 1.5 Goals and Objectives of this Study

Oxygen VSA is an established industrial process undergoing further development. The focus of this thesis is to develop an understanding of the thermal profiles identified by Collins and which have been the source of much consternation to the gas industry. It is hoped that an improved understanding of the underlying mechanisms will enable new strategies of optimisation of oxygen VSA.

This thesis is structured into four main chapters - modelling, experimental apparatus, experimental results, and optimisation. The literature review is introduced as needed at appropriate places in the thesis. This is in contrast to a more conventional approach of reviewing all the literature in a separate chapter. I believe that the approach adopted here considerably eases the readability of this thesis, and enables the complete treatment of relatively discrete sections.

The objectives of the four main chapters in this study are as follows:

Chapter 2 - Modelling

- Develop a non-isothermal numerical model for the simulation of oxygen VSA with a particular focus on heat transfer with the adsorber wall and the environment.
- Develop a number of simpler models for explaining and roughly predicting the CSS and dynamic thermal profiles in oxygen VSA
- Develop several perturbation techniques that are based on the premise that the ratio of the thermal capacitance of the gas and solid can be identified as a perturbation parameter. These perturbation techniques are presented as a useful heuristic device and as a possible acceleration scheme for numerical simulation of oxygen VSA. This exploration of perturbation technique is not exhaustive, and constitutes a significant area of mathematical endeavour where more work is possible.
- Develop an analytical technique for predicting the penetration of a water-loaded zone in oxygen VSA unit at CSS.

Chapter Three - Experimental Apparatus and Procedure

- Design, construct, commission and operate a laboratory scale oxygen VSA unit.
- Design and construct 'adiabatic' laboratory scale adsorption beds. Characterise these beds and compare them with metal and PVC columns with external insulation.

Chapter Four - Experimental Results and Discussion

- Investigate experimentally a range of operational, adsorbent, and adsorber parameters that impinge on the CSS and dynamic thermal profiles in oxygen VSA.
- Compare the experimental results with full numerical simulation, and with the simpler models developed in Chapter Two.

Chapter Five - Optimisation of Thermal Profiles

- Review the relevant patent literature that has sought to improve separation performance of oxygen PSA/VSA by modifying thermal profiles. These reported strategies include mitigating the axial thermal profile, optimising the axial thermal profile and reducing the cyclic temperature swing between adsorption and desorption.
- Develop a fundamental performance criterion by relating isotherm properties to sieve productivity and recovery and then linking these process performance parameters to adsorbent, blower and power costs.
- Outline some novel strategies for the thermal optimisation of oxygen VSA utilising cost based performance criteria.

# Chapter Two
# Modelling and Explaining Oxygen VSA Thermal Profiles

In order to understand the nature of thermal profiles in oxygen VSA it is necessary to understand intimately the oxygen VSA process. Oxygen VSA is a complex unit operation that involves combined heat and mass transfer in a cyclic process that is characterised by slow evolution to cyclic steady state (CSS). Numerical modelling of oxygen VSA can provide a powerful tool for understanding the process. This chapter starts with a description of a detailed numerical model used in this study called MINSA (Monash Integrated Numerical Simulator of Adsorption) and gives the approximations made in this model. MINSA is used throughout this study as a tool to help elucidate thermal profile information and can be used as a substitute for experimental data for conditions that are experimentally hard to achieve. In some limited instances ADSIM is also used for numerical simulation.

A significant limitation with numerical simulation is that it does not give 'engineering insight' into the nature and evolution of thermal profiles in oxygen VSA. This chapter offers some alternative models including qualitative, simple energy balance and perturbation models of thermal profiles in oxygen VSA. The benefits and limitations of these models are explored. These models are not a substitute for numerical simulation, but each assists in enhancing our understanding of the phenomena of thermal profiles in oxygen VSA. Lastly, the chapter develops a model to determine the penetration distance of a water-loaded zone into the prelayer of a VSA unit. The presence of a water-loaded zone can significantly alter the CSS temperature profile.

## 2.1 Modelling VSA - A Review

Bulk gas separations by PSA or VSA are complex unit operations. Considerable effort has been applied to develop models for the numerical simulation of these separation processes. This section reviews the modelling assumptions commonly made in bulk gas separation processes such as oxygen VSA. The focus of this review is on a 'typical' large scale industrial oxygen VSA system. This VSA system is compromised of 1, 2 or 3 identical vertical adsorption beds filled with nitrogen selective molecular sieve beads. The beds may be multi- or single layered with adsorptive beads of approximately 2-3.2 mm diameter. The bed length is 1.5-1.8m. The adsorption beds are subjected to an air feed of 1.4-1.3 bar (abs) and are evacuated to a vacuum of 0.4-0.3 bar (abs). The air is fed to the bottom of these beds and an enriched oxygen stream is withdrawn from the top of the bed. The adsorption beds contain no internal heaters. The total cycle time is of the order of one minute. The voidage at the bottom and top of the adsorption beds is small relative to the volume of the adsorption bed. Due to the symmetry between the beds, a VSA process can be modelled as a single adsorption bed. Figure 2.1 shows the typical pressure profile (140 kPa - 35 kPa) and step

times for a single adsorption bed in a typical 8 step cycle with a total cycle time of 60 seconds.

**Figure 2-1- One Bed Representation of Two Bed Cycle (with PE)**

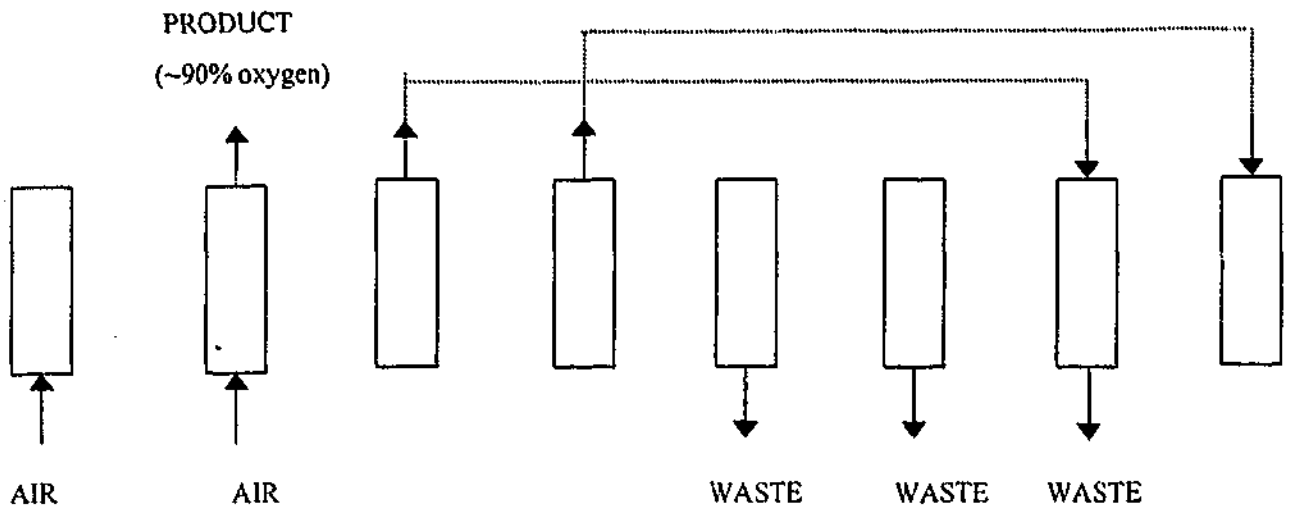


| Step 1 | Step 2 | Step 3 | Step 4 | Step 5 | Step 6 | Step 7 | Step 8 |
|---|---|---|---|---|---|---|---|
| Feed Repress.# | Feed | Provide Purge | Provide PE# | Evacuation | Evacuation | Receive Purge | Receive PE# |
| *130 kPa | 140 kPa | 105 kPa | 95 kPa | 50 kPa | 35 kPa | 50 kPa | 70 kPa |
| 12 sec | 10 sec | 5 sec | 3 sec | 12 sec | 10 sec | 5 sec | 3 sec |

Typical end of step pressures; # Feed Repress. = Feed Repressurisation, Provide PE = Provide Pressure Equalisation, Receive PE = Receive Pressure Equalisation
The dashed line (----) indicates the presence of bed-to-bed connections.

This is a typical cycle and pressure profile used for several experiments in this study which are detailed in Chapter Four.

The principle difference between this 'typical' industrial oxygen VSA unit, and a laboratory VSA, is that additional attention is required for modelling the thermal effects associated with heat loss and the column wall in the small diameter (laboratory) VSA unit.

### 2.1.1 Modelling Assumptions and Limitations

Restricting the investigation to this 'typical' oxygen VSA unit and its laboratory scale version enables a number of simplifying assumptions. These assumptions are adopted in MINSA (Monash Integrated Numerical Simulator of Adsorption) which is an adsorption simulator developed specifically to model this 'typical' oxygen VSA unit. Other adsorption simulators, ADSIM 6.1 (Aspentech, 1997), SIMPAC (Kumar, et.al., 1994), and MAUS (Hofmann, 1999) are based on a similar set of assumptions. These numerical simulators are an invaluable tool for modelling the behaviour of oxygen VSA systems, and generally achieve excellent agreement with both industrial and laboratory oxygen VSA data (Todd, et.al., 2000b; Kumar, et.al., 1994, Hofmann, 1999).

MINSA is used throughout this study. However one limitation with MINSA is the simplicity of its wall heat transfer model. In instances where a more complex wall model is required, ADSIM 6.1, a commercially available simulation package by ASPENTECH is utilised. The physical model that underpins MINSA is otherwise identical to that deployed in ADSIM.

**1 Dimensional Model:** There is no consideration of radial profiles in the vertical beds. This can be justified on the basis that there is no maldistribution in the flow within the bed, the adsorption beads are small relative to the bed diameter, and the heat loss from the adsorption bed is small. Work by Farooq and Ruthven (1990) and Lin, Farooq, and Tien (1999) has demonstrated the validity of modelling a bulk gas separation as a one-dimensional problem. Potentially, the only problem with this assumption relates to the radial heat profile in a small adsorption column. This is addressed in a subsequent section.

**Isotherm Model:** A binary dual-site Langmuir model is a suitable model of adsorption loading of nitrogen and oxygen on the microporous molecular sieves utilised in this study. Ideally, experimentally determined multicomponent isotherms should be used. However, where this is not possible, IAS (Ideal Adsorbed Solution) theory can be used to combine pure component data to derive multicomponent isotherms. It is important to note that argon is explicitly ignored in these binary isotherms. Instead, for the adsorbents used in this study it is assumed that argon behaves in the same way as oxygen (Choudray et.al., 2000, Jasra et.al., 1996). Obviously this approach would be invalid for high purity oxygen production (99%+) where argon/oxygen separation is critical.

The study also considers the adsorption of water to molecular sieve and activated alumina. Water is very strongly adsorbed and presents a highly favourable isotherm when adsorbed to NaX. A dual site Langmuir can describe this near rectangular isotherm. The model of water adsorbing to activated alumina is more complex (Chou et.al., 1998).

**Gas Properties and Flow Behaviour:** Given the physical properties of nitrogen and oxygen over the process envelope experienced in a VSA cycle, it is reasonable to assume the perfect gas law applies. The assumption of perfect gas behaviour ignores the Joule-Thompson effect. This can be justified due to small pressure window and physical properties of oxygen and nitrogen. The Joule-Thompson coefficient for nitrogen at one atmosphere and 25 $^{o}$C is 0.2217 (Perry, ed., 1984, p. 3-110). The gas viscosity and heat capacity of nitrogen and oxygen are functions of temperature.

A more significant assumption is that the gas flow is plug flow, and that axial dispersion can be neglected. The axial bed Peclet number determines the validity of this assumption.

$$Pe = \frac{uL}{E_z} \qquad (2\text{-}1)$$

where $E_z$ is the axial dispersion coefficient ($m^2$/sec)

u is superficial velocity (m/sec) (~0.5 m)

L is the bed length (m) (~2 m)

The following equation by Wakao (1976) can be used to calculate the axial dispersion coefficient.

$$E_z = 20\frac{D_{m,i}}{\varepsilon_b} + r_p u \qquad (2\text{-}2)$$

where $D_{m,i}$ is the multicomponent molecular diffusion coefficient based on the Chapman - Enskog equation at 1 bar , 300 K and air (6.9E-6 $m^2$/sec) (Bird, et.al., 1960, p.510)

$r_p$ is the pellet radius (~1.5E-3 m)

$\varepsilon_b$ is the interparticle voidage (~0.37)

Typical values for an oxygen VSA unit are shown in brackets. The resulting value for the axial dispersion coefficient $E_z$ = 0.00188 $m^2$/sec and the Peclet number is approximately 800. On this basis plug flow can be assumed and the second order axial dispersion term

neglected from the mass balance. This significant assumption may not be valid in other adsorptive separations.

**Adsorbent and Adsorbate physical properties:** Over the operating temperature range, the axial conductivity, density and the heat capacity of the adsorbent phase are treated as constant. The heat capacity of the adsorbate is assumed to be equal to the heat capacity of the gas. This last assumption is debatable (Liu and Ritter, 1998).

**Mass Transfer Kinetics:** While oxygen VSA is ostensibly an equilibrium separation, consideration of mass transfer kinetics is critical for determining separation performance, particularly with the emergence of faster VSA cycles. A linear driving force model is used to describe the mass transfer kinetics from the gas to the solid phase (Glueckauf and Coates, 1947, Glueckauf, 1955). The physical justification of this model is that oxygen VSA operates relatively close to equilibrium, and that the mass transfer resistance lies in the macropores of the molecular sieve (Ruthven and Xu, 1993; Karger and Ruthven, 1992). The resulting mass transfer coefficient, $k_i$, becomes :

$$k_i = \frac{60 D_{e,i}}{d_p^2} \text{ where } D_{e,i} = \frac{\varepsilon_p}{\alpha_p}\left(\frac{1}{\frac{1}{D_{m,i}} + \frac{1}{D_{K,i}}}\right) \qquad (2\text{-}3)$$

where $d_p$ is the adsorbent pellet diameter (m)

$D_{e,i}$ is the effective diffusion coefficient for component i ($m^2$/sec)

$\varepsilon_p$ is the adsorbent pellet porosity

$\alpha_p$ is the tortuosity of the pellet

$D_{K,i}$ is the Knudsen diffusion coefficient ($m^2$/sec)

The molecular and Knudsen diffusion coefficients are calculated by use of the standard expressions for these quantities (Sherwood et. al., 1975). The advantage of this assumption is that it makes computation relatively easy, and it is typically adopted for many adsorptive separations, including oxygen VSA. Limitations of this simple mass transfer model are the subject of current academic and industrial attention. For example, modelling rapid PSA process technology with much faster cycles operating further from equilibrium, probably warrants a more realistic mass transfer model, such as the dusty gas model (Todd, 2000a, Sotirchos and Serbezov, 1997a, Sotirchos and Serbezov, 1997b).

**Momentum Balance:** Oxygen VSA is a bulk gas separation with pressure driven flows through a porous medium. Velocity variations and the pressure drop within the bed are significant, and need to be calculated. Instead of endeavouring to solve the full momentum balance, the Ergun equation is used to relate pressure drop to velocity and other gas and bed properties. The Ergun equation is the most general of pressure drop correlations as it covers both laminar and turbulent flow regimes (Ergun, 1952, Todd et.al., 2001).

**Energy Balance:** One of the main simplifying assumptions in the development of the non-isothermal pressure swing adsorption models is thermal equilibrium between the gas and solid phase for a given axial position. The resulting energy balance is a single pseudo-homogeneous model written for both the gas and solid phase. The basis for this assumption is a high heat transfer coefficient between the solid and gas phases (Kumar and Sircar, 1986). The energy balance is also developed to include the thermal capacitance of the adsorbate. However in some sections of this study, further simplifying assumptions are made to ignore this term. The justification for neglecting this term is that the thermal capacitance of the adsorbate is small relative to the thermal capacitance of the solid. Axial conduction through the solid is also neglected due to the small thermal conductivity of molecular sieve (typically 0.25-0.3 W/mK). In addition, thermal conductivity has a dissipative effect in the thermal profile, and in some cases it is neglected, as it is not a causative mechanism in the evolution of thermal profiles.

The energy balance is also developed to include the term for the heat of compression of the gas phase. However for the typical VSA process conditions, this term can generally be neglected, as has been demonstrated by Psaras, Leach, and LaCava (1988). Some experimentation and analysis were also conducted to demonstrate that the heat of compression is small relative to the heat of adsorption for the pressure window investigated.

The model developed here has a number of different ways of estimating the heat of adsorption, the simplest being a constant heat of adsorption based on the parameters in the dual-site Langmuir model. This constant value can be based on a weighted average of the two adsorption sites, or more simply by the mean value of the two heats of adsorption. Alternatively a more rigorous estimation of the isosteric heat of adsorption can be made based on the Clausius-Clapeyron equation (Sircar, 1985).

**Wall Heat Transfer Coefficient ($h_{wi}$):** In order to model the thermal behaviour of oxygen VSA (in a small diameter column), one of the critical and complex parameters is the heat transfer coefficient between the adsorption bed and the wall. Correlations for this parameter are largely derived from the fixed bed reactor literature. For example, one commonly used correlation for determining $h_{wi}$ was developed by Li and Finlayson (1977) for non-adsorbing packed beds.

$$h_{wi} = \frac{2.03k_g\left(\frac{d_p u \rho_g}{\mu_g}\right)^{0.8}}{D}\exp\left(\frac{-6d_p}{D}\right) \qquad (2\text{-}4)$$

where D is the diameter of the adsorption bed (m)

$k_g$ is the thermal conductivity of the gas (W/m K)

$\rho_g$ is the density of the gas (kg/m$^3$)

$\mu_g$ is the viscosity of the gas (Pa sec)

$h_{wi}$ is the inside wall heat transfer coefficient (W/m$^2$ K)

This relatively simple correlation is utilised within MINSA. A similar form of this equation, the Leva correlation, is utilised by Ruthven (1984) and Park et.al. (1998).

More complex and detailed correlations have been developed based on the work of Dixon and Cresswell (Dixon, 1985, Dixon and Creswell, 1979), and subsequently utilised by Lin et.al. (1999). Lin et.al. (1999) sought to develop a correlation for $h_{wi}$ for an adsorbing bed. One of the main equations resulting from this work, involving the summation of the bed and wall resistances to determine the overall heat transfer coefficient, is as follows:

$$\frac{1}{h_{wi}} = \frac{1}{\alpha_w} + \frac{D}{2\nu k_{er}} \qquad (2\text{-}5)$$

where $\alpha_w$ is the two dimensional wall film heat transfer coefficient. (W/m$^2$ K)

$k_{er}$ is the effective radial conductivity based on both the fluid and solid phases(W/m K)

$\nu$ is an adjustable parameter to linearise the bed resistance term to account for the effect of the radial temperature distribution (Dimensionless)

Dixon (1985) proposed that ν varies between 3-6 depending on the operating conditions of a non-adsorbing bed. Lin et.al. (1999) considered a wider range of operating conditions for an adsorbing bed and developed an empirical correlation for ν based on 7 dimensionless groups. Based on this work the approximate value for ν for a typical oxygen VSA system is 10 and the approximate value of $h_{wi}$ is 50 W/m$^2$ K. However it should be stressed that the adsorption system considered by Lin et.al., differs to an oxygen VSA process markedly, and it is debatable whether the correlation is applicable.

Suzuki offers an alternative empirical correlation (Suzuki, 1990).

$$h_{wi} = \frac{k_{er}}{D}\left(a_1^2 + \frac{\delta(b)}{\xi}\right) \qquad (2\text{-}6)$$

where $a_1$, $\delta(b)$, and $\xi$ are parameters based on work by Yagi and Kunii (1961). Based on this correlation, a typical value of $h_{wi}$ for oxygen VSA operating conditions is 40 W/m$^2$ K.

Alternatively, an overall wall heat transfer coefficient can be obtained directly from empirical data for adsorption systems. For air purification by PSA, Mahle et.al. (1996) report a wall heat transfer coefficient of 93 W/m$^2$ K. Hwang, et.al. (1995) select a wall heat transfer coefficient of 42 W/m$^2$ K as a commonly reported value for activated carbon. Similarly, Murray (1996) in a one-bed RPSA study with 5A reports 42 W/m$^2$ K as the wall heat transfer coefficient. However it is unclear how this figure was determined.

This discussion highlights the need for further effort, to develop more detailed approaches to determine the wall heat transfer coefficient for oxygen VSA, and for adsorption processes in general. In some instances, $h_{wi}$ is a data fitted parameter, and this limits the scope of solely numerical simulator based investigations of adsorptive separations. In fact the absence of adequate wall heat transfer models is in part the justification for this research project. The need for 'adiabatic' laboratory scale beds is increased by the inability to adequately model the heat loss term to the wall. Unlike kinetic and isotherm parameters, which can reliably be predetermined by independent experimental techniques. current knowledge does not permit similar reliable and accurate determination of $h_{wi}$.

Based on the correlations sourced, when required, a constant value of 50 W/m$^2$ K will be assumed. This is obviously an approximation, but reflects the lack of reliable data available. It would be preferable not to use a constant value, but this is acceptable for numerical

simulations undertaken. Moreover, it should be stressed that this assumption does not impinge on the MINSA simulations, where (as detailed below) an overall heat transfer coefficient is utilised, which is dominated by the heat transfer resistance associated with the natural convection between the adsorption column outer wall and the ambient environment.

**The Wall and Heat Loss:** In modelling industrial VSA units, the explicit treatment of the wall can generally be neglected, and replaced with an overall heat loss term. This heat loss term is based on the temperature driving force between the system and the environment, and an overall lumped heat transfer coefficient. The overall heat transfer coefficient is based on the internal and external heat transfer coefficients, and the radial wall conductivity (Ruthven, 1984). The same approach is adopted in MINSA where the overall heat transfer coefficient is calculated as follows:

$$h_{wo} = \left[ \frac{1}{h_{wi}} + \frac{D \ln(D_o / D)}{2k_w} + \frac{1}{h_o} \right]^{-1} \qquad (2\text{-}7)$$

where $k_W$ is the thermal conductivity of the wall (W/m K)

$h_O$ is the heat transfer coefficient on the outside of the column ($W/m^2K$)

$h_{WO}$ is the overall wall heat transfer coefficient ($W/m^2K$)

$D_o$ is the outside diameter of the adsorption vessel (including the wall) (m)

Aside from the previously described difficulties in obtaining an accurate correlation for $h_{wi}$, determination of $h_{wo}$ is quite straight-forward.

However, the limitation of this simple approach can be important when considering a small diameter laboratory column. In such cases, as will be detailed in Chapter Three, the thermal effects of the wall can be more significant and require more detailed treatment. The wall can act as both a thermal sink and source, and can also be a prominent path for the axial conduction of heat. This has been recognised in the modelling literature, and several efforts have been made to more fully account for the thermal effects of the wall.

Farooq et.al., for example, have developed a single heat balance equation that includes both the wall and the adsorption bed (Farooq et.al, 1990, p. 1026). This energy balance equation essentially provides a cross sectional area average of the contribution of the column wall to the thermal capacitance and axial conduction of the adsorption bed.

$$\left(\frac{A_b}{A_t}\rho_g C_{pg} + \left(\frac{1-\varepsilon_b}{\varepsilon_b}\right)\frac{A_b}{A_t}\rho_s C_{ps} + \frac{A_w}{A_t \varepsilon_b}\rho_w C_{pw}\right)\frac{\partial T}{\partial t} =$$
$$-\left(k_b \frac{A_b}{A_t} + \frac{k_w}{\varepsilon_b}\frac{A_w}{A_t}\right)\frac{\partial^2 T}{\partial z^2} + u\rho_g C_{pg}\frac{\partial T}{\partial z} - (-\Delta H)\left(\frac{1-\varepsilon_b}{\varepsilon_b}\right)\frac{\partial n}{\partial t} + \frac{4h_{wo}}{\varepsilon_b D}(T - T_{ref}) = 0 \quad (2\text{-}8)$$

where $A_b$ is the cross sectional area of the bed ($m^2$)

$A_t$ is the total cross sectional area of the bed and adsorption column wall ($m^2$)

$A_w$ is the cross sectional area of the wall ($m^2$)

$k_b$ is the effective thermal conductivity of the bed (W/mK)

$k_w$ is the thermal conductivity of the wall (W/mK)

$\rho_w$ is the density of the wall ($kg/m^3$)

$C_{pw}$ is the specific heat capacity of the wall (J/kg K)

$C_{ps}$ is the specific heat capacity of the adsorbent (J/kg K)

$C_{pg}$ is the specific heat capacity of the gas (J/kg K)

T is the temperature (K)

It is evident from this equation that as the wall terms reduce to zero, the equation reverts to a typical form of the energy balance. This situation occurs in an industrial scale column based on the relative cross sectional area contributions of the wall and the bed. However in the case of a typical laboratory scale column, the wall could contribute significantly to the heat balance equation. From this equation, the influence of the wall can be minimised by reducing the wall thickness, and/or selecting a wall material with a low density, low specific heat, and low thermal conductivity.

One limitation of this approach is that, for a given axial position, the wall and adsorbent are assumed to be the same temperature, and in effect the wall heat transfer coefficient is assumed to be infinite. This would tend to dampen the cyclic adsorptive/desorptive temperature fluctuations unrealistically, and predict overly optimistic separation performance. With relatively short cycle times and the low thermal conductivity of typical molecular sieve, such a simple area average does not capture the full nature of the problem.

Instead of adopting an assumption of a uniform radial temperature profile across the bed and wall, a slightly different model is proposed by Rota and Wankat (1990), where the wall temperature is taken as the arithmetic average of the ambient temperature and the bed temperature.

A more rigorous approach to modelling the wall has been developed by Lee et.al. (1995) for a single breakthrough step, and by ADSIM for cyclic simulations (Aspentech, 1997). In these cases, a separate energy balance is written for the wall. In the case of ADSIM, this equation is as follows:

$$-k_w \frac{\partial^2 T_w}{\partial z^2} + \rho_w C_{pw} \frac{\partial T_w}{\partial t} - h_{wi} \frac{4D}{D_o^2 - D^2}(T - T_w) + h_o \frac{4D_o}{D_o^2 - D^2}(T_w - T_{amb}) = 0 \quad (2\text{-}9)$$

where $T_w$, $T_{amb}$ is the wall and ambient temperature respectively (K)

The equation captures the thermal capacitance and axial conductivity of the wall, and the heat exchange between the wall and the environment, and between the wall and the adsorption bed. This is still a one-dimensional heat balance. Any radial temperature gradient through the wall is neglected. This assumption will hold if the wall is thin and conductive i.e. metallic. The other complication is that the benefit of providing this more exacting treatment of the adsorber wall, is at the cost of increased computational time. The discretised form of this equation provides another set of N equations to solve, where N is the number of nodes resulting from the discretisation.

**Extra Column Effects:** In addition to modelling the adsorption column, it can also be necessary to model the voidages at both ends of the adsorption column. These volumes at the ends of the bed can contribute to variations in the performance. For example, the dead volume at the entrance of the adsorption bed contributes to a loss of oxygen recovery. There can also be heat loss from the end of bed voidages as well as the surrounding pipework.

It can also be important to model the product tank, as the pressure in the product tank determines the instantaneous product flow, and in one-bed cycles, product pressure determines the extent of product purge and pressurisation. Heat loss from the product tank can also be significant.

MINSA does not currently model these extra columns effects, but ADSIM 6.1 is capable of incorporating these effects, if required.

**Boundary Conditions and Bed-to-Bed Connections:** One of the significant complexities in modelling PSA separations is the frequent changes of boundary conditions over a cycle, and the presence of bed-to-bed connections. Four types of fixed flow boundary conditions are used - constant pressure, constant velocity, constant molar flowrate, and flow through a valve with a fixed Cv. The latter boundary condition incorporates a valve equation. Fixed composition and temperature boundary conditions are also used. The bed-to-bed steps, such as purge and pressure equalisation, are achieved by assuming symmetry between the adsorption beds, and storing pressure, velocity, and composition data into a vector for a 'provide' step, and using it as the boundary condition for the parallel 'receiving' step. This enables a multi-bed VSA unit to be modelled as a single bed, assuming perfect symmetry between the beds (Todd et.al., 2000b).

**Control Loops and CSS Determination:** Another important aspect of modelling PSA processes characterised by slow evolutionary behaviour, is to develop control schemes to achieve process set points, such as product flow, purity, and end of step pressures. Such control schemes are critical for optimisation studies, in order to enable direct comparison between different design conditions. In industrial practice, PID control is applied to achieve set point purity and pressure profiles in oxygen VSA. PID can also be applied to achieve control of the numerical simulation to the desired set points, through adjustment of valve Cv's and flows. Experience is required to align the appropriate manipulated and control variables, and to determine the appropriate PID values to achieve convergence and stability (Todd et.al., 2000b).

An alternative to PID control is manual manipulation of the boundary conditions (valve Cv's) to achieve pressure, purity and flow set points. The major benefit of PID control is in cases where tight tolerances are required in order to afford comparison between different operating conditions.

The slow evolutionary dynamics that characterise oxygen VSA also present problems for the determination of CSS. Closure of the mass and energy balances is required to within a tight tolerance along with periodicity of all state variables (Webley and He, 2000b).

### 2.1.2 The Resulting Model

Based on the preceding assumptions, the resulting total and component mole balances are as follows.

**Total mole balance:**

$$\frac{\partial p}{\partial t} = -\frac{\varepsilon_b T}{\varepsilon_t}\frac{\partial}{\partial z}\left(\frac{pv}{T}\right) - \frac{\rho_b RT}{\varepsilon_t}\left(\frac{\partial n_{N2}}{\partial t} + \frac{\partial n_{O2}}{\partial t}\right) + \frac{p}{T}\frac{\partial T}{\partial t} \qquad (2\text{-}10)$$

where p is the total pressure (bar)

$\varepsilon_t$ is the total voidage of the bed

R is the universal gas constant (83.1441E-6 $m^3$ bar/ mol K)

v is the interstitial velocity (m/sec)

$n_{N2}$, $n_{O2}$ are the adsorbate loading of nitrogen and oxygen respectively (mol /kg)

**Component mole balance (i):**

$$p\frac{\partial y_i}{\partial t} = -\frac{\varepsilon_b T}{\varepsilon_t}\frac{\partial}{\partial z}\left(\frac{py_i v}{T}\right) - \frac{\rho_b RT}{\varepsilon_b}\frac{\partial n_i}{\partial t} - y_i\frac{\partial p}{\partial t} + \frac{py_i}{T}\frac{\partial T}{\partial t} \qquad (2\text{-}11)$$

where $y_i$ is the mole fraction of component i

$n_i$ is the adsorbate loading of component i

$$\sum_{i=1}^{n} y_i = 1 \qquad (2\text{-}12)$$

**Dual-Site Langmuir Isotherm**

$$n_i^* = \frac{m_1 b_i p_i}{1 + \sum_{j=1}^{n} b_j p_j} + \frac{m_2 d_i p_i}{1 + \sum_{j=1}^{n} d_j p_j} \qquad (2\text{-}13)$$

where $b_i = b_{i,o}\exp\left(Q_{1,i}/RT\right)$ and $d_i = d_{i,o}\exp\left(Q_{2,i}/RT\right)$

where $m_1$, $m_2$, $b_{i,o}$, $d_{i,o}$, $Q_{1,i}$ $Q_{2,i}$ are Dual-site Langmuir parameters for nitrogen and oxygen.

**Mass Transfer Model - Linear Driving Force**

$$\frac{\partial n_i}{\partial t} = k_i(n_i^* - n_i) \qquad (2\text{-}14)$$

where $n_i^*$ is the equilibrium loading of component i at the specified T, p, $y_i$

**Ergun equation**

$$-\frac{\partial p}{\partial z} = \left[\frac{1.75(1-\varepsilon_b)\rho_g M_{wg}}{\phi_s \varepsilon_b d_p}\right] v^2 + \left[\frac{150\mu_g(1-\varepsilon_b)^2}{\phi_s{}^2 \varepsilon_b^2 d_p^2}\right] v \qquad (2\text{-}15)$$

where $\phi_S$ is the sphericity of the adsorbent bead or pellet

$M_{wg}$ is the molecular weight of the gas

**Energy Balance**

Unlike the mass balance, there are still some small differences in the formulations of energy balances used in adsorption research. This necessitates careful consideration to ensure the energy balance is internally and thermodynamically consistent. Appendix 1 provides a derivation of the energy balance.

$$\left(\rho_b \bar{C}_s + \rho_b \bar{C}_{ad} + \varepsilon_t \rho_g \bar{C}_{pg}\left(\frac{T_{ref}}{T}\right)\right)\frac{\partial T}{\partial t} +$$

$$\left(\varepsilon_t \rho_g \bar{C}_{pg}\left(\frac{T - T_{ref}}{p}\right) - \varepsilon_t\right)\frac{\partial p}{\partial t} + \left(\varepsilon_t \rho_g (T - T_{ref})(C_{pg,N2} - C_{pg,O2})\right)\frac{\partial y}{\partial t} = \qquad (2\text{-}16)$$

$$-\varepsilon_b \frac{\partial}{\partial z}\left(\rho_g v \bar{C}_{pg}(T - T_{ref})\right) + \rho_b \sum_{i=1}^{n}\left(\Delta H_i \frac{\partial n_i}{\partial t}\right) - \frac{4h_{wo}}{D}(T - T_{amb}) - \rho_b (T - T_{ref})\left(\sum_{i=1}^{n} C_{pg,i}\frac{\partial n_i}{\partial t}\right)$$

where $\rho_g = p/RT$ (Density based on perfect gas law) (mol/m$^3$)

$\bar{C}_{pg} = yC_{pg,N2} + (1\text{-}y)\, C_{pg,O2}$ (Average heat capacity of gas) (J/mol K)

$\bar{C}_{ad} = n_{N2} C_{pN2} + n_{O2} C_{pO2}$ (Ave. heat capacity of adsorbate) (J/kg K)

$\Delta H_i$ is the heat of adsorption for component i (J/mol)

**Heat of Adsorption**

There are a number of different options for the calculation of the heat of adsorption. The simplest is to assume constant values for the nitrogen and oxygen adsorption. A significant limitation with this assumption is that a dual site Langmuir model is premised on two adsorption sites with independent heats of adsorption. To overcome this problem, the constant heats of adsorption could be simple arithmetic averages or weighted averages of the heats of adsorption associated with the individual sites.

Alternatively the heat of adsorption can be calculated using the Clausius-Clapeyron equation.

$$\Delta H_i = -\frac{RT^2}{p_i}\left(\frac{\partial p_i}{\partial T}\right)_{n_{N2},n_{O2}} \qquad (2\text{-}17)$$

The term $(\partial p_i / \partial T)_{ni,nj}$ is determined through the isotherm relation $n_i^{eq} = n_i^{eq}(p_1, p_2, T)$ at a specific loading. However this requires significantly more computational time (Todd, et.al., 2000b).

### 2.1.3 Numerical Schemes - MINSA and ADSIM

A wide range of numerical techniques have been applied to solving the resulting mass and energy balance equations, including orthogonal collocation (Ruthven et.al. 1985; Ruthven, et.al. 1986; Farooq et.al. 1989; Aspentech, 1998), the method of lines (Chou and Huang, 1994), finite volume analysis (Todd et.al., 2000b; Hofmann et.al. 1999; Kumar et.al., 1994) and finite difference methods.

The two numerical simulators used in this study (MINSA and ADSIM 6.1) deploy different numerical schemes. MINSA involves spatial discretisation of the governing mass and energy balance equations, which are solved in the temporal domain using a time integrator - LSODA (backward difference, Livermore Solver for Ordinary Differential equations with Automatic switching method between stiff and non-stiff problems) (Petzold,1983).

A Finite Volume Method is used for the spatial discretisation. To integrate over volume element *k*, apply the following definitions.

$$\int_{k-\frac{1}{2}}^{k+\frac{1}{2}} \frac{\partial \alpha}{\partial t} dz = \Delta z \frac{d\bar{\alpha}}{dt} \qquad \textbf{(2-18a)}$$

and

$$\int_{k-\frac{1}{2}}^{k+\frac{1}{2}} \frac{\partial \alpha}{\partial z} dz = \left[ \alpha_{k+\frac{1}{2}} - \alpha_{k-\frac{1}{2}} \right] \qquad \textbf{(2-18b)}$$

Interpolation procedures for hyperbolic PDEs associated with central differencing can lead to stability problems, and upstream differencing to inaccuracies associated with numerical diffusion. To overcome this, a hybrid, conservative three-point upstream-weighted quadratic interpolation scheme, the so-called QUICK scheme (Quadratic Upstream Interpolation for Convective Kinematics, Leonard, 1979) is applied in MINSA to determine quantities at the boundary of each finite volume.

For modelling the gradient term $\partial\alpha/\partial z$ at the wall, use is made of the geometric property of parabolas that the slope half way between two points is equal to that of the chord joining these points. Hence:

$$\left.\frac{\partial \alpha}{\partial z}\right|_{k+\frac{1}{2}} = \frac{\alpha_{k+1} - \alpha_k}{\Delta z} \qquad \textbf{(2-19)}$$

To reduce numerical instability (i.e.oscillations) associated with the resolution of sharp wave fronts characteristic of hyperbolic PDEs, an additional smoothing procedure, the so called SMART scheme (Sharp and Monotonic Algorithm for Realistic Transport by convection), is applied.

ADSIM offers a wider range of numerical schemes than MINSA, however none of the schemes is conservative, like the FVM utilised by MINSA. ADSIM's numerical schemes include Upwind Finite Difference, Central Difference, Leonard Differencing, Quadratic Upwind Differencing, Mixed Differencing and Orthogonal Collocation. The time integration for these schemes is performed by SPEEDUP. For the purposes of this work, the simplest discretisation scheme was used , Upwind Finite Difference.

$$\frac{\partial \alpha_k}{\partial z} = \frac{\alpha_k - \alpha_{k-1}}{\Delta z} \qquad (2\text{-}20)$$

This scheme is fast and stable, but provides only first order accuracy, and gives a large amount of numerical dispersion. A very small node size is required to improve numerical accuracy. This scheme was used largely for demonstration purposes. For comparison with experimental data, the conservative numerical scheme underpinning MINSA is far more accurate.

### 2.1.4 Acceleration Schemes

One other complication with simulation of oxygen VSA is the slow convergence to CSS. Most numerical simulators, including MINSA and ADSIM involve successive substitution and faithfully model the slow dynamics of reality. This inability to accelerate numerical solutions has hampered the optimisation of oxygen VSA design and operation, and led to research efforts to accelerate the convergence of CSS.

Broadly, there are two classes of acceleration schemes - accelerated successive substitution and direct determination. These techniques differ fundamentally as to whether CSS periodicity is incorporated as an explicit equation (direct determination), or whether it is used as a check of CSS (accelerated successive substitution). Both classes of acceleration techniques have been successfully applied to oxygen VSA.

- Accelerated Successive Substitution - Cycle Jumping (Aspentech, 1997) and Node Adjustment (He and Webley, 1999)
- Direct Determination - Shooting Methods (Smith and Westerberg, 1992 and Croft and LeVan, 1994) and Complete Discretisation (Nilchan and Pantelides, 1998)

These alternate schemes have been applied with mixed success and this is an ongoing area of academic and industry interest. This work proposes another acceleration scheme based on a perturbation technique detailed in Section 2.5 and 2.6.

### 2.1.5 Modelling and the Need for Other Approaches

"PDEs if necessary, but not necessarily PDEs" Diran Basmadjian

Numerical simulators provide an invaluable tool for modelling the behaviour of oxygen VSA systems, and generally achieve excellent agreement with both industrial and laboratory oxygen VSA data (Todd et.al., 2000b; Kumar, et.al., 1994; Hofmann et.al., 1999). However numerical simulators have two distinct limitations. Firstly, as has been outlined, simulation times and convergence to CSS are painfully slow, even utilising current CPU processor power. Secondly, and more importantly, numerical simulations do not offer useful 'engineering insight' into the nature and dynamics of oxygen VSA operation. A principal motivation in this project, is to offer simplified explanations of the thermal profiles that offer more insights into the heat transfer mechanisms than detailed numerical simulation. A number of simple models are developed, both qualitative and quantitative. Initially a qualitative model or explanation of the evolution of thermal profiles is offered. Essentially this model seeks to enhance the gas industry knowledge that was elaborated in Chapter One.

## 2.2 A Simple Qualitative Description of Thermal Profiles in O2 VSA

In order to prevent the penetration of water and carbon dioxide into the main adsorbent layer of lithium or calcium based adsorbent, a prelayer of activated alumina or NaX adsorbent is used in oxygen VSA, for water and carbon dioxide removal (Kumar, 1996). The removal of these readily adsorbed trace components could be achieved in a separate unit operation, but there are significant capital cost benefits of integrating these steps in a single adsorption bed, and this is established industrial practice. In order to simplify this qualitative model, the prelayer can be considered inert to nitrogen and oxygen adsorption.

If a clean two layered bed with an inert prelayer undergoes adsorption, a step or discontinuity is formed between the inert layer and the adsorptive layer, based on the heat of adsorption in the main layer (Figure 2-2).

**Figure 2-2 – Initial Temperature Profile**

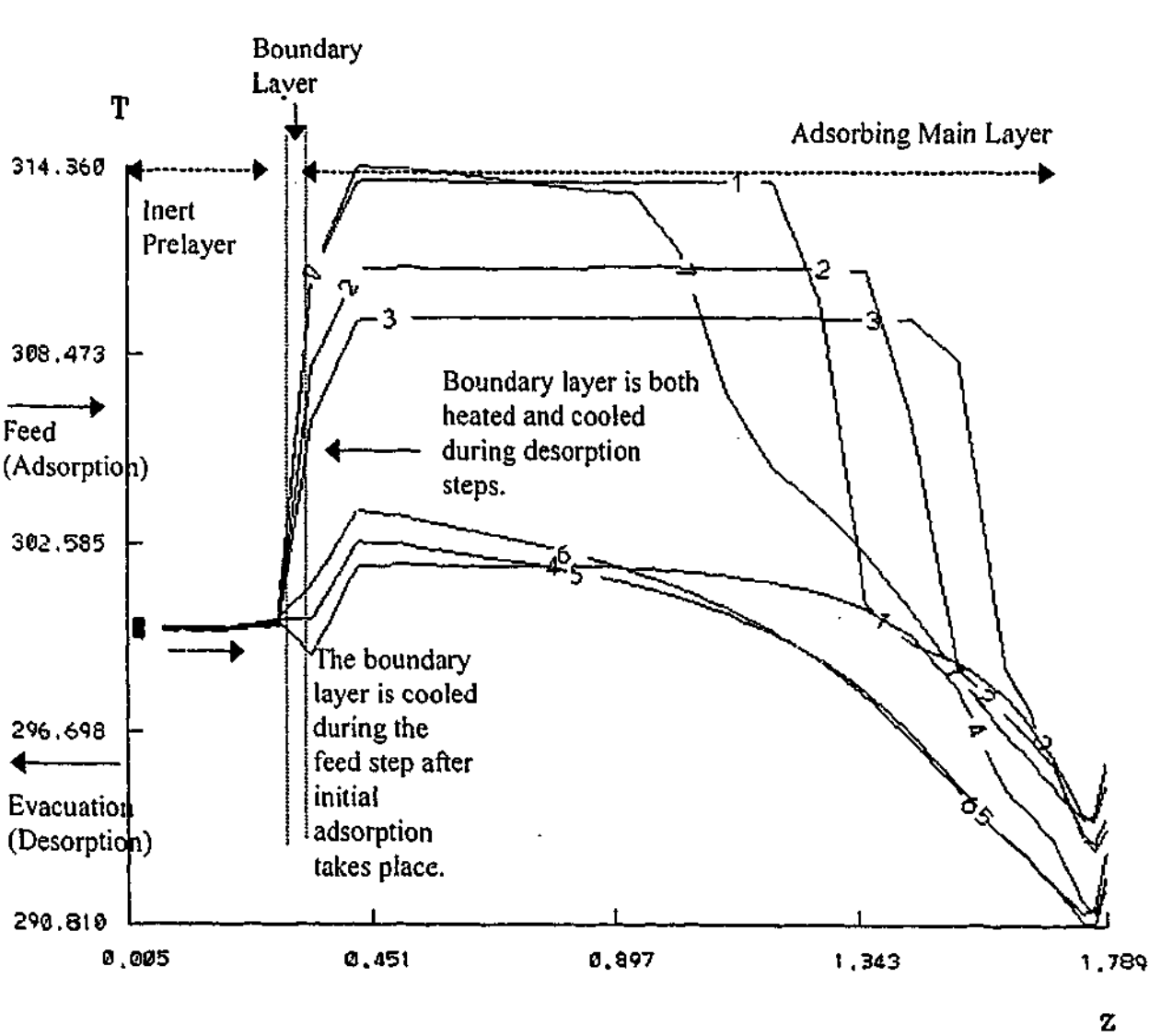

The numbers on Figure 2-2 indicate the temperature profile at the end of different steps and after one cycle. Step 1 is End of Feed, Step 2 is End of Provide Purge, Step 3 is End of Provide Pressure Equalisation, Step 4 is End of Evacuation (previously described as two steps), Step 5 is End of Receive Purge, Step 6 is End of Receive Pressure Equalisation, and Step 7 is End of Feed Repressurisation. This is the same cycle as described in Figure 2-1. However in Figure 2-1, the evacuation step is described as two steps.

As the feed gas is convected past the discontinuity, the temperature of a boundary layer in the adsorptive layer is reduced to the temperature of the feed gas. This boundary layer of the bed contains adsorbed gas, but has now been reduced in temperature to the feed gas temperature. When evacuation (depressurisation) occurs countercurrently, this boundary layer undergoes desorption of gas and is cooled. Simultaneously the boundary layer is also heated by desorbed gas that is passed over the boundary layer from further into the bed. This sequence of steps is shown in Figure 2-1. The numbers indicate the end of step temperatures. These profiles were generated with MINSA.

In general, when the mass flowrate of gas forward through the bed is greater than the mass flowrate of gas returned on desorption, there will be a net cooling of the boundary layer. As the boundary layer is cooled, the inert layer will be cooled below the feed gas temperature, and the inert layer will behave as a regenerative heat exchanger (Schmitt and Willmott, 1981). The desorbed gas will reduce the temperature of the inert layer, and this will in turn precool the feed gas as it enters in the next cycle. As this process continues, the thermal boundary layer shifts further into the adsorption bed, and the temperature profile evolves. A typical pattern of evolution is shown in Figure 2-3.

**Figure 2-3 Cycle 50 and Cycle 100 in the Evolution to a CSS Temperature Profile**

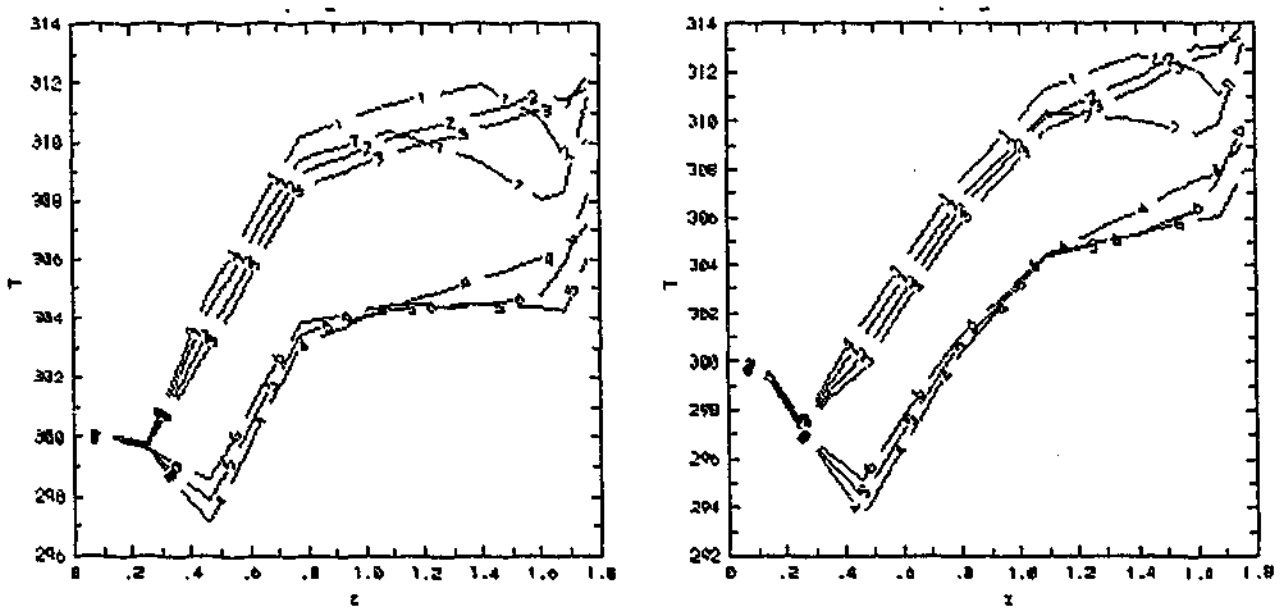

This process continues until CSS, when there is no net heating or cooling of any section of the adsorption bed over a cycle. The final temperature profile for this case is shown in Figure 2-4.

**Figure 2-4- Final CSS Temperature Profile - Cycle 4000**

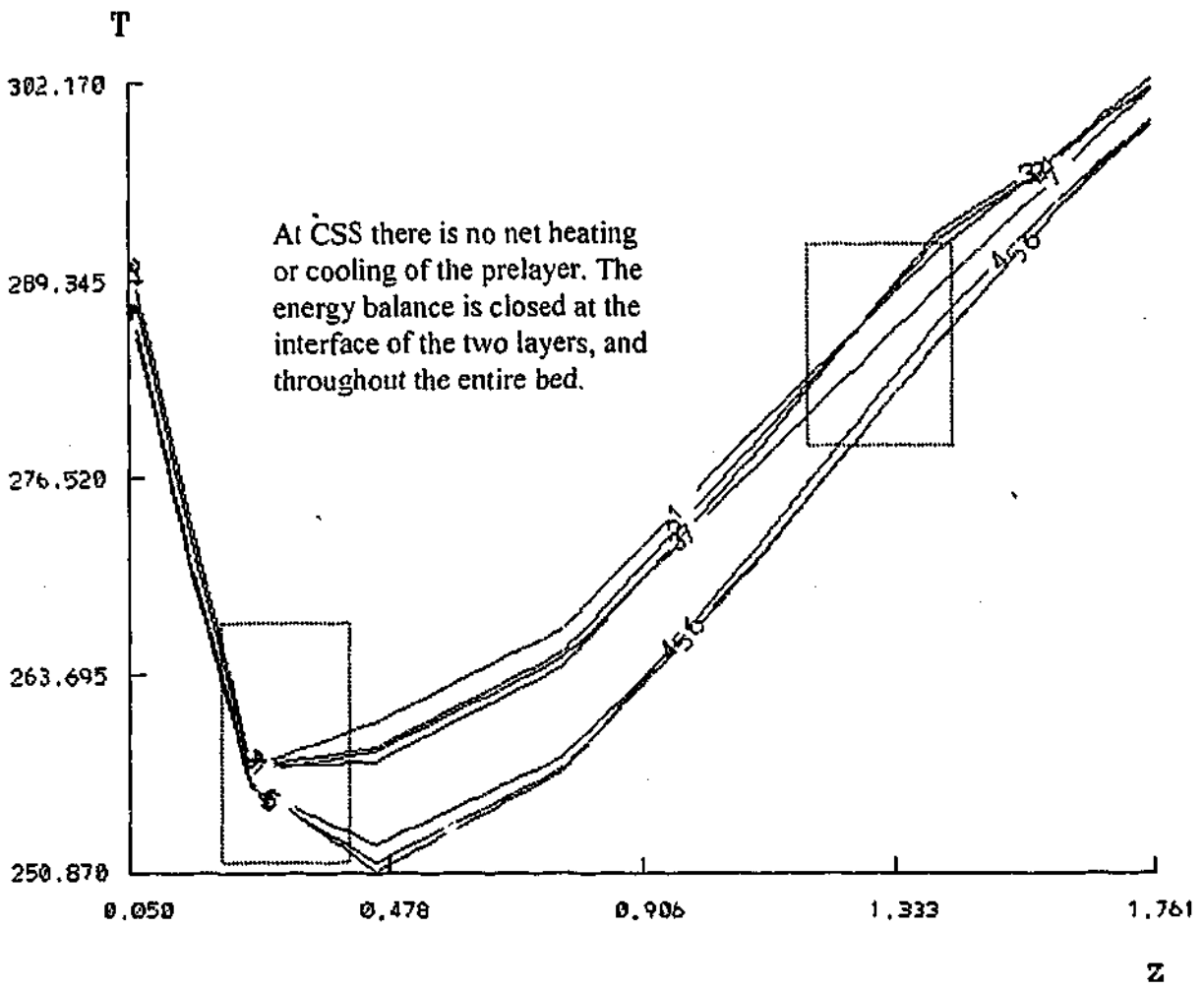


One important feature of Figure 2-4 is that the minimum bed temperature is just inside the adsorbent layer, adjacent to the inert layer. Under conditions of desorption, this section of the bed cools below the temperature of the inert. Hence the instantaneous coldest spot occurs just inside the main layer of adsorbent, even though during adsorption, as Figure 2-4 shows, the same section of bed gets hotter than the inert at the interface between the two layers.

It follows from this qualitative analysis that the 'cold spot' will be absent, if there is no inert prelayer acting as a regenerative heat exchanger. Furthermore, by the same argument, if there is no inert prelayer the bulk of the desorbed gas will exit the bed at a lower temperature than the feed gas. This is demonstrated numerically in Figure 2.7. In addition, an energy balance

around the adsorption bed, dictates that the product gas will leave the bed hotter than the feed gas.

This analysis of CSS temperature profiles differs fundamentally from the typical analysis of the velocity of composition and temperature waves in trace component breakthrough experiments, as has been reported by Ruthven, et.al. (1994), Basmadjian (1997) and many others. These studies result in equations 2-21 and 2-22, which together determine whether the composition and thermal waves will separate. The velocity of the composition wave, $w_c$, and the velocity of the thermal wave $w_t$ are given by the following equations.

$$w_c = \frac{v}{\left[1+\left(\frac{1-\varepsilon_b}{\varepsilon_b}\right)\frac{dn^*}{dT}\right]} \qquad (2\text{-}21)$$

$$w_t = \frac{v}{\left[1+\left(\frac{1-\varepsilon_b}{\varepsilon_b}\right)\frac{C_s}{C_{pg}}-\left(\frac{1-\varepsilon_b}{\varepsilon_b}\right)\left(\frac{-\Delta H}{C_{pg}}\right)\frac{dn^*}{dT}\right]} \qquad (2\text{-}22)$$

However the qualitative analysis of thermal profiles in this thesis is not concerned with the composition and thermal waves described in equations 2-21 and 2-22. Instead the causative effect of the 'cold spot' is the slow trailing convective wave, which is the result of the fixed temperature feed gas cooling or heating the adsorption bed. This effect is neglected in simple breakthrough experiments, but in a cyclic process such as VSA and PSA, this small cumulative effect dramatically shapes the CSS temperature profile, as has been described. In oxygen VSA systems there are leading composition and thermal waves, and these travel essentially at the same velocity, although the temperature wave is very slightly more dispersive due to second order effects (Todd, 1998). However, this is not the basis of the explanation of the mechanism causing the 'cold spot'.

In the presentation of this qualitative explanation, it is important to recognise that the initial conditions of the bed, the temperature, pressure, and loading all play a role in determining the evolutionary path to a CSS temperature profile. The qualitative explanation still holds, and a singular temperature profile evolves, based on the process conditions and adsorption bed configuration.

This qualitative model offers a simple account of the causes of the evolution of the temperature profiles and the ultimate convergence to CSS. It follows from this explanation, that any process condition affecting the heat of adsorption and the patterns of convection will shape the final CSS temperature profile. For example, changing cycle, step times, pressure envelopes, purge to feed ratios, recovery, product purity and sieve properties will all affect the CSS temperature profile to varying extents.

The temperature profiles in some other PSA systems have been investigated, but most of these studies have focused on single layer adsorption beds, and hence the 'cold spot' is not evident. However, two important studies advance the same qualitative explanation developed here, and apply it to a one layered adsorption bed. As stated before, such a system should display a CSS temperature profile where, during desorption, the entrance of the bed is cooler than the feed gas, and the product gas leaves the bed hotter than the feed gas. This assumes only slight heat exchange with the environment.

Lou et.al. (1999) investigated an adiabatic air drying PSA process with a single layered adsorption bed. Figure 2.5 shows the countercurrent desorbed gas exiting the bed at a temperature lower than the feed gas, and much of the product gas being warmer than the feed gas temperature.

**Figure 2-5 – CSS Thermal Profile for Air Drying**

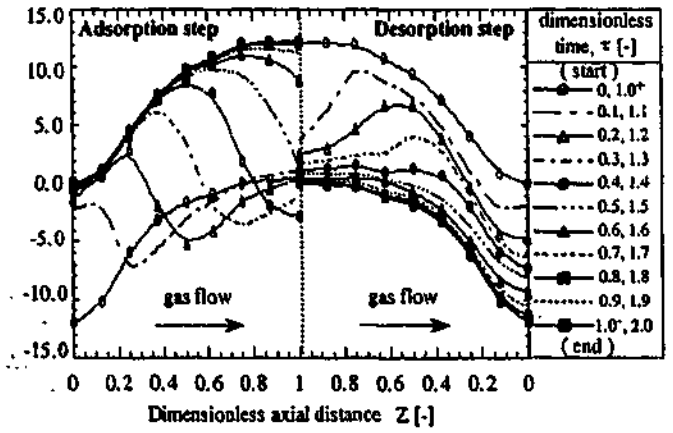


where z is the dimensionless length, and $\tau$ is the dimensionless time.

Lou et.al. (1999) show this as an inverted V-shaped axial CSS temperature profile containing both the adsorption and desorption temperature profiles. The figure also shows the movement of a temperature wave through the bed. A sharper temperature wave is evident during adsorption whereas the desorption step is characterised by dispersed waves.

The inverted V-shape is interpreted by Lou et.al as the superposition of two independent thermal effects i.e. a heat sink of precooled upstream adsorbent and a heat source by the generation of adsorption heat. This is essentially the same as the qualitative explanation developed for oxygen VSA except that there is no prelayer in the air drying system.

Similar experimental observations and the same explanation have been advanced by Mahle et.al. (1996) who studied an air-helium adsorptive separation on BPL carbon. They observed bed temperatures during desorption about 10 °C below the feed temperature.

**Figure 2-6 – CSS Temperature Profile for Air-Helium Separation**

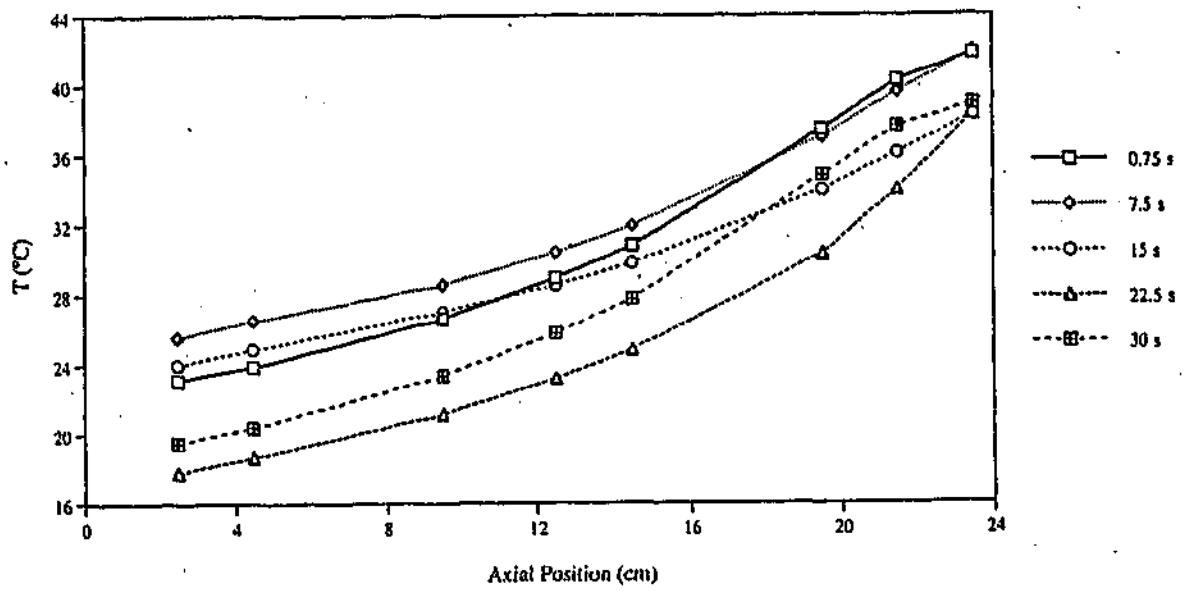


(Taken from Mahle et.al. 1996, p. 2352)

Figure 2-6 shows the CSS axial temperature profile for different times in the cycle. Mahle et.al. (1996) argue that this subcooling effect is caused by two factors. "First, adsorption or desorption of the carrier gas occurs over the whole as the bed is pressurised or depressurised. This leads to a uniform temperature cycling but, in itself, gives no net subcooling or wave character in the bed. Second, the imbalance of the molar flowrates, with higher rates for the feed step than for the purge step, drives the bed temperature toward the feed temperature.... This gives wave character to the bed profiles, with the temperature being close to the feed temperature over most of the bed during the feed step and subcooling in this region during the purge step" (Mahle et.al., 1996, p. 2353). This is the same causal mechanism to account for the 'cold spot' phenomenon, except that again, there is no inert prelayer to act as a regenerative heat exchanger in the helium-air PSA system devised by Mahle et.al. (1996).

## 2.3 Mapping Convective Heat Fluxes Through the Adsorption Bed

Examining more explicitly the convective heat fluxes through the adsorption bed, can further develop this qualitative analysis. It is evident that the axial CSS temperature profiles result from the interaction between the temperature swings due to adsorption and desorption, and the convection of this heat through the adsorption bed. With the aid of MINSA, it is possible to map explicitly the enthalpy flows through the bed for specific operating conditions. This can be a laborious process, but it provides further insight into the evolution of temperature profiles and the final CSS temperature.

The enthalpy fluxes through the adsorption bed can be described by the three separate quantities - the relative convective flux (RCF), cycle convective balance (CCB), and accumulated convective cycle balance (ACCB).

In the modelling of an adsorption bed, the adsorption bed can be divided or discretised into a series of nodes, or cells separated by walls.

**Figure 2-6 a – Nodes and Walls in Discretisation**

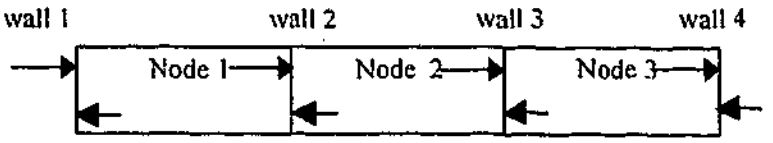


The arrows indicate that the relative convective fluxes are measured at the wall entering a node. The relative convective flux (RCF) indicates whether a node is being instantaneously heated or cooled by convected gas. It simply represents that difference in temperature between the temperature of a node, and the temperature of gas entering the node.

$$RCF = (\rho_g v C_{pg})_{in} (T_{n,wall,in} - T_{node}) \qquad (2\text{-}23)$$

where $T_{n,wall}$ and $T_{node}$ are the wall and node temperatures respectively (K)
RCF is the relative convective flux ($W/m^2$)

The gas velocity into the cell is defined as always positive (whether entering from the right or left), and only considers gas flows into a cell. If the RCF is negative, the node is being cooled by convected gas, and if the RCF is positive, the node is being heated by convected gas. The magnitude of the RCF measures the extent of heat or cooling of the node by convected gas.

The limitation of the relative convective flux (RCF) is that it does not provide a convective balance over the node. In order to develop a more complete model of the transient thermal behaviour, it is useful to undertake a convective balance over an entire cycle.

The Convective Cycle Balance (CCB) can be written as the balance of the convective fluxes into and out of a given cell over a given cycle.

$$CCB = \int_0^{\tau_c} \left[ C_{pg} \rho_g |v| (T_{n,wall} - T_{ref}) dt \right]_{in} - \int_0^{\tau_c} \left[ C_{pg} \rho_g |v| (T_{n,wall} - T_{ref}) dt \right]_{out}$$

$(J/m^2/cycle)$ **(2-24)**

The quantity CCB indicates whether the cell is undergoing a net positive or negative enthalpy change over an entire cycle. By contrast, the RCF indicates whether a cell is undergoing instantaneous and relative heating or cooling based on the gas convected into the cell only.[1]

A condition of CSS is that CCB converges to zero for all nodes throughout the bed. Under this condition there is no change in the temperature of a cell over an entire cycle and the temperature profile is periodic. The value of CCB indicates whether the cyclic cell temperature will be increasing or decreasing on the way to CSS. A negative CCB indicates that, over a specific cycle, the temperature of the node will be reduced, and conversely, a positive CCB denotes an increase in temperature of the node.

The convective cycle balance (CCB) calculated for each node can be accumulated over all cycles to determine the total extent of a temperature change of a cell in the transient period until CSS.

---

[1] The integral or summation of RCF will equal CCB if and only if:
- Upwind differencing is used in the discretisation, and
- Molar flows in and out of the cell are equal.

But this is not the case for the Finite Volume Method (FVM) and for bulk gas separations, such as oxygen VSA. RCF is still useful to give a qualitative guide to patterns of instantaneous heating and cooling due to gas convected into the cell.

$$ACCB = \int_0^N CCB \; dN \qquad (J/m^2) \tag{2-25}$$

At CSS the value of ACCB should converge to a constant. The quantity ACCB can be related to the temperature in the bed at a given time in the cycle, since:

$$T \approx \frac{ACCB}{\rho_s C_{ps}} + T_i \tag{2-26}$$

where $T_i$ is the initial temperature of the bed (K)

This indicates that the evolution of the temperature profile is proportional to ACCB.

The evolution of the RCF, CCB, and ACCB can be used to provide detailed insight into the evolution of temperature profiles and convergence to CSS. In effect, a detailed map of the convection of heat through the adsorption bed can be developed. This can be useful to explain the evolution of certain features of the axial CSS temperature profile, and how operating conditions impinge on the temperature profile. One example is offered here to demonstrate the evolution of the temperature profile of a single layered bed with a dry air feed.

The following diagram represents the typical CSS temperature profile for a dry air feed at 300 K and a single layered adsorption bed, with a two bed cycle, 8 step cycle and a typical VSA pressure profile, as described in Figure 2-1. The simulation was run with only 10 nodes to demonstrate the effect.

**Figure 2-7**

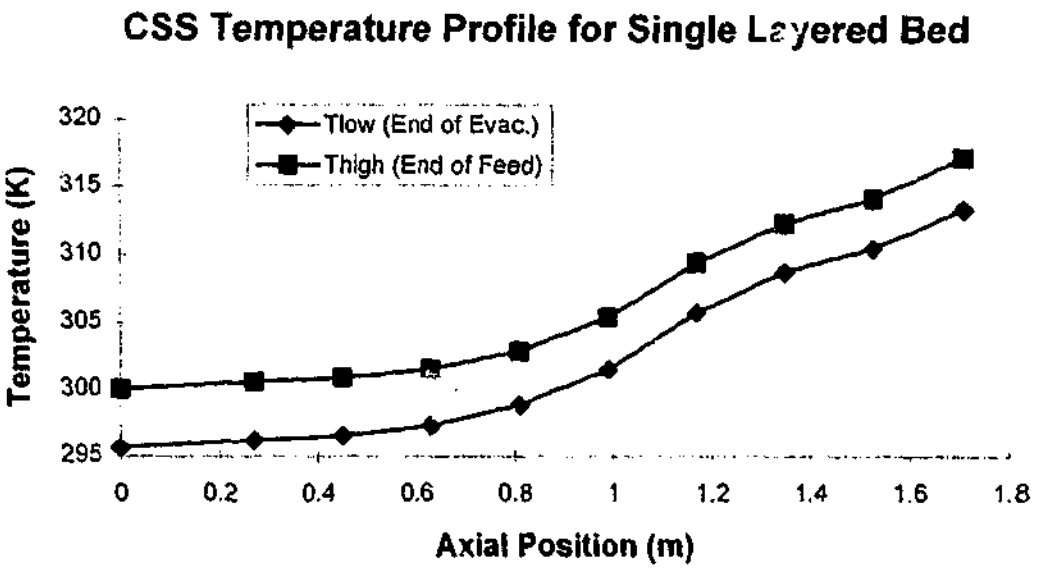

As expected, with a single layered bed with a dry air feed, there is an increasing temperature profile through the adsorption bed (no 'cold spot') and the temperature of desorbed gas leaving the bed is below the temperature of the feed gas temperature. The axial CSS temperature profile is similar in shape to that reported by Mahle et.al. (1996), although the adsorptive separations are different.

A plot of the CCB for selected nodes indicates that the net convection of heat into each node over a cycle converges to zero.

**Figure 2-8**

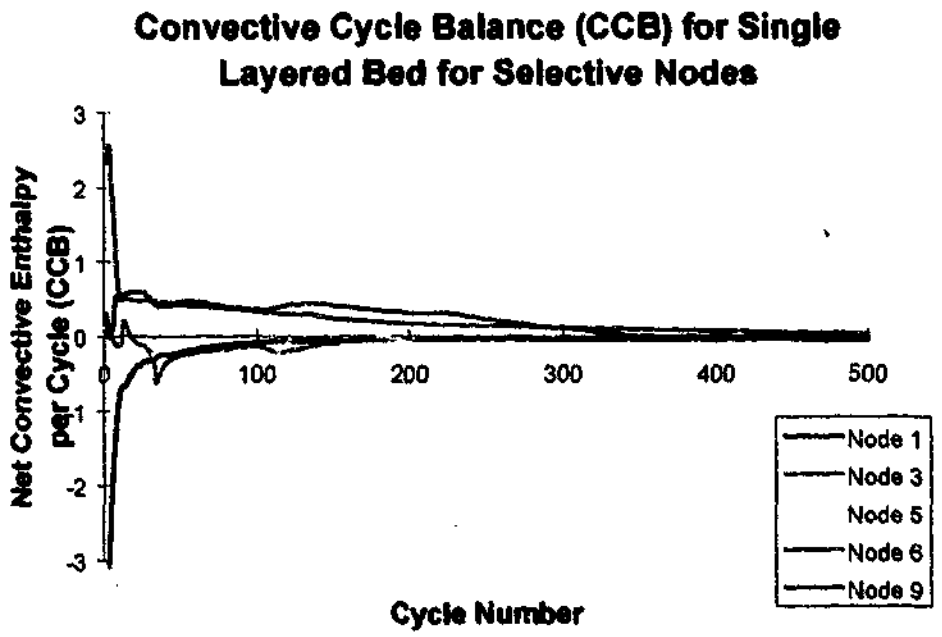


It is also evident that Node 1 undergoes slight cooling initially as does Node 3, whereas Node 6 and 9 are heated.

The plot of CCB does not completely converge to zero because a very coarse integration scheme was used in the calculation of CCB. Timesteps of 0.25 steps were used and this introduced some errors. For the same reason the ACCB did not converge to a constant. However the CCB does converge towards zero, and this was deemed as sufficient for the purpose of these qualitative explanations. A more exact overall convective balance (over the entire bed) could be calculated using much smaller timesteps within LSODA, the time integrator used by MINSA.

The limitation of the CCB plot is that it does not reflect the accumulative effect of the shifts of convected energy within the adsorption bed. These accumulative effects are displayed on the accumulative convected cycle balance (ACCB).

**Figure 2-9**

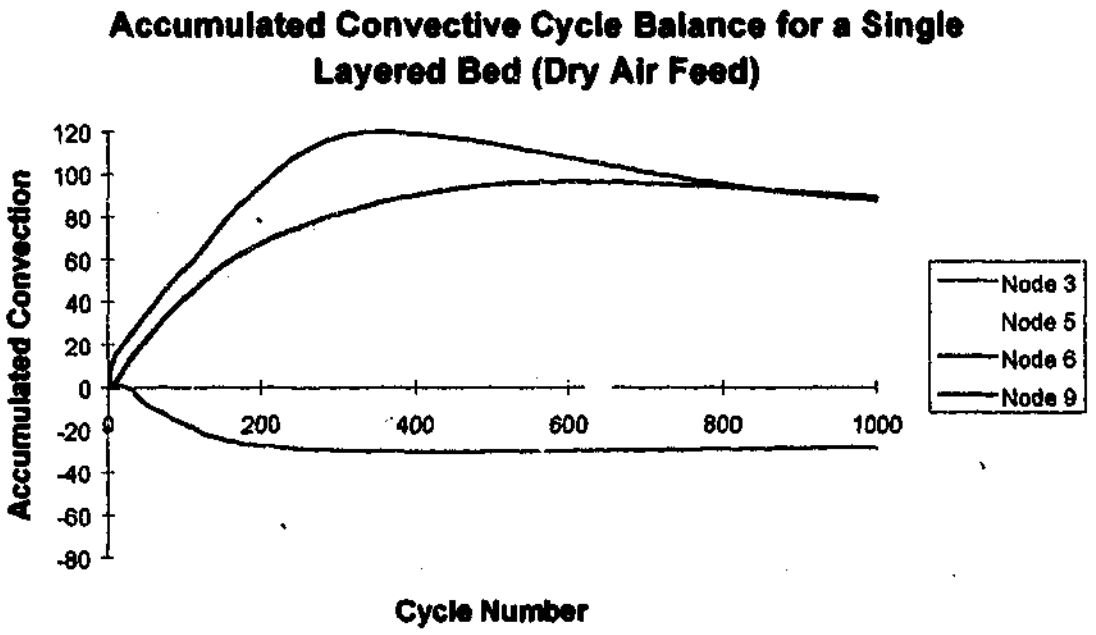


This plot clearly demonstrates the extent to which nodes in the bed are cooled or heated, and represents the evolutionary history of energy convected through the bed. The initial conditions of bed (pressure, loading and temperature) are contained within the ACCB plot. After 1000 cycles the ACCB plot displays similar features to the final CSS temperature plot.

The CCB and ACCB quantities provide 'cycle-by-cycle' history of the thermal evolution of the temperature profiles, and demonstrate the features of convergence to CSS temperature profiles. However, these plots do not reveal a key element of the explanation of the thermal profile. By contrast, the Relative Convective Flux (RCF) plot indicates the fate of each node during a cycle, and the extent of instantaneous heating or cooling. Limiting consideration to the first node in the adsorption bed, it is possible to map out the fate of Node 1.

**Figure 2-10**

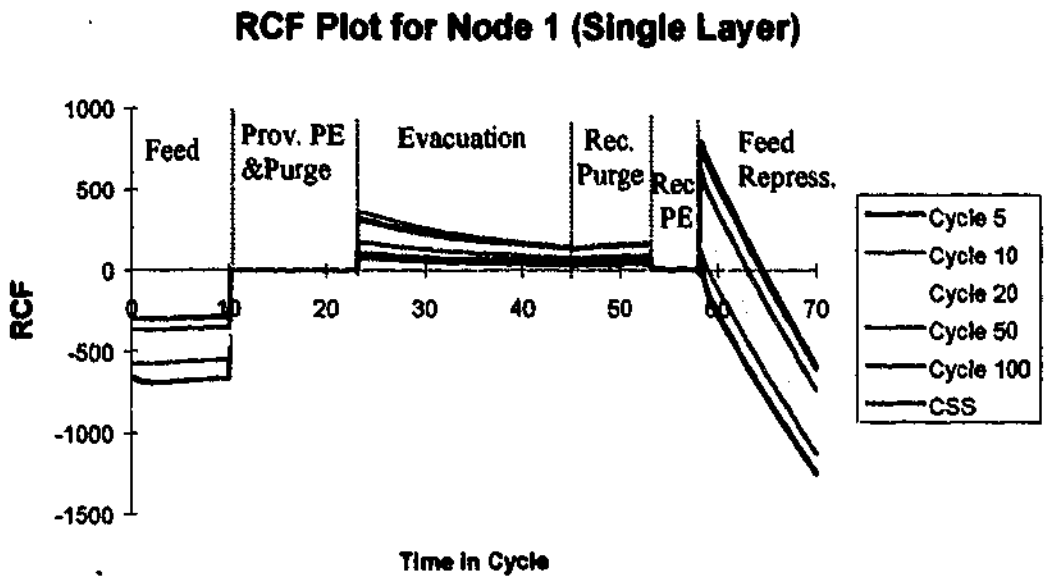


Node 1 is initially cooled by the feed gas on feed repressurisation (Step 8) and feed step (Step 1). The extent of cooling is greater than the heating caused by the evacuation and receive purge steps. As the cooling of the node continues it reaches temperatures below the feed gas temperature at the end of the evacuation and receive purge steps. When this occurs, the node is both partially heated and cooled during the feed repressurisation step. These conditions of combined heating and cooling by the feed gas give rise to a CSS temperature profile in Node 1. There is no regenerative heat exchanger that captures the colder desorbed gas, hence a temperature depression within a single layered bed will not occur.

The RCF, CCB, and ACCB quantities can be applied to provide a detailed account of the interaction of the convective fluxes through the adsorption bed, and explain the relationship between specific operating conditions and CSS temperature profiles. However this can be a laborious process and is reliant on numerical simulation to determine the different flux terms. The benefit of this approach is that it demonstrates there is no mystery to CSS temperature profiles, just a complex interaction of adsorptive/desorptive temperature swings and the convective enthalpy fluxes. A dynamic cell model is developed in Section 2.5 which displays similar patterns of thermal evolution to the RCF, CCB, and ACCB plots displayed here.

## 2.4 Simple Energy Balances To Predict the CSS Temperature Profile

The qualitative description of the evolution of the temperature profile, and mapping the convective enthalpy fluxes through the adsorption bed, provide a useful explanation of the CSS temperature profiles in oxygen VSA. However the qualitative explanation can appear as 'arm waving' and the mapping of convective fluxes can be too detailed and too reliant on the numerical simulation that underpins it. Neither approach offers a simple predictive model that identifies the key process parameters that determine the axial CSS temperature profile. The challenge here is to develop such a predictive model. However, such a model cannot hope to capture the entire range of process effects that shape the CSS temperature profile. For example, kinetic effects, the differences in the sharpening adsorptive waves, and dispersive desorptive waves, heat loss and the effect of bed-to-bed connection are all well beyond the scope of a simple predictive model. It is necessary to resort to a full numerical simulation to capture such effects.

### 2.4.1 Simple Regenerative Heat Exchanger Analysis

One such simple approach is to present the adsorption bed as an inert prelayer and main adsorbing layer, and perform simple mass and energy balances around the prelayer and the main layer at CSS. When combined with a series of assumptions, this enables the derivation of temperature profiles in the bed as a function of the key process parameters.

**Figure 2-11- Adsorption Bed with an Inert Prelayer**

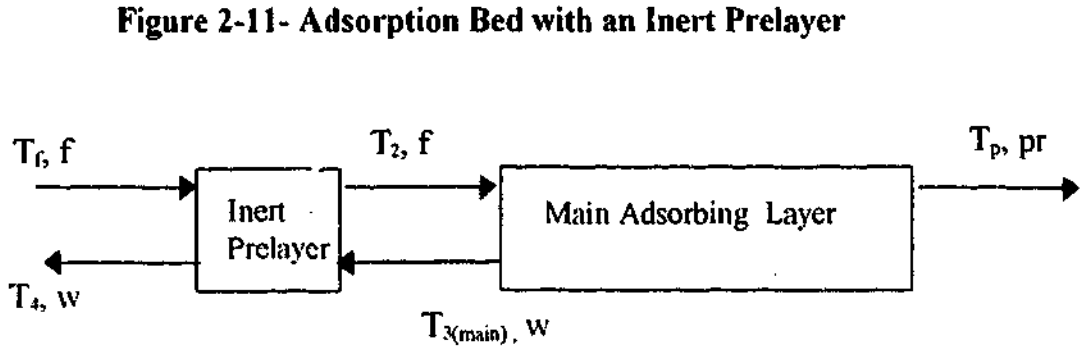


Where f, w, pr are instantaneous molar flows, and $T_f$, $T_2$, $T_{3(main)}$, $T_4$ and $T_p$ are the instantaneous temperatures of the gas entering or leaving the prelayer. The mass of the prelayer is $m_p$, and the heat capacity is $C_{sp}$ of the prelayer. The gas has a uniform molar specific heat capacity ($C_{pg}$). The mass of the main adsorbing layer is $m_m$, and the heat capacity is $C_{sm}$ of the main layer. The heat of adsorption in the main layer is $\Delta H$. The bed undergoes a simple cycle consisting of an adsorption step ($\tau_1$) and the desorption step ($\tau_2$).

### 2.4.2 Energy Balance Around the Prelayer *

The temperature of the gas entering the main adsorption bed after the prelayer $T_2$, is coupled to the temperature of the returning waste gas $T_{3(main)}$. As the thermal evolution towards CSS occurs, $T_2$ is gradually reduced, which in turn reduces $T_{3(main)}$. The coupling of the enthalpy fluxes for streams 2 and 3 gives rise to the sustained temperature depression evident in oxygen VSA. This coupling between the forward and reverse flows distinguishes the behaviour of an oxygen VSA unit from a typical industrial heat regenerator (Schmidt and Willmott, 1981). The relationship between streams 2 and 3 can be used to determine the temperature dip in the prelayer under different process conditions in the main layer, yet some further simplifying assumptions are required.

Figure 2-11 shows an inert prelayer which does not adsorb gas, and the gas phase accumulation is ignored, hence the molar flows f and w are unchanged through the prelayer. During the adsorption step in a cycle, feed gas enters the bed at $T_f$ and exits the bed at $T_2$. $T_f$ is a constant value, but $T_2$ increases until the end of the feed step. During the desorption step, gas enters the prelayer at $T_{3(main)}$ and leaves the prelayer at $T_4$. Half cycle energy balances can be written for both the adsorption and desorption steps for the prelayer.

$$m_p C_{sp} \Delta T_{prelayer} = C_{pg} \int_0^{\tau_1} f\left[T_f - T_2(t)\right] dt \qquad \text{(Adsorption Step)} \qquad (2\text{-}27)$$

$$-m_p C_{sp} \Delta T_{prelayer} = C_{pg} \int_{\tau_1}^{\tau_2} w\left[T_{3(main)}(t) - T_4(t)\right] dt \qquad \text{(Desorption Step)} \qquad (2\text{-}28)$$

The central assumption governing these two equations is that the entire prelayer undergoes a uniform swing in temperature ($\Delta T$) on adsorption and desorption. This is shown in Figure 2 –12 where the end of step temperature profiles are shown.

* A number of different modelling approaches are adopted in this work. Some nomeclature is unique to a particular modelling approach, however where possible common nomenclature is applied, such as $T_f$ for the temperature of the feed gas.

**Figure 2-12 End of Step Temperature Profiles in the Prelayer**

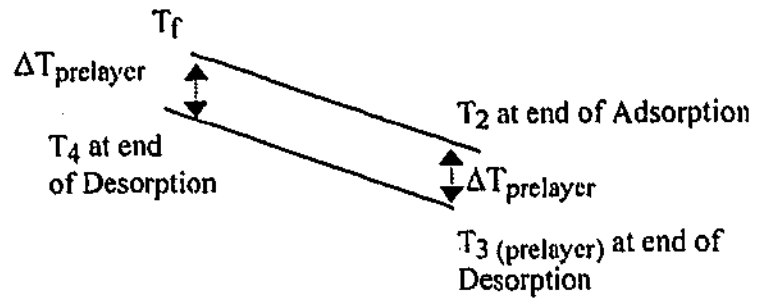


It is important to note that $T_{3(prelayer)}$ is different to the $T_{3(main)}$. $T_{3(main)}$ is the temperature of the gas entering the prelayer from the main layer, whereas $T_{3(prelayer)}$ is inside the prelayer. This is based on the assumption of a uniform $\Delta T$ within the prelayer.

To solve equation 2-27 and 2-28, it is necessary to make an additional assumption and solve these equations for average values of $T_2$, $T_4$, $T_3$.

$$T_4(t) \approx \overline{T_4} = \frac{T_f + T_{4,end}}{2} = T_{4,end} + \frac{\Delta T_{prelayer}}{2} \qquad (2\text{-}29)$$

$$T_2(t) \approx \overline{T_2} = \frac{T_{3(prelayer)} + T_{2,end}}{2} = T_{2,end} - \frac{\Delta T_{prelayer}}{2} \qquad (2\text{-}30)$$

Now the temperature of the gas entering the prelayer on the desorption step varies significantly over the duration of the desorption step.

$$T_{3(main)}(t) = \overline{T_2} - f(t) \qquad (2\text{-}31)$$

f(t) is a deviation temperature between the average temperature of gas entering into the main bed and the instantaneous temperature of waste gas entering the prelayer from the main layer.

Substituting these equations into equation 2-27 and 2-28 yields:

$$\frac{m_p C_{sp}}{C_{pg}} 2(T_f - \overline{T_4}) = (T_f - \overline{T_2}) \int_0^{\tau_1} f dt \qquad (2\text{-}32)$$

$$\frac{m_p C_{sp}}{C_{pg}} 2(T_f - \overline{T_4}) = E + (\overline{T_4} - \overline{T_2}) \int_{\tau_1}^{\tau_2} w dt \qquad (2\text{-}33)$$

where $E = \int_{\tau_1}^{\tau_2} w f(t) dt$ . This is the deviation enthalpy flux passed back through the prelayer, relative to the average temperature of gas entering the main layer.

$F = \int_0^{\tau_1} f dt$ , $Pr = \int_0^{\tau_1} Pr\, dt$ and $W = \int_{\tau_1}^{\tau_2} w dt$ . These are the totalised molar flows for the feed, product and waste respectively.

This results in:

$$\overline{T_2} = T_f - \frac{E}{F - W + \left(\frac{C_{pg} FW}{2 m_p C_{sp}}\right)} \qquad (2\text{-}34)$$

This is the average temperature of the gas entering the main adsorbing layer and is the temperature depression or 'cold spot'.

### 2.4.3 Implications of the Prelayer Energy Balance

There are a number of significant implications that can be made from Equation 2-34.

- The magnitude of the temperature depression translates vertically depending on the temperature of the feed gas. This assumes that E is unchanged. In practice the value of E is slightly dependent on the absolute temperature in the main bed; due to the temperature dependence of isotherms and gas properties, as is detailed in Chapter Four.

- As the mass of the prelayer increases the temperature depression converges to a minimum value. This indicates that for given E, F, W values a minimum temperature will occur. This is demonstrated in Figure 2-13 where a series of MINSA simulations were undertaken for the same cycle, and only the thickness of the prelayer was varied.

**Figure 2-13**

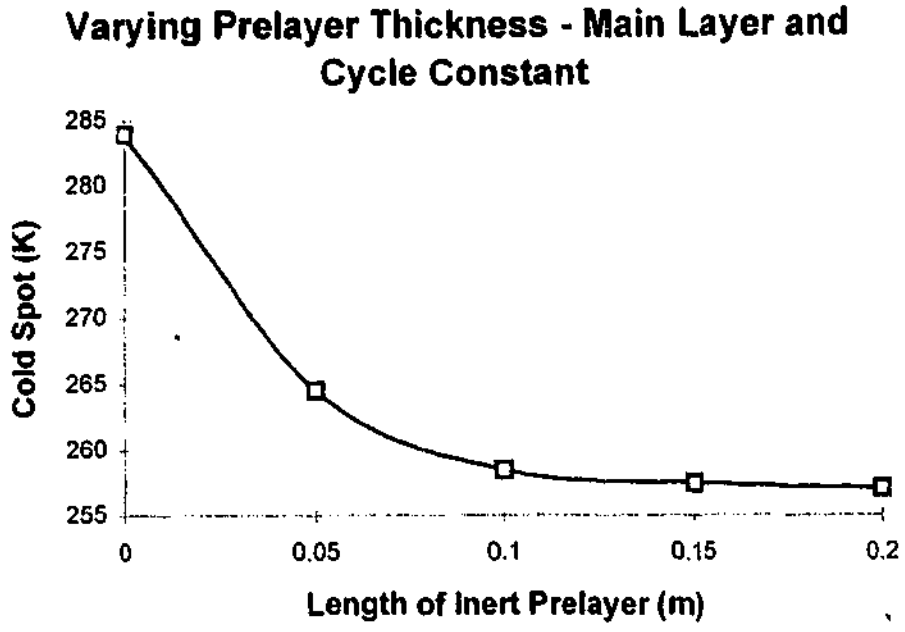


- If the total reverse enthalpy flux (E) is zero, there is no temperature gradient in the prelayer. Physically this will occur under conditions where there is no heat of adsorption in the main layer, there is no reverse flow, or the sum of the instantaneous reverse fluxes is zero.
- If the total forward molar flow (F) increases, without changing E and W, the extent of the temperature is reduced. This is the situation with low product purity and high recovery.
- If the oxygen recovery from the main process is low, as occurs with very high product purity ( i.e. F is approximately W), there will be an increase in the temperature depression ($T_f - \overline{T_2}$ ).

One of the limitations of Equation 2-34 is that the totalised reverse enthalpy flux parameter (E) cannot be calculated directly. This parameter is a complex function of the adsorption cycle and the properties of the main adsorbent bed. One approach is to determine the value of E by simulating a single layer case and determining the value of E relative to the feed gas temperature. A typical run was performed on MINSA for a single layered bed case for an adiabatic laboratory adsorption bed with the results shown in Table 2-1.

**Table 2-1 - Parameters for Single Layer Case, Adiabatic Beds, 7 Step Cycle**

| | MINSA Values (93%, VSA2-CaX) |
|---|---|
| Totalised Forward Molar Flow (F) (Moles/bed/cycle) | 2.1 |
| Totalised Reverse Molar Flow (W) (Moles/bed/cycle) | 1.9 |
| Feed Gas Temperature (K) | 288 |
| E Totalised Reverse Enthalpy relative to $T_f$ (mol. K) | 5.2 |

This value of E for the single layer case can be substituted into Equation 2-34 to enable the calculation of the temperature depression in the presence of an inert layer. For example, substituting these MINSA values into Equation 2-34 with an inert prelayer of 1.3 kg, the estimated temperature ( $\overline{T_2}$ ) was 266.7 K. This estimated value compares well with a full MINSA simulation with a 200 mm prelayer of activated alumina (1.3 kg), and all other process conditions as the single layer case. The equivalent two layer MINSA simulation calculated a 'cold spot' of 263 K. This is a reasonable comparison, but it is premised on a number of assumptions. For example, the effect of the absolute temperature of the gas entering the adsorption bed is ignored. Hence, assuming a constant value of E decouples the effect of the prelayer on the main layer adsorptive performance. At best the technique can only provide an estimate of the temperature profile, which in this case is quite good.

### 2.4.4 Energy Balance Around the Adsorbing Layer – The Reverse Enthalpy Flux

One of the limitations of Equation 2-34, is that the value of the key parameter, the deviation enthalpy flux (E), cannot be estimated from the energy balance around the prelayer. In the previous example, the value of E was determined by MINSA simulation. In practice, this enthalpy flux is a complex function of the cycle, the heat of adsorption, and molar flows through the main adsorption bed. It is possible however ,to derive a simplified expression for E based on mass and energy balance around the main adsorption layer.

Consider a simple 2 step cycle with a feed step and a countercurrent desorption step in a single layered adsorbing bed.

**Figure 2-14 – Balance Around Main Layer**

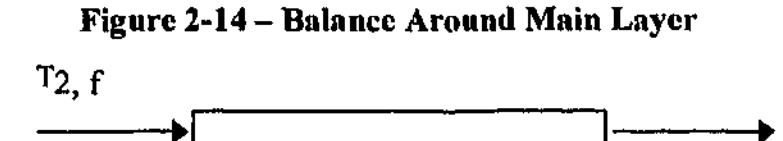


As in the energy balance around the prelayer, we ignore gas phase accumulation. It is further assumed that the adsorbate loading is not a function of the temperature, and there is a uniform temperature swing over the main layer of the adsorption bed. Based on these assumptions, the following mass and energy balances can be written.

$$F = Pr + W \tag{2-35}$$

$$C_{pg}F(T_2 - T_{ref}) = C_{pg}Pr(\overline{T_p} - T_{ref}) + C_{pg}W(\overline{T_3} - T_{ref}) \tag{2-36}$$

It is also possible to write mass and energy balances for the individual steps in the cycle.

**Adsorption/Feed:**

$$m_m C_{sm}\Delta T_{main} + C_{pg}(\overline{T_{ad}})(F - Pr) = \Delta H(F - Pr) + FC_{pg}(T_2 - T_{ref}) - Pr\,C_{pg}(\overline{T_p} - T_{ref}) \tag{2-37}$$

where $\overline{T_{ad}}$ is the average temperature of the adsorbed gas (K)

$\Delta T_{main}$ is the change in temperature over the bed during the step (K)

$\overline{T_p}$ is the average temperature of gas leaving the bed (K)

$m_m$ is the mass of the main layer (kg)

$C_{sm}$ is the heat capacity of the main layer (J/mol K)

$\overline{T_2}$ is the average temperature of gas leaving the bed (K)

This is shown diagrammatically in Figure 2-15.

**Figure 2-15**

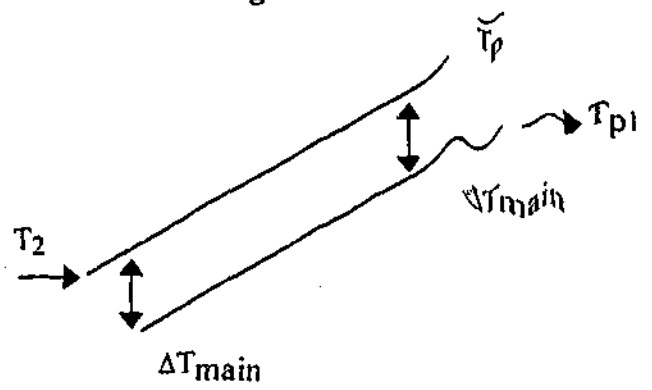


The temperature of the gas leaving the bed will be $T_{p1}$ for the bulk of the cycle, and only at breakthrough will there be any significant temperature rise of gas leaving the bed. Under these conditions it is reasonable to assume that $\overline{T_p} = T_{p1}$

The average temperature of the adsorbed phase is: $\overline{T_{ad}} = \frac{T_2 + T_{p1}}{2}$

For the other half of the cycle the energy balance can be written as:

**Desorption/Evacuation:**

$$-m_m C_{sm} \Delta T_{main} - C_{pg}(\overline{T_{ad2}})(F - Pr) = -\Delta H(F - P_r) + (F - Pr)C_{pg}(\overline{T_3} - T_{ref}) \quad \textbf{(2-38)}$$

where $\overline{T_{ad2}}$ is the average temperature of the adsorbed gas.

$\Delta T_{main}$ is the temperature change over the bed during the step.

$\overline{T_3}$ is the average temperature of gas leaving the bed.

**Figure 2-16**

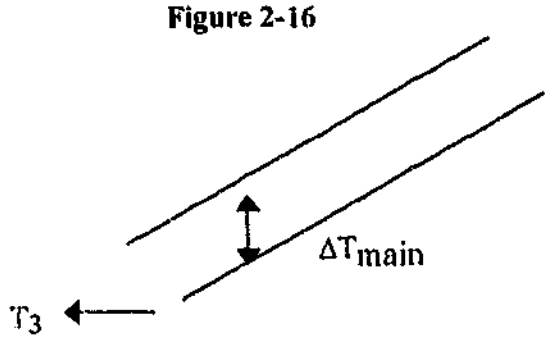


In this case the average temperature of the gas leaving the bed on desorption is:

$$\overline{T_3} = \overline{T_2} - \frac{\Delta T_{main}}{2} \qquad \textbf{(2-39)}$$

The aim of this analysis is to determine $\Delta T_{main}$ relative to $T_2$. This requires some additional simplifications ($T_2$=0, $T_{ref}$=0). The assumption is valid given that the loading is independent of the isotherms, and $\Delta T_{main}$ is a relative quantity.

The two energy balance equations can be solved to determine $\Delta T_{main}$ and $T_{pl}$.

$$\Delta T_{main} = \frac{\Delta H(F - Pr)\,Pr}{Pr\, m_m C_{sm} + \frac{(F - Pr)C_{pg}}{4}(F + Pr)} \qquad \textbf{(2-40)}$$

$$T_{pl} = \overline{T_2} + \frac{\Delta T_{main}}{2}\left(\frac{F}{Pr} - 1\right) \qquad \textbf{(2-41)}$$

A more detailed expression of $\Delta T_{main}$ can also be developed, if heats of adsorption of both components (nitrogen and oxygen) are considered to be different.

$$\Delta T_{main} = \frac{Pr\left(\Delta H_{N2}\left[Fy_f - Pr\left(1 - \frac{Rec\ F(1-y_f)}{PR}\right)\right] + \Delta H_{O2}\left[F - y_f F - Rec\ F + y_f\, Rec\ F\right]\right)}{Pr\, m_m C_{sm} + \left(\frac{(F - Pr)C_{pg}}{4}(F + Pr)\right)} \qquad \textbf{(2-42)}$$

where Rec is the recovery of oxygen in the product

$y_f$ is mole fraction of nitrogen in the feed gas

This enables the determination of an analytical expression for E. From the previous analysis,

$E = \int_{\tau_1}^{\tau_2} wf(t)dt$ and average values can be used for f(t). $f(t) = \frac{\Delta T_{main}}{2}$

The essence of this approximation is that desorbed gas is passed over the prelayer at some arithmetic average temperature. In practice the nature of this average will depend on the cycle and other process conditions.

These assumptions result in the following expression for E.

$$E = \left(\frac{F - Pr}{2}\right)\left(\frac{Pr\,\Delta H(F - Pr)}{Pr\,m_m C_{sm} + \frac{(F - Pr)C_{pg}}{4}(F + Pr)}\right) \qquad (2\text{-}43)$$

### 2.4.5 Accounting for Cycle Effects

One significant omission in this analysis is the effect of different cycles. The cycle type affects convective flows and impacts on the CSS temperature profile.

The cycle considered above is a simple hypothetical two step cycle (feed and countercurrent desorption). In practice more complex cycles are used and this can have a marked effect on the overall temperature profile. For example, the following 4 step cycle could be considered as more realistic.

**Figure 2-17 – Simplified Cycle**

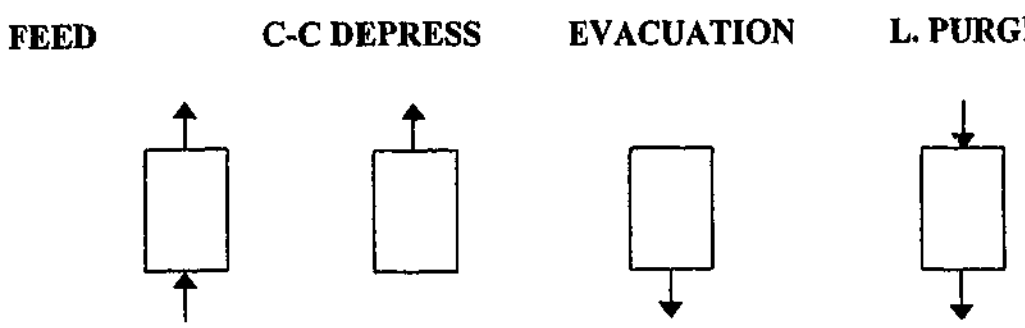


where C-C Depress (Cocurrent depressurisation), and L. Purge (Low Pressure Purge)

This cycle can be solved following the previously detailed method, through the inclusion of the energy balances for the cocurrent depressurisation and purge steps. However, this results in five simultaneous equations which can be solved, but it does not reduce to a simple analytical expression. Instead, a further simplification can be made, and a parameter $\alpha$ can be introduced to reflect the extent of low pressure purge.

$$\alpha = \frac{N_{waste,step4}}{N_{waste,total}} \qquad \textbf{(2-43 a)}$$

where $N_{waste,\ step4}$ is the moles of gas exiting the bed in step 4, and $N_{waste,\ total}$ is the moles of gas exiting the bed in step 3 and 4. In the case where $\alpha = 0$, this is the two step cycle. There is no cocurrent depressurisation or low pressure purge steps. When $\alpha = 1$, there is no flow under the evacuation step. The entire gas stream is desorbed cocurrently and used to purge the bed in step 4.

If we ignore the contribution of the purge (Step 4) to the temperature swing in the bed, and when $\alpha$=1, the entire countercurrent flow of gas occurs at $\Delta T$, not at some average $\Delta T/2$.

**For $\alpha$=1,**
$$E = (F - Pr)\frac{Pr\,\Delta H(F - Pr)}{Pr\,m_m C_{sm} + \left(\frac{(F - Pr)C_{pg}}{4}(F + Pr)\right)} \qquad \textbf{(2-44)}$$

Now based on the further assumption that the contribution of $\alpha$ can be treated linearly, the following general expression for E can be derived.

$$E = \frac{(F - Pr)}{2} \frac{Pr\,\Delta H(F - Pr)}{Pr\,m_m C_{sm} + \left(\frac{(F - Pr)C_{pg}}{4}(F + Pr)\right)}(1 + \alpha) \qquad (2\text{-}45)$$

When this expression for E is combined with the equation for the prelayer (Equation 2-34), the following two equations result.

$$\overline{T_2} = T_f - \frac{Pr\,\Delta H\ m_p C_{sp}\ (F - Pr)^2(1 + \alpha)}{\chi_1 \chi_2} \qquad (2\text{-}46)$$

where $\chi_1 = 4\,Pr\,m_m C_{sm} + (F + Pr)(F - Pr)C_{pg}$

$\chi_2 = 2\,Pr\,m_p C_{sp} + C_{pg} F(F - Pr)$

$$\overline{T_p} = T_f - \frac{Pr\,\Delta H\ m_p C_{sp}(F - Pr)^2(1 + \alpha)}{\chi_1 \chi_2} + \frac{Pr\,\Delta H(F - Pr)}{Pr\,m_m C_{sm} + \left(\frac{(F - Pr)C_{pg}}{4}(F + Pr)\right)} \frac{(1 + \alpha)}{2}\left(\frac{F}{Pr} - 1\right) \qquad (2\text{-}47)$$

The first equation describes the magnitude of the temperature depression, and the second equation describes the average temperature of the product gas leaving the bed.

This is a rough attempt to account for the effect of cycle type on temperature profile. Cycle effects are important, but difficult to account for, in such a simple model. The validity of this approach will be explored in Chapter Four. However, for much of the analysis with the simple energy balance, the contribution of cycle effects can be ignored.

Equations 2-46 and 2-47 can also be modified and stated in terms of adsorbate loading and pressure. For example, the critical working capacity of the adsorbent (F-Pr) can be stated in terms of loading as:

$$F - Pr = (WC)m_m = [n_f(P_f, T_f, y_f) - n_e(P_e, T_e, y_e)]m_m \qquad (2\text{-}48)$$

where WC is the working capacity or simply the quantity of gas loaded per cycle (mol/kg).
$n_f$ is the loading of the adsorbent at the end of feed step (mol/kg). $n_f$ is a function of the Pressure (P), temperature(T) and mole faction (y) at the end of feed step.
$n_e$ is the loading of the adsorbent at the end of evacuation step. (mol/kg) $n_e$ is a function of the Pressure (P), temperature(T) and mole faction (y) at the end of evacuation step.

In addition, F and Pr could be written in terms of the bed and upstream and downstream pressures, using a valve equation. The essential point here is that the derivation of the temperature profiles could be easily written in terms of pressure and adsorbate loading.

### 2.4.6 Conclusion and Implications of Energy Balance Analysis

A number of conclusions can be drawn from Equations 2-46 and 2-47. One of the less important conclusions is that there will be no temperature depression through the prelayer, if the heat of adsorption is zero, if there is no gas returned on desorption (W=0), or if no product gas is removed (total reflux) (Pr=0).

Some more substantial conclusions can be made by further manipulation of Equation 2-46. For example, the equation for $T_2$ can be differentiated with respect to Pr to determine the minimum temperature. The resulting equation is messy, but it does highlight the effect of product flow on the temperature depression.

$$\frac{d\overline{T_2}}{dPr} = \frac{4(\alpha+1)\Delta H m_p C_{sp}(F-Pr)}{\chi_2\chi_1}\left(F+Pr-\frac{(2m_pC_{sp}-FC_{pg})(F-Pr)Pr}{\chi_2}-\frac{(F-Pr)P(-C_{pg}(Pr+F))}{\chi_1}\right) \quad (2\text{-}49)$$

The significance of this equation is more pronounced when plotted using typical values for oxygen VSA flows and heats of adsorption.

**Figure 2-18**

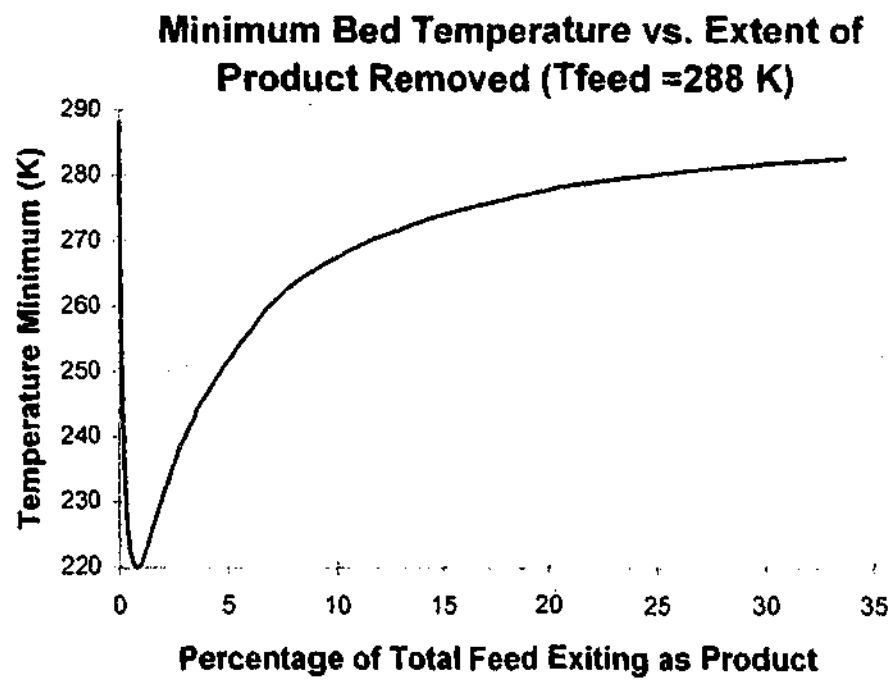


The plot demonstrates the effect of product removal on the extent of the temperature depression. It shows a highly non-linear relationship between product removal and the extent

of the 'cold spot'. In the limiting conditions where there is no product removal, or complete product removal, there is no temperature depression through the prelayer.

However, if only a very small quantity of gas is withdrawn, a very sharp and significant minimum can occur in the adsorption bed. For a typical oxygen VSA unit, the ratio of total product to the feed stream is approximately 11%. This predicted relationship is worthy of further investigation experimentally, and with full numerical simulation with MINSA.

Another interesting manipulation of the equation for the temperature depression (Equation 2-46) can address the issue - what is the ratio of main layer to prelayer that will give a minimum temperature depression for a fixed total bed length (and other fixed process conditions)? Equation 2-48 can be modified assuming that the total mass of the bed is fixed, and this fixed mass is a ratio of inert prelayer and adsorbing main layer.

$$\overline{T_2} = T_f - \frac{\Pr \Delta H\left((m_{tot} - m_m)C_{sp}\right)(WCm_m)^2(1+\alpha)}{\chi_3 \chi_4} \qquad \textbf{(2-50)}$$

where

$$\chi_3 = 4\Pr m_m C_{sm} + (WCm_m + \Pr)(WCm_m)C_{pg}$$

$$\chi_4 = 2\Pr(m_{tot} - m_m)C_{sp} + C_{pg}(\Pr + WCm_m)(WCm_m))$$

where $m_{tot}$ is the total mass of sieve in the bed (main and prelayers) (kg)
WC is the working capacity of the main layer (mol/kg)

This equation can be differentiated with respect to $m_m$, the resulting expression enabling the determination of the quantity of main layer and prelayer, that will cause a minimum temperature to occur in the bed. For typical oxygen VSA operating conditions, the minimum temperature arises with a ratio of 75% adsorbing layer and 25% inert prelayer by mass. This represents slightly more prelayer than is typically used in an industrial VSA unit.

These two examples demonstrate how simple manipulations of the equations for CSS temperature profiles can be usefully applied, to provide interesting insights into the thermal profiles in oxygen VSA. However, it should be noted that these equations for the CSS temperature profiles involve many simplifications, and it is important to acknowledge their resulting limitations. For example, the approach is predicated on the assumption of uniform

loading of adsorbate. However, in order to achieve oxygen purity, the mass transfer zone is generally held inside the bed. Other significant assumptions include ignoring bed-to-bed and cycle effects, ignoring kinetic effects, gas accumulation, ignoring heat loss from the column, assuming constant heats of adsorption, ignoring the effect of temperature on isotherms, and very importantly using very simplistic techniques to determine average temperatures.

The equations derived in this section can be applied to enable a better understanding of the axial CSS temperature profiles in oxygen VSA. This task is taken up in Chapter Four. It is up to the reader to decide the heuristic worth of this approach compared to full numerical simulation. It would be possible to extend this simple energy balance to incorporate other effects such as heat loss, an adsorbing prelayer, an inert at the top of the bed, but given the significant limitations with the approach, it is probably better to keep it simple.

## 2.5 A Dynamic Cell Model

It has been shown how a simple mass and energy balance around the adsorption bed and an inert prelayer. This simple mass and energy balance can predict the CSS temperature profiles for given process conditions and show how different process variables alter the temperature profile. However this analysis neglects an interesting and important aspect of the temperature profiles in oxygen VSA - the dynamic response. Oxygen VSA is characterised by the slow evolution to CSS. This was demonstrated using the flux plots - CCB and ACCB in Section 2.3. A simple dynamic cell model can also be useful in demonstrating the evolution to CSS, and in highlighting the underlying causes for the slow evolution.

A dynamic model can be developed using the same starting point as the simple energy balance - a cell model consisting of an inert prelayer and an adsorbing main layer. The distinction here is that the dynamic model consists of a series of coupled ODEs to describe the transient evolution to CSS. In order to achieve some slight improvement in the resolution of the temperature profile, two inert cells are used for the dynamic model. This is required since the cells are assumed to be CSTRs (Upwind Difference Scheme). While this is still not sufficient to describe a substantial or realistic temperature profile, the approach illustrates the transient behaviour of the temperature profile, and the analysis could be readily extended to incorporate more cells.

**Figure 2-19 - Adsorption Bed with an Inert Prelayer**

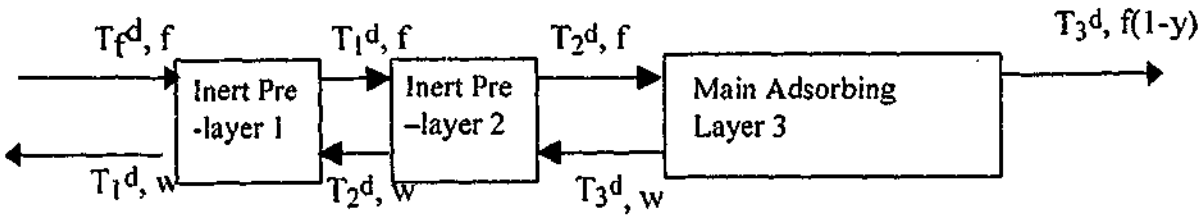


The superscript (d) is used to denote dynamic temperatures, to distinguish this analysis from the simple energy balance approach developed in Section 2-3.

Where f and w, are instantaneous molar flows, and $T_1^d$ and $T_2^d$ are the instantaneous temperatures of the gas entering or leaving the prelayer. One component is adsorbed (y), and there is a total recovery of the lighter component (f(1-y)). There is no accumulation in the gas phase. The mass of the prelayer is $m_p$, and the heat capacity is $C_{sp}$. The gas has a uniform molar specific heat capacity ($C_{pg}$). The mass of the main adsorbing layer is $m^d_3$, and the

heat capacity is $C_s$. The heat of adsorption in the main layer is $\Delta H$. $\tau_{ad}$ is the time of the adsorption step and $\tau_{de}$ is the time of the desorption step.

**Adsorption Step 1 ($0$-$\tau_{ad}$)**

Inert Cell 1: $$\frac{dT_1^d}{dt} = \phi_1(T_f^d - T_1^d) \quad \textbf{(2-51a)}$$

Inert Cell 2: $$\frac{dT_2^d}{dt} = \phi_1(T_1^d - T_2^d) \quad \textbf{(2-51b)}$$

Adsorbing Cell 3: $$\frac{dT_3^d}{dt} = \phi_3(T_2^d - T_3^d + y\psi) \quad \textbf{(2-51c)}$$

**Desorption Step ($0-\tau_{de}$)**

Inert Cell 1: $$\frac{dT_1^d}{dt} = \phi_1\omega(T_2^d - T_1^d) \quad \textbf{(2-52a)}$$

Inert Cell 2: $$\frac{dT_2^d}{dt} = \phi_1\omega(T_3^d - T_2^d) \quad \textbf{(2-52b)}$$

Adsorbing Cell 3: $$\frac{dT_3^d}{dt} = -\phi_3\omega\psi t \quad \textbf{(2-52c)}$$

where $$\phi_1 = \frac{fC_{pg}}{m_1^d C_s},\ \phi_3 = \frac{fC_{pg}}{m_3^d C_s},\ \psi = \frac{\Delta H}{C_{pg}},\ \omega = \frac{y\tau_{ad}}{\tau_{de}}$$

It is assumed that the two inert cells have the same mass. The adsorbed phase is included, but in order to simplify the equations, it is assumed that the mass of the adsorbent is much greater than the mass of the adsorbate. Inclusion of the adsorbate is critical for thermodynamic consistency for an isothermal system. In addition, the gas phase is ignored, adsorption occurs independent of temperature, and only one component is adsorbed. These simple coupled first order ODEs can be solved, resulting in the following six equations:

**Adsorption Step (Step 1)**

Inert Cell 1:
$$T_1^d(t) = T_f^d + \left(T_{1i}^d - T_f^d\right)e^{-\phi_1 t} \quad \textbf{(2-53a)}$$

Inert Cell 2:
$$T_2^d(t) = T_f^d + e^{-\phi_1 t}(T_{1i}^d - T_f^d)\phi_1 t + (T_{2i}^d - T_f^d)e^{-\phi_1 t} \quad \textbf{(2-53b)}$$

Adsorbing Cell 3:
$$T_3^d(t) = T_f^d + \psi y + e^{-\phi_2 t}\left(\left(\frac{(T_f^d - T_{1i}^d)\phi_1\phi_2}{{\phi_3}^2 - 2\phi_1\phi_3 + {\phi_1}^2}\right)\left[\left\{(\phi_1 - \phi_3)t + 1\right\}e^{(\phi_3 - \phi_1)t}\right\} - 1\right] + \left(\frac{(T_{2i}^d - T_f^d)\phi_3}{\phi_3 - \phi_1}\right)\left(e^{(\phi_3 - \phi_1)t} - 1\right) + T_{3i}^d - y\psi - T_f^d\right) \quad \textbf{(2-53c)}$$

**Desorption Step (Step 2)**

Adsorbing Cell 3:
$$T_3^d(t) = T_{3i}^d - \phi_3\omega\psi t \quad \textbf{(2-54a)}$$

Inert Cell 2:
$$T_2^d(t) = T_{3i}^d - \frac{\phi_3\psi(\phi_1\omega t - 1)}{\phi_1} + e^{-\phi_1\omega t}\left(T_{2i}^d - T_{3i}^d - \frac{\phi_3\psi}{\phi_1}\right) \quad \textbf{(2-54b)}$$

Inert Cell 1:
$$T_1^d(t) = e^{-\phi_1 tw}\left[T_{1i}^d - T_{3i}^d - \frac{2\phi_3\psi}{\phi_1} - t(\phi_1 T_{3i}^d - \phi_1 T_{2i}^d + \psi\phi_3)w\right] + T_{3i}^d + \frac{2\phi_3\psi}{\phi_1} - \phi_3\psi wt \quad \textbf{(2-54c)}$$

The initial temperature for the adsorption and desorption step are denoted by a subscript $_i$. The initial temperature for an adsorption step is determined as the end of the end of desorption, and vice versa.

The form of the equations reveals that the dynamic behaviour of the cells is related to the $\phi_1$ and $\phi_3$ parameters. The ratio of the thermal capacitance of the gas and solid phase dictates that these parameters will be small, thereby leading to slow evolution of the temperature profiles. Section 2-5 expands on this issue. The equations also highlight that the adsorbing cell undergoes linear cooling during desorption, due to the absence of convected gas into the cell. However, due to convection, the cell undergoes a more complex temperature evolution on adsorption.

The results of these equations can be presented graphically, to highlight the dynamic interaction between the heat of adsorption and convective fluxes. Figure 2-20 shows the temperature profiles for both inert cell 2 and the adsorbing cell, based on the following values:

$\phi_1 = 0.032\,\text{sec}^{-1}$, $\phi_3 = 0.000533\,\text{sec}^{-1}$, $\psi = 2000\text{K}$ y = 0.78, $\tau_{ad} = \tau_{de} = 20$ sec

**Figure 2-20**

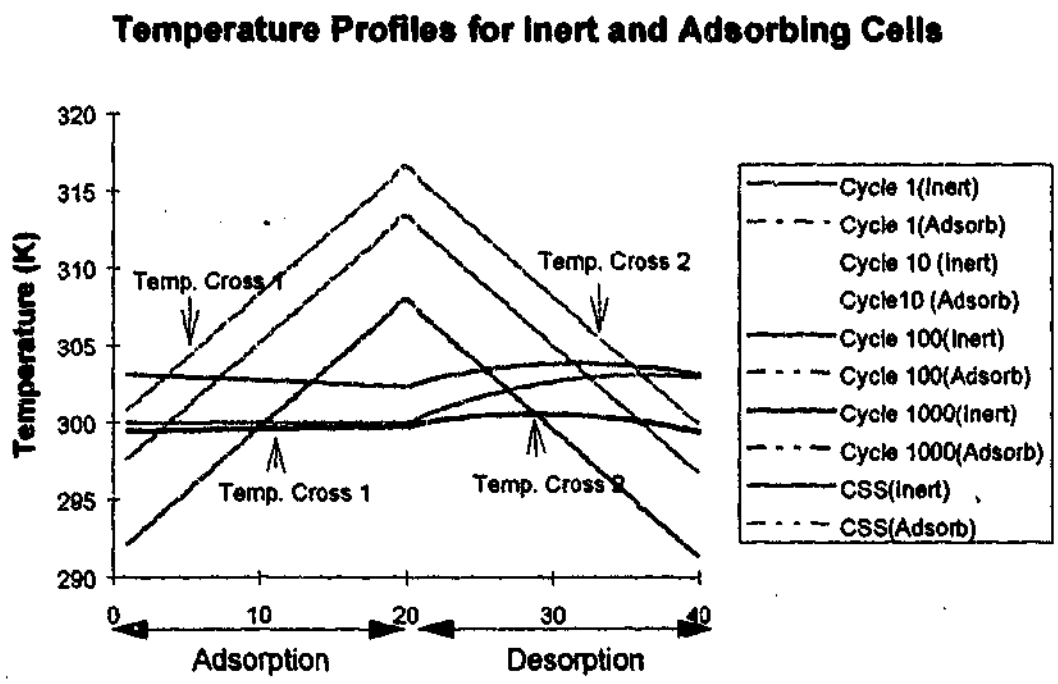


Figure 2-20 shows the temperature fluctuations in the adsorbing cell and inert prelayer. The initial temperature of both cells was 300 K. The adsorbing cell undergoes approximately 16 °C cyclic temperature swing compared with a much smaller temperature swing for the inert cell. A significant feature is the presence of a temperature cross during both the adsorption and desorption steps. This indicates the transition point where the temperature of the two adjacent cells is equal. Initially, the adsorbing cell is cooled by the inert cell during adsorption, and the inert cell is almost exclusively heated during desorption. This initially raises the temperature of the inert cell, but the feed gas also cools the inert cell, and its average temperature is gradually lowered. This results in a further reduction in the average temperature of the adsorbing cell. Convergence to CSS occurs when the location of the temperature crosses has shifted, such that there is no net cooling or heating of the cells over a cycle. At CSS over approximately the first 10 seconds, the adsorbing cell is heated by gas from the inert cell. After the temperature cross, the gas entering from the inert cell is cooling the adsorbing cell. In the initial 9 seconds of desorption, the inert cell is heated by gas from

the adsorbing cell. After the temperature cross and for the remaining 11 seconds in the cycle, the inert is cooling by gas from the adsorbing cell. This analysis parallels the development of the Relative Convective Flux (RCF) plot previously detailed in Section 2.3.

These results can also be plotted on a phase plane diagram.

**Figure 2-21**

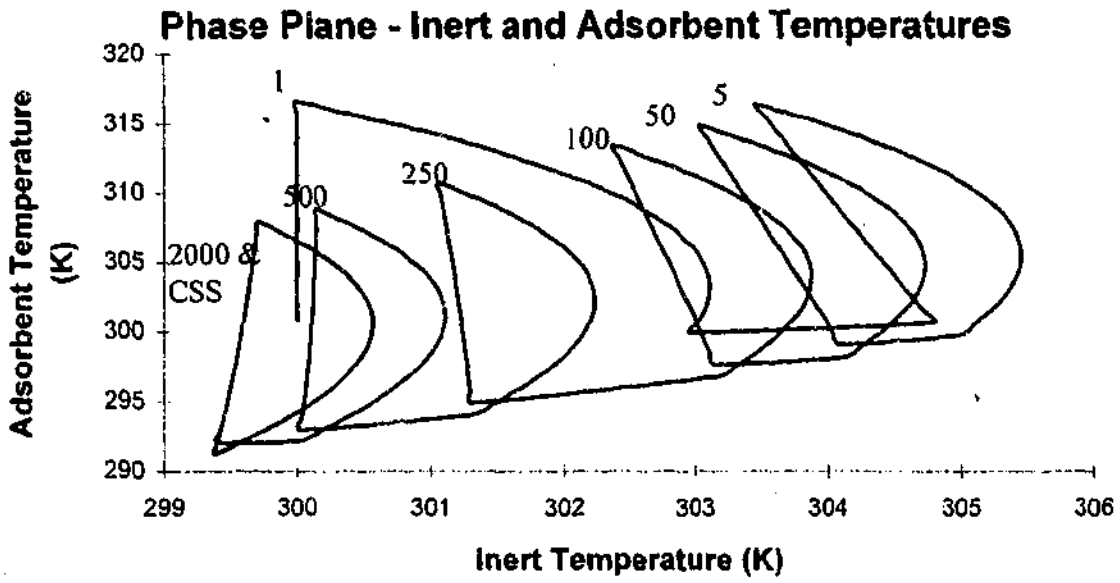


The phase plane diagram (Figure 2-21) shows the evolution of the temperature profiles and the convergence to CSS. Initially (Cycles 1 to 5), the inert layer undergoes net heating by the adsorbent cell. Subsequently, the inert and the adsorbing cell undergo net cooling and phase plane closes after several thousand cycles. Phase planes represent a useful means of tracking evolution to CSS.

This simple dynamic cell model cannot assist in the prediction of CSS temperature profiles. However the dynamic behaviour and the criteria for CSS closure are readily demonstrated with this model, as is the importance of the $\phi_1$ and $\phi_3$ parameters in shaping the dynamic behaviour of the VSA system.

## 2.6 Separation of Variables

Much of the previous analysis has been aimed at offering simple explanations of the axial CSS temperature profiles that occur in oxygen VSA. These explanations highlight the underlying causes of axial CSS temperature profiles, and the slow evolution to CSS. However, their simplicity also dictates that important effects are ignored, including kinetic and cycle effects. The next two sections of this Chapter focus on the development of perturbation techniques to more accurately predict axial CSS temperature profiles, and to accelerate the convergence to these solutions. This work represents an overview of perturbation techniques that could be applied to modelling oxygen VSA. The starting point for this analysis is an informal and experimental approach, based on a simple separation of variables. Beyond the separation of variables approach, more formal, mathematical approaches are developed - Krylov-Bogoliubov (K-B) method and Multiple Scale Analysis (MSA) in Section 2.7.

### 2.6.1 Observations of the Temperature Profiles in Oxygen VSA

The temperature profiles that arise in the operation of oxygen VSA are characterised by a short term fluctuation due to adsorption and desorption, and a longer term drift in temperature to CSS. Figure 2-22 and 2-23 display typical experimental data in the main part of the bed in the fast time (adsorptive) scale and slow time (convective) scale respectively. This work will be reported more fully in Chapter Four.

**Figure 2-22**

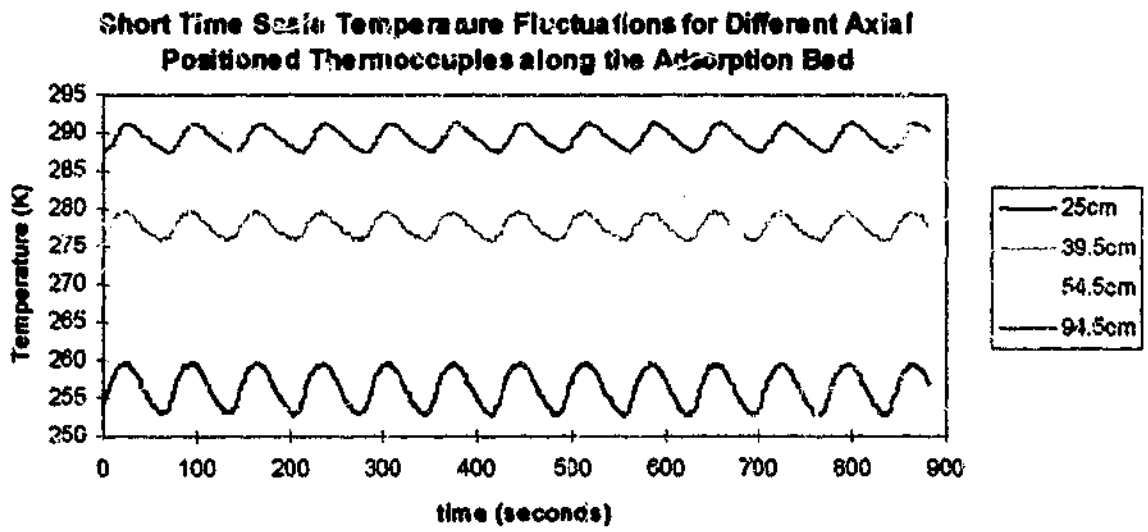


Figure 2-22 demonstrates that over a short time scale the temperature can be described as periodic. These periodic fluctuations are due to the cyclic VSA behaviour and the heat of

adsorption and desorption. One complete period corresponds to one cycle of operation of the VSA unit.

The slow time scale evolution of the temperature profile is caused by the gradual convection of heat through the adsorption bed. This gradual evolution can be witnessed in the following figure.

**Figure 2-23**

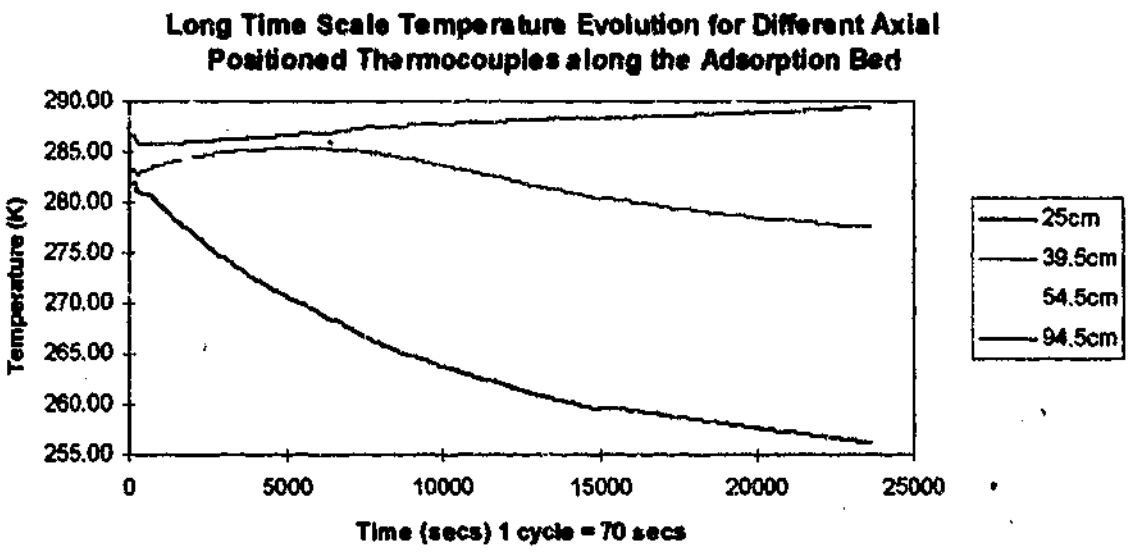


These long time scale temperature evolutions are similar in form to the ACCB plots developed in Section 2.3. Based on these temperature profiles, it is possible to represent the temperature term of the energy balance as the sum of two parts.

$$T = T_0 + T_l \qquad (2\text{-}55)$$

$T_0$ is the periodic temperature swing that is caused by adsorption and desorption and $T_l$ is the long time scale temperature shift. The physical basis for this decomposition of the temperature term into two parts, is that the convective term is essentially a small perturbation on the system, that only accumulates in the long time scale. The temperature cycling associated with adsorption and desorption, however, takes place in the fast time scale only.

### 2.6.2 Decoupling a Simplified Energy Balance– A Solution Strategy

It is possible to write a simplified energy balance based on the full energy balance equation (2-16). By order of magnitude analysis, this equation ignores gas accumulation, the adsorbed phase, heat of compression, and heat loss. These assumptions are typical of industrial oxygen VSA. This reduced equation includes solid accumulation, heat of adsorption and convection.

$$\rho_b C_{ps} \frac{\partial T}{\partial t} = -C_{pg} \frac{\partial}{\partial z}(\rho_g u T) + \rho_b \left( q_{N2} \frac{\partial n_{N2}}{\partial t} + q_{O2} \frac{\partial n_{O2}}{\partial t} \right) \qquad (2\text{-}56)$$

where $q_{N2}$ and $q_{O2}$ are the heats of adsorption for nitrogen and oxygen respectively (J/mol)

Based on the separation of the temperature term, it is possible to divide this equation into a short time scale equation, and a long time scale equation. In the short time scale, the convective term, and the accumulation of convective heat transfer can be ignored, thereby reducing the energy balance to the following.

$$\rho_b C_{ps} \frac{\partial T_0}{\partial t} = \rho_b \left( q_{N2} \frac{\partial n_{N2}}{\partial t} + q_{O2} \frac{\partial n_{O2}}{\partial t} \right) \qquad (2\text{-}57)$$

The long time scale equation can then be written as follows:

$$\rho_b C_{ps} \frac{\partial T_1}{\partial t} = -C_{pg} \frac{\partial}{\partial z}(\rho_g u T_1) - C_{pg} \frac{\partial}{\partial z}(\rho_g u T_0) \qquad (2\text{-}58)$$

The mass balance equations (2-10) and (2-11) and the energy balance (2-58) can be solved to determine the velocity profile and short time scale temperature profile, $T_0$. Only an approximate solution is required here, and this can be obtained after 50 cycles or so. This is measured by a very loose tolerance on the convergence. This is similar to the technique employed by Harriott and Tsirukis (1995).

This solution technique is based on the assumption that velocity, gas density and the short time temperature fluctuations are independent of the evolution of the long time scale temperature. Essentially this assumption ignores the temperature dependence of the isotherm,

and ignores that gas properties are a function of the long-time scale temperature profile, and can hence only provide an approximate solution. Some further iterative scheme is needed to account for the effect of the long time scale temperature profile on the short time scale properties, $\rho_b$, u, $T_0$.

The long time scale temperature ($T_1$) can be determined directly by assuming that the integration of equation 2-59 over a cycle period $\tau_c$ can be set to zero at CSS. This is equivalent to asserting that the net convective flux in and out of every node at CSS is zero, i.e. the energy balance closes.

$$0 = -\int_0^{\tau_c} C_{pg} \frac{\partial}{\partial z}(\rho_g u T_1)dt - \int_0^{\tau_c} C_{pg} \frac{\partial}{\partial z}(\rho_g u T_0)dt \qquad (2\text{-}59)$$

Now assuming that the long time scale temperature is essentially constant at CSS, and $C_{pg}$ is treated as constant, this equation can be reduced to:

$$0 = \frac{\partial}{\partial z} T_1 \int_0^{\tau_c} (\rho_g u)dt + \frac{\partial}{\partial z} \int_0^{\tau_c} (\rho_g u T_0)dt \qquad (2\text{-}60)$$

### 2.6.3 Comparison between Full Simulation and Separation of Variables

The separation of variables technique can readily be applied to predict the CSS temperature profile. Figure 2-24 presents the CSS temperature profile of the full numerical solution, and the temperature profile from the acceleration technique. The plot also displays the maximum and minimum axial temperatures over an adsorption cycle, for both full solution and the accelerated approximation technique. The simulation time for the full solution (3091 cycles) was 54495 seconds, whereas the acceleration technique (50 cycles) was 1239 seconds.

**Figure 2-24**

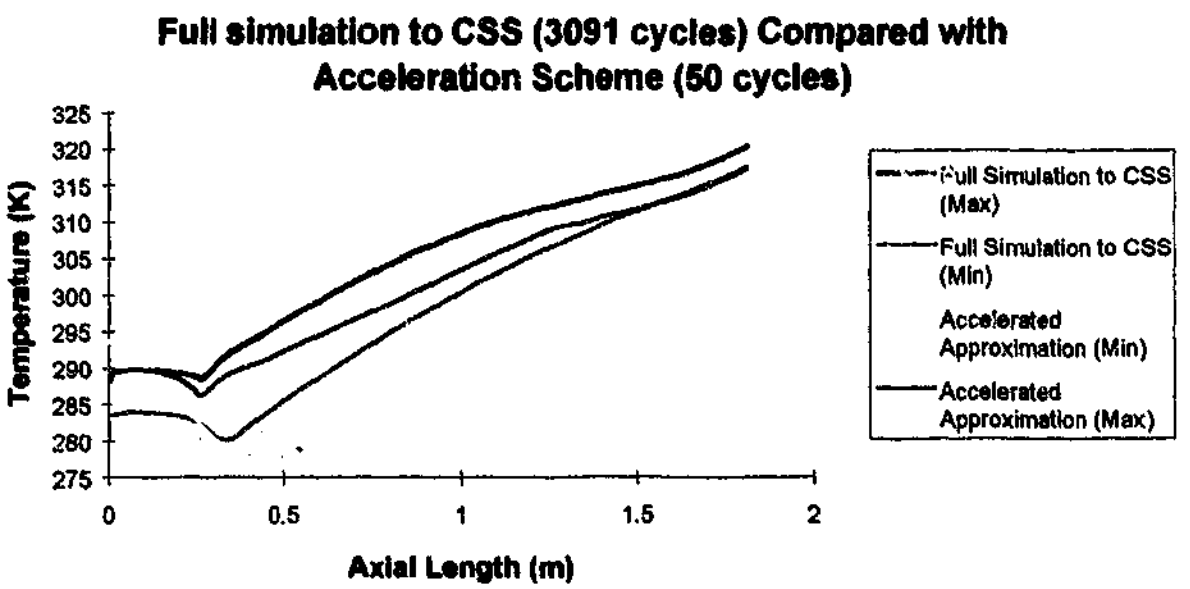


This comparison demonstrates a good correlation between the full CSS numerical solution and the accelerated approximate solution. The numeric values for the local minimum temperature at the interface between the two layers, and the maximum temperature at the end of the bed are similar.

It is also interesting to compare the temperature profiles when both the full simulation and the approximation technique have undergone 50 cycles of numerical simulation. When the initial conditions for the full numerical simulation are a clean bed at the feed gas temperature 288 K, it is apparent that there is a substantial difference between the two temperature profiles, as is indicated in Figure 2-25.

**Figure 2-25**

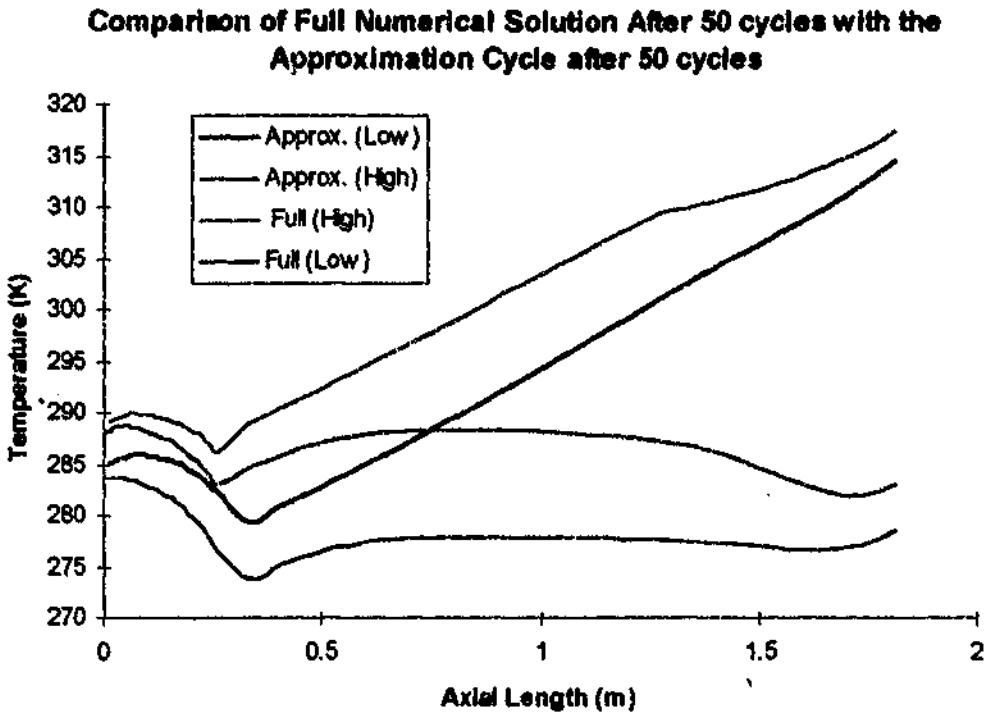


This suggests that the separation of variables technique could be used as an acceleration scheme. However even with a good prediction of the initial temperature profile using the approximation technique, there is still a significant time computationally in realising a closure of state variables within a specified tolerance. In the case above, using the ADSIM convergence tester with a tolerance of 4E-4, the following results were obtained for the full numerical model, taking the approximated temperature profile from Figure 2-24 as an initial condition to accelerate the solution.

**Table 2-2- Comparison of Simulation Times – Full Model vs. Acceleration Scheme**

| Simulation | Cycles to tolerance (4E-4) | CPU Time (166 MHz PI) |
|---|---|---|
| Full Numerical Model | 3091 | 54495 seconds |
| Accelerated Model | 2608<br>(+ 50 cycles to enable approximation of v, $\rho_g$, $T_o$) | 43063 seconds<br>1239 seconds<br>Total: 44302 seconds |

This represents a 19 % reduction in CPU time for the simulation, and demonstrates that even with a 'good' initial guess of the temperature profile, the incremental steps to achieve CSS are very slow. This scheme therefore only provides a modest acceleration to CSS, if we seek closure of all the state variables within a tight tolerance. Moreover, this example does not illuminate some of the limitations of this acceleration technique that require consideration.

Firstly, the generation of the short time scale data (density ($\rho_g$), velocity (u) and temperature fluctuation ($T_o$)) is generated numerically on the basis of the initial temperature and composition of the bed. Changing these initial conditions will change the numeric values of $\rho_g$, u and $T_o$, and hence also change the final long time scale CSS temperature profile. In order to compensate for this dependence on the initial conditions, it is necessary in some cases to develop an iterative scheme. In such a scheme, the long time scale temperature is used as the adsorption beds' initial conditions, to recalculate $\rho_g$, u and $T_o$. These are then used to calculate a better approximation of the final CSS temperature profile. This eliminates the effects of selection of the initial conditions (Refer Figure 2-27).

A second and more fundamental limitation with this separation of variables approximation technique, is that some of its assumptions are questionable for certain conditions. For example, if the prelayer of the beds is inert (e.g. activated alumina), it is assumed that there is no short time scale temperature swing in the prelayer. This is clearly not the case, as convected gas changes the temperature of the prelayer. As a result the approximation technique does not capture the magnitude of the 'cold spot'. Figure 2-26 shows the significant discrepancy between the predicted 'cold spot' using the separation of variables approximation and the full simulation, for the case of the inert prelayer. The difference in the minimum temperatures is approximately 15 °C.

**Figure 2-26**

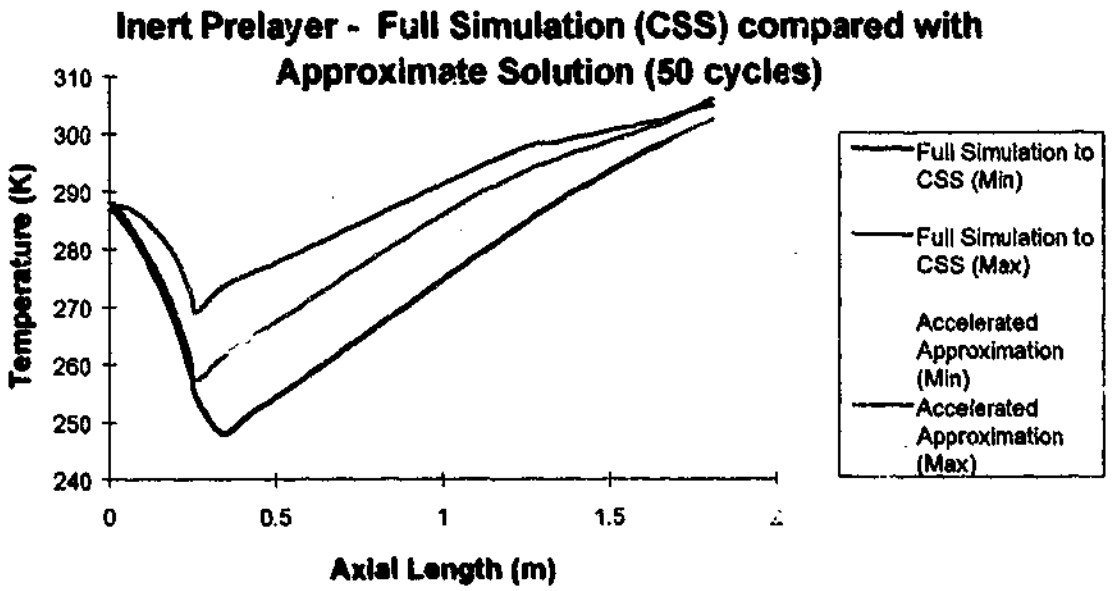

This comparison of temperature profiles can be improved by using the approximate solution as the initial conditions, to recalculate the short time scale molar flowrates and temperature swings. This is a means of eliminating the effect of the initial conditions. Figure 2-27 compares the minimum temperatures for the full simulation, the initial approximate solution and the iterated approximate solution.

**Figure 2-27**

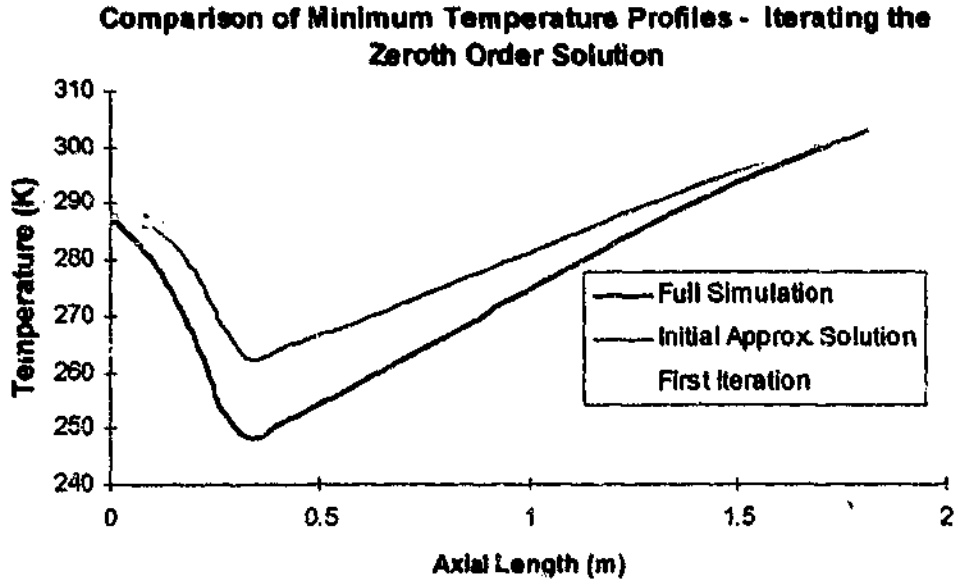


The iterated approximate solution is an improvement over the initial approximate solution. However this does not overcome the fundamental limitations with the zeroth order solution.

The prediction of the temperature depression with an inert prelayer by this technique is not related to the physical properties of the prelayer (thermal capacitance or depth). However from MINSA and ADSIM simulations and experiments detailed subsequently in Chapter Four, it is evident that these properties are critical for determining the cyclic temperature swing in the prelayer, and hence the overall temperature profile. Each of these examples highlights the limitations of a zeroth order technique, where convective effects are ignored in the short time scale.

Another more unusual limitation occurs with total reflux. This zeroth order technique cannot capture the temperature profile when the integral of the molar flow over a cycle is zero (total reflux), and hence the long term temperature fluctuation is indeterminate. It is also apparent that this zeroth order technique will not apply to cases where there is significant axial temperature gradient. i.e. where it cannot be assumed that the short time scale temperature fluctuations are caused solely by the adsorptive temperature swings.

It apparent that there is a range of process conditions for which the zeroth order separation of variables is not accurate, and the effects of important process variables are ignored. In addition, the CPU acceleration benefits of this technique as an acceleration scheme, are modest for a tight tolerance. However there are number of possible applications for the approach. For example, there is a strong argument that for design and optimisation purposes, instead of using all state variables as the measure of convergence and CSS, it would be more appropriate to solely examine convergence of performance criteria, such as bed sizing factor, power and oxygen recovery. Another application would be to enable quick and easy comparison of the temperature profiles of layering the bed with different molecular sieves. This is based on a recognition that the relative performance of molecular sieves is a function of temperature.

This review of the separation of variables highlights that the underlying zeroth order assumptions break down under a range of conditions. However, these limitations aside, the approach provides a useful heuristic technique for understanding the complex interaction between the heats of adsorption and convection. The task now is to formalise and further extend these approximation techniques.

## 2.7 Multiple Scale Analysis and Perturbation Techniques

### 2.7.1 Zeroth Order MSA Energy Balance

The separation of variables analysis resulting in equation 2-60 can be demonstrated to be the same as a zeroth order solution of a multiple scale analysis (MSA) approach. The application of MSA provides a more formal basis for understanding the two time scales that shape the evolution of the CSS temperature profile in oxygen VSA. Furthermore, the application of MSA highlights the level of approximation implicit in the solution, and provides a powerful technique whereby higher order solutions can be sought.

The starting point for this analysis is the simplified energy balance (Equation 2-57) written in dimensionless form.

$$\frac{\partial T^*}{\partial t^*} = -\frac{C_{pg}\rho_{g0}}{\rho_b C_{ps}}\frac{\partial}{\partial z^*}(\rho_g^* u^* T^*) + \left(\frac{q_{N2}\Delta n_{N2}}{\Delta T C_{ps}}\frac{\partial n_{N2}^*}{\partial t^*} + \frac{q_{O2}\Delta n_{O2}}{\Delta T C_{ps}}\frac{\partial n_{O2}^*}{\partial t^*}\right) \qquad (2\text{-}61)$$

where the following substitutions are made:

$$z^* = \frac{z}{L},\ u^* = \frac{u}{u_0},\ \rho_g^* = \frac{\rho_g}{\rho_{g0}},\ t^* = \frac{t}{t_0},\ T^* = \frac{T}{\Delta T},\ n_{N2}^* = \frac{n_{N2}}{\Delta n_{N2}},\ n_{O2}^* = \frac{n_{O2}}{\Delta n_{O2}}$$

where L = Adsorbent bed length (m) (2 m)

$u_0$ = Characteristic superficial velocity (m/sec) (1 m/sec)

$\rho_{g0}$ = Characteristic gas density at 1 bar and 298 K. (mol/m$^3$)

$\Delta n_{N2}$ = Characteristic swing in nitrogen loading (mol/kg)

$\Delta n_{O2}$ = Characteristic swing in oxygen loading (mol/kg)

$\Delta T$ = Characteristic swing in temperature over a cycle (5 $^oC$)

$t_0$ = Characteristic time (sec)

$$\frac{\partial T^*}{\partial t^*} = -\varepsilon\frac{\partial}{\partial z^*}(\rho_g^* u^* T^*) + H_{N2}\frac{\partial n_{N2}^*}{\partial t^*} + H_{O2}\frac{\partial n_{O2}^*}{\partial t^*} \qquad (2\text{-}62)$$

The resulting dimensionless groups can be understood as follows:

$\varepsilon = \frac{C_{pg}\rho_{go}}{\rho_b C_{ps}}$ ( Thermal capacitance of the gas to the thermal capacitance of the solid.)

$H_{N2} = \frac{q_{N2}\Delta n_{N2}}{\Delta T C_{ps}}$ (Heat generation by adsorption of N2 to accumulation of adsorptive heat.)

$H_{O2} = \frac{q_{O2}\Delta n_{O2}}{\Delta T C_{ps}}$ (Heat generation by adsorption of O2 to accumulation of adsorptive heat.)

Typical values of the dimensionless groups are $\varepsilon = 0.00125$, $H_{N2} = 0.9$, and $H_{O2} = 0.1$. This gives a physical basis to the MSA where there is a clearly identified perturbation parameter, $\varepsilon$. Taking this dimensionless form of the energy balance we can now embark on a MSA approach.

Using a multiple time scale expansion, a new slow time scale can be introduced as:

$$\tau^* = \varepsilon t^* \text{ (slow time scale)}$$

and we assume a perturbation expansion of the temperature term.

$$T^* = \sum_{n=0}^{N} \varepsilon^n T^{*(n)}(z^*, t^*, \tau^*) \qquad \text{(2-63)}$$
$$T^* = T^{*(0)} + \varepsilon T^{*(1)} + \varepsilon^2 T^{*(2)} + ..... + .....$$

Now the temporal derivatives can be transformed as:

$$\frac{\partial}{\partial t^*} \rightarrow \frac{\partial}{\partial t^*} + \varepsilon \frac{\partial}{\partial \tau^*} \qquad \text{(2-64)}$$

and considering only the first two terms of the perturbation expansion, realises the following form of the energy balance.

$$\frac{\partial T^{*(0)}}{\partial t^*} + \varepsilon\frac{\partial T^{*(1)}}{\partial t^*} + \varepsilon\frac{\partial T^{*(0)}}{\partial \tau^*} + \varepsilon^2\frac{\partial T^{*(1)}}{\partial \tau^*} =$$
$$-\varepsilon\frac{\partial}{\partial z^*}\left(\rho_g^* u^* (T^{*(0)} + \varepsilon T^{*(1)})\right) + H_{N2}\left(\frac{\partial n_{N2}^*}{\partial t^*} + \varepsilon\frac{\partial n_{N2}^*}{\partial \tau^*}\right) + H_{O2}\left(\frac{\partial n_{O2}^*}{\partial t^*} + \varepsilon\frac{\partial n_{O2}^*}{\partial \tau^*}\right) \quad \textbf{(2-65)}$$

Collecting like powers of $\varepsilon$:

$\varepsilon^0$ terms:

$$\frac{\partial T^{*(0)}}{\partial t^*} = H_{N2}\frac{\partial n_{N2}^*}{\partial t^*} + H_{O2}\frac{\partial n_{O2}^*}{\partial t^*} \quad \textbf{(2-66)}$$

$\varepsilon^1$ terms:

$$\frac{\partial T^{*(1)}}{\partial t^*} + \frac{\partial T^{*(0)}}{\partial \tau^*} = -\frac{\partial}{\partial z^*}\left(\rho_g^* u^* T^{*(0)}\right) \quad \textbf{(2-67)}$$

This is derived from the assumed periodicity of the loading in the short time scale such that:

$$\frac{\partial n_{N2}^*}{\partial \tau^*} = 0, \frac{\partial n_{O2}^*}{\partial \tau^*} = 0 \quad \textbf{(2-68)}$$

$\varepsilon^2$ terms:

$$\frac{\partial T^{*(1)}}{\partial \tau^*} = -\frac{\partial}{\partial z^*}(\rho_g^* u^* T^{*(1)}) \quad \textbf{(2-69)}$$

From Equation 2- 66, we can derive a general solution to the zeroth order term:

$$\boxed{T^{*(0)} = H_{N2} n_{N2}^* + H_{O2} n_{O2}^* + \varphi^{*(0)}(\tau^*, z^*)} \quad \textbf{(2-70)}$$

where $\varphi^{*(0)}(t^*, z^*)$ is a constant of integration that results from the integration of the zeroth order equation.

This equation has the same form as the separation of variables approach (Equation 2-60). The constant of integration is not a function of the short time scale, and can be considered the same as the long time scale component of the temperature profile. The $H_{N2}n_{N2}^* + H_{O2}n_{O2}^*$ term is clearly the adsorptive, or short time scale component of the temperature profile.

Substitution of this general solution into the first order Equation 2-69 yields the following equation.

$$\frac{\partial T^{*(1)}}{\partial t^*} + \frac{\partial T^{*(0)}}{\partial \tau^*} = -\frac{\partial}{\partial z^*}\left(\rho_g^* u^* (H_{N2}n_{N2}^* + H_{O2}n_{O2}^*)\right) - \frac{\partial}{\partial z^*}\left(\rho_g^* u^* \varphi^{*(0)}(\tau^*, z^*)\right) \tag{2-71}$$

Now this equation can be integrated over a cycle of period $\tau_c$.

$$\int_0^{\tau_c} \frac{\partial T^{*(1)}}{\partial t^*} dt^* + \int_0^{\tau_c} \frac{\partial \phi^{*(0)}}{\partial \tau^*} dt^* + \frac{\partial}{\partial z^*} \int_0^{\tau_c} \left(\rho_g^* u^* (H_{N2}n_{N2}^* + H_{O2}n_{O2}^*)\right) dt^* + \frac{\partial}{\partial z^*} \int_0^{\tau_c} (\rho_g^* u^* \phi^{*(0)}(\tau^*, z^*)) dt^* = 0 \tag{2-72}$$

Given the compatibility condition $\int_0^{\tau_c} \frac{\partial T^{*(1)}}{\partial t^*} dt^* = 0$, and making the additional approximation at CSS, that $\int_0^{\tau_c} \frac{\partial \varphi^{*(0)}}{\partial \tau^*} dt^* = 0$, the equation is reduced to:

$$\boxed{\frac{\partial}{\partial z^*} \int_0^{\tau_c} \rho_g^* u^* \left(H_{N2}n_{N2}^* + H_{O2}n_{O2}^*\right) dt^* + \frac{\partial}{\partial z^*} \varphi^{*(0)}(\tau^*, z^*) \int_0^{\tau_c} \rho_g^* u^* dt^* = 0} \tag{2-73}$$

This dimensionless equation is the same as equation (2-62) and enables the calculation of the zeroth order temperature solution, $T^{*(0)}$.

The utility of the MSA approach is that it provides a more formal basis for the experimental observations that led to the separation of variables approach. MSA demonstrates how we can decompose the evolution of CSS in oxygen VSA into two time scales, fast (adsorptive), and

slow(convective), and how the perturbation parameter ε explains the slow evolution of the CSS temperature profile.

As has been detailed previously, one fundamental limitation of this approach is that it provides only a zeroth order approximation of the temperature profile. Further work is required to utilise higher order terms in the temperature expansion. Moreover this preliminary application of the MSA does not even undertake an expansion of the velocity, composition and loading terms in the mass balance. In order to account for the alteration of performance of oxygen VSA as the temperature profile evolves, it is necessary to develop the perturbation expansion of the velocity, composition and loading, to account for the long time scale evolution of these variables. These limitations are addressed in the subsequent sections of this chapter.

### 2.7.2 Krylov- Bogoliubov (K-B) Method

Another perturbation technique can also be applied to solve the simplified energy balance - the Krylov- Bogoliubov (K-B) method (Huntley and Johnson, 1983). This technique involves setting the perturbation variable $\varepsilon$ to zero. This results in the same equation as the $\varepsilon^0$ term in equation (2-66)

$$\frac{\partial T^*}{\partial t^*} = H_{N2}\frac{\partial n^*_{N2}}{\partial t^*} + H_{O2}\frac{\partial n^*_{O2}}{\partial t^*} \qquad (2\text{-}74)$$

This equation can be integrated resulting in:

$$T^* = H_{N2}n^*_{N2} + H_{O2}n^*_{O2} + \kappa(z^*) \qquad (2\text{-}75)$$

The K-B method asserts that where $\varepsilon$ is small, $\kappa(z^*)$ is no longer a constant but a slowly varying function in time, and becomes $\kappa(t^*,z^*)$. This equation for $T^*$ is substituted back into the main energy balance resulting in:

$$\frac{\partial \kappa(t^*,z^*)}{\partial t^*} + \varepsilon\frac{\partial}{\partial z^*}\left[\rho^*_g v^*\left(H_{N2}n^*_{N2} + H_{O2}n^*_{O2} + \kappa(t^*,z^*)\right)\right] = 0 \qquad (2\text{-}76)$$

Now according to the K-B method the average value of $\kappa(t^*,z^*)$ at CSS will be constant. The average value of $\kappa(t^*,z^*)$ is determined by integration over a cycle at CSS.

$$\boxed{0 = \frac{\partial}{\partial z^*}\overline{\kappa(t^*,z^*)}\int_0^{\tau_c}\rho^*_g v^* dt^* + \frac{\partial}{\partial z^*}\int_0^{\tau_c}\left(\rho^*_g v^*\left(H_{N2}n^*_{N2} + H_{O2}n^*_{O2}\right)\right)dt^*} \qquad (2\text{-}77)$$

This is a method of averaging technique, and it results in the same solution as the separation of variables, and the zeroth order multiple scale analysis approach. However, as has been previously discussed, all techniques share the same significant flaw. In order to improve on the approach it is necessary to determine higher order terms via MSA.

### 2.7.3 First Order Multiple Scale Analysis

The principal limitation in the zeroth order MSA solution is that the convective effects are considered to occur in the long time scale only. This is incorrect. The introduction of higher order terms into the MSA approach yields an improved approximation of the overall temperature profile. Reintroducing the $\varepsilon^1$ term equation (Equation 2- 67) from the perturbation expansion results in:

$$\frac{\partial T^{*(1)}}{\partial t^*} + \frac{\partial T^{*(0)}}{\partial \tau^*} = -\frac{\partial}{\partial z^*}\left(\rho_g^* u^* T^{*(0)}\right) \qquad (2\text{-}78)$$

Now substituting the zeroth order solution into this equation and integrating over the short time scale results in the following equation.

$$\frac{\partial T^{*(1)}}{\partial t^*} + \frac{\partial\left(\varphi^{*(0)}(\tau^*, z^*)\right)}{\partial \tau^*} = -\frac{\partial}{\partial z^*}\left(\rho_g^* u^* (H_{N2} n_{N2}^* + H_{O2} n_{O2}^*)\right) \qquad (2\text{-}79)$$

$$-\frac{\partial}{\partial z^*}\left(\rho_g^* u^* \varphi^{*(0)}(\tau^*, z^*)\right)$$

$$T^{*(1)} = -\int_0^{t_1} \frac{\partial\left(\varphi^{*(0)}(\tau^*, z^*)\right)}{\partial \tau^*} dt^* - \frac{\partial}{\partial z^*}\int_0^{t_1}\left(\rho_g^* u^* (H_{N2} n_{N2}^* + H_{O2} n_{O2}^*)\right)dt^* \qquad (2\text{-}80)$$

$$-\frac{\partial}{\partial z^*}\int_0^{t_1}\left(\rho_g^* u^* \varphi^{*(0)}(\tau^*, z^*)\right)dt^* + \gamma(t^*, z^*)$$

where $\gamma(t^*,z^*)$ is a constant of integration and $t_1$ is the specific time in the short time scale. This equation is subject to the following boundary condition, $T^{*(1)} = 0$ at $t=0$. We can also apply the secularity condition:

$$\text{As } \begin{matrix} t_1 \longrightarrow \infty \\ \tau \longrightarrow \infty \end{matrix}$$

$$\text{Therefore } \frac{\partial\left(\varphi^{*(0)}(\tau^*, z^*)\right)}{\partial \tau^*} \longrightarrow 0 \qquad (2\text{-}81)$$

and this reduces the equation to:

$$T^{*(1)} = -\frac{\partial}{\partial z^*}\int_0^{t_1}\left(\rho_g^* u^* (H_{N2} n_{N2}^* + H_{O2} n_{O2}^*)\right)dt^* - \frac{\partial}{\partial z^*}\int_0^{t_1}\frac{\partial}{\partial z^*}\left(\rho_g^* u^* \varphi^{*(0)}(\tau^*, z^*)\right)dt^* \qquad (2\text{-}82)$$

This equation for $T^{*(1)}$ can be substituted back into the overall expression for $T^*$

$$T^* = T^{*(0)} + \varepsilon T^{*(1)} + .....$$

$$= H_{N2} n_{N2}^* + H_{O2} n_{O2}^* + \varphi^{*(0)}(\tau^*, z^*) - \varepsilon\frac{\partial}{\partial z^*}\int_0^{t_1}\left(\rho_g^* u^* (H_{N2} n_{N2}^* + H_{O2} n_{O2}^*)\right)dt^*$$

$$-\varepsilon\frac{\partial}{\partial z^*}\int_0^{t_1}\left(\rho_g^* u^* \varphi^{*(0)}(\tau^*, z^*)\right)dt^* \qquad (2\text{-}83)$$

Physically this indicates that the instantaneous temperature during a cycle at CSS is composed of four terms. The first is an adsorptive term ($H_{N2}n_{N2}^* + H_{O2}n_{O2}^*$) that is periodic over the cycle. The second is a baseline temperature $\varphi(\tau^*,z^*)$ that is fixed at CSS. These are the two temperature terms resulting from the separation of variables and zeroth order MSA. The additional two temperature terms are the effect of convection of the baseline term and the adsorptive term. This provides the instantaneous convective temperature change that was neglected in the zeroth order solution. Significantly the effect of these last two terms is damped by the perturbation parameter, $\varepsilon$.

The unknown on the right of this equation is $\varphi^{(0)}(\tau^*,z^*)$. This is found by substitution into the original energy balance which is integrated over a cycle at CSS. The resulting equation is:

$$\boxed{\frac{\partial}{\partial z^*}\int_0^{\tau_c}(\rho_g^* u^*[\chi_5 - \chi_6 - \chi_7]dt^* = 0} \qquad (2\text{-}84)$$

where $$\chi_5 = H_{N2} n^*_{N2} + H_{O2} n^*_{O2} + \varphi^{*(0)}(\tau^*, z^*)$$

$$\chi_6 = \varepsilon \frac{\partial}{\partial z^*} \int_0^{\tau_c} \left( \rho_g^* u^* (H_{N2} n^*_{N2} + H_{O2} n^*_{O2}) \right) dt^*$$

$$\chi_7 = \varepsilon \frac{\partial}{\partial z^*} \int_0^{\tau_c} \left( \rho_g^* u^* \varphi^{*(0)}(\tau^*, z^*) \right) dt^*$$

This equation can be solved for the unknown - $\varphi^{(0)}(\tau^*,z^*)$ and it is corrected for the short time scale effects of convection.

### 2.7.4 Comparison between the Full Simulation Solution and the First Order MSA Solution

When the first order term is incorporated into the perturbation solution, the result compares better with the full simulation solution, than the zeroth order solutions in Figure 2-27. The main effect of the inclusion of the first order term is to modify the short time scale enthalpy fluxes through the inert prelayer. This modifies the overall CSS temperature profile.

**Figure 2-28**

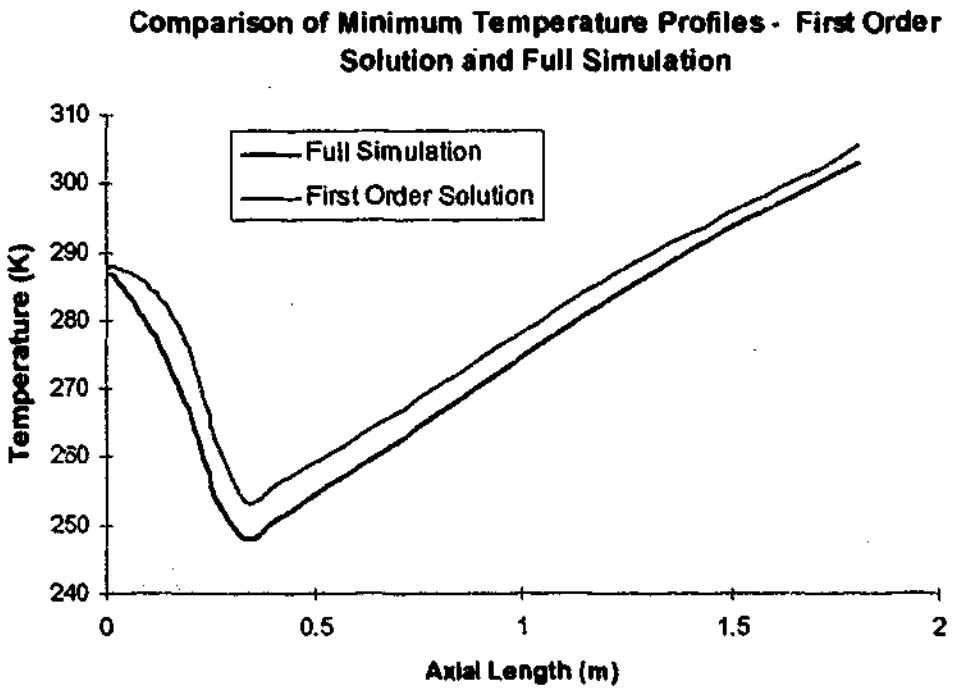

Figure 2-28 shows that the first order MSA solution is consistently approximately 5°C higher than the full simulation. This difference between the profiles is smaller than the zeroth order solution, particularly at the 'cold spot'(Full Solution ~248 K, First Order~253 K, Zeroth Order ~262 K). This indicates an improved approximation, but there are still consistent differences between the two results. The initial gradient in the prelayer is steeper for the full simulation, and this appears to result in a lower temperature profile through the entire bed. It appears that this initial difference accounts for the bulk of the difference in the two temperature profiles. This suggests there might be some difference in the treatment of the boundary conditions, or an issue with discretisation. This warrants some further investigation.

This example suggests that MSA might offer some potential benefits for acceleration of CSS, but this is only one example. More investigation is needed to confirm the veracity of this approach for other process conditions. The extension of this work is beyond the scope of this study. The aim here was largely to utilise the perturbation techniques as a heuristic device for better understanding CSS in oxygen VSA. It also demonstrates that the introduction of higher order terms can improve the approximate solution.

### 2.7.5 Dynamic Evolution of CSS via MSA

One important feature of a MSA perturbation approach is that unlike Poincare and Lindstedt's method (Holmes, 1995), MSA can capture the thermal evolution toward CSS. This potentially provides useful insights into the behaviour of the oxygen VSA process.

The starting point for this analysis is to modify the form of the integration constant, $\varphi^{*(0)}(\tau^*,z^*)$. The preceding analysis has essentially assumed a CSS approximation that the partial derivative of $\varphi^{*(0)}$ in the long time scale is zero. If this condition is relaxed, we can rewrite $\varphi^{*(0)}(\tau^*,z^*)$ as an explicit function in $\tau^*$ and $z^*$ subject to the secularity condition. The simplest functional form that meets both the initial conditions and the secularity conditions is:

$$\varphi^{*(0)}(\tau^*,z^*) = \left(T_i^* - \zeta(z^*)\right)e^{-\eta(\tau^*,z^*)} + \xi(z^*) \qquad (2\text{-}85)$$

where $\eta(0^*,z^*) = 0$ and $\eta(\infty, z^*) = \infty$ and $\varphi^{*(0)}(\tau^*,z^*) = \xi(z^*)$ as $t\to\infty$

A significant feature of this equation is that initial temperature does not effect the CSS. In effect the initial conditions are washed out of the bed. Now the overall zeroth order temperature term is given by:

$$T^{*(0)} = H_{N2}n_{N2}^* + H_{O2}n_{O2}^* + \zeta(z^*) + (T_i^* - \zeta(z^*))e^{-\eta(z^*,\tau^*)} \qquad (2\text{-}86)$$

The first term is adsorptive temperature swing, the second term is the baseline CSS temperature. The third term is the new term, which is the dynamic response of the temperature toward CSS. From the energy balance it is possible to derive the equation for $\eta(\tau^*,z^*)$:

$$\eta(\tau^*,z^*) = -\frac{1}{\left(T_i^* - \zeta(z^*)\right)\tau_c}\frac{\partial\left(\left[T_i^* - \zeta(z^*)\right]\int_0^{\tau_c}\rho_g{}^* u^* dt^*\right)}{\partial z^*}\varepsilon\tau^* \qquad (2\text{-}87)$$

This equation demonstrates how the dynamic behaviour of the VSA unit is a complex function of the initial conditions, the perturbation parameter (the ratio of the gas thermal

capacitance to solid thermal capacitance), and net convective enthalpy flux. Importantly it demonstrates that convergence to CSS is accelerated by higher values of ε, and greater net enthalpy fluxes through the adsorption bed, and shorter cycle times.

### 2.7.6 Inclusion of Additional Terms in Energy Balance (Axial Conduction and Heat Loss)

To this point the various perturbation techniques have been applied to a simplified energy balance, which considers only convection and heat generation by adsorption. It is possible to extend the analysis to include additional dissipative terms - axial conduction and heat loss. The energy balance with these terms included is:

$$\frac{\partial T^*}{\partial t^*} = -\varepsilon \frac{\partial}{\partial z^*}\left(\rho_g^* u^* T^*\right) + H_{N2}\frac{\partial n_{N2}^*}{\partial t^*} + H_{O2}\frac{\partial n_{O2}^*}{\partial t^*} - k_b^*\varepsilon\frac{\partial^2 T^*}{\partial z^{*2}} + h_{wo}^*\varepsilon\left(T^* - T_{amb}^*\right) \qquad (2\text{-}88)$$

where $k_b^*$ and $h_{wo}^*$ are scaled parameters of the axial conductivity and the heat transfer coefficient respectively. The significant point here is that the perturbation parameter ε appears in both these new terms. Following the method detailed previously the zeroth order solution to this equation is:

$$\boxed{\begin{aligned}&\frac{\partial}{\partial z^*}\int_0^{\tau_c}\rho_g^* u^* \chi_8 dt^* + \frac{\partial}{\partial z^*}\left(\varphi^{*(0)}\int_0^{\tau_c}\rho_g^* u^* dt^*\right) - h_{wo}^*\left(\tau_c\varphi^{*(o)} - \tau_c T_{amb}^* + \int_0^{\tau_c}\chi_8 dt^*\right)\\ &+ k_b^*\left(\int_0^{\tau_c}\frac{\partial^2\chi_8}{\partial z^{*2}}dt^* + \int_0^{\tau_c}\frac{\partial^2\varphi^{*(0)}}{\partial z^{*2}}dt^*\right) = 0\end{aligned}} \qquad (2\text{-}89)$$

where $$\chi_8 = H_{N2}n_{N2}^* + H_{O2}n_{O2}^*$$

This equation can be solved for $\varphi^{(0)}(\tau^*,z^*)$, as was previously undertaken with the separation of variables and zeroth order solution.

The inclusion of the thermal conductivity term is generally not required, based on an order of magnitude analysis, and the low thermal conductivity of adsorbent. Inclusion of the heat loss term is important when considering laboratory scale VSA units. Equation 2-89 is essentially derived to demonstrate how dissipative terms (heat loss and thermal conductivity) could be included in the perturbation analysis.

### 2.7.7 Full Application of MSA - Mass and Energy Balances

The major limitation in the application of perturbation techniques so far is that the mass balance and long time scale energy balances have been decoupled. It has been assumed that velocity, loading, pressure, and mole fraction are only a function of the short time scale, and are periodic functions in z and t. This ignores the effect of the long time scale temperature profile on oxygen VSA performance. It is possible to incorporate the effect of the long time scale energy balance, through an iterative process. The perturbation solution for the final CSS temperature profile can be used as an initial condition to calculate new pressure, velocity, mole fraction and loading profiles. This revised data can be used to calculate a new final CSS temperature profile. However, this is a laborious process that could be eliminated by a full MSA approach where additional terms are subjected to a perturbation expansion. This is closer to the formulation of the MSA approach as suggested by Harriott and Tsirukis (Unpublished). The following description outlines how a zeroth order full MSA approach could be devised. A number of additional simplifications are made to assist in the derivation of a solution.

Based on the K-B method the following three equations can be written:

$$\begin{aligned} P &= A_1(\tau,z)P'(t,z)+A_2(\tau,z) \\ y &= A_3(\tau,z)y'(t,z)+A_4(\tau,z) \\ T &= A_5(\tau,z)T'(t,z)+A_6(\tau,z) \end{aligned} \qquad (2\text{-}90)$$

where P', y', and T' are periodic functions in the short time scale. These functions are stretched and translated in long time scale ($\tau$) by the functions $A_i$. Based on the isotherm, it follows that the loading is a dependent function of P, y, and T. It is also assumed that the velocities through the adsorption bed are independent of $\tau$. The physical basis for this assumption is that at the ends of the adsorption bed, fixed velocities are imposed by Rootes type feed and vacuum blowers, and a fixed product withdrawal.

It also holds that at CSS $A_i$ for all i will be constants such that

$$\frac{\partial A_i}{\partial \tau} = 0 \text{ for all i}$$

The proposed solution involves solving the mass and energy (without convection) balances and P', y', and T' with $A_1, A_3, A_5 = 1$, and $A_2(0,z) = A_{20}$, $A_4(0,z) = A_{40}$, $A_6(0,z) = A_{60}$.

These periodic functions P', y', and T' can be substituted into the governing constitutive equations and imposing boundedness (secularity) on $A_i(\tau, z)$, the following equations result:

$$\frac{\partial}{\partial z}\int_0^{\tau_c}(A_1P'+A_2)u\,dt = 0 \qquad (2\text{-}91)$$

$$\frac{\partial}{\partial z}\int_0^{\tau_c}\left(\frac{A_1P'+A_2}{A_5T'+A_6}\right)u\,dt = 0 \qquad (2\text{-}92)$$

$$\frac{\partial}{\partial z}\int_0^{\tau_c}\left(\frac{A_1P'+A_2}{A_5T'+A_6}\right)(A_3y'+A_4)u\,dt = 0 \qquad (2\text{-}93)$$

Three additional equations are required in order to solve the six unknowns - $A_i$ for i =1 to 6.

Following the K-B and the method of averaging, half cycle equations result in:

$$\int_0^{\tau_c/2}\frac{A_1\partial P'}{\partial t}dt + \int_0^{\tau_c/2}\left(\frac{A_1P'+A_2}{A_5T'+A_6}\right)\frac{A_6\partial T'}{\partial t}dt = \int_0^{\tau_c/2} -(A_5T'+A_6)\frac{\partial}{\partial z}\left(u\frac{(A_1P'+A_2)}{A_5T'+A_6}\right)dt - \sum_{i=O2,N2}\frac{\rho_b R(A_5T'+A_6)}{\varepsilon_b}\frac{\partial n_i}{\partial t} \qquad (2\text{-}94)$$

$$\int_0^{\tau_c/2}\frac{A_1\partial(P'A_3y')}{\partial t}dt + \int_0^{\tau_c/2}\left(\frac{(A_1P'+A_2)(A_3y'+A_4)}{A_5T'+A_6}\right)\frac{A_6\partial T'}{\partial t}dt = \int_0^{\tau_c/2} -(A_5T'+A_6)\frac{\partial}{\partial z}\left(u\frac{(A_1P'+A_2)(A_3y'+A_4)}{A_5T'+A_6}\right)dt - \frac{\rho_b R(A_5T'+A_6)}{\varepsilon_b}\frac{\partial n_{N2}}{\partial t} \qquad (2\text{-}95)$$

$$\int_0^{\tau_c/2} \frac{A_5 \partial P'}{\partial t} dt = \int_0^{\tau_c/2} \frac{1}{C_{ps}} \left( q_{N2} \frac{\partial n_{N2}}{\partial t} + q_{O2} \frac{\partial n_{O2}}{\partial t} \right) dt \qquad (2\text{-}96)$$

The solution of the resulting 6 equations and 6 unknowns will not be undertaken in this study. This example has been presented to illustrate how a full (mass and energy) zeroth order perturbation technique could be applied through the introduction of P, y, and T functions, as described in equation 2-90. The basis of this derivation is that the period of the short-term oscillation is fixed by the cycle time, and these periodic functions are translated and shifted in the long time scale. This approach still suffers from the same limitations as the zeroth order analysis previously described. However, following the methods previously described, it would be possible to expand this approach to incorporate higher order terms. It is hoped that others will take up this task!

One problematic aspect of expanding the perturbation technique to include pressure and composition terms, involves dealing with the boundary conditions. It was assumed that the velocities were fixed boundary conditions, imposed by the feed and vacuum blowers, and a fixed product withdrawal. One further assumption might be to impose the same governing pressure profile on the cycle in addition to fixed velocities. The physical basis of this assumption is that, in practice, valves control the pressure profile. This would simplify the analysis, with only the composition and temperature not being periodic in the short time scale. However it would be important to ensure that the problem was not over constrained.

### 2.7.8 Conclusions, Limitations and Future Work for Perturbation Approaches

This section has sought to apply some different perturbation approaches to the problem of CSS closure in oxygen VSA. This endeavour was inspired largely by the ideas of Dr. George Harriott, and countless hours of watching convergence of the laboratory VSA to CSS. The principal realisation of all these approaches is that a perturbation parameter can be identified, based on the ratio of the thermal capacitance of the gas and the solid.

The potential benefits and limitations of these methods have been explored. Under certain process conditions, a zeroth order solution can quickly estimate the axial CSS temperature profile. However, ignoring the effect of convection in the short time scale can be perilous under other conditions. However the zeroth order solutions (separation of variables, K-B and MSA) are a heuristic device to better understand axial CSS temperature profiles, as a function of the process conditions and sieve arrangements that cause them.

The first order solutions yields a more accurate solution for the case of an inert prelayer. Future work is required to ascertain how these approaches can be combined with full numerical techniques to accelerate determination of CSS.

One significant limitation of applying these techniques to analysing experimental data, is that the velocity profile through the bed readily cannot be obtained from experimental measurements. The periodic temperature and pressure swings readily can be measured, but *in situ* velocity measurements are not so simple in a bulk gas separation system. Axial velocity, temperature and pressure data are required to apply these techniques to predict the CSS temperature profile, based on short time scale data. Local velocities could be measured by determination of differential pressures across small sections of the bed, and application of the Ergun equation.

## 2.8 Equilibrium Theory of the Penetration of a Water Loaded Zone

The modelling and descriptive approaches have sought to analyse the development of thermal profiles in oxygen VSA. This analysis has been based on a two component system (oxygen and nitrogen) where nitrogen is the heavier component. In practice, other trace components (water and carbon dioxide) adsorb even more strongly to the adsorbent, and displace the oxygen and nitrogen in a system of competitive adsorption. This necessitates the need for a prelayer to protect the main adsorption layer from water and carbon dioxide (Chou, et.al., 1998). Hitherto the prelayer has been treated as an inert, and this assumption enabled a variety of modelling approaches. The task now is to develop a technique to determine the penetration of water under oxygen VSA conditions. The effect of carbon dioxide is ignored for simplicity, and in accompanying experiments detailed in Chapter Four, carbon dioxide was removed prior to the VSA adsorption beds.

In industrial VSA units, determination of the length of the water loaded under different ambient and process conditions is very important, because it determines the length of the prelayer. Alternatively in cases where solely NaX is used as both the prelayer and main layer, the depth of the water penetration determines the amount of remaining adsorbent available for nitrogen and oxygen separation.

Water adsorption in the prelayer is modelled here using an equilibrium, isothermal, water balance based on a dual-site Langmuir model. This is similar to the development of LeVan (1995). Oxygen and nitrogen are treated as inert in the initial zone of the bed, where water adsorption occurs. It is well known that water is strongly adsorbed on X type zeolites, excluding nitrogen and oxygen adsorption (Hutson, et.al. 2000). The mass balance for water at a point in the bed is:

$$\frac{uP}{\varepsilon_t}\frac{\partial y_w}{\partial z}+\frac{\partial P y_w}{\partial t}+\frac{\rho_b RT}{\varepsilon_t}\frac{\partial n_w}{\partial t}=0 \qquad (2\text{-}97)$$

where $y_W$ is the mole fraction of water (Dimensionless)

$n_W$ is the adsorbate loading of water (mol/kg)

Since water is a trace component, it can be assumed that there are no axial pressure or velocity gradients in the water loaded zone. Water adsorbs strongly to both activated

alumina and NaX and its isotherm is highly favourable (Figure 2-29). A dual-site Langmuir model is used to describe the isotherm.

$$n_w = \frac{m_{w1} b_w P_w}{1 + b_w P_w} + \frac{m_{w2} d_w P_w}{1 + d_w P_w} \qquad (2\text{-}98)$$

where $b_w = b_{wo} \exp\left(\frac{Q_{w1}}{RT}\right)$ , $d_w = d_{wo} \exp\left(\frac{Q_{w2}}{RT}\right)$

where $m_{w1}$, $m_{w2}$, $b_o$, $d_o$, $Q_{w1}$, $Q_{w2}$ are the dual- site Langmuir parameters for water on NaX.

Using the appropriate isotherm parameters, the isotherm for water adsorption is shown in Figure 2-29 below (Aspentech, 1997). Consideration here is limited to water adsorption on NaX since the water- activated alumina is more complex than can be described by a Dual Site Langmuir model.

**Figure 2-29**

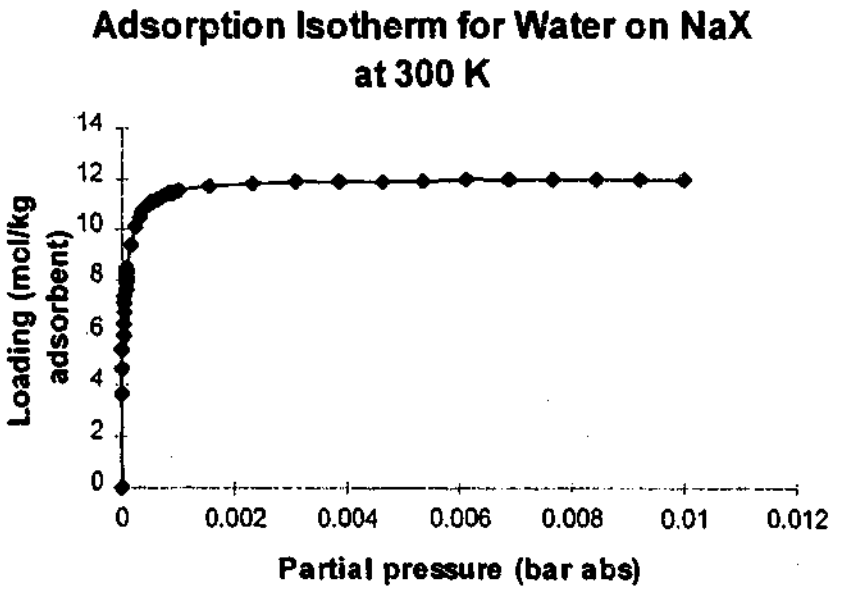

The plot shows an almost rectangular isotherm. There is a substantial range of partial pressures where the loading is essentially constant (i.e. $dn_w/dP_w$ is approximately zero), and a small region at low partial pressures, where the adsorbent undergoes substantial changes in loading for small changes in partial pressure.

Equation 2- 97 can be readily manipulated to yield the following equation for the characteristics.

$$\frac{dz}{dt} = \frac{u}{\varepsilon_t\left[1+\frac{\rho_b RT}{\varepsilon_t}\frac{dn_w}{dP_w}\right]} \qquad (2\text{-}99)$$

This equation can be used to determine the velocity of the water front during adsorption and desorption steps, for either constant or pressure varying steps. However, this equation alone does not enable determination of the position of the water loaded zone at CSS. At CSS, the water loaded zone penetrates to some final position into the bed, and shifts periodically between adsorption and desorption. We show this schematically in Figure 2-30.

**Figure 2-30**

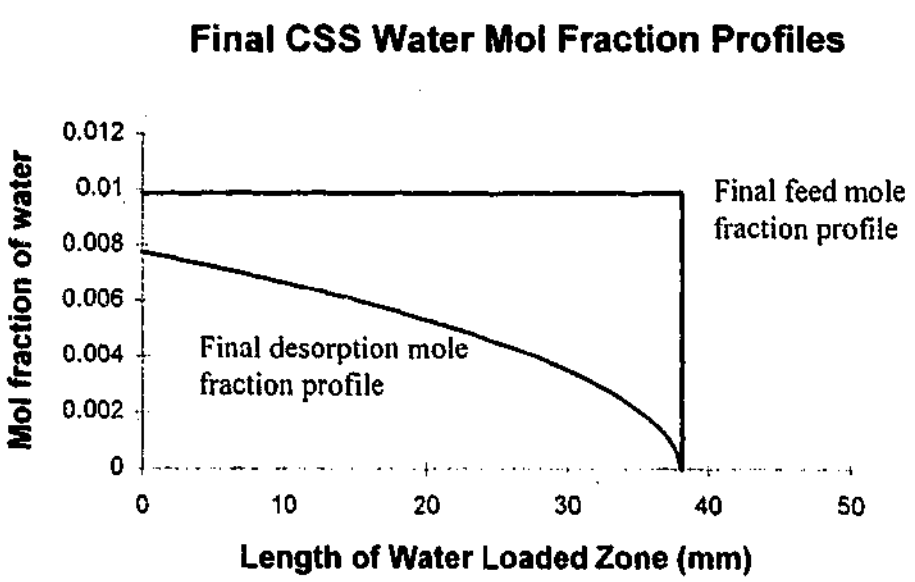


The adsorption front propagates as a shock wave, due to the highly favourable shape of the water isotherm, whereas the desorption front propagates as a simple or dispersive wave. CSS occurs when the quantity of water entering the bed during the feed repressurisation and feed steps, equals the water removed during desorption. This condition is described by equation 2 –100.

$$\int_0^{z_w} (n_{w,ad} - n_{w,de}) \frac{\rho_b \pi D^2}{4} dz = \int_0^{\tau_f} \frac{V_f P_w}{RT} dt \qquad (2\text{-}100)$$

where $V_f$ is the instantaneous volumetric flowrate of feed gas ($m^3$/sec)

$\tau_f$ is the total time of feed steps (feed and feed repressurisation) (sec)

$z_w$ is the length of the water loaded zone (m)

$n_{w,ad}$ is the water loading at the end of the adsorption step (mol/kg)

$n_{w,de}$ is the water loading at the end of the desorption step (mol/kg)

$P_w$ is the instantaneous partial pressure of water (bar)

where the left hand side of the equation is the change in water loading on the sieve between adsorption and desorption (ignoring gas phase accumulation), and the right hand side is the total moles of water entering the bed during the adsorption steps, which is known experimentally.

The solution technique involves calculating the total water fed per cycle per bed, given the experimentally determined flowrate and the relative humidity of the feed gas. This is the right hand side of equation 2-100. The unknown quantity is $z_w$ on the left hand side of equation 2-100. A value of $z_w$ is assumed and the water loading at the end of adsorption ($n_{w,ad}$) is calculated, assuming the water front is propagated as a shock front during adsorption. The final pressure and feed mole fraction of water are known. In order to determine the water loading at the end of desorption steps ($n_{w,de}$), it is necessary to solve equation 2-99 to determine the shape of the simple desorption wave, and ultimately the water loading as a function of z at the end of the desorption step. This requires experimental data to determine the pressure as a function of time, and the average gas velocity during the blowdown and purge steps. The approach detailed here is similar to previous work by LeVan (1995). However, in that work a constant pressure purge was assumed, and a more typical trace separation, such as air drying, was investigated. In such cases, feed and purge steps are long, and are interspersed by rapid pressurisation and depressurisation steps. However in the case of oxygen VSA, the process conditions are very different. The feed and blowdown steps are long and the purge step is short, and hence changes in pressure must be accounted for. The water loaded at the entrance of the adsorption bed undergoes an 'internal purge' with dry enriched nitrogen, during the blowdown and purge steps in the oxygen VSA cycle. Purge

conditions for the removal of water (trace component) are imposed by the process conditions for bulk separation of oxygen and nitrogen. This technique enables determination of the minimum prelayer thickness, and also enables characterisation of different oxygen VSA cycles, with respect to their purge to feed ratios over the prelayer. Equally importantly, this model enables estimation of the velocity of the water composition wave as a function of feed humidity. For example, the position of the water loaded zone before or after a period of humid weather could be estimated.

An alternative solution strategy is to solve equation 2-100 numerically over the water loaded zone for the evacuation step. The numerical technique involves estimating $z_W$ and calculating the moles of water desorbed from the water loaded zone over the desorption steps. When this calculated value equals the moles of water fed into the bed, the correct length of the water loaded zone has been found. This numerical approach used MINSA, but was simplified by using experimental pressure and velocity data, and hence only one equation, the water component balance (Equation 2-97) needed to be solved. Unlike the analytical solution, the numerical solution incorporates gas voidage into the calculation of the quantity of desorbed water.

One possible complication is that it is necessary to determine the initial conditions of the bed, at the end of the countercurrent desorption step. The pressure and mole fraction profile at the end of the feed step is known, but in some cycles additional cocurrent depressurisation steps occur prior to the countercurrent desorption. However for the partial pressure window investigated for these experiments, depressurisation occurs in the region of the isotherm, where $dn_w/dP_w$ is approximately zero. Under these conditions, it is assumed that the cocurrent depressurisation steps do not result in any change in the water mole fraction. In Chapter Four, the predictive capacity of this strategy for determining the penetration of the water loaded zone is assessed.

## 2.9 Alternative Modelling Approaches

Different models and approaches have been deployed to highlight different aspects of the 'thermal problem'. With this in mind it is useful to make brief mention of some alternate modelling approaches that were also considered, but not utilised. These approaches are mentioned here as a reference point for future work.

### 2.9.1 Method of Characteristics

The method of characteristics has found considerable scope for application in PSA, solving the governing hyperbolic conservation equations analytically. Isothermal solutions for bulk separations, such as oxygen VSA, have been developed by a number of researchers (Fernandez and Kenney 1983; Knaebel and Hill, 1985; Bossy and Tondeur, 1992; Chiang, 1996; Matz and Knaebel, 1988; Kayser and Knaebel, 1996; Subramanian and Ritter, 1998). Non-isothermal solutions for trace separations have been the focus of work by Davis and LeVan (1987). This suggests that the same techniques could be applied to non-isothermal bulk separations. However this proves difficult for a number of reasons.

Firstly, the bulk separation isothermal techniques were all based on a closed cycle. This was the case, even with the studies on incomplete purge (Matz and Knaebel, 1988). If the non-isothermal case is going to incorporate the slow thermal convective wave, a closed solution is not possible. Secondly, the technique proposed by Davis and LeVan (1987) for an isobaric, adiabatic, trace separation proved too difficult when applied to a non-isobaric, adiabatic, bulk separation. The reduction of the governing constitutive equations to three coupled hyperbolic equations is possible. However, further simplification to determine the characteristics did not prove possible.

The extension of Knaebel's work to consider the non-isothermal case remains beyond the scope of this thesis, but this task is the next obvious step in the further development of analytical techniques for PSA/VSA modelling. One hybrid approach is to combine Knaebel's isothermal work with the multiple scale analysis approach. Following Knaebel's work it is possible to derive loading, velocity and pressure data as a function of time over the cycle. This data can be substituted into the energy balance (without convection) to yield the adsorptive temperature swing. The long-term temperature profile can then be estimated.

### 2.9.2 Periodic Flow Reversal Reactors

One analogous unit operation to oxygen VSA is the periodic flow reversal reactor. A periodic flow reversal reactor (PFRR), as the name suggests, undergoes periodic changes in flow path of the reactants. This reactor scheme is applied for moderate exothermic reactions, where the hot effluent is used to heat up the cold feed to the required ignition temperature of the reaction. The switching of the feed ends periodically, enables a CSS profile where the ignition temperature can be achieved without external heat exchangers. Much of the work in this field has been pioneered by Matros (1989).

The PFRR scheme shares many aspects in common with oxygen VSA. Bidirectional flow and enthalpy fluxes resulting in a CSS temperature profile are features exhibited by both systems. Both also share the centrality of the concept of the regenerative heat exchanger as a storage device for heat, and the slow movement of the convective wave and gradual evolution of CSS. However there are many significant differences that limit the utility of the analogy. Firstly, the PFRR is symmetric with respect to all fluxes - mass and energy. Secondly, the PFRR is subject to constant mass flows and there is no accumulation of mass in the reactor, and no composition wave moving through the bed. This makes the modelling of the PFRR somewhat simpler.

One area of fruitful PFRR research has been investigation of multiple CSS. This topic has also attracted some attention in the adsorption literature (Kikkinides, E et.al., 1995). It is possible that the PFRR literature will provide a useful starting point for further adsorption research into the chaotic and bifurcation behaviour of some adsorptive separation systems.

## 2.1 Conclusions

This chapter has provided a far-reaching and eclectic approach to understanding both the dynamic and CSS nature of thermal profiles in oxygen VSA. Rather than this being a 'scatter gun' approach to modelling, it is felt that each approach developed provides a different focus on the problem, and each has different limitations. The initial qualitative explanation assists in demystifying the 'cold spot' phenomenon and draws attention to the heat storage effect of the prelayer. Mapping the convective enthalpy fluxes through the adsorption bed extends this insight. This explains the evolution and convergence to CSS. However, unlike a simple mass and energy balance around the adsorption bed, these approaches do not identify the key process parameters that shape the CSS temperature profile.

The simple energy balance results in overall equations for the temperature profile in oxygen VSA with an inert prelayer. This is useful, but limited. The effects of many important operating conditions, such as purge and pressure equalisation, cannot be explained with the simple energy balance. For such parameters, the importance of full numerical simulation cannot be underestimated. Numerical simulation, based on the model developed at the beginning of this chapter, remains the cornerstone for detailed analysis of oxygen VSA, and PSA in general. The validity of this model is assessed in Chapter Four against experimental data. One dimension of numerical modelling requiring further attention is determination of the wall heat transfer coefficient.

Another limitation of the simple energy balance approach is that the dynamic evolution to CSS is not captured. Instead, periodicity is an imposed condition to enable the derivation of the governing equations. An alternative approach is to develop a cell model, and derive coupled ODEs to determine the dynamic behaviour of a simplified oxygen VSA unit. These coupled ODEs can be solved analytically for a limited number of cells.

This chapter has also developed a number of perturbation approaches to modelling oxygen VSA based on some experimental insights. There is a sound physical basis for advancing this approach, and it provides useful insights into the evolution of CSS temperature profiles. MSA also presents a possible technique for the acceleration of CSS. A number of zeroth order approaches (separation of variables, K-B and MSA) result in the same solution. These have a number of limitations. Under certain process conditions, the effect of convection cannot be treated only as a perturbation effect. For example, if there is no adsorptive

temperature swing in the prelayer, or there is a very sharp temperature gradient, the effects of convective heat transfer cannot be considered only as a long time scale phenomenon. For other process conditions, such as those described in Figure 2-24 with an adsorbing prelayer, decoupling the time scales based on a perturbation variable is relatively successful.

Under circumstances where a zeroth order cannot be applied, there is a need for first order solutions based on MSA. Furthermore, the ultimate aim is the incorporation of perturbation of the mass balance, in addition to the energy balance. Some initial steps were taken in developing a full (mass and energy) MSA approach, and the challenge for future mathematical researchers is to further develop this work.

A technique for predicting the penetration of water into an oxygen VSA adsorption bed has also been proposed. This represents a useful technique for industrial gas companies, as predicting water penetration remains an important issue for two layered beds, where the prelayer protects the main layer from trace components, such as water and carbon dioxide.

Finally, a number of possible techniques or analogies have been highlighted. Analytic techniques using the method of characteristics have made an important contribution in the field of adsorption research. The next logical step for this work is a non-isothermal bulk separation. This is a challenge for future work. One simpler approach would be to combine an isothermal analytical solution following Knaebel and Hill (1985) with a perturbation approach. The analytically derived mass fluxes and loading profiles are used to estimate the final CSS temperature profiles.

Ultimately, the worth of this ensemble of approaches is measured by whether they assist in predicting and explaining oxygen VSA thermal profiles and performance. This task is further taken up in Chapter Four where experimental results are presented.

# Chapter Three

# Experimental Apparatus and Procedure - A Laboratory Scale Oxygen VSA Unit

One of the significant hurdles to understanding the 'cold spot' in oxygen VSA has been the inability of laboratory scale units to capture the magnitude of the temperature depression, due to heat exchange with the environment. This has made scale up difficult. This chapter details the design, construction and operation of a laboratory scale oxygen VSA unit.

## 3.1 Towards an Adiabatic Laboratory Column?

One aspect of this project is to endeavour to construct 'adiabatic' columns, to enable more reliable scale up of laboratory oxygen VSA unit results to industrial scale plants, and to enable investigation of thermal profiles in a laboratory unit. This has long been a goal of adsorption researchers, and the literature is scattered with proposed 'adiabatic' laboratory scale beds. In addition to thermal characteristics, in order to mimic industrial adsorbers, attention must also be paid to non-thermal scale up issues. The adsorption beds must also be mechanically robust and suitable for oxygen VSA process conditions. Furthermore the column diameter should not exceed 100 mm, in order to maintain suitability for laboratory investigation. If the diameter is much beyond 100 mm, the flowrates and valve sizes take the plant into the realm of pilot plant scale. This adds considerably to the cost of the unit with respect to both capital and operating costs.

This combination of required properties is not easy, and several design compromises are required. The following sections detail the rationale and final design of 'adiabatic' laboratory adsorption beds. In addition to this 'adiabatic' column, two other adsorption columns were also constructed. A PVC column was constructed as a more robust, but less adiabatic column. A typical metal column was also constructed to contrast with the 'adiabatic' column, and the PVC column.

### 3.1.1 Thermal Scale Up Issues

In efforts to develop an 'adiabatic' laboratory column it is important to analyse the different thermal conditions that generally arise in small and large adsorption columns. There are three principal thermal differences between metal laboratory scale columns and industrial scale columns. From Section 2.1.1 it is possible to summarise the following thermal differences.

**Heat loss from the bed** - Industrial scale columns have a high volume to surface area ratio, and as a result thermal behaviour is close to adiabatic. In contrast, in a small laboratory scale column with metal walls, there is more heat exchange with the environment. From the energy balance (Equation 2.21), in order to achieve similarity between the laboratory column and the industrial column, the following relationship must hold.

$$\left(\frac{h_{wo}}{D}\right)_{lab} = \left(\frac{h_{wo}}{D}\right)_{industrial} \qquad (3\text{-}1)$$

Typically the diameter of the industrial VSA is 2m, and hence the overall wall heat transfer coefficient of the laboratory scale unit must be approximately twenty times smaller than for the industrial scale unit.

**Axial Conduction along the wall** - In a metal laboratory scale column, the wall has significant thickness and a high conductivity, and any axial temperature profile in the bed will be dissipated along the bed, producing a less pronounced temperature depression. By comparison, the wall in an industrial column has a very small cross-sectional area, compared to the adsorption bed for axial heat conduction.

**Thermal capacitance of the wall** – As in the case of axial conduction, the thermal capacitance of the wall can also influence the temperature profile of the bed, by acting as a heat sink or source. With the cyclic nature of the PSA/VSA, the thermal capacitance of the wall can influence the ultimate temperate profiles that are established.

Based on these differences in the thermal behaviour of a small laboratory column and an industrial adsorption column, the challenge here is to build an innovative laboratory column that behaves thermally more like an industrial bed. It is also important to determine the

thermal characteristics of such a laboratory column. This is addressed in Section 3.1.7 and in the experiments.

### 3.1.2 Non-thermal Scale Up Issues

In addition to thermal differences, there are other potentially significant differences between laboratory and industrial VSA units that need to be considered. These differences are noted here to ensure that the problems of scale up encompass non-thermal issues as well.

As is well documented in the packed bed literature, the local packing of pellets immediately adjacent to the wall can differ in structure to the bulk packing within the bed, causing different flow patterns within the bed. In cases where the ratio bed/particle is small, these wall effects can be significant. In the case of the proposed laboratory scale column, the ratio is (100/4) or 25, and the industrial column ratio is 500. The ratio for the laboratory column is still significant, and this packing wall effect can probably be neglected.

Rota and Wankat use the term 'extra column effects' to describe the range of factors that require consideration in the scale up of VSA (Rota and Wankat, 1990). These effects include dead volume outside the bed (pipes, valves etc.), valve dynamics, and the nature of the gas distribution system. The voidage at the end of the beds is particularly important as it can influence oxygen recovery and other key performance parameters. Ideally the voidage at the end of beds should be kept small. The valve dynamics is not a critical issue for this study, as the step times are generally long, and the valve actuation time can be neglected. Good gas distribution is more easily achieved in a laboratory scale column than an industrial column, but it is unlikely there is any significant difference here.

Another possible area of difference between the laboratory and industrial columns, is the extent of heat loss from the pipework, since the diameter of the pipework is very different. Some consideration might be given to insulating the pipework in the laboratory scale column, to minimise the heat loss in this regard.

The pressure sources can also be different between the laboratory and industrial VSA units. The Rootes blowers used in the industrial unit have particular pressure-flow characteristics. These are invariably different from a house air supply and a control valve. This could lead to a difference in the pressure profiles between the two different scale units.

Not all of these extra column effects are accounted for in the design of the VSA unit because the focus of this study is on thermal profiles. However, if the aim was to develop a laboratory tool for very accurate (±0.5% performance) scaling up to industrial columns, it would be necessary to account for all of these 'extra column effects'.

### 3.1.3 Design Options

Based on the conclusions of Section 3.1.1, the proposed laboratory scale bed should have a combination of the following features - thin wall, very low radial and axial thermal conductivity and very low thermal capacitance. There is an obvious difficulty in achieving all these aims in the single adsorption column. A number of research laboratory units have been developed with the aim of achieving this end.

Carter (1968) developed an adiabatic column for adsorption studies. This column was composed of a thin walled polyethylene tube surrounded by polystyrene beads, all inside a metal case. Very similar designs have been utilised by Kaguei, Yu and Wakao (1985), Marcussen and Vinding (1982), Friday and Levan (1985) and LaCava et. al., (1988). Kaguei et.al.(1985) designed a very small adsorption column with internal walls produced of 3 cm polystyrene. This column had an overall heat transfer coefficient of 2.7 $W/m^2$ K. Marcussen and Vinding's design was based on a thin polyethylene wall surrounded by polystyrene insulation and LeVan and Friday used silica aerogel for insulation. They all suggest a small-scale unit with internal insulation to simulate the behaviour of an industrial scale adiabatic unit. The adsorption columns constructed for this project build on the efforts of these significant adsorption researchers.

An alternative strategy was pursued by Lou et.al. (1999) who developed a glass column surrounded by an evacuated jacket. The benefit of this design strategy is that the wall is more robust than the thin plastic walls described above, and this is required for the higher operating pressure in PSA air drying. One disadvantage is that it is not possible to use radial sample ports and thermocouples. To partially overcome this problem, Lou et.al.(1999b) used axial thermocouples which were pushed through the top of the bed. A number of alternate designs are also described in Appendix 2.

### 3.1.4 Design, Construction and Testing of the 'Adiabatic' Polyurethane Beds

The most 'adiabatic' column was designed and constructed as follows:

The column is 100 mm internal diameter and 2.2 m long. The wall of the column is 0.125 mm Mylar film. This inner column which contains the adsorbent is located within a Class 6 300 mm PVC pipe. The annulus between the pipe and column is filled with a rigid polyurethane foam. It is significant to note that the rigid closed cell polyurethane foam used has both lower thermal conductivity (17 mW/m K) and lower thermal capacitance (density 40 kg/m3) than both the polystyrene and the silica aerogel which have been used previously.

The column was constructed by wrapping Melinex (Mylar) 0.125 mm film around 100 mm OD aluminium tube. The Mylar was sealed onto itself with plastic glue (Loctite 401). The aluminium tube with wrapped Mylar was placed inside the PVC pipe. PFA sample tubes entered the bed radially through the PVC pipe, and were butted and glued against the Melinex film.

A 100 mm hole was machined in a PVC blank. This was bolted to the flange on the outer PVC tube. The aluminium tube (with Mylar) was forced through the 100 mm PVC hole. This provided a closed annulus to pour the polyurethane foam. When the rigid foam was set, the aluminium tube was removed. This required considerable force, but the polyurethane foam adhered strongly to the Mylar film holding it in place when the aluminium tube was removed.

**Figure 3-1 - Laboratory Scale Adsorption Column**

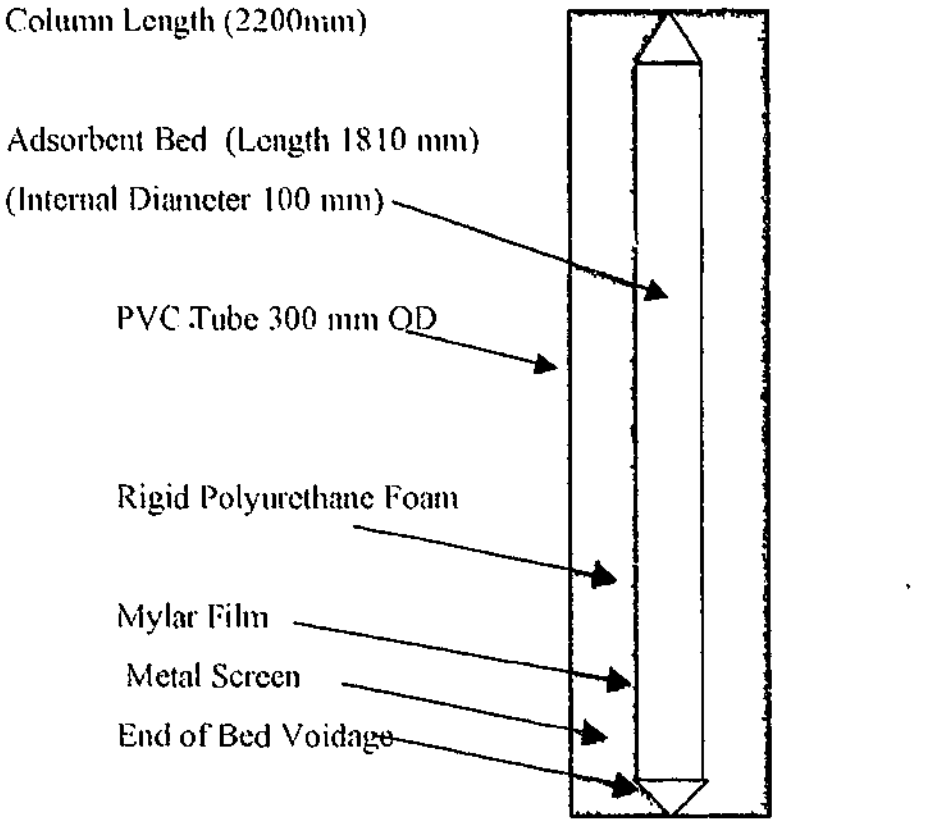


**Figure 3-2 – Cross Sectional Photo of Adiabatic Adsorption Column**

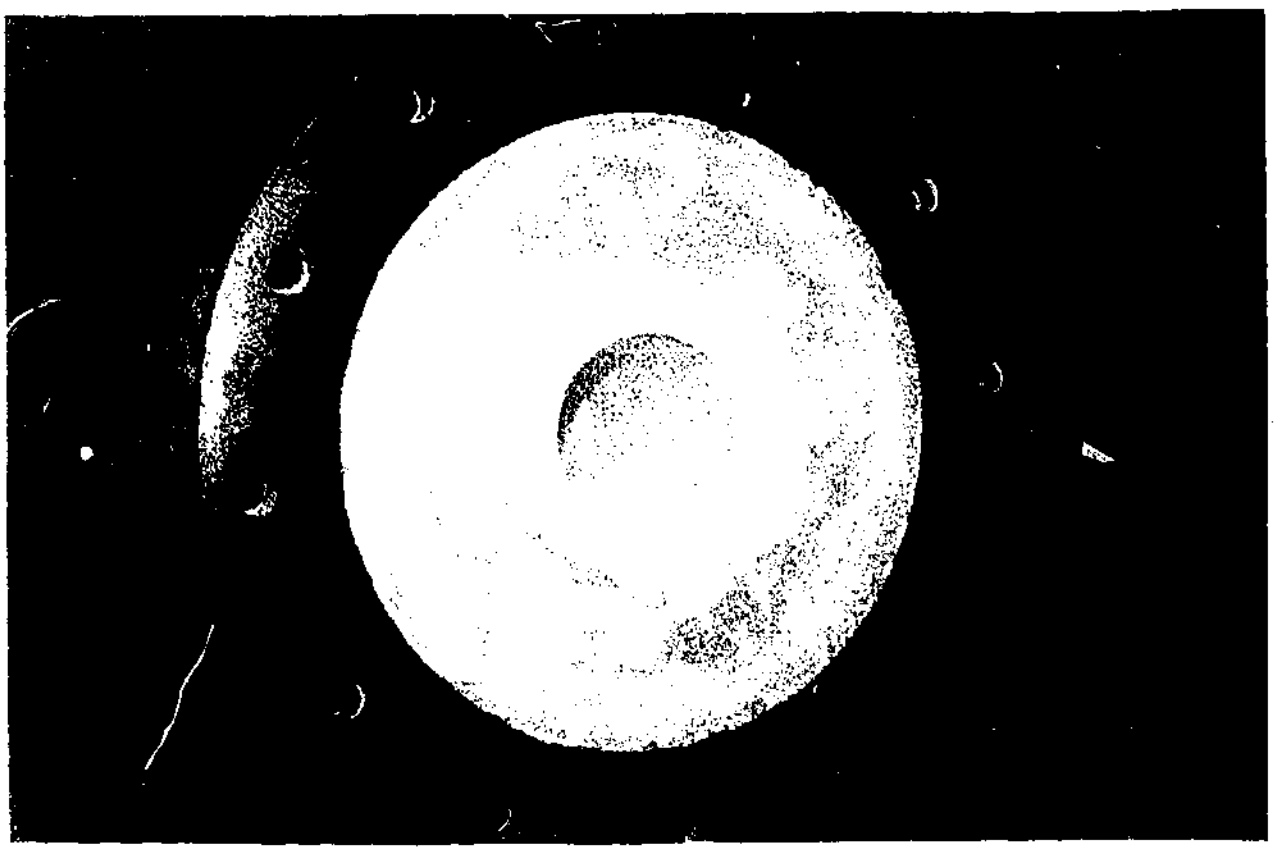

In addition to the thermal characterisation of the adsorption beds, a series of non-thermal (mechanical and chemical properties) tests were performed to determine the suitability of the design for oxygen VSA service.

The typical pressure range for the oxygen VSA operation is between 150 kPa abs. and 25 kPa abs. The column was pressure tested between 185 kPa abs. and 18 kPa abs. by cycling the bed pressure between these pressures for several hours. The column did not appear to suffer any changes caused by the positive and negative pressures. However the impact of repeated cycling over thousands of cycles could not be determined.

The column is also required to have appropriate chemical properties, to be suited to indirect contact with high concentrations of oxygen. This issue is dealt with at length in Appendix 6, which examines health and safety issues associated with the research project. There were some safety concerns associated with polyurethane and oxygen enriched air, and the possibility of a fire producing HCN.

The polyurethane columns represent a significant effort at designing an 'adiabatic' column, but in the pursuit of adiabaticity several trade-offs were made. Firstly, the mechanical robustness of the polyurethane columns is uncertain. Secondly, only a very limited number of radial thermocouples can be used for measuring the temperature. Thirdly, no additional thermocouple or sampling ports can be added to the polyurethane columns. Fourthly, there is a very remote safety concern associated with the polyurethane in the presence of oxygen. However, the oxygen is at near ambient temperature and pressure.

### 3.1.5 Design and Construction of Less 'Adiabatic' PVC Beds

Recognising the potential limitations with the polyurethane columns, some alternative columns were constructed that still sought to maintain the design principles of the 'adiabatic' columns, but were more mechanically robust.

These adsorption beds were constructed of thin walled (3mm) PVC tube (103.1 mm internal diameter) with PVC flanges and external Rockwell insulation. (Refer to Appendix 4 for diagram). PVC has a low thermal conductivity to reduce axial conduction of heat along the wall, and a low thermal capacitance to prevent storage and release of heat during a cycle. The external insulation minimises heat exchange with the environment. While this design is not as 'adiabatic' as the polyurethane columns, the rigid PVC walls have significant benefits for

experimentation. Firstly, compression fittings can be used for thermocouple and sample points, and there is no limit to the number of radial thermocouples. This proved particularly useful for sampling adsorbent from the column to determine the penetration of water. A sample point could be drilled, and sample removed, and then a PVC cover and solvent cement used to cover and reseal the sample point. This sampling procedure would have been impossible with the polyurethane columns. Secondly, the PVC columns are more robust and can be subjected to faster cycles and wider pressure windows without the possibility of any structural alteration. Thirdly, the PVC columns do not suffer the same oxygen compatibility issues that confront the polyurethane design. In short, the PVC columns are a more robust design, even if not the most adiabatic one!

As a consequence of these benefits, the PVC columns were used for much of the experimental work. Some experimental runs were conducted with both the polyurethane and PVC columns to compare the 'adiabaticity' of the different columns.

### 3.1.6 Construction of Metal Adsorption Beds

In addition to the polyurethane and PVC columns, some experiments were also conducted with uninsulated mild steel columns. These columns were designed to provide a point of comparison with the more 'adiabatic' columns.

The metal walled columns were constructed from mild steel pipe with an internal diameter of 102.3 mm and a wall thickness of 4 mm. The total column height was 2.2 m with a working bed height of 1.8-1.9 m.

## 3.2 Comparison of the Thermal Characteristics of the Different Adsorption Columns

The polyurethane columns were characterised using a method described by Kaguei, Yu and Wakao (1985), to determine the overall heat transfer coefficient of an adsorption bed using a steady heat input in an inert bed. By passing a constant gas flow at constant temperature through an inert bed, and measuring the heat loss along the bed, it is possible to determine the overall heat transfer. An experiment described in Appendix 3 was undertaken to determine the overall heat transfer coefficient for a polyurethane column. This experiment was undertaken with a prototype column with an outside diameter of 250 mm, and a 100 mm annulus. The overall heat transfer coefficient for the experiment conducted was 0.22 $W/m^2$ K, which clearly demonstrates that the largest resistance to heat transfer exists in the polyurethane insulation. The solution corresponded to an effective thermal conductivity of the polyurethane of 11 mW/m K. This is lower than the reported value of 17 mW/m K, but is subject to errors in the estimation of the physical parameters and variations in the polyurethane pour.

### 3.2.1 Comparison of Columns – Adiabatic, Polyurethane, PVC and Metal

Utilising Equation 2-9, a simple comparison of overall heat transfer coefficients can also be made for comparing the three different types of adsorption columns. The approximate values are polyurethane (0.3), PVC (1.1) and metal (3.9). These results are not surprising. However, this analysis ignores some important properties - axial conduction and the thermal capacitance of the wall. In order to incorporate these effects more fully, a cycle simulation can be undertaken using ADSIM, and the more detailed wall model is described in Section 2.1.1. The current version of MINSA does not contain a wall model of the same complexity as ADSIM.

For a typical oxygen VSA cycle it is possible to compare these cases (polyurethane, PVC and metal) with the adiabatic case, where there is no heat loss to the wall. Figure 3-3 describes the axial CSS temperature profiles for the three cases and the adiabatic run at the end of the purge step.

**Figure 3-3**

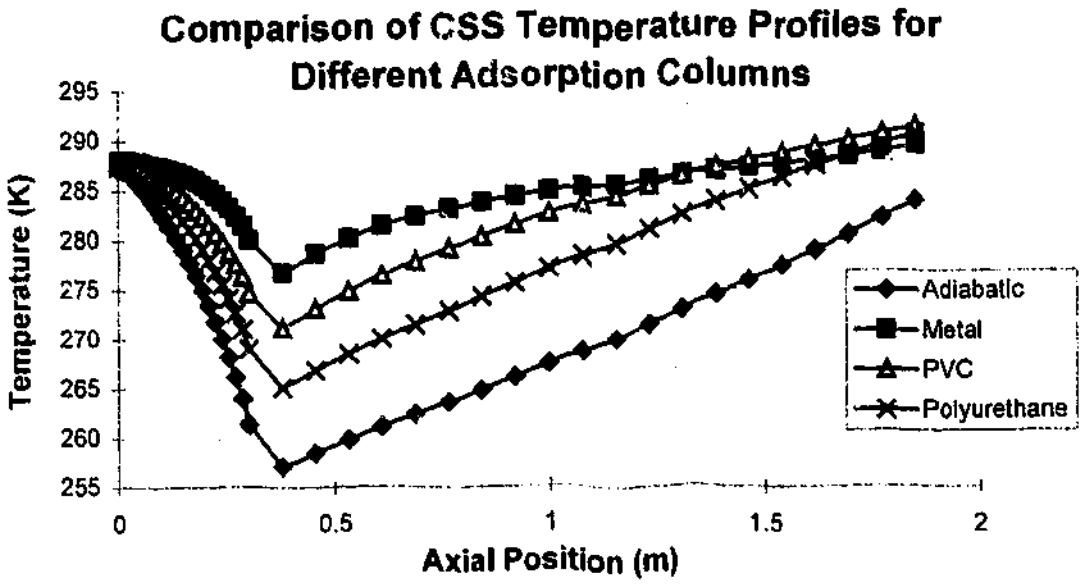


The wall heat transfer ($h_{wi}$) coefficient used for this simulation was 50 W/m$^2$ K. As expected, the extent of the 'cold spot' is most pronounced in the adiabatic case, followed by the polyurethane columns, the PVC columns, and the metal walled columns. The heat exchange with the environment dissipates the axial CSS temperature profile.

These cases can be understood largely in terms of overall heat exchange with the environment. However, other process conditions require a separate energy balance for the wall, as developed in ADSIM.

### 3.2.2 Perfect External Insulation – The Impact of the Wall with Heat Loss to the Environment

It is instructive to compare the previous example with the case of the metal adsorption bed surrounded by a perfect insulator. In this case, the metal wall acts as a heat sink and source during the cycle, and dampens the temperature swing. Three different cases can be considered. In all cases there is no heat exchange with the environment.

1. Metal wall surrounded by a perfect insulator. The heat transfer co-efficient between the wall and the adsorbent is 50 W/m$^2$K.
2. Quasi-bed wall where the wall is incorporated into the bed (Equation 2-10). This represents the case of an infinite heat transfer coefficient between the wall and the adsorbent. In this case the wall is not considered explicitly, and instead the thermal mass of the wall is incorporated into the adsorbent. Again there is no heat exchange with the environment.

3. No wall. This represents the adiabatic case where there is no heat exchange to the wall from the adsorption bed.

These three cases were simulated with ADSIM, and the results are displayed in Figure 3-4.

**Figure 3-4**

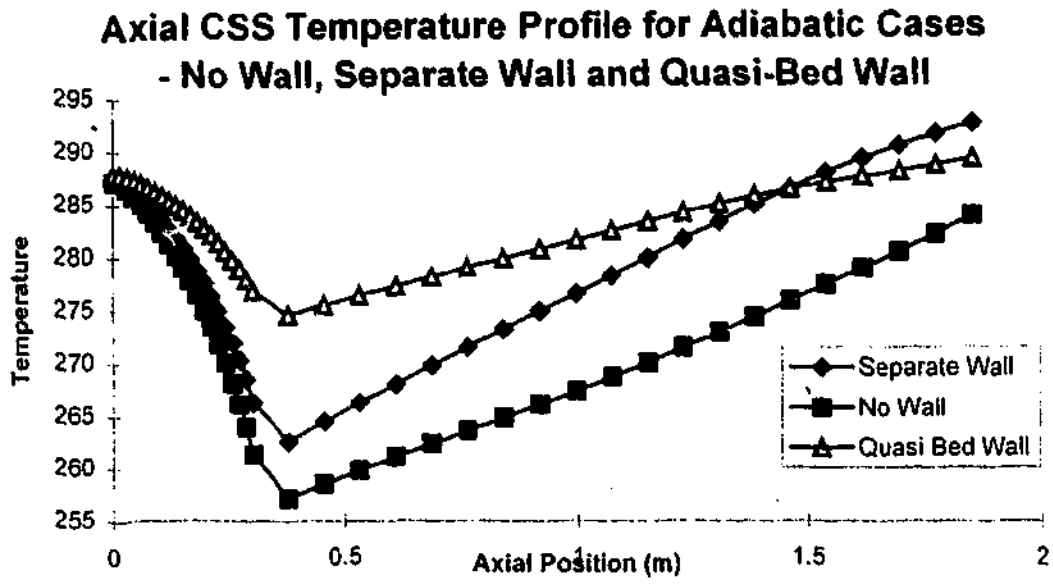


Figure 3-4 demonstrates the limitation of the quasi-bed wall approach where the wall is not treated explicitly. The CSS axial temperature profile is dissipated due to the fact that the cyclic temperature swing between adsorption and desorption is dramatically reduced. The average cyclic temperature swing through the main layer of adsorbent was 4 °C(quasi-bed wall), 7.3 °C(separate wall), and 7.7 °C (no wall). The effect of the quasi-bed wall model also exaggerates the separation performance, compared to an explicit treatment of the wall. The CSS product purity for the quasi-bed wall model was 92% compared with 88% in the other cases.

Figure 3-4 also demonstrates that even if there is no heat loss to the environment, the wall can act as a sink and source for heat, and alter the axial CSS temperature profile. This highlights the limitations of insulating a metal laboratory scale adsorption column, and justifies the effort to eliminate the thermal capacitance of the wall, through the design of a novel laboratory scale adsorption column.

## 3.3 Design, Construction, Operation of the VSA Unit

Beyond the attempts to develop adiabatic adsorption beds, at the core of this experimental investigation is a laboratory scale oxygen VSA unit. The main features of this VSA unit are detailed below and further details are provided in the appendices.

### 3.3.1 Overview of the VSA Unit

**Figure 3-5 - Schematic Diagram of Laboratory Oxygen VSA Unit**

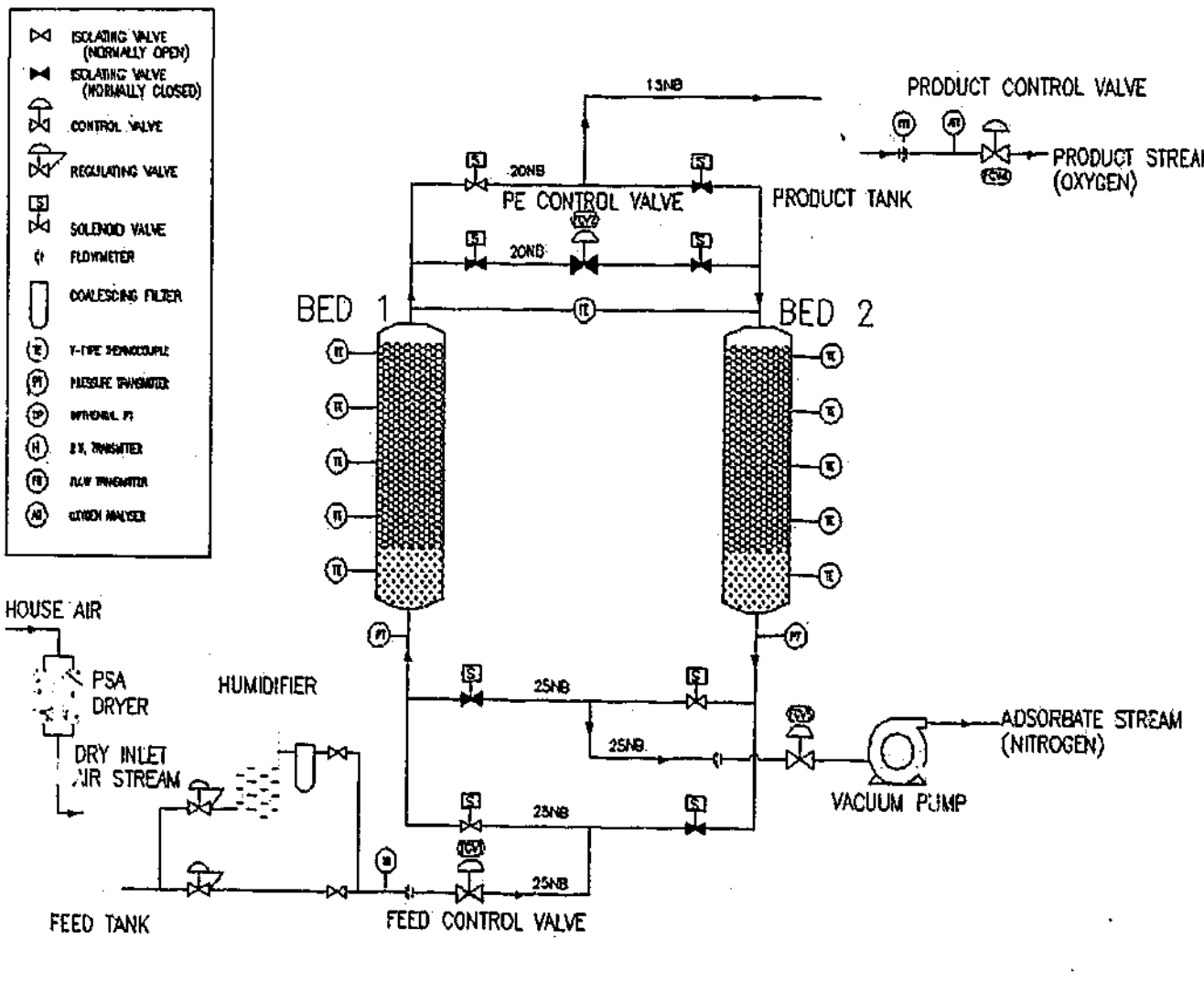

**Instrumentation**

Along the length of the adsorption beds are junction-exposed type T thermocouples that enter the bed radially for temperature monitoring. Thermocouples are also located throughout the pipework to monitor the process gas streams. The location of pressure transducers is also shown on the equipment schematic. A paramagnetic oxygen analyser is located after the 60 litre product surge tank, to monitor the product oxygen concentration. Flowmeters are also located on the feed, vacuum and product lines. The product line is a small differential pressure type flowmeter, while the feed and vacuum lines are measured with annubar flowmeters. The product line flow was verified with a Dry Test Meter (DTM). For the one bed cycle (without cocurrent depressurisation), an additional flowmeter was required to measure the blowdown step to atmospheric pressure.

**Valves**

The feed and vacuum valves at the bottom of the adsorption beds are pneumatically actuated one inch (GEMU) valves. All other solenoid valves are three quarter inch pneumatically actuated (GEMU) valves. The control valves (Badger Research) enable the control of the flows through all cycle steps.

**Feed Air**

The feed air is supplied at a dew point of -58 $^{o}$C. This is achieved through the use of a two bed desiccant dryer, which also removes carbon dioxide and trace hydrocarbons. The feed air is supplied after a surge tank and a regulator valve, at an approximate pressure of 1.5 bar absolute. It is important to note that the adsorbent in the dryer is NaX. Even with the slow cycles (~4 minutes) this leads to a very slight oxygen enrichment prior to the oxygen VSA unit. The inlet oxygen concentration to the VSA unit was 22%. This figure was confirmed with frequent measurements. Hence, when simulated with MINSA on a two component basis (with oxygen and argon treated as a single component), the feed gas was treated as 77% nitrogen and the balance (23%) oxygen/argon.

Some wet air experiments were conducted. In these cases the feed gas is passed through a humidifier, which increases its humidity to 35%-40% relative humidity. The humidity was monitored on-line using a Vaisala humidity meter.

**Vacuum Pump and PLC/SCADA**

A rotary vane vacuum pump is used to enable evacuation of the adsorption beds. The control and monitoring of the VSA unit is performed by PLC and SCADA software.

A more detailed description of the equipment items in provided in Appendix 4.

### 3.3.2 VSA Cycles

Three different VSA cycles were used in the experimental program.

- **Cycle 1** - Two bed six step cycle with feed repressurisation and cocurrent depressurisation without feed. The total cycle time was 55 seconds. This represents a simplified industrial cycle.

**Figure 3-6 – Cycle 1 – Two Bed (No Pressure Equalisation)**

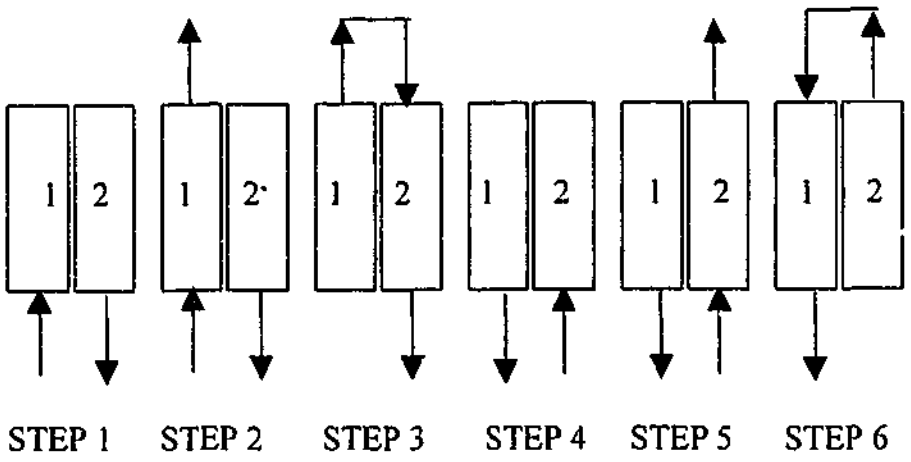


**Table 3-1 – Steps and Cycle Time for Cycle 1**

| Step | Step 1 | Step 2 | Step 3 | Step 4 | Step 5 | Step 6 |
|---|---|---|---|---|---|---|
| Bed 1 | Feed Repress.# | Feed | Provide Purge | Evacuation | Evacuation | Receive Purge |
| Bed 2 | Evacuation | Evacuation | Receive Purge | Feed Repress.# | Feed | Provide Purge |
| Step Time | 5 sec | 12.5 sec | 10 sec | 5 sec | 12.5 sec | 10 sec |

Feed Repress. # = Feed Repressurisation

The same two bed six step cycle can also be presented as a one bed model with the dashed line (---) representing the bed-to-bed connection.

**Figure 3-7 – Symmetric One Bed Representation of Two Bed Cycle**

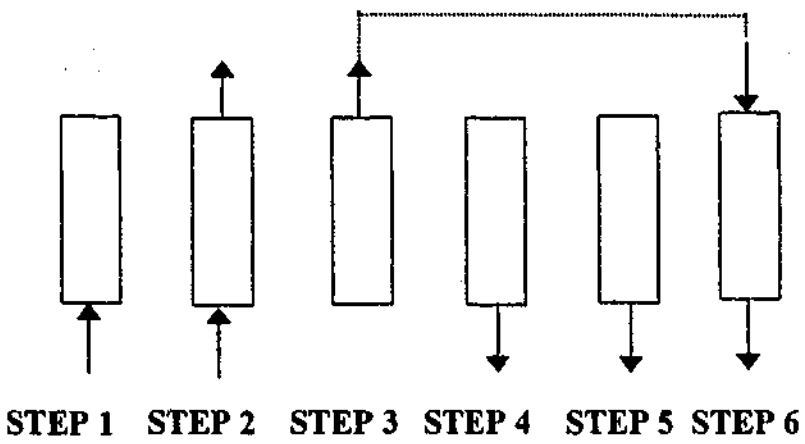

**Cycle 2** - Two bed eight step cycle. This cycle is similar to cycle 1 except a pressure equalisation step is included in order to improve recovery. The total cycle time varied between 60-70 seconds. The cycle can also be represented as a single model. The dashed lines (---) indicate the bed-to-bed connections.

**Figure 3-8 - Cycle 2 – Two Bed (with Pressure Equalisation)**

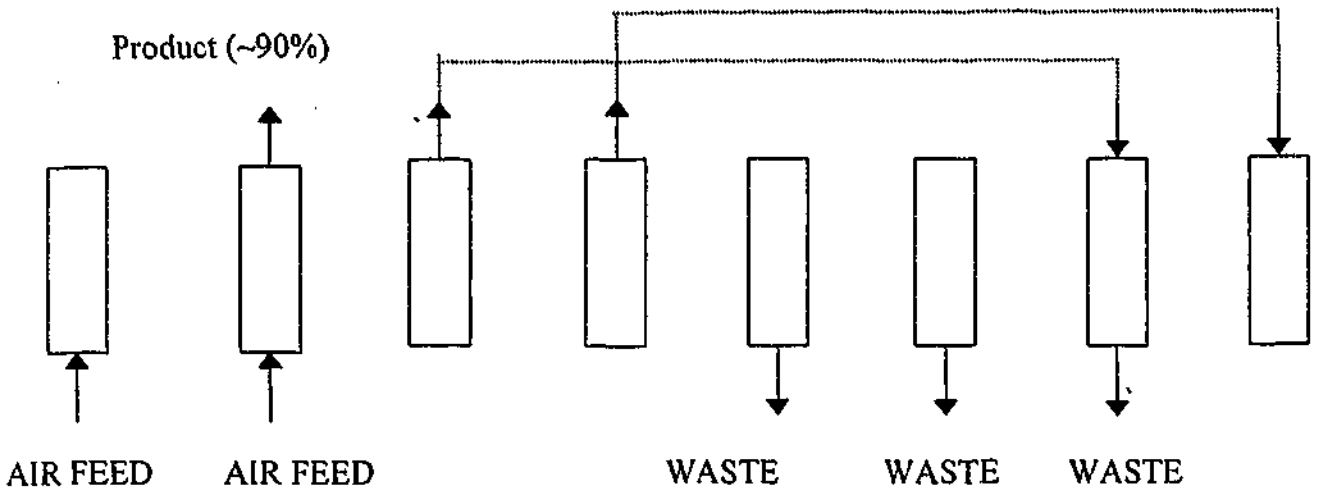


**Table 3-2 – Steps and Cycle Time for Cycle 2**

| Step 1 | Step 2 | Step 3 | Step 4 | Step 5 | Step 6 | Step 7 | Step 8 |
|---|---|---|---|---|---|---|---|
| Feed Repress.# | Feed | Provide Purge | Provide PE# | Evacuation | Evacuation | Receive Purge | Receive PE# |
| 12 sec | 10 sec | 8 or 5 sec | 5 or 3 sec | 12 sec | 10 sec | 8 or 5 sec | 5 or 3 sec |

# Feed Repress. = Feed Repressurisation, Provide PE = Provide Pressure Equalisation, Receive PE = Receive Pressure Equalisation

- **Cycle 3** - One bed five step cycle. Increasingly one bed VSA units are used for the production of low tonnage oxygen (below 10 tpdc). A limitation with this cycle is the absence of a cocurrent depressurisation step reduced recovery, although this could be achieved by cocurrent depressurisation into an additional and separate tank. The total time of this cycle was 56 seconds. This cycle also presents a process difficulty. The vacuum pump should not be operated with a suction pressure above atmospheric pressure. In the absence of cocurrent depressurisation, the bed is at feed pressure when countercurrent evacuation occurs. This necessitates countercurrent blowdown to atmosphere followed by evacuation with the vacuum pump. This requires an additional flowmeter for measuring the blowdown to atmosphere. An additional DTM flowmeter was used for this purpose. An additional difficulty with the one bed cycle is that, ideally,

they require a larger product tank to buffer the flows, and provide gas for purge. Unlike a two bed cycle, purge gas is required from an additional tank, in this case the product tank. The absence of bed-to-bed connections is also a benefit, as it reduces the complexity of the process and the extent of interactions.

These cycles are shown diagrammatically as follows:

**Figure 3-9 – Cycle 3 – One Bed Cycle**

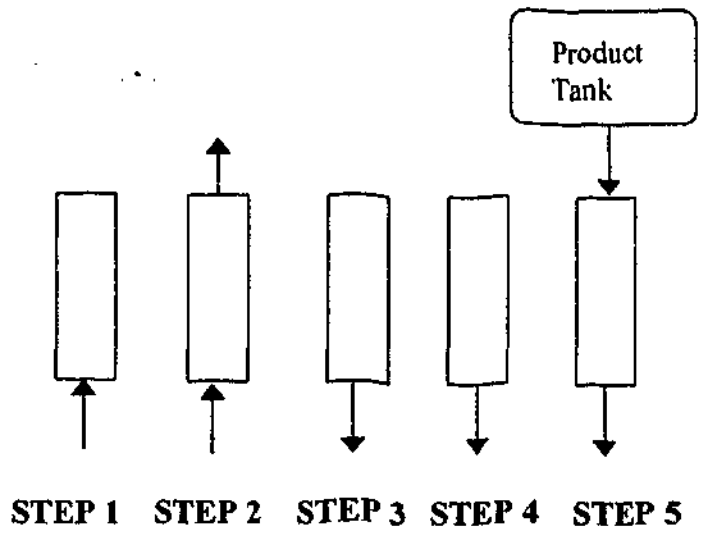


**Table 3-3 – Steps and Cycle Time for One Bed Cycle**

| Step | Step 1 | Step 2 | Step 3* | Step 4 | Step 5 |
|---|---|---|---|---|---|
| Bed 1 | Feed Repress.# | Feed | Evacuation | Evacuation | Receive Purge |
| Step Time | 10 sec | 13 sec | 2 sec | 25 sec | 6 sec |

- Step 3 is a blowdown step to atmospheric pressure prior to evacuation by the vacuum pump (Step 4).

### 3.3.3 VSA Control Scheme

As is typical of VSA operation, the basic control scheme involved valve switching based on fixed step times. While PID control was implemented, for typical operation the flow controls were manually adjusted, to achieve the desired pressure profiles, and product flows and purities. Given the absence of load disturbances, manual control was deemed sufficient for this study. An additional benefit of manual control is that it eliminated the possibility of complex loop interactions that can characterise VSA operation. A disadvantage of the absence of purity control was that comparison of different experimental runs was made difficult where the product purity varied slightly.

The absence of feed temperature control was another limitation of this study. Subsequently a feed heat has been incorporated into the VSA unit. Controlled feed temperature eliminates one important source of process fluctuation, and would assist in optimisation studies of VSA.

The PLC/SCADA system provided a range of additional supervisory functions including alarms, trips, process performance and mass balance calculations and CSS checks. Appendix 5 and 10 provide a more detailed description of these functions.

Control of oxygen VSA is a complex task. The VSA process is essentially a combination of highly coupled batch or semi-batch steps. This is not the domain of traditional chemical engineering control. Full PID control has been applied to the oxygen VSA unit at Monash University with some success (Beh, et.al., 2000). Currently research is underway in the Monash University Adsorption Research Group by Chris Beh to ascertain the benefits of neural networks as an alternative control scheme to traditional PID.

### 3.3.4 Adsorbents Used and Adsorbent Characterisation

A range of different adsorbents was used in this study. Table 3-4 details the adsorbents used in this study, and the supplier of the adsorbents.

**Table 3-4 - Adsorbents Utilised**

| Adsorbent | Supplier |
|---|---|
| (3/16") F200 Activated Alumina | Alcca |
| 13X (NaX) APG (1/16") pellets | UOP |
| PSO2HP (NaX) beads | UOP |
| VSA6 beads | UOP |
| VSA2 beads | UOP |
| LiLSX | APCI |

13X APG and PSO2HP are both essentially NaX. They differ with respect to their shape (pellets vs. beads) and the nature and amount of binder. Either can be used as a prelayer for water and carbon dioxide removal. VSA2 (CaX) is an early generation VSA adsorbent. It is characterised by a highly non-linear (favourable) isotherm with respect to nitrogen adsorption. The disadvantages of VSA2 are the extent of oxygen co-adsorption, and the deep vacuum needed to achieve the nitrogen working capacity. VSA6 contains a combination of calcium and sodium and hence the isotherm is slightly more linear. LiLSX represents the current generation of industrial adsorbents, and it has very little oxygen co-adsorption, and is quite linear with respect to nitrogen loading.

The vendor provided isotherm data for the materials. Some dual site Langmuir isotherms were provided by APCI. In other cases single site Langmuir isotherms were obtained from pure component isotherm measurements and IAS theory.

### 3.3.5 Determination of CSS

The slow evolution to CSS that characterises oxygen VSA makes determination of CSS difficult. This also arises as a problem for numerical simulation (He and Webley, 2000). However, experimental VSA has the added complication of minor fluctuations in the ambient temperature, feed gas temperature and the atmospheric pressure. All of these impinge on the process and further complicate the determination of CSS. In addition, instrumentation errors and accuracy hamper accurate determination of CSS.

The PLC program utilised a CSS check routine, and that checked the convergence of the mass balance within a specific tolerance, and the convergence of the performance parameters and temperature. The 'long time scale' temperatures proved to be the most useable measure of CSS, which is akin to closure of the energy balance. CSS was achieved if the long time scale temperature change for all thermocouples was less than 1 $^{o}$C over a two hour period. In some cases this was difficult to achieve due to fluctuations in the ambient temperature.

The principle limitation with using the mass balance and performance parameters as measures of CSS was that they would close too quickly within the required tolerance. If the tolerance was too tight, instrumental errors would prevent closure at all.

### 3.3.6 Quality Assurance & Experimental Error Analysis

In order to maintain the validity of the experimental program, a number of quality assurance procedures were developed related to the instrumentation, adsorbent performance, and the integrity of the adsorption beds and pipework. These procedures are outlined in Appendix 7. In addition some experimental runs were repeated in order to demonstrate repeatability of results.

**Table 3-5 – Primary Measurement Errors**

| Instrument Analog | Accuracy/Error |
|---|---|
| Pressure Transducers (Bourdon Sedeme) | Accuracy: ±0.2% of Full Scale; Repeatability: ±0.05% Full Scale Hysteresis: ±0.1% Full Scale; Response time < 3 mSec |
| DP Cells | Accuracy: ±0.1% Full Scale<br>Typical error for Yokogawa, Rosemount and Foxboro DP cells |
| Oxygen Analyser (1440 C Servomex) | Repeatability: ±0.1%; Linear Error ±0.1%; The paramagnetic flowmeter does not have backpressure compensation and as a result the error in the reading is directly proportional to changes in the ambient pressure. Also the ambient temperature can adjust the reading by 0.3% per 10 $^{o}$C with the operating range.<br>Global estimate: ±1% |
| Flowmeters (Annubar with DP) | Accuracy ±1% of flow coefficient; Repeatability ±0.1%<br>An additional complication with the assessment of the flowmeter errors is the dynamic response of the DP cell during the feed repressurisation step. The equipment supplier error ignores the transient response of the flow. This is compounded by the damped response of the DP cells ( ~1sec) Ultimately the flowmeter accuracy is measured by the mass balance error |
| Flowmeters (Product DP) | Accuracy ±1% of full scale |
| Flowmeters (Product DTM) | Accuracy ±0.5% reading over operating range |

| | |
|---|---|
| Flowmeters (Blowdown DTM) | Accuracy ±3% of reading. This flowmeter was only required for 1 bed cycles for blowdown to atmospheric pressure prior to evacuation by vacuum pump |
| Thermocouples | Type T thermocouples with PLC cold junction compensation<br>Accuracy: ±1 °C (maximum); Accuracy: ±0.5 °C (typical)<br>Response Time: <1 sec<br>This is not a measure of the differential error measured over a cycle. |
| Humidity Meter HMI 33 (Vaisala) | Temperature Accuracy: ±0.3 °C; Relative Humidity Accuracy: ±2% of 100 %<br>This unit cannot accurately measure the humidity of air from the desiccant dryer, but is suitable for measuring humidified air. |
| Flow Control Valves (Badger Research) | Rangeability of Control Valves (50:1%) This means the maximum controllable flow is 50 times greater than the minimum controllable flow. |
| I/P Transducers | Accuracy ±0.1% of output span (typical); ±0.25% output span (max.)<br>Hysteresis ±0.01% of output span (typical) ±0.1% output span (max.)<br>Repeatability ±0.01% of output span (typical) ±0.1% output span (max.) |

**Table 3-6 - Secondary Errors**

| Secondary Measurement | Accuracy/Error |
|---|---|
| Feed Flow and Vacuum Flow | Accuracy ±2% of reading |
| Product Flow | Accuracy ±3% of reading |
| BSF | Accuracy ±3% |
| Recovery | Accuracy ±3% |

In addition to consideration of the direct instrument, 12-bit accuracy was used for analog to digital conversion by the PLC. This system is able to provide robust, industry relevant data with mass balance closures typically to within 3% as is detailed in Appendix 9.

However, in a limited number of cases for experimental runs PuAA400NaX#and PuAANaXVSA6#, the mass balance closures were slightly worse. In these experimental runs, EMCO turbine flowmeters were used on the feed and vacuum lines. The major limitation with the turbine flowmeters was their inability to pick up the spikes in the flow that characterise VSA/PSA operation. Also the turndown of the turbine flowmeters was such that for the low flows there was a slightly non-linear response of the flowmeters. However, these experimental runs are significant terms in the large temperature depressions that were achieved with the polyurethane columns, and the temperature, pressure and product flow data is reliable.

**Other Errors**

The precise axial location of the thermocouples in the adsorption bed is a potentially significant error. The junction exposed thermocouples were located radially into the column, but no account was taken of any movement of the thermocouple junction axially. The filling of the columns with adsorbent and the movement of adsorbent due to cycle operation could deflect the thermocouples ±20 mm from the measured axial position. The settling of adsorbent can also influence the location of thermocouples.

## 3.4 Conclusion

This chapter has detailed the design, construction and thermal characterisation of three types of adsorption columns – Polyurethane, PVC, and metal. The polyurethane columns are the closest to adiabatic, but not the most mechanically robust. All three columns are used in the experimental investigation, but the PVC columns proved to be the most suitable compromise between the required mechanical and thermal properties.

The VSA unit developed in this study is essentially the same as an industrial VSA unit, except that it has more instrumentation, and no feed blower. The level of instrumentation should afford good comparison with numerical simulations on MINSA.

# Chapter Four

# Experimental Results and Discussion –

# Thermal Profiles in Oxygen VSA

To date there has been some experimental investigation of axial CSS temperature profiles in PSA separations, but very little published investigation of oxygen VSA/PSA thermal profiles. A range of experiments was conducted to assess the validity of the modelling approaches and to understand the scope of parameters that shape thermal profiles in oxygen VSA. The parameters that were investigated were operational parameters (such as pressure window, product purity and flow, extent of purge, feed temperature), column effects (whether the adsorption column is metal, PVC or polyurethane), adsorbent/prelayer effects (such as different prelayers and different types of prelayers), and wet air feed effects (where a quasi-inert prelayer is created by the strong adsorption of water).

Both the simpler models and MINSA were compared with these experiments. Assessments are made of the explanatory and predictive power of these different models developed in Chapter Two.

## 4.1 Existing Experimental Data of Axial CSS Temperature Profiles in PSA

The 'cold spot' temperature profile identified by Collins in his seminal patents in the 1970s has been often quoted in the adsorption textbooks (Ruthven, et.al. (1994), Wankat (1990), and Yang (1987)), and is presented as Figure 1.1 in Chapter One of this study. Kumar et.al. have also presented experimental evidence of the temperature depression in oxygen VSA, but for only a single process condition (Kumar, et.al., 1994).

Other experimental observations of the 'cold spot' have been prominent in the patent literature (Armond (1997), Notaro et.al.(1997), Ackley et.al. (2000), Leavitt (1992), Watson et.al. (1995)).However, neither the textbooks, the patent literature nor Kumar's paper have undertaken an experimental investigation of the wide variety of process parameters that effect the axial CSS temperature profile.

There have been experimental investigations of the axial CSS temperature profile in other PSA separations. Lou et.al. (1999) investigated the effect of pressure ratio, velocity and cycle time on the CSS temperature profiles in an adiabatic air drying system. Mahle et.al. (1996) undertook an experimental investigation of a PSA process using BPL to separate air and helium. Both these studies involved single layered adsorption beds and were detailed in Chapter Two.

Similar single layered bed PSA experiments have been undertaken by Liu et.al. (1998) and Yang and Doong (1985), but these studies did not offer explanations of the axial CSS temperature profile. Liu et.al. (1998) investigated temperature profiles in a PSA solvent vapor recovery process with a single layered adsorption bed of activated carbon (Liu et.al., 1998b; Liu and Ritter, 1998a). Their experimental study identified six process parameters (volumetric purge-to-feed, purge pressure, volumetric feed flow rate, feed concentration, cycle time, and pressurisation/blowdown step time) that shaped the CSS temperature and mole fraction profiles.

**Figure 4-1- CSS Temperature Profile for SVR**

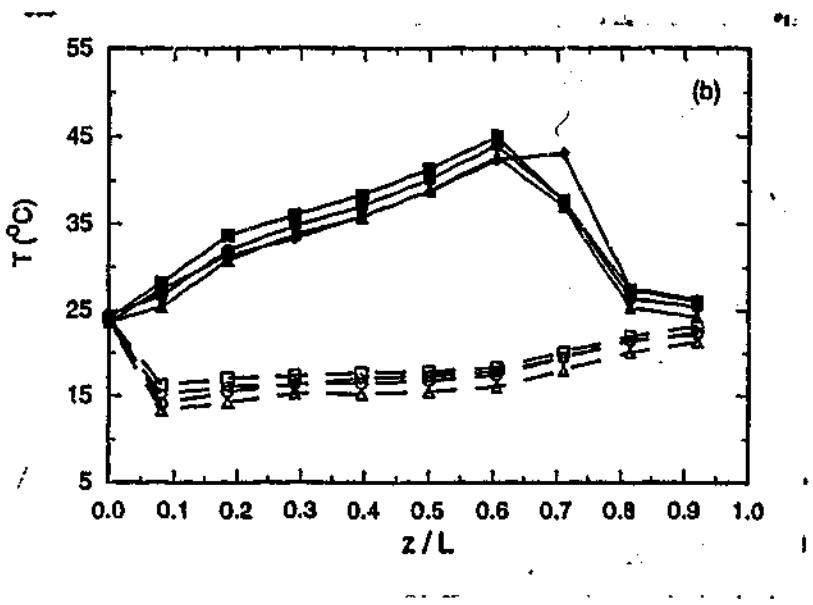


(Taken from Liu et.al., 1998b, p. 2457)

Figure 4-1 shows the characteristic temperature swing between adsorption and desorption, and the positive temperature gradient axially through the bed. The different profiles show the effect of changing pressurisation quantities and purge time on the CSS temperature profile. This also demonstrates that the desorption temperature is well below the feed gas temperature (25 °C). It is unclear whether the thermocouple at z/L=0 is exposed to the desorbed gas. However, in the PSA-SVR system, like the air drying system, there is no inert prelayer, and hence no 'cold spot'. The markedly smaller temperature swing at the end of the bed is the result of the adsorption front not breaking through the end of the bed. While, unlike oxygen VSA, this was a single layered study, the scope of the investigation ensures that some of its conclusions are relevant to oxygen VSA.

A study by Yang and Doong (1985) of the bulk separation of hydrogen and methane by PSA displayed a similar shaped temperature profile (Figure 4-2). The feed temperature was 25 °C, and the temperature of gas leaving the bed at the end of the countercurrent blowdown and purge steps was approximately –10 °C. The cyclic temperature swing is approximately 35 °C! If an inert layer was included in this system, the predicted magnitude of the 'cold spot' would be very large!

**Figure 4-2 – CSS Temperature for Hydrogen – Methane PSA Separation**

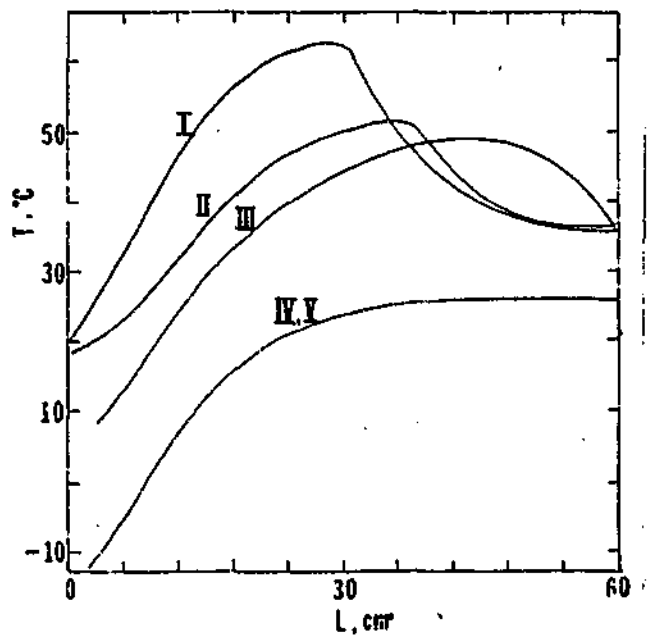


(Taken from Yang and Doong (1985) p. 1840)

Unlike these works, Park et.al. (1998) investigated a multilayered adsorption bed for hydrogen PSA. However, the study offered little explanation of some interesting temperature profiles that displayed slight dips at the interface between the layers.

**Figure 4-3 – CSS Temperature Profiles for Multilayered Hydrogen PSA**

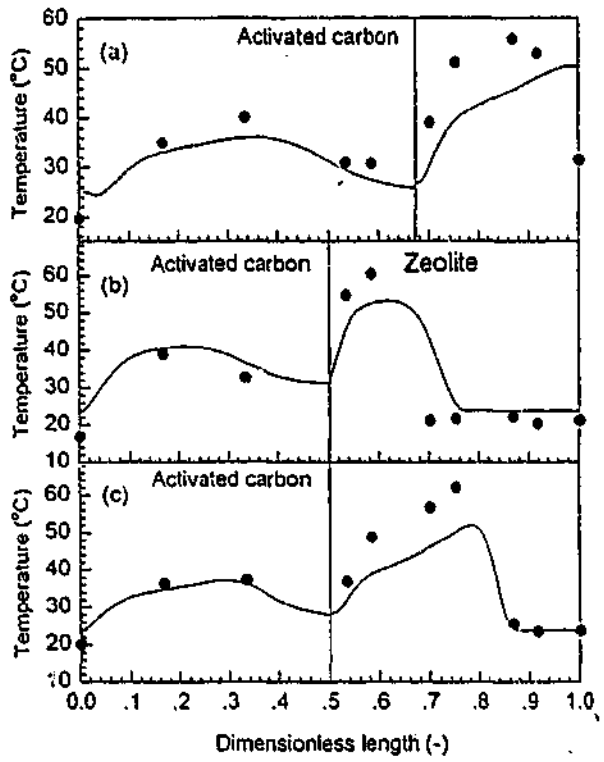


This brief review demonstrates that while some experimental investigation of axial thermal profiles in PSA systems has been undertaken recently, oxygen VSA has been hardly investigated in the open literature. This further demonstrates the need for the detailed experimental investigation of oxygen VSA axial thermal profiles in this Chapter.

## 4.2 Experimental Program to Investigate Axial Temperature Profiles

In order to validate the models developed in Chapter Two a wide ranging experimental program was undertaken. The scope of this work involved the investigation of several different classes of effects - operational effects, adsorbent effects, and dynamic effects. In addition to presenting the results of this experimental investigation, the predicted outcomes (qualitative and/or quantitative) of the models are also presented.

One complication here is that a variety of models of different complexity have been developed. The simpler models cannot capture the effect of all the process variables that impinge on oxygen VSA thermal profiles. For example, the role of varying purge cannot be determined by reference to the simple energy balance technique, which assumes uniform adsorption. However is hoped that the utility of these simpler approaches will be apparent in other cases. The strategy pursued here is akin to the principle of Occam's Razor. Preference will be given to the simplest model to explain the observed experimental temperature profile and VSA performance. Many process conditions elude simple analytic tools, and in these cases numerical simulation techniques (MINSA and ADSIM) will be utilised.

Verification of MINSA has been reported in previous literature (Todd et.al., 2000b; Webley et.al., 2000c). This work involved verifying MINSA against experimental data, constant pattern solutions, and analytical solutions based on the work of Knaebel and Hill (1985). In this chapter comparisons are made between the experimental results and numerical simulation to demonstrate the veracity of the physical model that underpins MINSA in capturing the thermal effects evident in oxygen VSA. One of the particular complications with numerical simulation is the determination of appropriate dual site Langmuir parameters, and mass transfer coefficients. This was particularly difficult for the LiLSX adsorbent that was used in some experiments. The absorbent has not been fully characterised and this has made simulation difficult. For simulation purposes, the isotherm parameters for a generic LiX adsorbent were used to simulate the LiLSX, even though there was some small differences between the two. However there are significant benefits in using LiLSX for the experimental investigations, in that the higher loading capacity tends to increase the magnitude of the 'cold spot' and the severity of the overall temperature profile. By contrast, NaX is better characterised and more easily simulated, but does not feature the loading capacity of LiLSX.

Importantly, effects not captured by the models are also highlighted, and some effort is made to explain these effects and draw out the limitations of the models. Full experimental results are detailed in Appendix 9. In this chapter, key temperature, pressure, and performance profiles are presented. In some cases several sets of experimental results illustrate the same point. In these instances much of the experimental data is noted as supporting results. The reader is directed to Appendix 9 for these results.

The experimental program and the fundamental research question addressed can be summarised as follows:

**Table 4-1 - Experimental Parameters Investigated**

| Parameter Investigated | Model Prediction |
|---|---|
| **4.3 Preliminary** | |
| Single Layered Bed with Dry Air Feed | Models predict that the temperature depression will not be evident in single layered bed with dry air feed. |
| Multilayered Bed with Inert Prelayer and Dry Air Feed | Models predict temperature depression will be evident. |
| **4.4 Operational Effects** | |
| Effect of Pressure Window | Models predict that a wider pressure window will result in a more pronounced temperature depression. |
| Effect of Product Flow and Purity | Product purity and flow affect the adsorptive loading and the convective fluxes through the adsorption bed. It is predicted that increased purity will result in more pronounced temperature profiles. |
| Effect of Purge | Purge plays a critical role in oxygen VSA performance. Adjusting the quantity of purge will alter the temperature profile. However the effect of purge is neglected in the simple energy balance. |
| Effect of Pressure Equalisation | The qualitative model predicts that cocurrent depressurisation will increase the magnitude of the 'cold spot' |
| Oxygen Recovery | Oxygen recovery is often used as a parameter for characterising oxygen VSA performance. However a specific oxygen recovery (and pressure window) does not result in a unique axial CSS temperature profile. |
| Effect of Feed Temperature | The simple models and Collins' work predicts that changes in the feed temperature will lead to a vertical translation of the axial CSS temperature profile |
| Effect of Cycle | It is predicted that different cycles will result in different CSS temperature profiles due to differing convective flows. |

| | |
|---|---|
| **4.5 Column Effects** | |
| Effect of Metal Walled Columns | It is predicted that with a metal walled column the axial CSS temperature profile will be dissipated due to axial conduction and heat loss to the environment. |
| Effect of Polyurethane Column vs. PVC Column | Numerical modelling suggests that the CSS temperature profile will be more severe in the polyurethane columns than in the PVC columns. |
| **4.6 Adsorbent/Prelayer Effects** | |
| Effect of Main Layer Adsorbent | Newer lithium based adsorbents have a larger nitrogen working capacity causing larger cyclic temperature swings. Models predict that this should result in a more pronounced axial temperature profile compared to NaX with the same pressure window. |
| Effect of Thickness of Prelayer | The simple energy balance model predicts that increasing the length of the prelayer will cause a bigger cold spot due to an increased regenerative heat exchanger effect. The model suggests that there will be an asymptotic minimum. |
| Effect of an Adsorbing Prelayer – NaX | The simple models are based on an inert prelayer. Qualitatively it is predicted that an adsorbing prelayer will mitigate the cold spot. |
| Effect of Higher Capacity Prelayer – LiLSX - 'Hot Spot' Effect | If the loading capacity and heat generation is greater in the prelayer than the main layer, it is speculated that a 'hot spot' (an inverted 'cold spot') will occur in a one-bed cycle. |
| Effect of an Inert to Mitigate the Cyclic Temperature Swing | Reducing the cyclic temperature swing should increase performance and reduce the magnitude of the axial CSS temperature profile. |
| **4.7 Transient Effects** | |
| Transient Temperature Profiles with Dry Air Feed | Multiple Scale Analysis predicts that the interaction between the short time scale cyclic temperature fluctuations and the long time scale temperature drift will result in a CSS temperature profile. |
| **4.8 Wet Air Feed Effects** | |
| Effect of Wet Air Feed on CSS Temperature Profile | Collins and Kumar's work suggests water loading forms a quasi-inert zone at the entrance of the adsorption bed resulting in a temperature depression in a single layered adsorption bed |
| Transient Effect of Water Adsorption | The initial loading of water on a 'clean' bed should produce a transient temperature spike, which will eventually dissipate. |
| **4.9 Total Reflux and Curious Effects** | |
| Total Reflux - Internal and External | Simple models predict that there will be no temperature gradient through the prelayer. Numerical modelling of this proves difficult. This is a difficult experiment to undertake due to heat losses. |

This list of experimental parameters is not exhaustive, but represents the main parameters of interest for elucidating the nature of thermal profiles in oxygen VSA. A number of other experimental parameters affect the extent of the temperature depression. For example, it is expected that much shorter cycles would limit the extent of the nitrogen adsorption and reduce the temperature swing, and hence reduce the severity of the 'cold spot'. A more detailed examination of the pressure window would also be possible. The study could also have been extended to a more thorough investigation of the effect of cycle, of different adsorbent types and pressure windows.

However, the parameters investigated experimentally combined with MINSA simulations provide sufficient examples to gain a thorough understanding of the temperature profiles.

## 4.3 Preliminary Experiments

Two simple preliminary experiments were conducted to demonstrate that the temperature depression that characterised oxygen VSA is caused by the presence of an inert prelayer, or prelayer with reduced adsorptive capacity (or temperature swing) compared to the main adsorbent layer. A single layered bed with a dry air feed does not display the temperature depression typically associated with oxygen PSA/VSA. Similarly it is easy to demonstrate that when a 300 mm inert prelayer is included (with a dry air feed) the 'cold spot' is present. These two simple experiments provide a starting point for a more thorough investigation, and render implausible Wankat's explanation about gas density effects (Wankat, 1990), and other postulated explanations that the effect is due to water adsorption (Stegmaier, 1996).

### 4.3.1 Single Layered Adsorption Bed with Dry Air Feed

The simplest axial CSS temperature profile results from a single layered adsorption bed with a dry air feed. This is not a realistic industrial scenario, but provides a useful starting point for this experimental investigation.

**Model Prediction:** A single layered bed with a dry air feed will not manifest a temperature depression, since there is no regenerative heat exchanger effect. At CSS, the desorbed gas will leave at a lower temperature than the feed gas. The qualitative model also predicts that the temperature of the product gas will be higher than the feed gas. MINSA simulations support these observations, as is demonstrated in Chapter 2.3.

The simple energy balance (without the prelayer) results in the following expression for the temperature of the product gas leaving the bed.

**(2-49)**

$$T_p = T_f + \frac{2\Delta H(F - Pr)Pr}{\left(Pr\, m_m C_{sm} + \left(\frac{(F - Pr)C_{pg}}{4}(F + Pr)\right)\right)\left(\frac{F}{Pr} - 1\right)}$$

**Experiment:** Numerous experiments were conducted with a dry air feed and a single layered bed. It is critical the feed air has a very low dew point to ensure that a water loaded zone is not created. For all dry air experiments the dew point of the feed air was -58 $^{o}$C at ambient temperature and pressure.

**Result(s):**

**Figure 4-4**

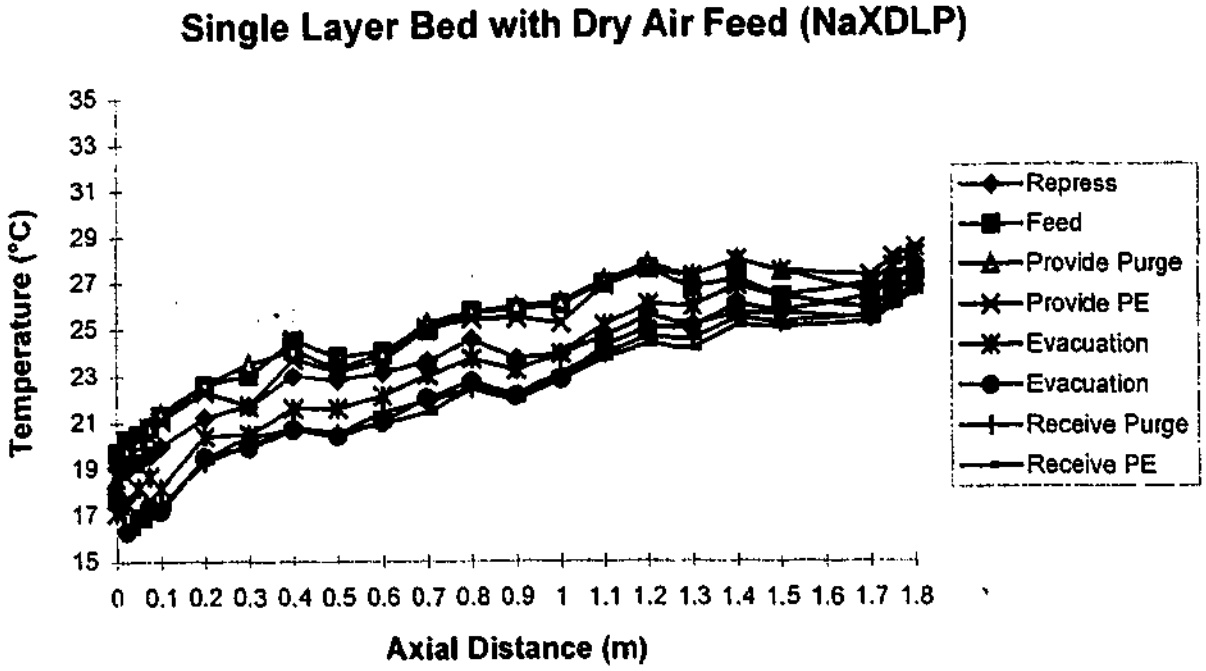


Figure 4-4 shows the axial CSS temperature profile for a single layered bed of NaX undergoing two bed VSA cycle (Cycle 2) with PVC adsorption bed with a pressure profile of 136-36 kPa. The oxygen product purity is 80.1%. The different temperatures represent the end of step temperatures in the bed. At the end of the feed step the main section of the bed is hottest, and coldest during the desorption steps - evacuation and receive purge. The feed temperature was 19.5 $^{o}$C. The average temperature swing over the cycle is 3.3 $^{o}$C, but the temperature swing at the end of the bed is smaller (2 $^{o}$C), due to reduced nitrogen adsorption at the end of the bed. The temperature profile shows that the nitrogen front breaks through on the provide purge and provide pressure equalisation steps. This is typical for purity control in a two-bed cycle. This highlights how temperature profiles can be a useful diagnostic to reveal the movement of composition waves through the adsorption bed.

As the simple qualitative theory suggests, there is no 'cold spot' observed, and the temperature of the desorbed gas leaving the bed is lower than the feed temperature.

Based on the simple energy balance, the average temperature of the gas leaving the adsorption bed is 29.8 $^{o}$C. This compares well with the experimental result of 27 $^{o}$C, remembering that the simple model ignores heat loss.

**Supporting Results:** A number of single layered bed experiments with dry air feed were conducted (LSX1, LSX2, LSX3, NaXDHP). The CSS temperature profiles vary, but absence of a 'cold spot' is a common feature. The variation in the process conditions and adsorbents alters the overall temperature profile, and this issue is further explored.

**Conclusion:** The 'cold spot' can only result if the adsorption bed is not homogeneous with respect to its adsorptive properties. This CSS temperature profile with a single layered oxygen VSA is very similar in shape to the CSS axial thermal profiles observed in other single layered PSA systems, as was detailed in Section 4.1 and Section 2.2 (Lou et.al. (1999), Mahle et.al. (1996), Liu et.al. (1998) and Yang and Doong (1985)).

### 4.3.2 A Simple Multilayered Bed

In practice, due to the need to prevent the penetration of trace components (water and carbon dioxide) onto lithium and calcium based adsorbents, there is a need to have a multilayered adsorption bed. The simplest multilayered adsorption bed is an inert prelayer followed by the main nitrogen selective adsorbent.

**Model Prediction:** The simple models treating an inert prelayer as a regenerative heat exchanger predict that there will be a temperature depression at the interface between prelayer and the main layer, caused by the asymmetries in the mass and enthalpy flows through the adsorption bed.

**Result(s):**

**Figure 4-5**

**Activated Alumina (300 mm) and LiLSX Main Layer**
**( 1 Bed Cycle) (AA300LSX4)**

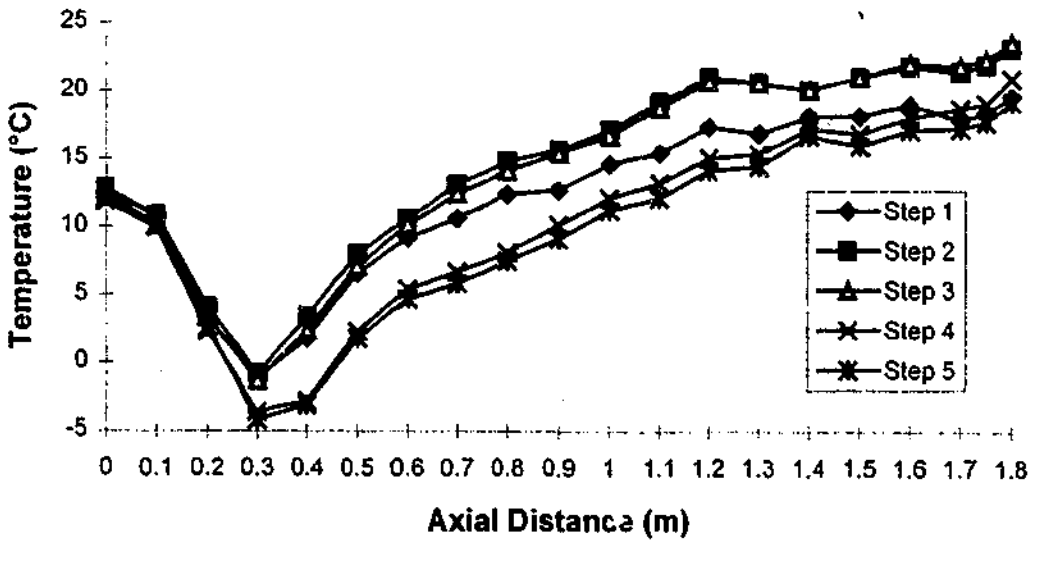


Figure 4-5 describes the axial CSS temperature profile for a 1 bed cycle (Cycle 1) with a 300 mm prelayer of activated alumina and a main layer of 1550 mm of LiLSX and the PVC adsorption beds. The pressure window was 140-41 kPa and a oxygen product purity of 85.6 %. The minimum temperature at the interface is approximately 17 $^{o}$C below the feed temperature, and the temperature of product gas is approximately 7 $^{o}$C above the feed temperature.

This represents a typical two layered bed that can be successfully simulated with MINSA. Table 4-2 describes experimental run AA300LSX4 and its numerical simulation.

**Table 4-2 - Comparison between Experimental Run and Simulation (AA300LSX4)**

| | **Experimental (AA300LSX4)** | **MINSA Simulation** |
|---|---|---|
| Pressure Profile (kPa) (Step 1/2/4/5) | 134.1/140.2/41.1/45.4 | 134/140.3/42.2/46.7 |
| Product Purity*(%) | 89.5 ±0.5 | 89.4 |
| Feed Flow (mmol/cycle) | 3896±77 | 4170 |
| Product Flow(mmol/cycle) | 332±10 | 336 |
| Recovery (%) | 33.4±2.0 | 31.3 |
| Temperature Minimum(°C) (Cold Spot) | -4.3 ±1.0 | -4.0 |
| Temperature at End of Bed (°C) | 23.4 ±1.0 | 20.5 |

*As with all MINSA simulations the product purity is on a two component basis where oxygen and argon are assumed to behave similarly and are treated as a single component. The term product purity is used to refer to oxygen and argon. Oxygen purity refers solely to the oxygen concentration.

The MINSA simulation compares well with respect to most process variables except the feed flow (~7%). This is most probably due to the use of a generic LiX isotherm, rather than the specific LiLSX adsorbent used. Table 4-2 highlights that the experimental and simulation results compare well with respect to the temperature profile. Interestingly, like subsequent examples, the experimentally observed end of bed temperature is higher than the simulation value.

**Supporting Results:** The presence of the 'cold spot' was observed in all cases with an inert prelayer (e.g. AA300NaX1 through to AA300NaX20). It was also evident when there was a quasi-inert water-loaded prelayer (e.g. NaXWLP), and an adsorbing prelayer, such as NaX where the main layer was VSA6 or LiLSX ( e.g. NaX300LSX1 and PuNaXVSA61).

**Conclusion:** The presence of the 'cold spot' was consistently observed with all experiments undertaken where the temperature swing due to adsorption/desorption was larger in the main layer than in the prelayer. This is consistent with the qualitative explanation developed in Section 2.2.

## 4.4 Operational Effects

The preliminary experiments demonstrate the effect of the presence and absence of an inert prelayer in an oxygen VSA bed. The task now is to move beyond these preliminary experiments, and investigate operational parameters that can effect the extent and magnitude of the temperature profile. These parameters include pressure window, product flow, extent of purge and pressure equalisation, recovery, gas feed temperature and cycle type.

### 4.4.1 Effect of the Pressure Window

Power is the major operating cost for oxygen VSA. Power consumption is intimately related to the pressure window of operation. The equations for the feed and vacuum blower are detailed in Appendix 10. The current trend in VSA operation is to reduce the power consumption by reducing the pressure window, specifically by using shallower vacuums for desorption.

**Model Prediction:** The pressure window is a critical parameter in determination of the extent of the temperature depression, and the overall temperature profile. The pressure window in combination with the adsorbent isotherm determines the extent of adsorption and the working capacity of the adsorbent. The working capacity and the heat of adsorption associated with the adsorbent, determine the cyclic temperature swing. For the case of a bed with an inert prelayer, as the pressure window is increased, it is expected that the magnitude of the temperature depression will increase. The following equation developed in Chapter 2.4 can be applied to estimate changes to the temperature depression, when the pressure window is adjusted and the product flow kept constant. This alters both the working capacity of the adsorbent, and the totalised feed flow (F).

**(2-48)**

$$\overline{T2} = T_f - \frac{Pr\,\Delta H(m_p C_{sp})(WCm_m)^2(1+\alpha)}{(4\,Pr\,m_m C_{sm} + (F+Pr)(WCm_m)Cpg)(2\,Pr\,m_p C_{sp} + C_{pg}F(WCm_m))}$$

It is important to note that due to the non-linear and favourable shape of most oxygen VSA isotherms, the pressure window must be specified in absolute terms (e.g. 140-40 kPa), rather than the difference between $P_{high}$ and $P_{low}$ (e.g. 100 kPa). This is because the absolute

working capacity will vary considerably depending on the specific pressures. However for a linear isotherm such distinctions are unnecessary.

**Experiment:** In order to illustrate the effect of the pressure window on the temperature depression, three different experimental runs were conducted. In each case the end of feed pressure (126±0.5 kPa) and product flow (482±16 mmol/cycle) were fixed, and the end of evacuation pressure was varied between 32, 41 and 53 kPa.

**Result(s):**

**Table 4-3 - Effect of Pressure Window on Temperature Profile**

| | AA300NaX5 | AA300NaX6 | AA300NaX7 |
|---|---|---|---|
| Evacuation Pressure (kPa) | 32 | 41 | 53 |
| Oxygen Purity (%) | 91.0 | 72.9 | 57.2 |
| Inlet Feed Temperature (°C) | 20.0 | 22.0 | 20.3 |
| Cold Spot (°C) | 1.2 | 8.6 | 10.2 |
| ΔT (Feed - Cold Spot) (°C) | 18.8 | 13.4 | 10.1 |
| Average Temperature Swing in Main Layer (°C)* | 3.8 | 3.0 | 2.6 |

*The mass transfer zone (MTZ) at the end of the bed was ignored and measured between 0.3 and 1.3 m.

As the evacuation pressure is increased (the pressure window is reduced), there is less nitrogen adsorption resulting in lower product purity, and a reduced temperature swing associated with adsorption and desorption. This reduced temperature swing in the main layer results in a reduced magnitude of the CSS temperature depression. The simple energy balance model described in Equation 2-48 predicts this. Table 4-4 details the predictions of the simple energy balance.

**Table 4-4 - Simple Energy Balance Prediction of Temperature Depression**

| | AA300NaX5 | AA300NaX6 | AA300NaX7 |
|---|---|---|---|
| Feed Gas (mmol/bed/cycle) | 2120 | 1880 | 1640 |
| Loading ($WCm_m$)(F-Pr) (mmol/bed/cycle) | 1900 | 1650 | 1410 |
| Cyclic Temperature Swing (°C) | 4.4 | 3.8 | 3.3 |
| Feed Temperature (°C) | 20.0 | 22.0 | 20.3 |
| Product Temp (above feed) (°C) | 4.0 | 2.4 | 1.6 |
| Cold Spot (°C) | 0.5 (1.2)* | 6.5 ( 8.6)* | 8.6 (10.2)* |
| ΔT (Feed - Cold Spot) (°C) | 19.5 (18.8)* | 15.5 ( 13.4)* | 11.7 (10.1)* |

* The experimental results are indicated in brackets.

Table 4-4 is consistent with the experimental results. As the working capacity of the adsorbent increases through increasing the pressure window, the magnitude of the 'cold spot' is increased (keeping all other process variables constant). It should be noted that the simple energy balance contains a number of significant assumptions including that there is no heat loss, no gas phase accumulation, one component and a single heat of adsorption. The heat of adsorption used for this calculation was 20,000 J/mol based on main nitrogen loading on NaX. While the comparison with experimental results is good in this case, such assumptions may not be valid in all cases. More importantly, the simple equation (Equation 2-48) correctly discerns the trend that as the pressure window is reduced, the extent of the 'cold spot' is also reduced.

These three experimental runs can also be simulated numerically with MINSA. NaX is a well characterised adsorbent which should enable good comparison with the experimental results.

**Table 4-5- Comparison of experimental and simulation results for AA300NaX5**

| | Experimental AA300NaX5 | Simulation AA300NaX5 | Pressure | Experimental AA300NaX5 | Simulation AA300NaX5 |
|---|---|---|---|---|---|
| Feed Gas (mmol/cycle) | 4249±84 | 4381 | Step 1 | 122.0±0.5 | 122.2 |
| Waste Gas (mmol/cycle) | 3730±74 | 3937 | Step 2 | 126.5±0.5 | 127.1 |
| Product Gas (mmol/cycle) | 463±14 | 444 | Step 3 | 96.5±0.5 | 97.8 |
| Product purity (%) | 95.1±0.5 | 94.6 | Step 4 | 87.2 ±0.5 | 86.3 |
| Product Recovery (%) | 45.1±2.0 | 41.7 | Step 5 | 32.6±0.5 | 32.7 |
| Product Rate (kg/day) | 19±0.6 | 19 | Step 6 | 48.3±0.5 | 46.6 |
| Mass Balance Error (%) | 1.3±2 | <1E-6 | Step 7 | 59.9 ±0.5 | 60.6 |

**Table 4-6 - Comparison of experimental and simulation results for AA300NaX6**

| | Experimental AA300NaX6 | Simulation AA300NaX6 | Pressure | Experimental AA300NaX6 | Simulation AA300NaX6 |
|---|---|---|---|---|---|
| Feed Gas (mmol/cycle) | 3765±76 | 3903 | Step 1 | 124.7±0.5 | 124.1 |
| Waste Gas (mmol/cycle) | 3164±64 | 3390 | Step 2 | 127.7±0.5 | 127.5 |
| Product Gas (mmol/cycle) | 498±15 | 513 | Step 3 | 98.3±0.5 | 99.2 |
| Product purity (%) | 76.3±0.5 | 76.35 | Step 4 | 90.1±0.5 | 88.8 |
| Product Recovery (%) | 43.9±2.0 | 43.6 | Step 5 | 41.7 ±0.5 | 41.7 |
| Production rate (kg/day) | 17±0.5 | 18 | Step 6 | 57.7±0.5 | 56.8 |
| Mass Balance Error (%) | 2.8±2 | <1E-6 | Step 7 | 68.6±0.5 | 69.1 |

**Table 4-7 - Comparison of experimental and simulation results for AA300NaX7**

| | Experimental AA300NaX7 | Simulation AA300NaX7 | Pressure | Experimental AA300NaX7 | Simulation AA300NaX7 |
|---|---|---|---|---|---|
| Feed Gas (mmol/cycle) | 3289±66 | 3234 | Step 1 | 122.7±0.5 | 122.0 |
| Waste Gas (mmol/cycle) | 2763±55 | 2734 | Step 2 | 127.1±0.5 | 126.5 |
| Product Gas (mmol/cycle) | 486±15 | 500 | Step 3 | 101.3±0.5 | 101.3 |
| Product purity (%) | 59.8±0.5 | 60.0 | Step 4 | 94.5±0.5 | 92.4 |
| Product recovery (%) | 38.4±2 | 40.3 | Step 5 | 53.5±0.5 | 53.5 |
| Production rate (kg/day) | 13±0.4 | 14 | Step 6 | 67.8±0.5 | 67.9 |
| Mass Balance Error (%) | 1.22±2.0 | <1E-6 | Step 7 | 78.0±0.5 | 78.1 |

There is good correlation between MINSA and the experimental runs with respect to the flows and pressure window. Likewise Table 4-8 highlights, the correlation with respect to the temperature profiles is reasonable.

**Table 4-8 - Comparison between experimental and simulated temperature profiles**

| | Experimental AA300NaX5 | Sim. | Experimental AA300NaX6 | Sim. | Experimental AA300NaX7 | Sim. |
|---|---|---|---|---|---|---|
| Cyclic Temp. Swing (°C)* | 3.8±0.5 | 3.9 | 3.0±0.5 | 3.5 | 2.6±0.5 | 3.2 |
| Feed Temperature (°C) | 20.0±1.0 | 20.0 | 22.0±1.0 | 22.0 | 20.3±1.0 | 20.3 |
| End of Bed Temp. (°C) | 24.9±1.0 | 20.8 | 27.4±1.0 | 21.6 | 23.8±10.0 | 20.7 |
| Temperature Min. (°C) | 1.2±1.0 | 0.5 | 8.6±1.0 | 5.8 | 10.2±1.0 | 8.3 |

*Average cyclic temperature swing between 0.3 and 1.3 m

Table 4-8 shows a reasonable correlation between the experimental runs and simulation runs with respect to the minimum bed temperatures. Interestingly, the simulated temperature profile is consistently lower than the experimental value. Curiously the same trend is evident in the work by Kumar et.al. (1996) and Webley et.al. (2000), probably the result of limitations in modelling the heat loss associated with the adsorption column wall.

However there is a more significant discrepancy when comparing the end of bed temperatures and the cyclic temperature swings. The MINSA predicted temperature swings are consistently greater than the experimental results. This could be due to the simulation error associated with the two heats of adsorption of the adsorbent. This could be caused by parameter estimation for the dual site Langmuir isotherms, or errors associated with approximating $\Delta H$ rather than using the rigorous isosteric heats of adsorption. Or the discrepancy could be based on the model assumption of thermal equilibrium between the solid and the gas. An alternative explanation is that the physical properties of the adsorbent (bed density, heat capacity, and voidage) used for MINSA simulation are incorrect. However, it is unlikely that the bed density and voidage are incorrect, because the pressure profile and flows compare very well between the simulation and experimental results. It is possible that the estimated heat capacity of the adsorbent is incorrect, and a higher value should be used in the MINSA simulations. However, the specific heat capacity of the adsorbent of 1000 J/Kg K is based on industry data supplied by APCI. This issue is not completely resolved in this thesis.

A further possible explanation is that thermocouple measurements are the source of the difference between the simulation and experimental results. The estimated response time of the junction exposed type T thermocouples was 1 second (90% response) which indicates that the severity of the cyclic temperature swing could be marginally underestimated. However for a 60 second cycle the consequences of the response time will be minimal. Another possible difference could be due to absolute errors with the thermocouples, but this is also unlikely since the measurement of the differential temperature change over a cycle is likely to be less than ±0.5 °C.

Another important and significant difference between the experimental and MINSA results relates to the temperature at the end of the bed. The experimental temperatures at the end of the bed are consistently slightly higher than the MINSA predicted values. This difference cannot be explained by thermocouple error. This difference suggests that the adsorber heat loss model utilised could be refined to account for heat loss, where the convective flows at the end of the bed are quite small.

**Supporting Results:** The same result is evident when comparing AA300LSX1 and AA300LSX3. These experimental runs had the same product valve positions, (and similar product flows), the same amount of purge, and the same end of feed pressure (140 kPa), but differing minimum bed pressures (AA300LSX1~30 kPa, AA300LSX4~40 kPa). Like the previous example, this translated into very different axial CSS temperature profiles as is shown in Figure 4-6.

**Figure 4-6**

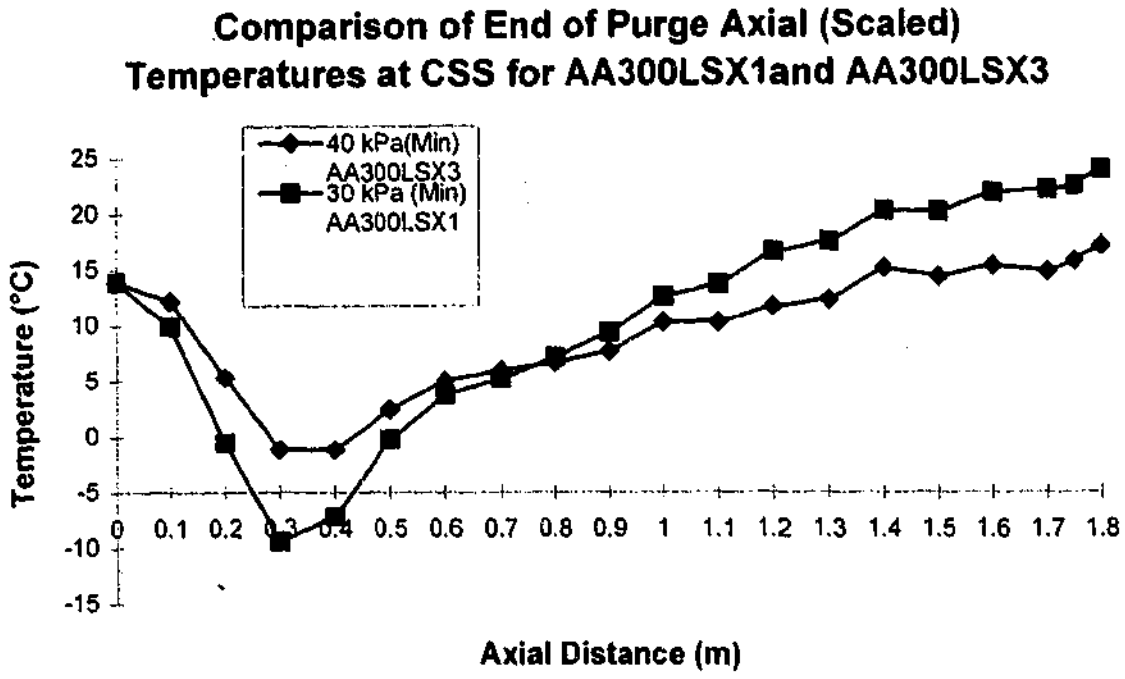


The temperature profiles have been scaled to the feed temperature of AA300LSX3 to eliminate the effect of the feed temperature on the CSS axial temperature profile. The figure shows that the case with a wider pressure window (AA300LSX1) (140-30 kPa) results not only in a more pronounced 'cold spot' (approximately 10 $^{o}$C lower), but also a steeper gradient in the temperature profile through the main layer. This is consistent with the simple energy balance.

The effect of the pressure window on the CSS axial temperature profile is also evident with some of the polyurethane column runs. PuAANaXVSA6-9 and PuAANaXVSA6-10 are similar experimental results except the pressure window is slightly wider for Run PuAANaXVSA6-9 (137 –37.5) compared to PuAANaXVSA6-10 (136-44 kPa). As expected, the experimental run that has the deeper vacuum has a more pronounced 'cold spot': (-20.2 $^{o}$C compared with –16 $^{o}$C).

**Figure 4-7**

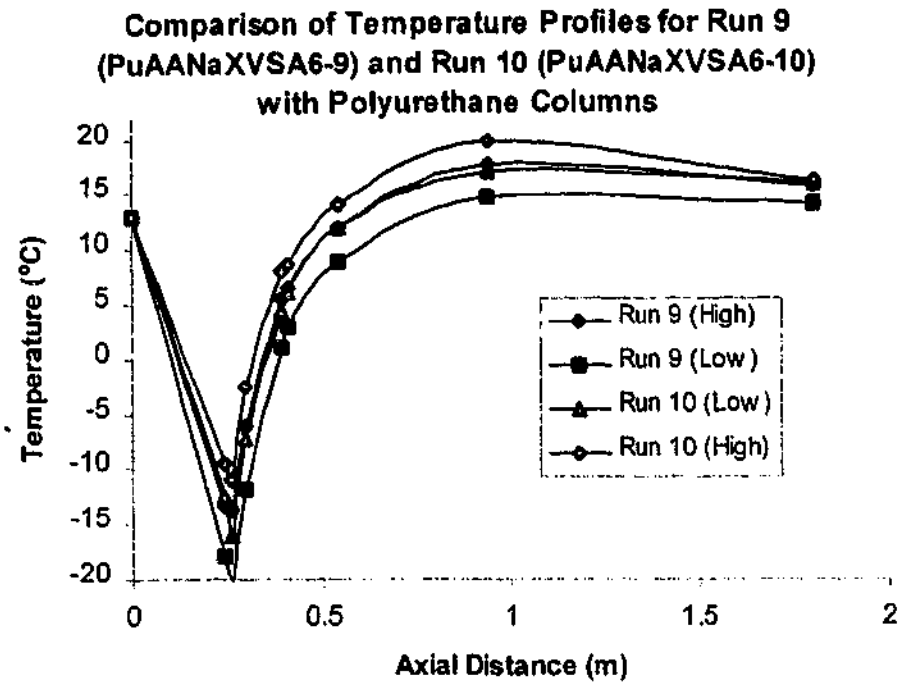


Figure 4-7 also highlights a severe 'cold spot' evident with a two bed cycle and the polyurethane columns. This plot also demonstrates that the polyurethane columns have insufficient thermocouples for clear resolution of the temperature profile through the entire bed.

**Conclusion:** Each of these examples has shown that an increased pressure window increases the cyclic temperature swing which in turn increases the extent of the temperature depression, and the severity of the temperature profile. However, it should be noted that the key parameter is not solely the pressure window, but the working capacity of the adsorbent i.e. the quantity of nitrogen adsorbed. As will be demonstrated in Section 4.6.1, for the same pressure window, adsorbents with different isotherms will lead to different temperature profiles.

### 4.4.2 Effect of Product Flow (& Purity) - Ratio of Forward/Reverse Flow

Current industrial VSA produces oxygen at purities 90-93%. The maximum possible oxygen purity is 95.5%, due to argon contamination. Future market opportunities for enriched oxygen could be as low as 40% oxygen. Purity control is typically achieved by adjusting the position of the product control valve. Where all other process variables are kept constant, reduced product flow results in higher product purity.

**Model Prediction:** The simple energy balance model predicts that reducing the product flow, and keeping all other process conditions identical, will increase the magnitude of the temperature depression. This does not apply to miniscule or zero product flows, where the extent of the temperature depression will not be as pronounced. (Refer Figure 2-17)

**Experiment:** Comparing three experimental runs (AA300LSX3, AA300LSX4 and AA300LSX8) where the pressure window was approximately constant ($\Delta P$=99 kPa), and the extent of purge was similar, but the amount of product flow was varied.

**Result(s):**

**Table 4-9 - Effect of Varying the Product Flow (AA300LSX)**

| | AA300LSX3 | AA300LSX4 | AA300LSX8 |
|---|---|---|---|
| Oxygen Purity (%) | 69.8 | 85.6 | 94.6 |
| Product Valve Cv (%) | 30 | 20 | 10 |
| Product Flow (mmol/cycle) | 448 | 333 | 200 |
| Feed Flow (mmol/cycle) | 3960 | 3896 | 3906 |
| Evacuated Flow (mmol/cycle) | 3510 | 3546 | 3574 |
| Recovery (%) | 36.0 | 33.0 | 22.7 |
| Average Feed Temperature ($^{o}$C) | 13.3 | 12.1 | 11.4 |
| Cold Spot ($^{o}$C) | -1.2 | -4.2 | -6.3 |
| $\Delta$T (Feed - Cold Spot) ($^{o}$C) | 14.5 | 16.3 | 17.7 |

This demonstrates that, even when the minor difference in feed temperature is accounted for the effect of reducing the product flow (while maintaining other process variables constant) is to increase the extent of the 'cold spot'.

**Supporting Results:** A similar result is evident when comparing NaX300LSX1, NaX300lSX4, and NaX300LSX5.

**Table 4-10 - Effect of Varying Product Flow (NaX300LSX)**

| | NaX300LSX1 | NaX300LSX4 | NaX300LSX5 |
|---|---|---|---|
| Oxygen Purity (%) | 88.5 | 87.8 | 60.5 |
| Product Valve Cv (%) | 20 | 20 | 50 |
| Product Flow (mmol/ cycle) | 336 | 323 | 623 |
| Recovery (%) | 33.0 | 31.3 | 38.8 |
| Average Feed Temperature (°C) | 10.8 | 11.5 | 11.9 |
| Feed Flow (mmol/cycle) | 4232 | 4197 | 4357 |
| Evacuated Flow(mmol/cycle) | 3764 | 3806 | 3797 |
| 'Cold Spot' (°C) | 4.2 | 4.7 | 7.3 |

Run NaX300LSX1 and NaXLSX4 represent quality assurance runs to demonstrate the repeatability of the data for the same process conditions (except for a minor difference in feed temperature). Table 4-10 demonstrates that increasing the product flow (NaX300LSX5) (and maintaining all other process variables constant) diminishes the extent of the temperature depression.

Another supporting result is evident with comparing AA300NaX2, AA300NaX3, and AA300NaX4. Like the previous example, the pressure profiles are the same, and only the product valve position (FCV4) is varied between these three experimental runs.

**Table 4-11 - Effect of Varying Product Flow (AA300NaX)**

| | AA300NaX2 | AA300NaX3 | AA300NaX4 |
|---|---|---|---|
| Oxygen Purity (%) | 95.3 | 86.9 | 71.4 |
| Product Valve Cv (%) | 18.0 | 30.0 | 50.0 |
| Product Flow (mmol/ cycle) | 301 | 474 | 682 |
| Recovery (%) | 33.4 | 44.8 | 49.0 |
| Average Feed Temperature(°C) | 22.6 | 20.6 | 20.5 |
| Feed Flow (mmol/cycle) | 3897 | 4186 | 4529 |
| Evacuated Flow(mmol/cycle) | 3503 | 3642 | 3810 |
| Cold Spot (°C) | 4.2 | 6.2 | 8.4 |
| ΔT (Feed - Cold Spot) (°C) | 18.4 | 14.4 | 12.1 |

In addition to considering the effect of the product flow (hence purity) on the cold spot, it is also instructive to look at the effect on the overall temperature profile, rather than simply the 'cold spot'. For example, comparison of a low purity (NaXDLP) and a high purity (NaXDHP) case for a single layer bed (NaX) with dry feed air demonstrates the significant difference in the temperature profiles.

**Figure 4-8**

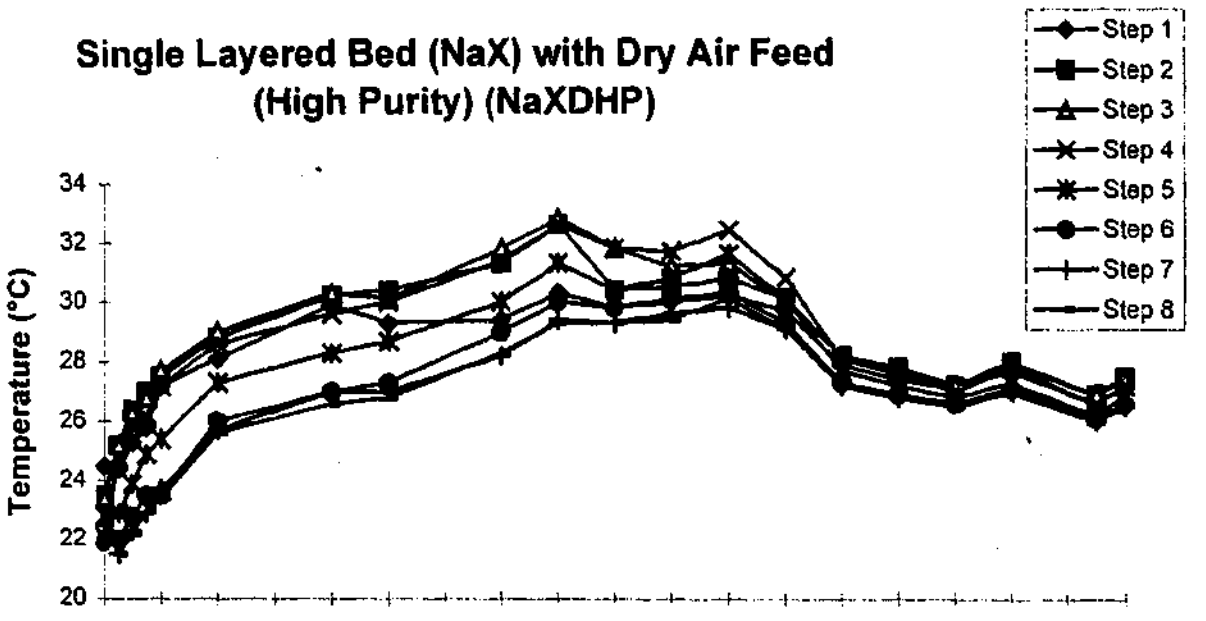


**Figure 4-9**

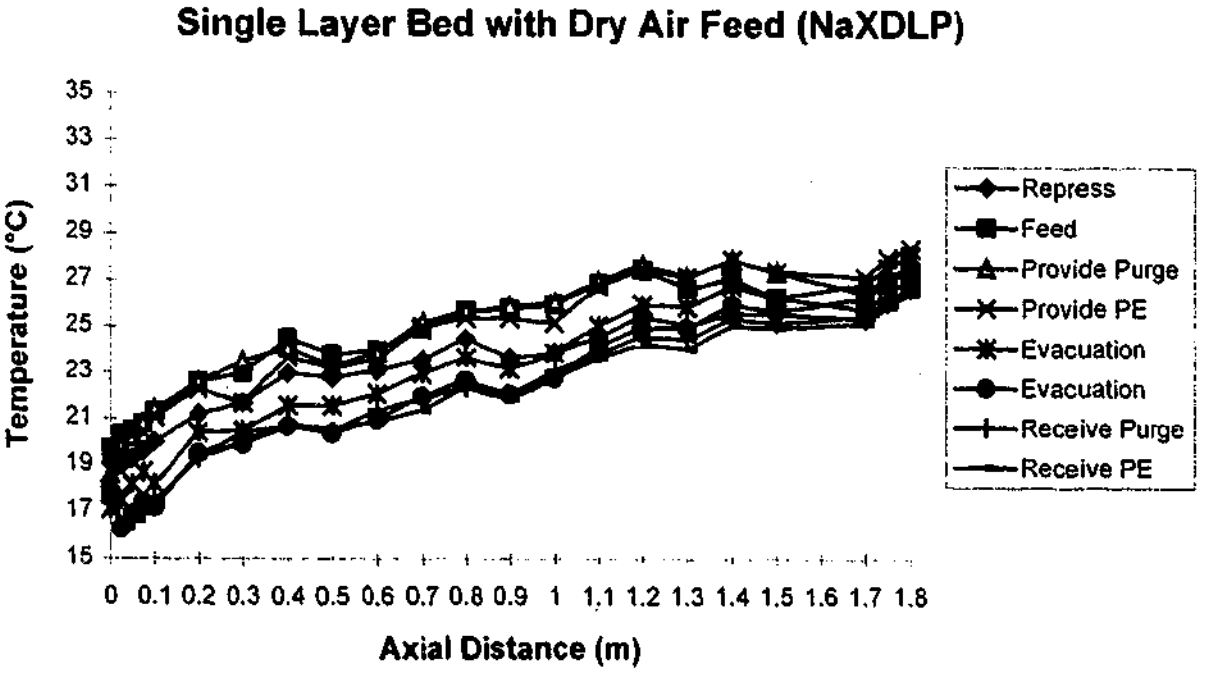

The shapes of these two temperature profiles are different. In the high purity case, there is a local maximum in the temperature profile near the middle of the bed, and a much reduced temperature swing through the end of the bed. In effect the mass transfer zone is held back inside the bed, and there is little nitrogen adsorption over the last 0.5 metres of the bed. This highlights one significant problem with the simple energy balance model that assumes uniform nitrogen adsorption over the entire main layer. However, the simple energy balance model can be modified to include the effects of holding the mass transfer zone well inside the bed, by modelling an inert zone. This situation can be modelled as a regenerative heat exchanger at the end of the bed, and fixing the temperature boundary condition at the end of the bed as the ambient temperature. The resulting approximation is:

$$\Delta T_{post} \approx \frac{C_{pg}\,Pr(T_p - T_{amb})}{m_{post}C_{spost} + \left(\frac{Pr\,C_{pg}}{2}\right)} \qquad (4\text{-}1)$$

where $\Delta T_{post}$ = Temperature swing in the inert (post-layer) at the end of the bed (K)

$m_{post}$ = Mass of the inert (post-layer) at the end of the bed (kg)

$Cs_{post}$ = Heat capacity of inert (post layer) at the end of the bed (kJ/kg K)

The equation shows that in the absence of adsorption at the top of the bed, there is a small temperature swing associated with convection. This equation is based on the assumption that the ambient temperature in purge and other countercurrent steps does not influence $T_p$. It is also assumed that oxygen is not adsorbed in the top section of the bed. Both these assumptions are questionable, but the equation does serve to highlight that when the nitrogen front is kept well back inside the bed, there is an end zone of the bed that undergoes a reduced temperature swing, and the resulting maximum bed temperature is located well inside the bed.

By contrast, the temperature profile of the low purity run (NaXDLP) shows a constantly increasing temperature profile through the bed, and significant nitrogen loading at the end of the bed. Interestingly, the $\Delta T$ across the adsorption bed for both the high and low purities cases, is similar when the difference in feed temperatures is accounted for.

**Supporting Results:** This difference between NaXDLP and NaXDHP is also evident in the other experimental runs that were undertaken at high purity and low purity conditions - (NaXWLP, NaXWHP), (AA38NaXLP, AA38NaXHP), (AA300NaXDLP, AA300NaXDHP) and (AA300NaXWLP, AA300NaXWHP).

**Conclusion:** The effect of reducing the product flow, and keeping other process variables constant, is seen to exacerbate the 'cold spot'. This potentially has significant implications for oxygen VSA operation. Under certain operating conditions, if purity cannot be achieved, typically the product flow is reduced. This increases the 'cold spot' which may in turn further reduce performance. The VSA control system can respond by further reducing the product flow, and exacerbating the problem.

### 4.4.3 Effect of Purge

In order to achieve product purity, purge is a critical step in oxygen VSA. The extent of purge is an important process variable for controlling the performance which can also effect the CSS temperature profile.

**Model Prediction:** The extent of purge principally adjusts the partial pressures (loading) through the adsorption bed. Qualitatively increasing the amount of purge will increase the extent of nitrogen loading and unloading, and hence increase the temperature depression. This is akin to increasing the pressure window. Howeve the effect of purge is "neven on the bed due to the dispersive nature of the purge composition wave. This makes it difficult to utilise the equations of the simple energy balance developed in Chapter Two, which is based on uniform loading of a single component. Instead it is necessary to resort to full numerical simulation.

**Experiment:** Three experimental runs were conducted with different levels of purge- AA300LSX5, AA300LSX6, AA300LSX10. Each run was conducted with approximately the same overall pressure window, but the extent of purge in Step 5 was varied. Adjusting FCV3 (purge valve) and holding the position of the FCV5 (vacuum valve) constant can vary the amount of purge. The extent of purge can be measured by the change in bed pressure during the purge step. The following table summarises these three experimental runs.

**Result(s):**

**Table 4-12 - Effect of Varying Extent of Purge (AA300LSX)**

| | AA300LSX5 | AA300LSX6 | AA300LSX10* |
|---|---|---|---|
| FCV3 (Purge Valve Position) | 13% | 17% | 0% |
| kPa (Increase) during Purge | 4 | 8 | 0 |
| Feed flow (mmol/cycle) | 3896 | 3976 | 3271 |
| Product flow (mmol/cycle) | 361 | 307 | 332 |
| Oxygen Purity (%) | 85.6 | 92.4 | 45.7 |

* Run AA300LSX10, the purge step was neglected entirely.

Table 4-12 demonstrates, purge plays a critical role in achieving product purity. For similar pressure profiles (~140-40 kPa), the absence of purge (AA300LSX10) substantially reduces the product purity. Figure 4.10 shows that the extent of purge also significantly shapes the

CSS temperature profile. The pressure profile in run AA300LSX10 was slightly smaller (137-43 kPa)

**Figure 4-10**




Run AA300LSX6 has a significantly more pronounced temperature depression than either of the other experimental runs. The temperature swing over the main section of the bed (ignoring the mass transfer zone at the end of the bed) is largest in the Runs AA300LSX6 (6.2 $^{o}$C), AA300LSX5 (5.8 $^{o}$C), and AA300LSX10 (4.5 $^{o}$C). This higher temperature swing and the higher feed flow, demonstrates that more adsorption occurs in Run AA300LSX6.

The product flowrate is higher in Runs AA300LSX5 and AA300LSX10. This is simply because the increased purge gas reduces the pressure in the product tank, and for the same valve Cv less product gas is taken. This is one of the complications in the analysis of causative effects on the CSS temperature profiles. The interrelationship between process variables makes it difficult to isolate single variables for analysis.

**Figure 4-11**

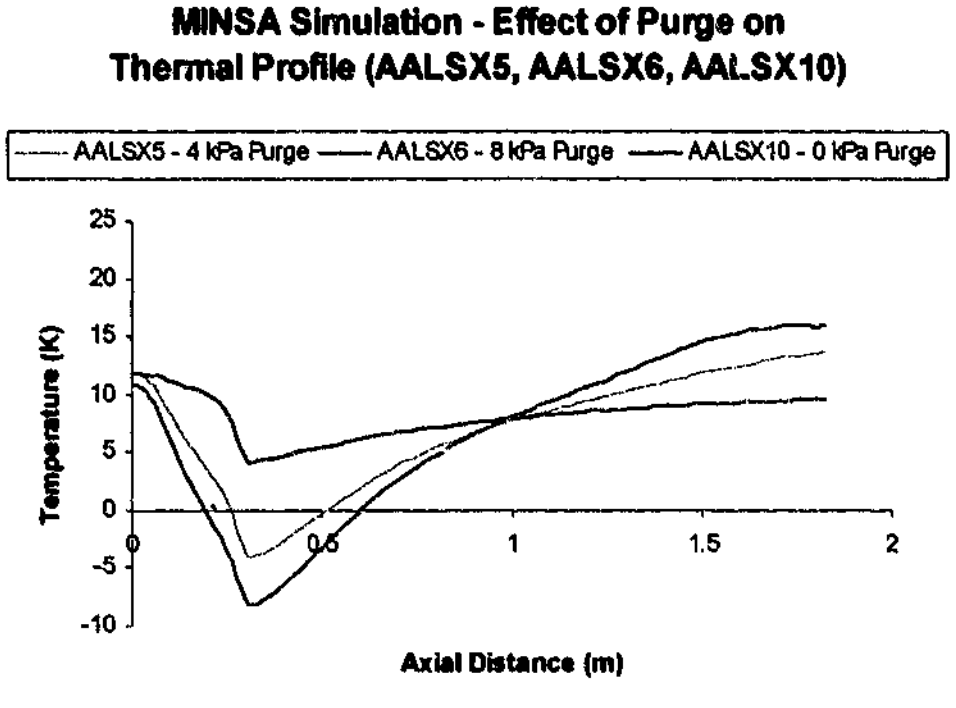


Figure 4-11 shows an excellent comparison between the experimental and MINSA simulation temperature profiles for Runs AALSX5, AALSX6 and AALSX10.

One interesting observation from these temperature profiles in Figure 4-10 is the different location of the temperature minimum. In AA300LSX6 the temperature minimum is located at 300 mm - the interface between the prelayer and the main layer. In AA300LSX5, the temperature at 300 mm and 400 mm are almost identical, and in the case of the least severe temperature profile (AA300LSX10) the temperature minimum is located at 400 mm position.

This observation is quite consistent with the explanation that the minimum bed temperature is just inside the adsorbent layer, not in the inert. Under conditions of desorption, the adsorbent adjacent to the inert will be colder than the inert prelayer. However the thermocouples used to measure the temperature profile measure discrete axial locations, and hence it can appear that the 'cold spot' can shift inside the adsorbent. This can be shown diagrammatically.

**Figure 4-12 – Comparison of Deep and Shallow Temperature Profiles**

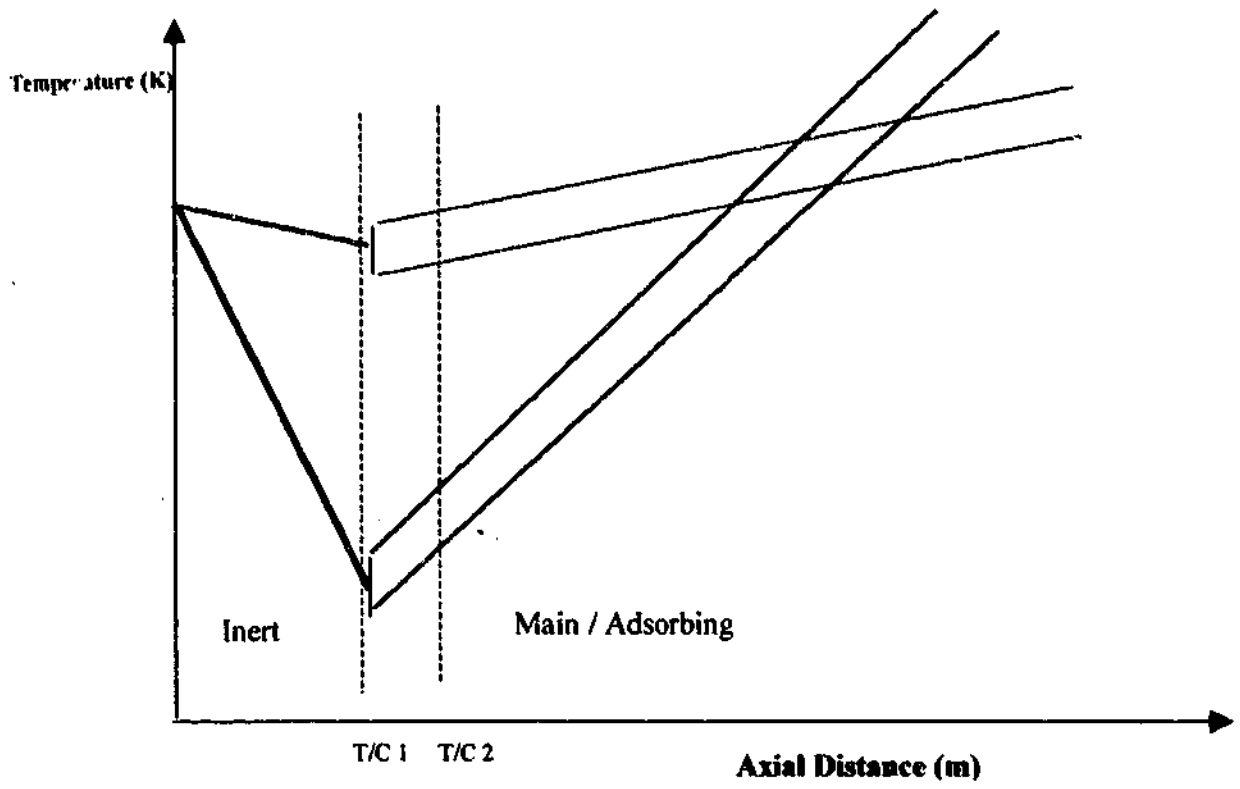


Figure 4-12 shows two different axial CSS temperature profiles. The temperature profile through the prelayer is shown with a thicker line. The temperature swing through the main layer is represented by the end of the adsorption and desorption temperatures. The axial location of two thermocouple positions is shown with a dashed line. Thermocouple 1 is located just inside the inert layer and Thermocouple 2 is located 100 mm into the main adsorbent layer. For the more severe temperature profile (black), it is apparent that T/C 1< T/C 2. However the converse is true for the flatter temperature where T/C 1>T/C 2 at the end of desorption. However in both cases the absolute minimum temperature occurs just inside the adsorbent layer under conditions of desorption (purge and/or evacuation). An experimental complication is that this precise point cannot readily be measured with discrete thermocouples. Settling of the adsorption bed and the possible axial deflection of the thermocouple introduce some uncertainty as to the precise location of the thermocouples.

These observations about the precise location of the temperature minimum apply to the experimental study. For the experiments conducted with a 300 mm inert prelayer, in the case of a severe temperature profile, the minimum temperature was located at the 300 mm thermocouple position. However, for flatter temperature profiles, the temperature minimum was generally located at the 400 mm thermocouple position.

**Conclusion:** It is evident that the extent of purge plays a critical role for oxygen VSA performance and affects the CSS temperature profile. Increasing the extent of the purge reduces the partial pressure at the end of the cycle, and leads to an increasing partial pressure window over the cycle. This has the same effect as increasing the total pressure window, as described in 4.4.1.

One significant limitation with the simple energy balance model is that it is based on one component, and hence effect of purge, and partial pressure (as opposed to total pressure) cannot be described.

### 4.4.4 Effect of Pressure Equalisation (PE)

Recent industrial oxygen VSA cycles have incorporated cocurrent depressurisation and 'top-to-top' pressure equalisation (PE) as steps to improve oxygen recovery. It is worthwhile ascertaining whether PE (top-to-top) influences the axial CSS temperature profile.

**Model Prediction:** As in the case of purge, PE steps have complex effects on mass transfer zones and enthalpy fluxes that cannot be determined with reference to the simple models developed in Chapter Two. MINSA simulation is required to demonstrate the effect of PE on axial CSS temperature profiles.

**Experiment:** In order to assess the effect of the extent of PE on the axial CSS temperature profile, two different experimental Runs (AA300NaX17 and AA300NaX18) were conducted, where the valve position of FCV2 (Pressure Equalisation valve) was varied during the PE step. In addition, in order to maintain the same overall pressure window, control valves FCV1 (Feed Valve) and FCV5 (Vacuum Valve) were adjusted for the different runs. With the exception of the PE step (both receive and provide), the pressure profiles varied by less than ± 0.5 kPa.

**Result(s):** Table 4-13 details the experimental Runs AA300NaX17 and AA300NaX18. In AA300NaX17, there is increased PE leading to improved recovery.

**Table 4-13 - Effect of Varying Extent of Pressure Equalisation (AA300NaX)**

| | **AA300NaX17** | **AA300NaX18** |
|---|---|---|
| Pressure Window (kPa) | 140/32 | 140/32 |
| PE Control Valve (FCV2)% | 25 | 10 |
| ΔP for PE step (kPa) | 13 | 3 |
| Feed Flow (mmol/cycle) | 4622 | 5192 |
| Product Flow (mmol/cycle) | 577 | 592 |
| Oxygen Purity (%) | 85.5 | 85.5 |
| Oxygen Recovery (%) | 48.6 | 44.0 |

From a performance point of view, increasing the extent of PE significantly improves oxygen recovery. Increasing the amount of PE also increases the magnitude of the temperature depression as in evident in Figure 4-13. The temperature difference between the feed and the cold spot is 25.6 $^{o}$C (AA300NaX17) and 22.6 $^{o}$C (AA300NaX18).

**Figure 4-13**

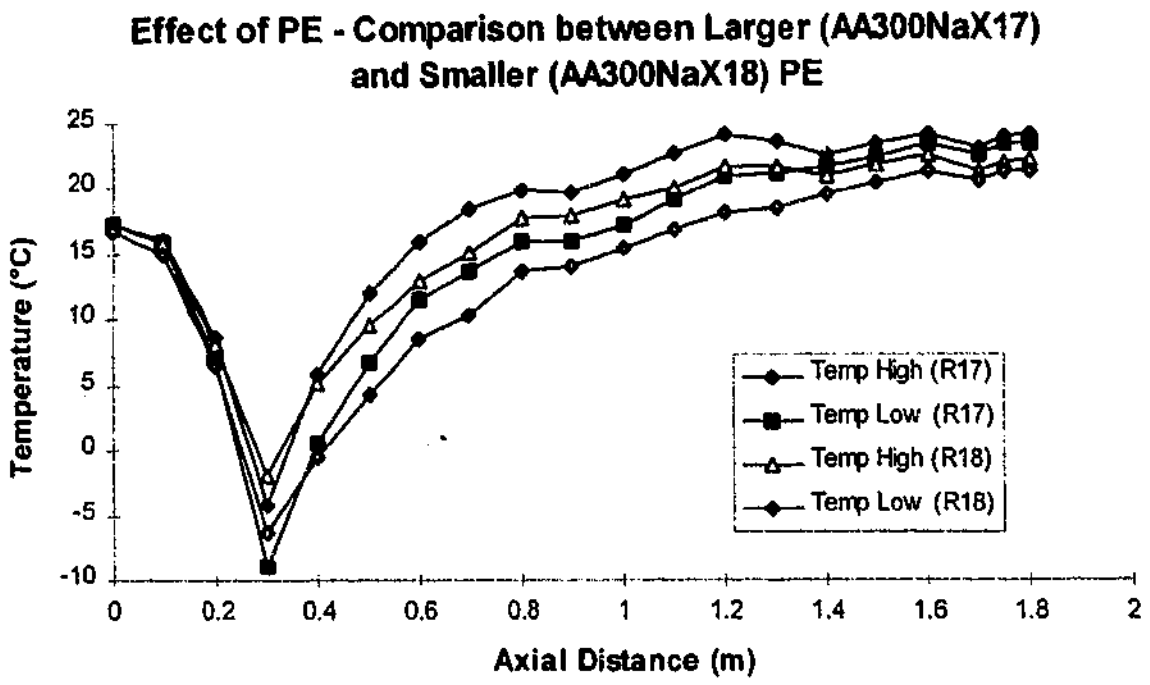


The temperature profiles are very similar, however the severity of the temperature depression is more pronounced for the case with the larger PE (AA300NaX17), and the temperature profile through the main layer is slightly hotter. This same result is evident when both experimental runs are simulated with MINSA. When simulated, the 'cold spot" for AA300NaX17 is –4.2 °C compared to 1.3 °C for AA300NaX18. While both these temperatures are higher than the experimental values, the trend and the difference between the values is the same. The larger pressure equalisation step resulted in a slightly more pronounced temperature profile.

The effect of varying amounts of PE cannot be explained using the simplified energy balance model. However it is possible to offer an explanation as to why the temperature depression is more pronounced for the experimental run with more PE (AA300NaX17). In terms of enthalpy fluxes, the effect of cocurrent depressurisation is to convect forward some hotter gas towards the end of the bed, which has the net effect of increasing the cooling effect over the prelayer. This can be demonstrated by numerical simulation. (Refer Section 4-4-7 on cycle effects). In the case of the smaller PE (AA300NaX18), the feed flow is higher. As has been discussed, a higher feed flow with the same extent of adsorption, will tend to flatten the temperature profile. Both these mechanisms contribute towards a slight difference in the temperature profiles.

Both AA300NaX17 and AA300NaX18 can be reasonably well simulated with MINSA as is detailed in Table 4-14 and Table 4-15.

**Table 4-14- Experimental and MINSA comparison for Run AA300NaX17**

| | Experimental AA300NaX17 | Simulation | Pressure | Experimental (kPa) | Simulation (kPa) |
|---|---|---|---|---|---|
| Feed Gas (mmol/cycle) | 4622±92 | 4683 | Step 1 | 134.2±0.5 | 134.5 |
| Waste Gas (mmol/cycle) | 3981±80 | 4143 | Step 2 | 139.8±0.5 | 139.0 |
| Product Gas (mmol/cycle) | 577±17 | 540 | Step 3 | 100.7±0.5 | 101.7 |
| Product purity (%) | 89.4±0.5 | 89.8 | Step 4 | 88.2±0.5 | 88.1 |
| Oxygen Recovery (%) | 48±2 | 45 | Step 5 | 32.6±0.5 | 33.2 |
| Oxygen Product. (kg/day) | 23±0.6 | 22.0 | Step 6 | 54.0±0.5 | 53.0 |
| Mass Balance Error (%) | 1.4±2 | <1E-6 | Step 7 | 69.3±0.5 | 69.0 |

**Table 4-15 - Experimental and MINSA comparison for Run AA300NaX18**

| | Experimental AA300NaX18 | Simulation AA300NaX18 | Pressure | Experimental (kPa) | Simulation (kPa) |
|---|---|---|---|---|---|
| Feed Gas (mmol/cycle) | 5192±104 | 4848 | Step 1 | 134.3±0.5 | 134.5 |
| Waste Gas (mmol/cycle) | 4595±92 | 4348 | Step 2 | 140.4±0.5 | 139.7 |
| Product Gas (mmol/cycle) | 592±18 | 500 | Step 3 | 101.5±0.5 | 103.8 |
| Product purity (%) | 89.3±0.5 | 89.5 | Step 4 | 98.9±0.5 | 96.9 |
| Oxygen Recovery (%) | 44±2.0 | 40.2 | Step 5 | 32.4±0.5 | 33.4 |
| Oxygen Product. (kg/day) | 23±0.7 | 21 | Step 6 | 52.3±0.5 | 51.8 |
| Mass Balance Error (%) | 0.1±2 | <1E-6 | Step 7 | 58.5±0.5 | 61.7 |

**Conclusion:** Varying the amount of PE and keeping all other process conditions uniform has an effect on the overall temperature profile. However in order to achieve the same product purity, and pressure window, there are limits as to the extent of pressure equalisation. Too much PE will cause a reduction in product purity. Within the range of typical pressure differences for pressure equalisation, there is only a small effect of the overall temperature profile.

### 4.4.5 Recovery - A Useful Process Variable?

As is detailed in Chapter Five, recovery is often used as a performance parameter for oxygen VSA. However, there are some limitations with using recovery as a causative process variable in determination of CSS temperature profiles. The same recovery at CSS can occur for varied process conditions and hence different CSS temperature profiles.

**Model Prediction:** For two component adsorption, in order to determine the CSS temperature profile it is necessary to fix the product purity, and the recovery. Recovery alone cannot be used to predict the temperature profile.

**Experimental:** In the case of AA300LSX6 and AA300LSX7, both runs are subject to the same pressure profile (140-40 kPa) and the same product valve position. The experimental runs only differ with respect to the quantity of purge - AA300LSX6 undergoes more purge.

**Result(s):**

**Table 4-16 - Effect of Recovery on Temperature Profile**

| | AA300LSX6 | AA300LSX7 |
|---|---|---|
| FCV3 (Cv Purge Valve) | 17% | 13% |
| Recovery (%) | 32.4 | 32.8 |
| Product Purity(%) | 96.6 | 88.6 |
| Product Flow (mmol/cycle) | 307 | 331 |
| Feed Flow (mmol/cycle) | 3977 | 3888 |

**Figure 4-14**

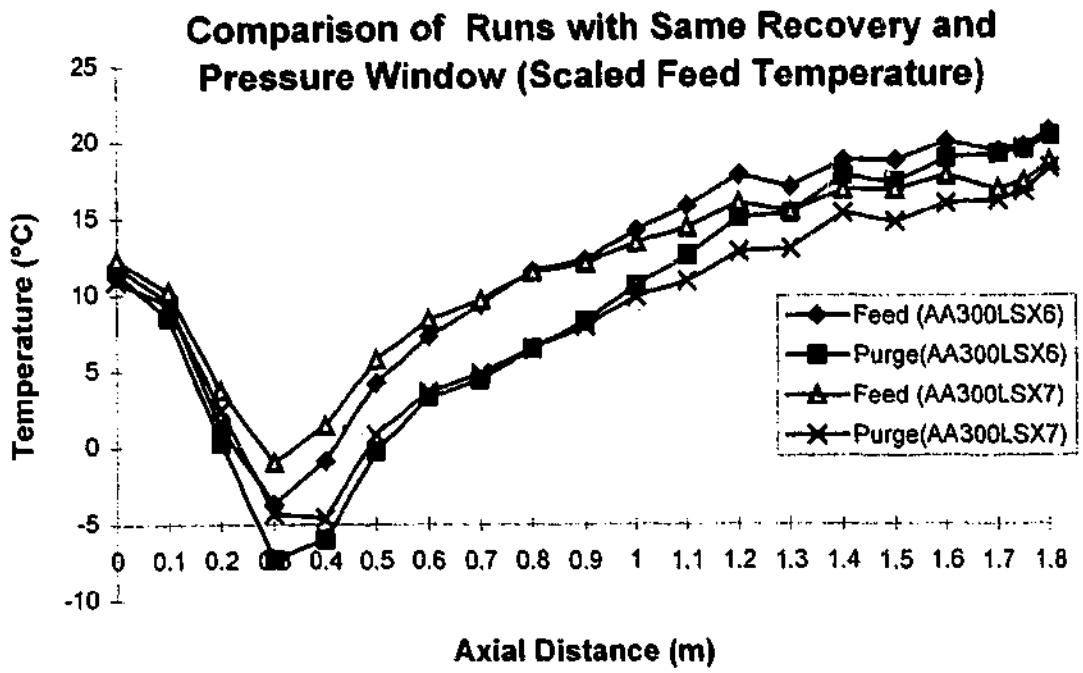


In Figure 4-14, the feed gas temperatures are scaled to enable more accurate comparison between the two different experimental runs. The minimum temperature is 4 $^{o}$C lower in the higher purity case (AA300LSX6), and the top of the bed is 2 $^{o}$C hotter.

These thermal profiles are similar, but it is evident that the same recovery and pressure window does not necessitate the same axial temperature profile. This is due to the fact that different process conditions, resulting in different convective flows and cyclic temperature swings, can have the same recovery.

**Supporting Results:** A more extreme example of the case where two different experimental runs can have different temperature profiles, but the same oxygen recovery, is evident in Runs AA300LSX8 and AA300LSX10. The pressure profiles varied slightly between these two experimental Runs - AA300LSX8 (140-41 kPa) and AA300LSX10 (138-44 kPa)

**Table 4-17 - Effect of Recovery on Temperature Profile (AA300LSX)**

| | AA300LSX8 | AA300LSX10 |
|---|---|---|
| FCV3 (Cv Purge Valve) | 17% | 0% |
| Recovery | 21.9 | 23.0 |
| Product Purity(%) | 98.6 | 52.2 |
| Product Flow (mmol/cycle) | 200 | 332 |
| Feed Flow (mmol/cycle) | 3906 | 3271 |

**Figure 4-15**

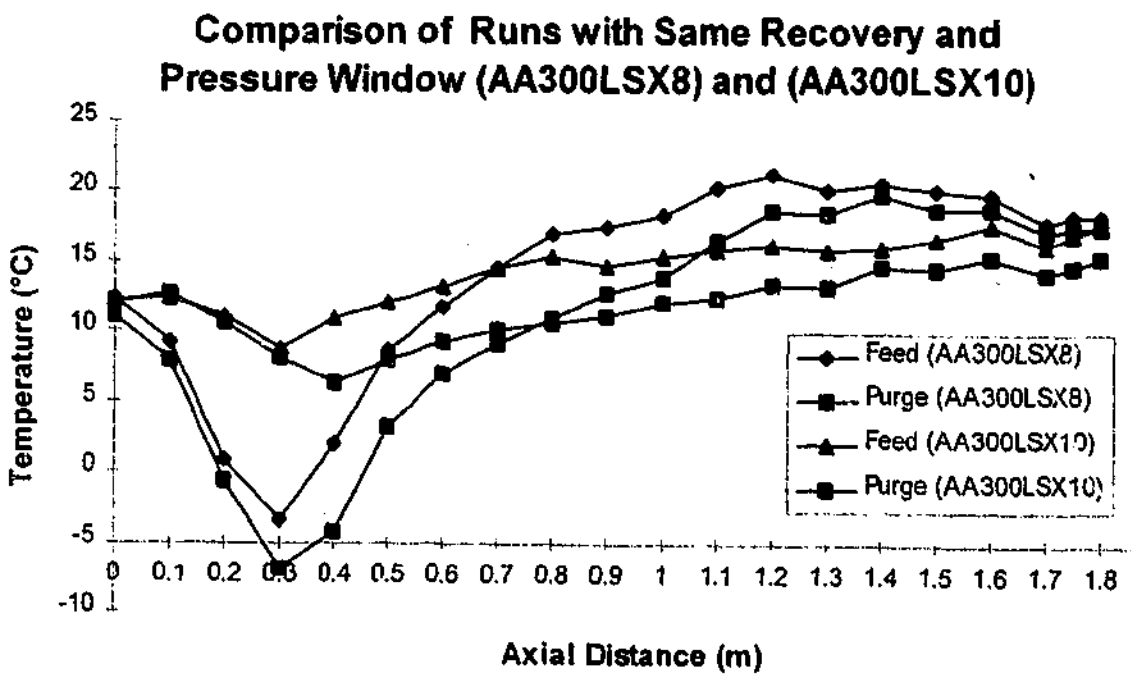


Figure 4-15 clearly demonstrates that recovery without reference to product purity is not a useful variable for analysing CSS temperature profiles. This also shows that in the high purity case (AA300LSX8) there is little adsorption at the end of the bed, and the characteristic temperature maximum is located well inside the bed.

**Conclusion:** Oxygen recovery without reference to purity does not assist in predicting the temperature profile.

### 4.4.6 Effect of Feed Temperature

There are several environmental conditions that can impinge on oxygen VSA performance, most importantly - barometric pressure, humidity, and ambient temperature. The ambient temperature affects the temperature of the feed gas entering the adsorption bed after compression, and this can have a significant effect on the CSS temperature profile.

**Model Prediction:** Both the simple energy balance model and the work of Collins, suggest that changing the feed temperature will lead to a vertical translation of the axial temperature gradient, depending on the feed temperature.

**(2- 34)**

$$\overline{T_2} = T_f - \frac{E}{F - W + \left(\frac{C_{pg} F W}{2 m_p C_{sp}}\right)}$$

**Experiment:** One difficulty with this experiment is that there was no feed heater or temperature control on the feed line. However, diurnal and seasonal variation in the feed temperature did occur, enabling some investigation of the effect of the feed temperature on the axial CSS temperature profile. Subsequent modifications to the oxygen VSA unit have included the addition of a feed heater with temperature control.

**Result(s):**

**Figure 4-16**

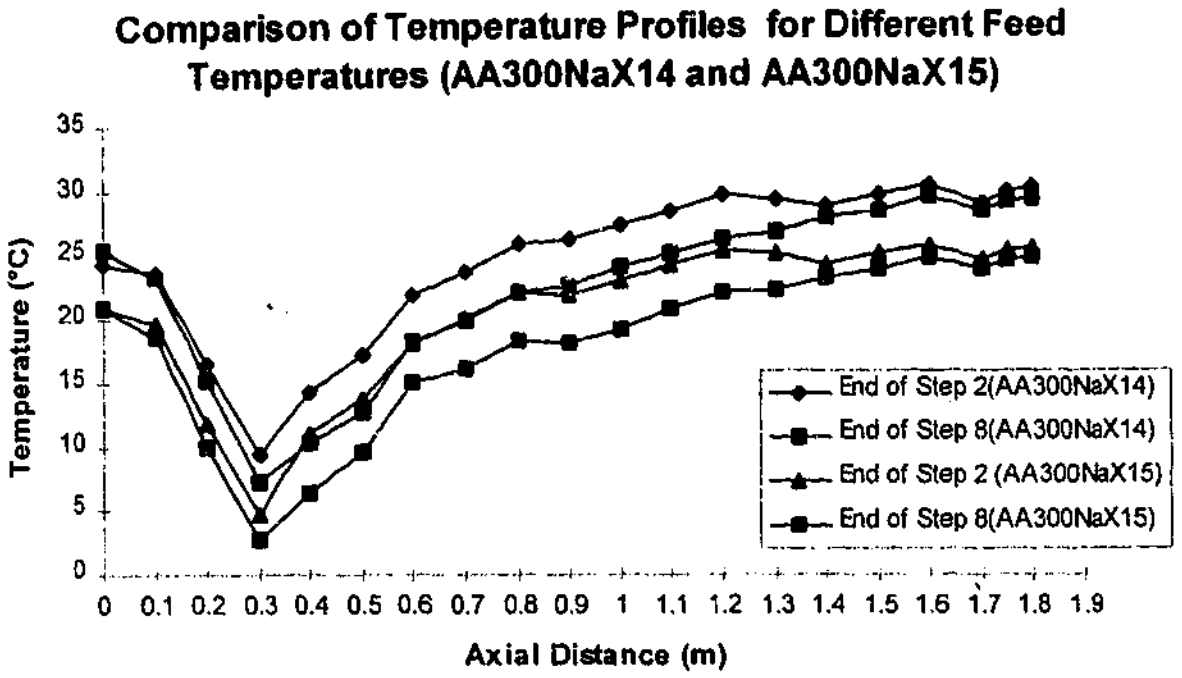


Figure 4-16 highlights that for a 5 °C difference in the feed temperature, the axial temperature profile is uniformly displaced by the same margin. This is consistent with the simple energy balance and Collin's earlier observations.

**Supporting Results:** The effect of the vertical translation of the axial CSS temperature based on the feed gas temperature was also evident in experimental Runs PuAA400NaX1, PuAA400NaX2 and PuAA400NaX3 (Wilson, et.al., 1998).

The absence of temperature control on the feed line limited the scope of the investigation of the effect of the feed temperature on axial CSS temperature profile and the overall VSA performance. Over the limited temperature range explored, the simple model correctly predicted the behaviour. However, this model ignores the temperature dependence of the isotherms. Over a larger range of feed temperatures, it is probable the feed temperature will not simply lead to a vertical translation of the temperature profile, but will also alter the separation performance. This effect can be investigated with MINSA.

It is possible to envisage three different VSA units operating in very different climatic conditions - Calgary (Canada), Kalgoorlie and Melbourne (Australia). The assumed ambient temperature in Calgary is –20 °C, Kalgoorlie is 40 °C, and Melbourne is 20 °C. Adiabatic

feed blower compression is assumed to increase the feed gas temperature by 20 °C. While, in practice, either pre-heating or pre-cooling might be utilised to mitigate these harsh climatic variations, it is interesting to simulate these different cases.

Figure 4- 17 highlights that the axial temperature profiles are translated vertically depending on the feed temperature. However, it is also evident that the temperature difference between the feed temperature and the 'cold spot' is most pronounced in the Calgary case (35°C), compared to (18.4 °C) Melbourne, and (13.2 °C) Kalgoorlie. This is due to the temperature dependency of the isotherm, and the different feed temperatures alter the performance significantly. For the same boundary conditions (valve settings and tank pressures) there was marked variation in the product flow and purity. These differences affect the extent of the 'cold spot'.

**Figure 4-17**

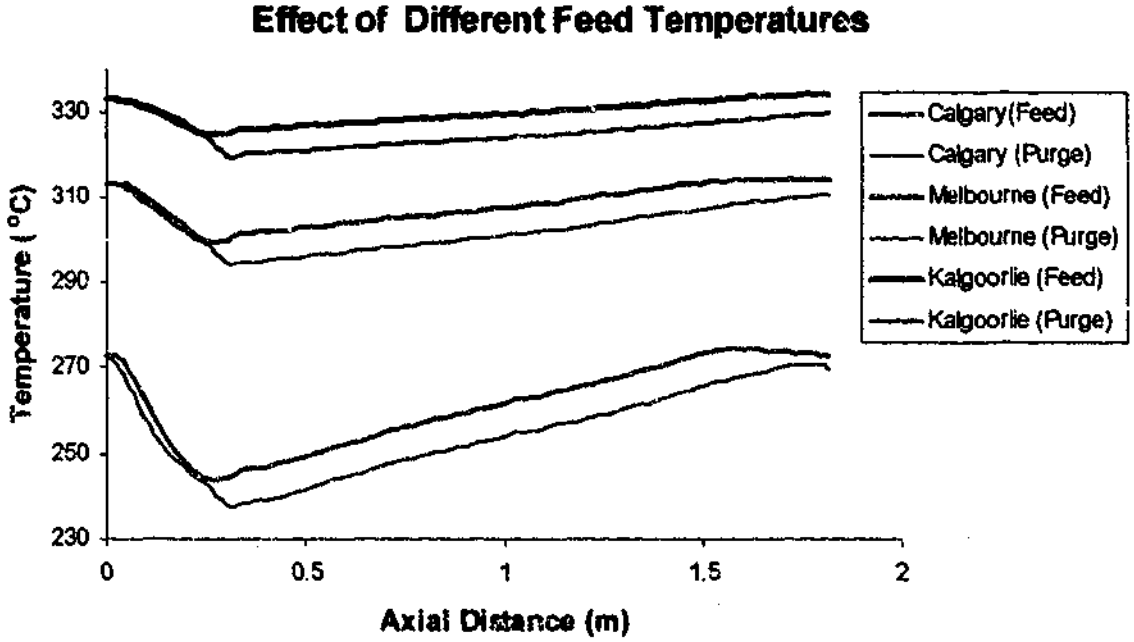


This case demonstrates a significant assumption with the simple energy balance model, which ignores the temperature dependence of the isotherms. In practice, the hotter feed gas results in less adsorption, and the difference between the gas feed temperature and the 'cold spot' is reduced, as this example shows. The approximation that the temperature profile is only shifted axially is essentially only valid over a small temperature range.

**Conclusion:** Adjusting the feed temperature is a simple approach to altering the axial CSS temperature profile. This was patented by Collins and has been reported by others. However preheating or precooling requires additional equipment and cost.

### 4.4.7 Effect of Cycle Type

One area of significant innovation in oxygen VSA has been cycle development. The trend to reduce the number of adsorption beds, and introduce new steps, such as cocurrent depressurisation, has necessitated the development of new cycles. Some of these new cycles have obvious effects on the thermal profiles in oxygen VSA. For example, in a one-bed cycle with purge from the product tank, the temperature of the gas (the temperature boundary condition) entering the top of the bed is fixed at ambient temperature. This contrasts with a bed-to-bed purge step in a two bed cycle, where this boundary condition is not fixed. Other effects are less obvious, but it is clear the cycle type will affect the convective fluxes and heats of adsorption, thus altering the axial CSS temperature profiles.

**Experiments:** The effect of cycle type can be demonstrated by running two different experiments with the same pressure windows ($P_{high}$ and $P_{low}$) and product purity, but with different cycles. A two bed 60 second cycle (with PE) (AA300NaX13) was compared with a 56 second single bed cycle (B1AA300NaX3).

**Model Prediction:** The simple energy balance equations developed in Section 2-4 contain a parameter $\alpha$. This parameter is a very rough approximation to recognise the effect of cycle type on axial CSS temperature profile. However, the complication with this parameter is that it requires an estimation of the extent of flow from top-to-top of the adsorption beds. In order to demonstrate this effect an estimate of $\alpha$ can be obtained, based on typical flows derived from MINSA. A typical value for $\alpha$ for the two bed cycle is 0.35.

**Result(s):**

Figure 4- 18 highlights that the introduction of top-to-top purge and PE leads to a more severe temperature profile than a one bed cycle, for the same pressure profile and product purity.

**Figure 4-18**

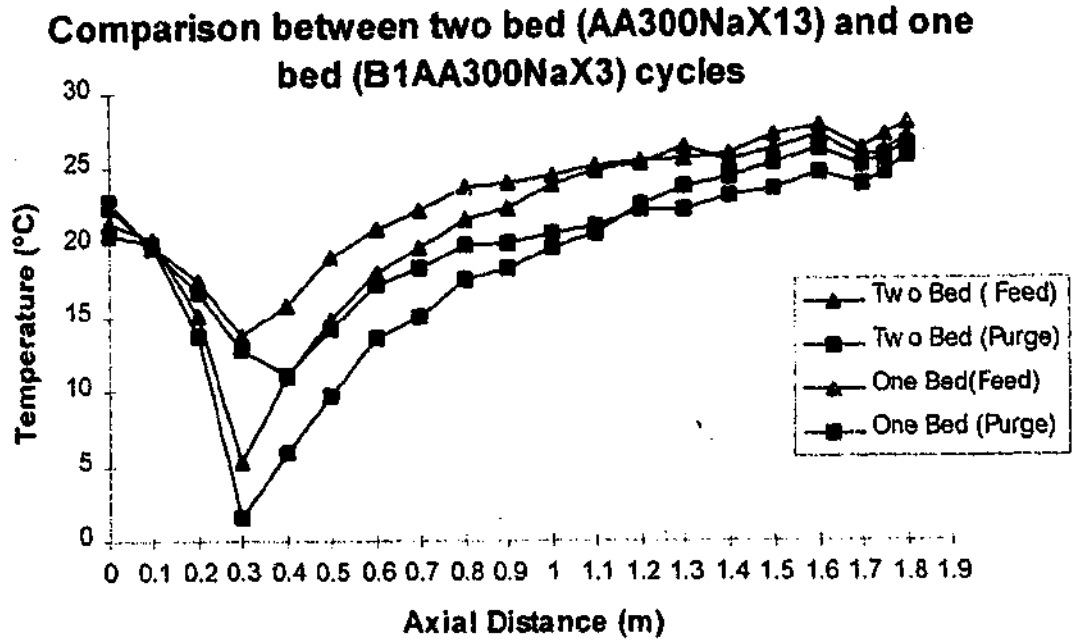


**Table 4-18 – Performance comparison of One Bed and Two Bed**

| | **B1AA300NaX3** | **AA300NaX13** |
|---|---|---|
| Number of Beds and Cycle Time | 1 ( 56 sec) | 2 (60 sec) |
| Average Pressure Profile (kPa) | 133.9/138.2/ 33.0/36.3 | 134.2/140.4/107.2/96.7/ 51.3/34.0/50.6/64.2 |
| Feed (mmol/cycle/bed) | 3321 | 2375 |
| Product (mmol/cycle/bed)@ Oxygen(%) | 251@83.0% | 307@83.0% |
| Oxygen Recovery (%) and BSF(kg/TPDc) | 27.3 (807) | 46.6 (725) |
| Average Feed Temperature($^{o}$C) | 22.0 | 20.6 |
| Max Product Temperature($^{o}$C) | 28.1 | 28.2 |
| Cold Spot ($^{o}$C) | 10.7 | 1.5 |
| $\Delta$T (Feed - Cold Spot) ($^{o}$C) | 11.3 | 19.1 |
| $\Delta$T (Max Prod. – Minimum) ($^{o}$C) | 17.4 | 26.7 |

The pressure windows for the two cycles are not identical. The pressure window for the two bed cycle is 2 kPa higher, and 1 kPa shallower, than the one bed cycle. The combined effect is a 1% difference in the width of the pressure windows.

From a process engineering point of view, the most significant feature of these two cycles is the far higher oxygen recovery of the two bed cycle. This demonstrates the value of bed-to-bed steps and the benefit of cocurrent depressurisation. Chapter Five details the effect of higher oxygen recovery on lower power costs and capital costs.

Figure 4-19 demonstrates that the temperature profile is more severe for the two bed cycle, and qualitatively this makes sense. However the simple treatment of the bed-to-bed steps through the $\alpha$ parameter is not adequate, as is shown in Table 4-19.

**Table 4-19 – Temp. Profiles for One Bed and Two Bed Cycles (Simple Energy Balance)**

| | **B1AA300NaX3** | **AA300NaX13** |
|---|---|---|
| Average Cyclic Temperature Swing over main adsorbent layer (°C) | 3.5 | 3.4 |
| Feed Temperature (°C) | 22.0 | 20.6 |
| Cold Spot (°C) | 5.7 (10.7) * | 7.0 (1.5)* |
| Product Temp (°C) | 28.8 (27.2)* | 22.0 (28.2)* |

*Experimental values are in brackets

Table 4-19 shows that the simple energy balance equations do not adequately account for the effect of the bed-to-bed steps on the severity of the temperature profile. It is clear that if all other process variables are held constant, the effect of $\alpha$ is to increase the extent of the temperature depression. However, other parameters also vary between the two cycles. The feed and product flows vary, and these all impinge on the temperature profile. This example shows the limitations of the simple energy balance approach, and highlights that cycle effects cannot be accounted for using this approach. In such cases it is necessary to rely on numerical techniques.

This example also demonstrates that the effect of cycle is difficult to isolate because different cycles necessitate different feed flows, purge rates and recoveries, even if the pressure profile is held constant. In order to attempt to isolate the effect of the cycle on temperature profiles, it is necessary to consider a much simpler cycle. Consider a single component gas being fed into a two layered (AA/LiLSX) single adsorption bed. The bed is subject to a three step cycle (feed

repressurisation, feed, and evacuation) over a fixed pressure window (1.4-0.4 bar). The cycle contains no cocurrent depressurisation and purge. An alternative two bed cycle can be devised with the same pressure window, and product removal rate, but this cycle contains cocurrent depressurisation and purge. Obviously, for a single component system, a purge step has no practical purpose. These two different cycles can be run on MINSA to demonstrate the effect of cocurrent depressurisation on the CSS thermal profile.

**Table 4-20 – MINSA Simulation – One Component Feed – One Bed and Two Bed Cycles**

| | One Bed | Two Bed with Co-current depress. |
|---|---|---|
| $P_{high}/P_{low}$ | 1.4/0.4 | 1.4/0.4 |
| Feed/Bed/Cycle (mmol) | 4431 | 4477 |
| Product/Bed/Cycle (mol) | 380 | 385 |
| Co-current Depress/Bed/Cycle (mmol) | 0 | 403 |

While the overall pressure profiles and flows are very similar for the one bed and two bed cases, the presence of the bed-to-bed cocurrent depressurisation has a marked effect on the overall temperature profile, as is demonstrated in Figure 4-19.

Figure 4-19

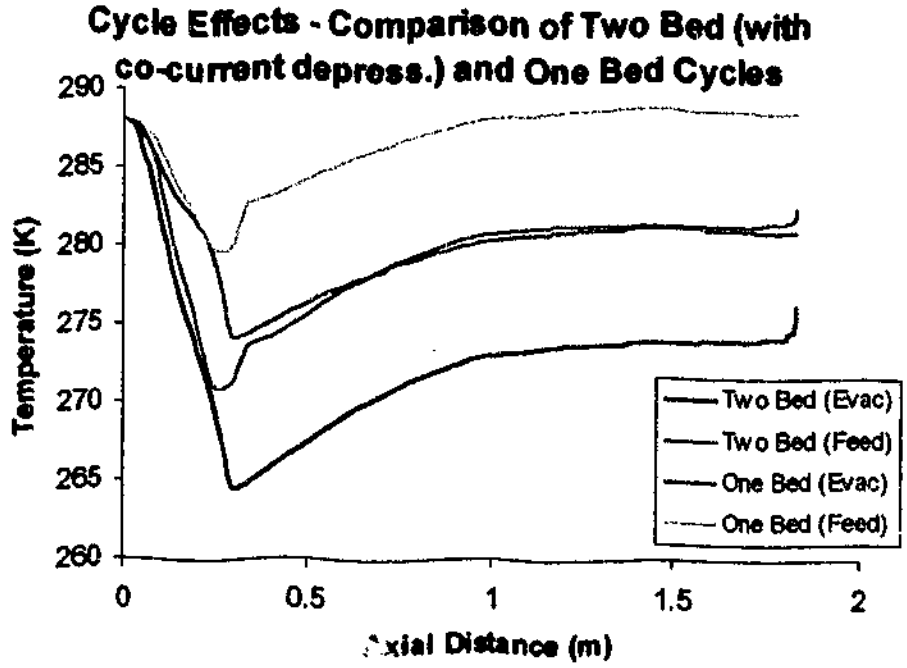

This result is consistent with the experimental data presented in Figure 4-18. The effect of cocurrent depressurisation (bed-to-bed connection) is to increase significantly the magnitude of the 'cold spot'. This is expected qualitatively, but the magnitude of the difference cannot be accounted for by the proposed α parameter described in Section 2.4.5. The simple treatment of the cycle effect predicts, in this case, a minor difference between the two temperature profiles, but the MINSA simulation shows the effect to be far more substantial. In conclusion, it is apparent that the simple energy balance model is not capable of predicting the impact of cycle effects on the CSS temperature profiles.

Aside from the extent of the temperature depression, the temperature profiles are very similar, and are different to the typical two component profiles. In the case of a single component there is no composition wave and leads to uniform loading over the main adsorbent layer.

**Supporting Results:** Run AA300NaX5 and Run B1AA300NaX7 show very similar results. Thus for the same $P_{high}$ and $P_{low}$, and the same product purity, the two bed cycle (with co-depressurisation) displayed a far more severe temperature profile than the one bed cycl

**Conclusion:** Cycle type can have a marked effect on the CSS temperature profile. However, the effect cannot readily be explained by the simple energy balance equations. Numerical simulator tools are required.

## 4.5 Column Effects

### 4.5.1 Effect of Axial Conduction and Heat Loss - Metal Walled Columns

In Section 3.1 consideration was given to the impact of the adsorption column on the axial CSS temperature profile. Heat loss, axial conduction along the wall, and the wall acting as a thermal sink and source over a cycle were all identified as issues that impinge on the CSS temperature profile.

**Model Prediction:** In the case of an uninsulated metal walled column, there will be increased heat exchange with the environment and axial conduction of heat along the walls. Both these effects will flatten the axial CSS temperature profile and reduce the extent of the 'cold spot'.

**Experiment :** A series of experimental runs were undertaken using the metal walled columns described in Section 3.3.

**Result(s):** Experimental Run MAACAX 1 describes a multilayered bed with 200 mm of activated alumina followed by 1.7 m of CaX (VSA2), with a 2 bed cycle and pressure profile of 132-44 kPa, and a product purity of approximately 90%.

**Figure 4-20**

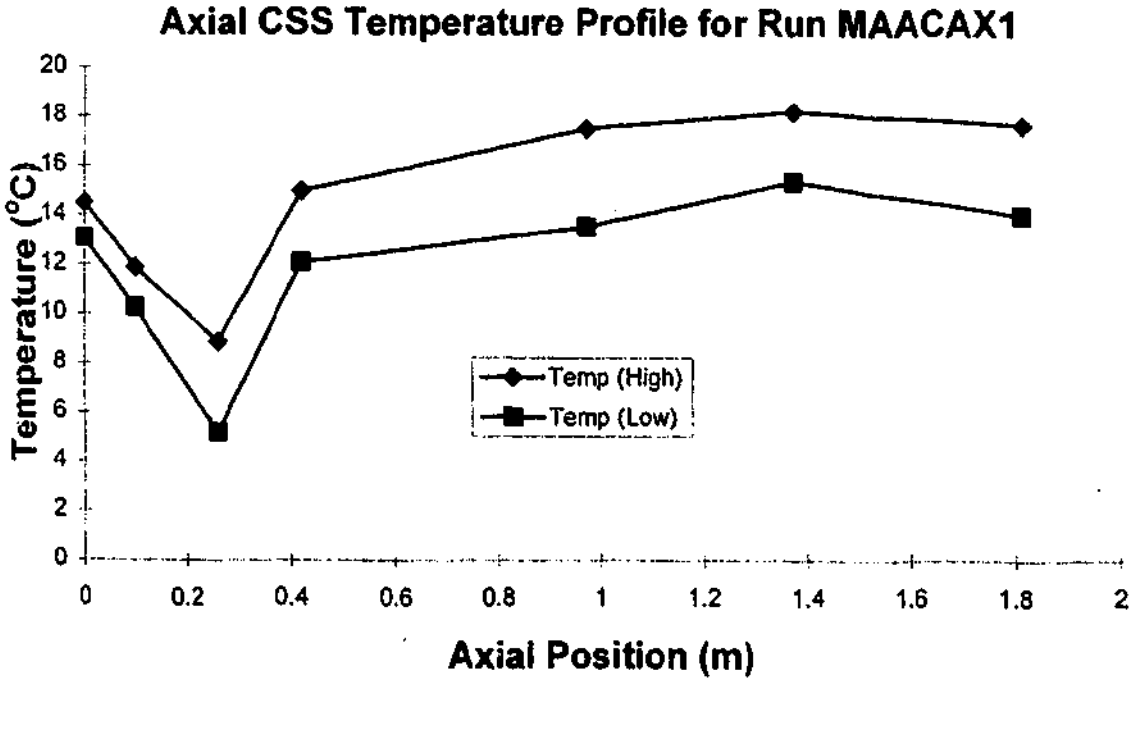

This axial CSS temperature profile presents only the maximum and minimum temperatures over a cycle, rather than the end of step temperatures. As expected with the use of the metal walled column, the magnitude of the 'cold spot' is reduced significantly, and temperature profile through the main bed is relatively flat. For a similar pressure profile, with the polyurethane columns, the minimum temperature in the bed was -16 °C (PuAANaXVSA610). However there were some differences between these two runs. The prelayer was thicker in the polyurethane bed, and different forms of CaX were used (VSA2 in the metal walled columns and VSA6 in the polyurethane column).

This experimental run was also simulated numerically, and the results reported in Webley et.al. (2000). Table 4-21 reports both the experimental and MINSA CSS results.

**Table 4-21 - Comparison of Numerical and Simulation Results - MAACaX1**

| | Experimental | Sim. | | Experimental Pressure | Sim. |
|---|---|---|---|---|---|
| Feed Gas (mmol/cycle) | 3990±30 | 4350 | Step 1 | 125.5±1.3 | 127 |
| Waste Gas (mmol/cycle) | 3624±30 | 3982 | Step 2 | 131.7±1.5 | 131.8 |
| Product Gas (mmol/cycle) | 401±10 | 368 | Step 3 | 107.5±0.8 | 108.7 |
| Oxygen purity (%) | 89.5±0.8 | 89.7 | Step 4 | 88.1±1.6 | 88.5 |
| Oxygen Recovery (%) | 41.1±1.2 | 34.5 | Step 5 | 45.2±0.5 | 45.3 |
| Oxygen Product. (kg/day) | 16.5±0.5 | 15.2 | Step 6 | 54.1±1.3 | 55.5 |
| Mass Balance Error (%) | 0.96 | <1e-6 | Step 7 | 72.7±1.1 | 74.1 |

This is reported as a 7 step cycle, rather than an 8 step cycle. The evacuation step has been compressed to one step (Step 5), whereas in the PLC logic (experimentally) it is treated as two steps.

Table 4-21 demonstrates a reasonable correlation between the experimental and simulated CSS data. Slightly higher experimental product flow (8.5%) is the major discrepancy between the two results. The temperature profiles are similar. The minimum temperature at the interface for the MINSA run is 0.0 °C, compared to 5.1 °C for the experiment. This discrepancy is probably due to the absence of a wall model in MINSA to accurately model the heat loss to the wall, and the axial conduction of heat along the metal wall. This aside, both demonstrate the substantial effect of a metal walled column on the axial CSS temperature profile, when the same cycle is run with MINSA, and the bed is modelled as adiabatic, the temperature minimum in the bed is -15 °C.

**Supporting Results:** All other metal walled runs displayed a reduced temperature cold spot, and a flatter temperature profile through the main adsorbent layer (MAACaX2 and MAACaX3).

**Conclusion:** The use of a metal walled column reduced the extent of the temperature depression and flattened the temperature profile through the adsorption bed.

### 4.5.2 Effect of Polyurethane Column vs. PVC Column

A motivation for part of this study was to construct an adiabatic adsorption column. Due to difficulties previously described, the polyurethane columns were used for only limited experimentation. However some experiments were conducted to enable comparison between the thermal profiles in the polyurethane columns and the PVC columns.

**Model Prediction:** Based on heat transfer models, it is predicted that the temperature profiles evident in polyurethane columns will be more severe than the PVC columns, due to reduced heat loss and reduced axial conduction.

**Experimental:** The slightly different internal diameter of the polyurethane (100 mm) and the PVC (103 mm) columns leads to slightly different masses of adsorbent in the columns and different end of bed voidages. In order to achieve the same mass fluxes and pressure profiles, the valve positions needed adjustment.

**Result(s):**

**Table 4-22 - Comparison of Temperature Profiles for PU and PVC Columns**

| | PULSX4 (Polyurethane) | AA300LSX1 (PVC) |
|---|---|---|
| Inlet Temperature (°C) | 13 | 11.1 |
| Temperature @ 400 mm (°C) | -12.6 | -10.1 |
| ΔT(feed –T@400mm) (°C) | 25.6 | 21.2 |
| Maximum Temperature (°C) | 34.5 | 24.2 |

**Table 4-23 - Comparison of Temperature Profiles for PU and PVC Columns**

| | PULSX3 (Polyurethane) | AA300LSX4 (PVC) |
|---|---|---|
| Inlet Temperature (°C) | 14.1 | 12.5 |
| Temperature @ 400 mm(°C) | -6.2 | -3.1 |
| ΔT(feed –T@400mm) (°C) | 20.3 | 15.6 |
| Maximum Temperature (°C) | 30.9 | 23.4 |

Both these cases demonstrate that the temperature profile is more severe for the polyurethane columns than the PVC columns. The difference between the feed temperature and the temperature at the axial position of 400 mm, is approximately 5 °C greater with the

polyurethane columns. Furthermore the maximum temperatures in the polyurethane columns are significantly hotter. This demonstrates that heat exchange with the environment will reduce not only the extent of the 'cold spot', but also reduce the severity of the profile through the entire bed.

**Conclusion:** These examples confirm that the polyurethane columns are significantly more 'adiabatic' than the PVC columns.

## 4.6 Adsorbent and Prelayer Parameters

In addition to operational effects, the axial temperature profiles in oxygen VSA can be significantly affected by the properties of the main layer and prelayer adsorbent properties.

### 4.6.1 Effect of Main Layer Adsorbent

The development of lithium based adsorbents has been the major innovation in industrial oxygen VSA over the last five years. LiLSX adsorbents are significantly reducing specific power and BSF numbers (typically reduced 33-50% compared to calcium and sodium based adsorbents). The BSF is the Bed Sizing Factor (kg adsorbent / TPDc Oxygen) and is the reciprocal of the sieve or adsorbent productivity.

These new sieves have significantly higher loading capacities causing larger cyclic temperature swings. This will affect the CSS temperature profile.

**Model Prediction:** The simple energy balance method results in the following equation to determine the extent of the temperature depression.

**(2-48)**

$$\overline{T2} = T_f - \frac{Pr\,\Delta H(m_p C_{sp})(WCm_m)^2(1+\alpha)}{\left(4\,Pr\,m_m C_{sm} + (F+Pr)(WCm_m)C_{pg}\right)\left(2\,Pr\,m_p C_{sp} + C_{pg}F(WCm_m)\right)}$$

It is evident from this equation that as the heat of adsorption (ΔH) increases, the extent of the temperature depression increases linearly. However specific adsorbents are characterised not only in terms of the ΔH, but importantly the quantity of adsorption that occurs, i.e. the absolute heat generation for a given pressure swing. For example, VSA6 and LiX have similar heats of adsorption (ΔH), but VSA6 has a lower loading capacity than LiX for the same pressure window and product flow. It is expected that the temperature depression would be more pronounced for LiX than VSA6. The same argument can be applied when comparing LiX and NaX. However in this case both the heats of adsorption and loading will be higher with LiX.

**Experiment:** In order to demonstrate the effect of the main layer adsorbent on the temperature profile, experiments were conducted with the same prelayer, prelayer thickness, same cycle and pressure window, but the main adsorbent layer was varied. In one case, LiLSX was used as the main adsorbent, in the other case NaX. Since the pressure profile is held constant, the flows vary considerably between the NaX and LiLSX adsorbents, due to the higher loading capacity of the LiLSX. Two experimental runs were conducted with the NaX. In Run B1AA300NaX1, the product purity was adjusted to be the same as the LiLSX. In Run B1AA300NaX2, the product flow was adjusted to be the same as the LiLSX case.

**Result(s):**

**Figure 4-21**

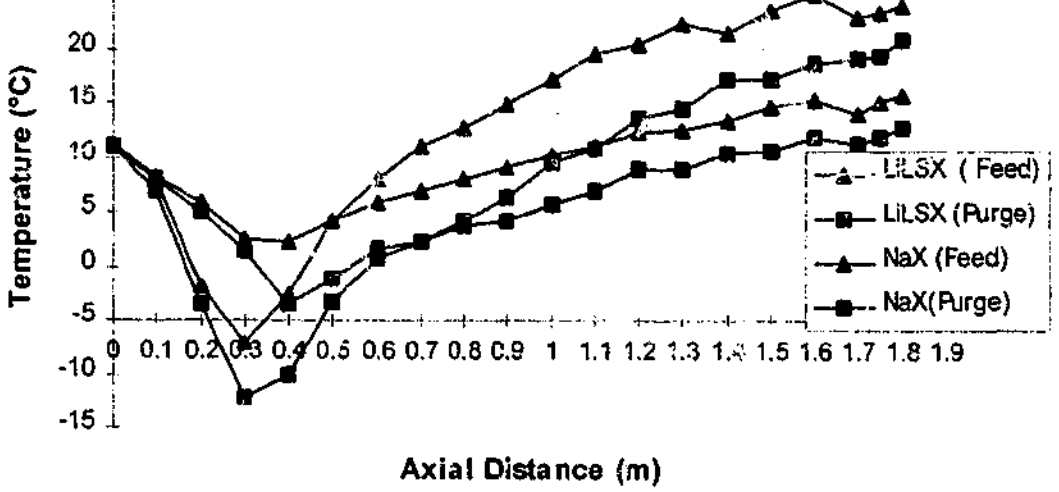


In Figure 4-21, the temperature profile of B1AA300NaX2 is shifted vertically so the feed temperature of the two experimental runs is the same (11.1 °C). This aids comparison between the data sets. Figure 4-21 confirms that the 'cold spot' and overall temperature profile are more severe with the LiLSX adsorbent.

Table 4-24 reports the experimental results for Runs B1AA300NaX1, B1AA300NaX2 and AA300LSX1. The simple energy balance can be applied to predict the temperature profile for these three experimental runs.

**Table 4-24 - Comparison between different types of main adsorbent layers**

| | B1AA300NaX1 | B1AA300NaX2 | AA300LSX1 |
|---|---|---|---|
| Adsorbing Layer | NaX | NaX | LiLSX |
| Pressure Profile (kPa) | 133.7/138.2/ 30.4/34.5 | 135/140/ 30.8/34.4 | 134.6/140.6/ 30.4/34.0 |
| Feed (mmol/cycle) | 3505 | 3709 | 4647 |
| Product (mmol/cycle) | 229 | 480 | 440 |
| Oxygen Purity (%) | 89.5 | 62.13 | 90.6 |
| Average Feed Temperature(°C) | 20.6 | 21.5 | 11.1 |
| Max Product Temperature(°C) | 27.2 | 28.0 | 24.1 |
| Average Temp. Swing (°C)* | 5.1 | 4.45 | 7.9 |
| Cold Spot (°C) | 6.8 | 9.9 | -12.3 |
| ΔT (Feed - Cold Spot) (°C) | 13.8 | 11.6 | 23.4 |
| ΔT (Max Prod. – Cold Spot) (°C) | 20.4 | 18.1 | 36.4 |

* Temperature swing determined between 0.3 – 1.3 m length of bed. Not including MTZ.

One of the major complications with the technique of simple energy balance is the estimation of the appropriate heat of adsorption. In this study, a two component dual site Langmuir isotherm is applied, resulting in four specific heats of adsorption. In some cases where the heats of adsorption are significantly different between oxygen and nitrogen, and between the two sites, it is difficult to select a characteristic heat of adsorption. In this case, to overcome this limitation, the heat of adsorption was adjusted, so that, the average experimental cyclic temperature swing between feed and purge, was the same used for the simple energy balance calculations.

**Table 4-25- Simple Energy Balance Comparison between Different Main Layers**

| | B1AA300NaX1 | B1AA300NaX2 | AA300LSX1 |
|---|---|---|---|
| Feed Gas (mmol/bed/cycle) | 3505 | 3709 | 4647 |
| Loading (F-Pr) (mol/bed/cycle) | 3280 | 3220 | 4207 |
| Average Cyclic Temperature Swing over main adsorbent layer (°C) | 3.8 | 4.0 | 6.8 |
| Feed Temperature (°C) | 20.6 | 21.5 | 11.1 |
| Cold Spot (°C) | 0.5 (6.8) | 10.2 (9.9) | -13.7 (-12.3) |
| Product Temp (°C) | 29.3 (27.2) | 23.9 (28.0) | 20.6 (24.1) |
| ΔT (Feed - Cold Spot) (°C) | 20.1 (13.8) | 11.3 (11.6) | 24.8 (23.4) |
| ΔT (Product – Cold Spot) (°C) | 28.8 (20.4) | 13.7 (18.1) | 34.4 (36.4) |

*Bracketed are the experimental values.

The simple energy balance predicts the trend of the temperature profiles. The results are very good for B1AA300NaX2 and AA300LSX1, but not as good for B1AA300NaX1.

**Supporting Results:** The severity of the temperature depression was less in all cases for the one bed runs, with NaX as the main adsorbent compared with LiLSX for the same pressure window. (1BAA300NaX3, 1BAA300NaX3)

One complication in the analysis of the effect of adsorbent properties on the extent of the depression, is that different adsorbents have different heats of adsorption and different isotherms, which leads to a different balance of convection and cyclic temperature swings. It is impossible in reality to isolate the effect of heats of adsorption, since other variables are altered. However this is easy to achieve with MINSA. In MINSA the adsorptive properties of a fictitious adsorbent can be fixed and independent of temperature, but the heat of adsorption varied. This enables isolation of the effect of heat of adsorption on the CSS temperature profile. Under such conditions, the flows and performance should be almost independent of the heat of adsorption selected, except for a minor effect on the gas properties. However the temperature profile should differ markedly. The simple energy balance model asserts the following relationship.

$$\overline{T_2} = T_f - G\ \Delta H \qquad (4\text{-}2)$$

where G is a function of flows, loading, thermal properties of the main layer and prelayer, and the heat capacity of the gas.

MINSA simulations were conducted with isotherms independent of temperature, and with three different heats of adsorption (ΔH) – 5000 J/mol, 10,000 J/mol, and 20,000 J/mol. All other process conditions were identical. In order to simplify the analysis, an adiabatic system was selected, so that complications associated with heat loss could be neglected. Table 4-26 demonstrates near identical performance for these three simulations.

**Table 4-26 – Comparison of Temperature Profiles for Different Heats of Adsorption**

| Heat of Adsorption (J/mol) | **5,000** | **10,000** | **20,000** |
|---|---|---|---|
| Feed Flow (mmol/cycle) | 5181 | 5186 | 5194 |
| Product Flow (mol/cycle) | 338 | 338 | 339 |
| Product Purity (%) | 97.8 | 97.8 | 97.7 |
| Average Cyclic Temperature Swing (°C)* | 3.1 | 6.1 | 12.3 |
| Cold Spot (K) | 280.2 | 272.5 | 257.2 |

*Average cyclic temperature swing ignoring the mass transfer zone between 0.3-1 m.

As predicted, the thermal profiles and cyclic temperature swings varied considerably between the three simulations. Table 4-26 shows that the average cyclic temperature swing varies proportionally with the heat of adsorption. Figure 4-22 demonstrates that the magnitude of the temperature depression increases linearly with an increase in the heat of adsorption. This is consistent with the simple energy balance model prediction.

**Figure 4-22**

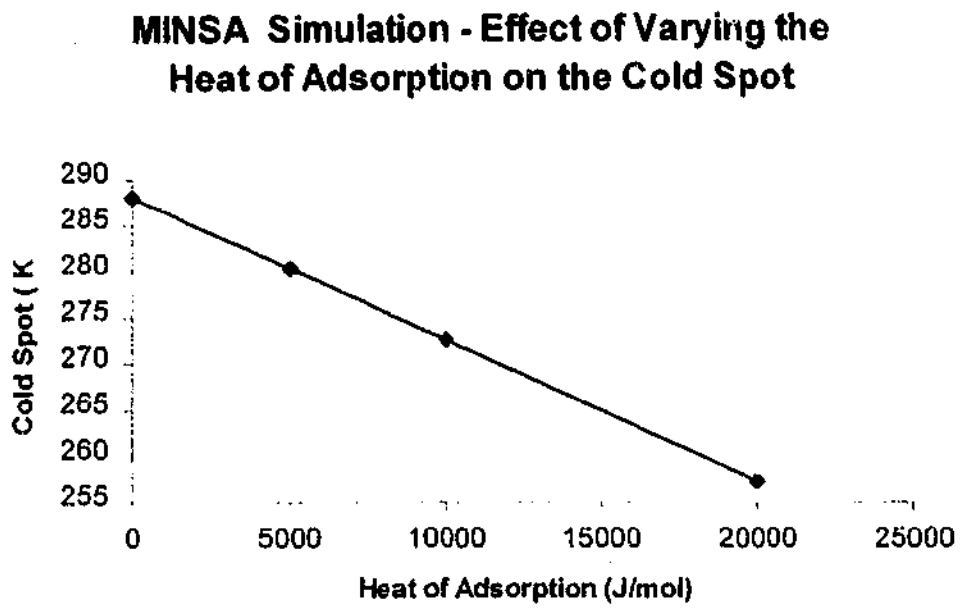


**Conclusion**: The temperature swing associated with adsorption and desorption is a critical parameter in determining the extent of the 'cold spot'. The magnitude of this temperature swing is increased by an adsorbent with a larger adsorptive capacity, and/or where the heat of adsorption is higher. New adsorbents, such as LiLSX have a larger adsorptive capacity (over a given pressure window), hence the cold spot will be more pronounced. This was demonstrated with experimental run AA300LSX1, compared with the experiments with NaX as the main adsorbent.

For the numerical simulation where the heat of adsorption was adjusted, but the adsorptive capacity held constant, there was a very simple linear effect demonstrated on the magnitude of the 'cold spot'. This is consistent with the simple energy balance model.

### 4.6.2 Effect of Prelayer Thickness

The prelayer is required to prevent the penetration of water and carbon dioxide into the main adsorbent layer. The prelayer has to be of sufficient depth for complete removal of these trace components. The prelayer also causes the development of the 'cold spot'.

**Model Prediction:** The simple energy balance around an inert prelayer results in the following equation.

$$\overline{T_2} = T_f - \frac{E}{F - W + \left(\frac{C_{pg} F W}{2 m_p C_{sp}}\right)} \qquad \textbf{(2- 34)}$$

An implication of this equation is that, as the thermal capacitance of the prelayer increases (with all other process variables constant), the 'cold spot' asymptotes to a minimum value.

**Experiment:** Three experiments were undertaken with an inert prelayer of activated alumina of 25 mm, 115 mm, and 300 mm respectively. The main layer of adsorbent (LiLSX) was essentially a constant mass, and all other process conditions were the same in each run.

**Result(s):**

**Figure 4-23**

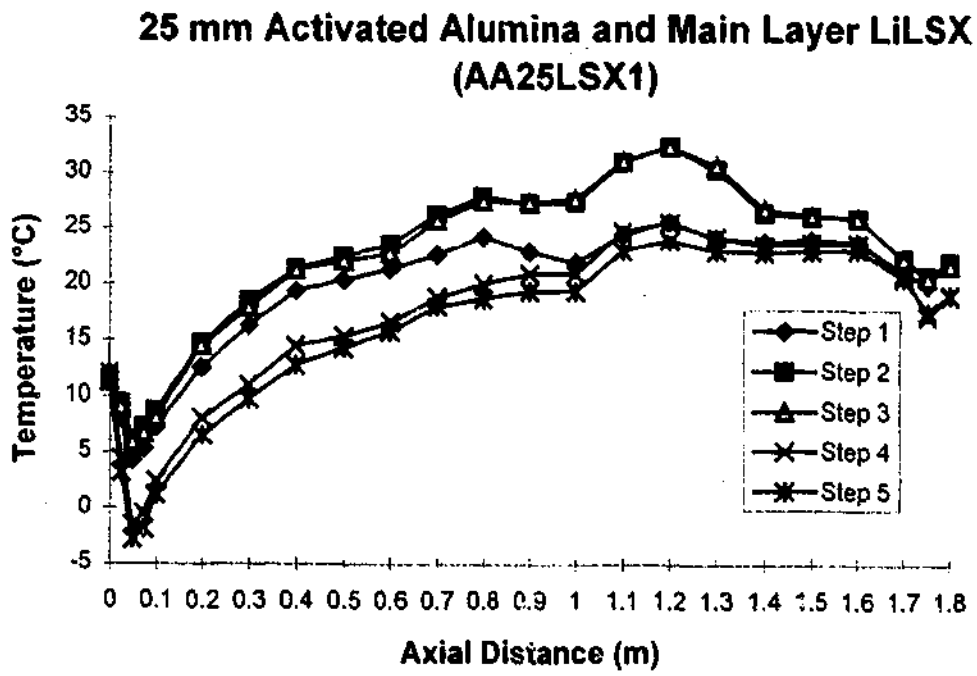


Figure 4-23 shows the temperature profile for Run AALSX25. In this case there is only a small temperature depression located just inside the adsorption bed. Figure 4-24 shows the effect of increasing the thickness of the prelayer, and plots the end-of-purge temperature

profiles for three different prelayers – 25 mm, 115 mm, and 300 mm. The location of the minimum correlates with the thickness of the prelayer, although in the case of the 115 mm prelayer, the minimum appears at 200 mm, as no thermocouple was located at 115 mm.

**Figure 4-24**

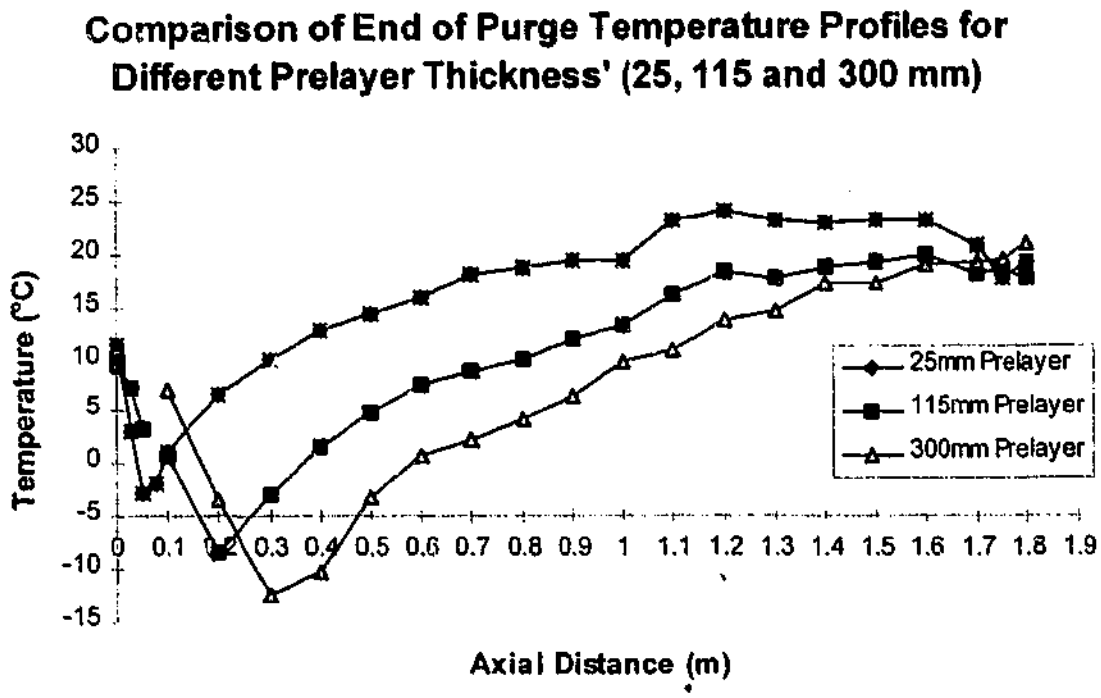


One complication with the temperature profiles at the end of the bed is that the total bed length was different in each case, since the main adsorbent layer was fixed (1550 mm) and the prelayer was varied between 25mm and 300 mm. The temperature profiles are deceptive, because it *appears* that the composition front is held further back in the 25 mm prelayer case (AA25LSX). This is not the case. It is simply that thermocouples at axial position 1.6 m and above are actually located outside the adsorption bed. The temperature swing in this void space is the result of gas compression and expansion. When adjusted for the total bed length, the location of the composition wave is similar, suggesting similar product purities.

The temperature minimum for these three experimental runs can be plotted against the depth of prelayer (Figure 4-25). This plot displays the asymptotic behaviour predicted by the simple energy balance and the MINSA runs. One significant source of experimental error is that it is difficult to locate the thermocouple precisely, in relation to the interface between the activated alumina and LiLSX. This introduces some uncertainty as to the precise extent of the temperature depression, but the predicted asymptotic behaviour is still observed.

**Figure 4-25**

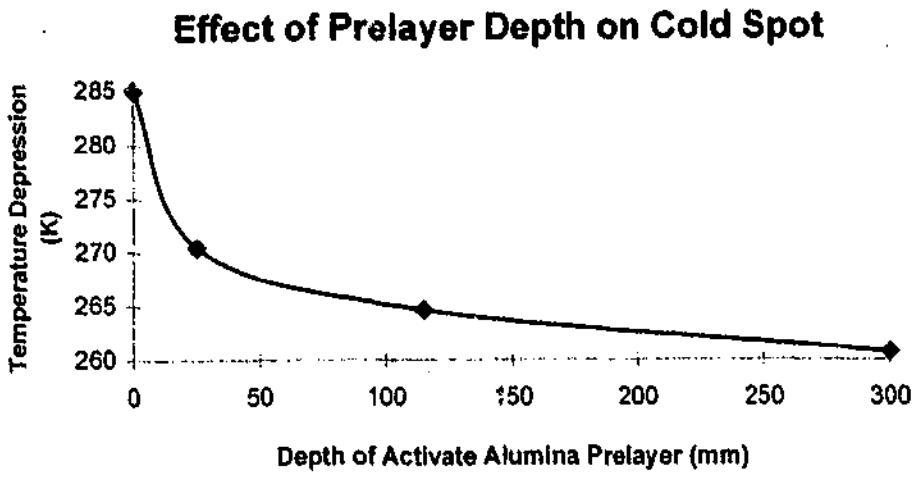


The performance for each run was almost identical, suggesting that a slight difference in the operating temperature (in the temperature range investigated) has only a slight effect on the adsorptive behaviour and selectivity of LiLSX. This issue is explored further in Chapter Five.

**Table 4-27 - Performance Comparison for Different Prelayer Thickness' (AALSX)**

| | AA25LSX | AA115LSX | AA300LSX1 |
|---|---|---|---|
| Pressure window (kPa) High/Low | 140.4/31.6 | 140.5/31.6 | 140.6/30.4 |
| Oxygen Purity (%) | 90.0 | 90.2 | 90.6 |
| Product Flow (mmol/cycle) | 437 | 440 | 440 |
| BSF (kg/TPDc) | 403.1 | 407.7 | 401.9 |
| Recovery (%) | 38.4 | 38.5 | 38.9 |

It should be stressed that the average temperature of the LiLSX adsorbent only varied slightly for these three runs ( AA25LSX - average LiLSX temperature 15.0 $^{o}$C, AA115LSX - average temperature 10.8 $^{o}$C, AA300LSX1 - average temperature 8.7 $^{o}$C). Hence it is reasonable to expect that the performance will be similar.

**Supporting Results:** Other experiments were undertaken varying the length of the activated alumina prelayer and NaX as the main layer (38 mm and 300 mm) (AA38NaXLP and AA300NaX1). These runs displayed the same trend - as the prelayer increased in length, the temperature dip was more pronounced. However in these experiments, the length of the main layer was varied, to achieve the same total bed length. As a result the total mass of active adsorbent was varied making comparison between the temperature profiles and performance figures difficult.

A further conclusion from equation 2-34 is that for inert materials with different densities and heat capacities, the same temperature dip is possible, if the length of the prelayer is adjusted to achieve the same thermal capacitance. This was confirmed by simulation with MINSA. Figure 4-26 describes near identical temperature profiles for two different runs, where only the prelayer was adjusted. In one case the prelayer was 200 mm with a density of 3000 kg/m$^3$, and in the other, the prelayer was 714 mm with a density of 840 kg/m$^3$. The specific heat capacity in both cases was the same, hence the total thermal mass of both prelayers was the same. The length of both prelayers was scaled to unity in order to aid comparison. Obviously without scaling the prelayers, the minimum for the higher density (3000 kg/m$^3$) case would be at 200 mm, and for the lower density case (840 kg/m$^3$) would be at 714 mm. The performance figures were nearly identical for both cases, since the mass of active adsorbent is the same, and the temperature and pressure profiles the same. The main difference is the bed voidage is slightly larger for the lower density case.

**Figure 4-26**

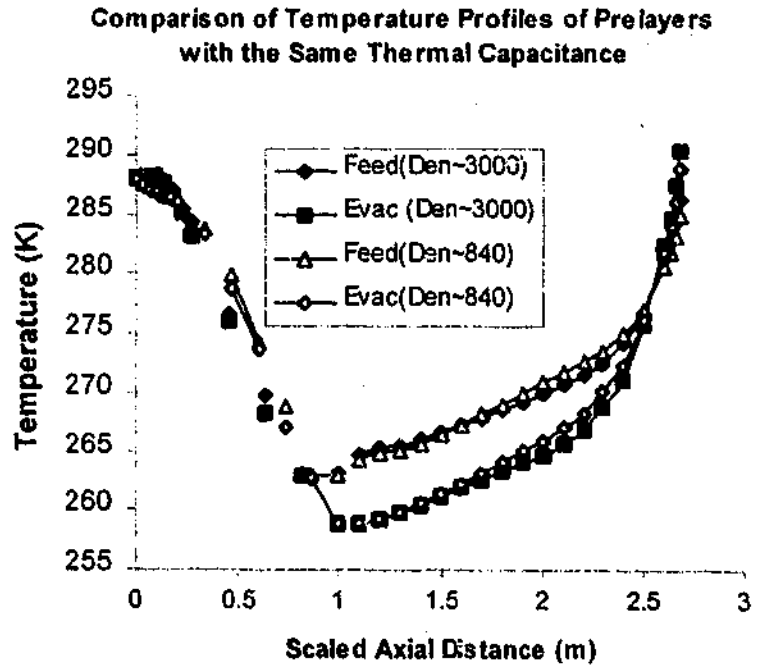


Figure 4-26 shows the length of the prelayer in both cases is scaled to unity to aid comparison. The figure demonstrates that thermal mass or thermal capacitance of the prelayer is a critical property for determining the extent of the 'cold spot'. This was also confirmed with a very different prelayer configuration (400 mm and a prelayer density of 25 kg/m$^3$ compared with 200 mm and a prelayer density of 50 kg/m$^3$). The scaled temperature profiles were almost identical in this case, where the absolute thermal mass is very small. In order to ensure the validity of these simulations it is necessary to ensure appropriate

discretisation of the prelayer, so that any difference in the temperature profiles is not a numerical artifact.

This functionality between the 'cold spot' and the thermal mass of the prelayer ignores the area of heat transfer. This is based on the assumption of thermal equilibrium between the gas and the adsorbent. This assumption may not be valid for all prelayers as the following example illustrates.

This comparison of prelayers with different physical properties, but the same thermal capacitance,.was also attempted experimentally with 150 mm of plastic packing used as a prelayer in place of the activated alumina. This was thermally equivalent to 25 mm of activated alumina. However, there was a substantial difference in the CSS axial temperature profiles and the extent of the temperature depressions. In the plastic packing case there was only a very slight temperature depression. It is speculated that there are two reasons for this. Firstly, the plastic packing was very porous and there was insufficient heat transfer between the waste gas and the packing for the model to be valid. Secondly, the porosity of the packing allowed the migration of some active adsorbent from the main layer into the prelayer. This led to heat being generated in the region of plastic packing, and hence invalidated the assumption that it was inert. In effect the experiment with the plastic packing behaved more like a single layered bed. The CSS temperature profile supports this conclusion.

**Conclusion:** Subsequent experimentation could be undertaken utilising silica gel or some other inert with a dry air feed, and adjusting the thickness of the prelayer to achieve the same thermal capacitance as the case of the activated alumina. An alternative inert prelayer that could be tested is NaX that had been thermally cracked (850 $^{o}$C), thereby collapsing its internal porosity, and eliminating its adsorptive properties. This 'killed' sieve is significantly denser than activated alumina due to its lower internal porosity.

The principle conclusion here is that the properties of the prelayer and length of the prelayer are design variables that can be used to adjust the extent of the temperature depression. This is obviously subject to the constraint that the prelayer must retain sufficient adsorptive capacity for water and carbon dioxide removal.

### 4.6.3 Effect of Adsorbing Prelayer - NaX Prelayer

One simple strategy to mitigate the extent of the temperature depression is to replace the inert prelayer with an adsorbing prelayer.

**Model Prediction:** The simple analysis undertaken using the regenerative heat exchanger model is complicated by the presence of an adsorbing prelayer. Qualitatively, it is apparent that the heat generated in the adsorbing prelayer should mitigate the extent of the 'cold spot'.

**Experiment:** Five different experimental runs were undertaken with a 300 mm prelayer of NaX APG pellets and a main layer of 1550 mm of LiLSX. A range of different pressure profiles was explored.

**Result(s):** Figure 4-27 presents the axial CSS temperature profile for Run NaX300LSX2 for a pressure window of 140-29.3 kPa and a product purity of 91.5%.

**Figure 4-27**

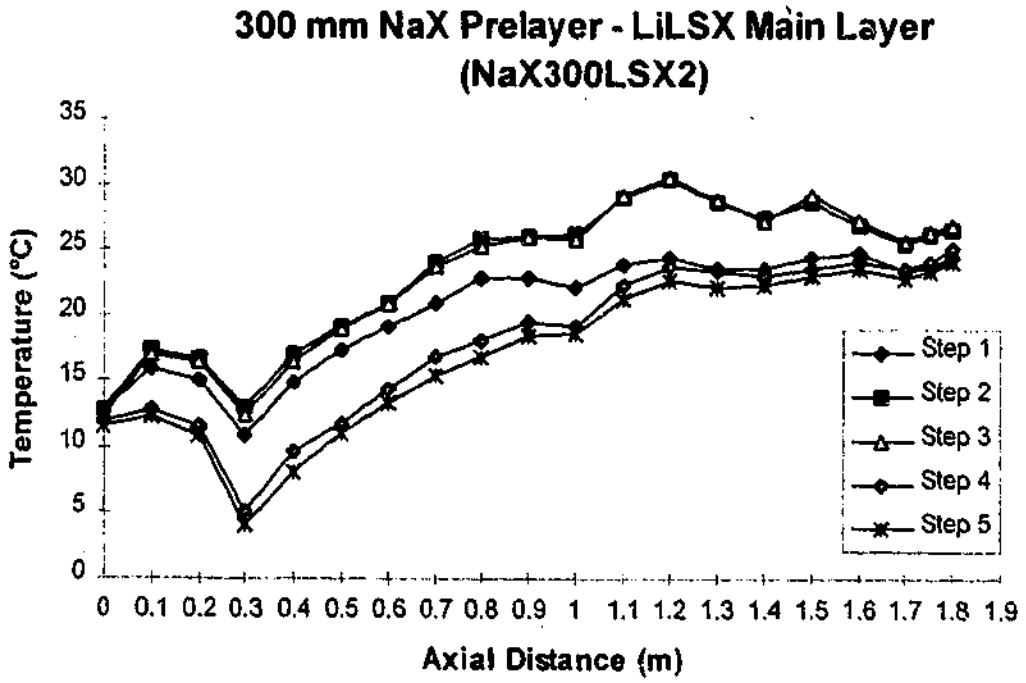


The most apparent difference between this profile and the case of the inert prelayer is the significant temperature swing through the prelayer, due to nitrogen loading on NaX. The effect of this loading is to markedly reduce the overall magnitude of the temperature depression. Experimental Run NaX300LSX2 and Run AA300LSX1 share the same process conditions, except the prelayers are different - NaX and Activated Alumina.

**Table 4-28 - Effect of Prelayer Adsorbent**

| | NaX300LSX2 | AA300LSX1 |
|---|---|---|
| 300 mm Prelayer | NaX(APG) | Activated Alumina |
| Inlet Feed Temperature (°C) | 13.6 | 11.1 |
| Average Temp. Swing in Prelayer(°C) | 5.6 | 1.9 |
| Ave. Temp. Swing in Main Layer*(°C) | 7.7 | 7.8 |
| Cold Spot (°C) | 3.7 | -12.3 |
| ΔT (Feed to Cold Spot) (°C) | 9.9 | 23.4 |

* This calculated average temperature swing was determined over the same bed length and ignored the mass transfer zone at the end of the bed where less adsorption (temperature swing) takes place.

Table 4-28 demonstrates that there is a marked difference in the extent of the 'cold spot'. The presence of an adsorptive prelayer ensures that there is a significant temperature swing in the prelayer, diminishing the difference between the prelayer and main layer. An interesting aspect of the temperature profile through the NaX prelayer is its curved shape.

The performance of the adsorption bed with the NaX (300NaXLSX2) is slightly better than the alumina prelayer case (300ALSX1) with respect to purity. The production rates are similar, but the purity is 1% higher in the case of Run NaX300LSX2. This is to be expected given the additional nitrogen adsorptive capacity of the NaX prelayer.

The simple modelling approaches developed in Chapter Two are based on assumption of an inert prelayer. These models are not applicable to the case of an adsorbing prelayer, and we need to rely on numerical techniques for modelling this case.

A simulation run was undertaken based on experimental Run NaX300LSX1. As has been mentioned previously, there was some difficulty characterising the isotherm of the LiLSX, and hence a generic LiX dual sited Langmuir isotherm was used instead.

**Figure 4-28**

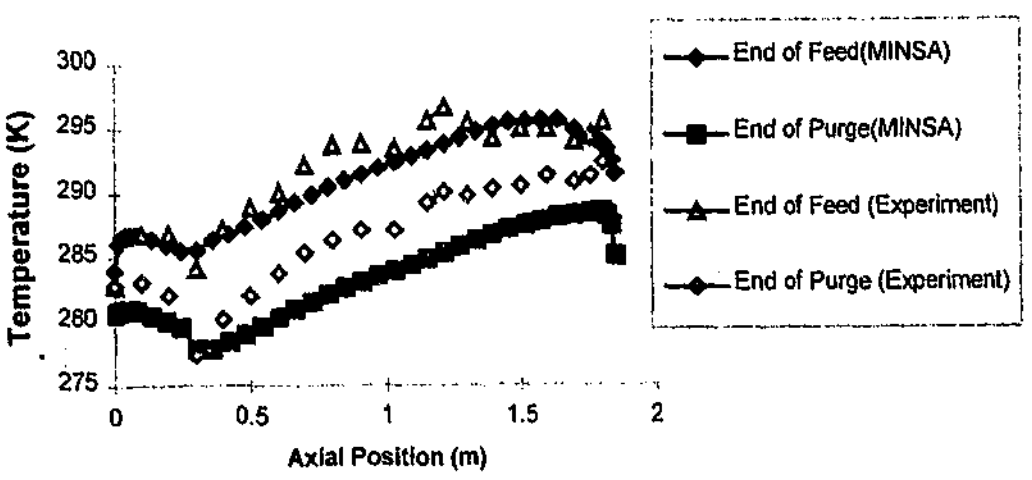


The experimental run and the MINSA simulation show the same reduced temperature depression compared with an inert prelayer. Comparing the simulation and experimental data, the overall temperature profiles are similar, but the cyclic temperature swings are slightly different, confirming some discrepancy between the simulation isotherms, most probably associated with the heats of adsorption. This difference is also evident in Table 4-29 comparing the experimental and simulation results.

**Table 4-29 - Comparison between experiment and simulation (NaX300LSX1)**

| | NaX300LSX1 | MINSA |
|---|---|---|
| End of Step Pressures (kPa) (For step 1, 2, 4,5) | (135±0.5, 140±0.5, 40±0.5, 44±0.5) | (138, 140, 38, 43) |
| Production (kgPDc) | 15±0.4 | 17 |
| Product Purity(%) | 92.6±0.5% | 92.6% |
| Feed Flow (mmol/cycle) | 4230±84 | 4900 |
| Recovery (%) | 33%±2% | 30% |

Most importantly, it is evident that the numerical model (and its underlying physical model) accurately capture the reduced magnitude of the 'cold spot' with an adsorbing prelayer.

**Supporting Results:** The reduced temperature depression was observed in all experimental runs with NaX as the prelayer(Na300LSX3, Na300LSX4, Na300LSX5). One important point is that altering the pressure window with an adsorbing prelayer, does not have as pronounced an effect on the temperature depression as is the case with an inert prelayer. For example,

comparing NaX300LSX1 (Pressure window ~140 kPa - 40 kPa) and NaX300LSX2 (Pressure window ~140-30 kPa). There is only a marginal difference in the temperature profiles.

This is largely due to the fact that, as the temperature swing in the main layer increases due to the increase in the pressure window, so does the temperature swing in the adsorbing prelayer. However, in the case of an inert prelayer there is no change in the temperature swing due to the pressure window.

**Conclusion:** The presence of an adsorbing prelayer, such as NaX, mitigates the extent of the temperature depression. However, in practice, with a wet air feed, a water-loaded zone will form at the entrance of the prelayer that is devoid of nitrogen loading capacity. The temperature profile evident in Figure 4-27 can only occur with a dry air feed.

### 4.6.4 Effect of Higher Capacity Prelayer - LiLSX - 'Hot Spot' Effect

An alternative and purely hypothetical adsorbent arrangement is to place LiLSX as the prelayer and NaX the main layer. The main purpose of this adsorbent configuration is to demonstrate that the once misunderstood 'cold spot' is simply the result of the balance of heats of adsorption (and cyclic temperature swings) and convective fluxes throughout the bed. Replacing the inert prelayer with a prelayer of adsorptive capacity greater than the main layer should create a 'hot spot' as opposed to a cold spot.

**Model Prediction:** The effect of a LiLSX prelayer cannot be predicted with the simple energy balance model, which assumes an inert prelayer. Qualitatively, it is expected that there will be a temperature 'hump' instead of the characteristic temperature 'dip'.

**Result(s):**

**Figure 4-29**

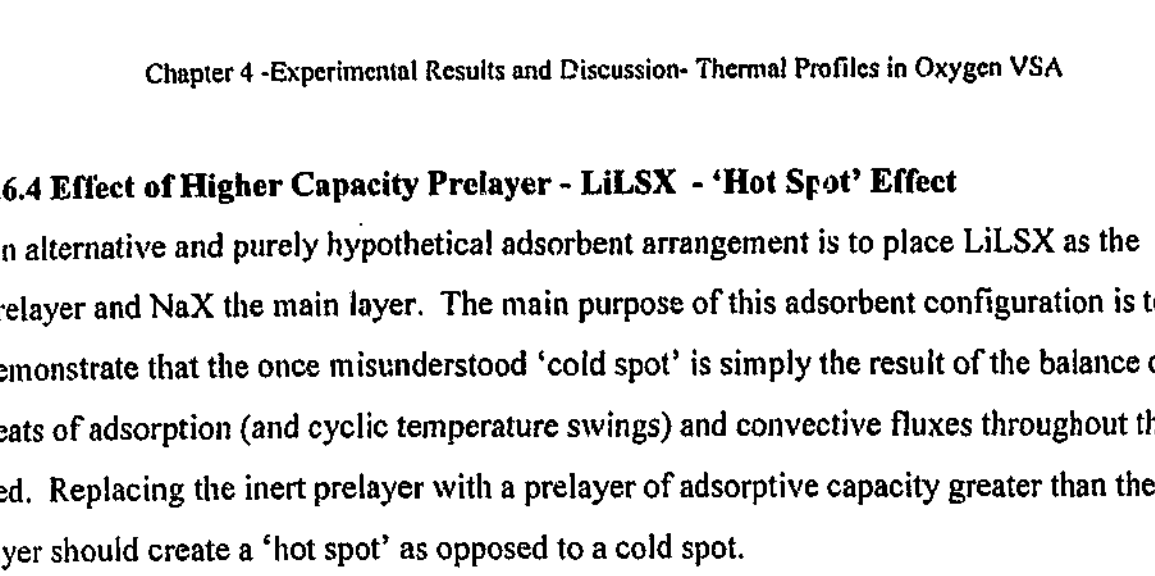


Figure 4-29 indicates that the hottest point in the bed is at the interface between the prelayer of LiLSX and the main layer of NaX. In effect an inverted 'cold spot' results from the interaction between the heats of adsorption and the convective fluxes. In the limiting case this can be considered analogous to an adsorbing single layer followed by an inert prelayer. This is not dissimilar to a high purity cycle where the composition front is kept well back inside the adsorption bed.

**Figure 4-30**

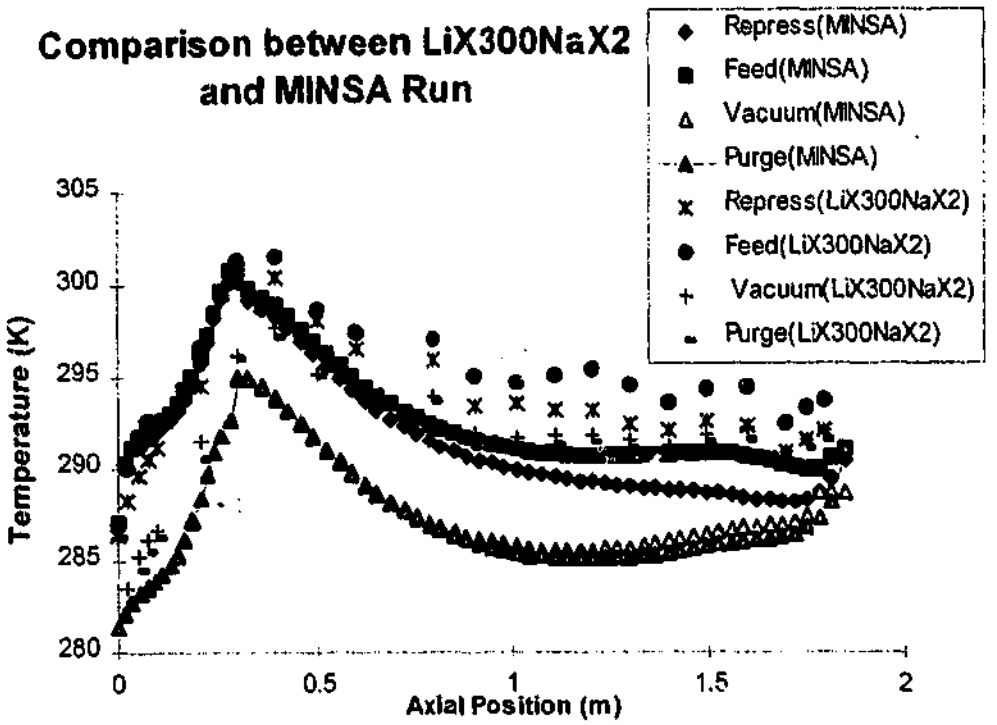


It is useful to simulate the case of the LiLSX prelayer, to confirm that the numeric model captures the interesting effect of the 'hot spot' observed experimentally. Figure 4-30 compares the CSS temperature profiles for experimental run (LSX300NaX2) and its MINSA simulation.

Both the experimental profile and MINSA simulation display the 'hot spot' to a similar magnitude, although the profiles through the main layer are different. The experimental profile is slightly hotter (average 3.8 $^{o}$C), and flatter than the simulation result. The profile through the main bed for the simulation run is slightly more concave. This discrepancy is due to the magnitude of the cyclic temperature swings. As has been previously detailed the LiLSX adsorbent was not thoroughly characterised, and instead an isotherm for a generic LiX isotherm was used. Furthermore a constant heat of adsorption was used for the main layer, which also contributes to the difference in cyclic temperature swings. These differences aside, the simulation accurately captures the experimental performance results.

**Table 4-30 - Temperature Profiles – LSX300NaX2 and MINSA Simulation**

| | LSX300NaX2 | MINSA Simulation |
|---|---|---|
| Average Prelayer Temperature Swing ($^{O}$C) | 7.3 | 8.0 |
| Average Main Layer Temperature Swing ($^{O}$C) | 4.3 | 5.1 |
| Oxygen Product (mmol/cycle) | 203 | 207 |
| Feed (mmol/cycle) | 3589 | 3884 |
| Product Purity (%) | 93.3% | 93.3% |

**Supporting Results:** This result is consistent with cases of a LiLSX prelayer (LSX300NaX2 and LSXNaX3) which also display the 'hot spot' with slightly different process conditions. One interesting aspect of the 'hot spot' effect was that, the pressure window did not significantly affect it. This is due to the fact that with both an adsorbing prelayer and the main layer, changing the pressure window affects both layers, and depending on the shapes of the isotherms, both layers undergo an increased or decreased temperature swing associated with adsorption and desorption. For example, both NaX and LiLSX isotherms are quite linear over the pressure range in question, so that an increase in the pressure window corresponds to the same relative increase in loading, and the same increase in the temperature swing. The absolute difference in the temperature swing between the two layers is increased, but the relative difference remains similar.

**Conclusion:** Like the 'cold spot', the nature and extent of the 'hot spot' will also be affected by the process conditions. However the detailed demonstration of the nature of the 'hot spot' is beyond the scope of this project, as it is purely a hypothetical case with reference to current oxygen VSA. Suffice it to say that the 'hot spot' arises when the cyclic temperature swing in the prelayer is greater than the cyclic temperature swing in the main layer.

This investigation has focused on a one-bed cycle with a LiLSX prelayer. This created a hot spot. However the temperature profile would be different for an adiabatic two bed cycle. The temperature gradient would continue to rise through the main layer, but the gradient would be steepest through the LiLSX prelayer.

### 4.6.5 Effect of an Inert to Mitigate the Cyclic Temperature Swing

One strategy for improving the performance of oxygen VSA is to dampen the cyclic temperature fluctuation associated with adsorption and desorption, and thereby increase the working capacity of the adsorbent. The history and rationale for this optimisation strategy are outlined in more detail in Chapter Five.

**Model Prediction:** The inclusion of some thermal diluent should reduce the cyclic temperature swing, and thereby reduce the severity of the CSS axial temperature gradient, and improve the performance of the VSA unit.

**Experiment Undertaken:** A previous experimental run (Run AA115LSX1) was undertaken with a 115 mm prelayer of activated alumina and main layer of LiLSX. To assess the role of the diluent, four kilograms of copper pellets were mixed with the main layer of adsorbent. The pellets were approximately 2mm in length and 1.6mm in diameter. Copper was selected as a thermal diluent due to its high heat capacity, density and thermal conductivity. For the same process conditions, the temperature profiles and performance were compared with the case of no copper diluent (Run AA115LSX1), and copper added (Run AA300LSXCu).

**Result(s):** The CSS axial temperature profile for Run AA300LSXCu presents a very slightly reduced temperature depression compared with the run without the copper diluent.

**Figure 4-31**

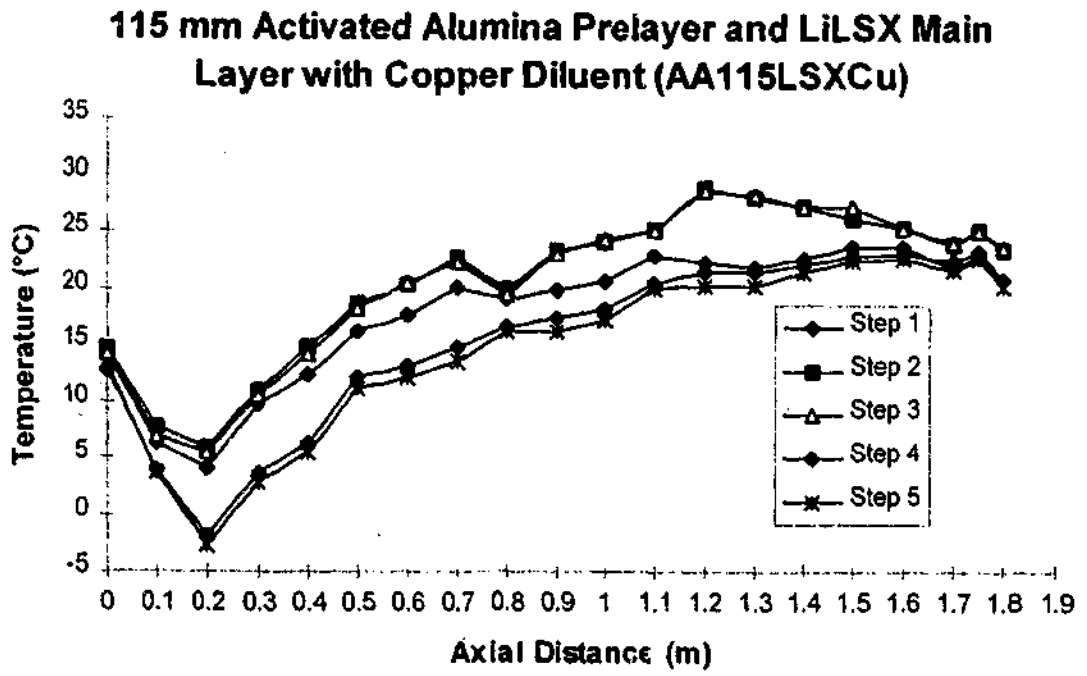

**Table 4-31 - Temperature comparison between experimental runs (with and without copper diluent)**

| | AA115LSXCu | AA115LSX |
|---|---|---|
| Thermal Diluent | 4 kg Copper Pellets | None |
| Feed Temperature | 14.2 | 10.6 |
| Cold Spot (°C) | -2.8 | -8.5 |
| ΔT(Feed to Cold Spot) (°C) | 17.0 | 19.1 |
| ΔT(Max.Temp – Cold Spot) (°C) | 31.6 | 35.1 |

This indicates that the presence of the diluent at a concentration of 9% v/v has a slight effect on the extent of the temperature depression and the severity of the temperature profile. The temperature difference across the bed is reduced by 3.5 °C in the case with the copper diluent. The average temperature swing between adsorption and desorption for the case with the copper diluent was 6.1 °C compared to 6.5 °C. In most cases there was little difference in the temperature swing. The difference was only pronounced at the axial position of 0.8 and 1.1 m where there was an appreciably smaller temperature swing for the copper diluent run (3.7 and 5.2 °C). This suggests that unless the adsorbent is in intimate contact with the thermal diluent, the effect is marginal. As a result, in order to achieve a marked impact on the overall thermal profile, and reduce the cyclic temperature swing substantially, more copper needs to be added, or the thermal diluent must be incorporated into the adsorbent pellet.

**Table 4-32 – Performance comparison between experimental runs (with and without copper diluent)**

| | AA115LSXCu | AA115LSX |
|---|---|---|
| Thermal Diluent | 4 kg Copper Pellets | None |
| Pressure Profile(kPa) | 135.5/141.2/31.4/35.5 | 133.76/140.5/31.6/34.8 |
| Product Purity* (%) | 94.1 | 94.3 |
| Feed (mmol/cycle) | 4731 | 4684 |
| Product (mmol/cycle) | 455 | 440 |
| Recovery (%) | 39.3 | 38.5 |
| BSF (kg/TPDc) | 374 | 386 |
| Specific Power (kW/TPDc) | 9.8 | 10.0 |

* Two component basis.

Table 4-32 demonstrates that for a marginally wider pressure window, the adsorbent bed with the copper diluent has slightly better performance (~0.8% higher recovery, and a reduced BSF by ~12 kg/TPDc), but the results are very similar. In fact it is possible that other experimental variables might have been the source of this performance difference. The ambient temperatures (and hence feed temperatures) were different, the ambient pressure was possibly different, the pressure profiles differed by 0.7 kPa, and the product purities differed by 0.2%. In sum it is possible that the performance improvement was the result of minor differences in these other process variables, and not attributable to the copper pellets at all. However, perhaps more importantly, even if these minor differences are neglected, the presence of the copper pellets only marginally improved VSA performance. The implications of this conclusion are explored in Chapter Five.

One commonly adopted assumption is that the thermal diluent can be treated as part of the adsorbent, and the specific heat capacity of the adsorbent can be adjusted to take account of the thermal mass of the diluent. For example, the effect of adding 4 kg of copper pellets to 7.91 kg of adsorbent can be assumed to increase the specific heat capacity of the adsorbent from 1000 kJ/kg K to 1200 kJ/kg K. MINSA simulation of AA115LSX and AA115LSXCu can be performed. In the case of AA115LSXCu, the heat capacity of the adsorbent is adjusted to be 1200 kJ/kg K.

**Table 4-33- Experimental and MINSA Simulation without Thermal Diluent**

| | AA115LSX | MINSA |
|---|---|---|
| Pressure Profile (kPa.) | 133.8/140.5/31.6/34.8 (±0.5) | 133.3/140.7/31.8/34.9 |
| Product Purity (%) | 94.3±0.5 | 94.3 |
| Feed Flow (mmol/cycle) | 4684±94 | 4987 |
| Product Flow (mmol/cycle) | 440±13 | 435 |
| Product Recovery (%) | 38.5 | 35.7 |
| Cold Spot at 200 mm (°C) | -8.5 | -12.1 |
| ($T_{feed} - T_{cold\ spot}$) (°C) | 18.7 | 22.3 |

**Table 4-34 Experimental and MINSA Simulation with Thermal Diluent**

| | AA115LSXCu | MINSA |
|---|---|---|
| Pressure Profile (kPa.) | 135.5/141.2/31.4/35.5 (±0.5) | 136.3/140.2/31.3/35.4 |
| Product Purity (%) | 94.1±0.5 | 94.1 |
| Feed Flow (mmol/cycle) | 4731±95 | 5106 |
| Product Flow (mmol/cycle) | 455±14 | 479 |
| Product Recovery (%) | 39.3 | 38.4 |
| Cold Spot at 200 mm (°C) | -2.8 | -5.4 |
| $\Delta(T_{feed} - T_{cold\ spot})$(°C) | 17.2 | 19.8 |

There is a reasonable correlation between MINSA and experimental results. The most significant discrepancy lies in the feed flow, where the MINSA predictions are 6-7% higher than experimental values. This difference is most probably due to slight errors in the estimation of the dual-site Langmuir parameters.

Two important trends are shared by both the simulated and experimental values. In both cases, the addition of a thermal diluent improves separation performance and reduces the extent of the temperature depression. These effects are more pronounced with the MINSA simulations. For example, the adjustment of the specific heat capacity from 1000 J/kg K to 1200 J/kg K in representing the addition of a thermal diluent, increases the product flow by 9%. However, experimental results suggest the addition of the copper pellets only achieves a 3% increase in flow. This indicates that the technique of adjusting the specific heat capacity to account for the addition of an inert thermal diluent, leads to overly optimistic predictions

of performance improvement. This approach is based on the assumption that there is no resistance to heat transfer between the adsorbent and the inert pellets, and that the inert pellets are well mixed through the adsorbent bed. It can be concluded that a more realistic model is required to account for the heat transfer resistances. A full pellet model based on the non-isothermal version of the Dusty Gas Model is currently being developed at Monash University to address this issue.

For the MINSA simulations, adjusting the specific heat capacity from 1000 to 1200 J/kg K, reduces the magnitude of the cyclic temperature swing between adsorption and desorption by 16%. This is consistent with experimental observations. Along with this, increasing the specific heat capacity to 1200 J/kg K increases the change in the nitrogen loading (working capacity) over the bed by 2%. The slightly increased purge amount for the case with the copper diluent (AA115LSXCu) also contributes slightly to the improved performance and higher feed flow. The significant conclusion remains that the thermal diluent has a small effect on the performance improvement, and the simple adjustment of the specific heat capacity provides an overly optimistic prediction of the benefits of a thermal diluent, since the resistance to heat transfer and inert pellet mixing is ignored.

**Conclusion:** The presence of a thermal diluent reduced the severity of the axial thermal profile. However the thermal diluent had little impact on the overall performance of the oxygen VSA unit.

## 4.7 Transient Effects

### 4.7.1 Transient Temperature Profiles with Dry Air Feed

This study has largely focused on CSS temperature profiles. The transient behaviour is an interesting aside. Furthermore transient temperature profiles can provide useful process information about the dynamic behaviour of the VSA system.

**Model Prediction:** The perturbation techniques and the dynamic model developed in Chapter Two predict a slow evolution to a CSS temperature profile, where the temperature profiles will be periodic.

**Experiments:** All experiments that were satisfactorily run to CSS provide data of the thermal evolution of the VSA unit. One example is Run 1BAA300NaX.

**Result(s):** The thermal evolution of experimental Run B1AANaX is presented in Figure 4-32 for selected thermocouple locations. The temperatures were sampled once per cycle at the same point in the cycle. Hence at CSS, the temperatures in Figure 4-32 should remain unchanged since the VSA unit behaviour is periodic, with a frequency of the cycle time.

**Figure 4-32**

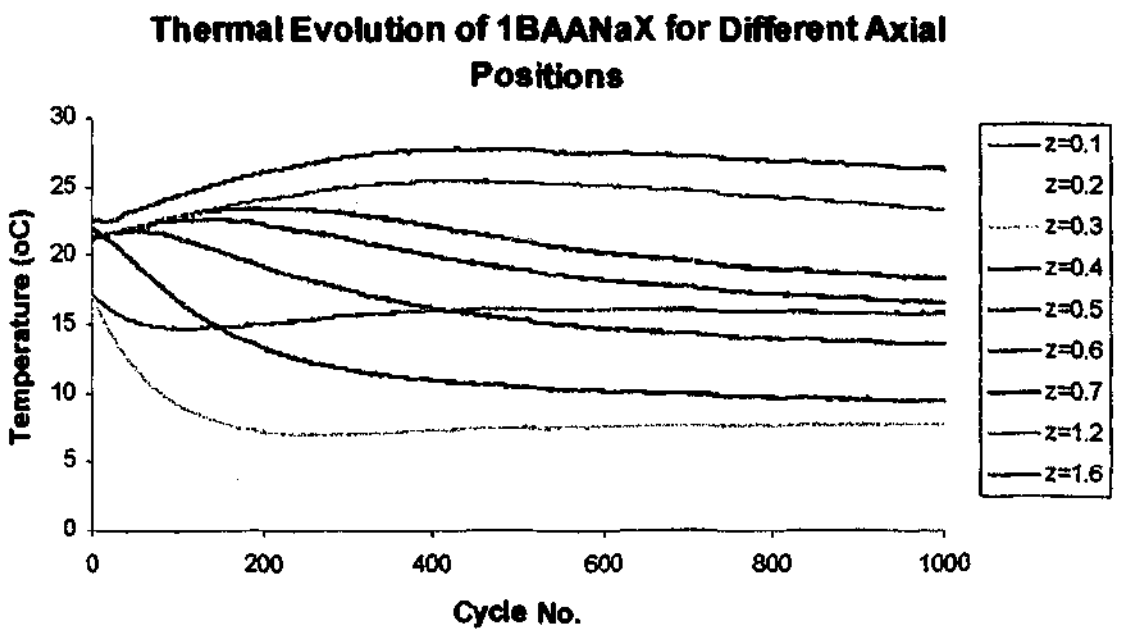

This demonstrates the slow evolution to CSS. One complication with demonstrating CSS is fluctuations in the temperature profile due to diurnal fluctuations in the ambient and feed gas temperatures.

This thermal evolution can also be simulated on MINSA. Figure 4-33 presents a comparison between the thermal evolution for experimental runs and MINSA simulation for selected thermocouples.

**Figure 4-33**

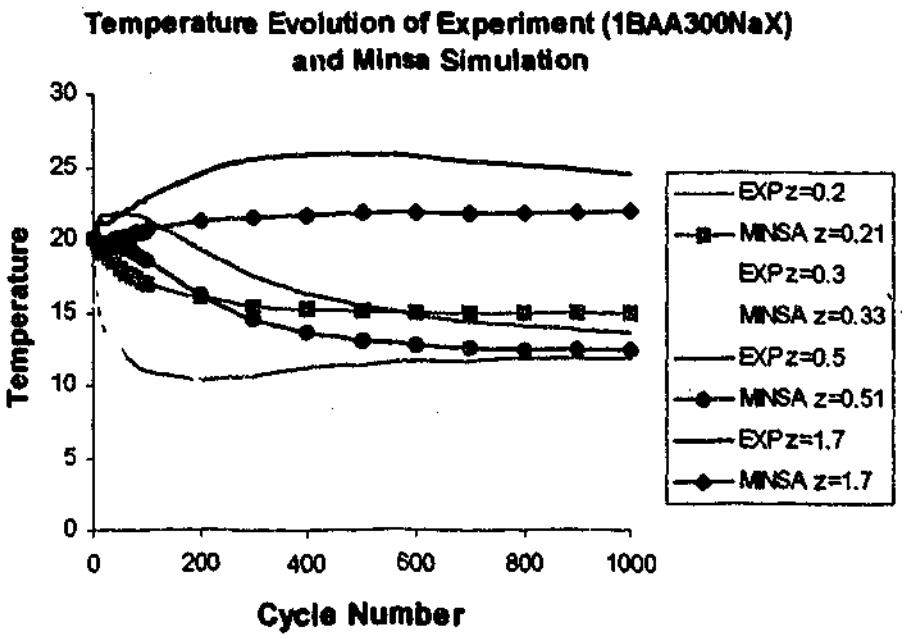


Figure 4-33 shows similar evolutionary profiles for both the experimental results and MINSA. The dynamic response of the experimental run is slightly faster than the MINSA simulation, and there is a slight discrepancy in the absolute temperatures at CSS. The difference in the dynamic response is most probably due to different initial conditions, and to discrepancies in the precise location of thermocouples around the interface between the prelayer and the adsorbing layer. However, it can still be concluded that MINSA captures the slow thermal evolution of an oxygen VSA unit. Table 4-35 provides the CSS mass flows and 'cold spot' temperature for Run 1BAA300NaX.

**Table 4-35- MINSA Simulation and Experimental Results – 1BAA300NaX**

| | Experimental | MINSA Simulation |
|---|---|---|
| Pressure Profile (kPa) | 133.7/138.4/30.5/34.5 | 134.6/139.0/30.0/34.6 |
| Feed (mol/cycle) | 3505 | 3284 |
| Product (mol/cycle) | 228 | 208 |
| Product Purity (%) | 93.5 | 93.5 |
| Cold Spot (°C) | 6.9 | 7.8 |
| Product Temperature (°C) | 25.9 | 25.0 |

In addition to the slow evolution, the cyclic temperature swing between adsorption and desorption shows truly periodic behaviour at CSS as is shown in Figure 4- 34 for selected thermocouples.

**Figure 4-34**

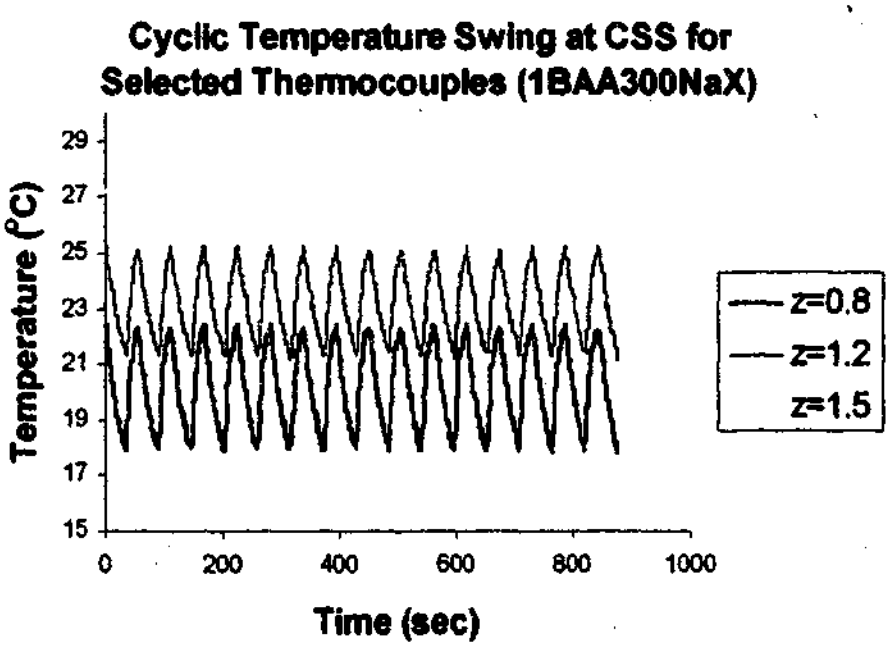


**Supporting Results:** Figures 2- 21 and 2- 22 are also supporting temperature profiles showing the evolution to CSS.

**Conclusion:** Oxygen VSA operation is characterised by the slow evolution of thermal profiles based on the ratio of the thermal capacitance of the gas to the adsorbent. This provided the basis for the perturbation techniques developed in Chapter Two. It has been

demonstrated that the MINSA simulation and experiment 1BAA300NaX show a similar dynamic response.

Some interesting future experiments concerning the dynamic behaviour of the VSA unit would be to start with different initial conditions (mole fraction, or temperature), and plot the different path of thermal evolution to the same unique CSS. One of the significant implications of this slow evolution to CSS is that it can make process control of oxygen VSA difficult, as the final result of valve position changes can take several hundred, if not a thousand cycles (Beh et.al., 2000).

## 4.8 Wet Air Feed Effects

The preceding examination of thermal effects in oxygen VSA has been limited to consideration of dry air feed. However, industrial practice is to feed ambient (wet) air to the VSA unit. This introduces a number of complications since the feed stream now contains water, carbon dioxide and other trace components. Developing techniques to determine the penetration of water into the adsorption bed is vital for the design of industrial VSA units. The dynamic effect of the introduction of wet air feed is also assessed. This work is presented in Wilson et.al. (2001).

### 4.8.1 Effect of Wet Air Feed on CSS Temperature Profile

**Model Prediction:** The effect of water as a strongly adsorbed trace component is to create a quasi-inert zone, where no or very reduced nitrogen adsorption occurs (Kumar, 1996). It follows that there will be temperature depression in a single layered bed of NaX. It is possible to determine the length of the water loaded, by applying a water balance at CSS as described in Chapter 2-8.

**Experiments:** A humidifier was placed in the feed line, and air with a relative humidity of 40% ±2% (measured at ambient temperature and pressure) was introduced into the VSA unit with a single layer of dry NaX. The unit was run to CSS.

The technique to determine the penetration of the water loaded zone was to extract small (~2 g) samples of adsorbent from the bed at predefined axial distances, and to measure the nitrogen adsorption capacity of these samples on a Micromeritics ASAP2010M analyser. The samples were extracted by drilling into the PVC column. Each sample was then degassed at ambient conditions prior to the measurement of nitrogen capacity. We thus infer the presence of water on a sample by the reduction in nitrogen loading at 810 mmHg nitrogen and 295 K. It is important not to degas the sample at elevated temperature, since this fully restores the nitrogen adsorption capacity.

The use of reduced nitrogen capacity to infer the extent of water loading was considered preferable to TGA analysis, which would have determined percent water loading on the sampie. The latter does not give information on the extent of nitrogen loading, which is the critical issue addressed in this work.

**Result(s):** Run NaXWLP describes a single layered bed fed with wet air. This run only differs to Run NaXDLP, described in Section 4.3.1 with respect to the introduction of wet air. The resulting CSS temperate profile displays a clear temperature depression.

**Figure 4-35**

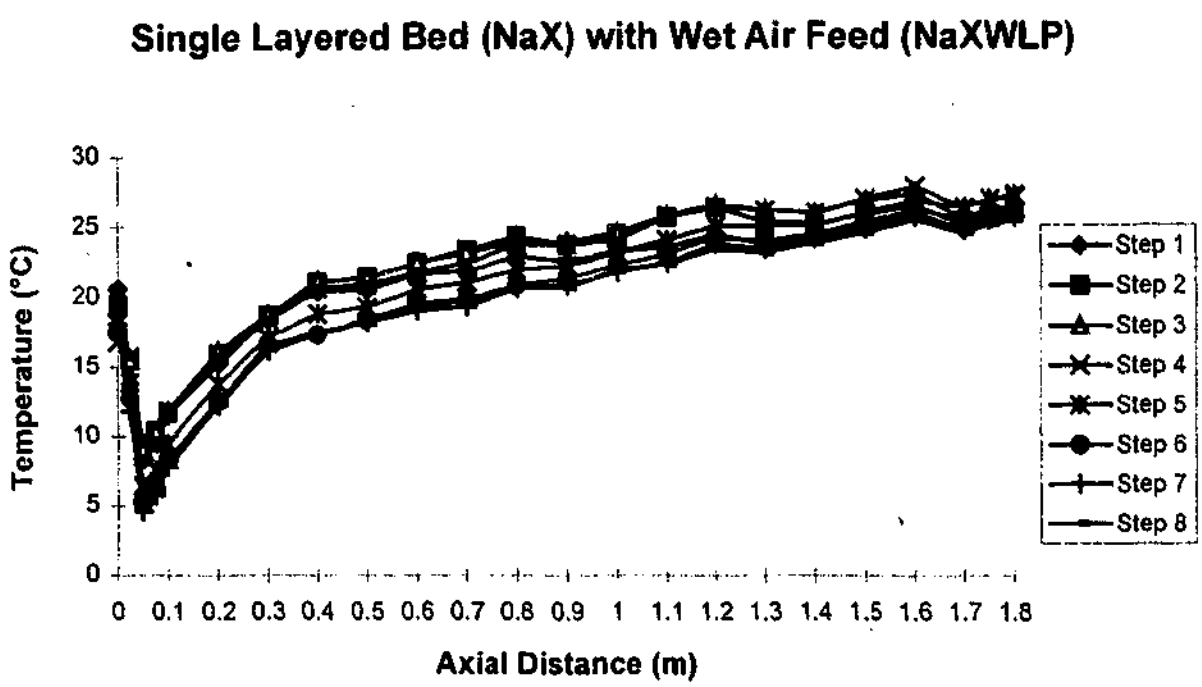


A prominent temperature depression forms over the first 50 mm of bed. A temperature drop from the feed temperature to about 5 °C occurs, followed by a rise in temperature thereafter. The models suggest that this depression is due to reduced nitrogen loading capacity in the first 50mm.

The length of the water loaded zone was determined by measuring reduced nitrogen loading capacity at different axial positions. Figure 4-35 shows the nitrogen loading capacity at different axial positions along the adsorption bed, after the process had reached CSS.

**Figure 4-36**

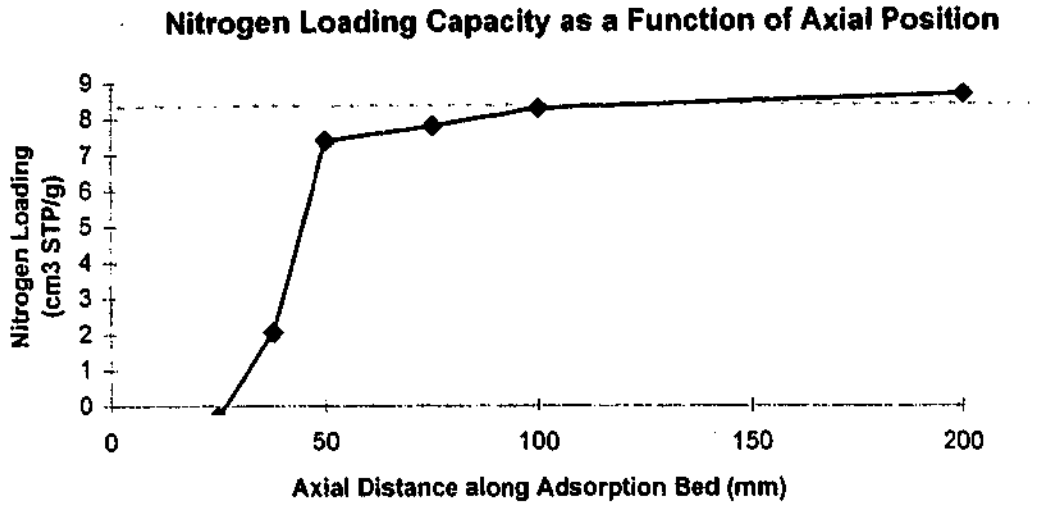


Figure 4-36 indicates the water-loaded zone is approximately 25-40 mm from the inlet of the column, and no nitrogen loading occurs in this zone. Thereafter the nitrogen loading increases over approximately 20 mm to near full adsorption capacity. There is a slight tail in this plot that could be attributed to a mass transfer zone, that is not accounted for in the simple equilibrium model. However, there is still a sharp transition point that justifies an equilibrium model to a first approximation. The position of the 'inert' zone corresponds well to the location of the temperature depression shown in Figure 4-35.

Based on the equation 2-99 and using the experimentally determined pressure and velocity profiles for the desorption step, the z-t plot shown in Figure 4-37 was generated. This plot describes lines of constant mole fraction over the duration of the countercurrent desorption steps. Bed pressure is also plotted on the graph. During the major part of the desorption step the pressure in the bed decreases exponentially, and then increases slightly during the purge step.

**Figure 4-37 - Lines of Constant Mole Fraction during the Desorption Steps**

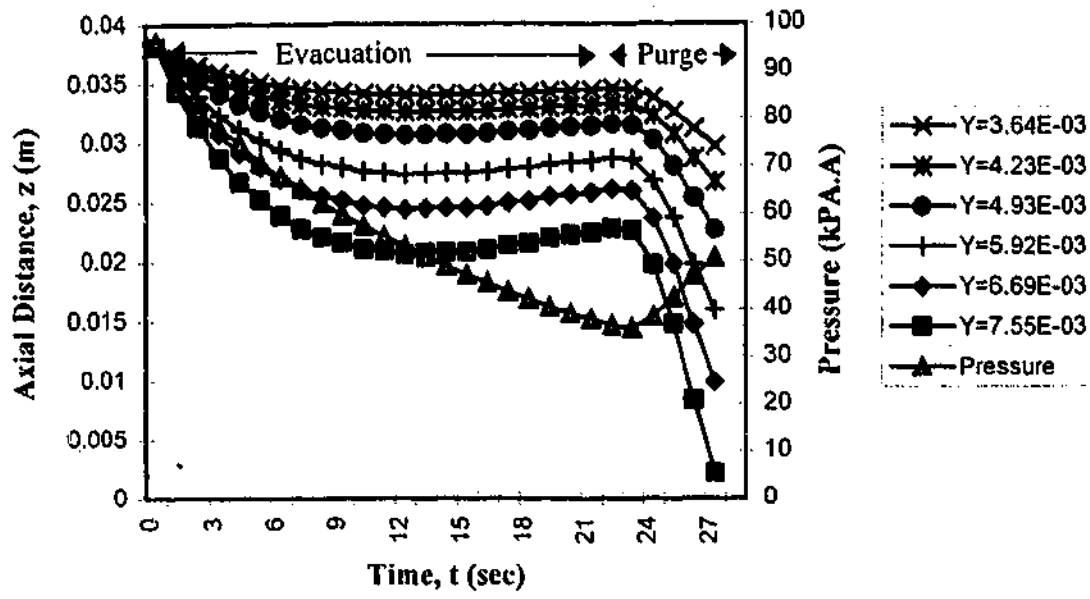


Based on these lines of constant mole fraction combined with Equation 2-95, the penetration of the water loaded zone was calculated to be 38 mm. The relative humidity of the feed air was 40% at 18 °C and atmospheric pressure. The pressure profile and the required velocity data for calculation of the length of the water-loaded zone were taken from the low purity run for Run NaXWLP. The numerical solution using MINSA was calculated to be 36 mm. The MINSA calculation includes the change in water mole fraction within the gas phase between the desorption and adsorption steps.

An additional feature of the using MINSA (a successive substitution simulator) is that the evolution of the water loaded zone can be determined (Refer Figure 4-38).

**Figure 4-38**

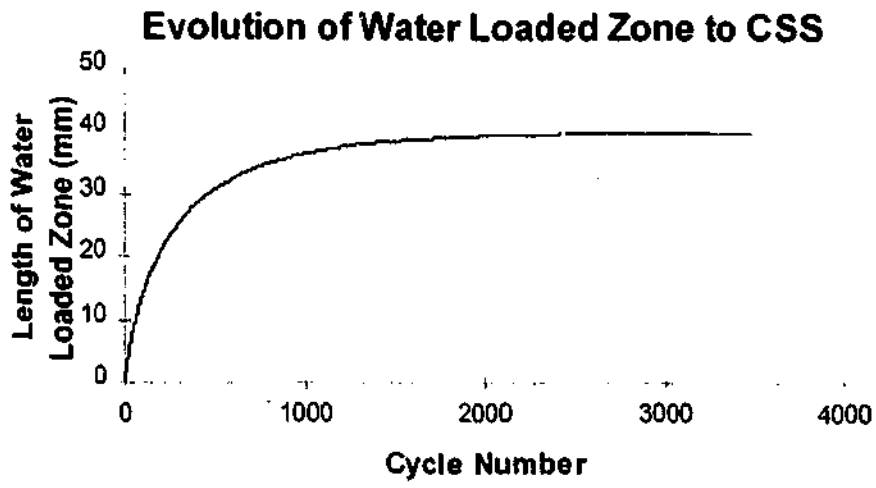

Both the analytical and MINSA results compare well with the experimental result of between 25-40 mm. However, this large uncertainty in the experimental result highlights a limitation of the experimental technique applied, for determining the location of the water front. As a result, it is difficult to account for the shape of the experimental water mass transfer zone with sufficient accuracy, to ascertain whether the equilibrium assumption is valid. MRI (Magnetic Resonance Imaging) is an alternative technique that has been recently applied for the determination of the position of a water front in chromatographic studies (Karsten-Bar, Balcom, Ruthven, 2000). Potentially MRI offers much improved accuracy that would enable an improved comparison between experimental and modelling results.

Within experimental error, it appears that a simple equilibrium model, solved by characteristics or a numerical technique, provides a useful design tool for determining the thickness of the water-loaded zone. The technique could also be used for investigating the impact of process parameters (feed humidity, internal purge velocity, and pressure profile) on the CSS position of the water front. For example, the same VSA cycle, except with the feed gas having a relative humidity of 90% at 30 °C and atmospheric pressure, results in a calculated water penetration zone of 280mm. This is reasonably consistent with current industrial practice, where a 300 mm prelayer of NaX might be used, although in practice an industrial unit would be subjected to higher purge to feed ratios. It should be noted that if activated alumina were to be used, a shorter prelayer would be possible due to increased adsorptive capacity for water. It also suggests that in tropical environments with closer to 100% relative humidity and higher ambient temperatures, pretreatment of the feed gas may be warranted to reduce the water load to the adsorption bed. Alternatively one could use a two layered prelayer with an activated alumina layer first, then NaX.

This analysis also highlights the need to develop VSA cycles that provide sufficient internal purge to ensure the water front cannot penetrate beyond the design prelayer. For example, there are dangers of producing more product gas at lower purities, because this reduces the ratio of internal purge to feed, and as a consequence the water front will penetrate further into the bed, and possibly break through the prelayer. This is a critical issue for the future of low purity Rapid PSA.

This analysis has demonstrated the presence of a water loaded zone that displaces nitrogen, but ignores the heat generation associated with the adsorption and desorption of water in this section of the bed. As shown in Figure 4-36, the temperature swing due to adsorption is less in the water-loaded zone than the main bed, but is still not zero. The temperature swing associated with water in the prelayer can be calculated from solving an energy balance equation including convection and the heat of adsorption associated with water over the water loaded zone. An approximate solution to the energy balance equation gives a temperature swing of 2.3 $^{o}$C which is less than the swing in the nitrogen layer (approximately 4.3 $^{o}$C in the single layered bed with a dry air feed). This analysis suggests that one possible simplified model is to treat the water-loaded zone as an inert prelayer and ignore the heat effects associated with water adsorption/desorption. This idea is explored in the following experimental runs - AA38NaXLP, AA300NaXDLP and AA300NaXWLP.

In AA38NaXLP, dry air feed was used and a short prelayer of activated alumina was placed at the entrance of the adsorption bed, to simulate an inert zone as measured earlier. The thickness of the prelayer was 38 mm, which was based on the experimentally determined thickness of the water prelayer in NaXWLP. The resulting CSS temperature profile shown in Figure 4-39 is similar to the profile for NaXWLP, suggesting that wet loaded NaX and the dry alumina cause similar thermal profiles, because both prelayers do not adsorb nitrogen. Evidently, the effect of heat generation due to water adsorption/desorption plays only a minor role in the formation of the overall thermal profile.

Unfortunately, the feed temperature was not the same for experimental runs AA38NaXLP and NaXWLP. However, as was demonstrated in Section 4.4.6, over a small temperature range, different feed temperatures lead to a near uniform vertical translation of the entire profile. Therefore it is more important to look at the temperature drop when comparing results. For NaXWLP, a temperature drop of 15 $^{o}$C was observed whereas a 10 $^{o}$C drop was observed for AA38NaXLP. Part of this difference is due to uncertainty of the thickness of the water-loaded zone, as shown below.

**Figure 4-39**

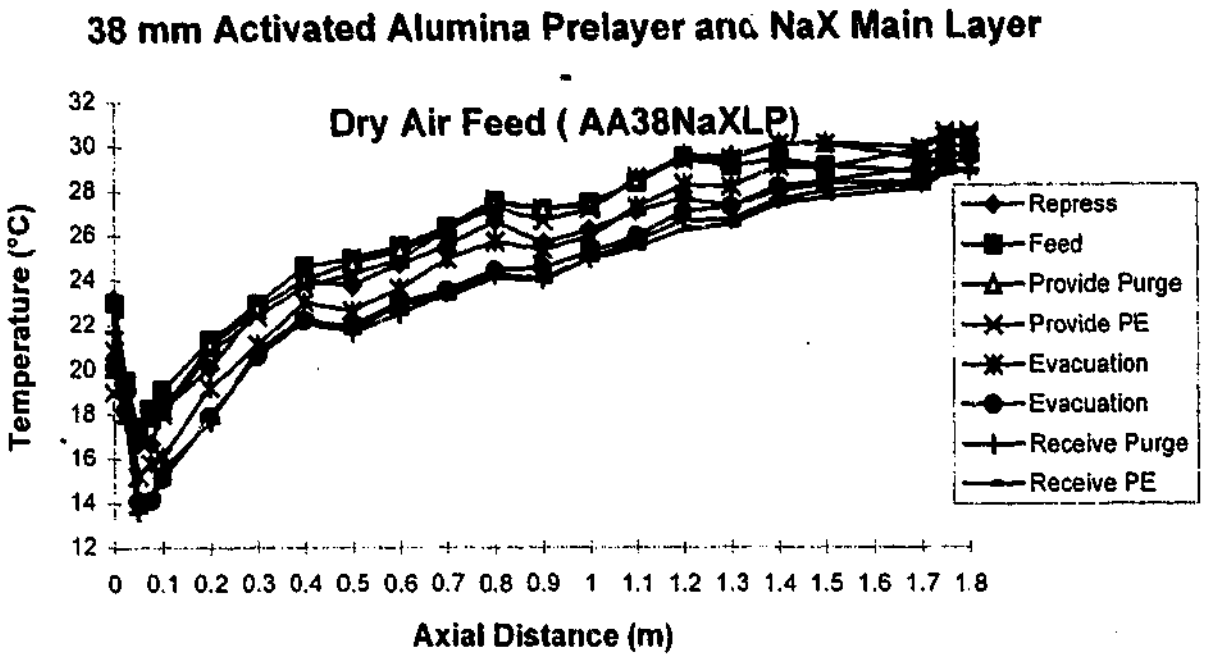


One limitation with this analysis is that the exact thickness of the water-loaded zone could not be determined, and the effect of any water mass transfer zone in NaXWLP has not been taken into account. In order to overcome this, additional experiments were performed with a long prelayer of activated alumina with dry (AA300NaXDLP) and wet (AA300NaXWLP) feed air. The objective of these experiments is to consider only the effect of water adsorption in the prelayer, and to ensure the prelayer is sufficiently thick so that water cannot penetrate through to the main nitrogen adsorbing layer. Any thermal effects due to water adsorption in the overall thermal profiles are isolated by these experiments. The resulting CSS temperature profiles shown in Figure 4-40 and 4-41 are compelling. These plots are very similar and confirm that water loading on activated alumina has only a marginal effect on the overall temperature profile. This confirms that formation of a 'cold spot' is determined by differences in adsorptive capacity of the two layers, and that the heat of adsorption of water plays only a minor role.

**Figure 4-40**

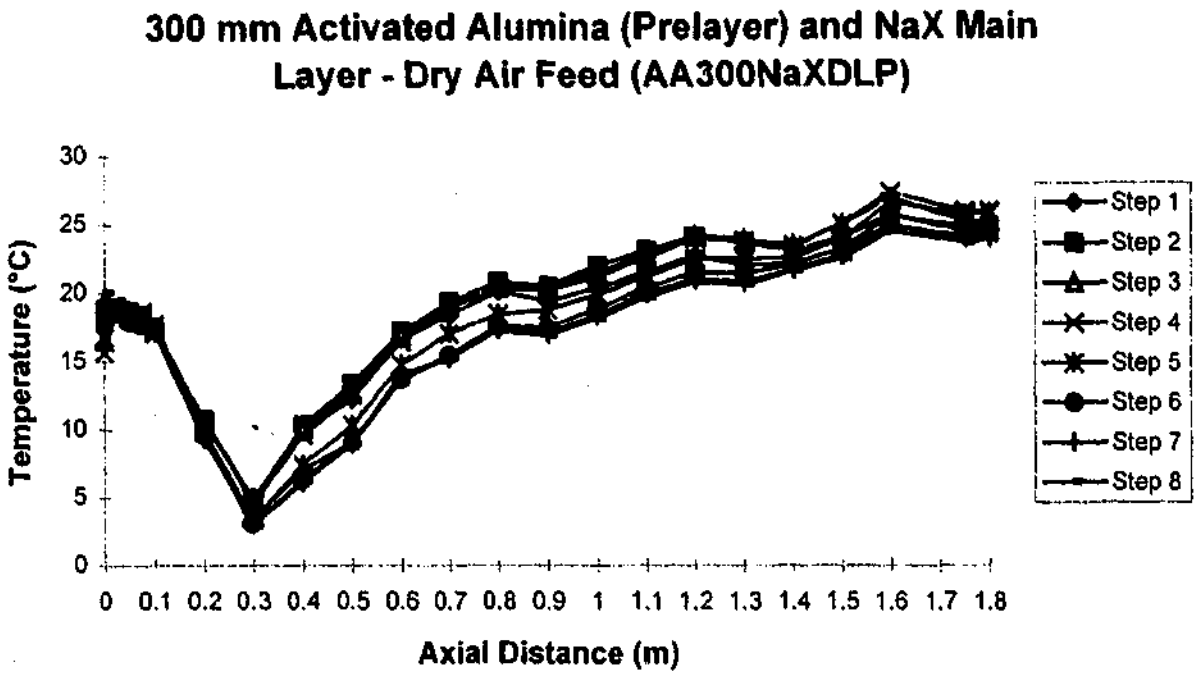


**Figure 4-41**

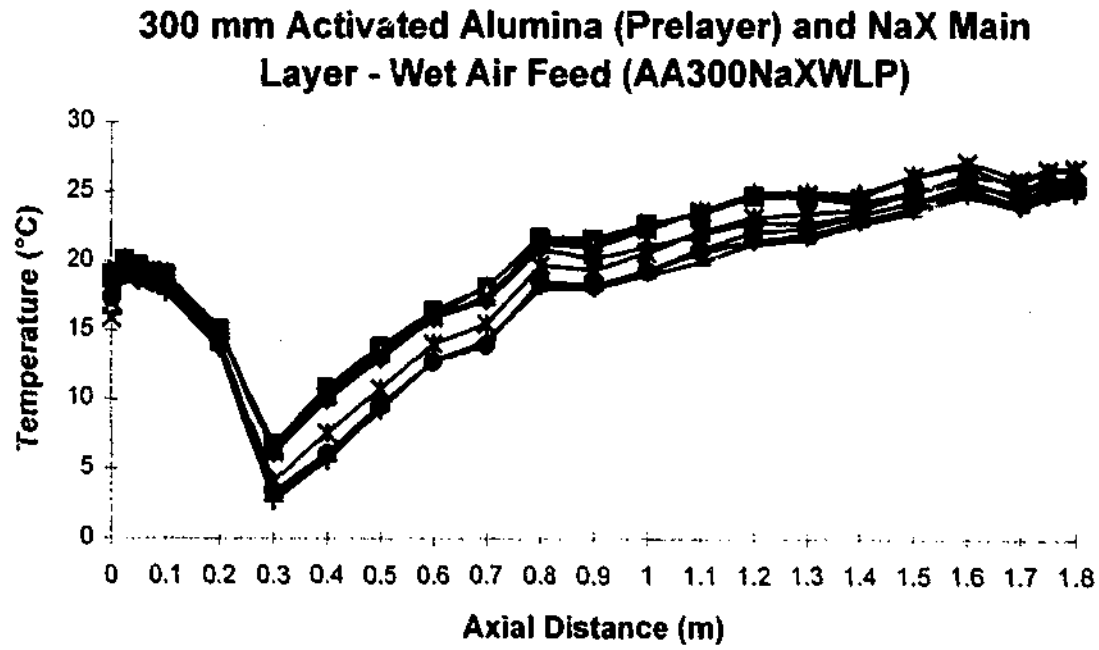

An interesting difference in the temperature profiles is that the temperature swing at the entrance of the bed for the wet feed (1.4 $^{o}$C) is greater than for the dry air feed (0.4 $^{o}$C), and there is a slight increase in the temperature of the bed above the feed temperature in the wet air feed case. Also, the temperature minimum for the dry air feed case is slightly lower than for the wet air feed case. These results are consistent with the fact that water loading is occurring. However, this has only a minor effect on the overall temperature profile.

Figure 4-40 and 4-41 (AA300 NaXDLP and AA300NaXWLP) also display more pronounced 'cold spots' than the previous cases as a consequence of a thicker prelayer, as was detailed in Section 4.6.2.

**Conclusion:** These experiments with wet air clearly confirm that a water loaded zone penetrates into a prelayer of NaX some finite distance. This creates a quasi-inert zone (with respect to nitrogen loading capacity) that causes the formation of a 'cold spot'. The analytical technique and MINSA predicted the length of this water loaded zone. There is considerable scope to further develop this technique and to determine the length of the water-loaded zone under different process conditions : different humidities, and different purge to feed rates. It also would be useful to further assess the assumption of a very sharp water mass transfer zone. The experimental results suggest that there is a slightly broader mass transfer zone. Some recent work by Karsten-Bar et.al. (2000) using MRI could be instructive in this regard. Importantly, the shape of this mass transfer zone will change with the move to shorter cycle times, and higher gas velocities, and will smear out, necessitating the need for thicker prelayers.

### 4.8.2 Transient Effect of Water Adsorption on Temperature Profiles

The introduction of wet air (relative humidity ~40%) will also produce a transient effect, where considerable heat will be generated when water adsorbs on to 'clean' dry activated alumina.

**Model Prediction:** The models developed in Chapter Two did not address the transient thermal effect of water adsorption, but it is apparent that there should be a temperature spike as water initially loads on to clean adsorbent, due to the high heat of adsorption of water on activated alumina or NaX. It is speculated that this effect will diminish in significance as the length of the water loaded zone increases.

**Experiment:** In order to assess the dynamic effect of the introduction of wet air feed, the VSA unit was fed dry air to CSS, and then switched to wet air of relative humidity ~40%, and the VSA unit continued operating to a new CSS. 300mm of activated alumina was used, to ensure the water loaded zone stayed inside the activated alumina prelayer.

**Result(s):**

Figure 4-42 displays a very sharp temperature increase at the front of the bed as wet feed gas initially contacts a dry prelayer of 300 mm of alumina. The VSA unit was at CSS with dry air feed (AA300NaXDLP) when it was switched to wet air feed (cycle zero). Immediately there was a sharp increase in the temperature profiles resulting from water adsorption on to 'clean' activated alumina.

**Figure 4-42**

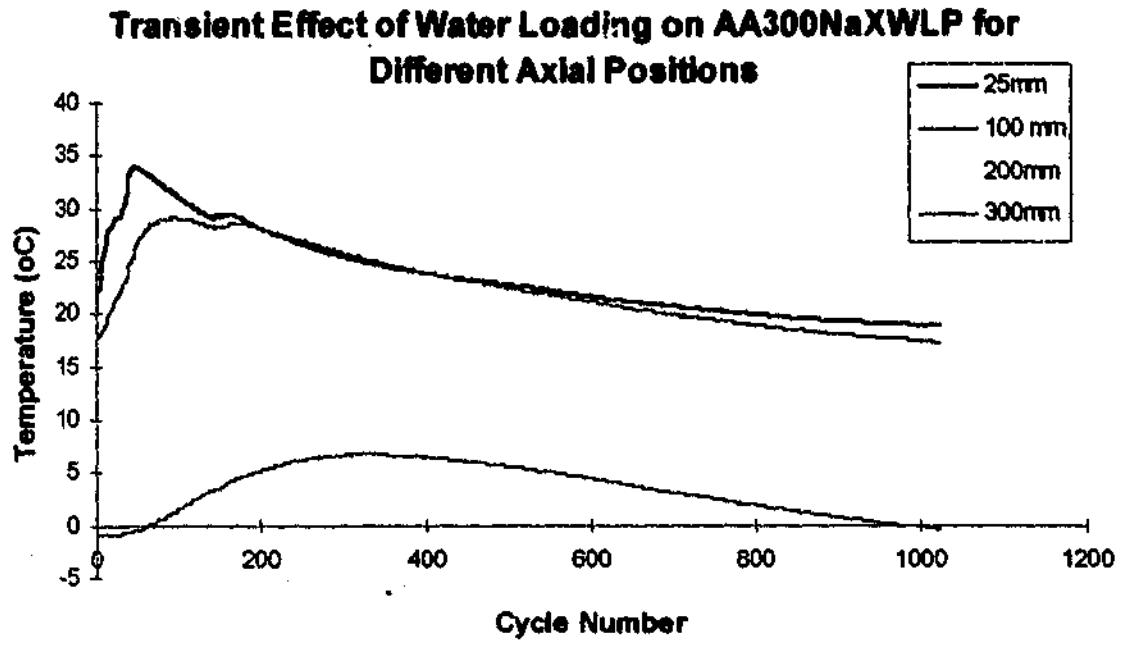


Over a thousand cycles this sharp temperature rise is convected through the front section of the bed, (as shown by thermocouples downstream) and largely disappears. This transient behaviour is not evident with dry feed air cases. The overall effect is an axial temperature profile at cycle zero very similar to the profile at cycle 1000. This confirms, as previously observed, that the CSS profiles are very similar for the dry and wet feed cases where there is an inert prelayer. However, the CSS profiles neglect this important difference in the transient behaviour in the wet and dry feed cases. The implications of this transient profile are important for understanding the effect of varying humidity on temperature profiles in the bed.

The observed temperature 'spike' results from the significant heat of adsorption of water initially, in a very thin section of clean bed, giving a substantial temperature rise. The heat of adsorption will be highest on a clean bed, due to the large isoteric heat of adsorption at zero loading. This heat is convected through the bed and the temperature 'spike' is slowly dissipated. The thermal wave travels slowly due to the slow speed of the convection of thermal energy through the adsorption bed. This temperature wave resulting from water adsorption is decoupled from the water composition wave that is held inside the initial section of the bed. As the water loaded zone increases in length, the absolute thermal capacitance of the water loaded zone increases. In effect, the heat generated by water

adsorption occurs over a larger mass of sieve, leading to a much smaller temperature increase at CSS.

**Conclusion:** This transient thermal 'spike' has little effect on oxygen VSA operation. It is an effect only evident at plant start-up, or in process conditions where there is a significant increase in ambient humidity. One safety concern is that the temperature 'spike' could melt plastic columns used in laboratory scale VSA units. In order to prevent this the feed humidity should be increased gradually, after the adsorption bed has an established axial temperature profile.

## 4.9 Total Reflux and Curious Effects

Total reflux represents a simple and totally theoretical cycle where no product gas is removed from the adsorption bed. There are two different cases of total reflux - internal and external. The total internal reflux case represents, simply, feed repressurisation followed by countercurrent evacuation. In the total external reflux case, bed-to-bed steps are included such as purge and pressure equalisation, but no product is taken. Considering the case of adiabatic adsorption beds, mass and energy flows in and out of the bottom of the adsorption beds are equal. Total reflux represents an interesting limiting case for theoretical investigation, and a useful test for numerical simulators.

### 4.9.1 Total Reflux - Internal and External

**Model Prediction:** The simple energy balance predicts that there will no average temperature gradient through the prelayer for both cases. Qualitatively for both cases, internal and external reflux, the mean temperature in an inert prelayer will be the temperature of the feed gas, as there is no net heating or cooling of the prelayer. The simple energy balance predicts likewise. However the zeroth order MSA and separation of variables approaches are less helpful. It is not possible to determine the long time scale temperature through the prelayer, since the integral of the mass flow over the cycle is zero when no product is taken.

The case of adiabatic total reflux also proves to be a difficult one for numerical simulation, particularly for the external reflux case. A typical temperature profile for the internal reflux case is described in Figure 4-43. This is based on an ADSIM simulation.

**Figure 4-43**

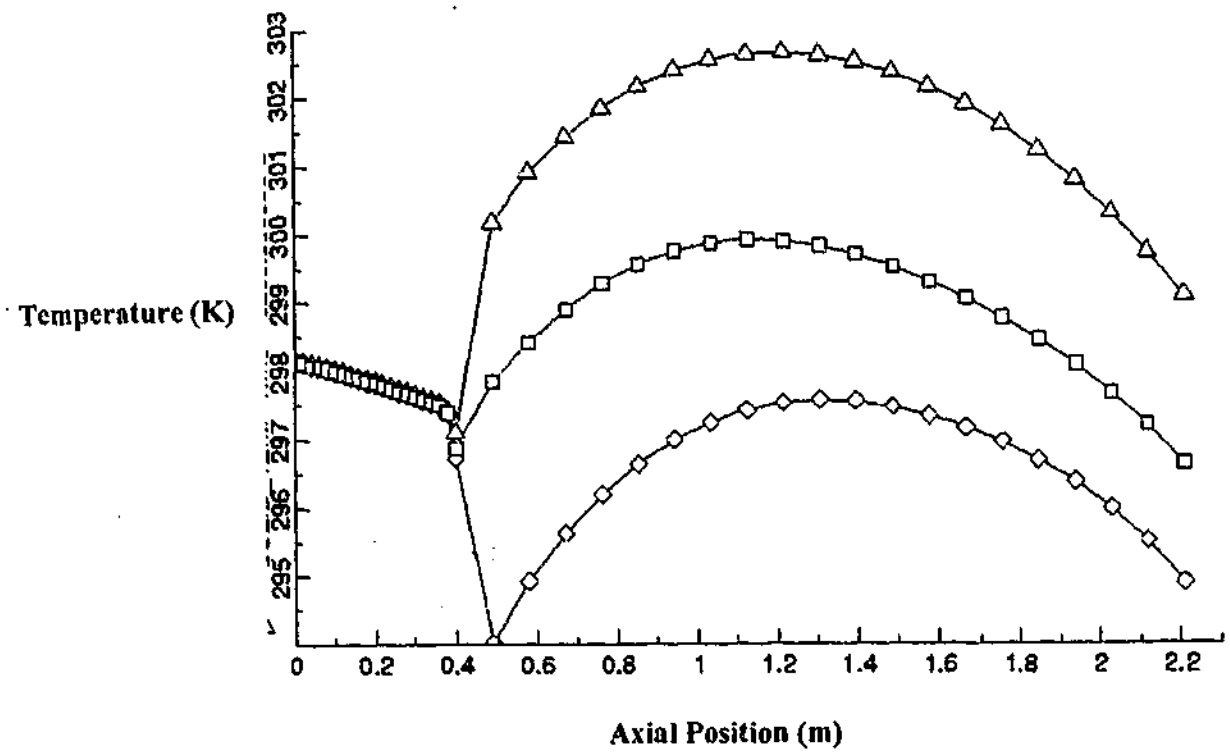


This presents an axial temperature gradient at CSS. There is only a slight temperature gradient through the prelayer (0.5 $^{o}$C) whereas the simpler models predict no mean temperature gradient. The slight temperature gradient is the result of numerical effects, and failure to close the mass and energy balances within tight tolerances. For practical purposes it is still possible to conclude that there is essentially no axial temperature gradient through the prelayer. It is also evident in the numerical simulation that the profile in the main bed is dominated by the cyclic adsorptive/desorptive temperature fluctuation. There is no appreciable long time scale gradient through the prelayer. This situation arises because there is no convected heat through the end of the adsorption bed, in the case of total internal reflux, and as a result the temperature at the end of the bed is essentially fixed. The slight hump in the middle of the bed arises due to the fact that heat is held inside the bed.

While the models still predict that there will be no net temperature gradient through the prelayer, the case of total external reflux is more complicated. The evolution of the axial temperature profile is particularly slow. In one simulation case, it required 134,000 cycles to converge within the specified MINSA tolerances! The introduction of the bed-to-bed step increases the complexity of the interaction between convective heat fluxes and heat of adsorption. Figure 4-44 shows the axial temperature profiles for an 8 step VSA cycle (Cycle 2) with a pressure window of 1.4-0.45 bar with an inert prelayer and a main layer of VSA2, at CSS after 1340,000 cycles (at CSS) and after 3000 cycles (not at CSS).

**Figure 4-44**

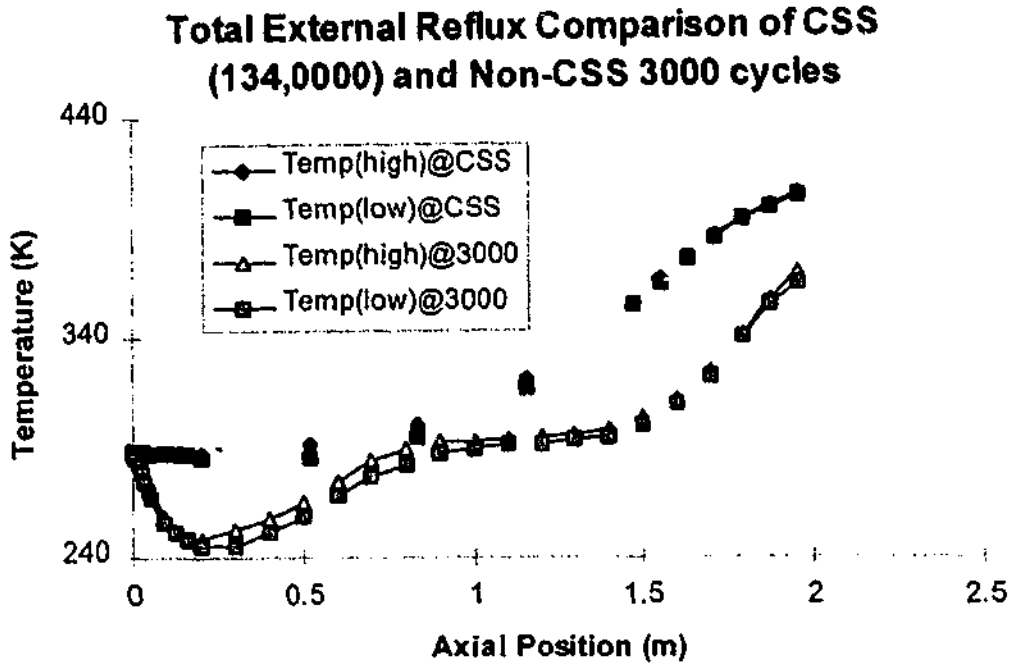


Figure 4-44 shows that initially there is a sustained temperature depression (after 3000 cycles), but as the profile evolves, the end of the bed is progressively heated, and the entire temperature profile is lifted. This process continues until there is closure of the energy balance. At CSS there is no temperature gradient through the prelayer, and the end-of-bed temperature is 404 K. This limiting case highlights the importance of a conservative numerical scheme, where closure of the mass and energy balances can be achieved to very tight (and specified) tolerances. This hypothetical example also highlights the danger of assuming CSS based on real world 'rules of thumb' about cycles to CSS. The absence of real world dissipative second order terms can greatly increase the time to CSS.

**Experiments:** The experimental investigation of total internal and external reflux is complicated by two factors. Firstly, there is a safety issue associated with the rotary vane vacuum pump. As no oxygen enriched product is withdrawn, there is the possibility of enriched oxygen gas being passed through the vacuum pump. This risk was averted by operating with the gas ballast open on the vacuum pump, which then continuously draws approximately 60 litre/min of air through the vacuum pump and thereby dilutes any oxygen enriched process gas.

Secondly, all the models are predicated on the assumption of adiabatic beds. In practice this is not the case, and the introduction of a heat loss term is likely to cause a profile through the inert prelayer.

**Result(s):** The CSS profile differs significantly from the simulation runs - there is a marked temperature gradient through the prelayer and the temperature profile through the top of the bed is flat. These differences can be explained as a result of the heat exchange with the environment in the experimental run.

Heat exchange occurs along the length of the bed, but also from the product tank and product pipework. This, combined with the composition front being held well back, leads to the CSS profile.

The effect of product removal can also be ascertained by comparing AA300LSX9, AA300LSX10, and AA300LSXINT. The pressure window of these three runs was approximately the same (137-44 kPa). No purge step was employed in any cycle. The sole effective difference in these cycles was the amount of product removed.

**Table 4-36 - Effect of Internal Total Reflux or Small Product Removal**

| | AA300LSXINT | AA300LSX9 | AA300LSX10 |
|---|---|---|---|
| Product Flow (mmol/cycle) | N/A | 100 | 332 |
| Oxygen Purity (% $O_2$) | N/A | 50.0% | 45.7% |
| Average Feed Temp (°C) | 12.0 | 11.2 | 11.5 |
| Cold Spot (°C) | 7.4 | 4.4 | 6.3 |
| ΔT (Feed - Cold Spot) (°C) | 4.6 | 6.8 | 5.2 |

Interestingly, there is a minimum 'cold spot', as was observed with the simple energy balance model (Figure 2-17). There is a quantity of product removal that corresponds to a minimum temperature.

It is also possible to compare the temperature profiles for the case of total internal and external reflux. As is evident from Table 4-37, external reflux displays a far more significant temperature profile than internal reflux. This is also demonstrated in the adiabatic simulated case in Figure 4-44, where after 3000 cycles there is a significant temperature profile through both the prelayer and main layer. This is similar to the experimental result

(AA300LSXEXT). However, unlike the MINSA simulation, in the experimental run heat loss prevents very high temperatures at the end of the bed, and there is a persistent temperature gradient through the prelayer at CSS. By contrast, no significant temperature gradient ever appears in the total internal reflux case, because there is no enthalpy flux through the end of the adsorption bed.

**Table 4-37 – Comparison of Temperature Profiles (Internal vs. External Reflux)**

| | **AA300LSXINT** | **AA300LSXEXT** |
|---|---|---|
| Feed Flow (mmol/cycle) | 2743 | 3708 |
| Pressure Profile (kPa) | 136.7/44.8 | 135.3/141.1/41.1/45.6 |
| Average Feed Temp (°C) | 12.7 | 13.7 |
| Cold Spot (°C) | 6.8 | -5.1 |
| Max Bed Temp.(°C) | 12.7 | 36.6 |
| ΔT(Max-Cold Spot) (°C) | 5.9 | 41.7 |

Table 4-37 also shows a significantly increased feed gas flow for the total external reflux case (AA300LSXEXT), due to the effect of purge. This is apparent even when the slight difference in pressure windows is accounted for.

**Conclusion:** Total reflux (internal and external) represents an interesting limiting case for analysis, and a useful test for numerical simulators. The case of total internal reflux (without heat loss) is relatively easy to understand. At CSS the enthalpy fluxes forward and reverse through the prelayer are equal, and hence there is no temperature gradient. The temperature at the end of the bed is 'relatively' fixed, since no gas is convected through the end of the bed.

The total external reflux is more complex. Like the case of the total internal reflux, at CSS the enthalpy fluxes forward and reverse through the prelayer are equal, hence there is no temperature gradient. However prior to CSS, the cocurrent steps and the 'bed-to-bed' connection cause a substantial temperature depression and significant heating at the end of the bed. As this process of heating the top of the bed continues, the 'cold spot' is reduced, until there is no temperature gradient through the prelayer, but an extremely high temperature at the end of the bed. Obviously heat loss from the adsorption bed and from 'bed-to-bed' connections would in reality prevent such high temperatures.

## 4.10 Conclusion

This Chapter has compared experimental data for the CSS temperature profiles with the simple energy balance, qualitative explanations and MINSA simulations. A range of parameters were investigated and some of the main results can be briefly summarised as follows:

- The working capacity of the adsorbent strongly effects the severity of the temperature profile. If the working capacity is increased, through increasing the pressure window, or increasing the extent of purge, the 'cold spot' will be more severe.
- The amount of product flow also impacts on the temperature profile. Increasing the product flow tends to flatten the temperature profile.
- The extent of pressure equalisation also effects the temperature profile, but this is limited since the extent of PE is limited.
- The feed gas temperature will tend to translate the temperature profile vertically. The resulting temperature profiles will be different due to the temperature dependence of the isotherms.
- The specific cycle can impact significantly on the overall temperature profile. The extent of top-to-top (bed-to-bed) interaction tends to increase the severity of the 'cold spot'.
- In laboratory scale oxygen VSA, the thermal profiles are more severe in the polyurethane columns, than in the PVC columns. The metal columns gave the flattest temperature profiles. The main limitation with the polyurethane columns was their lack of mechanical robustness.
- Increasing the adsorptive properties of the main layer, and/or increasing the heat of adsorption of the main layer adsorbent will increase the severity of the 'cold spot'.
- The thermal mass of the inert prelayer causes the 'cold spot'. Increasing the thermal mass of the prelayer increases the magnitude of the temperature depression. However the temperature asymptotes to a given value for the specific enthalpy fluxes through the main adsorption bed.
- An adsorbing prelayer significantly reduces the extent of the temperature depression.
- In the case where the temperature swing in the adsorbing prelayer is larger than the main layer, the temperature profile will exhibit a 'hot spot' in a one bed cycle.
- The addition of an inert thermal diluent can mitigate the severity of the temperature profile. However for experiments undertaken with the copper diluent, the performance and thermal profile alteration was relatively small.

- Oxygen VSA exhibits slow evolution to CSS. This transient response can be modelled well with the dynamic simulator MINSA.
- Water can play a critical role in creating the preconditions for a 'cold spot' by creating a quasi-inert water loaded zone with virtually no nitrogen adsorptive capacity. The depth of this water loaded zone can be successfully described as a function of feed flow, humidity, purge volume, and the properties of the adsorbent. This relationship can be described analytically.
- When loaded on dry pristine adsorbent, water can also cause a transient temperature spike. Over a thousand cycles this temperature spike is dissipated through the adsorption bed.
- Total reflux represents a curious limiting case. In the case of total internal reflux, the temperature profile through the prelayer and main layer remains relatively flat. By contrast, with total external reflux, the convection of heat through the bed leads to a significant transient 'cold spot' that slowly recedes as the top section of the bed is progressively heated.

MINSA has been successfully demonstrated to be a powerful tool for predicting the VSA performance and axial CSS temperature profile. The major discrepancies between MINSA and the experimental results occurred for the simulation of LiLSX which had not been adequately characterised, so a generic LiX adsorbent was used for these simulations. This reinforces the critical role of the multicomponent isotherm measurements for reliable PSA/VSA simulations. However with the well characterised NaX, MINSA very accurately predicted the performance of the VSA unit, and the axial temperature profile. Flows correlated to within less than 5%, pressure profiles to within less than 2%, oxygen purities to within less than 0.5%.

Two areas of difference between the MINSA simulation and the experimental results related to the temperatures at the end of the bed, and the cyclic temperature swing. MINSA consistently over-predicted the measured cyclic temperature swings, and consistently under-predicted the CSS temperature at the end of the adsorption bed. Several reasons have been postulated for these differences. Cyclic temperature swing may have been over predicted due to the incorrect estimate of the heat of adsorption, or adsorbent heat capacity. This requires further investigation, but it should not detract from the fact of generally excellent correlation between MINSA and the experimental results.

Chapter Three described in detail the goal of the development of adiabatic adsorption columns. The results with these columns were mixed. As expected, the polyurethane columns achieved more marked temperature profiles than were observed in the metal or PVC columns. In addition, the lowest bed temperatures were achieved with the polyurethane columns.

However, the polyurethane columns were not sufficiently mechanically robust to be used for most experiments. The repeated cyclic pressure swings led to a delaminating of the mylar film from the polyurethane foam. It is also possible that a secondary effect caused by oxygen aging may have assisted this process of degrading the polyurethane columns.

Another problem with the polyurethane columns was that they limited the number of radial thermocouples that could be used to monitor the temperature profile. In a different prototype polyurethane column with extensive thermocouple ports (~20 thermocouples per bed), there was severe delaminating of the bed and marked short-circuiting and channelling of air through the polyurethane insulation, rather than through the adsorbent. Also, unlike the PVC columns, sample points and additional thermocouples could not simply be drilled into the polyurethane columns.

Another ongoing concern with the polyurethane columns was the risk of fire with unattended operation. As is detailed in Appendix 6, a byproduct of the combustion of polyurethane foam is HCN. Although the risk assessment deemed the probability of fire to be very low, the combination of oxygen and polyurethane foam is not ideal.

Some alternative adiabatic column designs are detailed in Appendix 2. However it was felt that the PVC columns represented a suitable compromise between mechanical, non-isothermal performance, and ease of temperature measurement and gas and solid sampling.

One significant omission from this study is a detailed investigation of the performance impact of different CSS temperature profiles. In the case investigated in Section 4-6-2 (AA25LSX1, AA115LSX, and AA300LSX1), where the thickness of the inert prelayer was varied and the mass adsorbent was held constant, there was little difference in the separation performance. This is due to the fact that the average bed temperature was similar for all three cases. Furthermore as shall be detailed in Chapter Five, for LiLSX over the temperature range in question, separation performance is reasonably constant. The conclusion is that

small variations in average bed temperature do not necessarily impact on oxygen VSA separation performance.

However in order to demonstrate experimentally that temperature profiles can in other instances impact markedly on separation performance, several modifications to the experimental procedure would be required:

- A heater and cooler on the feed line, and/or the adsorption bed. This would enable adjustment of the temperature profile, without relying on the inert prelayer. Subsequent to this experimental work, a heater has been added to the oxygen VSA unit.
- Investigate the effect with single layer beds. This would ensure the same mass of adsorbent in all cases, and the same end of bed voidages. In several experiments undertaken in this study, where the temperature profiles differed, the mass of adsorbent was not held constant, and hence it is not possible to isolate the performance effect of different temperature profiles.
- Alter the control scheme to adjust the feed and vacuum flow control valves during the steps, to achieve constant velocities akin to constant volume blowers (Rootes blowers) typically used in oxygen VSA. This would enable direct comparison of the separation performance, assuming fixed blower size, which is a more realistic industrial scenario.
- The control scheme also needs to be improved to achieve the same purities and purge flowrates between different experimental runs, to enable better direct comparison.
- Careful adsorbent selection would also assist in observing the effect of CSS temperature profiles on oxygen VSA separation performance. For example, Chapter Five demonstrates that NaX and CaCHA separation performance is a stronger function of temperature than LiLSX.

These modifications would assist to enable further investigation of the effect on performance of CSS temperature profiles in a laboratory scale VSA unit. Instead this study utilises MINSA in Chapter Five to more fully investigate these effects. It is felt that this is a reasonable approach, given that the accuracy of MINSA has been thoroughly demonstrated in this chapter. The application of MINSA also enables investigation of the process conditions that could not easily be achieved in the laboratory unit. For example, feed temperature well away from ambient (both hot and cold) cannot be easily achieved in the laboratory unit.

# Chapter Five

# Optimisation of Thermal Profiles in Oxygen VSA

The presence of the 'cold spot' in oxygen VSA and PSA is well recognised in the gas industry. It is appreciated that both the cyclic temperature fluctuations associated with adsorption and desorption, and significant axial temperature profiles can have a marked impact on the overall performance of the VSA unit. Patents and the academic literature report both performance improvement and deterioration due to the presence of the 'cold spot'. The absence of well-defined performance criteria has complicated this situation. This chapter develops fundamental performance criteria by relating isotherm properties to sieve productivity (1/BSF) and recovery and then linking these process performance parameters to adsorbent, blower and power costs.

This chapter also reviews the gas industry's response to the 'cold spot' in oxygen VSA/PSA. From early efforts at mitigating the thermal profile, more recent patents have sought to optimise the CSS axial thermal profile. Other researchers have sought to reduce the cyclic adsorption/desorption temperature swing in order to improve performance. Based on the performance criteria developed in this chapter, and drawing on the modelling and experimental work in the preceding chapters, a number of new strategies of thermal optimisation are proposed.

## 5.1 - Differences in Performance and Different Performance Criteria

An ongoing difficulty with the thermal optimisation of oxygen PSA/VSA has been the absence of clearly defined performance criteria. This has led to apparently conflicting conclusions about the consequences of severe thermal profiles, and preferred operating conditions. This situation has also been compounded by the fact that general conclusions have been drawn, when the impact of operating inside a temperature zone is highly specific to a given adsorbent, pressure window and cycle.

A measure of this uncertainty is evident from the conclusions of several different adsorption researchers. Skarstrom (1966) states that room temperature is preferred for PSA using zeolites. Likewise Collins (1977) demonstrates that in the case of oxygen PSA with NaX, sub-ambient operating temperatures result in reduced oxygen recovery. While investigating CaA, Karwat (1967) reports that the preferred operating temperature for oxygen enrichment is 300 K. However these conclusions conflict with the significant work of Izumi et.al. (1989) who argued that some types of a molecular sieve perform better at temperatures well below ambient (NaX at -30 $^{o}$C), while molecular sieves with alkaline earth cations (Ca and Sr) showed best separation performance at near room temperature. Leavitt (1992) and Yanagi

and Qui (1998) draw similar conclusions to Izumi and argue that for VSA cycles with NaX, subambient operating temperatures are preferred.

These apparently conflicting conclusions can only be reconciled by developing more specific process performance criteria, and recognising that performance is a function of operating conditions, sieve type, and cycle. This situation is highlighted by the work of Collins who argues that the 'cold spot' impacts negatively on recovery for oxygen PSA using NaX. Collin's focus on recovery as the measure of performance ignores the importance of sieve productivity (1/BSF). (BSF is the Bed Sizing Factor (kg adsorbent/TPDc Oxygen and the reciprocal of BSF is a measure of the sieve productivity.) The importance of recovery becomes only apparent when a VSA/PSA plant has been built and the blowers' size is fixed because in this case, the recovery becomes a direct measure of production rate. To highlight this issue, consider the following MINSA simulation runs for a single layered adiabatic bed composed of LiLSX with an 8 step cycle (Cycle 2), and dry air feed, and a pressure window of 1.25-0.48 bar.

**Table 5-1- Comparison of Performance for Different Feed Temperature**

| **Feed Gas Temperature into Main Layer** | **200 K** | **250 K** | **300 K** |
|---|---|---|---|
| Total Feed (mmol) | 7720 | 5630 | 4900 |
| Total product (mmol) | 1010 | 700 | 770 |
| Oxygen production (kgpdc) | 43 | 30 | 33 |
| Recovery (%) | 52.7 | 50.0 | 63.4 |
| Purity (%) | 92.8 | 92.9 | 93.1 |

Table 5.1 illustrates the situation that Collins and others in the gas industry faced. Industrial plants were designed and built on the basis of the laboratory scale data with feed gas temperatures of approximately 300 K, corresponding to a recovery of 63.4%. Blowers were sized on the basis of this oxygen recovery derived from these laboratory scale results, but when scaled up to industrial (adiabatic) adsorption beds, such recoveries (and hence production rates) were not achieved due to the presence of the severe axial temperature profile. For example, Collins (1977) reports an oxygen recovery of 45.5% (feed temperature of 70 °F) in a 4 inch bed, compared with 39.4% recovery (feed temperature 50 °F) in a 26 inch bed. This problem resulted in a number of patents and other strategies, (detailed in Section 5.5) that sought to mitigate the severe axial temperature profiles.

Once the presence of the 'cold spot' was better understood, this enabled approaches that sought to optimise the effect, rather than mitigate it. Typically this required performance measures that included sieve productivity, rather than solely recovery (Watson et.al., 1996). Subsequently, a Praxair patent developed a more detailed measure of adsorbent performance as a function of temperature for a specified pressure window (Notaro et.al., 1997). This patent develops an Adsorption Figure of Merit (AFM) for different adsorbents at different temperatures. The identified parameters that make up the AFM are:

- $n_{N2,ad} - n_{N2,de}$ - The difference in nitrogen loading between adsorption and desorption conditions.
- $\alpha_{N2,ad}$ - The selectivity of the adsorbent for nitrogen at the adsorption conditions.
- $\alpha_{N2,de}/\alpha_{O2,de}$ - The selectivity of the adsorbent for nitrogen at the adsorption conditions divided by the selectivity for oxygen at the desorption conditions.

The product of these three parameters is presented as the adsorbent performance number (AFM). This is an arbitrary measure of performance.

A similar measure of performance utilised in the gas industry is sieve productivity per unit mass of adsorbent (1/BSF). The BSF can be simply derived from a mass balance around the VSA unit over a cycle.

$$BSF = \frac{\left(\frac{1-y_{O2,f}}{y_{O2,f}} - \frac{1-y_{O2,pr}}{y_{O2,pr}}\right)}{WC_{N2} - WC_{O2}\left(\frac{1-y_{O2,f}}{y_{O2,f}}\right)} \qquad (5\text{-}1)$$

where WC is the working capacity of the adsorbent with respect to nitrogen and oxygen. (change in mol loading/kg adsorbent) If the voidage of the adsorbent is ignored this is simply the difference in loading capacity between the end of feed (f) and the end of evacuation (e) conditions.

$$WC_{N2} = n_{feed}(P_f, T_e, y_{N2,f}) - n_{evac}(P_e, T_e, y_{N2,e}) \qquad (5\text{-}2)$$

The pressure and mole fraction differ at the end of feed and the end of evacuation. For the isothermal case, the temperature ($T_e$) is unchanged. The same equation can be written to determine the working capacity with respect to oxygen. A binary system is assumed and nitrogen ($y_{N2,f}$) is 0.78 and the balance is oxygen. i.e. oxygen and argon are treated as a

single component. The evacuation mole fraction of nitrogen ($y_{N2,e}$) could be determined analytically (Knaebel and Hill, 1985). However for this analysis, like Notaro et.al. (1997) the nitrogen mole fraction on evacuation is assumed to be 0.95.

For the typical case, where the product purity is 90% oxygen, and an air feed, the reciprocal of this equation (1/BSF) provides a measure of the sieve productivity.

$$\frac{1}{BSF} = \frac{WC_{N2} - 3.76WC_{O2}}{3.65} \text{ (mol of oxygen product per cycle / kg of adsorbent)} \qquad (5\text{-}3)$$

This equation can also be written in more units incorporating cycle time explicitly.

$$\frac{1}{BSF} = \left(\frac{WC_{N2} - 3.76WC_{O2}}{3.65}\right) Mw_{O2} \frac{0.0864}{\tau_c} \text{ (TPDc/kg adsorbent)} \qquad (5\text{-}4)$$

Dimensional consistency dictates which equation (either 5-3 or 5-4) is utilised as a measure of sieve productivity. Given that the cycle time is fixed in this analysis, either equation can be used to compare the productivity of different adsorbents.

A limitation with these equations is that the oxygen working capacity may increase relative to the nitrogen working capacity thereby resulting in a negative sieve productivity (1/BSF) number. Under this condition, it is not possible to achieve a product purity of 90%.

It also follows from the mass balance that the oxygen recovery (Rec) can be written as:

$$Rec^* = \frac{\frac{1}{BSF}}{WC_{O2} + \frac{1}{BSF}} \qquad (5\text{-}5)$$

*Rec is generally stated throughout this chapter as a fraction, not as a percentage. In Chapter 4, oxygen recoveries were generally reported as percentages, which is common industrial practice.

If the total working selectivity of the adsorbent S is defined as the ratio of the nitrogen working capacity to the oxygen working capacity ( $S = WC_{N2} / WC_{O2}$ ), the sieve productivity can be rewritten as:

$$\frac{1}{BSF} = \frac{WC_{N2}(S - 3.76)}{3.65S} \qquad (5\text{-}6)$$

This equation, like the AFM shows a direct proportionality between sieve productivity and nitrogen working capacity. The equations differ with respect to their treatment of selectivity. However in many cases, where selectivity is not a strong function of temperature, both performance parameters correlate well. Figure 5-1 presents the plot (1/BSF) and AFM where the maximum values of both are scaled to unity to aid comparison.

**Figure 5-1**

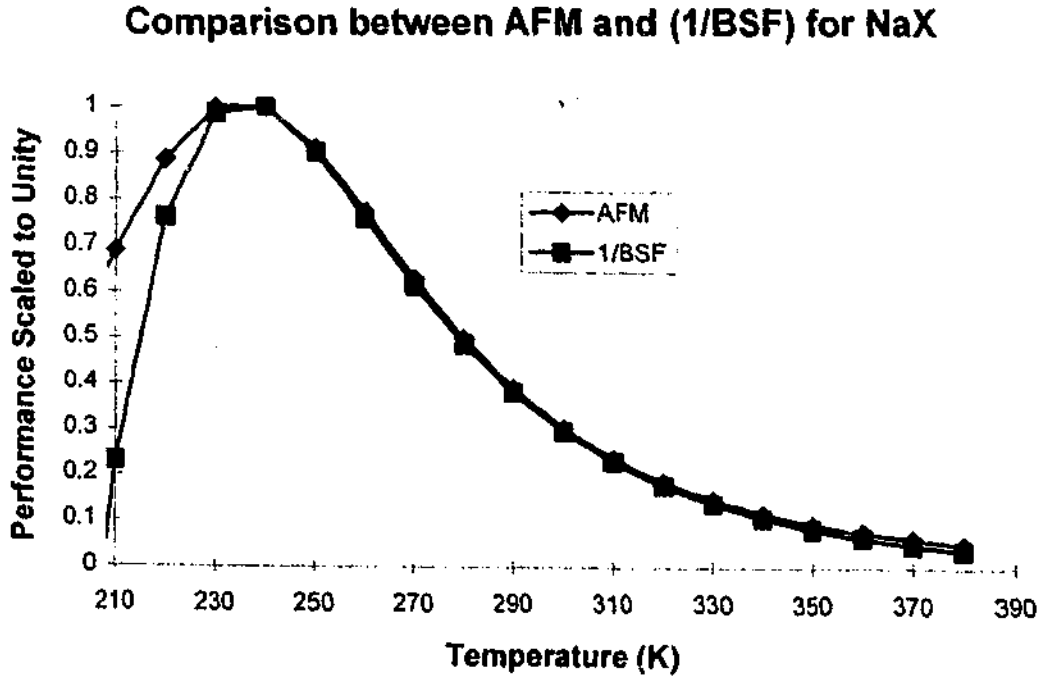


In other cases, where selectivity alters significantly with temperature, there are marked disparities between the two different performance measures as shown in Figure 5-2 for CaCHA.

**Figure 5-2**

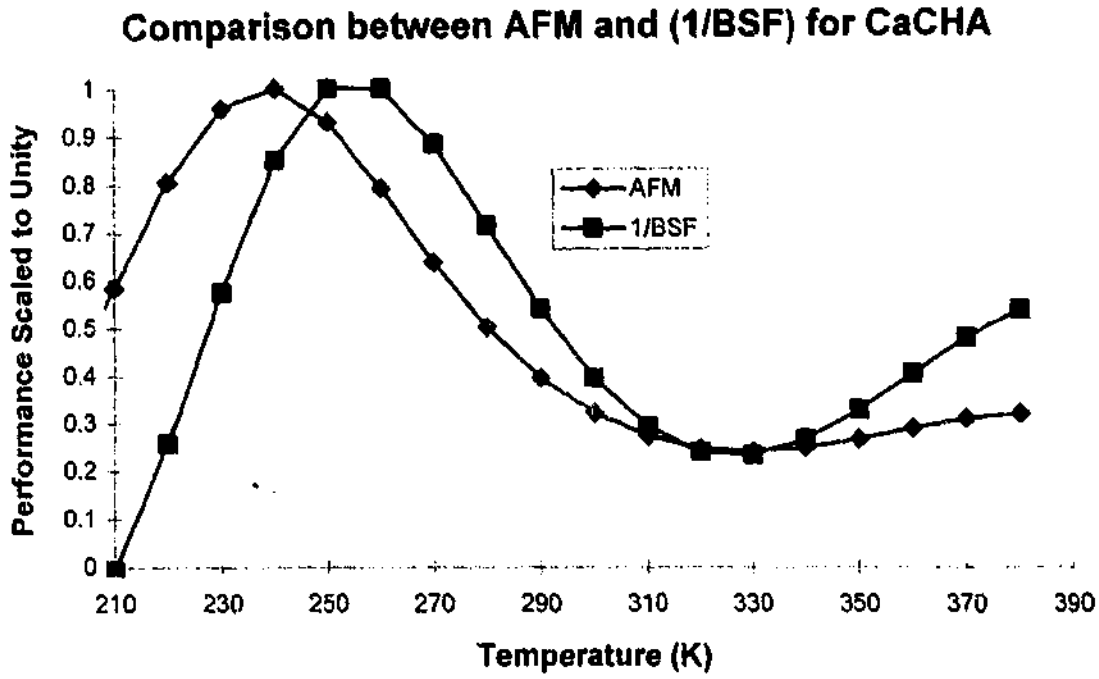


One interesting feature of these performance parameters is that the location of the sieve productivity maximum shifts for different pressure windows. For example, there is some apparent discrepancy between Collins and Leavitt regarding the performance of NaX at different mean temperatures. However Collins considered a PSA cycle (say 6-1 bar abs) where Leavitt considered a subatmospheric VSA cycle. The optimum operating temperature for an isothermal cycle is 270 K for the PSA cycle, whereas the optimum for the VSA cycle is 240 K as is shown in Figure 5-3. This suggests that both Leavitt and Collins may be correct for the given pressure windows that they investigated.

**Figure 5-3**

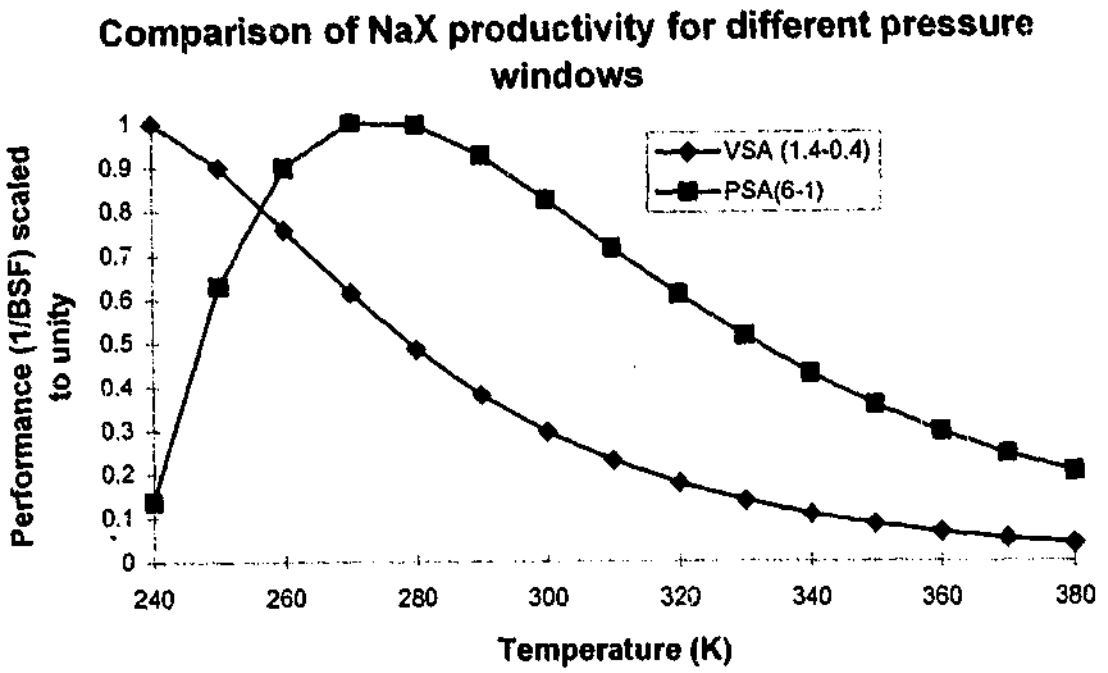


One important observation from the preceding figures is that the local performance maximum for some adsorbents occurs at very low temperatures, approximately 200 K. This is significantly below typical operating conditions, and approximately the operating conditions proposed by Yanagi and Qui (1998). There are several possible explanations for sieve productivity improvement at very low temperatures. Firstly, these performance parameters and the work of Yanagi and Qui (1998) are derived on the basis of isothermal operation. Adiabatic operation will significantly shift the location of the performance maximum. Secondly, these plots of sieve productivity at very low temperature operation could be correct, but these conditions probably coincide with significantly lower oxygen recovery. The trade off between (1/BSF) and recovery may not be favourable.

This suggests that an adiabatic measure of performance is required instead of an isothermal one. Ackley et.al. (2000) acknowledge the need for an adiabatic performance measure and propose the following adiabatic performance measures: (a) nitrogen working capacity, (b) nitrogen working capacity divided by oxygen working capacity (adiabatic separation efficiency), or the product of (a) and (b). Importantly, the temperature difference between adsorption and desorption is accounted for in this work. Ackley et.al. (2000) suggest the temperature difference can be determined from experiment, adiabatic process simulation, or estimated by applying a simple energy balance. The approach adopted here is to assume a very simple equation to calculate the temperature rise associated with adsorption (Equation 5.8).

Incorporating adiabaticity is important, but the performance measures proposed by Ackley et.al. (2000) share many of the limitations of the AFM and the simple 1/BSF. These limitations include:

- The working capacity of the sieve as previously defined was limited to the difference in the adsorptive loading of nitrogen at adsorptive conditions and desorptive conditions. This ignores losses associated with voidage. To more accurately determine performance, the working capacity must include voidage. In fact, as sieve productivity improves, the contribution of voidage becomes a more significant component of separation inefficiency.
- None of these plots (AFM, adiabatic separation efficiency or 1/BSF) include the cost of different adsorbents. The sole basis of any performance indicator must be cost. On this basis 1/BSF provides a more realistic performance parameter because it is related to the quantity of adsorbent, and hence capital cost required, for a given production rate.
- In addition to sieve productivity there is also a need to consider the oxygen recovery for different adsorbents. Oxygen recovery is critical because it determines the size and power consumption of the feed and vacuum blowers, and the sizes of pipework and valves. The importance of recovery is often neglected, because unlike most other adsorptive separations, the feed gas for oxygen VSA is free (at ambient pressure and temperature).

## 5. 2 Revised process and economic performance criteria

The identified limitations with Praxair's AFM and adiabatic separation efficiency, and the simple isothermal 1/BSF can be overcome. However, even this revised performance criteria does not include all the process variables that impinge on overall VSA performance. A full optimisation of design and process variables is beyond the scope of this project. The aim here is to outline the relationship between the process performance criteria and the total cost (operating and capital), and hence enable direct cost comparison between different adsorbents based on their isotherms.

Central to this task is the development of a more realistic measure of sieve productivity that includes voidage and cyclic temperature fluctuations associated with adsorption and desorption. There is also a need to include oxygen recovery as a key process parameter. Oxygen recovery directly impinges on feed blower and vacuum blower sizing and power.

Together these two performance parameters, recovery and sieve productivity (1/BSF), can be related to the cost of adsorbent and the cost of the feed and vacuum blowers, and related to the power costs.

$$\text{Capital Cost} = \text{Fixed Capital Cost} + \text{Adsorbent} + \text{Blowers}$$

$$\text{Operating Cost} = \text{Fixed Operating Cost} + \text{Power}$$

Without detailing the fixed capital and fixed operating costs, it is possible to make a direct comparison between different adsorbents with respect to sieve productivity (1/BSF) and recovery. These fixed costs are assumed, independent of the adsorbent selected.

The adsorbent cost is the quantity of adsorbent required multiplied by the cost of the adsorbent. Both the feed and vacuum blowers are constant volume Rootes blowers, and size of the blowers is a function of the recovery, and the pressure window and cycle time. For the case considered here the pressure window and cycle are fixed. It is assumed that the cost of the feed and vacuum blowers can be scaled linearly with size. The feed blower is a single stage blower, and it is assumed that the vacuum blower requires two stages. The variable operating cost of the oxygen VSA is power. The equations for power for the feed and vacuum blowers can be found in Appendix 10.

In order to apply these performance criteria, it is necessary to fix a number of process variables. The variables that can be fixed include the number of beds (2), pressure window (1.4 - 0.4 bar absolute), nitrogen mole fraction window (0.78 (feed) - 0.95 (evacuation)), the product purity (90%), the cycle (Cycle 2), the cycle time (60 sec), the feed time (22 sec), the pump down time (27 sec), and the production rate (50 TPDc). The analysis also assumes that the bed is uniformly saturated at the end of feed conditions, and the effect of axial concentration gradients and any kinetics effects are ignored. It is reiterated that in a full optimisation, these variables cannot be fixed, but this does not adversely effect the comparison of the thermal performance of different adsorbents.

### 5.2.1 Revised Sieve Productivity and Recovery

The revised adiabatic sieve productivity measure (1/BSF) including the effects of voidage can be derived in a similar manner to its isothermal counterpart. However, now the working capacity of the adsorbent with respect to nitrogen between the end of feed (f) and the end of evacuation(e) conditions is redefined as:

$$WC_{N2}^{adi,v} = n_{feed}(P_f, T_f, y_{N2,f}) - n_{evac}(P_e, T_e, y_{N2,e}) + \left(\frac{\varepsilon_t}{R\rho_b}\right)\left(\frac{P_f y_{N2,f}}{T_f} - \frac{P_e y_{N2,e}}{T_e}\right) \quad (5\text{-}7)$$

The superscript (adi,v) denotes calculation of the working capacity that includes adiabaticity and voidage. The last term is the gas phase contribution to the working capacity. The effect of voidage on performance is becoming increasingly important with new adsorbents, such as LiLSX, where very little oxygen coadsorption occurs. The relative contribution of voidage to the working capacity of oxygen increases with such adsorbents. The total porosity ($\varepsilon_t$) of all adsorbents is taken as 0.6.

The analogous equation can also be written for oxygen working capacity ($WC^{adi,v}_{O2}$). The loading is now calculated, not simply at different pressures and compositions, but also different temperatures. The temperature rise associated with adsorption is approximated as:

$$T_f = \frac{\sum_{i=N2,O2} \Delta H_i (n_{f,i} - n_{e,i})}{C_{ps}} + T_e \quad (5\text{-}8)$$

This approximation ignores the effects of convection and heat accumulation in the gas phase. These revised working capacities are substituted into the previous equation for (1/BSF) (Equation 5-4) to determine the adiabatic sieve productivity. Likewise, the determination of the oxygen recovery remains unchanged, however the revised oxygen working capacity ($WC^{adi,v}{}_{O2}$) is used.

### 5.2.2 Feed and Vacuum Blower Sizing

In addition to the adsorbent cost, it is necessary to consider the cost of the feed and vacuum blowers, and power costs, to determine the totalised costs of different adsorbents. This necessitates sizing the blowers, and developing a functional relationship between blower size and recovery.

The instantaneous feed blower flowrate can be calculated from the mass balance on a VSA as:

$$V_{f,inlet} = \left(\frac{X}{Rec}\right)\left(\frac{RT_{amb}}{P_{atm}}\right)\left(\frac{1}{0.22Mw_{O2}}\right)\left(\frac{10^6}{86400}\right)\left(\frac{\tau_c}{2\tau_f}\right) = \frac{X}{Rec}1.035\left(\frac{\tau_c}{2\tau_f}\right) \qquad (5\text{-}9)$$

where X is the scale of the plant in tonne per day contained. (TPDc). The inlet flow rate $V_{f,\,inlet}$ is measured at ambient temperature and pressure.

Considering the case where X =50 TPDc and the oxygen VSA is operating with a two bed cycle this reduces to:

$$V_{f,inlet} = \frac{2.82}{Rec} \text{ (actual } m^3/sec) \qquad (5\text{-}10)$$

This expression can be used to determine the size and power requirements of the feed blower. This ignores the case where feed air may bypass the feed blower at the beginning of feed repressurisation (when the bed pressure is below atmospheric pressure). However any idle step is accounted for in terms of the feed time as a fraction of the cycle time.

The instantaneous vacuum blower flowrate is be calculated as follows:

$$V_{e,inlet} = \frac{X\left(\frac{10^6}{\left(\frac{86400}{\tau_c}\right)Mw_{O2}}\right)\left(\frac{1}{2}\right)\left(\frac{1}{y_{O2,f}\,Rec} - \frac{1}{y_{O2,pr}}\right)R}{\int_{\tau_{evac}} \frac{P_e}{T_e}dt} \text{ (actual m}^3\text{/sec)} \quad \textbf{(5-11)}$$

Considering the 50 TPDc VSA unit, this reduces to:

$$V_{e,inlet} = \frac{4510\left(\frac{4.76}{Rec} - 1.1\right)}{\int_{\tau_{evac}} \frac{P_e}{T_e}dt} \text{ (actual m}^3\text{/sec)} \quad \textbf{(5-12)}$$

In this case the inlet volumetric flowrate to the vacuum blower is not only a function of the recovery, but also the pressure profile associated with the evacuation steps. The integration of the pressure profile occurs only during the time of the evacuation. For a typical pressure profile, this equation reduces to:

$$V_{e,inlet} \approx \frac{4.1}{Rec} - 1 \text{ (actual m}^3\text{/sec)} \quad \textbf{(5-13)}$$

### 5.2.3 Power Requirements

The feed and vacuum flowrates, and the pressure profile determine the power requirements for the blowers. For the VSA cycle and pressure window detailed, the power requirements for the feed blower is given by:

Specific Feed Blower Power (kW/TPDc)

$$=2.78(10^{-4})\left(\frac{k}{k-1}\right)\frac{101.325}{\eta_f}\left(\frac{2.82}{Rec}\right)3600\left(\frac{2}{X\tau_c}\right)\int_0^{\tau_f}\left[\left(\frac{P_f}{P_{atm}}\right)^{\frac{k-1}{k}}-1\right]dt \qquad (5\text{-}14)$$

where $\eta_f = 0.7$, k= 1.395, and X = 50 TPDc. For a typical two bed pressure profile, with pressurisation to 1.4 bar, the additional approximation can be made:

$$\int_0^{\tau_f}\left[\left(\frac{P_f}{P_{atm}}\right)^{\frac{k-1}{k}}-1\right]dt \approx 1.45 \qquad (5\text{-}15)$$

The resulting equations are:

$$\text{Specific Feed Blower Power (kW/TPDc)} = \frac{1.4}{Rec} \qquad (5\text{-}16)$$

$$\text{Total Feed Blower Power (kWhr/day)} \approx \frac{1685}{Rec} \qquad (5\text{-}17)$$

When the bed is lower than atmospheric pressure during a feed repressurisation step, and when the feed blower is idling, it is assumed that the power requirement is zero.

The analogous equations can be written for the vacuum blower.

Specific Vacuum Blower Power (kW/TPDc)

$$=2.78(10^{-4})\left(\frac{k}{k-1}\right)\frac{1}{\eta_v}3600\left(\frac{4.1}{Rec}-1\right)\left(\frac{2}{X\tau_c}\right)\int_{\tau_e}^{P_c}\left[\left(\frac{P_{atm}}{P_e}\right)^{\frac{k-1}{k}}-1\right]dt \qquad (5\text{-}18)$$

For a typical two bed pressure profile, the following approximation can be made.

$$\int_{\tau_c} P_{evac}\left[\left(\frac{P_{atm}}{P_c}\right)^{\frac{k-1}{k}} - 1\right] dt \approx 250 \qquad (5\text{-}19)$$

Hence the equation for the resulting power equation for the vacuum blower are:

$$\text{Specific Vacuum Blower Power (kW/TPDc)} \approx \frac{3.45}{Rec} - 0.84 \qquad (5\text{-}20)$$

$$\text{Total Vacuum Blower Power (kWhr/day)} \approx 1009\left(\frac{4.1}{Rec} - 1\right) \qquad (5\text{-}21)$$

## 5.3 Relating Recovery and Sieve Productivity to Cost

In order to convert these process parameters (quantity of adsorbent, blower sizes, and power requirements) to a cost basis, the following cost information is assumed. These are arbitrary costs used to illustrate the concepts used in this study.

**Table 5-2 - Cost of Adsorbents**

| Adsorbent | P (Price US$/kg) |
|---|---|
| NaX | 4.00 |
| 5A | 8.00 |
| MgA | 8.00 |
| VSA 6 (CaNaX) | 8.50 |
| LiX | 17.00 |
| LiLSX | 20.00 |

The dual-site Langmuir isotherms for these adsorbents were supplied by APCI and ADSIM.

Feed Blower Cost ($) $=18{,}000V_{f,\,inlet}$ **(5-22)**

Vacuum Blower Cost ($) $=10{,}000V_{e,\,inlet} + 90{,}000$ **(5-23)**

Power: $0.04/kWhr

It should be stressed these are notional costs for the purpose of demonstrating the technique. This enables the determination of the following costs on the basis of recovery and sieve productivity. From Equation 5-4, the total adsorbent cost is as follows:

$$\text{Total Adsorbent Cost} = \left(\frac{3960}{WC_{N2} - 3.76WC_{O2}}\right)\text{Cost} \qquad \textbf{(5-24)}$$

$$\text{Feed Blower Cost (\$)} = 18{,}000\left(\frac{2.82}{Rec}\right) \qquad \textbf{(5-25)}$$

$$\text{Vacuum Blower Cost (\$)} = 10{,}000\left(\frac{4.1}{Rec} - 1\right) + 90{,}000 \qquad \textbf{(5-26)}$$

$$\text{Feed Blower Power Cost (\$/day)} = \frac{67.4}{Rec} \qquad \textbf{(5-27)}$$

$$\text{Vacuum Blower Power Cost (\$/day)} = 40.4\left(\frac{4.1}{Rec} - 1\right) \qquad \textbf{(5-28)}$$

The total power cost/day is simply the summation of these two terms, and it is assumed that the plant runs 350 days per year. The variable capital and operating costs can be combined to determine the total cost over a ten-year period based on Net Present Cost calculations. The effects of inflation are ignored. It is assumed that the nominal interest rate is 8%.

$$\text{(NPC) Net Present Cost (Variable Component)} = \sum_{t=1,10} \frac{\text{Cost in year t}}{(1+ir)^t} \qquad \textbf{(5-29)}$$

$$NPC = \frac{\text{Adsorbent Cost} + \text{Blower Cost} + \text{Annual Power}}{(1+ir)} + \sum_{t=2,10} \frac{\text{Annual Power Cost}}{(1+ir)^t} \qquad \textbf{(5-30)}$$

$$NPC = \frac{\left(\frac{3960}{WC_{N2} - 3.76WC_{O2}}\right)P + 18{,}000\left(\frac{2.82}{Rec}\right) + 10{,}000\left(\frac{4.1}{Rec} - 1\right)}{(1+ir)} + \frac{90{,}000 + 350\left(\frac{67.4}{Rec} + 40.4\left(\frac{4.1}{Rec} - 1\right)\right)}{(1+ir)} + \sum_{t=2,10} \frac{350\left(\frac{67.4}{Rec} + 40.4\left(\frac{4.1}{Rec} - 1\right)\right)}{(1+ir)^t} \qquad \textbf{(5-31)}$$

5-31 directly relates total cost (capital and operating) over 10 years to oxygen recovery and sieve productivity (1/BSF). Cost can now be deployed as the criteria to compare different adsorbents at different operating temperatures. However before proceeding, several caveats are required.

This cost analysis involves several simplifications. For example, there is no cost penalty associated with vessel and pipe sizes. A less productive sieve would necessitate larger adsorption vessels and feed and vacuum lines, but this additional cost is neglected from the analysis. Larger adsorption vessels also have the added disadvantage of greater pipe and vessel voidage, which in turn reduces oxygen recovery. These effects are also excluded from the analysis.

The objective of this performance analysis is to minimise the unit cost of oxygen through reducing the capital and operating costs. However in practice there are other qualitative factors requiring consideration, for example, process controllability is important (Ackley

et.al., 2000, p.13). The performance of some adsorbents can change significantly with small shifts in temperature. This can make start up and control difficult. For example, the diurnal or season fluctuation in temperature may cause significant shifts in performance, requiring new and more expensive control schemes (Beh et.al, 2000).

## 5.4 Application of Process Performance and Economic Criteria

These revised process performance criteria (adiabatic sieve productivity and recovery) and the related cost index together provide a powerful tool for analysis of oxygen VSA systems.

### 5.4.1 Isothermal vs. Adiabatic Performance

Isothermal measures of sieve productivity favour lower temperature operation because the heat of adsorption is ignored. This dramatically increases the nitrogen working capacity of the adsorbent. For example, in Figure 5-4 the isothermal sieve productivity of VSA6 appears to increase dramatically with a reduction in temperature. However when an adiabatic performance measure is used, no such improvement is evident. This demonstrates the need to use the adiabatic measure for VSA operation. Figure 5-4 also shows the large potential benefits of isothermal operation.

**Figure 5-4**

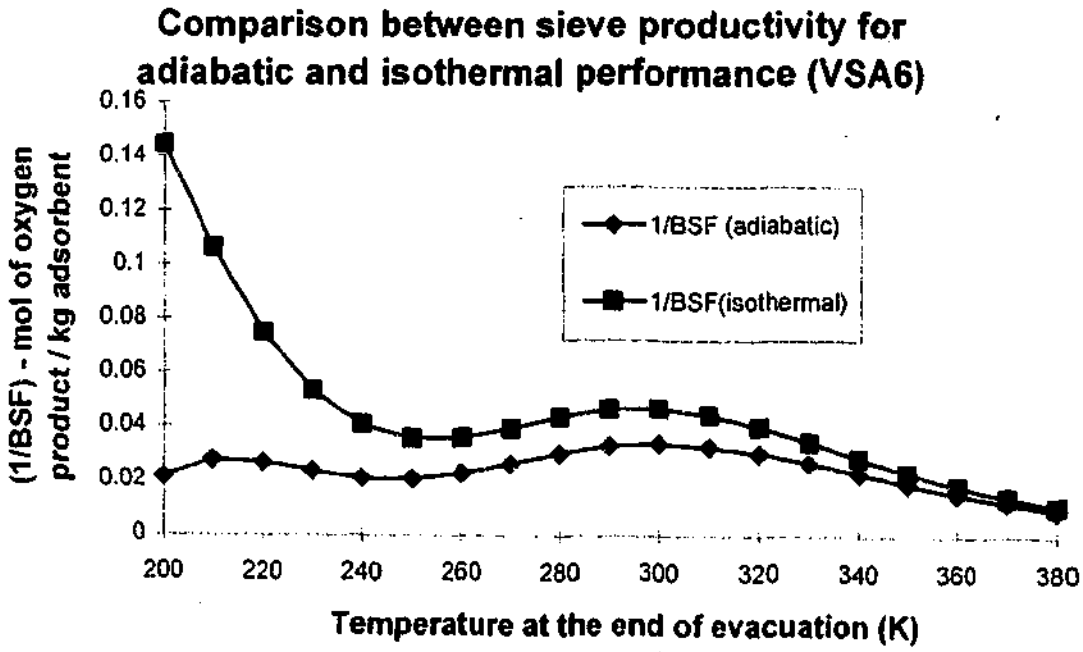


This approach can be readily applied to assessing the potential benefits of adsorbent modification to achieve dampened temperature fluctuation and improved performance. For example, Figure 5-5 compares the sieve productivity of 'adiabatic' LiX, 'isothermal' LiX and 'modified' LiX. In the case of the modified adsorbent, the heat capacity has been tripled to represent the effect of an inert thermal diluent inside the adsorbent pellet. The sieve productivity number is on the basis of kilograms of active adsorbent.

**Figure 5-5**

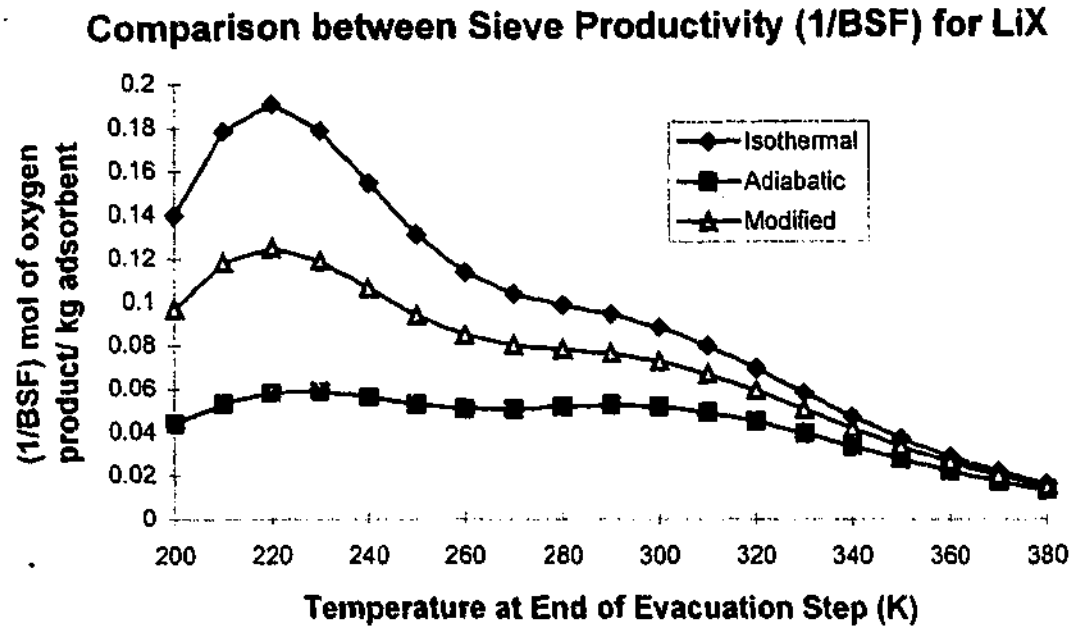


The economic benefits of such adsorbent modification can be readily determined by reference to cost. Figure 5-6 shows the cost of 'isothermal' LiX adsorbent/kg in order to breakeven with the total cost of current 'adiabatic' adsorbent. This provides some insight into the economic scope for adsorbent modification.

**Figure 5-6**

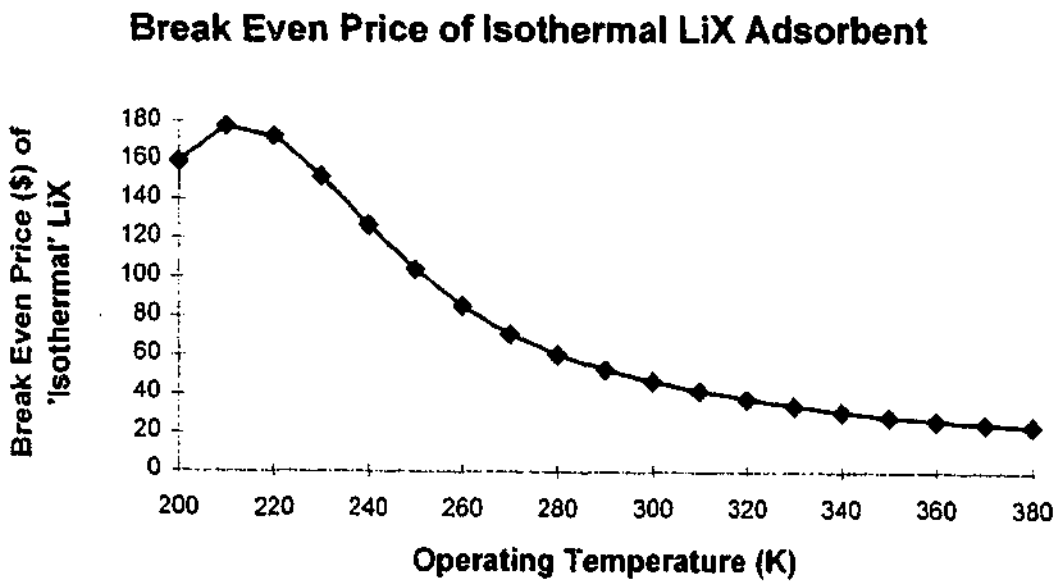

### 5.4.2 Mixed Adsorbents

This technique also enables investigation of composite adsorbents of different zeolite crystals. For example, VSA6 is a composite adsorbent composed of NaX and CaX formulated by limiting the extent of cation exchange and achieving a fixed ratio of Na to Ca. The motivation for the development of VSA6 was to overcome the limitations of CaX's highly non-linear isotherm, and the cost penalty of deep vacuums.

A composite adsorbent can be postulated based on a given mass ratio of two or more different adsorbents. For example, a 50/50 mix of NaX and LiX would show the following sieve productivity compared to undiluted NaX and LiX:

**Figure 5-7**

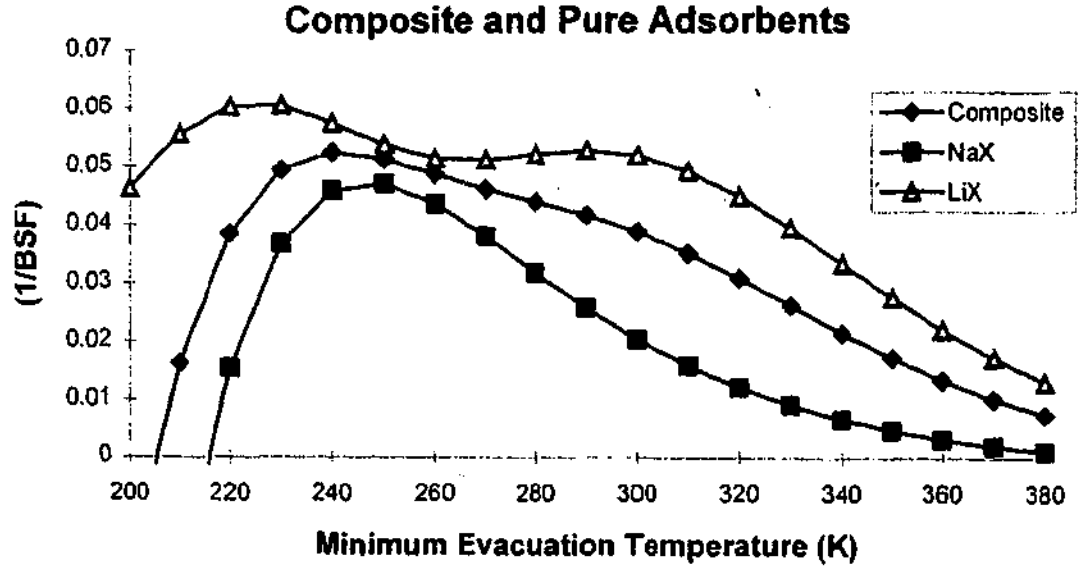


A full assessment of the benefits of this composite NaX/LiX adsorbent would require estimation of the cost for limited lithium ion exchange. The adiabatic temperature swing for the composite is reduced compared to pure LiX. NaX acts as both an adsorbent, and thermal diluent. This is further addressed in Section 5.5.5.

This technique ignores the scope of interaction between the different cations in the zeolite cage. It assumes the effect of the different cations is linear and additive. In practice there are crystallographic reasons why this simplification is crude. It remains to be investigated under what circumstances this approach is unrealistic.

### 5.4.3 Recovery and Sieve Productivity

In addition to sieve productivity (1/BSF), it has been proposed that the recovery must also be recognised as a key performance parameter. This is important because there can be a trade off between sieve productivity (1/BSF) and oxygen recovery for some operating regimes. For example, LiLSX displays different maxima for sieve productivity and oxygen recovery. In order to aid comparison of the maximum values of the recovery and 1/BSF are scaled to unity.

**Figure 5-8**

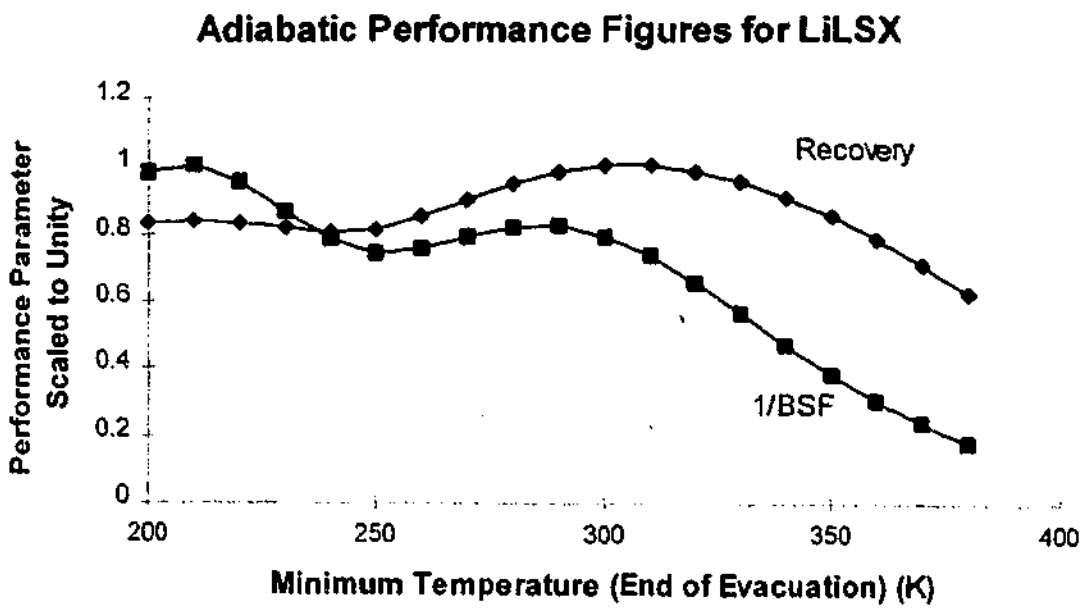


The maximum for recovery is at 300 K while the maximum for sieve productivity (1/BSF) is at 210 K. The optimal operating temperature can only be determined with reference to total cost. Figure 5-9 identifies that for the cost structure previously detailed, the optimum operating temperature is 300 K.

**Figure 5-9**

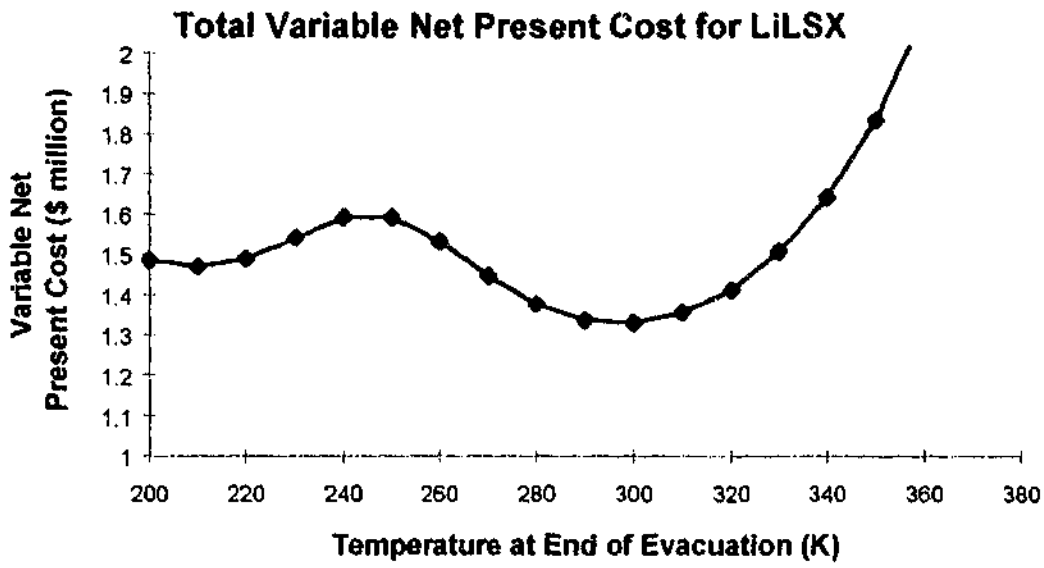


This shows the cost significance of recovery. The challenge for optimisation is to achieve close to the optimal temperature in the entire adsorption bed. This challenge is taken up later in this chapter.

### 5.4.4 Performance Comparisons of Adsorbents

It is interesting to compare the process performance of different adsorbents as a function of temperature. Current industrial practice utilises LiLSX as the preferred adsorbent. The following figures of sieve productivity (1/BSF) and recovery confirm the technical performance benefits of LiLSX.

**Figure 5-10**

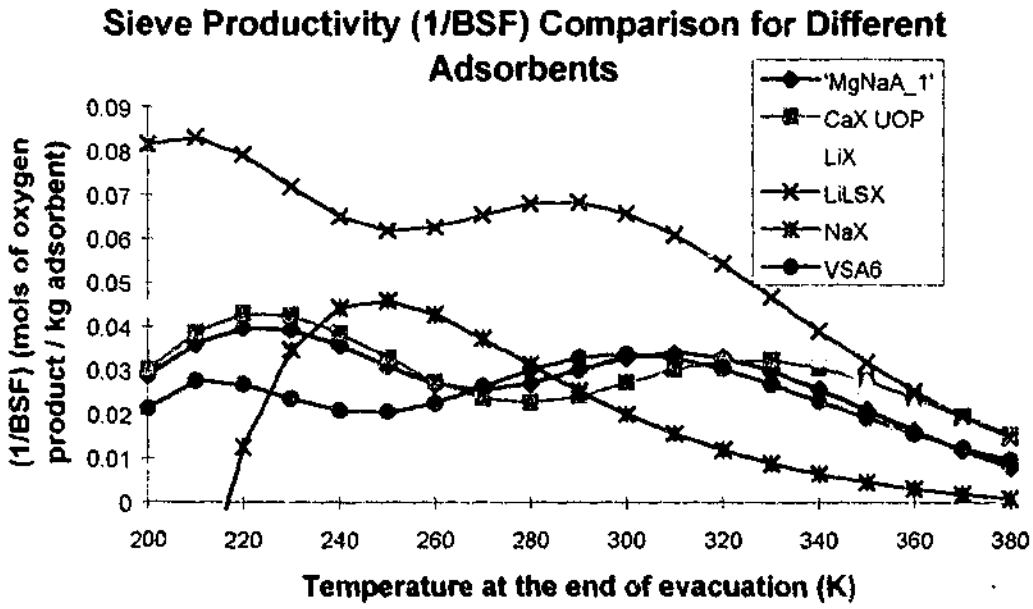

**Figure 5-11**

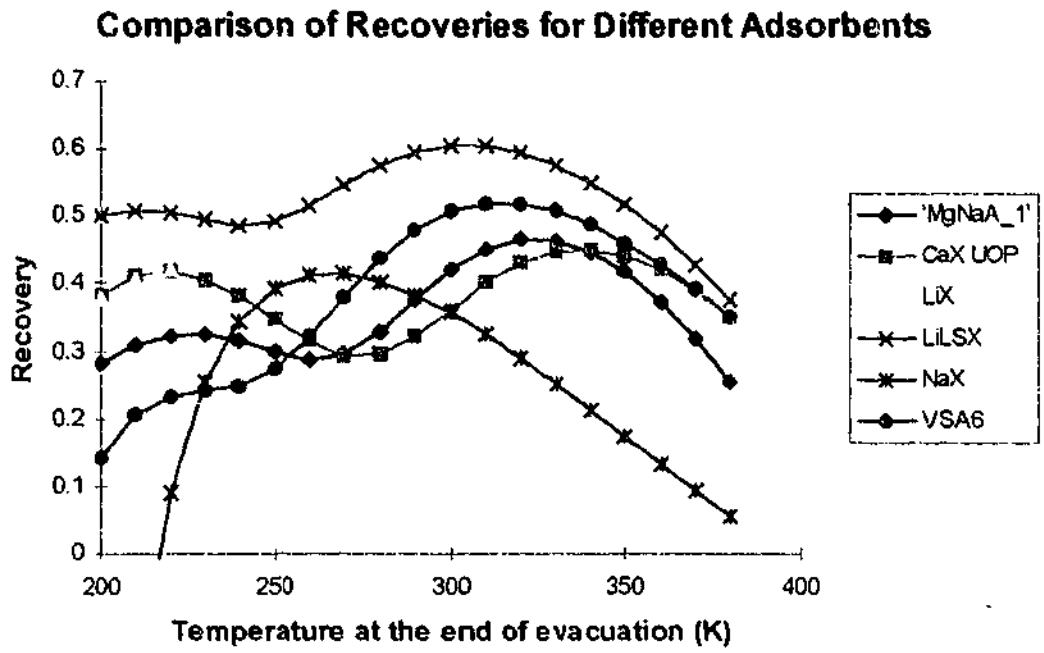


These figures are compelling. LiLSX is the preferred adsorbent, but also the most expensive. Together Figure 5-10 and 5-11 show that around 260 K, NaX shows a maximum for both sieve productivity and recovery. Is it possible that at 260 K, NaX is a preferred adsorbent to LiLSX on a cost basis? Figure 5-12 shows that this is not the case for the presently assumed cost structure. Over almost the entire temperature range (except above 350 K), LiLSX is the lowest total cost adsorbent. Again this shows the benefits of high recovery for lowering power costs. The substantial conclusion here is that, if LiLSX is available, and the outlined cost structure applicable, there is no benefit in layering adsorption beds as previously described by Notaro et.al. (1997).

**Figure 5-12**

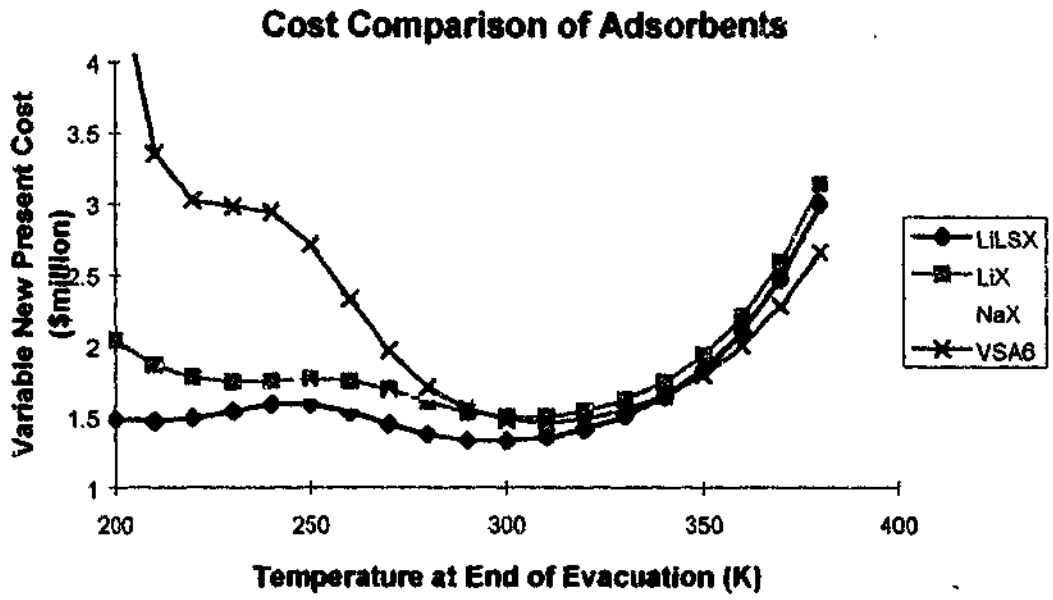


Figure 5-13 shows that across a wide temperature range both NaX and VSA6 have zones of preferential operation. Section 5.6 tackles the question of what strategies are available to achieve optimum VSA operation, recognising these different zones of preferred operation.

**Figure 5-13**

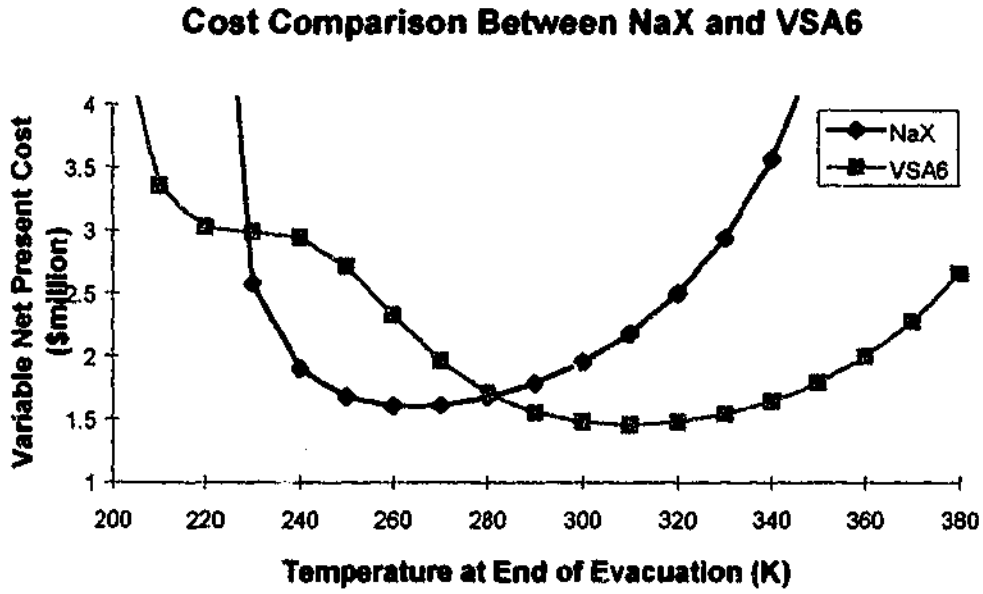


This section has developed an approach for comparing different adsorbents based on sieve productivity and recovery, and relating these parameters to a totalised cost. In order to achieve this aim, a range of assumptions is required, and these have been detailed. Important, if not critical issues, such as kinetics, cycles, pressure drop, number of beds, bed geometry, the importance of purge for purity have all been ignored. This has led to optimistic

process performance parameters. However, the modelling approach successfully draws out several significant conclusions.

- There are unparalleled process and economic benefits of LiLSX across all typical operating temperature ranges for the pressure windows considered (1.4-0.4 bar abs.) It does not follow that LiLSX will exceed all other adsorbents for different pressure windows. This conclusion is specific to the process conditions, and the assumed cost structure.
- There are potential benefits of operating LiLSX close to ambient temperature (300 K). The performance deteriorates below 0 $^{o}$C and above 40 $^{o}$C. If half the adsorption bed operates outside this narrow temperature band, the additional contribution to the totalised (10 year) cost would be in excess of $50,000.
- Some adsorbents' process performance is highly temperature dependent e.g. NaX. There is a relatively narrow temperature zone, beyond which the performance deteriorates markedly. Awareness of this strong functionality is critical for process design and control. Equally importantly, the Li based adsorbents retain similar performance (sieve productivity and recovery) across a range of temperatures. This improves controllability, and performance is less dependent on the ambient temperature fluctuations.
- Recovery is important to overall cost. Typically oxygen VSA installations are generally leased to the client who supplies (and pays for) power. Potentially this biases oxygen VSA design toward minimising capital costs, and neglecting the critical importance of power. The recovery impacts on the size of the blowers (capital cost) and the power. Based on this analysis, increasing the recovery 50% to 51% reduces the cost of the blowers by $3600, and reduces the annual power cost by $3200. Interestingly, if power was neglected from the cost analysis, at operating temperatures between 250-260 K, NaX is a significantly lower cost option (~50% lower capital cost).
- The performance and cost criteria demonstrate the wide scope for substantial performance enhancement, by reducing the temperature swing associated with adsorption and desorption. The subsequent section reviews a number of questionable attempts to achieve this potential improvement.
- These process and economic performance criteria were developed on the basis of a uniform end of evacuation temperature through the bed. In practice, there will obviously be a temperature gradient due to the interplay between convective fluxes and heats of adsorption. This dictates that the optimal cost will be a weighted average based on the fraction of the bed at different temperatures.

This work is not a substitute for a detailed optimisation of oxygen VSA, but it is hoped that this analysis provides a performance and cost criteria for comparing different adsorbents as a function of operating temperature. These measures of performance are of little utility, if the thermal profile in oxygen VSA cannot be adjusted or modified. Modification of thermal profiles in oxygen VSA has been the source of numerous patents by the gas industry. The following section critically reviews these efforts, and finally proposes some new optimisation strategies.

## 5.5 Three Approaches of Thermal Profile Modification

There are essentially three approaches to dealing with thermal profiles in oxygen PSA/VSA. The first approach that was originally pursued by the gas industry was mitigation of the axial CSS temperature profile. Collins and others devised a range of strategies based on the premise that the presence of the 'cold spot' reduced oxygen recovery. Subsequently, there was a shift in thinking, and several adsorption researchers sought to exploit the 'cold spot' to improve separation, recognising that the behaviour of different adsorbents can be a strong function of temperature. Thirdly, and most fundamentally, other adsorption researchers have sought to improve performance by focussing on the cyclic temperature swing between adsorption and desorption, rather than the overall axial temperature profile. These three different strategies are explored below. In addition to published strategies, possible alternatives are also outlined, based on the models and experiments in the preceding chapters.

### 5.5.1 Minimising the Axial Temperature Profile - Mitigation Strategies

One strategy proposed by Collins involves bypassing the feed compressor aftercooler to increase the temperature of the feed gas and reduce the temperature minimum, and thereby improve oxygen recovery (Collins, 1976). This is an obvious strategy to reduce the temperature minimum, but it also increases the temperature at the top of the bed, which may not be desirable.

Another mitigation strategy proposed by Collins uses metal rods or plates to conduct the heat axially and moderate the severity of the temperature profile, and improve oxygen recoveries (Collins, 1977). The objective of this invention was to achieve oxygen recoveries in commercial size plants equivalent to those obtained in small pilot plants.

In addition to these patented and published strategies to reduce the severity of the temperature profile, the preceding chapters suggest a range of alternative strategies. In some cases, there is anecdotal evidence that these strategies have been pursued industrially.

The principle mechanism by which the severe temperature profile arises is the interaction between temperature swing of desorption/adsorption and convective fluxes. It follows that altering the patterns of convection in the bed will alter the CSS temperature profile. There are two simple applications of this idea. Firstly, reducing the reverse (desorptive) gas flow over

the prelayer, and secondly, replacing the 'top-to-top' pressure equalisation (PE) step with 'top-to-bottom' PE step.

Additional valving and pipework above the prelayer would allow for the removal of some desorbed gas above the prelayer. This would dissipate or flatten the temperature depression. However, the volume of desorbed gas passed over the prelayer is critical for water removal from the prelayer, and a deeper prelayer may be required to prevent the penetration of water into the main layer.

Alternatively, the current practice of 'top-to-top' pressure equalisation (PE) could be modified to 'top-to-bottom' pressure equalisation (PE). This would modify the enthalpy fluxes through the bed and reduce the severity of the temperature depression, and limit the gradient through the bed. Table 5-3 compares the axial CSS temperatures for the cases of 'top-to-bottom' PE and 'top-to-top' PE.

**Table 5-3 – Comparison of the effect of different types of PE on thermal profiles**

| | 'Top-to-Bottom' PE | 'Top-to-Top' PE |
|---|---|---|
| Feed Temperature (K) | 300 | 300 |
| Minimum Temperature (Cold Spot) (K) | 284 | 280 |
| End of Bed Temperature (K) | 300 | 305 |
| Maximum $\Delta T$ across Bed (K) | 16 | 25 |

The severity of the temperature profile across the bed is reduced. However, the effect is not substantial, as the absolute enthalpy flux associated with the PE step is small compared with the other steps. The PE flow was approximately 5% of the total feed flow into the bed. Furthermore, the introduction of a 'top-to-bottom' PE also modifies the composition patterns within the bed, and this introduces a further level of complexity to the process.

A similar strategy would involve heating the gas entering the bed on purge and pressure equalisation steps. This would tend to lift the axial temperature profile and reduce the minimum temperature. Again this would increase the complexity (and cost) of the process.

Experimental results in Chapter Four revealed that the replacement of the prelayer of activated alumina with a prelayer of NaX, significantly reduced the extent of the temperature depression for cases with a dry air feed. Even though activated alumina and NaX (when

water loaded) behave similarly as inert prelayers, by using NaX as the prelayer, the minimum length of inert bed is used. The additional effects of the reduced density of NaX, and slightly higher water loading capacity of activated alumina will tend to offset each other.

### 5.5.2 A Proposed Mitigation Strategy for LiLSX

Based on the temperature behaviour of LiLSX, there is scope to apply partial mitigation strategies to achieve the entire CSS temperature profile within the range 0-40 °C.

- The aim of operating in this temperature range (0 - 40 °C) makes the presence of a prelayer desirable, even if dry air was available. Without a prelayer (and after adiabatic compression), the average temperature of feed gas entering the adsorption bed is approximately 40 °C. Hence without a prelayer, the entire bed would be outside the optimal operating temperature region!

- Prelayer selection is one aspect of this mitigation strategy. For example, if the average ambient temperature was 15 °C, NaX could be used as a prelayer to mitigate the temperature depression. However, for higher ambient temperatures activated alumina could be utilised.

- The depth and properties of the prelayer can be adjusted to optimise the temperatures through the main layer. However, one of the limitations of using a prelayer to adjust the temperature is that the prelayer properties are design variables, not operating or process variables. So, if there are significant fluctuations in the ambient temperature this may lead to sub-optimal performance, by shifting the temperature of the main adsorbent layer. Under some circumstances, in climates with large ambient temperature variations, the addition of a feed air cooler or heater could be justified.

- The cost profile for LiLSX indicates that the optimal operating temperature is 300 K. This suggests that axial copper rods, as patented by Collins, might be applicable to maintain the entire adsorption bed as close to 300 K as possible.

The cost of such mitigation strategies must be justified, based on a reduction in the unit cost of oxygen. For a given CSS temperature profile, it is possible to calculate the unit cost of oxygen, through discretising the bed into a series of sections at different temperatures and calculating the cost at specific temperatures, and then determining an overall cost.

### 5.5.3 Exploiting the 'Cold Spot' - Existing Strategies

In marked contrast to the mitigation strategies, the patent and published literature also contains a number of ideas where the 'cold spot' phenomenon or severe axial temperature profiles can be exploited to improve performance.

For example, while not utilising the mechanism of internal heat regeneration to lower the temperature of the main adsorbent, Izumi et.al.(1989) and Yanagi and Qui (1998) advocate the use of external cooling to precool the feed air entering the adsorbent bed. Izumi et.al. (1989) suggest external refrigeration equipment to reduce the temperature of the feed air and internal cooling coils to reduce the temperature of the bed.

More radically, Yanagi and Qui (1998) propose cooling the inlet air with liquid hydrogen to temperatures as low as 200 K, and feeding the air to a single layered bed of 13X or 5A. They argue that a prelayer is not required, as the carbon dioxide and water are condensed at the lower feed temperatures. One significant problem with the Yanagi and Qui (1998) study is that it assumes isothermal operation, which is a significant failing, when considering the alleged improvements in nitrogen working capacities at lower temperatures.

Leavitt pursued the approach of Izumi et.al., but sought to achieve lower operating temperatures by the use of internal heat regenerators (Leavitt, 1992). He proposed an arrangement where, in addition to the drying prelayer, additional heat regenerator zones are located above and below the drying layer. These regenerator zones are comprised of metal spheres to enhance the regenerative heat exchanger effect of the prelayer, and utilise rather than disregard, the heating effects that occur in the course of cyclic PSA operations (Leavitt, 1992). Leavitt also proposed external insulation on the adsorbent bed to prevent heat transfer from the environment, and achieve lower temperature operation.

One novel aspect of the patent is the inclusion of an inert regenerator prior to the drying layer. Leavitt argues that this layer of metal balls captures the refrigeration effect of desorbed water during the evacuation and purge steps. According to the patent, when the first regenerator is performing well and the drying layer itself is acting as a heat regenerator, no second regenerator between the drying layer and the main adsorbent layer will be required.

Armond (1997) also incorporates the ideas of Izumi et.al. (1989) in a recent patent. The patent divides the adsorption bed into three sections. The first section is an activated alumina

prelayer for water and carbon dioxide removal. The second section contains adsorbent selected for optimum operational efficiencies at a temperature between -35 °C to -45 °C. The top section contains adsorbent selected for optimum operational efficiencies at ambient temperatures. In addition the top section contains metal plates that dissipate temperature profiles, in order to achieve ambient conditions in the top section. The patent also promotes the use of heaters in the top section to achieve ambient operating temperatures.

A patent by Watson et.al. (1996) also promotes the layering of adsorption bed based on the recognition that adsorbent performance is a function temperature. Watson et.al. suggest that the higher capacity zeolites, such as CaX, lose selectivity and develop a high capacity for oxygen at lower temperatures (below 50 °F). The patent therefore proposes using a lower capacity zeolite, such as NaX, in the cold section of the bed, to reduce the extent of co-adsorption of oxygen, and thereby increase the recovery. In the top section of the bed (above 50 °F), a zeolite with a high capacity, such as CaX, should be used. For VSA processes, the patent recommends that 20-50% of the total air separation is achieved by NaX. In addition it is suggested that the prelayer for water and carbon dioxide removal is also NaX. The reported benefits of this multilayer strategy are improved recovery and production, the extent and severity of the temperature depression is reduced, and the load on the vacuum blower is decreased.

A more recent patent by Praxair (Notaro et al., 1997) offers a more systematic and detailed approach to the layering of the adsorption beds, to exploit the temperature dependence of different adsorbents' performance. Using the previously discussed Adsorption Figure of Merit (AFM) coupled with an approximate means of determining temperature profiles, Notaro et.al. (1997) outline where different adsorbents should be located axially through the adsorption bed.

One approximation with this patent is that the temperature of the air exiting the prelayer is fixed at 260 K. This is an assumption, since as has been demonstrated throughout this project, the temperature of the gas leaving the prelayer is a function of many process variables, and should not be assumed to be constant (unless for some simplifying demonstration purpose.) However, this patent stands as a significant attempt to develop a rational methodology for layering adsorption beds, recognising that some adsorbents' performance is a strong function of temperature.

### 5.5.4 Proposed Strategy to Optimise the Axial Temperature Profile

One obvious strategy for adjusting the 'cold spot' is to adjust the properties of the prelayer. Leavitt (1992) originally pursued this idea. However, based on the simple modelling in Chapter Two, a wider range of strategies is available to adjust the extent of the temperature depression. For example, increasing the thickness of an inert prelayer, or using a prelayer with a higher thermal capacitance, would reduce the temperature minimum in the adsorption bed. Likewise the extent of the temperature depression could be minimised by reducing the length of the prelayer. This approach would be subject to the constraint of maintaining a minimum thickness for water and carbon dioxide removal in the prelayer. Another approach might involve mixing activated alumina and NaX in the prelayer to achieve a desired temperature minimum.

These strategies can be combined with the idea of layering proposed by Praxair (Notaro et.al., 1997) and APCI (Watson et.al., 1996). The approach to bed layering developed here is informed by the modelling and experimental work in this study, and the revised process and economic performance criteria. The technique for determining the optimal bed layer is best illustrated by example. Consider the cost curves for VSA6 and NaX*(Figure 5-14) where NaX* is a hypothetical adsorbent with a profile similar to NaX, but with slightly enhanced performance in the temperature range 250-280 K.

**Figure 5-14**

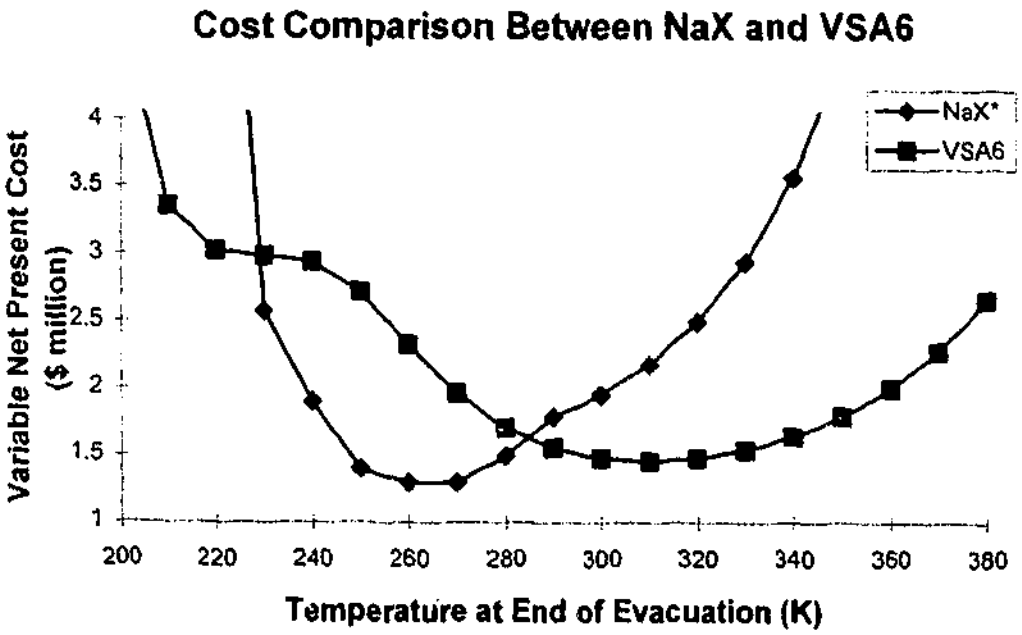


There is a low temperature region (250- 280 K) where NaX* is the preferred adsorbent, and above 280 K VSA6 is preferable. It is apparent the NaX* should be located closer to the prelayer, and VSA6 at the top of the bed. However numerous design issues remain. How

much prelayer? What sort of prelayer? What ratio of NaX/VSA? How is the optimum design confirmed? The following procedure could be utilised to address these questions.

1. Assume a composition of the main bed (say 40% NaX / 60% VSA6)
2. Use a multiple scale analysis procedure to determine the main bed CSS temperature profile ignoring the inert prelayer. (using $P_f$ and $P_e$) and estimating the velocity profile).
3. Use the simple energy balance model to adjust the location of the temperature minimum to 250 K and calculate the required thickness of the prelayer.
4. Estimate the cost based on an integration of the cost surface to determine the minimum cost.
5. Adjust the ratio of NaX/VSA6 and iterate 2 through 4 until the lowest cost is determined.

This technique only provides an estimate of the cost. Subsequent confirmation is required by full MINSA simulation. MINSA enables direct determination of adsorbent quantity, recovery and power. These values can be directly substituted into the cost equation 5-31. The numerical simulation importantly incorporates kinetics, cycle effects, and bed geometry effects. Ultimately these are all required for an accurate determination of cost. However the estimate of cost based working capacity provides a useful heuristic for understanding the effects of temperature on adsorbent performance. And importantly, the technique provides a strong clue to attractive adsorbent configurations.

For example, it is interesting to compare the performance of an adsorption bed composed of half NaX and half VSA6 (by mass) using MINSA. In one case, the layers are sequenced so that NaX is adjacent to the 'cold spot'. In the other case, VSA6 is first. The feed temperature is assumed to be 260 K. This is only a rough approximation of the effect of an inert prelayer (as adopted by Notaro, et.al., 1997). Obviously in practice, the order of the adsorbents in the main layer will effect the extent of the temperature depression. However for demonstration purposes this approximation is acceptable. The cycle simulated was a two bed 8 step cycle. The pressure window was 1.4 – 0.4 bar, and the pressure profiles matched within 0.5 kPa. The total bed length was 1.8 m comprised of 0.92 m VSA6, and 0.88 m NaX. The total mass of adsorbent (NaX and VSA6) was 19.8 kg for both beds.

**Table 5-4- Comparison of performance based on order of adsorbents (NaX/VSA6 vs. VSA6/NaX)**

| | NaX/VSA 6 | VSA6/NaX |
|---|---|---|
| Product Purity | 93.9% | 93.9% |
| Recovery | 47.8 | 42.0 |
| BSF (kg/TPDc) | 660 | 872 |
| Power (kW/TPDc) | 7.07 | 8.2 |

Table 5-4 demonstrates that placing the NaX in the coldest section of the bed, and VSA6 at the top of the bed improves adsorbent performance considerably. The BSF is lower and recovery 5.8% higher. This is consistent with Figure 5-13.

This difference in performance is due to the significantly higher nitrogen working capacity (approximately 22%) for the total adsorbent with the NaX/VSA6 configuration. This adsorbent configuration also has slighter higher oxygen working capacity (approximately 5%). However the substantial benefit in increased nitrogen working capacity more than offsets the effect of slightly increased oxygen co-adsorption.

### 5.5.5 Minimising the Cyclic Temperature Swing - Towards Isothermal Operation

Given the preoccupation with the 'cold spot' and axial CSS temperature profiles, many approaches have tended to ignore the performance impact of the temperature swing associated with adsorption and desorption. The extent of adsorption and desorption are both significantly limited by this temperature swing, and some researchers have sought to increase the 'isothermality' of PSA/VSA systems in order to improve performance.

Yang and Cen (1986) have suggested a shell-tube heat exchanger system whereby the tube side is one adsorber and the shell side, a second adsorption column. The aim is to achieve heat transfer between the two columns (the tube and shell sides) and limit the cyclic temperature swing. The numerical modelling undertaken demonstrates some performance improvements, and the magnitude of the cyclic temperature swing is approximately halved. However, as Rege and Yang acknowledge, this approach "is not very attractive since it adds to the complexity of the multibed adsorptive process" (Rege and Yang, 1997, p.5364). Moreover, Yang and Cen investigated $H_2/CH_4$ and $H_2/CO$ separations using activated carbon in a 4 cm inside tube with a 6.55 cm shell (Yang and Cen, 1986). On such a small scale, the extent of heat exchange between the tube and shell side will be maximised. On a large scale typical of oxygen VSA (2-3 m diameter beds) the approach is completely infeasible, as there will be insufficient area for heat transfer, unless there was a vast number of tubes in a tube bundle. In essence the low thermal conductivity of the adsorbent limits the rate of the heat transfer over a cycle.

In order to overcome this problem, Yang and Cen (1986) and Rege and Yang (1997) have proposed the inclusion of inert iron particles (of nearly the same size as that of the zeolite particles) mixed through with the adsorbent. The aim is to dampen the cyclic temperature fluctuation and improve the isothermality of operation. Based on LiX, Rege and Yang (1997) report the results of numerical simulations where through the addition of an inert, the temperature swing was reduced by almost 60% compared to the case of pure adsorbent. Rege and Yang (1997) concluded that for a fixed total volume bed the optimum volume of inert was approximately 10%.

Gaffney et.al (1993) have proposed a similar idea, where an inert or diluent of similar heat capacity to the adsorbent is added with the adsorbent (Gaffney et.al., 1993). This patent recommends that the inert diluent constitute at least 5% of the total mass of adsorbent and

diluent. It is also recommended that the diluent be integrated with the active adsorbent phase, but it is not explained how this should occur.

Lou et.al. (1999b) describe an experiment with an air drying PSA unit, where inert steel balls of 2 mm diameter were included with the adsorbent to increase the total heat capacity of the adsorbent bed by a factor of four! This successfully reduced the cyclic temperature swing and improved the separation efficiency. However based on the lower heat capacity of metal compared with adsorbent, this involves a mass of steel balls approximately seven times the original mass of adsorbent!

Fuderer proposed reducing the cyclic temperature swing by doping activated carbon with inert denser alumina (Fuderer, 1985). The net effect was to increase the thermal capacitance and reduce the thermal swing and improve recovery.

Another proposal to reduce the thermal swing was advanced by Walter (1996) using a single vessel with multiple internal compartments, each containing adsorbent. The compartments are in thermal contact, and arranged so that the adjacent compartments are in adsorption and desorption simultaneously. Heat is transferred from the adsorbing compartments to the desorbing compartments.

Ackley et.al. (2000) suggest using another adsorbent as an inert diluent to lower the thermal swing. For example, it is proposed that a mixture of 20% NaX and 80% LiX is used in preference to 100% LiX, because the temperature swing associated with adsorption on the NaX is 6 $^{o}$C compared to 14 $^{o}$C on the LiX. In effect the NaX is a thermal diluent, but not an inert one. This is a mixture of beads or pellets, not a partially exchanged composite adsorbent, as described in Section 5.4.2.

Ackley et.al. (2000) argue that this is preferable to using an inert, because the NaX still contributes to adsorption and maintains low bed sizes, whereas an inert is accompanied by disadvantages of greater pressure drop, larger vessels and higher unit power consumption for a given feed flow. It is also suggested that inert materials with a high heat capacity are generally dense materials that can be quite expensive, and may necessitate the need for higher strength bed supports and foundations (Ackley et.al., 2000).

Interestingly, Ackley et.al. (2000) offer some pilot plant performance data supporting the benefit of mixtures of NaX and LiX as opposed to straight LiX (Ackley, et.al., 2000, p.12). The plant data presents a 20/80 mix of NaX and LiX beads which performs only marginally worse than 100% LiX. The patent suggests that this small difference in performance is due to the thermal diluting effect of the NaX. However the analysis neglects to include the effect of the 'cold spot'. The authors do not separate out how much performance alteration can be attributed to reducing of the thermal cycling, as opposed to the effect of the CSS axial temperature profile. In fact, based on the plots presented of adiabatic separation efficiency, it would appear more beneficial to layer an adsorption bed with NaX (20%) followed by LiX (80%), than mix the two adsorbents through the entire length of the adsorbent bed as Praxair proposed in an earlier patent (Notaro, et.al., 1997).

The evidence for mixing different adsorbents presented by Ackley et.al. (2000) would be more compelling if the pilot plant CSS temperature profiles were presented. This way it would be possible to reduce if the mixture of adsorbents had an effect on both the thermal swing and the CSS temperature profile.

The optimisation criteria selected by Rege and Yang also requires modification. Rather than assuming a fixed volume bed and adjusting the mix of adsorbent and inert, it would be preferable to optimise the total cost, and include the cost of the adsorbent and the cost of inert.

A major drawback with the work of Gaffney et.al., Yang and coworkers, and Ackley et.al. is the assumption that the presence of an inert or adsorbing diluent uniformly dampens the cyclic heat generation term (Rege and Yang, 1997, p. 5364; Gaffney et.al. ,1993; Ackley et.al., 2000). The approach simply assumes that an effective specific heat can be calculated, based on the weighted summation of the thermal capacitance of both the inert and the adsorbent, or the mixture of adsorbents. The issue of the mechanism and timescale of heat transfer between the inert and the adsorbent (or mixture of adsorbents) is ignored. This leads to overly optimistic predictions of the benefit of the inclusion of diluent (inert or otherwise). This was observed in Section 4.6.5 where an experiment with copper pellets (AA115LSXCu) shows that only modest gains were achieved at an inert concentration of 9%v/v. To more accurately determine the effect of the inclusion of an inert on damping the cyclic temperature swing, a more complex model is required that includes the mechanisms of heat transfer within the bead, and from the bead to the inert (or a lower temperature adsorbent).

There are potentially large benefits to be gained by reducing the cyclic temperature fluctuation. Separation performance will improve, and the overall CSS temperature profile will flatten. However, as yet there is no evidence that these techniques have been successfully applied in industrial oxygen VSA.

While recognising the limitations of any simple adjustment of the specific heat capacity to account for the presence of a thermal diluent, this approach can be used to ascertain the maximum possible performance improvement available, and to assess the economic viability of this approach to thermal management in oxygen VSA. Table 5-5 reports MINSA simulations where the adsorbent heat capacity is altered between 1000 kJ/kg K and infinity (isothermal operation). For a one bed simulation with a pressure profile (138.0/141.3/31.0/35.0) and product purity (95.4%) were held constant in all cases. PID control loops were used in MINSA to achieve these set point pressures and purity. This eliminates some of the uncertainty of the experimental results and isolates the performance improvement of the thermal diluent.

**Table 5-5- Performance Comparison with Different Adsorbent Specific Heat Capacities**

| Adjusted Cp (J/kg K) | 1000 | 1200 | 2000 | 10,000 | Isothermal |
|---|---|---|---|---|---|
| Feed Flow (mmol/cycle) | 4991 | 5189 | 5492 | 5954 | 6048 |
| Product Flow (mmol/cycle) | 445 | 477 | 522 | 592 | 603 |
| BSF (kg/TPDc) | 377.4 | 352.1 | 321.7 | 283.7 | 278.5 |
| Recovery (%) | 37.0 | 38.1 | 39.4 | 41.2 | 41.0 |
| Power (kW/TPDc) | 8.5 | 8.4 | 8.1 | 8.0 | 7.9 |
| Cold Spot (°C) | -11.0 | -7.8 | 0.2 | 11.3 | 14.4 |

Table 5-5 demonstrates that over the cycle and adsorbent investigated, oxygen VSA separation performance increases with increasing specific heat capacity of the adsorbent. However, the recommendations of Rege and Yang and Gaffney et.al. in relation to the addition of small quantities of inert thermal diluent do not appear useful. Furthermore, it should be remembered that this is the "maximum" effect, which ignores the resistance to heat transfer between the adsorbing pellet and the inert thermal diluent pellet.

The addition of a large quantity of small metal balls will improve the separation efficiency, but there is a large cost associated with this strategy. The cost of a thermal diluent, along with any additional civil and mechanical works to support the much heavier adsorption beds

must be taken into account. Coupled with this would be an increased pressure drop through the adsorption bed, as well as a corresponding increase in power consumption. For current oxygen VSA technology these additional costs cannot be justified. The main problem is that while metal pellets are dense, the specific heat capacity of metal is low.

Despite the fact that this analysis ignores the problems of heat transfer resistance between the adsorbent and thermal diluent, it is apparent that adjustment of the specific heat capacity through the addition of metal balls and inert adsorbent cannot be justified on financial grounds. In order to achieve a large increase in thermal capacitance required to maintain near-isothermal operation, it is necessary to use a phase change material (PCM) as the thermal diluent. The larger heat sink offered by a solid-solid PCM would enable the system to operate more isothermally without the additional mass associated with metal pellets. For example, 91% Neopentyl Glycol (NPG)/ 9% Trihydroxy Methyl-Aminomethane (TAM) has a solid-solid phase transition between 30-39 $^{o}$C and a heat transition of 143-150 kJ/kg (Wang, et.al., 2000). If the temperature of the adsorption bed cycles over the transition range of the solid-solid PCM, the addition of 1 kg PCM to 7.91 kg adsorbent would adjust the specific heat capacity of the adsorbent to be 20,000 J/kg K. This would effectively achieve isothermal operation, along with the corresponding performance benefits.

It is interesting to note (using an analysis of the Biot numbers for oxygen VSA) that the controlling resistance to heat transfer resides in the external film. This suggests that any thermal conductivity of the PCM, even in pellet form, is not critical to achieving the required isothermal behaviour.

However, there are a number of potential problems with using PCMs for thermal management. Firstly, the adsorption bed, or sections of the adsorption bed, operate outside the transition temperature range of the PCM, and consequently will have minimal effect as a thermal diluent in these regions. Secondly, if the PCM is effective at achieving near isothermal operation, additional cooling may be required after the feed compressor, given that there will be no 'cold spot' reducing the temperature of the air entering the main layer of adsorbent. Thirdly, the NPG/TAM polyalcohol PCM could not be incorporated within the pellet due to the extreme temperatures in the calcination process. As a result, it will be necessary to consider the heat transfer resistance between a sorbent pellet and the adjacent PCM.

## 5.6 Conclusion

This Chapter has examined the impact of thermal profiles on oxygen VSA performance with a view to establishing optimal thermal profiles. It has sought to refine and improve some existing strategies based on a more detailed cost equation.

The benefit of LiLSX and importance of recovery have been highlighted. The ability of the prelayer to adjust the temperature profile has also been demonstrated. The depth and type of the prelayer are important variables for optimising the temperature profiles for LiLSX.

Importantly it has also been concluded there is no benefit in layering LiLSX. The potential benefits of layering can only be realised when in different temperature regions there are different preferred adsorbents.

The techniques proposed do not substitute for full numerical simulation. Too many important effects (kinetic, cycle, pressure drop, bed geometry, composition profiles) have been neglected from this simplified analysis. However it has been argued that the cost surfaces developed provide a powerful guide to suggest particular thermal optimisation strategies.

This chapter also reveals an unfortunate reality for bulk PSA adsorptive separation. The adsorptive temperature rise seriously limits the separation potential. The possibility of achieving more isothermal operation is attractive, but thwart with difficulties. Much of the published literature pursuing this optimisation strategy neglects the complexity of this problem. The application of solid-solid PCM warrants further investigation.

# Chapter 6
# Conclusions, Future Research and Recommendations

## 6.1 Conclusions

This study has undertaken a wide-ranging investigation of thermal profiles in oxygen VSA. Each of the preceding chapters has provided detailed conclusions about VSA modelling, the experimental investigation and optimisation strategies. Some of the more important conclusions can be briefly restated.

- There is no mystery surrounding thermal profiles, and the 'cold spot' in oxygen VSA. The underlying reasons for these thermal profiles are evident in other PSA systems. The uniqueness of oxygen VSA thermal profiles is largely the result of the regenerative heat exchanger effect caused by the presence of an inert prelayer.

- A simple energy balance around the adsorbent bed identifies key process parameters that shape the CSS temperature profile. Some important process parameters including cycle, kinetic and adsorbing prelayer effects cannot be captured by the simple energy balance.

- The slow dynamic response of oxygen VSA is due to the ratio of the gas to adsorbent thermal capacitance, and the resulting slow propagation of a trailing thermal wave. This enables the identification of the perturbation parameter ($\varepsilon$), and is a prominent quantity in study of the dynamic behaviour of oxygen VSA.

- The length of a water-loaded zone with NaX can be predicted analytically and this result is consistent with experimental observations (within the accuracy of the experimental sampling procedure).

- The physical model underpinning MINSA, and the Finite Volume Method with a QUICK scheme and SMART smoothing can reasonably accurately capture the performance and thermal profiles of the laboratory scale oxygen VSA unit.

- The project has designed, constructed, commissioned, and operated a laboratory scale oxygen VSA unit. The polyurethane columns sustained severe temperature profiles, but did not prove sufficiently mechanically robust. The PVC columns were a suitable compromise between adiabaticity and mechanical reliability.

- The VSA unit was well instrumented and provided mass balance closures routinely within 3%.

- A wide ranging experimental investigation was undertaken that identified a range of experimental parameters that shape the CSS temperature profile. These parameters have been detailed in Chapter Two.

- The performance of oxygen VSA can be markedly affected by the local adsorbent temperature. This was thoroughly demonstrated with numerical simulation.

- The cost criterion developed for adsorbent performance provides a powerful technique for comparing different adsorbents and provides a rational basis for adsorbent selection and optimal temperature for operation.

- A number of thermal optimisation strategies were reviewed and considered. There are significant potential benefits to be gained from thermal optimisation, and an approach was outlined to assess these strategies.

## 6.2 Future Research

This study has provided a broad overview of oxygen VSA. One consequence of the breadth of this study is that it pointed to several areas that could be explored for future research.

- One of the reasons for the need for the development of an adiabatic adsorption bed is a deficiency in heat transfer models. This study has highlighted the elements of a detailed wall heat transfer model. As yet this model has not been included in MINSA, and has not been verified. An important element of such a heat transfer model is a method for accurately determining the inside wall heat transfer coefficient. This is a fundamental area of chemical engineering requiring further investigation.

- The perturbation techniques developed in this study have provided a technique for better understanding CSS and conditions for closure of the energy balance, and a possible acceleration technique. However for this work to be of more than passing interest it is necessary to further develop this approach. From the mathematical literature, it is unclear whether this will be possible. Perturbation solutions to PDEs is a reasonably new field in mathematics and it is unclear whether this work would be possible, particularly given the complex boundary conditions associated with PSA/VSA processes.

- The polyurethane column design for adiabatic adsorption beds was limited in a number of respects. The lack of mechanical robustness suggests some modification to these columns is required. Possibly a higher density polyurethane foam would overcome these problems. Alternatively a complete redesign might be required. Perhaps the most feasible alternative design is thin walled PVC columns with an evacuated jacket for insulation. The principle limitation with this design is that temperature probes and gas and adsorbent sampling become more problematic. If sampling is required, the current PVC columns with external Rockwell insulation are acceptable.

- The analytic technique for the determination of the water loaded zone correlated well with the full numerical solution and the experimentally determined depth. Future work could be undertaken to explore the water penetration for a wider range of process conditions (air

humidity, feed and purge rates). This work could also refine the experimental technique for more accurate determination of the depth of the water-loaded zone.

- Numerical investigation has confirmed that oxygen VSA performance can be a strong function of temperature. Experimentally, this was not demonstrated effectively. The subsequent addition of a feed heater on the laboratory VSA unit should make experimental investigation of the temperature effect on performance much easier.

- The cost criterion that has been developed for oxygen VSA needs to be combined with the strategy outlined in Chapter Five for determining the best adsorbent configuration. One simple extension to this work is to consider the adsorbent performance as a function of pressure window, and operating temperature. However ultimately this work needs to be combined with other aspects of oxygen VSA optimisation (cycle, cycle time, bed length, pellet size) and subject to the same cost criterion. This work is currently being pursuing this work at Monash University.

- Assess the potential application of solid-solid phase change materials (PCM) for reducing the cyclic temperature swings between adsorption and desorption.

## 6.3 Recommendations for Industrial Practice

Commercial confidentiality makes it difficult to assess the current state of gas industry knowledge about oxygen VSA. There is much in-house knowledge of the 'cold spot' problem and patents proposing thermal optimisation strategies. However, a number of recommendations flow from this study.

- This study has shown that CSS temperature profiles reveal much about the operation of the VSA unit. The location and movement of the nitrogen front and the water-loaded front can be readily determined by reference to the CSS temperature profile. This fact shows that temperature profiles are a powerful diagnostic tool for understanding the performance of specific oxygen VSA units. Operational problems such as unbalanced beds, adsorbent with a reduced adsorptive capacity, and low purity product can all be diagnosed by reference to the CSS temperature profiles. Plant start-up time could also be reduced if detailed axial temperature profiles were available. Unlike composition probes that require a fast response oxygen analyzer (mass spectrometer or zirconia oxide probe), thermocouples are cheap and easily inserted into an adsorption bed. In practice these thermocouples would not require logging by the PLC. Instead, the thermocouples could be monitored as required, using manual readings.

- The potential benefits of isothermal operation have been well documented in this study. However in practice it is debatable whether this is possible. This study has questioned the value of several of the patents that endeavour to reduce the temperature swing between adsorption and desorption. More isothermal operation becomes a possibility with structured adsorbents (monoliths), where the substrate can be used to dissipate the heat of adsorption. The advent of ultra fast cycles (300 cycles/min) resulting in much smaller adsorbent quantities may also present opportunities for more isothermal operation. If more isothermal operation were achievable, there would be considerable scope for low temperature operation.

# Appendices

# Appendix 1 - Derivation of the Energy Balance for a Two Component System

Several energy balances appear in the adsorption literature, which are not conservative and do not close at CSS. Detailed below is the derivation of an energy balance that is thermodynamically consistent, and closes at CSS. This is the energy balance used in MINSA.

This derivation ignores axial conduction for the reasons detailed in Chapter Two. Axial conduction could be readily included, and may be required for adsorptive separations, other than oxygen VSA. The energy balance is developed for a two component system.

Applying the First Law over a differential volume of adsorption bed:

**Appendix 1- 1**

$$dU = h_{in}\dot{F}_{in}\delta t - h_{out}\dot{F}_{out}\delta t + \delta Q - \delta W$$

where dU is the change in the total internal energy of the system (J)

$h_{in}$ is specific enthalpy of inlet gas (J/mol)

$h_{out}$ is specific enthalpy of exit gas (J/mol)

$F\delta t$ is flow of moles of gas in or out of volume over time $\delta t$

$\delta Q$ is the differential heat into the system over time $\delta t$ (J)

$\delta W$ is the differential work done by the system over time $\delta t$ (J)

The total internal energy of the system can also be expressed as the sum of the internal energy of the separate phases - solid, adsorbed, and gas.

**Appendix 1- 2**

$$U = U_S + U_g + U_{ad.}$$

**Appendix 1- 3**

$$U = A\delta z\left(\frac{P\varepsilon_l}{RT}\right)\hat{U}_g + \hat{U}_s\rho_b A\delta z + A\delta z\rho_b n\hat{U}_{ad}$$

where A is the cross-sectional area of the differential volume ($m^2$)

U is the total internal energy of the system (J)

$U_g$ , $U_{ad}$, $U_s$ is the internal energy of the gas, adsorbed, and solid phases respectively (J)

$\hat{U}_g$ is the specific internal energy of the gas phase (J/mol of gas)

$\hat{U}_{ad}$ is the specific internal energy of the adsorbed phase (J/mol of adsorbate)

$\hat{U}_s$ is the specific internal energy of the solid phase (J/kg adsorbent)

Some additional simplifications can be made for the gas, solid and adsorbed phases:

**Gas Phase**

The enthalpy of the gas phase can be related to the internal energy of the gas phase assuming perfect gas behaviour.

**Appendix 1- 4**

$$\hat{U}_g = \hat{H}_g - \frac{P}{\rho_g}$$

**Appendix 1- 5**

$$\hat{H}_g = y_1 h_1^* + (1 - y_1)h_2^* \text{ where } h_1^* = h_1^o + C_p(T - T_{ref})$$

where $h_i^*$ is the enthalpy of pure i at $T_{ref}$

$h_i^o$ is the enthalpy of pure i at T

Reference state: Pure i at To and P has enthalpy = 0.

**Appendix 1- 6**

$$d\hat{H}_g = \sum C_{pg,i}(T - T_{ref})dy_i + \sum y_i C_{pg,i}dT$$

where $C_{pg,i}$ is the specific heat capacity of gas component i (J/mol K)

$y_i$ is the mole fraction of component i

**Solid (Adorbent) Phase**

The internal energy of the solid can be rewritten as:

**Appendix 1- 7**

$$\hat{U}_s = C_s(T - T_{ref}) \text{ and } d\hat{U}_s = C_s dT$$

where $C_s$ is the heat capacity of the adsorbent (kJ/kg K)

**Adsorbate Phase**

From Sircar (1985) it has been shown that:

**Appendix 1- 8**

$$\hat{U}_{ad} = \hat{H}_{ad}$$

**Appendix 1- 9**

$$d(n\hat{U}_{ad}) = \left(\frac{\partial \hat{H}_{ad}}{\partial T}\right)_{n_1,n_2} dT + \left(\frac{\partial \hat{H}_{ad}}{\partial n_1}\right)_{T,n_2} dn_1 + \left(\frac{\partial \hat{H}_{ad}}{\partial n_2}\right)_{T,n_1} dn_2$$

**Appendix 1- 10**

$$\left(\frac{\partial \hat{H}_{ad}}{\partial n_1}\right)_{T,n_2} = -\Delta H_1 + C_{pg,1}(T - T_{ref})$$

**Appendix 1- 11**

$$d(n\hat{U}_{ad}) = \left(\frac{\partial \hat{H}_{ad}}{\partial T}\right)_{n_1,n_2} dT + -\Delta H_1 + C_{pg,1}(T - T_{ref}) + -\Delta H_2 + C_{pg,2}(T - T_{ref})$$

Again from Sircar (1985):

**Appendix 1- 12**

$$\left(\frac{\partial \hat{H}_{ads}}{\partial T}\right)_{n_1,n_2} = \frac{\partial}{\partial T}\left(n_1 h_1^* + n_2 h_2^* + \Phi - T\left(\frac{\partial \Phi}{\partial T}\right)_{P,y_i}\right)_{n_1,n_2}$$

where $\Phi$ is the surface potential defined by Sircar (1985).

**Appendix 1- 13**

$$\left(\frac{\partial \hat{H}_{ads}}{\partial T}\right)_{n_1,n_2} = n_1 C_{pg,1} + n_2 C_{pg,2} + \frac{\partial \Phi}{\partial T}_{n_1,n_2} + \frac{\partial T\left(\frac{\partial \Phi}{\partial T}\right)_{P,y_i}}{\partial T}_{n_1,n_2}$$

where $\bar{c}_{ad} = n_1 C_{pg,1} + n_2 C_{pg,2}$ (Average heat capacity of adsorbate) (J/ kg K)

**Appendix 1- 14**

$$\zeta \equiv \frac{\partial \Phi}{\partial T}_{n_1,n_2} + \frac{\partial T\left(\frac{\partial \Phi}{\partial T}\right)_{P,y_i}}{\partial T}_{n_1,n_2}$$

**Appendix 1- 15**

$$\left(\frac{\partial \hat{H}_{ads}}{\partial T}\right)_{n_1,n_2} = \bar{c}_{ad} + \zeta$$

**Heat Loss from the System**

**Appendix 1- 16**

$$Q_{loss} = \frac{4h_{wo}}{D}\left(T - T_{amb}\right)$$

**Combining Expressions and Substituting into Equation Appendix 1-1 yields:**

**Appendix 1- 17**

$$\left(\rho_b cs + \rho_b \bar{c}_{ad} + \rho_b \zeta + \varepsilon_t \rho_g \bar{c}_{pg} \frac{T_{ref}}{T}\right)\frac{\partial T}{\partial t} +$$

$$\left(\varepsilon_t \rho_g \bar{c}_{pg}\left(\frac{T - T_{ref}}{p}\right) - \varepsilon_t\right)\frac{\partial p}{\partial t} + \left(\varepsilon_t \rho_g (T - T_{ref})(c_{pg,1} - c_{pg,2})\right)\frac{\partial y}{\partial t} =$$

$$-\varepsilon_b \frac{\partial}{\partial z}\left(\rho_g v \bar{c}_{pg}(T - T_{ref})\right) + \rho_b \sum_{i=1}^{2}\left(\Delta H_i \frac{\partial n_i}{\partial t}\right) - \frac{4h_{wo}}{D}(T - T_{amb}) - \rho_b (T - T_{ref})\left(\sum_{i=1}^{2} c_{pg,i} \frac{\partial n_i}{\partial t}\right)$$

This represents the complete energy balance. One simplification in the MINSA form of this equation is that the $\zeta$ term is neglected, and hence the surface potential of the adsorbed phase is ignored. This is done for ease of computation, but it does not effect the conservative form of the equation.

# Appendix 2 - Alternative Designs of Adiabatic Columns

This study sought to develop an 'adiabatic' adsorption column using polyurethane insulation and mylar. A number of alternative column designs were considered. Given the limitations of the polyurethane columns, these alternatives are noted for future consideration.

- A column using evacuated aluminised mylar insulation around a thin wall PVC pipe. The aim is to achieve an adiabatic bed with little axial conduction along the column wall. The thermal conductivity of evacuated aluminised mylar is measured in miro-Watts per metre Kelvin. This is similar to the column design of Hou et.al. (1999b) who used a glass walled column surrounded by an evacuated jacket. One limitation with this design is the difficulty in radial sampling of the column. It would be necessary to use axial thermocouples to monitor the temperature profile. Also the inside wall material would have to have low thermal capacitance and low thermal conductivity. Either glass or PVC would be suitable in this respect.

- Very thin steel inner wall with an opening between the column and the internal space. In this configuration there would be no pressure difference across the steel wall, hence the wall could be ultra thin. However, the working volume of the adsorption would be significantly greater and this may pose control problems, and also free convection in the annulus would need to be accounted for.

- A very thin walled vessel with some control strategy to maintain the pressure on both sides of the wall. This could involve having an additional vacuum pump to reduce the pressure in the annulus. An alternative approach would be to have a diaphragm system connecting the inner and outer sections so that their respect pressures could be equalized.

- In addition to these possibilities, a more radical approach would be to have external heating /cooling around the adsorption column which ensures that there is no local temperature driving force between the column and the environment, hence achieving adiabatic operation. The problem with this system is that with rapid cycle times, control would be a problem. This would all complicate the interpretation of laboratory scale results.

- Operating the adsorption within a second adsorption column (i.e. pipe-in-pipe). Again there would be no temperature driving force. However the pipework and other equipment for this system would be very complicated, and costly.

Each of these alternative designs presents new complications. As a result, the PVC columns with external Rockwell insulation were selected as a much simpler, and more mechanically robust design. These PVC columns were demonstrated experimentally and by numerical simulation, not to be as adiabatic as the polyurethane columns. The challenge of developing a laboratory scaled column that is both mechanically robust and adiabatic remains!

# Appendix 3 - Experimental Determination of the Overall Heat Transfer Coefficient for the Polyurethane Columns

The overall heat transfer coefficient of the polyurethane columns was assessed following the method of Kaguei, Yu and Wakao (1985). This involves passing a constant gas flow at fixed temperature through an inert bed and measuring the heat loss/gain to determine the overall heat transfer. In this case, the polyurethane column was filled with BPL carbon and fed with cooled nitrogen.

The principle equation for this analysis is:

$$\frac{T_z - T_{amb}}{T_{ref} - T_{amb}} = \exp[\lambda(z - z_{ref})]$$

$$\text{where } \lambda = \frac{v}{2\alpha}\{1 - \sqrt{(1 + \frac{8\alpha h_{wo}}{v^2(D/2)\varepsilon_b C_{pg}\rho g})} \text{ and } \alpha = \frac{k_e^o}{\varepsilon_b C_g \rho_g} + 0.5 d_p v$$

where

$T_{ref}$ = Reference temperature ($^oC$ )

$z_{ref}$ = Reference position (m)

$T_{amb}$ = Ambient temperature (33.3 $^oC$)

v = Interstitial fluid velocity (7.26E-02 m/sec)

$k_e^o$:= Stagnant axial conductivity (0.12 W/m K)

$\alpha$ = Axial fluid dispersion coefficient (3.82E-04 m2/sec)

D= Column Diameter (0.1 m)

$\varepsilon_b$ = Bulk void fraction of adsorption bed (0.5)

$C_{pg}$:= Specific heat capacity of gas (1000 J/kg K)

$\rho_g$: = Gas density (1.29 kg/m3)

$d_p$ = Adsorbent particle diameter (5mm) (4-10 mesh)

For a full derivation of this equation refer to Kaguei, Yu and Wakao (1985).

Appendix 3 - Experimental Determination of the Overall Heat Transfer Coefficient

**Experimental Results**

The following table reports the experimental temperature data, and the required manipulation to determine the overall heat transfer co-efficient.

| Point | Temp | Z (m) | $(T_{feed}-T_{amb})$ $/(T_{ref}-To)$ | $(z-z_{ref})$ | $Ln((T_{feed} T_{amb})$ $/(T_{ref}-T_{amb}))$ |
|---|---|---|---|---|---|
| 1 | 21.64 | 0 | 0 | 0 | 0 |
| 2 | 22.22 | 0.4 | 0.95 | 0.4 | -0.05102 |
| 3 | 23.1 | 0.8 | 0.87 | 0.8 | -0.13378 |
| 4 | 23.85 | 1.2 | 0.81 | 1.2 | -0.21015 |

Based on this data the calculated value of the overall heat transfer co-efficient ($h_{wo}$) is 0.22 $W/m^2$ K. In this case the outside diameter of the polyurethane column wall was 250 mm.

This technique could be used more extensively to confirm the estimated overall heat transfer co-efficients used for MINSA simulations.

# Appendix 4 - Equipment List for Oxygen VSA Unit

Attached is a detailed list for equipment utilised in the oxygen VSA unit. Also attached is a series of photographs of the elements of the VSA unit.

# Appendix 4 - Instrumentation and Equipment Specification

| Description | Tag | Type | Model | Manufacturer | Size |
|---|---|---|---|---|---|
| Vacuum Blower and Electric Motor | | Rotary Vane | KSV65 | Kinney | |
| Air Dryer with Filtration System | | PSA Dryer | Pneudri, DM015 | Domnick Hunter | |
| Humidity Meter | AIT4 | | | Viasala | |
| Oxygen Analyser | AIT2 | Paramagnetic | 1440C | Servomex | |
| Vacuum Line Filter | | 100 micron filter | | | |
| Feed Supply Tank | | Carbon Steel | | | 60 ltr |
| Product Surge Tank | | Carbon Steel | | | 60 ltr |
| Feed Pressure Transmitter | P1 | | 22D7 | Bourdon Sedeme | 1/2" |
| Pressure Transmitter | P2 | | 22D7 | Bourdon Sedeme | 1/2" |
| Product Pressure Transmitter | P4 | | 23D7 | Bourdon Sedeme | 1/2" |
| Vacuum Pressure Transmitter | P5 | | 22D7 | Bourdon Sedeme | 1/2" |
| Product Tank Pressure Transmitter | P6 | | 22D7 | Bourdon Sedeme | 1/2" |
| Bed-Bed Pressure Transmitter | P7 | | 22D7 | Bourdon Sedeme | 1/2" |
| Feed Tank Pressure Transmitter | | | GS4200 | Genspec | 1/4" |
| Bed 1 Pressure Transmitter | PB1 | | 22D7 | Bourdon Sedeme | 1/2" |
| Bed 2 Pressure Transmitter | PB2 | | 22D7 | Bourdon Sedeme | 1/2" |
| Bed 3 Pressure Transmitter | PB3 | | 22D7 | Bourdon Sedeme | 1/2" |
| Bed- Bed DP Transmitter | DP1 | | EJA110 | Yokogawa | 1/4" |
| Feed DP Transmitter | DP2 | | IDP10-A22A21D-M1 | Foxboro | 1/4" |
| Vacuum DP Transmitter | DP4 | | IDP10-A22A21D-M1 | Foxboro | 1/4" |
| Feed Flow Meter | FIT1 | Pitot Tube | Annubar, GNT-10 | Fisher Rosemount | 1/2" |
| Product Flow Meter | FIT4 | Laminar Plate | PVHL-50LPM | Cole Palmer | 1/2" |
| Vacuum Flow Meter | FIT5 | Pitot Tube | Annubar, GNT-10 | Fisher Rosemount | 1/2" |
| Feed Control Valve | FCV1 | Linear Trim 4,CV=4.0, ATO, 3-15 psig | | Badger Meter, Inc. | 3/4" |
| Bed-Bed Control Valve | FCV2 | Linear Trim 4,CV=4.0, ATO, 3-15 psig | | Badger Meter, Inc. | 3/4" |
| Product Repress Control Valve | FCV3 | Linear Trim A,CV=2.5, ATO, 3-15 psig | | Badger Meter, Inc. | 1/2" |
| Product Control Valve | FCV4 | Linear Trim H,CV=0.13, ATO, 3-15 psig | | Badger Meter, Inc. | 1/4" |
| Vacuum Control Valve | FCV5 | Linear Trim 5,CV=5.0, ATO, 3-15 psig | | Badger Meter, Inc. | 1" |

| Description | Tag | Type | Model | Manufacturer | Size |
|---|---|---|---|---|---|
| Thermocouple T1 through T24 | T1 | T-Type | Exposed Wire | RS Components | |
| Bed 1 Pressure Relief Valve | PRV1 | Relief @ 160 kPa.A | | | 1/4" |
| Bed 2 Pressure Relief Valve | PRV2 | Relief @ 160 kPa.A | | | 1/4" |
| Bed 3 Pressure Relief Valve | PRV2 | Relief @ 160 kPa.A | | | 1/4" |
| Vacuum Pressure Relief Valve | VRV5 | Relief @20 kPa.A | | | 1" |
| Product Repress Isolation Valve | KV1 | Manual Ball | 3 piece, S.S. | Kingston | 3/4" |
| Feed Isolation Valve | KV2 | Manual Ball | 3 piece, S.S. | Kingston | 1" |
| Vacuum Isolation Valve | KV3 | Manual Ball | 3 piece, S.S. | Kingston | 1" |
| Vacuum Isolation Valve | KV4 | Manual Ball | 3 piece, S.S. | Kingston | 1" |
| Product Isolation Valve | KV5 | Manual Ball | 3 piece, S.S. | Kingston | 1/4" |
| Product Isolation Valve | KV6 | Manual Ball | 3 piece, S.S. | Kingston | 1/4" |
| Product Isolation Valve | KV7 | Manual Ball | 3 piece, S.S. | Kingston | 1/4" |
| Vacuum Isolation Valve | KV8 | Manual Ball | 3 piece, S.S. | Kingston | 1" |
| Bed 1 Feed Valve On/Off | KV11 | Actuated Angle Seat | 554-25D195-1-1 | Gemu | 1" |
| Solenoid Valve for KV11 (and other KVs) | | Single Acting | 324-2M1254-1-24VDC | Gemu | |
| Bed 1 Vacuum Valve On/Off | KV12 | Actuated Angle Seat | 554-25D195-1-1 | Gemu | 1" |
| Bed 1 Product Valve On/Off | KV13 | Actuated Angle Seat | 554-20D195-1-0 | Gemu | 3/4" |
| Bed 1 Purge Valve On/Off | KV14 | Actuated Angle Seat | 554-20D195-1-0 | Gemu | 3/4" |
| Bed 2 Feed Valve On/Off | KV21 | Actuated Angle Seat | 554-25D195-1-1 | Gemu | 1" |
| Bed 2 Vacuum Valve On/Off | KV22 | Actuated Angle Seat | 554-25D195-1-1 | Gemu | 1" |
| Bed 2 Product Valve On/Off | KV23 | Actuated Angle Seat | 554-20D195-1-0 | Gemu | 3/4" |
| Bed 2 Purge Valve On/Off | KV24 | Actuated Angle Seat | 554-20D195-1-0 | Gemu | 3/4" |
| Bed 3 Feed Valve On/Off | KV31 | Actuated Angle Seat | 554-25D195-1-1 | Gemu | 1" |
| Bed 3 Vacuum Valve On/Off | KV32 | Actuated Angle Seat | 554-25D195-1-1 | Gemu | 1" |
| Bed 3 Product Valve On/Off | KV33 | Actuated Angle Seat | 554-20D195-1-0 | Gemu | 3/4" |
| Bed 3 Purge Valve On/Off | KV34 | Actuated Angle Seat | 554-20D195-1-0 | Gemu | 3/4" |
| | | | | | |
| **PLC/SCADA** | | | | | |
| CPU | | 90-30 Series | IC693CPU352 | GE-Fanuc | |
| Power Supply | | | IC693PWR321 | GE-Fanuc | |

| Description | Tag | Type | Model | Manufacturer | Size |
|---|---|---|---|---|---|
| Thermocouple Module | | | HE693THM884 | GE-Fanuc | |
| Ethernet InterfaceModule | | | IC693CMM321 | GE-Fanuc | |
| Analogue Input/Output Module, 2 Out/4 In | | | IC693ALG442 | GE-Fanuc | |
| Analogue Output Module, 8 Channel | | | IC693ALG392 | GE-Fanuc | |
| Analogue Input Module, 16 Channel | | | IC693ALG223 | GE-Fanuc | |
| Digital Input Module | | | IC693MDL634 | GE-Fanuc | |
| Digital Output Module | | | IC693MDL940 | GE-Fanuc | |
| | | | | | |
| Citect 5.2 SCADA on 166 MHz P1 | | | | CiTechnologies | |

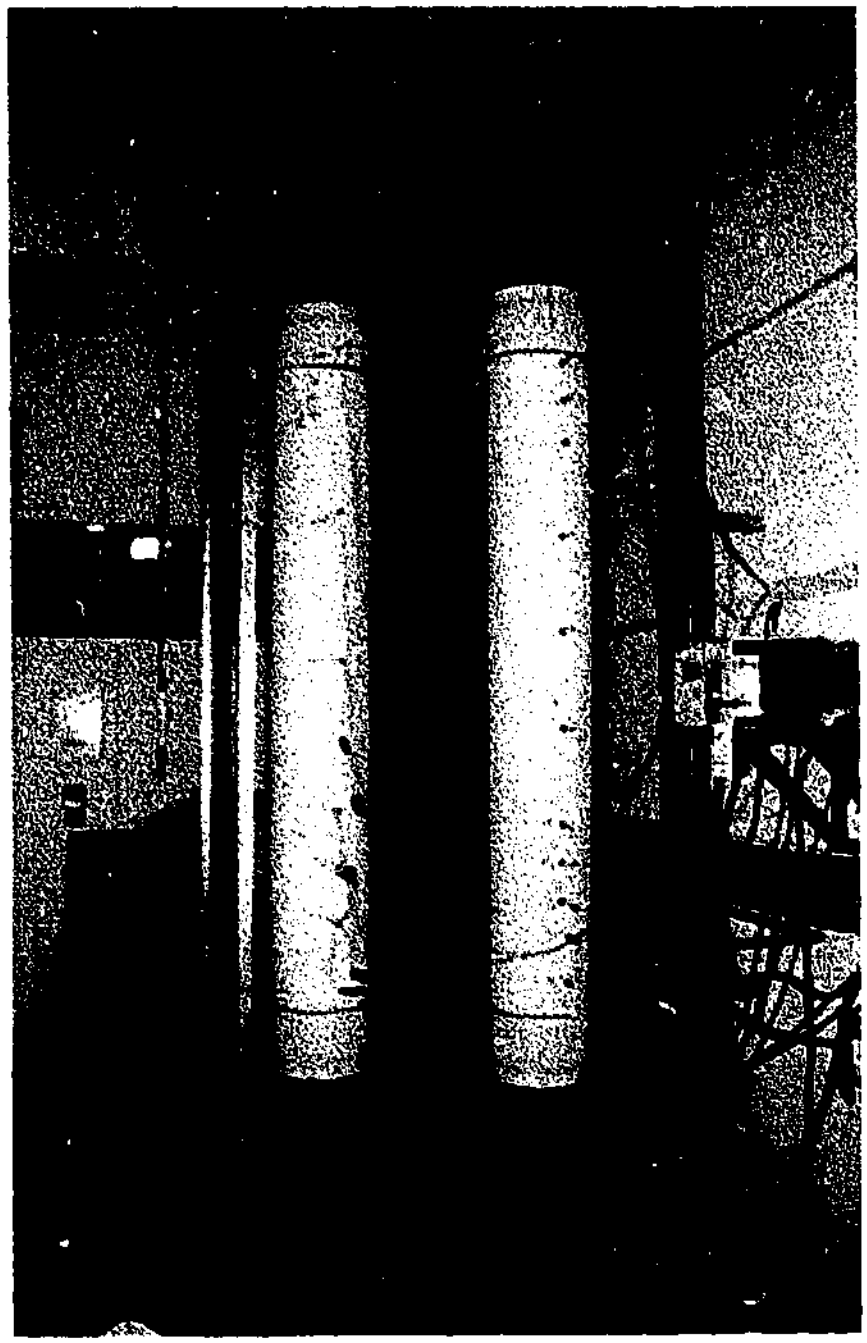

Two Bed VSA Unit with Polyurethane Columns
(SCADA screen in background)

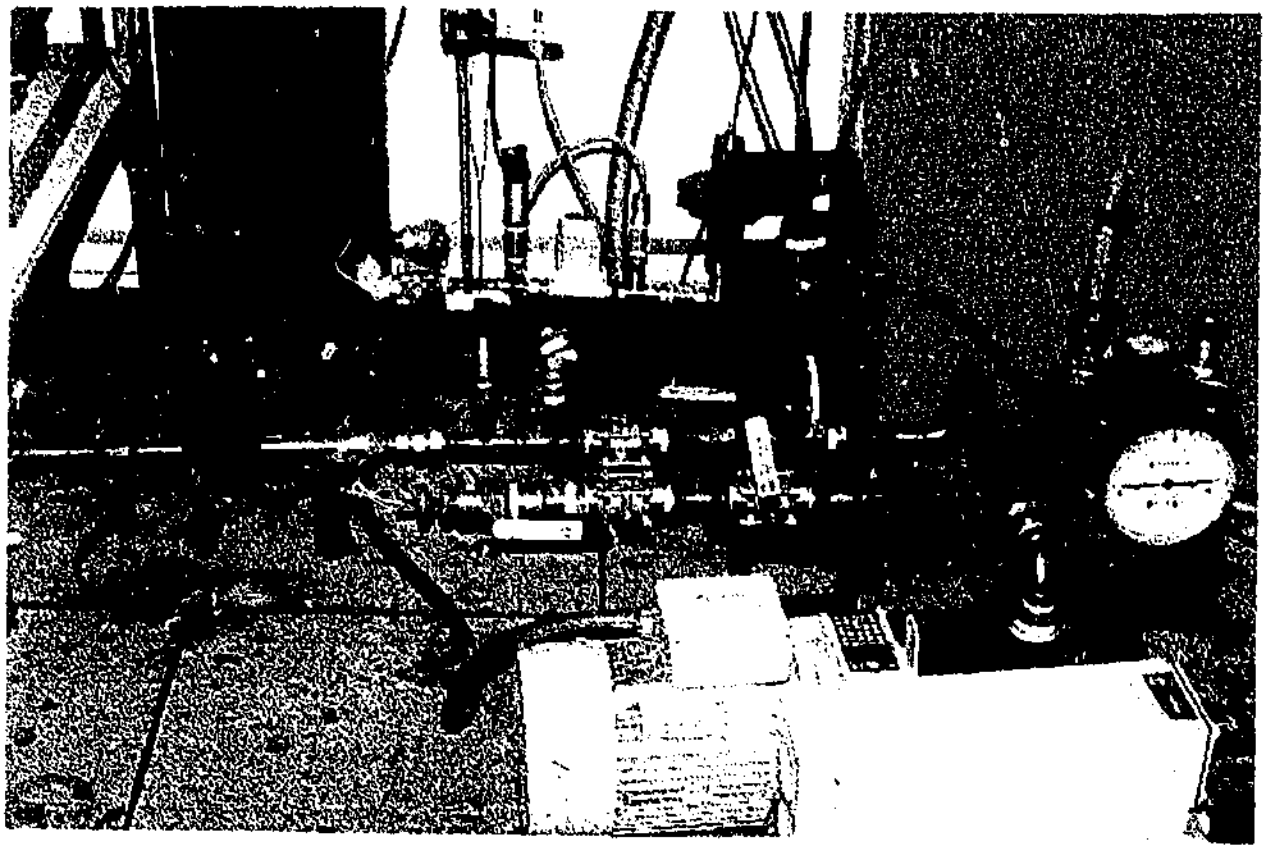

**Product and Vacuum Manifolds with Instrumentation**

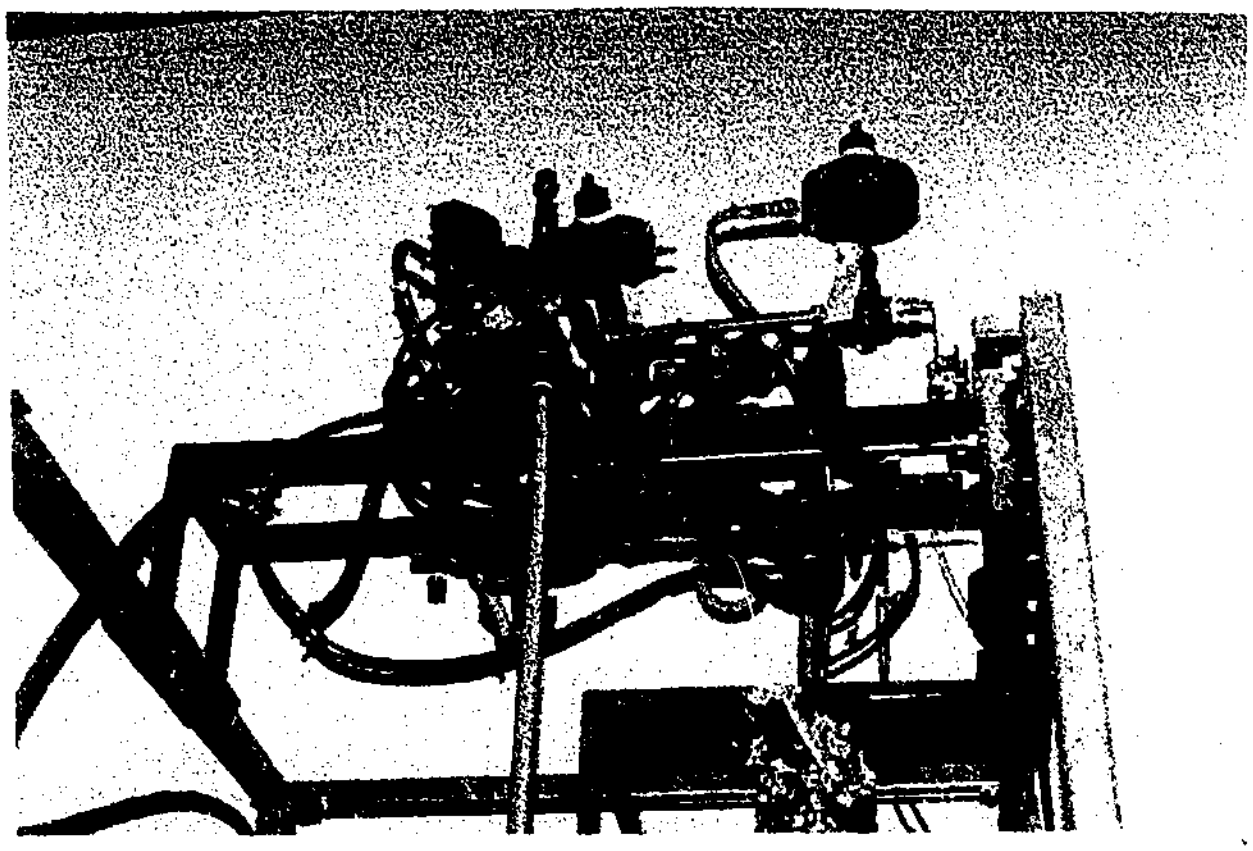

**Top Manifold and Valving**

# Appendix 4 – PVC Column with External Insulation and Thermocouple Probes

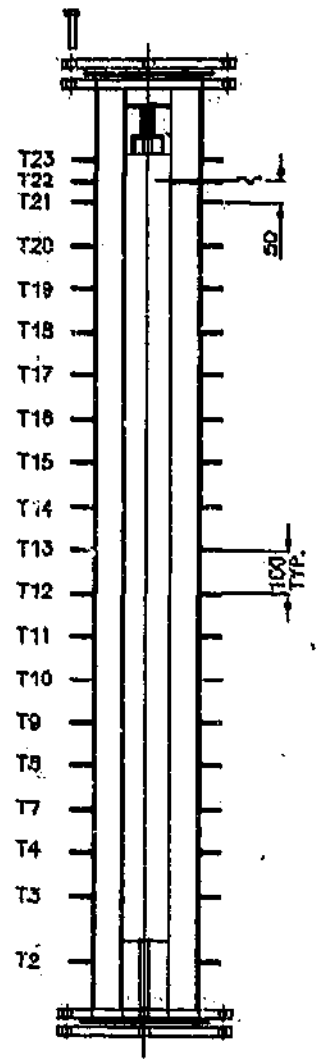

# Appendix 5 - Control System for the Oxygen VSA Unit

The VSA Unit is controlled by a GE-Fanuc 90-30 PLC with an Ethernet connection to a PC based SCADA (Citect) system. This control system is similar to an industrial VSA unit, except the laboratory unit has more instrumentation, and more control valves.

Detailed below is a description of the control philosophy for the VSA unit.

## Normal Operation

### Valve Cycling

The sequencing of the valves is performed by the PLC automatically. The step times and cycle are inputted to the PLC via the SCADA system. The logic of these cycles is tested prior to running the VSA unit.

### Control Valves

There are five control valves used to control the flows, pressures and product purity within the VSA unit.

FCV1 is the feed control valve.
FCV2 is the purge and pressure equalisation control valve.
FCV3 is the product repressurisation and purge control valve.
FCV4 is the product line control valve. This valve is used to control the product purity and the flow. A cascaded PID loop using the product oxygen analyzer (master) and the FIT4 product flowmeter (slave) can be used on FCV4.
FCV5 is in the vacuum line and controls the rate of evacuation. Valve position is adjusted to ensure that the bed is pumped down to the required pressure within the available step time.

PID control can be implemented on any these valves, or they can be adjusted manually.

**Manual Operation**

Due to the complexity of the valve sequencing in the VSA cycles, the solenoid ON/OFF valves are not adjusted manually except for off-line testing. However, the flow control valves can be adjusted manually to achieve desired pressure and flow profiles.

Manual operation of the vacuum pump and compressor can be achieved by selecting the MANUAL selector switch on the PLC cubicle. When selected to MANUAL, the drives (vacuum pump (and compressor) can be started and stopped using the stop/start buttons on the front of the PLC cubicle.

**Start-Up**

In order to start up the oxygen VSA unit:

1. The vacuum pump is selected to AUTO via the switch selectors on the PLC cubicle.
2. Select the UNIT AVAILABLE button on the SCADA interface (relay KV40).
3. Press the hardware START button on the front of the cubicle selected.

Under these conditions the vacuum pump will be running, but the VSA unit will only commence cycling valves after selecting the UNIT RUNNING button on the SCADA interface.

This start up configuration is to ensure that the VSA unit cannot be started remotely, and if the unit is shutdown it cannot restart automatically.

**Shutdown**

Shutdown can be achieved by:

1. Software shutdown via the SCADA system
2. Hardware shutdown by pressing the STOP button of the front of the PLC cubicle

## Alarm Conditions and SCADA/PLC Responses

Due to the extended unattended operation of the VSA unit, the following alarm conditions were coded into the PLC.

There are two different ALARM conditions:
- **Priority 1 Alarms** that cause a shutdown to the VSA unit.
- **Priority 2 Alarms** are logged as alarms within the SCADA/PLC system, but do not shutdown the VSA Unit.

Most alarm conditions are Priority 1 Alarms causing the VSA unit to shut down. This approach is adopted as this is a research project and there is no significant penalty for a shutdown.
In the event of a Priority One alarm, the VSA unit, the unit can only be restarted after locally pressing the START button located on the front of the PLC.

Listed below are a variety of ALARMS conditions that are incorporated into the control system for the VSA unit.

## PRIORITY 1 ALARMS

### Loss of Mains Power (415/240 VAC)

In the event of the loss or disruption of the power supply, the PLC and PLC circuits and solenoids will lose power, and the VSA unit will be shutdown.

### Loss of Air to Solenoid Valve

In the event of loss of pilot air to the pneumatically actuated valves, the solenoid would continue to operate and it would appear to be operating normally. Hence it is necessary to make provision within the PLC software to recognise flow deviations and pressure changes that would result from the air loss to an actuated valve. Since all the valves are air-to-open (ATO), the loss of air will result in closure of a valve.

**Loss of Signal**

When the PLC detects a loss of signal from any of the instruments, or drives, or the loss of a PLC module, the VSA unit will be shut down. Possible causes of a loss of signal will be field wiring, circuit breakers or fuses, or failure of the 24V regulated power supply. These alarms are internal to the PLC logic.

**High Pressure Alarm**

It is possible to envisage conditions where the unit may be exposed to higher than design pressures. Possible causes would be failure or incorrect adjustment of the inlet air regulator. The unit and beds are protected from high bed pressures by software alarms in the PLC which cause the unit to shut down, as well as pressure relief valves. The software alarms are set at 150 kPa abs., and the relief valve are set at 169 kPa abs.

**High Vacuum Alarm**

Under certain conditions a high vacuum could, both software alarms and the vacuum relief valve will protect the beds. Like the situation with the high positive pressures, the software alarms will be activated prior to the vacuum relief valve and shut the VSA unit down. The vacuum relief valve is set at 20 kPa abs.

**Flow, Pressure and Temperature Deviation Alarms**

Flow, pressure and temperature deviation alarms are also included in the PLC/SCADA system. These alarms are activated when a process variable deviates from a specific range. For example, for a one bed cycle, if the product tank pressure is lower than 105 kPa, the unit is stopped to prevent the possibility of back flow through the product flowmeter in a one bed cycle where the product tank is used for purge.

**PRIORITY 2 ALARMS**

In addition to the Priority 1 alarms to ensure the safe operation of the VSA unit that cause the shutdown of the unit, a SCADA/PLC software will also address a variety of other conditions that will result in Priority 2 alarms. These alarms will be logged, but not cause the shutdown of the unit. Typical Priority 2 alarms involve fluctuations in the performance of the VSA unit such as changes to the product flow or concentration outside a desired range. These alarms are logged to assist in understanding the performance of the unit, and trouble shooting.

**Interlocks**

In addition to the alarms, the PLC program also contains an INTERLOCK subroutine. This subroutine, for example, ensures that the feed valve and the vacuum valve cannot be opened on the same bed simultaneously. Other interlocks protect the VSA unit from similar undesirable valve configurations. This subroutine will protect the system from inadvertently programming the PLC with incorrect and possibly damaging cycles.

**SCADA System and Monitoring the VSA Unit**

The SCADA system based on CITECT 5.2 was designed to trend all key variables, and enable online control. All data is sampled every second. The SCADA system also provided reports detailing all the process parameters at a given time. These report files can be automatically outputted when the VSA unit achieves a predefined criteria of CSS. A sample report is provided in Appendix 8.

Attached is a typical GUI page from Citect.

# Citect GUI Page

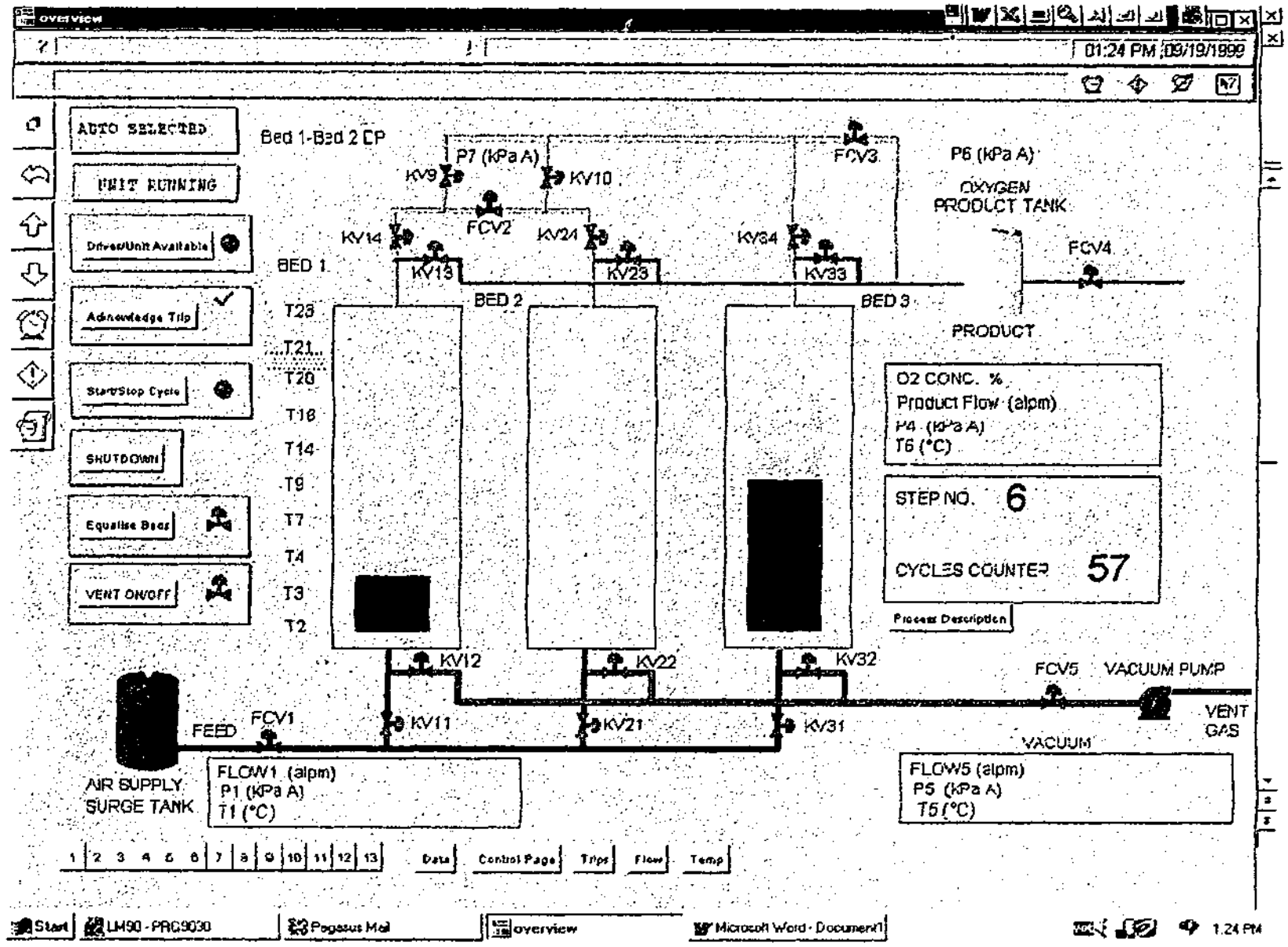

# Appendix 6 - Safety and Risk Assessment For Oxygen VSA Unit

This appendix summarises the most significant conclusions from the HAZOP and risk assessment conducted for this project. Like any process with high purity oxygen, fire was the principle risk, even though the operating pressure and temperature of the VSA unit are close to ambient conditions.

## Summary of Fire Risks

Two principal fire risks were identified in the risk assessment.

- Possible ignition associated with the vacuum pump and high concentrations of oxygen.
- Possible ignition within the adsorption columns.

The risk of the ignition associated with the vacuum pump is minimised by using an appropriate oxygen compatible oil and a 5 micron filter before the vacuum pump. This is a proven strategy for minimising this risk. Both the pump and oil have been used by Air Products and Chemicals Inc. (APCI) on a similar unit. Also the risk assessment of the vacuum pump is dealt with at length in ASTM G63 - Standard Guide for Evaluating Nonmetallic Materials for Oxygen Service. In effect this hazard is well known and has been controlled.

An additional safeguard was to operate the rotary vacuum pump with the ballast open to draw a quantity of air into the pump, and reduce the possibility of any high oxygen concentrations. Under typical operating conditions this would not occur, but if a bed were over purged, it would be possible that an oxygen enriched stream may enter the vacuum pump.

Given the low operating pressure and temperature of the VSA unit, the valves, piping and instrumentation were not purchased 'cleaned for oxygen service'. Instead equipment was cleaned with acetone and dried with nitrogen prior to installation.

Unlike the vacuum pump, the pipework, valves, and instrumentation, there is no historic data or standards to easily assess this risk for the polyurethane columns. These columns are not constructed out of oxygen compatible materials with respect to their Auto Ignition Temp (AIT) or Oxygen Index. In fact, in the event of a fire the combustion of the polyurethane foam could release some toxic (HCN) gases. However from a risk assessment for the columns, the risk of ignition is very low. Friction, particle impact, and static electricity have been assessed as highly improbable/impossible sources of ignition. As a result, it was concluded that the polyurethane columns were acceptable for service, even if not ideal.

**Oxygen Aging Experiment**

In addition to considering the AIT and combustion properties of different materials, it is also important to examine the more general behaviour of materials in an enriched oxygen environment. The German organisation, BAM, developed an oxygen-aging test to evaluate to the suitability of materials for oxygen service.[1]

A modified aging experiment was conducted at 74 C, 100% oxygen and 110 K Pa g for 5 hours. This temperature and pressure considerably exceed the maximum operating conditions in the VSA unit. The sample included polyurethane foam, loctite adhesive, mylar, and nylon tube. The result of the aging experiment was only a very slight reduction in weight, and no discernible change in the properties of the materials. Based on this experiment these materials appear suitable for the service in the VSA unit.

## Hazards

A summary of the major hazards associated with the operation of the VSA unit are presented in the following table:

[1] Wegner, W., Binder, Carlton., Hengstenberg,P., Herrmann, K., and Weinert,D., Tests to Evaluate the Suitability of Materials for Oxygen Service, Flammability and Sensitivity of Materials in Oxygen-Enriched Atmospheres, Thrid Volume, ASTM STP986, D.W. Schroll, Ed., American Society for Testing and Materials, Philadelphia, 1988, pp. 268-278

# Appendix 6 - Major Hazard Summary

| Item | Origin/Cause | Consequences | Protection/Action/Comment |
|---|---|---|---|
| High oxygen concentration | Leak from column or product pipework. | Fire from some ignition source external to the column | Vent oxygen and nitrogen together. Confirm the integrity of the pipework. External PVC columns rated to 6 bar |
| Fire | Combination of oxygen and some ignition source in the VSA unit. Or any fire source within the building. | Fire including combustion of the polyurethane columns and release to toxic gas. Major fire within the laboratory is possible. | Very thorough HAZOP detailing risk. Fire extinguishers present and fire safety training. Signs indicating fire risk and elevated oxygen levels. Hardwired relay to stop VSA unit if fire occurs. |
| High nitrogen concentration | Leak from column or pipework | Insufficient oxygen in the local environment causing respiratory failure. | Confirm integrity of columns and pipework to 6 bar g. Ensure good ventilation to prevent the build up of nitrogen gas. |
| Electrical shock | Short circuit, Earth leak, Poor wiring, Poor work practices | Electrocution<br><br>Fire | Ensure properly grounded wiring. 24 VDC is used for solenoid actuated valves and instrumentation and control valves. |
| High pressure air | Failure of pipework or pressure vessel prior to pressure reducing valve causing release of high pressure air | Damage to equipment and personnel | Ensure all pipework and pressure vessels are adequately pressure rated. Test pressure relief valve on air compressor. Wear safety glasses at all times. |
| Zeolite inhalation or dust release | Incorrect handling of zeolite during transfer to column | Personal injury to lungs or skin caused by heating of zeolite with adsorption of water | Wear personal protective equipment (dust mask, safety goggles, gloves) when handling zeolite. |
| Overheating of column | Slug of saturated water enters pristine adsorption bed or humid air. | Damage to columns. | Drier operating at dew point temperature of -40 C prior to VSA unit and there is a no possible source of bulk water. When humidifier used, PLC shut down of VSA unit on high temperature alarm. |

# Appendix 7 - Quality Assurance and Adsorbent Characterisation

## Calibration of Instrumentation

The output of the instrumentation was checked through the PLC in all cases. This ensures that any changes in instrument performance, or the PLC input, or PLC analog-to-digital conversion are captured by these checks.

## Oxygen Analysers

The oxygen analyser was tested once a fortnight using a single point calibration. This involved testing with 90% oxygen or pure oxygen. If the analyser was reading greater than 0.2% from the standard, the instrument was recalibrated using a two point calibration.(Nitrogen and Oxygen).

## Pressure Transducers

The pressure transducers were checked against themselves, and against atmospheric pressure once per week. Recalibration of the pressure transducers was achieved by adjusting the zero and the span in the SCADA system.

## Flowmeters

The accuracy of the flowmeters was checked in three ways. Firstly, the closure of the mass balance at CSS provides an indication of the flowmeters' accuracy. Secondly, the flowmeters were checked against DTM and soap bubble flowmeters. Thirdly, the flowmeters were recalibrated by NATA registered suppliers.

## FIT1 and FIT5

Both the feed flowmeter (FIT1) and the vacuum flowmeter (FIT5) were both annubar flowmeters inline. Once every two weeks these flowmeters were checked against each other. If the deviation was greater than 2%, the flowmeters and the DP cells were recalibrated.

Once every two months FIT1 and FIT5, were checked against a DTM flowmeter.

**Product Flow (FIT4)**

In addition to the product flowmeter (FIT4), there was also a DTM flowmeter reading that was manually recorded. If the deviation was greater than 2% between the flowmeters, FIT4 was recalibrated.

At low flows FIT4 was checked against a bubble soap flowmeter. At higher flows, the DTM flowmeter was used.

**Thermocouples**

The thermocouples were initially checked against known standards – dry ice, water at 0°C, and a temperature bath at 30 °C. Only thermocouples within ±1 °C were used.

When the VSA unit was not operating, it was possible to check that all thermocouples correctly read the same ambient temperature within ±1 °C.

**Humidity Meter**

The humidity meter was used to confirm the performance of the PSA Dryer located before the VSA unit. The humidity meter was also used to check the air humidity for the wet air experiments described in Chapter Four. The Australian Pulp and Paper Institute calibrated the humidity meter once per month.

**Testing Pipework and Adsorption Beds**

The pipework and adsorption beds were initially leak tested, and tested every time the adsorption beds were repacked. This testing was to ensure the beds were properly sealed, and to see if valve seats were leaking.

The presence of an adsorbent in the bed makes pressure testing slightly complex, and the bed pressure will fluctuate depending on the temperature, as more or less gas is loaded on the adsorbent.

The adsorbent bed, valve seat and pipework integrity was deemed acceptable, when the pressure drop in the adsorption bed was less than 3 kPa over one hour from an initial pressure of 140 kPa.

**Adsorbent Performance**

To confirm the quality of the adsorbent used, single component (Nitrogen) isotherms were obtained at ambient temperature using the Micromeretics ASAP2010. The procedure involved an ambient degas of a sample of adsorbent from the drum, and the measurement of isotherms at ambient temperature (Sample A). The sample was then degassed at elevated temperature for 12 hours at 460 °C in order to measure the 'pristine' isotherm (Sample B). Any difference in the isotherms between Sample A and B can be attributed to water or carbon dioxide loading. If the difference in the nitrogen loading capacity between the two samples was greater than 5%, the molecular sieve was deemed unsuitable for use, and required regeneration or return to the supplier.

**Other Measured Variables**

The masses of adsorbent were determined with scales that are checked by a registered supplier, once every six months. The height of the adsorbent was measured with a tape measure.

Additional adsorbent characterisation (e.g. internal porosity, bulk porosity, heat capacity) required for simulation was performed by APCI, or taken from adsorption and vendor literature.

## Appendix 8 - Sample Report

Below is a sample report outputted from Citect recording all measured variables and some key performance parameters.

# Oxygen VSA Report File

**Time:** 07:32:11 AM
**Date:** Friday, August 11, 2000

**Step No.:** 4
**Cycle No.:** 1079

**Prelayer:** AA, 2.06 kg
**Molecular Sieve:** LiLSX, 7.91 kg Total
**Cycle Type:** Single Bed, 5 step
**Total Cycle Time:** 56

Is the Process at Cyclic Steady State? Yes

**Step Times (sec):**

| Step 1 | Step 2 | Step 3 | Step 4 |
|---|---|---|---|
| 10 | 13 | 2 | 25 |

Step 5
6

**End of Step Control Valve Positions:**
With Vacuum Valve, FCV5, 44.00 % open

| | FCV1(%) | FCV2(%) | FCV3(%) | FCV4(%) |
|---|---|---|---|---|
| Step 1 | 62.00 | | 0.00 | 30.00 |
| Step 2 | 38.00 | | 0.00 | 30.00 |
| Step 3 | | 0.00 | 0.00 | 30.00 |
| Step 4 | | 0.00 | 0.00 | 30.00 |
| Step 5 | 0.00 | | 13.00 | 30.00 |

**End of Step Bed Pressures (kPa.A):**

| | Bed 1 |
|---|---|
| Step 1 | 134.57 |
| Step 2 | 140.66 |
| Step 3 | 100.96 |
| Step 4 | 30.39 |
| Step 5 | 34.05 |

**End of Step Product Pressure (kPa.A):**

| | |
|---|---|
| Step 1 | 109.46 |
| Step 2 | 137.00 |
| Step 3 | 135.74 |
| Step 4 | 123.55 |
| Step 5 | 110.52 |

**End of Step Temperatures (°C):**

| Thermocouple | T2 | T3 | T4 | T7 | T8 |
|---|---|---|---|---|---|
| Axial Pos. (m) | Bed Inlet | 0.1 | 0.2 | 0.3 | 0.4 |
| Dimless Axial Pos. | 0 | 0.0552 | 0.1105 | 0.1657 | 0.2210 |
| Step 1 | 11.70 | 8.60 | -2.00 | -7.30 | -3.20 |
| Step 2 | 11.10 | 8.50 | -1.30 | -6.60 | -2.00 |
| Step 3 | 10.90 | 8.10 | -1.90 | -7.00 | -2.70 |
| Step 4 | 11.60 | 7.40 | -3.00 | -11.40 | -9.10 |
| Step 5 | 11.00 | 7.00 | -3.50 | -12.30 | -10.20 |

| Thermocouple | T9 | T10 | T11 | T12 | T13 |
|---|---|---|---|---|---|
| Axial Pos. (m) | 0.5 | 0.6 | 0.7 | 0.8 | 0.9 |
| Dimless Axial Pos. | 0.2762 | 0.3315 | 0.3867 | 0.4420 | 0.4972 |
| Step 1 | 3.30 | 6.40 | 8.70 | 11.00 | 11.60 |
| Step 2 | 4.90 | 8.10 | 11.20 | 13.30 | 14.90 |
| Step 3 | 4.30 | 8.00 | 11.00 | 12.70 | 14.80 |
| Step 4 | -2.30 | 1.70 | 3.40 | 5.40 | 7.90 |
| Step 5 | -3.30 | 1.20 | 2.60 | 4.20 | 6.50 |

| Thermocouple | T14 | T15 | T16 | T17 | T18 |
|---|---|---|---|---|---|
| Axial Pos. (m) | 1.0 | 1.1 | 1.2 | 1.3 | 1.4 |
| Dimless Axial Pos. | 0.5525 | 0.6077 | 0.6630 | 0.7182 | 0.7735 |
| Step 1 | 14.20 | 15.20 | 16.70 | 16.50 | 18.40 |
| Step 2 | 16.90 | 19.90 | 20.60 | 22.40 | 21.60 |
| Step 3 | 16.80 | 19.60 | 20.60 | 22.40 | 21.60 |
| Step 4 | 11.00 | 12.80 | 14.90 | 15.90 | 17.90 |
| Step 5 | 10.00 | 11.10 | 13.60 | 14.50 | 17.30 |

| Thermocouple | T19 | T20 | T21 | T22 | T23 |
|---|---|---|---|---|---|
| Axial Pos. (m) | 1.5 | 1.6 | 1.7 | 1.75 | 1.8 |
| Dimless Axial Pos. | 0.8287 | 0.8840 | 0.9392 | 0.9669 | 0.9945 |
| Step 1 | 18.90 | 20.20 | 19.70 | 20.10 | 21.20 |
| Step 2 | 23.70 | 24.60 | 22.60 | 23.10 | 24.00 |
| Step 3 | 23.80 | 25.20 | 22.90 | 23.40 | 24.20 |
| Step 4 | 18.00 | 19.60 | 20.10 | 20.40 | 21.80 |
| Step 5 | 17.10 | 18.80 | 19.10 | 19.50 | 20.80 |

| Thermocouple | T24 Radial | Inlet | Vacùum | Product | Top of Bed |
|---|---|---|---|---|---|
| Step 1 | 14.80 | 11.10 | 12.30 | 12.60 | |
| Step 2 | 14.90 | 11.10 | 12.20 | 12.30 | |
| Step 3 | 14.90 | 11.00 | 12.20 | 12.40 | |
| Step 4 | 14.70 | 11.70 | 13.00 | 13.00 | |
| Step 5 | 14.90 | 11.20 | 12.40 | 12.50 | |

**Cyclic Values:**

Feed Gas: 4647.72 mmol/cycle
Vacuum Gas: 3406.92 mmol/cycle
Product Gas: 451.81 mmol/cycle
Manual Check on Product Flow using DTM: 10.33 l/cycle @ 12.6 and 101 kPa ( 440.54 mmol/cycle)

Manual Recorded Blowdown to Atmospheric pressure : 19 al/cycle ( 810.56 mmol/cycle)
This is added to the vacuum gas to determine the totalised waste gas.

Oxygen in Feed Gas: 1022.50 mmol/cycle
Oxygen in Product Gas: 409.22 mmol/cycle

Product Purge Gas: 329.15 mmol/cycle

Blower Power: 2.48 W/cycle
Vacuum Power: 8.76 W/cycle

**Performance Factors:**

| | |
|---|---|
| Oxygen Purity: | 90.58% |
| Oxygen + Argon in Product | 94.69% |
| N2 in Product | 5.31% |
| Recovery: | 38.94 % |
| TPDc: | 0.020 |
| BSF: | 401.90 kg sieve/TPDc |
| Total Power: | 9.93 kW/TPDc |
| | |
| Mass Balance Error: | -0.22% |

## Appendix 9 - Experimental Data Summary Sheets

This appendix provides a summary of the experiments undertaken in the course of this project. A summary sheet is provided of the CSS values for each experimental run. These sheets provide all pressure and temperature profiles and performance data. Mass balance errors are also recorded.

# Appendix 9 - Experimental Data

| Run # | Description |
|---|---|
| AA300NaX1 | 2 Bed - Cycle 2 - 300 mm AA- 1550 mm NaX - Purity ~95%, Pwindow - 128 kPa -33 kPa |
| AA300NaX2 | 2 Bed - Cycle 2 - 300 mm AA - 1550 mm NaX - Purity ~95%, Pwindow - 128 kPa -33 kP |
| | (Same as A300NaX1) |
| AA300NaX3 | 2 Bed - Cycle 2 - 300 mm AA - 1550 mm NaX - Purity ~87%, Pwindow - 127 kPa -34 kP |
| | (Higher product flow and lower purity compared with AA300NaX1 and AA300NaX2) |
| AA300NaX4 | 2 Bed - Cycle 2 - 300 mm AA - 1550 mm NaX - Purity ~71%, Pwindow - 126 kPa -32 kP |
| | (Higher product flow and lower purity compared with AA300NaX1 and AA300NaX2) |
| AA300NaX5 | 2 Bed - Cycle 2 - 300 mm AA- 1550 mm NaX - Purity ~91%, Pwindow - 126 kPa -32 kPa |
| AA300NaX6 | 2 Bed - Cycle 2 - 300 mm AA- 1550 mm NaX - Purity ~95%, Pwindow - 128 kPa -41 kPa |
| | (Higher evacuation pressure ( 41 kPa) compared with A300NaX5 ~ lower puirty) |
| AA300NaX7 | 2 Bed - Cycle 2 - 300 mm AA- 1550 mm NaX - Purity ~57%, Pwindow - 128 kPa -33 kPa |
| | (Higher evacuation pressure ( 53 kPa) compared with A300NaX5 ~ lower puirty) |
| AA300NaX8 | 2 Bed - Cycle 2 - 300 mm AA- 1550 mm NaX - Purity ~83%, Pwindow - 127 kPa -30 kPa |
| | (Same P window as A300NaX5 except increased purge) |
| AA300NaX9 | 2 Bed - Cycle 2 - 300 mm AA- 1550 mm NaX - Purity --83%, Pwindow - 128 kPa -33 kPa |
| | (Same P window as A300NaX5 except reduced purge) |
| AA300NaX10 | 2 Bed - Cycle 2 - 300 mm AA- 1550 mm NaX - Purity ~89%, Pwindow - 127 kPa -31 kPa |
| | (QA run for comparison with A300NaX5) |
| AA300NaX11 | 2 Bed - Cycle 2 - 300 mm AA- 1550 mm NaX - Purity ~95%, Pwindow - 141 kPa -33 kPa |
| AA300NaX12 | 2 Bed - Cycle 2 - 300 mm AA- 1550 mm NaX - Purity ~78%, Pwindow - 134 kPa -35 kPa |
| AA300NaX13 | 2 Bed - Cycle 2 - 300 mm AA- 1550 mm NaX - Purity ~83%, Pwindow - 140 kPa -33 kPa |
| AA300NaX14 | 2 Bed - Cycle 2 - 300 mm AA- 1550 mm NaX - Purity ~80%, Pwindow - 141 kPa -31 kPa |
| AA300NaX15 | 2 Bed - Cycle 2 - 300 mm AA- 1550 mm NaX - Purity ~84%, Pwindow - 141 kPa -33 kPa |
| AA300NaX16 | 2 Bed - Cycle 2 - 300 mm AA- 1550 mm NaX - Purity ~83%, Pwindow - 140 kPa -33 kPa |
| AA300NaX17 | 2 Bed - Cycle 2 - 300 mm AA- 1550 mm NaX - Purity ~86%, Pwindow - 140 kPa -32 kPa |
| AA300NaX18 | 2 Bed - Cycle 2 - 300 mm AA- 1550 mm NaX - Purity ~86%, Pwindow - 140 kPa -32 kPa |
| AA300NaX19 | 2 Bed - Cycle 2 - 300 mm AA- 1550 mm NaX - Purity ~83%, Pwindow - 139 kPa -31 kPa |
| AA300NaX20 | 2 Bed - Cycle 2 - 300 mm AA- 1550 mm NaX - Purity ~81%, Pwindow - 139 kPa -31 kPa |
| AA300NaX21 | 2 Bed - Cycle 2 - 300 mm AA- 1550 mm NaX - Purity ~76%, Pwindow - 139 kPa -35 kPa |
| AA300NaX22 | 2 Bed - Cycle 2 - 300 mm AA- 1550 mm NaX - Purity ~95 %, Pwindow - 141 kPa -31 kP |
| AA300LSX1 | 1 Bed - Cycle 3 - 300 mm AA, 1550 mm LiLSX - 140-30 kPa, Purity ~90% |
| AA300LSX2 | 1 Bed - Cycle 3 - 300 mm AA, 1550 mm LiLSX - 140-31 kPa, Purity ~90% |
| | (Same as 300ALSX1) |

| | |
|---|---|
| AA300LSX3 | 1 Bed - Cycle 3 - 300 mm AA, 1550 mm LiLSX - 140-42 kPa, Purity ~70% |
| AA300LSX4 | 1 Bed - Cycle 3 - 300 mm AA, 1550 mm LiLSX - 140-41 kPa, Purity ~86% |
| AA300LSX5 | 1 Bed - Cycle 3 - 300 mm AA, 1550 mm LiLSX - 140-41 kPa, Purity ~92% |
| AA300LSX6 | 1 Bed - Cycle 3 - 300 mm AA, 1550 mm LiLSX - 140-41 kPa, Same as 300ALSX4 |
| AA300LSX7 | 1 Bed - Cycle 3 - 300 mm AA, 1550 mm LiLSX - Repeat of 300ALSX4 |
| AA300LSX8 | 1 Bed - Cycle 3 - 300 mm AA, 1550 mm LiLSX - 140-41 kPa, Purity ~95%, low prod. |
| AA300LSX9 | 1 Bed - Cycle 3 - 300 mm AA, 1550 mm LiLSX - No Purge (1% Product Cv) |
| AA300LSX10 | 1 Bed - Cycle 3 - 300 mm AA, 1550 mm LiLSX - No Purge (20% Product Cv) |
| AA300LSX11 | 1 Bed - Cycle 3 - 300 mm AA, 1550 mm, Low Feed Pressure, Purity ~46% |
| AA300LSXEX | 1 Bed - Cycle 3 - 300 mm AA, 1550 mm LiLSX - Total Internal Reflux |
| AA300LSXINT | 1 Bed - Cycle 3 - 300 mm AA, 1550 mm LiLSX - Total External Reflux |
| AA115LSX1 | 1 Bed - Cycle 3 - 115 mm AA, 1550 mm LiLSX - Same P and Purity as AA300LSX1 |
| AA25LSX1 | 1 Bed - Cycle 3 - 25 mm AA, 1550 mm LiLSX - Same P and Purity as AA300LSX1 |
| AA115LSXCu | 1 Bed - Cycle 3 - 115 mm AA, 1550 mm LiLSX - 140-31 kPa, Purity ~90%, Cu Diluen |
| LSX1 | 1 Bed - Cycle 3 - Single Layer of LiLSX - P Window 140 -29 kPa |
| LSX2 | 1 Bed - Cycle 3 - Single Layer of LiLSX - P Window 139.8-28.6, 53 sec cycle |
| LSX3 | 1 Bed - Cycle 3 - Single Layer of LiLSX - P Window 139.4-30.1, 53 sec cycle |
| NaX300LSX1 | 1 Bed - Cycle 3 - 300 mm NaX, 1550 mm LiLSX - P window 140 - 40 kPa ~ 88.5 % purit |
| NaX300LSX2 | 1 Bed - Cycle 3 - 300 mm NaX, 1550 mm LiLSX - P window 141-29 kPa ~ 91.5 % purity |
| | (Deeper vacuum compared with NaX300LSX1) |
| NaX300LSX3 | 1 Bed - Cycle 3 - 300 mm NaX, 1550 mm LiLSX - P window 140-32 kPa ~ 92.7% purit |
| | (More purge than NaX300LSX2) |
| NaX300LSX4 | 1 Bed - Cycle 3 - 300 mm NaX, 1550 mm LiLSX - P window 141 - 40 kPa ~ 88 % purit |
| | (Repeat NaX300LSX1) |
| NaX300LSX5 | 1 Bed - Cycle 3 - 300 mm NaX, 1550 mm LiLSX - P window 141-40 kPa ~ 60 % purity |
| | (Lower Purity, More Product) |
| LSX300NaX1 | 1 Bed - Cycle 3 - 300 mm LiLSX, 1550 mm NaX - P window 141-38 kPa ~ 90 % purity |
| LSX300NaX2 | 1 Bed - Cycle 3 - 300 mm LiLSX, 1550 mm NaX - P window 141- 38 kPa ~ 90 % purit |
| LSX300NaX3 | 1 Bed - Cycle 3 - 300 mm LiLSX, 1550 mm NaX - P window 140- 30 kPa ~ 80 % purit |
| PL100LSX1 | 1 Bed - Cycle 3 - 100 mm Plastic packing, 1550 mm LiLSX -140- 31 kPa ~ 89 % purity |

| | |
|---|---|
| AA300LSXPU1 | 1 Bed - Cycle 3 - 300 mm AA, 1550 mm LiLSX - 124-40 kPa, Purity ~93%, PU Bed |
| AA300LSXPU2 | 1 Bed - Cycle 3 - 300 mm AA, 1550 mm LiLSX - 140-41 kPa, Purity~ 87%, FCV4 18 |
| AA300LSXPU3 | 1 Bed - Cycle 3 - 300 mm AA, 1550 mm LiLSX - 124-41 kPa, Purity ~93%, FCV4 10 |
| AA300LSXPU4 | 1 Bed - Cycle 3 - 300 mm AA, 1550 mm LiLSX - 139-30 kPa, Purity ~91%, FCV4 27 |
| NaXDLP | 2 Bed - Cycle 2 - Dry Air Feed Single Layer 13X, Low Purity - 137-37 kPa, Purity~ 80% |
| NaXDLP2 | 2 Bed - Cycle 2 - Dry Air Feed Single Layer 13X, Low Purity - 137 - 36 kPa, Purity ~82 |
| NaXDHP | 2 Bed - Cycle 2 - Dry Air Feed Single Layer 13X, High Purity - 142-34 kPa, Purity ~95% |
| NaXDHP2 | 2 Bed - Cycle 2 - Dry Air Feed Single Layer 13X, High Purity - 140-33 kPa, Purity ~96% |
| NaXWLP | 2 Bed - Cycle 2 - Wet Air Feed Single Layer 13X, Low Purity - 137-35 kPa, Purity ~82% |
| NaXWHP | 2 Bed - Cycle 2 - Wet Air Feed Single Layer 13X, High Purity - 138-34 kPa, Pur. ~96% |
| NaXWHP2 | 2 Bed - Cycle 2 - Wet Air Feed Single Layer 13X, High Purity - 138-34 kPa, Purity ~95% |
| AA38NaXLP | 2 Bed - Cycle 2 - Dry Air Feed - 38 mm AA, NaX - Low Purity -80% - 138-35 kPa |
| AA38NaXHP | 2 Bed - Cycle 2 - Dry Air Feed - 38 mm AA, NaX - High Purity ~95% - 140-33 kPa |
| AA300NaX-DLP | 2 Bed - Cycle 2 - Dry Air Feed - 300 mm AA, NaX - Low Purity ~78% - 134-35 kPa |
| AA300NaX-DHP | 2 Bed - Cycle 2 - Dry Air Feed - 300 mm AA, NaX - High Purity ~96% - 140-33 kPa |
| AA300NaX-DLP | 2 Bed - Cycle 2 - Wet Air Feed - 300 mm AA, NaX - Low Purity ~80% - 135-34 kPa |
| AA300NaX-DHP | 2 Bed - Cycle 2 - Wet Air Feed - 300 mm AA, NaX - High Purity ~95% - 141-33 kPa |
| MAACaX1 | 2 Bed Cycle 2 - Metal Columns, 200 mm AA, 1750 mm CaX, 132 - 43 kPa, Purity~90% |
| MAACaX2 | 2 Bed Cycle 2 - Metal Columns, 200 mm AA, 1750 mm of CaX , 140 - 56 kPa, Pur. ~65 |
| MAACaX3 | 2 Bed Cycle 2 - Metal Columns, 200 mm AA, 1750 mm of CaX, 129-46 kPa, Purity ~93% |
| B1AA300NaX1 | 1 Bed Cycle, PVC Columns, 300 mm AA, 1550 mm NaX - 138-30 kPa, Purity ~89% |
| B1AA300NaX2 | 1 Bed Cycle, PVC Columns, 300 mm AA, 1550 mm NaX - 140-31 kPa, Purity ~62% |
| B1AA300NaX3 | 1 Bed Cycle, PVC Columns, 300 mm AA, 1550 mm NaX - 138-33 kPa, Purity ~87% |
| B1AA300NaX4 | 1 Bed Cycle, PVC Columns, 300 mm AA, 1550 mm NaX - 140-31 kPa, Purity ~75% |
| B1AA300NaX5 | 1 Bed Cycle, PVC Columns, 300 mm AA, 1550 mm NaX - 140-30 kPa - Purity ~94% |
| B1AA300NaX6 | 1 Bed Cycle, PVC Columns, 300 mm AA, 1550 mm NaX - 141-29 kPa, Purity ~94.4% |
| B1AA300NaX7 | 1 Bed Cycle, PVC Columns, 300 mm AA, 1550 mm NaX - 126-31 kPa, Purity ~90.5% |

| | |
|---|---|
| PuAA400NaX1 | 2 Bed - Cycle 1- 400 mm AA- 1400 mm NaX (P window 128-55 kPa) |
| PuAA400NaX2 | 2 Bed - Cycle 1 - 400 mm AA- 1400 mm NaX (P window 132-60 kPa) ~ Higher ambient |
| PuAA400NaX3 | 2 Bed - Cycle 1 - 400 mm AA- 1400 mm NaX (P window 131-45 kPa) ~ Deeper vacuum |
| PuAANaX-VSA69 | 2 Bed - Cycle 2 (70 sec) - 260 mm AA-180 mm NaX-1380 mm VSA6 (P window 138-38 kPa) Purity ~89% |
| PuAANaX-VSA610 | 2 Bed - Cycle 2 (70 sec) - 260 mm AA-180 mm NaX-1380 mm VSA6 (P window 135-45 kPa) Purity ~89% |
| PuAANaX-VSA611 | 2 Bed - Cycle 2 (70 sec) - 260 mm AA-180 mm NaX-1380 mm VSA6 ( P window 135-45) Purity ~55% |
| PuAANaX-VSA612 | 2 Bed - Cycle 2 (70 sec) - 260 mm AA-180 mm NaX-1380 mm VSA6 ( P window 135-46) Purity ~67% |
| PuAANaX-VSA613 | 2 Bed - Cycle 2 (70 sec) - 260 mm AA-180 mm NaX-1380 mm VSA6 ( P window 136-46) Purity ~93% |
| PuNaXVSA61 | 2 Bed - Cycle 2 (70 sec) - 310 mm NaX-1500 mm VSA6 ( P window 128-40) Purity ~89 |
| Notes: | * The experimental data sheets report a temperature profile for one bed, and the pressure profile for both beds. |
| | * Mass balances were not as reliable for Runs PUAA400NaX1 through to PUNaXVSA61 due to the use of turbine flowmeters. In some cases the vacuum flow was measured with a DTM flowmeter after the vacuum pump. The temperature and pressure profiles are correct in all cases. |
| | * All runs are dry air feed unless stated. |
| | * The three cycles used are described in Chapter 3. |

## Run Number AA300NaX1

**Description of Experiment**

Two bed with 300 mm prelayer of activated alumina, main layer NaX, PVC beds
60 second cycle

| Sieve Arrangement and Bed | | |
|---|---|---|
| Type of Prelayer | AA | AA |
| Type of Main Layer | NaX | NaX |
| Bed | PVC | PVC |
| | **Bed 1** | **Bed 2** |
| Mass of Prelayer (kg) | 1.882 | 1.862 |
| Mass of Main layer(kg) | 8.4882 | 8.508 |
| Height of Prelayer (mm) | 300 | 300 |
| Height of Main layer(mm) | 1550 | 1550 |

| End of Step Press. at CSS (kPa) | Bed 1 | Bed 2 |
|---|---|---|
| Step 1 | 123.6 | 49.9 |
| Step 2 | 128.0 | 34.2 |
| Step 3 | 96.8 | 50.5 |
| Step 4 | 87.9 | 61.2 |
| Step 5 | 49.3 | 124.3 |
| Step 6 | 33.4 | 129.1 |
| Step 7 | 50.3 | 97.1 |
| Step 8 | 60.6 | 88.1 |

| Mass Balance at CSS (Total millimole per cycle) | | | |
|---|---|---|---|
| Feed flow | 3612.1 | Evacuation flow | 3346.4 |
| Product flow | 313.7 | Mass Balance Error (%) | -1.3 |

| Key Performance Parameters | | | |
|---|---|---|---|
| Oxygen Recovery (%) | 37.5 | BSF (kg/TPDc) | 1242.3 |
| Power: (kW/TPDc) | 11.4 | Oxygen Purity (%): | 95.1 |

| End of Step CSS Temperature Profile (°C) | | | | | | | | |
|---|---|---|---|---|---|---|---|---|
| z (m) | Step 1 | Step 2 | Step 3 | Step 4 | Step 5 | Step 6 | Step 7 | Step 8 |
| 0 | 22.4 | 21.6 | 20.7 | 18.8 | 20.6 | 21 | 21.5 | 22.5 |
| 0.1 | 20.8 | 21.2 | 20.6 | 20.6 | 20.6 | 20.2 | 20.7 | 20.7 |
| 0.2 | 14.4 | 14.6 | 14.3 | 14.3 | 13.5 | 13.3 | 13.3 | 13.3 |
| 0.3 | 5.6 | 6.3 | 5.9 | 5.6 | 4.4 | 3.2 | 3.3 | 3.5 |
| 0.4 | 15.9 | 16.7 | 16 | 15.8 | 13.4 | 12.3 | 12.2 | 12.3 |
| 0.5 | 21.3 | 22 | 21.6 | 21.1 | 19.5 | 18.5 | 18.2 | 18.5 |
| 0.6 | 22.7 | 23.2 | 23 | 22.6 | 21.2 | 20.1 | 19.9 | 19.7 |
| 0.7 | 24.1 | 24.9 | 24.7 | 24.3 | 22.9 | 21.7 | 21.3 | 21.1 |
| 0.8 | 26.2 | 27.2 | 26.8 | 26.5 | 25 | 23.9 | 23.3 | 23.2 |
| 0.9 | 25.9 | 27.1 | 27.1 | 26.8 | 25.6 | 24.4 | 23.9 | 23.7 |
| 1 | 25.8 | 27.7 | 28 | 27.8 | 26.5 | 25.1 | 24.7 | 24.4 |
| 1.1 | 27 | 28.8 | 29.5 | 29.7 | 28.3 | 27 | 26.4 | 26.2 |
| 1.2 | 27.9 | 28.7 | 30.1 | 30.3 | 29.2 | 28.1 | 27.4 | 27.4 |
| 1.3 | 27.4 | 27.8 | 29.1 | 29.6 | 28.7 | 27.5 | 27.1 | 26.9 |
| 1.4 | 26.4 | 26.5 | 26.8 | 27.4 | 26.7 | 26.3 | 26.2 | 26.2 |
| 1.5 | 26.2 | 26.4 | 26.4 | 26.6 | 26 | 25.7 | 25.7 | 25.7 |
| 1.6 | 26.4 | 26.8 | 26.7 | 26.8 | 26.3 | 25.9 | 25.9 | 25.9 |
| 1.7 | 23.9 | 24 | 24 | 24 | 23.7 | 23.6 | 23.7 | 23.7 |
| 1.75 | 24.6 | 24.8 | 24.7 | 24.7 | 24.2 | 23.9 | 23.9 | 24 |
| 1.8 | 24.9 | 25.2 | 25.1 | 25.1 | 24.5 | 24.2 | 24.3 | 24.3 |

# Run Number AA300NaX2

**Description of Experiment**

Two bed with 300 mm prelayer of activated alumina, main layer NaX, PVC, 60 second cycle

| Sieve Arrangement and Bed | | |
|---|---|---|
| Type of Prelayer | AA | AA |
| Type of Main Layer | NaX | NaX |
| Bed | PVC | PVC |
| | **Bed 1** | **Bed 2** |
| Mass of Prelayer (kg) | 1.882 | 1.862 |
| Mass of Main layer(kg) | 8.4882 | 8.508 |
| Height of Prelayer (mm) | 300 | 300 |
| Height of Main layer(mm) | 1550 | 1550 |

| End of Step Press. at CSS (kPa) | Bed 1 | Bed 2 |
|---|---|---|
| Step 1 | 123.2 | 48.9 |
| Step 2 | 127.4 | 33.4 |
| Step 3 | 95.8 | 50.0 |
| Step 4 | 86.8 | 60.8 |
| Step 5 | 48.4 | 123.4 |
| Step 6 | 32.6 | 128.3 |
| Step 7 | 49.6 | 96.1 |
| Step 8 | 60.2 | 87.0 |

| Mass Balance at CSS (Total millimole per cycle) | | | |
|---|---|---|---|
| Feed flow | 3896.8 | Evacuation flow | 3503.5 |
| Product flow | 300.9 | Mass Balance Error (%) | 2.4 |

| Key Performance Parameters | | | |
|---|---|---|---|
| Oxygen Recovery (%) | 33.4 | BSF (kg/TPDc) | 1292.5 |
| Power: (kW/TPDc) | 12.7 | Oxygen Purity (%): | 95.3 |

| End of Step CSS Temperature Profile (°C) | | | | | | | | |
|---|---|---|---|---|---|---|---|---|
| z (m) | Step 1 | Step 2 | Step 3 | Step 4 | Step 5 | Step 6 | Step 7 | Step 8 |
| 0 | 24.1 | 23.7 | 21.4 | 20.6 | 22.2 | 22.4 | 22.9 | 23.7 |
| 0.1 | 22.4 | 22.1 | 22 | 21.8 | 22 | 22 | 21.2 | 21.3 |
| 0.2 | 15.7 | 15.6 | 15.4 | 15.3 | 14.8 | 14.6 | 14.3 | 14.3 |
| 0.3 | 6.8 | 7.1 | 6.8 | 6.5 | 5.5 | 4.6 | 3.8 | 3.9 |
| 0.4 | 17.3 | 18.1 | 17.3 | 16.8 | 15 | 13.9 | 13.6 | 13.7 |
| 0.5 | 22.5 | 23.2 | 22.9 | 22.4 | 20.9 | 20.1 | 19.6 | 19.8 |
| 0.6 | 23.9 | 24.5 | 24.2 | 23.7 | 22.1 | 21 | 21.1 | 20.7 |
| 0.7 | 25.3 | 26.1 | 26.3 | 25.6 | 24.3 | 23 | 22.8 | 22.6 |
| 0.8 | 27.3 | 28.3 | 28.1 | 27.9 | 26.2 | 25.1 | 24.7 | 24.5 |
| 0.9 | 26.8 | 27.9 | 28 | 27.8 | 26.6 | 25.6 | 25.2 | 24.9 |
| 1 | 26.9 | 28.6 | 28.9 | 28.7 | 27.8 | 26.3 | 25.8 | 25.5 |
| 1.1 | 28.2 | 29.8 | 30.5 | 30.7 | 29.9 | 28.2 | 27.7 | 27.4 |
| 1.2 | 29 | 29.7 | 31.2 | 31.4 | 30.4 | 29.2 | 28.7 | 28.6 |
| 1.3 | 28.4 | 28.9 | 30 | 30.6 | 29.6 | 28.6 | 28.1 | 28 |
| 1.4 | 27.4 | 27.5 | 27.8 | 28.3 | 27.6 | 27.3 | 27.1 | 27.1 |
| 1.5 | 27.3 | 27.4 | 27.4 | 27.5 | 27 | 26.8 | 26.7 | 26.8 |
| 1.6 | 27.6 | 27.9 | 28 | 27.9 | 27.4 | 27.2 | 27.1 | 27.1 |
| 1.7 | 25.1 | 25.2 | 25.2 | 25.1 | 24.8 | 24.8 | 24.7 | 24.7 |
| 1.75 | 25.9 | 26.1 | 26.1 | 26 | 25.5 | 25.2 | 25.2 | 25.2 |
| 1.8 | 26.2 | 26.5 | 26.4 | 26.4 | 25.9 | 25.6 | 25.6 | 25.6 |

## Run Number AA300NaX3

**Description of Experiment**
Two bed with 300 mm prelayer of activated alumina, main layer NaX, PVC beds
60 second cycle

| Sieve Arrangement and Bed | | |
|---|---|---|
| Type of Prelayer | AA | AA |
| Type of Main Layer | NaX | NaX |
| Bed | PVC | PVC |
| | **Bed 1** | **Bed 2** |
| Mass of Prelayer (kg) | 1.882 | 1.862 |
| Mass of Main layer(kg) | 8.4882 | 8.508 |
| Height of Prelayer (mm) | 300 | 300 |
| Height of Main layer(mm) | 1550 | 1550 |

| End of Step Press. at CSS (kPa) | Bed 1 | Bed 2 |
|---|---|---|
| Step 1 | 122.2 | 51.0 |
| Step 2 | 126.6 | 35.2 |
| Step 3 | 96.5 | 50.6 |
| Step 4 | 88.8 | 61.2 |
| Step 5 | 49.9 | 123.4 |
| Step 6 | 34.2 | 127.8 |
| Step 7 | 50.4 | 97.6 |
| Step 8 | 60.7 | 89.8 |

| Mass Balance at CSS (Total millimole per cycle) | | | |
|---|---|---|---|
| Feed flow | 4185.5 | Evacuation flow | 3642.2 |
| Product flow | 474.2 | Mass Balance Error (%) | 1.7 |

| Key Performance Parameters | | | |
|---|---|---|---|
| Oxygen Recovery (%) | 44.8 | BSF (kg/TPDc) | 898.80 |
| Power: (kW/TPDc) | 8.81 | Oxygen Purity (%): | 86.90 |

| End of Step CSS Temperature Profile (°C) | | | | | | | | |
|---|---|---|---|---|---|---|---|---|
| z (m) | Step 1 | Step 2 | Step 3 | Step 4 | Step 5 | Step 6 | Step 7 | Step 8 |
| 0 | 22.1 | 22 | 19.3 | 18.3 | 20.6 | 20.8 | 21.5 | 22.1 |
| 0.1 | 21.4 | 21.4 | 21.2 | 21.1 | 21 | 21.1 | 20.4 | 20.4 |
| 0.2 | 16.2 | 16.1 | 16.1 | 16 | 15.3 | 15.2 | 14.8 | 14.9 |
| 0.3 | 6.6 | 7.1 | 7.4 | 7.3 | 5.6 | 4.6 | 4.3 | 4.3 |
| 0.4 | 13.1 | 13.8 | 13.5 | 13 | 10.9 | 9.8 | 9.3 | 9.6 |
| 0.5 | 16.4 | 17.3 | 16.9 | 16.5 | 14.5 | 13.3 | 13 | 13.3 |
| 0.6 | 19.4 | 20 | 19.3 | 19.3 | 17.2 | 16.3 | 16.4 | 16.3 |
| 0.7 | 20.6 | 21.5 | 20.9 | 21 | 19 | 17.8 | 18.1 | 17.9 |
| 0.8 | 23.1 | 23.8 | 23.6 | 23.4 | 21.6 | 20.6 | 20.4 | 20.3 |
| 0.9 | 22.6 | 23.7 | 23.4 | 23.4 | 22.1 | 21 | 20.6 | 20.7 |
| 1 | 23.5 | 24.4 | 24.4 | 24.2 | 22.8 | 22 | 21.6 | 21.5 |
| 1.1 | 24.2 | 25.5 | 25.5 | 25.6 | 24.4 | 23.3 | 22.9 | 22.7 |
| 1.2 | 25 | 26.6 | 26.8 | 26.8 | 25.6 | 24.4 | 23.8 | 23.7 |
| 1.3 | 24.8 | 26.3 | 26.8 | 26.6 | 25.6 | 24.7 | 24.1 | 23.8 |
| 1.4 | 25 | 25.4 | 26.2 | 26.1 | 25.4 | 25 | 24.6 | 24.5 |
| 1.5 | 25.7 | 26.2 | 27.1 | 27.3 | 26.5 | 25.8 | 25.3 | 25.2 |
| 1.6 | 27.1 | 27.6 | 28.4 | 29 | 28.6 | 27.8 | 27.1 | 26.8 |
| 1.75 | 26.1 | 26.2 | 26.5 | 27.2 | 27 | 26.2 | 25.7 | 25.6 |
| 1.8 | 26.3 | 26.4 | 26.5 | 26.9 | 26.8 | 26.2 | 25.8 | 25.7 |

# Run Number AA300NaX4

**Description of Experiment**

Two bed with 300 mm prelayer of activated alumina, main layer NaX, PVC bed
60 second cycle

| Sieve Arrangement and Bed | | |
|---|---|---|
| Type of Prelayer | AA | AA |
| Type of Main Layer | NaX | NaX |
| Bed | PVC | PVC |
| | **Bed 1** | **Bed 2** |
| Mass of Prelayer (kg) | 1.882 | 1.862 |
| Mass of Main layer(kg) | 8.4882 | 8.508 |
| Height of Prelayer (mm) | 300 | 300 |
| Height of Main layer(mm) | 1550 | 1550 |

| End of Step Press. at CSS (kPa) | Bed 1 | Bed 2 |
|---|---|---|
| Step 1 | 122.3 | 48.9 |
| Step 2 | 125.7 | 32.8 |
| Step 3 | 97.2 | 46.4 |
| Step 4 | 89.6 | 57.6 |
| Step 5 | 48.0 | 122.8 |
| Step 6 | 32.0 | 126.5 |
| Step 7 | 46.4 | 97.8 |
| Step 8 | 57.3 | 90.4 |

| Mass Balance at CSS (Total millimole per cycle) | | | |
|---|---|---|---|
| Feed flow | 4528.8 | Evacuation flow | 3809.7 |
| Product flow | 682.3 | Mass Balance Error (%) | 0.8 |

| Key Performance Parameters | | | |
|---|---|---|---|
| Oxygen Recovery (%) | 49.0 | BSF (kg/TPDc) | 759.4 |
| Power: (kW/TPDc) | 8.2 | Oxygen Purity (%): | 71.4 |

| End of Step CSS Temperature Profile (°C) | | | | | | | | |
|---|---|---|---|---|---|---|---|---|
| z (m) | Step 1 | Step 2 | Step 3 | Step 4 | Step 5 | Step 6 | Step 7 | Step 8 |
| 0 | 21.5 | 20.6 | 19.7 | 18.7 | 19.3 | 19.7 | 21.6 | 22.6 |
| 0.1 | 21.4 | 21.4 | 21.9 | 21.8 | 21.2 | 21.2 | 21.5 | 21.7 |
| 0.2 | 16.4 | 16.5 | 16.8 | 16.8 | 16 | 15.8 | 15.8 | 15.9 |
| 0.3 | 10.4 | 10.5 | 10.5 | 10.4 | 9.3 | 8.8 | 8.4 | 9.2 |
| 0.4 | 13.8 | 14.3 | 14.3 | 14 | 11.7 | 10.6 | 10.8 | 11.2 |
| 0.5 | 15.5 | 16 | 15.9 | 15.8 | 13.6 | 12.6 | 12.4 | 12.3 |
| 0.6 | 18.6 | 19.4 | 18.9 | 18.8 | 17.3 | 16.3 | 16.4 | 16.2 |
| 0.7 | 19.8 | 20.9 | 20.9 | 20.4 | 19.2 | 17.9 | 17.6 | 17.6 |
| 0.8 | 21.9 | 22.6 | 22.5 | 22 | 20.5 | 19.4 | 19 | 19.3 |
| 0.9 | 21.7 | 22.7 | 22.4 | 22.3 | 20.8 | 19.7 | 19.6 | 19.3 |
| 1 | 22.7 | 23.8 | 23.8 | 23.3 | 21.9 | 20.7 | 20.3 | 20.2 |
| 1.1 | 23.6 | 24.6 | 24.7 | 24.3 | 23 | 22.2 | 21.6 | 21.5 |
| 1.2 | 24.4 | 25.7 | 25.7 | 25.5 | 24.2 | 23.4 | 22.9 | 22.7 |
| 1.3 | 23.9 | 25.5 | 25.7 | 25.4 | 24.2 | 23.2 | 22.8 | 22.5 |
| 1.4 | 24 | 24.9 | 25.2 | 25 | 24.3 | 23.8 | 23.6 | 23.4 |
| 1.5 | 25 | 25.9 | 26.6 | 26.4 | 25.4 | 24.8 | 24.4 | 24.2 |
| 1.6 | 26.5 | 27.3 | 28.4 | 28.6 | 27.9 | 27.1 | 26.4 | 26.1 |
| 1.75 | 26.1 | 26.3 | 27.2 | 27.7 | 27.3 | 26.5 | 25.8 | 25.6 |
| 1.8 | 26.6 | 26.6 | 27.1 | 27.7 | 27.5 | 26.7 | 25.9 | 25.9 |

# Run Number AA300NaX5

**Description of Experiment**

Two bed with 300 mm prelayer of activated alumina, main layer NaX, PVC bed
60 second cycle

| Sieve Arrangement and Bed | | |
|---|---|---|
| Type of Prelayer | AA | AA |
| Type of Main Layer | NaX | NaX |
| Bed | PVC | PVC |
| | **Bed 1** | **Bed 2** |
| Mass of Prelayer (kg) | 1.882 | 1.862 |
| Mass of Main layer(kg) | 8.4882 | 8.508 |
| Height of Prelayer (mm) | 300 | 300 |
| Height of Main layer(mm) | 1550 | 1550 |

| End of Step Press. at CSS (kPa) | Bed 1 | Bed 2 |
|---|---|---|
| Step 1 | 121.8 | 48.6 |
| Step 2 | 125.9 | 33.1 |
| Step 3 | 96.3 | 48.4 |
| Step 4 | 86.8 | 60.2 |
| Step 5 | 47.7 | 121.8 |
| Step 6 | 32.1 | 126.9 |
| Step 7 | 48.3 | 96.8 |
| Step 8 | 59.6 | 87.6 |

| Mass Balance at CSS (Total millimole per cycle) | | | |
|---|---|---|---|
| Feed flow | 4248.8 | Evacuation flow | 3730.1 |
| Product flow | 463.3 | Mass Balance Error (%) | 1.3 |

| Key Performance Parameters | | | |
|---|---|---|---|
| Oxygen Recovery (%) | 45.1 | BSF (kg/TPDc) | 878.5 |
| Power: (kW/TPDc) | 9.3 | Oxygen Purity (%): | 91.0 |

| End of Step CSS Temperature Profile (°C) | | | | | | | | |
|---|---|---|---|---|---|---|---|---|
| z (m) | Step 1 | Step 2 | Step 3 | Step 4 | Step 5 | Step 6 | Step 7 | Step 8 |
| 0 | 20.9 | 20.3 | 18.5 | 16.8 | 18.4 | 19.2 | 20 | 20.9 |
| 0.1 | 19.3 | 20 | 19.3 | 19.3 | 19.1 | 19.3 | 19 | 18.9 |
| 0.2 | 13.7 | 13.9 | 13.7 | 13.7 | 13.1 | 12.7 | 12.6 | 12.6 |
| 0.3 | 4 | 5 | 4.5 | 4.4 | 2.5 | 1.7 | 1.2 | 1.3 |
| 0.4 | 11 | 12.3 | 11.5 | 11.2 | 9.1 | 7.5 | 7.6 | 7.8 |
| 0.5 | 15.2 | 16 | 15.7 | 15.4 | 13.3 | 12 | 11.9 | 11.8 |
| 0.6 | 18.3 | 19.1 | 18.3 | 18.2 | 16.2 | 15.1 | 15.4 | 15.4 |
| 0.7 | 19.9 | 20.7 | 20.1 | 19.7 | 17.9 | 16.9 | 16.8 | 17 |
| 0.8 | 22.2 | 23.1 | 22.6 | 22.4 | 20.8 | 19.7 | 19.4 | 19.1 |
| 0.9 | 21.8 | 22.7 | 22.8 | 22.4 | 21 | 20.1 | 19.6 | 19.6 |
| 1 | 22.3 | 23.5 | 23.6 | 23.5 | 21.9 | 21.1 | 20.6 | 20.3 |
| 1.1 | 23.3 | 24.8 | 25 | 25.1 | 23.4 | 22.6 | 22 | 21.5 |
| 1.2 | 23.9 | 25.8 | 26.2 | 25.9 | 24.6 | 23.6 | 23 | 22.6 |
| 1.3 | 23.8 | 25.3 | 26 | 26 | 24.8 | 23.8 | 23.3 | 23 |
| 1.4 | 24 | 24.4 | 25.2 | 25.2 | 24.5 | 24 | 23.7 | 23.6 |
| 1.5 | 24.7 | 25.1 | 25.8 | 26.3 | 25.4 | 24.6 | 24.3 | 24.1 |
| 1.6 | 25.8 | 26.2 | 26.9 | 27.7 | 27.3 | 26.4 | 25.8 | 25.5 |
| 1.75 | 24.3 | 24.6 | 24.7 | 25.1 | 25 | 24.2 | 23.9 | 23.8 |
| 1.8 | 24.5 | 24.8 | 24.8 | 25 | 24.7 | 24.2 | 23.9 | 23.9 |

# Run Number AA300NaX6

**Description of Experiment**

Two bed with 300 mm prelayer of activated alumina, main layer NaX, PVC bed
60 second cycle

| Sieve Arrangement and Bed | | |
|---|---|---|
| Type of Prelayer | AA | AA |
| Type of Main Layer | NaX | NaX |
| Bed | PVC | PVC |
| | **Bed 1** | **Bed 2** |
| Mass of Prelayer (kg) | 1.882 | 1.862 |
| Mass of Main layer(kg) | 8.4882 | 8.508 |
| Height of Prelayer (mm) | 300 | 300 |
| Height of Main layer(mm) | 1550 | 1550 |

| End of Step Press. at CSS (kPa) | Bed 1 | Bed 2 |
|---|---|---|
| Step 1 | 124.3 | 57.6 |
| Step 2 | 127.2 | 42.4 |
| Step 3 | 97.6 | 58.0 |
| Step 4 | 89.3 | 69.3 |
| Step 5 | 56.4 | 125.1 |
| Step 6 | 41.3 | 128.1 |
| Step 7 | 57.3 | 99.0 |
| Step 8 | 67.9 | 90.9 |

| Mass Balance at CSS (Total millimole per cycle) | | | |
|---|---|---|---|
| Feed flow | 3765.3 | Evacuation flow | 3163.9 |
| Product flow | 498.5 | Mass Balance Error (%) | 2.7 |

| Key Performance Parameters | | | |
|---|---|---|---|
| Oxygen Recovery (%) | 43.9 | BSF (kg/TPDc) | 1018.7 |
| Power: (kW/TPDc) | 7.7 | Oxygen Purity (%): | 72.9 |

| End of Step CSS Temperature Profile (°C) | | | | | | | | |
|---|---|---|---|---|---|---|---|---|
| z (m) | Step 1 | Step 2 | Step 3 | Step 4 | Step 5 | Step 6 | Step 7 | Step 8 |
| 0 | 22.9 | 22.3 | 21.2 | 19.9 | 21 | 21.1 | 23.2 | 23.9 |
| 0.1 | 22.6 | 22.6 | 23.2 | 23.2 | 22.3 | 22.2 | 23 | 22.9 |
| 0.2 | 18.8 | 18.9 | 19 | 19 | 18.3 | 18.1 | 18.2 | 18.2 |
| 0.3 | 10.4 | 10.9 | 11.1 | 11 | 9.6 | 8.6 | 8.7 | 9 |
| 0.4 | 14.7 | 15.4 | 15.6 | 15.2 | 12.9 | 11.7 | 12.2 | 12.5 |
| 0.5 | 17.6 | 18.1 | 17.9 | 17.4 | 15.7 | 14.8 | 14.6 | 15.1 |
| 0.6 | 20 | 20.3 | 19.9 | 19.7 | 18.4 | 17.7 | 17.6 | 17.9 |
| 0.7 | 21 | 21.7 | 21.4 | 21.4 | 20.1 | 18.9 | 19 | 19 |
| 0.8 | 23.2 | 23.7 | 23.4 | 23 | 21.7 | 20.9 | 20.8 | 21 |
| 0.9 | 22.9 | 23.8 | 23.6 | 23.3 | 22.3 | 21.3 | 21.1 | 21 |
| 1 | 23.9 | 25 | 24.8 | 24.2 | 23.2 | 22 | 21.9 | 22.1 |
| 1.1 | 24.8 | 25.7 | 25.7 | 25.4 | 24.1 | 23.2 | 22.9 | 22.8 |
| 1.2 | 25.5 | 26.7 | 26.5 | 26.4 | 25.2 | 24.4 | 24.2 | 23.9 |
| 1.3 | 25.1 | 26.4 | 26.5 | 26.2 | 25.3 | 24.5 | 24.1 | 23.9 |
| 1.4 | 25.3 | 26 | 26.3 | 26.2 | 25.6 | 25.2 | 25 | 24.9 |
| 1.5 | 26.2 | 26.8 | 27.6 | 27.4 | 26.7 | 26.2 | 25.8 | 25.5 |
| 1.6 | 27.5 | 28.2 | 29.1 | 29.3 | 28.8 | 28.1 | 27.5 | 27.2 |
| 1.75 | 26.9 | 27.2 | 27.9 | 28.4 | 28.3 | 27.6 | 26.9 | 26.6 |
| 1.8 | 27.3 | 27.6 | 28 | 28.5 | 28.6 | 28 | 27.2 | 27 |

# Run Number AA300NaX7

**Description of Experiment**

Two bed with 300 mm prelayer of activated alumina, main layer NaX, PVC bed
60 second cycle

| Sieve Arrangement and Bed | | |
|---|---|---|
| Type of Prelayer | AA | AA |
| Type of Main Layer | NaX | NaX |
| Bed | PVC | PVC |
| | **Bed 1** | **Bed 2** |
| Mass of Prelayer (kg) | 1.882 | 1.862 |
| Mass of Main layer(kg) | 8.4882 | 8.508 |
| Height of Prelayer (mm) | 300 | 300 |
| Height of Main layer(mm) | 1550 | 1550 |

| End of Step Press. at CSS (kPa) | Bed 1 | Bed 2 |
|---|---|---|
| Step 1 | 122.0 | 68.4 |
| Step 2 | 126.4 | 54.3 |
| Step 3 | 100.3 | 68.7 |
| Step 4 | 93.4 | 77.7 |
| Step 5 | 66.7 | 123.4 |
| Step 6 | 52.8 | 127.9 |
| Step 7 | 66.8 | 102.3 |
| Step 8 | 75.3 | 95.6 |

| Mass Balance at CSS (Total millimole per cycle) | | | |
|---|---|---|---|
| Feed flow | 3289.4 | Evacuation flow | 2763.3 |
| Product flow | 486.0 | Mass Balance Error (%) | 1.2 |

| Key Performance Parameters | | | |
|---|---|---|---|
| Oxygen Recovery (%) | 38.4 | BSF (kg/TPDc) | 1334.2 |
| Power: (kW/TPDc) | 6.6 | Oxygen Purity (%): | 57.2 |

| End of Step CSS Temperature Profile (°C) | | | | | | | | |
|---|---|---|---|---|---|---|---|---|
| z (m) | Step 1 | Step 2 | Step 3 | Step 4 | Step 5 | Step 6 | Step 7 | Step 8 |
| 0 | 22.2 | 22 | 19.9 | 18.7 | 20.2 | 20.1 | 22 | 22.7 |
| 0.1 | 21.3 | 21.4 | 21.1 | 21.8 | 21.7 | 21.3 | 21.3 | 21 |
| 0.2 | 18.4 | 18.6 | 18.3 | 18.6 | 18.2 | 18 | 17.8 | 17.8 |
| 0.3 | 11.5 | 12.4 | 11.7 | 11.7 | 11.2 | 10.3 | 10.2 | 10.3 |
| 0.4 | 15 | 15.4 | 15.1 | 14.9 | 13.5 | 12.7 | 12.2 | 12.5 |
| 0.5 | 16.6 | 17.3 | 17 | 16.5 | 15.5 | 14.5 | 14.5 | 14.8 |
| 0.6 | 18.6 | 19 | 18.7 | 18.5 | 17.3 | 16.8 | 16.7 | 16.8 |
| 0.7 | 19.6 | 20.2 | 20 | 19.7 | 18.1 | 17.5 | 17.5 | 17.4 |
| 0.8 | 20.4 | 21 | 20.6 | 20.4 | 19.5 | 18.6 | 18.9 | 18.8 |
| 0.9 | 20.4 | 21 | 20.7 | 20.5 | 19.5 | 19 | 18.7 | 19 |
| 1 | 20.8 | 21.8 | 21.6 | 21.4 | 20.2 | 19.3 | 19.1 | 19.3 |
| 1.1 | 21 | 22 | 21.9 | 21.9 | 21 | 19.8 | 19.6 | 19.8 |
| 1.2 | 21.9 | 22.9 | 22.6 | 22.5 | 21.6 | 20.8 | 20.6 | 20.5 |
| 1.3 | 21.8 | 22.9 | 22.7 | 22.5 | 21.6 | 20.9 | 20.7 | 20.6 |
| 1.4 | 22.6 | 23.2 | 23.2 | 23.1 | 22.6 | 22.3 | 22.1 | 22 |
| 1.5 | 23.2 | 24 | 24.2 | 24.1 | 23.4 | 23 | 22.7 | 22.4 |
| 1.6 | 23.7 | 24.6 | 25.2 | 25.3 | 24.7 | 24.1 | 23.7 | 23.4 |
| 1.7 | 23 | 23.2 | 23.6 | 23.7 | 23.3 | 23.1 | 22.7 | 22.7 |
| 1.75 | 23.5 | 23.9 | 24.6 | 25 | 24.7 | 24.1 | 23.5 | 23.2 |
| 1.8 | 24.2 | 24.4 | 25 | 25.4 | 25.3 | 24.8 | 23.9 | 23.8 |

## Run Number AA300NaX8

**Description of Experiment**

Two bed with 300 mm prelayer of activated alumina, main layer NaX, PVC beds
60 second cycle

| Sieve Arrangement and Bed | | |
|---|---|---|
| Type of Prelayer | AA | AA |
| Type of Main Layer | NaX | NaX |
| Bed | PVC | PVC |
| | **Bed 1** | **Bed 2** |
| Mass of Prelayer (kg) | 1.882 | 1.862 |
| Mass of Main layer(kg) | 8.4882 | 8.508 |
| Height of Prelayer (mm) | 300 | 300 |
| Height of Main layer(mm) | 1550 | 1550 |

| End of Step Press. at CSS (kPa) | Bed 1 | Bed 2 |
|---|---|---|
| Step 1 | 124.5 | 44.9 |
| Step 2 | 127.2 | 30.3 |
| Step 3 | 88.8 | 52.9 |
| Step 4 | 79.4 | 65.4 |
| Step 5 | 43.7 | 125.3 |
| Step 6 | 29.1 | 128.0 |
| Step 7 | 51.4 | 90.7 |
| Step 8 | 63.2 | 81.3 |

| Mass Balance at CSS (Total millimole per cycle) | | | |
|---|---|---|---|
| Feed flow | 3826.6 | Evacuation flow | 3203.9 |
| Product flow | 528.1 | Mass Balance Error (%) | 2.5 |

| Key Performance Parameters | | | |
|---|---|---|---|
| Oxygen Recovery (%) | 52.0 | BSF (kg/TPDc) | 845.8 |
| Power: (kW/TPDc) | 8.9 | Oxygen Purity (%): | 83.0 |

| End of Step CSS Temperature Profile (°C) | | | | | | | | |
|---|---|---|---|---|---|---|---|---|
| z (m) | Step 1 | Step 2 | Step 3 | Step 4 | Step 5 | Step 6 | Step 7 | Step 8 |
| 0 | 27.8 | 27.9 | 24.9 | 23.5 | 26 | 25.9 | 28.1 | 28.5 |
| 0.1 | 27.7 | 27.2 | 27.5 | 27.3 | 26.8 | 27.4 | 27.2 | 27 |
| 0.2 | 22.3 | 22.3 | 22.4 | 22.2 | 21.5 | 21.5 | 21.3 | 21.4 |
| 0.3 | 12.5 | 13.2 | 12.6 | 12.7 | 11.2 | 10.2 | 10.4 | 10.2 |
| 0.4 | 20.3 | 20.8 | 20.4 | 19.9 | 17.7 | 16.9 | 16.9 | 17 |
| 0.5 | 24.2 | 24.7 | 24.5 | 23.9 | 22 | 21.3 | 21 | 21.2 |
| 0.6 | 26.9 | 27.6 | 27.2 | 26.9 | 25.2 | 24.6 | 24.2 | 24.2 |
| 0.7 | 28.3 | 29.6 | 28.9 | 28.9 | 27.3 | 26.3 | 26.1 | 26.2 |
| 0.8 | 29.8 | 30.4 | 30.2 | 29.6 | 28.3 | 27.5 | 27.2 | 27.3 |
| 0.9 | 29.3 | 30.2 | 30.1 | 29.9 | 28.7 | 27.7 | 27.7 | 27.6 |
| 1 | 30.2 | 31.3 | 31.1 | 31.2 | 29.6 | 28.8 | 28.6 | 28.3 |
| 1.1 | 31.1 | 32.5 | 32.4 | 32.3 | 30.8 | 30 | 29.7 | 29.6 |
| 1.2 | 31.7 | 33.5 | 33.6 | 33.1 | 32.1 | 31.3 | 30.8 | 31 |
| 1.3 | 31.6 | 32.8 | 33.3 | 33.2 | 32.2 | 31.5 | 31.1 | 30.9 |
| 1.4 | 31.8 | 32.1 | 32.8 | 32.7 | 32.1 | 31.8 | 31.5 | 31.4 |
| 1.5 | 32.5 | 32.8 | 33.6 | 33.8 | 33 | 32.3 | 32.2 | 32 |
| 1.6 | 33.7 | 34.2 | 35 | 35.4 | 35 | 34.3 | 33.8 | 33.5 |
| 1.75 | 32.8 | 33 | 33.3 | 34 | 33.9 | 33.3 | 32.7 | 32.5 |
| 1.8 | 33.2 | 33.3 | 33.4 | 34.1 | 34.1 | 33.5 | 32.9 | 32.8 |

# Run Number AA300NaX9

**Description of Experiment**

Two bed with 300 mm prelayer of activated alumina, main layer NaX, PVC beds
60 second cycle

| Sieve Arrangement and Bed | | |
|---|---|---|
| Type of Prelayer | AA | AA |
| Type of Main Layer | NaX | NaX |
| Bed | PVC | PVC |
| | **Bed 1** | **Bed 2** |
| Mass of Prelayer (kg) | 1.882 | 1.862 |
| Mass of Main layer(kg) | 8.4882 | 8.508 |
| Height of Prelayer (mm) | 300 | 300 |
| Height of Main layer(mm) | 1550 | 1550 |

| End of Step Press. at CSS (kPa) | Bed 1 | Bed 2 |
|---|---|---|
| Step 1 | 123.3 | 50.9 |
| Step 2 | 127.0 | 34.3 |
| Step 3 | 103.5 | 44.2 |
| Step 4 | 93.3 | 56.6 |
| Step 5 | 50.3 | 122.9 |
| Step 6 | 33.4 | 127.4 |
| Step 7 | 45.7 | 102.5 |
| Step 8 | 57.8 | 93.6 |

| Mass Balance at CSS (Total millimole per cycle) | | | |
|---|---|---|---|
| Feed flow | 4117.9 | Evacuation flow | 3572.1 |
| Product flow | 517.4 | Mass Balance Error (%) | 0.7 |

| Key Performance Parameters | | | |
|---|---|---|---|
| Oxygen Recovery (%) | 47.20 | BSF (kg/TPDc) | 866.70 |
| Power: (kW/TPDc) | 8.49 | Oxygen Purity (%): | 82.65 |

| End of Step CSS Temperature Profile (°C) | | | | | | | | |
|---|---|---|---|---|---|---|---|---|
| z (m) | Step 1 | Step 2 | Step 3 | Step 4 | Step 5 | Step 6 | Step 7 | Step 8 |
| 0 | 27.4 | 26.7 | 25.2 | 25.1 | 25.2 | 25.5 | 26.5 | 28.3 |
| 0.1 | 26.5 | 26.6 | 26.6 | 27 | 26.3 | 26.2 | 26.2 | 26.7 |
| 0.2 | 23 | 23.1 | 23 | 23.1 | 22.4 | 22.2 | 22.1 | 22.3 |
| 0.3 | 15 | 15.5 | 15.4 | 15.6 | 13.9 | 13 | 12.7 | 13.1 |
| 0.4 | 19 | 19.9 | 19.6 | 19.5 | 17.3 | 16 | 15.8 | 16.4 |
| 0.5 | 21.7 | 22.4 | 22.1 | 21.9 | 20.1 | 18.8 | 18.6 | 18.8 |
| 0.6 | 24.2 | 24.9 | 24.5 | 23.9 | 22.6 | 21.7 | 21.4 | 21.4 |
| 0.7 | 25.1 | 26.2 | 25.5 | 25.5 | 23.8 | 23 | 22.8 | 22.6 |
| 0.8 | 28.5 | 29.3 | 29.3 | 29 | 27.3 | 26.5 | 26.2 | 26.3 |
| 0.9 | 28.2 | 28.9 | 28.9 | 28.7 | 27.6 | 26.6 | 26.1 | 26.2 |
| 1 | 29 | 30 | 29.7 | 29.7 | 28.4 | 27.5 | 26.7 | 26.7 |
| 1.1 | 29.4 | 30.8 | 30.9 | 30.5 | 29.3 | 28.7 | 27.9 | 27.7 |
| 1.2 | 30.1 | 31.8 | 31.9 | 31.4 | 30.3 | 29.5 | 29 | 28.7 |
| 1.3 | 30 | 31.6 | 31.9 | 31.8 | 30.6 | 29.7 | 29.3 | 29.1 |
| 1.4 | 30.4 | 31.1 | 31.5 | 31.5 | 30.8 | 30.4 | 30.1 | 30 |
| 1.5 | 31.2 | 31.8 | 32.5 | 32.8 | 31.8 | 31.2 | 30.8 | 30.7 |
| 1.6 | 32.4 | 32.9 | 33.6 | 34.2 | 33.7 | 32.9 | 32.4 | 32.1 |
| 1.75 | 31.3 | 31.6 | 31.8 | 32.2 | 32.2 | 31.5 | 31.1 | 31 |
| 1.8 | 31.6 | 31.9 | 31.8 | 32.1 | 32.1 | 31.5 | 31.1 | 31.1 |

# Run Number AA300NaX10

**Description of Experiment**

Two bed with 300 mm prelayer of activated alumina, main layer NaX, PVC beds
60 second cycle

| Sieve Arrangement and Bed | | |
|---|---|---|
| Type of Prelayer | AA | AA |
| Type of Main Layer | NaX | NaX |
| Bed | PVC | PVC |
| | **Bed 1** | **Bed 2** |
| Mass of Prelayer (kg) | 1.882 | 1.862 |
| Mass of Main layer(kg) | 8.4882 | 8.508 |
| Height of Prelayer (mm) | 300 | 300 |
| Height of Main layer(mm) | 1550 | 1550 |

| End of Step Press. at CSS (kPa) | Bed 1 | Bed 2 |
|---|---|---|
| Step 1 | 122.8 | 47.31 |
| Step 2 | 126.6 | 31.69 |
| Step 3 | 95.8 | 47.69 |
| Step 4 | 86.2 | 59.81 |
| Step 5 | 46.3 | 123.38 |
| Step 6 | 30.63 | 127.63 |
| Step 7 | 47.63 | 96.56 |
| Step 8 | 59.25 | 87.38 |

| Mass Balance at CSS (Total millimole per cycle) | | | |
|---|---|---|---|
| Feed flow | 4159.3 | Evacuation flow | 3608.1 |
| Product flow | 485.8 | Mass Balance Error (%) | 1.6 |

| Key Performance Parameters | | | |
|---|---|---|---|
| Oxygen Recovery (%) | 47.3 | BSF (kg/TPDc) | 855.1 |
| Power: (kW/TPDc) | 9.2 | Oxygen Purity (%): | 89.2 |

| End of Step CSS Temperature Profile (°C) | | | | | | | | |
|---|---|---|---|---|---|---|---|---|
| z (m) | Step 1 | Step 2 | Step 3 | Step 4 | Step 5 | Step 6 | Step 7 | Step 8 |
| 0 | 23 | 23 | 20.5 | 19.4 | 21 | 22 | 22.5 | 23.7 |
| 0.1 | 22.4 | 22.9 | 22.3 | 22.4 | 22.2 | 22.3 | 22.1 | 22 |
| 0.2 | 17.8 | 18.1 | 17.8 | 17.8 | 17.1 | 17 | 16.8 | 16.8 |
| 0.3 | 8.4 | 9.3 | 8.8 | 8.6 | 7.4 | 6.1 | 6.3 | 6 |
| 0.4 | 15.2 | 16 | 15.4 | 15.2 | 12.7 | 11.5 | 11.4 | 11.8 |
| 0.5 | 18.7 | 19.3 | 19 | 18.8 | 16.4 | 15.6 | 15.3 | 15.6 |
| 0.6 | 21.7 | 21.9 | 21.7 | 21.1 | 19.5 | 18.6 | 18.3 | 18.9 |
| 0.7 | 22.8 | 23.9 | 23.7 | 23.1 | 21.7 | 20.2 | 20.1 | 20.3 |
| 0.8 | 25.9 | 26.4 | 26.2 | 25.8 | 24.5 | 23.6 | 23.2 | 23.2 |
| 0.9 | 25.2 | 26.3 | 26.1 | 26 | 24.5 | 23.5 | 23.3 | 23.1 |
| 1 | 25.7 | 27.1 | 27.2 | 27.1 | 25.2 | 24.3 | 23.9 | 23.7 |
| 1.1 | 26.4 | 28.1 | 28.4 | 28.3 | 26.9 | 26.1 | 25.3 | 25.2 |
| 1.2 | 27.4 | 29.2 | 29.3 | 29.2 | 28.2 | 27.2 | 26.6 | 26.5 |
| 1.3 | 27.2 | 28.6 | 29.2 | 29.1 | 28 | 27.1 | 26.6 | 26.3 |
| 1.4 | 27.1 | 27.4 | 28.2 | 28.2 | 27.5 | 27.1 | 26.8 | 26.7 |
| 1.5 | 27.9 | 28.2 | 29 | 29.4 | 28.5 | 27.8 | 27.5 | 27.3 |
| 1.6 | 29.4 | 29.8 | 30.5 | 31.3 | 30.8 | 30 | 29.3 | 29.1 |
| 1.75 | 28.1 | 28.3 | 28.5 | 29.1 | 29 | 28.3 | 27.8 | 27.7 |
| 1.8 | 28.3 | 28.5 | 28.5 | 28.8 | 28.7 | 28.2 | 27.8 | 27.8 |

## Run Number AA300NaX11

**Description of Experiment**

Two bed with 300 mm prelayer of activated alumina, main layer NaX, PVC beds
60 second cycle

| Sieve Arrangement and Bed | | |
|---|---|---|
| Type of Prelayer | AA | AA |
| Type of Main Layer | NaX | NaX |
| Bed | PVC | PVC |
| | **Bed 1** | **Bed 2** |
| Mass of Prelayer (kg) | 1.882 | 1.862 |
| Mass of Main layer(kg) | 8.4882 | 8.508 |
| Height of Prelayer (mm) | 300 | 300 |
| Height of Main layer(mm) | 1550 | 1550 |

| End of Step Press. at CSS (kPa) | Bed 1 | Bed 2 |
|---|---|---|
| Step 1 | 134.6 | 51.8 |
| Step 2 | 140.5 | 34.4 |
| Step 3 | 106.4 | 51.0 |
| Step 4 | 96.3 | 62.9 |
| Step 5 | 51.2 | 135.3 |
| Step 6 | 33.0 | 141.6 |
| Step 7 | 50.3 | 106.3 |
| Step 8 | 62.2 | 95.8 |

| Mass Balance at CSS (Total millimole per cycle) | | | |
|---|---|---|---|
| Feed flow | 4441.8 | Evacuation flow | 4010.2 |
| Product flow | 251.5 | Mass Balance Error (%) | 4.1 |

| Key Performance Parameters | | | |
|---|---|---|---|
| Oxygen Recovery (%) | 24.6 | BSF (kg/TPDc) | 1541.8 |
| Power: (kW/TPDc) | 17.2 | Oxygen Purity (%): | 95.6 |

| End of Step CSS Temperature Profile (°C) | | | | | | | | |
|---|---|---|---|---|---|---|---|---|
| z (m) | Step 1 | Step 2 | Step 3 | Step 4 | Step 5 | Step 6 | Step 7 | Step 8 |
| 0 | 21.7 | 21.6 | 19.3 | 18.5 | 19.9 | 19.9 | 20.6 | 21.5 |
| 0.1 | 18.7 | 19.1 | 18.6 | 19 | 19.4 | 19.6 | 19.1 | 19.4 |
| 0.2 | 10.4 | 10.1 | 9.9 | 10.1 | 11.5 | 11.4 | 11.3 | 11.2 |
| 0.3 | 0.3 | -0.5 | -0.9 | -0.7 | 2 | 2.7 | 2.3 | 2.2 |
| 0.4 | 12.6 | 11.7 | 10.9 | 11.2 | 15.3 | 15.9 | 15.3 | 14.9 |
| 0.5 | 18.1 | 16.7 | 16.2 | 16.2 | 20.3 | 21.1 | 20.8 | 20.4 |
| 0.6 | 21.1 | 19.7 | 19.6 | 19.3 | 23.2 | 23.9 | 23.3 | 23.1 |
| 0.7 | 23.6 | 21.9 | 21.7 | 21.4 | 25.1 | 25.5 | 25.3 | 25.2 |
| 0.8 | 25.1 | 23.7 | 23.2 | 23.1 | 26.2 | 27.2 | 27 | 26.7 |
| 0.9 | 25.6 | 24.6 | 23.6 | 23.4 | 26.4 | 27.6 | 27.7 | 27.5 |
| 1 | 27.3 | 26 | 25.3 | 24.9 | 26.9 | 28.6 | 29.1 | 29 |
| 1.1 | 28.5 | 27.1 | 26.2 | 26.3 | 27.2 | 28.8 | 30.3 | 30.1 |
| 1.2 | 28.6 | 27.5 | 27.2 | 27.1 | 27.7 | 28.1 | 29.3 | 29.6 |
| 1.3 | 28.7 | 27.5 | 27.1 | 27 | 27.6 | 28 | 28.8 | 29.5 |
| 1.6 | 25.7 | 26 | 26 | 25.9 | 25.4 | 25 | 25 | 25 |
| 1.75 | 23.6 | 23.2 | 23.2 | 23.2 | 23.9 | 24.2 | 24.1 | 24 |

# Run Number AA300NaX12

**Description of Experiment**

Two bed with 300 mm prelayer of activated alumina, main layer NaX, PVC beds
60 second cycle

| Sieve Arrangement and Bed | | |
|---|---|---|
| Type of Prelayer | AA | AA |
| Type of Main Layer | NaX | NaX |
| Bed | PVC | PVC |
| | **Bed 1** | **Bed 2** |
| Mass of Prelayer (kg) | 1.882 | 1.862 |
| Mass of Main layer(kg) | 8.4882 | 8.508 |
| Height of Prelayer (mm) | 300 | 300 |
| Height of Main layer(mm) | 1550 | 1550 |

| End of Step Press. at CSS (kPa) | Bed 1 | Bed 2 |
|---|---|---|
| Step 1 | 129.9 | 53.1 |
| Step 2 | 133.9 | 36.0 |
| Step 3 | 104.1 | 49.9 |
| Step 4 | 96.0 | 61.1 |
| Step 5 | 51.9 | 130.0 |
| Step 6 | 34.8 | 134.8 |
| Step 7 | 49.9 | 104.7 |
| Step 8 | 61.0 | 96.9 |

| Mass Balance at CSS (Total millimole per cycle) | | | |
|---|---|---|---|
| Feed flow | 4802.6 | Evacuation flow | 4119.3 |
| Product flow | 607.7 | Mass Balance Error (%) | 1.6 |

| Key Performance Parameters | | | |
|---|---|---|---|
| Oxygen Recovery (%) | 45.2 | BSF (kg/TPDc) | 776.5 |
| Power: (kW/TPDc) | 8.5 | Oxygen Purity (%): | 78.5 |

| End of Step CSS Temperature Profile (°C) | | | | | | | | |
|---|---|---|---|---|---|---|---|---|
| z (m) | Step 1 | Step 2 | Step 3 | Step 4 | Step 5 | Step 6 | Step 7 | Step 8 |
| 0 | 20.4 | 18.9 | 17.1 | 15.9 | 17.9 | 18 | 19.4 | 20.6 |
| 0.1 | 19 | 19 | 19 | 19 | 18.5 | 18 | 18 | 18.6 |
| 0.2 | 13.9 | 14 | 14 | 14 | 13.3 | 12.8 | 12.6 | 12.8 |
| 0.3 | 4.9 | 5.5 | 5.3 | 4.8 | 3.1 | 1.8 | 1.5 | 2 |
| 0.4 | 8.8 | 9.9 | 9.6 | 9.3 | 6.7 | 4.8 | 4.6 | 5 |
| 0.5 | 12.3 | 12.9 | 12.6 | 12.2 | 9.9 | 8.4 | 8.4 | 8.5 |
| 0.6 | 14.9 | 15.4 | 15.5 | 14.6 | 13 | 11.6 | 11.7 | 11.9 |
| 0.7 | 16.1 | 17.2 | 17.1 | 16.5 | 14.7 | 13.4 | 13 | 13.4 |
| 0.8 | 19.8 | 20.8 | 20.3 | 20 | 18.4 | 17.3 | 16.9 | 17 |
| 0.9 | 19.5 | 20.5 | 20.5 | 20.3 | 18.8 | 17.4 | 17.2 | 17 |
| 1 | 20.6 | 21.6 | 21.7 | 21.4 | 19.6 | 18.3 | 18.4 | 18.2 |
| 1.1 | 21.4 | 22.8 | 22.7 | 22.4 | 21 | 19.8 | 19.5 | 19.4 |
| 1.2 | 22.1 | 23.7 | 23.8 | 23.6 | 22.2 | 21.1 | 20.6 | 20.4 |
| 1.3 | 22.1 | 23.9 | 24.1 | 23.8 | 22.6 | 21.5 | 21 | 20.7 |
| 1.4 | 22.4 | 23.2 | 23.7 | 23.5 | 22.7 | 22.2 | 21.9 | 21.7 |
| 1.5 | 23.2 | 24.1 | 25 | 24.9 | 23.9 | 23.2 | 22.7 | 22.4 |
| 1.6 | 24.2 | 24.8 | 25.9 | 26 | 25 | 24.3 | 23.7 | 23.6 |
| 1.7 | 23.3 | 23.7 | 24.4 | 25 | 24.8 | 23.9 | 23.2 | 22.9 |
| 1.75 | 24.1 | 24.5 | 25.2 | 25.8 | 25.6 | 24.8 | 23.9 | 23.7 |
| 1.8 | 24.4 | 24.7 | 25.1 | 25.7 | 25.6 | 24.8 | 23.9 | 23.8 |

# Run Number AA300NaX13

**Description of Experiment**

Two bed with 300 mm prelayer of activated alumina, main layer NaX, PVC beds
60 second cycle

| Sieve Arrangement and Bed | | |
|---|---|---|
| Type of Prelayer | AA | AA |
| Type of Main Layer | NaX | NaX |
| Bed | PVC | PVC |
| | **Bed 1** | **Bed 2** |
| Mass of Prelayer (kg) | 1.882 | 1.862 |
| Mass of Main layer(kg) | 8.4882 | 8.508 |
| Height of Prelayer (mm) | 300 | 300 |
| Height of Main layer(mm) | 1550 | 1550 |

| End of Step Press. at CSS (kPa) | Bed 1 | Bed 2 |
|---|---|---|
| Step 1 | 134.3 | 51.9 |
| Step 2 | 139.8 | 34.7 |
| Step 3 | 107.1 | 50.4 |
| Step 4 | 96.3 | 64.3 |
| Step 5 | 50.8 | 134.3 |
| Step 6 | 33.6 | 140.8 |
| Step 7 | 50.8 | 107.3 |
| Step 8 | 64.2 | 97.1 |

| Mass Balance at CSS (Total millimole per cycle) | | | |
|---|---|---|---|
| Feed flow | 4749.5 | Evacuation flow | 4153.1 |
| Product flow | 615.2 | Mass Balance Error (%) | -0.4 |

| Key Performance Parameters | | | |
|---|---|---|---|
| Oxygen Recovery (%) | 46.70 | BSF (kg/TPDc) | 725.90 |
| Power: (kW/TPDc) | 8.67 | Oxygen Purity (%): | 82.93 |

| End of Step CSS Temperature Profile (°C) | | | | | | | | |
|---|---|---|---|---|---|---|---|---|
| z (m) | Step 1 | Step 2 | Step 3 | Step 4 | Step 5 | Step 6 | Step 7 | Step 8 |
| 0 | 21.1 | 21.4 | 18.6 | 17.9 | 19.9 | 19.2 | 21.2 | 22.5 |
| 0.1 | 19.8 | 20.4 | 20 | 20.2 | 20.8 | 20.2 | 20.5 | 20.4 |
| 0.2 | 14.1 | 14.1 | 13.7 | 13.8 | 15.2 | 15.1 | 15.3 | 15.3 |
| 0.3 | 2.8 | 2.2 | 1.5 | 1.9 | 4.7 | 5.3 | 5.4 | 5.2 |
| 0.4 | 7.3 | 6.2 | 5.9 | 6.1 | 10.2 | 11 | 10.9 | 10.5 |
| 0.5 | 11.3 | 10.1 | 9.7 | 10.1 | 13.7 | 14.8 | 14.3 | 14 |
| 0.6 | 14.7 | 13.9 | 13.6 | 13.6 | 16.8 | 18 | 17.4 | 16.7 |
| 0.7 | 16.6 | 15.5 | 15 | 15.4 | 18.3 | 19.7 | 19.1 | 18.8 |
| 0.8 | 19 | 17.8 | 17.5 | 17.7 | 20.5 | 21.5 | 21.2 | 21 |
| 0.9 | 19.9 | 18.6 | 18.3 | 18.1 | 21 | 22.2 | 22.1 | 21.6 |
| 1 | 21.4 | 20.4 | 19.7 | 19.6 | 22.1 | 23.8 | 23.6 | 23 |
| 1.1 | 22.2 | 21.2 | 20.6 | 20.6 | 22.8 | 24.7 | 24.3 | 24 |
| 1.2 | 23.8 | 22.9 | 22.4 | 22.3 | 23.7 | 25.2 | 25.4 | 25.2 |
| 1.3 | 25.2 | 24.2 | 23.6 | 23.4 | 24.5 | 26.3 | 26.8 | 26.6 |
| 1.4 | 25.2 | 24.8 | 24.3 | 24.2 | 24.8 | 25.4 | 26.2 | 26.1 |
| 1.5 | 26.3 | 25.7 | 25.2 | 25 | 25.6 | 23.2 | 27.3 | 27.5 |
| 1.6 | 27.4 | 26.7 | 26.2 | 26.1 | 26.5 | 27 | 27.9 | 28.4 |
| 1.7 | 26.5 | 25.8 | 25.1 | 24.8 | 25.1 | 25.5 | 26.3 | 27 |
| 1.75 | 27.1 | 26.4 | 25.6 | 25.4 | 25.7 | 26 | 26.3 | 27.2 |
| 1.8 | 28.1 | 27.3 | 26.5 | 26.3 | 26.6 | 26.9 | 27.4 | 28.2 |

## Run Number AA300NaX14

**Description of Experiment**
Two bed with 300 mm prelayer of activated alumina, main layer NaX, PVC beds
60 second cycle

| Sieve Arrangement and Bed | | |
|---|---|---|
| Type of Prelayer | AA | AA |
| Type of Main Layer | NaX | NaX |
| Bed | PVC | PVC |
| | **Bed 1** | **Bed 2** |
| Mass of Prelayer (kg) | 1.882 | 1.862 |
| Mass of Main layer(kg) | 8.4882 | 8.508 |
| Height of Prelayer (mm) | 300 | 300 |
| Height of Main layer(mm) | 1550 | 1550 |

| End of Step Press. at CSS (kPa) | Bed 1 | Bed 2 |
|---|---|---|
| Step 1 | 136.3 | 48.4 |
| Step 2 | 140.8 | 32.4 |
| Step 3 | 99.1 | 55.9 |
| Step 4 | 88.4 | 70.3 |
| Step 5 | 47.1 | 137.5 |
| Step 6 | 31.3 | 142.0 |
| Step 7 | 54.5 | 101.0 |
| Step 8 | 68.2 | 90.0 |

| Mass Balance at CSS (Total millimole per cycle) | | | |
|---|---|---|---|
| Feed flow | 4501.7 | Evacuation flow | 3813.9 |
| Product flow | 656.3 | Mass Balance Error (%) | 0.7 |

| Key Performance Parameters | | | |
|---|---|---|---|
| Oxygen Recovery (%) | 53.2 | BSF (kg/TPDc) | 703.4 |
| Power: (kW/TPDc) | 8.7 | Oxygen Purity (%): | 80.3 |

| End of Step CSS Temperature Profile (°C) | | | | | | | | |
|---|---|---|---|---|---|---|---|---|
| z (m) | Step 1 | Step 2 | Step 3 | Step 4 | Step 5 | Step 6 | Step 7 | Step 8 |
| 0 | 25.3 | 24.3 | 21.8 | 21.3 | 23.3 | 23.7 | 25.3 | 25.5 |
| 0.1 | 24 | 23.7 | 23.5 | 23.9 | 23.8 | 23.8 | 23.7 | 23.2 |
| 0.2 | 16.2 | 16.5 | 16.4 | 16.6 | 15.8 | 15.6 | 15.2 | 15.2 |
| 0.3 | 9.1 | 9.3 | 8.9 | 8.3 | 7 | 6.8 | 6.9 | 7.2 |
| 0.4 | 13.8 | 14.2 | 13.6 | 13.3 | 11.1 | 10.1 | 10.1 | 10.2 |
| 0.5 | 16 | 17.1 | 16.4 | 16.1 | 13.9 | 12.6 | 12.7 | 12.7 |
| 0.6 | 21.1 | 21.8 | 21.2 | 20.9 | 19.1 | 18.3 | 18.3 | 18.2 |
| 0.7 | 22.3 | 23.6 | 23.4 | 23 | 21.3 | 19.9 | 19.4 | 19.9 |
| 0.8 | 24.9 | 25.8 | 25.3 | 25.1 | 23.6 | 22.5 | 22.1 | 22.1 |
| 0.9 | 24.9 | 26.1 | 25.6 | 25.5 | 23.9 | 23 | 22.7 | 22.5 |
| 1 | 26 | 27.3 | 27.3 | 26.8 | 25.2 | 24.5 | 23.9 | 24 |
| 1.1 | 26.3 | 28.3 | 28.5 | 28 | 26.7 | 25.6 | 25 | 25.1 |
| 1.2 | 27.3 | 29.5 | 29.5 | 29.3 | 28 | 26.9 | 26.4 | 26.2 |
| 1.3 | 27.5 | 29.2 | 29.7 | 29.5 | 28.3 | 27.4 | 27 | 26.7 |
| 1.4 | 28.3 | 28.7 | 29.5 | 29.4 | 28.7 | 28.3 | 28 | 27.8 |
| 1.5 | 29.1 | 29.5 | 30.4 | 30.5 | 29.6 | 29.1 | 28.6 | 28.4 |
| 1.6 | 29.9 | 30.3 | 31 | 31.4 | 30.6 | 30 | 29.5 | 29.4 |
| 1.7 | 28.6 | 28.9 | 29.3 | 30.1 | 29.9 | 29.3 | 28.5 | 28.3 |
| 1.75 | 29.4 | 29.7 | 30.1 | 30.9 | 30.7 | 30 | 29.2 | 29 |
| 1.8 | 29.9 | 30.1 | 30.2 | 31.1 | 31 | 30.3 | 29.5 | 29.3 |

# Run Number AA300NaX15

**Description of Experiment**

Two bed with 300 mm prelayer of activated alumina, main layer NaX, PVC beds
60 second cycle

| Sieve Arrangement and Bed | | |
|---|---|---|
| Type of Prelayer | AA | AA |
| Type of Main Layer | NaX | NaX |
| Bed | PVC | PVC |
| | **Bed 1** | **Bed 2** |
| Mass of Prelayer (kg) | 1.882 | 1.862 |
| Mass of Main layer(kg) | 8.4882 | 8.508 |
| Height of Prelayer (mm) | 300 | 300 |
| Height of Main layer(mm) | 1550 | 1550 |

| End of Step Press. at CSS (kPa) | Bed 1 | Bed 2 |
|---|---|---|
| Step 1 | 135.9 | 67.0 |
| Step 2 | 140.5 | 33.4 |
| Step 3 | 101.0 | 55.1 |
| Step 4 | 90.9 | 68.4 |
| Step 5 | 48.8 | 136.9 |
| Step 6 | 32.6 | 141.6 |
| Step 7 | 54.0 | 102.1 |
| Step 8 | 67.0 | 91.9 |

| Mass Balance at CSS (Total millimole per cycle) | | | |
|---|---|---|---|
| Feed flow | 4658.7 | Evacuation flow | 4013.0 |
| Product flow | 608.4 | Mass Balance Error (%) | 0.8 |

| Key Performance Parameters | | | |
|---|---|---|---|
| Oxygen Recovery (%) | 49.9 | BSF (kg/TPDc) | 723.7 |
| Power: (kW/TPDc) | 8.9 | Oxygen Purity (%): | 84.1 |

| End of Step CSS Temperature Profile (°C) | | | | | | | | |
|---|---|---|---|---|---|---|---|---|
| z (m) | Step 1 | Step 2 | Step 3 | Step 4 | Step 5 | Step 6 | Step 7 | Step 8 |
| 0 | 21 | 20.9 | 18.1 | 16.9 | 18.9 | 18.8 | 20.1 | 20.9 |
| 0.1 | 19 | 19.7 | 19.4 | 19.6 | 19 | 18.9 | 18.5 | 18.6 |
| 0.2 | 11.2 | 11.7 | 11.5 | 11.6 | 10.7 | 10.2 | 10 | 10 |
| 0.3 | 4.1 | 4.7 | 4.3 | 4.1 | 2.4 | 2.4 | 2.2 | 2.7 |
| 0.4 | 10.1 | 11 | 9.9 | 9.6 | 7.3 | 6.1 | 6 | 6.4 |
| 0.5 | 12.8 | 13.8 | 13.3 | 13.1 | 10.7 | 9.4 | 9.2 | 9.6 |
| 0.6 | 17.6 | 18 | 17.6 | 17.5 | 15.9 | 14.6 | 14.7 | 14.9 |
| 0.7 | 19 | 20 | 20 | 19.7 | 17.9 | 16.4 | 16.2 | 16.1 |
| 0.8 | 21 | 22.1 | 21.7 | 21.3 | 19.5 | 18.5 | 18.3 | 18.3 |
| 0.9 | 20.6 | 21.8 | 21.5 | 21.4 | 19.7 | 18.5 | 18.2 | 18 |
| 1 | 21.6 | 22.9 | 22.8 | 22.4 | 21 | 19.8 | 19.4 | 19.1 |
| 1.1 | 22.2 | 24.2 | 24.4 | 23.9 | 22.7 | 21.3 | 21.1 | 20.7 |
| 1.2 | 23.3 | 25.2 | 25.6 | 25.3 | 23.7 | 22.6 | 22.2 | 22.1 |
| 1.3 | 23.3 | 25 | 25.6 | 25.4 | 24.1 | 23.1 | 22.5 | 22.2 |
| 1.4 | 23.7 | 24.2 | 25.1 | 25 | 24.1 | 23.6 | 23.3 | 23.1 |
| 1.5 | 24.5 | 25 | 26.1 | 26.2 | 25.2 | 24.5 | 24 | 23.8 |
| 1.6 | 25.4 | 25.7 | 26.6 | 27.1 | 26.2 | 25.4 | 25 | 24.8 |
| 1.7 | 24.3 | 24.5 | 25 | 25.8 | 25.7 | 24.9 | 24.1 | 23.8 |
| 1.75 | 25.1 | 25.3 | 25.8 | 26.6 | 26.5 | 25.7 | 24.9 | 24.6 |
| 1.8 | 25.3 | 25.5 | 25.7 | 26.6 | 26.5 | 25.7 | 24.9 | 24.8 |

## Run Number AA300NaX16

**Description of Experiment**

Two bed with 300 mm prelayer of activated alumina, main layer NaX, PVC beds
60 second cycle

| Sieve Arrangement and Bed | | |
|---|---|---|
| Type of Prelayer | AA | AA |
| Type of Main Layer | NaX | NaX |
| Bed | PVC | PVC |
| | **Bed 1** | **Bed 2** |
| Mass of Prelayer (kg) | 1.882 | 1.862 |
| Mass of Main layer(kg) | 8.4882 | 8.508 |
| Height of Prelayer (mm) | 300 | 300 |
| Height of Main layer(mm) | 1550 | 1550 |

| End of Step Press. at CSS (kPa) | Bed 1 | Bed 2 |
|---|---|---|
| Step 1 | 133.3 | 51.8 |
| Step 2 | 139.7 | 34.5 |
| Step 3 | 100.3 | 55.8 |
| Step 4 | 95.1 | 64.4 |
| Step 5 | 50.8 | 134.1 |
| Step 6 | 33.6 | 140.8 |
| Step 7 | 54.8 | 101.8 |
| Step 8 | 63.4 | 96.0 |

| Mass Balance at CSS (Total millimole per cycle) | | | |
|---|---|---|---|
| Feed flow | 4780.7 | Evacuation flow | 4189.1 |
| Product flow | 603.1 | Mass Balance Error (%) | -0.2 |

| Key Performance Parameters | | | |
|---|---|---|---|
| Oxygen Recovery (%) | 47.4 | BSF (kg/TPDc) | 742.5 |
| Power: (kW/TPDc) | 8.8 | Oxygen Purity (%): | 82.8 |

| End of Step CSS Temperature Profile (°C) | | | | | | | | |
|---|---|---|---|---|---|---|---|---|
| z (m) | Step 1 | Step 2 | Step 3 | Step 4 | Step 5 | Step 6 | Step 7 | Step 8 |
| 0 | 21.2 | 21.2 | 18.8 | 17 | 18.5 | 19.5 | 20.2 | 20.9 |
| 0.1 | 19.4 | 20.2 | 19.4 | 19.5 | 19.5 | 19.2 | 19.5 | 19.3 |
| 0.2 | 13 | 13.5 | 13.1 | 13.1 | 12.5 | 12.2 | 11.9 | 11.8 |
| 0.3 | 2.1 | 3.4 | 3 | 2.6 | 0.9 | -0.7 | -0.7 | -0.5 |
| 0.4 | 8.3 | 9.8 | 8.9 | 8.5 | 6.1 | 4.7 | 4.4 | 4.8 |
| 0.5 | 13 | 14 | 13.7 | 13.3 | 10.9 | 9.4 | 9.5 | 9.3 |
| 0.6 | 16.6 | 17.7 | 17.1 | 17 | 14.9 | 13.4 | 13.8 | 13.8 |
| 0.7 | 18.8 | 20.1 | 19.3 | 19.3 | 17 | 15.7 | 15.8 | 15.9 |
| 0.8 | 21.3 | 22.3 | 21.7 | 21.6 | 19.9 | 18.8 | 18.4 | 18.5 |
| 0.9 | 21 | 22.1 | 21.9 | 21.5 | 20.2 | 19 | 18.6 | 18.7 |
| 1 | 21.7 | 23.1 | 23 | 22.9 | 21.5 | 20.1 | 19.8 | 19.8 |
| 1.1 | 22.8 | 24.3 | 24.4 | 24.4 | 22.8 | 21.9 | 21.4 | 21 |
| 1.2 | 23.7 | 25.6 | 25.8 | 25.5 | 23.9 | 22.9 | 22.4 | 22.1 |
| 1.3 | 23.6 | 25.4 | 25.8 | 25.6 | 24.3 | 23.3 | 22.7 | 22.4 |
| 1.4 | 24 | 24.7 | 25.3 | 25.1 | 24.3 | 24 | 23.6 | 23.4 |
| 1.5 | 24.8 | 25.5 | 26.5 | 26.5 | 25.6 | 24.9 | 24.4 | 24.1 |
| 1.6 | 25.7 | 26.2 | 27.2 | 27.4 | 26.5 | 25.8 | 25.3 | 25.1 |
| 1.7 | 24.5 | 25 | 25.6 | 26.3 | 26 | 25.2 | 24.5 | 24.2 |
| 1.75 | 25.3 | 25.8 | 26.4 | 27.1 | 26.8 | 26 | 25.2 | 25 |
| 1.8 | 25.6 | 25.9 | 26.3 | 27.1 | 26.8 | 26 | 25.2 | 25.1 |

## Run Number AA300NaX17

**Description of Experiment**

Two bed with 300 mm prelayer of activated alumina, main layer NaX, PVC beds
60 second cycle

| Sieve Arrangement and Bed | | |
|---|---|---|
| Type of Prelayer | AA | AA |
| Type of Main Layer | NaX | NaX |
| Bed | PVC | PVC |
| | **Bed 1** | **Bed 2** |
| Mass of Prelayer (kg) | 1.882 | 1.862 |
| Mass of Main layer(kg) | 8.4882 | 8.508 |
| Height of Prelayer (mm) | 300 | 300 |
| Height of Main layer(mm) | 1550 | 1550 |

| End of Step Press. at CSS (kPa) | Bed 1 | Bed 2 |
|---|---|---|
| Step 1 | 133.8 | 48.7 |
| Step 2 | 139.3 | 33.1 |
| Step 3 | 100.1 | 54.6 |
| Step 4 | 87.4 | 70.3 |
| Step 5 | 47.6 | 134.7 |
| Step 6 | 32.1 | 140.3 |
| Step 7 | 53.4 | 101.4 |
| Step 8 | 68.4 | 89.0 |

| Mass Balance at CSS (Total millimole per cycle) | | | |
|---|---|---|---|
| Feed flow | 4622.1 | Evacuation flow | 3981.4 |
| Product flow | 577.2 | Mass Balance Error (%) | 1.4 |

| Key Performance Parameters | | | |
|---|---|---|---|
| Oxygen Recovery (%) | 48.6 | BSF (kg/TPDc) | 749.7 |
| Power: (kW/TPDc) | 9.2 | Oxygen Purity (%): | 85.6 |

| End of Step CSS Temperature Profile (°C) | | | | | | | | |
|---|---|---|---|---|---|---|---|---|
| z (m) | Step 1 | Step 2 | Step 3 | Step 4 | Step 5 | Step 6 | Step 7 | Step 8 |
| 0 | 17.7 | 17.3 | 15.7 | 13.2 | 16.2 | 15.5 | 17.2 | 19.3 |
| 0.1 | 16.5 | 16 | 16.2 | 16.5 | 15.5 | 15.8 | 15.8 | 15.3 |
| 0.2 | 8.5 | 8.6 | 8.5 | 8.6 | 7.3 | 7.1 | 6.9 | 6.6 |
| 0.3 | -4.7 | -4.2 | -4.2 | -4.3 | -7.3 | -8.3 | -9 | -8.6 |
| 0.4 | 5.4 | 5.9 | 5.3 | 5.2 | 1.8 | 0.6 | 0.6 | 0.5 |
| 0.5 | 11 | 11.9 | 11.3 | 10.7 | 8.2 | 6.7 | 6.7 | 6.6 |
| 0.6 | 14.8 | 15.9 | 15 | 14.8 | 12.6 | 11.1 | 11.4 | 11.3 |
| 0.7 | 16.9 | 18.4 | 17.8 | 17.3 | 15.5 | 13.7 | 13.6 | 13.8 |
| 0.8 | 18.8 | 19.8 | 19.2 | 18.9 | 17 | 15.9 | 15.8 | 15.8 |
| 0.9 | 18.4 | 19.6 | 19.6 | 19 | 17.5 | 16.3 | 15.9 | 15.9 |
| 1 | 19.6 | 20.9 | 21.1 | 20.6 | 18.8 | 17.5 | 17.1 | 16.9 |
| 1.1 | 20.8 | 22.5 | 22.6 | 22.2 | 20.6 | 19.5 | 19.1 | 18.9 |
| 1.2 | 21.8 | 23.9 | 24 | 23.7 | 22.2 | 21.2 | 20.8 | 20.5 |
| 1.3 | 21.7 | 23.5 | 24 | 23.9 | 22.4 | 21.5 | 20.9 | 20.7 |
| 1.4 | 21.8 | 22.3 | 23.2 | 23.2 | 22.1 | 21.8 | 21.4 | 21.3 |
| 1.5 | 22.7 | 23.2 | 24.2 | 24.5 | 23.4 | 22.7 | 22.2 | 22.1 |
| 1.6 | 23.5 | 24 | 24.8 | 25.5 | 24.4 | 23.7 | 23.2 | 23.1 |
| 1.7 | 22.5 | 22.9 | 23.3 | 24.2 | 24 | 23.3 | 22.4 | 22.2 |
| 1.75 | 23.3 | 23.8 | 24.2 | 25.2 | 25 | 24.2 | 23.3 | 23.1 |
| 1.8 | 23.5 | 24 | 24.1 | 25 | 25 | 24.2 | 23.3 | 23.1 |

# Run Number AA300NaX18

**Description of Experiment**

Two bed with 300 mm prelayer of activated alumina, main layer NaX, PVC beds
60 second cycle

| Sieve Arrangement and Bed | | |
|---|---|---|
| Type of Prelayer | AA | AA |
| Type of Main Layer | NaX | NaX |
| Bed | PVC | PVC |
| | **Bed 1** | **Bed 2** |
| Mass of Prelayer (kg) | 1.882 | 1.862 |
| Mass of Main layer(kg) | 8.4882 | 8.508 |
| Height of Prelayer (mm) | 300 | 300 |
| Height of Main layer(mm) | 1550 | 1550 |

| End of Step Press. at CSS (kPa) | Bed 1 | Bed 2 |
|---|---|---|
| Step 1 | 133.8 | 50.9 |
| Step 2 | 139.5 | 32.8 |
| Step 3 | 100.9 | 52.6 |
| Step 4 | 98.6 | 59.0 |
| Step 5 | 50.0 | 134.9 |
| Step 6 | 32.1 | 140.6 |
| Step 7 | 52.0 | 102.1 |
| Step 8 | 58.0 | 99.3 |

| Mass Balance at CSS (Total millimole per cycle) | | | |
|---|---|---|---|
| Feed flow | 5192.2 | Evacuation flow | 4595.5 |
| Product flow | 592.2 | Mass Balance Error (%) | 0.1 |

| Key Performance Parameters | | | |
|---|---|---|---|
| Oxygen Recovery (%) | 44.3 | BSF (kg/TPDc) | 732.1 |
| Power: (kW/TPDc) | 9.6 | Oxygen Purity (%): | 85.5 |

| End of Step CSS Temperature Profile (°C) | | | | | | | | |
|---|---|---|---|---|---|---|---|---|
| z (m) | Step 1 | Step 2 | Step 3 | Step 4 | Step 5 | Step 6 | Step 7 | Step 8 |
| 0 | 19.8 | 19.8 | 17.6 | 16.5 | 18.1 | 18.3 | 19.3 | 19.7 |
| 0.1 | 18.1 | 18.3 | 18.1 | 18 | 17.2 | 17.5 | 17.5 | 17.2 |
| 0.2 | 10.4 | 10.7 | 10.4 | 10.5 | 9.4 | 9.2 | 9 | 8.9 |
| 0.3 | -0.6 | 0.6 | 0.4 | 0.2 | -2.5 | -3.5 | -3.8 | -3.9 |
| 0.4 | 6.5 | 7.6 | 6.8 | 6.6 | 3.7 | 2.3 | 2 | 2.3 |
| 0.5 | 10.8 | 12 | 11.6 | 11.1 | 8.6 | 7 | 6.8 | 6.9 |
| 0.6 | 14.4 | 15.3 | 14.8 | 14.5 | 12.3 | 11.1 | 10.9 | 11 |
| 0.7 | 16.5 | 17.5 | 17 | 16.6 | 14.5 | 13.1 | 12.8 | 12.8 |
| 0.8 | 19.2 | 20.2 | 19.6 | 19.4 | 17.8 | 16.4 | 16 | 16 |
| 0.9 | 19 | 20.3 | 19.9 | 19.8 | 18.1 | 16.8 | 16.5 | 16.3 |
| 1 | 20.1 | 21.5 | 21.5 | 21.1 | 19.2 | 17.9 | 17.8 | 17.4 |
| 1.1 | 21.1 | 22.4 | 22.9 | 22.3 | 20.9 | 19.4 | 19.3 | 18.6 |
| 1.2 | 22 | 23.9 | 24 | 23.7 | 22.1 | 21 | 20.5 | 20.2 |
| 1.3 | 22 | 23.9 | 24.2 | 24.1 | 22.6 | 21.5 | 20.9 | 20.6 |
| 1.4 | 22.6 | 23.3 | 24 | 23.7 | 22.8 | 22.3 | 21.9 | 21.9 |
| 1.5 | 23.5 | 24.1 | 25.3 | 25.2 | 24 | 23.3 | 22.8 | 22.6 |
| 1.6 | 24.4 | 24.8 | 26.1 | 26.1 | 25.1 | 24.2 | 23.7 | 23.7 |
| 1.7 | 23.2 | 23.6 | 24.4 | 25.1 | 24.5 | 23.7 | 22.9 | 22.7 |
| 1.75 | 23.9 | 24.3 | 25.2 | 25.8 | 25.2 | 24.4 | 23.7 | 23.4 |
| 1.8 | 24.2 | 24.5 | 25.1 | 25.7 | 25.2 | 24.4 | 23.7 | 23.6 |

## Run Number AA300NaX19

**Description of Experiment**

Two bed with 300 mm prelayer of activated alumina, main layer NaX, PVC beds
60 second cycle

| Sieve Arrangement and Bed | | |
|---|---|---|
| Type of Prelayer | AA | AA |
| Type of Main Layer | NaX | NaX |
| Bed | PVC | PVC |
| | **Bed 1** | **Bed 2** |
| Mass of Prelayer (kg) | 1.882 | 1.862 |
| Mass of Main layer(kg) | 8.4882 | 8.508 |
| Height of Prelayer (mm) | 300 | 300 |
| Height of Main layer(mm) | 1550 | 1550 |

| End of Step Press. at CSS (kPa) | Bed 1 | Bed 2 |
|---|---|---|
| Step 1 | 134.0 | 46.88 |
| Step 2 | 138.8 | 32.19 |
| Step 3 | 98.8 | 55 |
| Step 4 | 81.4 | 75.19 |
| Step 5 | 45.8 | 135.19 |
| Step 6 | 31.31 | 140 |
| Step 7 | 53.94 | 100.5 |
| Step 8 | 73.94 | 83.25 |

| Mass Balance at CSS (Total millimole per cycle) | | | |
|---|---|---|---|
| Feed flow | 4233.3 | Evacuation flow | 3572.6 |
| Product flow | 599.7 | Mass Balance Error (%) | 1.4 |

| Key Performance Parameters | | | |
|---|---|---|---|
| Oxygen Recovery (%) | 53.40 | BSF (kg/TPDc) | 744.30 |
| Power: (kW/TPDc) | 8.92 | Oxygen Purity (%): | 83.05 |

| End of Step CSS Temperature Profile (°C) | | | | | | | | |
|---|---|---|---|---|---|---|---|---|
| z (m) | Step 1 | Step 2 | Step 3 | Step 4 | Step 5 | Step 6 | Step 7 | Step 8 |
| 0 | 21.1 | 20.4 | 19.1 | 16.4 | 18.8 | 19 | 21.6 | 22.6 |
| 0.1 | 19.8 | 19.9 | 20.5 | 20.5 | 19.6 | 19.4 | 20.1 | 20 |
| 0.2 | 13 | 13.2 | 13.3 | 13.2 | 12.2 | 11.8 | 11.7 | 11.7 |
| 0.3 | -0.7 | 0.1 | 0.4 | 0.1 | -2.8 | -4.2 | -4 | -3.7 |
| 0.4 | 7.9 | 8.7 | 8.5 | 7.7 | 4.7 | 3.2 | 3.5 | 3.8 |
| 0.5 | 13.4 | 14.2 | 13.5 | 12.8 | 10.6 | 9.2 | 9.1 | 9.6 |
| 0.6 | 17.4 | 18.1 | 17.5 | 16.6 | 15 | 13.7 | 13.6 | 13.9 |
| 0.7 | 19 | 20 | 20 | 19.2 | 17.2 | 15.9 | 15.9 | 15.8 |
| 0.8 | 21.9 | 22.8 | 22.6 | 21.9 | 20.2 | 19.3 | 19.2 | 19.3 |
| 0.9 | 21.5 | 22.9 | 22.5 | 22.3 | 20.8 | 19.9 | 19.4 | 19.2 |
| 1 | 22.3 | 24.1 | 23.9 | 23.6 | 22.1 | 21.1 | 20.6 | 20.5 |
| 1.1 | 23.3 | 25.1 | 25.3 | 24.9 | 23.9 | 22.6 | 22 | 22.1 |
| 1.2 | 24.5 | 25.9 | 26.5 | 26.3 | 25.2 | 24.1 | 23.7 | 23.6 |
| 1.3 | 24.3 | 25.4 | 26.5 | 26.3 | 25.2 | 24.4 | 23.9 | 23.7 |
| 1.4 | 24.4 | 24.9 | 25.7 | 25.8 | 24.9 | 24.5 | 24.2 | 24.1 |
| 1.5 | 25.2 | 25.6 | 26.3 | 26.8 | 25.9 | 25.4 | 24.9 | 24.7 |
| 1.6 | 26 | 26.3 | 26.7 | 27.5 | 26.8 | 26.2 | 25.7 | 25.5 |
| 1.7 | 24.8 | 25.1 | 25.2 | 25.8 | 26 | 25.4 | 24.6 | 24.4 |
| 1.75 | 25.5 | 25.8 | 25.9 | 26.6 | 26.7 | 26.2 | 25.3 | 25.1 |
| 1.8 | 25.8 | 26.1 | 26.1 | 26.6 | 26.8 | 26.2 | 25.3 | 25.3 |

# Run Number AA300NaX20

**Description of Experiment**

Two bed with 300 mm prelayer of activated alumina, main layer NaX, PVC beds
60 second cycle

| Sieve Arrangement and Bed | | |
|---|---|---|
| Type of Prelayer | AA | AA |
| Type of Main Layer | NaX | NaX |
| Bed | PVC | PVC |
| | **Bed 1** | **Bed 2** |
| Mass of Prelayer (kg) | 1.882 | 1.862 |
| Mass of Main layer(kg) | 8.4882 | 8.508 |
| Height of Prelayer (mm) | 300 | 300 |
| Height of Main layer(mm) | 1550 | 1550 |

| End of Step Press. at CSS (kPa) | Bed 1 | Bed 2 |
|---|---|---|
| Step 1 | 134.9 | 47.13 |
| Step 2 | 139.2 | 32.5 |
| Step 3 | 98.9 | 55.44 |
| Step 4 | 81.8 | 75.56 |
| Step 5 | 45.9 | 135.94 |
| Step 6 | 31.25 | 140.5 |
| Step 7 | 54.38 | 100.69 |
| Step 8 | 74.25 | 83.63 |

| Mass Balance at CSS (Total millimole per cycle) | | | |
|---|---|---|---|
| Feed flow | 4222.4 | Evacuation flow | 3559.2 |
| Product flow | 611.5 | Mass Balance Error (%) | 1.2 |

| Key Performance Parameters | | | |
|---|---|---|---|
| Oxygen Recovery (%) | 53.40 | BSF (kg/TPDc) | 746.30 |
| Power: (kW/TPDc) | 8.92 | Oxygen Purity (%): | 81.18 |

| End of Step CSS Temperature Profile (°C) | | | | | | | | |
|---|---|---|---|---|---|---|---|---|
| z (m) | Step 1 | Step 2 | Step 3 | Step 4 | Step 5 | Step 6 | Step 7 | Step 8 |
| 0 | 21.9 | 21.5 | 18.9 | 17.1 | 20 | 20.5 | 21.2 | 22.5 |
| 0.1 | 21.2 | 21.2 | 20.7 | 20.6 | 20.6 | 20.6 | 20.2 | 20.2 |
| 0.2 | 14.3 | 14.6 | 14.2 | 14.2 | 13.3 | 13 | 12.8 | 12.8 |
| 0.3 | 1.5 | 2 | 2.2 | 1.5 | -0.9 | -2 | -2.6 | -2.3 |
| 0.4 | 9.6 | 10.5 | 9.8 | 8.9 | 6.2 | 4.9 | 5.2 | 5.6 |
| 0.5 | 14.5 | 15.7 | 15.2 | 14.3 | 11.9 | 10.7 | 10.7 | 10.9 |
| 0.6 | 18.5 | 19.2 | 18.8 | 17.8 | 16.2 | 14.8 | 14.9 | 15 |
| 0.7 | 20.5 | 21.2 | 20.9 | 20.1 | 18.5 | 17.1 | 16.9 | 17.2 |
| 0.8 | 22.8 | 23.9 | 23.6 | 23 | 21.4 | 20.3 | 20.2 | 20.1 |
| 0.9 | 22.3 | 23.7 | 23.7 | 23.2 | 21.6 | 20.7 | 20.6 | 20.3 |
| 1 | 23.3 | 25 | 25 | 24.7 | 23.1 | 22 | 22 | 21.8 |
| 1.1 | 24.5 | 26.5 | 26.4 | 26.2 | 25.1 | 23.8 | 23.6 | 23.6 |
| 1.2 | 25.6 | 27.1 | 27.9 | 27.4 | 26.2 | 25.5 | 24.9 | 24.8 |
| 1.3 | 25.6 | 26.7 | 27.7 | 27.6 | 26.5 | 25.6 | 25.2 | 25 |
| 1.4 | 25.6 | 26.1 | 26.9 | 26.9 | 26.2 | 25.7 | 25.4 | 25.3 |
| 1.5 | 26.4 | 26.8 | 27.5 | 28 | 27.2 | 26.4 | 26.2 | 26 |
| 1.6 | 27.2 | 27.6 | 28 | 28.7 | 28.1 | 27.3 | 27 | 26.8 |
| 1.7 | 26.2 | 26.4 | 26.5 | 27.2 | 27.3 | 26.7 | 26.1 | 25.8 |
| 1.75 | 26.9 | 27.2 | 27.3 | 28.1 | 28.2 | 27.4 | 26.7 | 26.5 |
| 1.8 | 27.2 | 27.4 | 27.3 | 27.9 | 28.2 | 27.4 | 26.7 | 26.7 |

## Run Number AA300NaX21

**Description of Experiment**
Two bed with 300 mm prelayer of activated alumina, main layer NaX, PVC beds
60 second cycle

| Sieve Arrangement and Bed | | |
|---|---|---|
| Type of Prelayer | AA | AA |
| Type of Main Layer | NaX | NaX |
| Bed | PVC | PVC |
| | **Bed 1** | **Bed 2** |
| Mass of Prelayer (kg) | 1.882 | 1.862 |
| Mass of Main layer(kg) | 8.4882 | 8.508 |
| Height of Prelayer (mm) | 300 | 300 |
| Height of Main layer(mm) | 1550 | 1550 |

| End of Step Press. at CSS (kPa) | Bed 1 | Bed 2 |
|---|---|---|
| Step 1 | 129.4 | 53.6 |
| Step 2 | 139.2 | 36.8 |
| Step 3 | 106.1 | 52.4 |
| Step 4 | 95.3 | 67.0 |
| Step 5 | 52.4 | 129.9 |
| Step 6 | 35.7 | 140.3 |
| Step 7 | 52.4 | 106.8 |
| Step 8 | 66.5 | 96.3 |

| Mass Balance at CSS (Total millimole per cycle) | | | |
|---|---|---|---|
| Feed flow | 4608.5 | Evacuation flow | 4067.9 |
| Product flow | 662.5 | Mass Balance Error (%) | -2.6 |

| Key Performance Parameters | | | |
|---|---|---|---|
| Oxygen Recovery (%) | 49.6 | BSF (kg/TPDc) | 736.3 |
| Power: (kW/TPDc) | 8.2 | Oxygen Purity (%): | 75.9 |

| End of Step CSS Temperature Profile (°C) | | | | | | | | |
|---|---|---|---|---|---|---|---|---|
| z (m) | Step 1 | Step 2 | Step 3 | Step 4 | Step 5 | Step 6 | Step 7 | Step 8 |
| 0 | 20.2 | 19.2 | 17.6 | 15.5 | 17.6 | 17.9 | 19.3 | 20.8 |
| 0.1 | 18.6 | 19.1 | 19.2 | 19.3 | 18.6 | 18.3 | 18.4 | 18.1 |
| 0.2 | 13.9 | 14.2 | 14.2 | 14.3 | 13.5 | 13.1 | 13 | 12.8 |
| 0.3 | 3.5 | 4.7 | 4.7 | 4.4 | 2 | 0.6 | 0.2 | 0.5 |
| 0.4 | 7.9 | 9.1 | 8.8 | 8.8 | 6.1 | 4.1 | 4 | 4.3 |
| 0.5 | 11.4 | 12.8 | 12.2 | 11.7 | 9.4 | 8.1 | 7.7 | 8.2 |
| 0.6 | 14.5 | 15.6 | 15.2 | 14.7 | 12.8 | 11.4 | 11.4 | 11.7 |
| 0.7 | 16.2 | 17.1 | 17.3 | 16.7 | 14.8 | 12.9 | 13.3 | 13.3 |
| 0.8 | 19.4 | 20.5 | 20.2 | 19.8 | 18.2 | 17.1 | 16.8 | 16.8 |
| 0.9 | 18.8 | 20.2 | 19.9 | 19.7 | 18.1 | 17 | 16.7 | 16.4 |
| 1 | 20.1 | 21.6 | 21.4 | 21.1 | 19.3 | 18.4 | 18 | 17.8 |
| 1.1 | 21 | 23 | 23 | 22.7 | 21.1 | 20.1 | 19.2 | 19.3 |
| 1.2 | 22 | 23.9 | 24 | 23.8 | 22.4 | 21.3 | 20.7 | 20.6 |
| 1.3 | 21.7 | 23.7 | 24.1 | 23.9 | 22.6 | 21.6 | 21 | 20.7 |
| 1.4 | 22.3 | 23.1 | 23.8 | 23.7 | 22.8 | 22.4 | 21.9 | 21.8 |
| 1.5 | 23.2 | 23.9 | 25.2 | 25.2 | 24 | 23.4 | 22.8 | 22.6 |
| 1.6 | 24.2 | 24.9 | 25.9 | 26.2 | 25.2 | 24.5 | 24 | 23.8 |
| 1.7 | 23.3 | 23.6 | 24.3 | 25.1 | 25 | 24.1 | 23.3 | 23 |
| 1.75 | 24.2 | 24.5 | 25.2 | 26 | 25.9 | 25.1 | 24.2 | 23.9 |
| 1.8 | 24.6 | 24.8 | 25.1 | 26.1 | 25.9 | 25.2 | 24.1 | 24 |

# Run Number AA300NaX22

**Description of Experiment**

Two bed with 300 mm prelayer of activated alumina, main layer NaX, PVC beds
60 second cycle

| Sieve Arrangement and Bed | | |
|---|---|---|
| Type of Prelayer | AA | AA |
| Type of Main Layer | NaX | NaX |
| Bed | PVC | PVC |
| | **Bed 1** | **Bed 2** |
| Mass of Prelayer (kg) | 1.882 | 1.862 |
| Mass of Main layer(kg) | 8.4882 | 8.508 |
| Height of Prelayer (mm) | 300 | 300 |
| Height of Main layer(mm) | 1550 | 1550 |

| End of Step Press. at CSS (kPa) | Bed 1 | Bed 2 |
|---|---|---|
| Step 1 | 127.7 | 49.3 |
| Step 2 | 140.8 | 32.1 |
| Step 3 | 104.9 | 49.1 |
| Step 4 | 93.4 | 62.4 |
| Step 5 | 48.4 | 127.9 |
| Step 6 | 30.9 | 141.8 |
| Step 7 | 48.8 | 105.1 |
| Step 8 | 62.1 | 93.4 |

| Mass Balance at CSS (Total millimole per cycle) | | | |
|---|---|---|---|
| Feed flow | 4253.4 | Evacuation flow | 4132.2 |
| Product flow | 245.1 | Mass Balance Error (%) | -2.9 |

| Key Performance Parameters | | | |
|---|---|---|---|
| Oxygen Recovery (%) | 24.8 | BSF (kg/TPDc) | 1597.0 |
| Power: (kW/TPDc) | 19.4 | Oxygen Purity (%): | 94.7 |

| End of Step CSS Temperature Profile (°C) | | | | | | | | |
|---|---|---|---|---|---|---|---|---|
| z (m) | Step 1 | Step 2 | Step 3 | Step 4 | Step 5 | Step 6 | Step 7 | Step 8 |
| 0 | 21.9 | 21.6 | 19.4 | 18.5 | 20 | 20.6 | 21 | 22.1 |
| 0.1 | 19.2 | 19.5 | 18.9 | 19 | 18.2 | 18.7 | 17.9 | 18.3 |
| 0.2 | 10 | 10.4 | 10 | 10 | 8.9 | 8.7 | 8.4 | 8.6 |
| 0.3 | 0.1 | 0.6 | 0.7 | 0.5 | -1.9 | -2.8 | -3.6 | -3.6 |
| 0.4 | 14 | 15.4 | 14.6 | 14.2 | 11.5 | 10.2 | 9.7 | 9.7 |
| 0.5 | 18.3 | 19.7 | 19.2 | 18.9 | 16.5 | 14.9 | 14.5 | 14.4 |
| 0.6 | 20.9 | 22 | 21.2 | 21.1 | 19 | 17.9 | 17.4 | 17.4 |
| 0.7 | 22 | 23.5 | 22.8 | 22.4 | 20.4 | 19.1 | 18.4 | 18.7 |
| 0.8 | 24.7 | 26 | 25.7 | 25.5 | 23.7 | 22.4 | 21.8 | 21.4 |
| 0.9 | 23.6 | 25.5 | 25.8 | 25.5 | 23.9 | 22.6 | 21.9 | 21.8 |
| 1 | 23.8 | 26.4 | 27.2 | 27.2 | 25.7 | 24.2 | 23.6 | 23.2 |
| 1.1 | 25.8 | 26.7 | 28.5 | 28.8 | 27.1 | 26.2 | 25.4 | 24.9 |
| 1.2 | 25.6 | 26.2 | 28 | 28.4 | 27.1 | 25.9 | 25.2 | 25 |
| 1.3 | 24.4 | 24.9 | 25.7 | 26.8 | 25.7 | 24.3 | 24 | 23.9 |
| 1.4 | 23.3 | 23.6 | 23.5 | 23.9 | 23.3 | 23 | 22.9 | 22.9 |
| 1.5 | 23.2 | 23.5 | 23.3 | 23.3 | 22.8 | 22.5 | 22.5 | 22.6 |
| 1.6 | 23.7 | 24 | 23.8 | 23.8 | 23.3 | 23.1 | 23.1 | 23.2 |
| 1.7 | 22.2 | 22.7 | 22.5 | 22.5 | 22 | 21.6 | 21.5 | 21.6 |
| 1.75 | 22.9 | 23.4 | 23.3 | 23.3 | 22.7 | 22.2 | 22.2 | 22.3 |
| 1.8 | 23.7 | 24.3 | 24.1 | 24 | 23.4 | 23 | 23.1 | 23.1 |

# Run Number AA300LSX1

**Description of Experiment**

One bed with 300 mm prelayer of activated alumina, main layer LiLSX, PVC bed 56 second cycle

| Sieve Arrangement and Bed | |
|---|---|
| Type of Prelayer | AA |
| Type of Main Layer | LiLSX |
| Bed | PVC |
| Mass of Prelayer: | 2.06 kg |
| Mass of Main layer: | 7.92 kg |
| Height of Prelayer: | 300 mm |
| Height of Main layer: | 1550 mm |

| End of Step Pressures at CSS (kPa) | |
|---|---|
| Step 1 | 134.6 |
| Step 2 | 140.7 |
| Step 3 | 101.0 |
| Step 4 | 30.4 |
| Step 5 | 34.1 |

| Mass Balance at CSS (Total millimole per cycle) | | | |
|---|---|---|---|
| Feed flow | 4647.7 | Evacuation flow | 4217.5 |
| Product flow | 440.5 | Mass Balance Error (%) | -0.2 |

| Key Performance Parameters | | | |
|---|---|---|---|
| Oxygen Recovery (%) | 38.94 | BSF (kg/TPDc) | 401.90 |
| Power: (kW/TPDc) | 9.93 | Oxygen Purity (%): | 90.60 |

| End of Step CSS Temperature Profile (°C) | | | | | |
|---|---|---|---|---|---|
| z (m) | Step 1 | Step 2 | Step 3 | Step 4 | Step 5 |
| 0 | 11.9 | 11.4 | 11.2 | 11.6 | 11 |
| 0.1 | 8.8 | 8.4 | 8.1 | 7.5 | 7 |
| 0.2 | -1.9 | -1.2 | -1.7 | -3 | -3.5 |
| 0.3 | -7.2 | -6.8 | -7.1 | -11.2 | -12.3 |
| 0.4 | -3.2 | -1.6 | -2.6 | -8.8 | -10.1 |
| 0.5 | 3.6 | 5 | 4.3 | -2.2 | -3.2 |
| 0.6 | 6.9 | 8.2 | 8 | 1.8 | 0.8 |
| 0.7 | 9 | 11.3 | 11.1 | 3.5 | 2.2 |
| 0.8 | 10.8 | 13.3 | 12.8 | 5.4 | 4.2 |
| 0.9 | 11.6 | 15 | 14.8 | 8 | 6.4 |
| 1 | 14 | 17 | 17.1 | 10.7 | 9.6 |
| 1.1 | 15 | 19.5 | 19.5 | 12.4 | 10.7 |
| 1.2 | 16.6 | 20.6 | 20.5 | 14.8 | 13.6 |
| 1.3 | 16.5 | 22.3 | 22.3 | 15.9 | 14.5 |
| 1.4 | 18.4 | 21.6 | 21.5 | 17.9 | 17.2 |
| 1.5 | 18.9 | 23.8 | 23.7 | 18 | 17.1 |
| 1.6 | 20.1 | 24.6 | 25.1 | 19.6 | 18.8 |
| 1.7 | 19.7 | 22.6 | 22.9 | 20.1 | 19.1 |
| 1.75 | 20.1 | 23.2 | 23.3 | 20.5 | 19.4 |
| 1.8 | 21.2 | 24.1 | 24.1 | 21.9 | 20.8 |

# Run Number AA300LSX2

**Description of Experiment**

One bed with 300 mm prelayer of activated alumina, main layer LiLSX, PVC bed
56 second cycle

| Sieve Arrangement and Bed | |
|---|---|
| Type of Prelayer | AA |
| Type of Main Layer | LiLSX |
| Bed | PVC |
| Mass of Prelayer: | 2.06 kg |
| Mass of Main layer: | 7.92 kg |
| Height of Prelayer: | 300 mm |
| Height of Main layer: | 1550 mm |

| End of Step Pressures at CSS (kPa) | |
|---|---|
| Step 1 | 135.3 |
| Step 2 | 140.8 |
| Step 3 | 101.1 |
| Step 4 | 31.3 |
| Step 5 | 35.0 |

| Mass Balance at CSS (Total millimole per cycle) | | | |
|---|---|---|---|
| Feed flow | 4622.1 | Evacuation flow | 4145.7 |
| Product flow | 442.9 | Mass Balance Error (%) | 0.7 |

| Key Performance Parameters | | | |
|---|---|---|---|
| Oxygen Recovery (%) | 39.33 | BSF (kg/TPDc) | 403.90 |
| Power: (kW/TPDc) | 9.67 | Oxygen Purity (%): | 89.65 |

| End of Step CSS Temperature Profile (°C) | | | | | |
|---|---|---|---|---|---|
| z (m) | Step 1 | Step 2 | Step 3 | Step 4 | Step 5 |
| 0 | 11.4 | 11.3 | 11.2 | 11.8 | 11 |
| 0.1 | 8.4 | 8.9 | 8.7 | 7.9 | 7.3 |
| 0.2 | -1.6 | -0.8 | -1.3 | -2.3 | -2.9 |
| 0.3 | -7 | -6.1 | -6.4 | -10.5 | -11.7 |
| 0.4 | -3.4 | -1.8 | -2.3 | -8.5 | -10 |
| 0.5 | 3.3 | 4.8 | 3.9 | -2.5 | -3 |
| 0.6 | 6.6 | 8.4 | 7.6 | 1.6 | 1.1 |
| 0.7 | 8.9 | 11.2 | 10.8 | 3.6 | 2.3 |
| 0.8 | 10.7 | 13.2 | 12.6 | 5.3 | 4.1 |
| 0.9 | 11.5 | 14.7 | 14.6 | 8 | 6.6 |
| 1 | 14 | 16.9 | 16.8 | 11 | 9.7 |
| 1.1 | 14.7 | 19.3 | 19.1 | 12.5 | 10.8 |
| 1.2 | 16.4 | 20.6 | 20.4 | 14.7 | 13.4 |
| 1.3 | 16.4 | 21.9 | 22 | 15.7 | 14.4 |
| 1.4 | 18.3 | 21.4 | 21.4 | 17.8 | 17.1 |
| 1.5 | 18.7 | 23.4 | 23.5 | 17.9 | 16.9 |
| 1.6 | 20 | 24.4 | 24.8 | 19.4 | 18.5 |
| 1.7 | 19.7 | 22.8 | 23.2 | 20.2 | 19.1 |
| 1.75 | 20.1 | 23.3 | 23.7 | 20.5 | 19.4 |
| 1.8 | 21.2 | 24.2 | 24.5 | 22 | 20.8 |

# Run Number AA300LSX3

**Description of Experiment**

One bed with 300 mm prelayer of activated alumina, main layer LiLSX, PVC bed 56 second cycle

| Sieve Arrangement and Bed | |
|---|---|
| Type of Prelayer | AA |
| Type of Main Layer | LiLSX |
| Bed | PVC |
| Mass of Prelayer: | 2.06 kg |
| Mass of Main layer: | 7.92 kg |
| Height of Prelayer: | 300 mm |
| Height of Main layer: | 1550 mm |

| End of Step Pressures at CSS (kPa) | |
|---|---|
| Step 1 | 133.8 |
| Step 2 | 140.7 |
| Step 3 | 101.1 |
| Step 4 | 41.9 |
| Step 5 | 44.7 |

| Mass Balance at CSS (Total millimole per cycle) | | | |
|---|---|---|---|
| Feed flow | 3962.4 | Evacuation flow | 3510.1 |
| Product flow | 448.8 | Mass Balance Error (%) | 0.1 |

| Key Performance Parameters | | | |
|---|---|---|---|
| Oxygen Recovery (%) | 36.0 | BSF (kg/TPDc) | 512.0 |
| Power: (kW/TPDc) | 7.9 | Oxygen Purity (%): | 69.8 |

| End of Step CSS Temperature Profile (°C) | | | | | |
|---|---|---|---|---|---|
| z (m) | Step 1 | Step 2 | Step 3 | Step 4 | Step 5 |
| 0 | 14.1 | 13.6 | 13.3 | 14 | 13.9 |
| 0.1 | 12.6 | 12.4 | 12.2 | 12.4 | 12.2 |
| 0.2 | 6.3 | 6.5 | 6.2 | 5.6 | 5.3 |
| 0.3 | 1.7 | 2 | 1.7 | -0.7 | -1.2 |
| 0.4 | 3.7 | 4.9 | 4.2 | -0.9 | -1.2 |
| 0.5 | 7.2 | 8.8 | 7.9 | 3 | 2.4 |
| 0.6 | 8.9 | 10.7 | 10.1 | 5.3 | 5 |
| 0.7 | 9.8 | 12.7 | 12.4 | 6.7 | 5.9 |
| 0.8 | 11.4 | 13.6 | 13.2 | 7.5 | 6.6 |
| 0.9 | 11.4 | 14.2 | 13.7 | 8.5 | 7.6 |
| 1 | 13.4 | 15.7 | 15.5 | 11 | 10.2 |
| 1.1 | 13 | 16.5 | 16.2 | 11.3 | 10.2 |
| 1.2 | 14.6 | 18 | 17.7 | 12.5 | 11.6 |
| 1.3 | 14.7 | 18 | 18 | 12.9 | 12.2 |
| 1.4 | 16.3 | 18 | 18 | 15.5 | 15 |
| 1.5 | 16.5 | 18.7 | 18.7 | 15 | 14.2 |
| 1.6 | 17.4 | 19.7 | 19.7 | 16.1 | 15.2 |
| 1.7 | 15.7 | 19.3 | 19.4 | 16.2 | 14.7 |
| 1.75 | 16.3 | 20 | 20.3 | 16.9 | 15.6 |
| 1.8 | 17.3 | 21.9 | 22.1 | 19 | 17 |

# Run Number AA300LSX4

**Description of Experiment**

One bed with 300 mm prelayer of activated alumina, main layer LiLSX, PVC bed, 56 second cycle

| Sieve Arrangement and Bed | |
|---|---|
| Type of Prelayer | AA |
| Type of Main Layer | LiLSX |
| Bed | PVC |
| Mass of Prelayer: | 2.06 kg |
| Mass of Main layer: | 7.92 kg |
| Height of Prelayer: | 300 mm |
| Height of Main layer: | 1550 mm |

| End of Step Pressures at CSS (kPa) | |
|---|---|
| Step 1 | 134.1 |
| Step 2 | 140.2 |
| Step 3 | 101.1 |
| Step 4 | 41.1 |
| Step 5 | 45.4 |

| Mass Balance at CSS (Total millimole per cycle) | | | |
|---|---|---|---|
| Feed flow | 3896.0 | Evacuation flow | 3546.1 |
| Product flow | 333.0 | Mass Balance Error (%) | 0.4 |

| Key Performance Parameters | | | |
|---|---|---|---|
| Oxygen Recovery (%) | 33.4 | BSF (kg/TPDc) | 562.6 |
| Power: (kW/TPDc) | 9.2 | Oxygen Purity (%): | 85.6 |

| End of Step CSS Temperature Profile (°C) | | | | | |
|---|---|---|---|---|---|
| z (m) | Step 1 | Step 2 | Step 3 | Step 4 | Step 5 |
| 0 | 12.7 | 12.9 | 12.2 | 11.9 | 12.7 |
| 0.1 | 10.9 | 10.9 | 10.1 | 10 | 10.1 |
| 0.2 | 3.3 | 4.1 | 3.3 | 2.3 | 2.6 |
| 0.3 | -1.1 | -0.8 | -1.3 | -3.6 | -4.2 |
| 0.4 | 1.8 | 3.4 | 2.4 | -2.8 | -3.1 |
| 0.5 | 6.6 | 8 | 7.1 | 2.3 | 1.8 |
| 0.6 | 9.2 | 10.6 | 10.1 | 5.4 | 4.7 |
| 0.7 | 10.6 | 13.1 | 12.4 | 6.7 | 5.8 |
| 0.8 | 12.4 | 14.8 | 14.1 | 8.1 | 7.5 |
| 0.9 | 12.7 | 15.6 | 15.4 | 10.1 | 9.1 |
| 1 | 14.6 | 17.1 | 16.7 | 12.1 | 11.2 |
| 1.1 | 15.4 | 19.1 | 18.7 | 13.2 | 12.1 |
| 1.2 | 17.3 | 20.9 | 20.6 | 15 | 14.1 |
| 1.3 | 16.8 | 20.5 | 20.5 | 15.3 | 14.4 |
| 1.4 | 18.1 | 20 | 20 | 17.2 | 16.7 |
| 1.5 | 18.1 | 20.9 | 20.9 | 16.8 | 15.9 |
| 1.6 | 18.9 | 21.7 | 21.9 | 18 | 17.1 |
| 1.7 | 17.8 | 21.3 | 21.7 | 18.6 | 17.2 |
| 1.75 | 18.3 | 21.8 | 22.2 | 19 | 17.7 |
| 1.8 | 19.5 | 23 | 23.4 | 20.8 | 19.1 |

# Run Number AA300LSX5

**Description of Experiment**

One bed with 300 mm prelayer of activated alumina, main layer LiLSX, PVC bed 56 second cycle

| Sieve Arrangement and Bed | |
|---|---|
| Type of Prelayer | AA |
| Type of Main Layer | LiLSX |
| Bed | PVC |
| Mass of Prelayer: | 2.06 kg |
| Mass of Main layer: | 7.92 kg |
| Height of Prelayer: | 300 mm |
| Height of Main layer: | 1550 mm |

| End of Step Pressures at CSS (kPa) | |
|---|---|
| Step 1 | 134.1 |
| Step 2 | 140.2 |
| Step 3 | 101.1 |
| Step 4 | 41.1 |
| Step 5 | 45.4 |

| Mass Balance at CSS (Total millimole per cycle) | | | |
|---|---|---|---|
| Feed flow | 3896.0 | Evacuation flow | 3546.1 |
| Product flow | 361.5 | Mass Balance Error (%) | -0.3 |

| Key Performance Parameters | | | |
|---|---|---|---|
| Oxygen Recovery (%) | 36.0 | BSF (kg/TPDc) | 518.3 |
| Power: (kW/TPDc) | 9.2 | Oxygen Purity (%): | 85.6 |

| End of Step CSS Temperature Profile (°C) | | | | | |
|---|---|---|---|---|---|
| z (m) | Step 1 | Step 2 | Step 3 | Step 4 | Step 5 |
| 0 | 12.7 | 11.7 | 11.7 | 12.6 | 11.5 |
| 0.1 | 11 | 11 | 11 | 11 | 10.2 |
| 0.2 | 5.8 | 5.8 | 5.4 | 5.1 | 4.7 |
| 0.3 | 1.7 | 2 | 2 | -0.5 | -1.3 |
| 0.4 | 4.4 | 5.5 | 5.1 | 0.2 | -1.2 |
| 0.5 | 8.1 | 9.4 | 9 | 3.8 | 3.2 |
| 0.6 | 10.1 | 11.7 | 11.3 | 6.4 | 6 |
| 0.7 | 11.9 | 14.4 | 13.7 | 7.9 | 7.4 |
| 0.8 | 13.4 | 15.9 | 15.3 | 9.3 | 8.5 |
| 0.9 | 13.6 | 16.1 | 16 | 10.4 | 9.6 |
| 1 | 15 | 17.1 | 16.8 | 11.8 | 11.5 |
| 1.1 | 15.5 | 19 | 18.6 | 13 | 12.4 |
| 1.2 | 16.6 | 20.1 | 19.9 | 14.3 | 13.5 |
| 1.3 | 15.7 | 19.3 | 19.3 | 14.1 | 13.3 |
| 1.4 | 16.6 | 18.3 | 18.2 | 15.7 | 15.3 |
| 1.5 | 16.8 | 18.9 | 18.9 | 15.2 | 14.6 |
| 1.6 | 17.5 | 19 | 19 | 15.9 | 15.3 |
| 1.7 | 15.8 | 18.2 | 18.2 | 15.2 | 14.1 |
| 1.75 | 16.3 | 18.9 | 18.9 | 15.8 | 14.8 |
| 1.8 | 17 | 20.3 | 20.4 | 17.4 | 15.9 |

# Run Number AA300LSX6

**Description of Experiment**

One bed with 300 mm prelayer of activated alumina, main layer LiLSX, PVC bed 56 second cycle

| Sieve Arrangement and Bed | |
|---|---|
| Type of Prelayer | AA |
| Type of Main Layer | LiLSX |
| Bed | PVC |
| Mass of Prelayer: | 2.06 kg |
| Mass of Main layer: | 7.92 kg |
| Height of Prelayer: | 300 mm |
| Height of Main layer: | 1550 mm |

| End of Step Pressures at CSS (kPa) | |
|---|---|
| Step 1 | 135.3 |
| Step 2 | 140.0 |
| Step 3 | 101.1 |
| Step 4 | 41.3 |
| Step 5 | 49.7 |

| Mass Balance at CSS (Total millimole per cycle) | | | |
|---|---|---|---|
| Feed flow | 3976.8 | Evacuation flow | 3654.7 |
| Product flow | 307.4 | Mass Balance Error (%) | 0.4 |

| Key Performance Parameters | | | |
|---|---|---|---|
| Oxygen Recovery (%) | 32.6 | BSF (kg/TPDc) | 564.5 |
| Power: (kW/TPDc) | 9.6 | Oxygen Purity (%): | 92.4 |

| End of Step CSS Temperature Profile (°C) | | | | | |
|---|---|---|---|---|---|
| z (m) | Step 1 | Step 2 | Step 3 | Step 4 | Step 5 |
| 0 | 11.9 | 10.5 | 10.4 | 11.3 | 11.5 |
| 0.1 | 9.6 | 8.8 | 9.3 | 8.7 | 8.5 |
| 0.2 | 1.2 | 1.5 | 1.1 | 0.5 | 0.3 |
| 0.3 | -3.7 | -3.5 | -3.5 | -6.6 | -7.3 |
| 0.4 | -0.9 | -0.6 | -1 | -5.4 | -6 |
| 0.5 | 4.2 | 5.8 | 5.1 | 0.2 | -0.3 |
| 0.6 | 7.2 | 8.8 | 8.4 | 3.8 | 3.2 |
| 0.7 | 9.3 | 11.4 | 11.1 | 5.4 | 4.4 |
| 0.8 | 11.5 | 13.4 | 12.9 | 6.9 | 6.4 |
| 0.9 | 12.2 | 15.2 | 14.9 | 9.5 | 8.2 |
| 1 | 14.1 | 16.8 | 16.5 | 11.6 | 10.5 |
| 1.1 | 15.7 | 19.4 | 19.3 | 13.7 | 12.5 |
| 1.2 | 17.7 | 21.9 | 21.9 | 16.2 | 14.9 |
| 1.3 | 16.9 | 21.9 | 22 | 16.6 | 15.2 |
| 1.4 | 18.6 | 21.4 | 21.3 | 18.4 | 17.6 |
| 1.5 | 18.6 | 23.1 | 23.2 | 18.4 | 17.2 |
| 1.6 | 19.8 | 24 | 24.4 | 19.7 | 18.7 |
| 1.7 | 19.2 | 21.8 | 22.1 | 19.9 | 19 |
| 1.75 | 19.5 | 22.3 | 22.5 | 20.2 | 19.3 |
| 1.8 | 20.5 | 22.7 | 22.8 | 21.1 | 20.2 |

# Run Number AA300LSX7

**Description of Experiment**

One bed with 300 mm prelayer of activated alumina, main layer LiLSX, PVC bed 56 second cycle

| Sieve Arrangement and Bed | |
|---|---|
| Type of Prelayer | AA |
| Type of Main Layer | LiLSX |
| Bed | PVC |
| Mass of Prelayer: | 2.06 kg |
| Mass of Main layer: | 7.92 kg |
| Height of Prelayer: | 300 mm |
| Height of Main layer: | 1550 mm |

| End of Step Pressures at CSS (kFa) | |
|---|---|
| Step 1 | 134.2 |
| Step 2 | 140.0 |
| Step 3 | 101.1 |
| Step 4 | 41.8 |
| Step 5 | 46.0 |

| Mass Balance at CSS (Total millimole per cycle) | | | |
|---|---|---|---|
| Feed flow | 3888.5 | Evacuation flow | 3593.2 |
| Product flow | 331.1 | Mass Balance Error (%) | -0.9 |

| Key Performance Parameters | | | |
|---|---|---|---|
| Oxygen Recovery (%) | 32.5 | BSF (kg/TPDc) | 571.6 |
| Power: (kW/TPDc) | 9.2 | Oxygen Purity (%): | 84.7 |

| End of Step CSS Temperature Profile (°C) | | | | | |
|---|---|---|---|---|---|
| z (m) | Step 1 | Step 2 | Step 3 | Step 4 | Step 5 |
| 0 | 13.6 | 13.3 | 12.8 | 12.2 | 12.2 |
| 0.1 | 11.5 | 11.7 | 11.2 | 10.4 | 10.7 |
| 0.2 | 5 | 5.5 | 5 | 4 | 3.7 |
| 0.3 | 0.3 | 1 | 0.3 | -2.5 | -3 |
| 0.4 | 2.7 | 4.1 | 3.1 | -2.4 | -3.3 |
| 0.5 | 7 | 8.2 | 7.6 | 2.5 | 2.1 |
| 0.6 | 9.6 | 10.8 | 10.5 | 6 | 4.9 |
| 0.7 | 10.9 | 13.1 | 12.8 | 7.2 | 6.1 |
| 0.8 | 12.7 | 15 | 14.6 | 8.6 | 7.7 |
| 0.9 | 13.3 | 15.7 | 15.7 | 10.4 | 9.2 |
| 1 | 14.6 | 17.1 | 16.8 | 12.3 | 11.1 |
| 1.1 | 15.6 | 19.2 | 18.8 | 13.3 | 12.1 |
| 1.2 | 17.2 | 20.6 | 20.5 | 15.1 | 14 |
| 1.3 | 16.6 | 20.3 | 20.4 | 15.3 | 14.2 |
| 1.4 | 18 | 19.9 | 19.9 | 17.1 | 16.5 |
| 1.5 | 18 | 20.7 | 20.9 | 16.7 | 15.9 |
| 1.6 | 18.9 | 21.8 | 21.9 | 18.1 | 17.1 |
| 1.7 | 18 | 21.4 | 21.7 | 18.7 | 17.3 |
| 1.75 | 18.5 | 22 | 22.2 | 19.1 | 17.9 |
| 1.8 | 19.8 | 23.5 | 23.7 | 21.1 | 19.4 |

# Run Number AA300LSX8

**Description of Experiment**

One bed with 300 mm prelayer of activated alumina, main layer LiLSX, PVC bed 56 second cycle

| Sieve Arrangement and Bed | |
|---|---|
| Type of Prelayer | AA |
| Type of Main Layer | LiLSX |
| Bed | PVC |
| Mass of Prelayer: | 2.06 kg |
| Mass of Main layer: | 7.92 kg |
| Height of Prelayer: | 300 mm |
| Height of Main layer: | 1550 mm |

| End of Step Pressures at CSS (kPa) | |
|---|---|
| Step 1 | 135.1 |
| Step 2 | 140.0 |
| Step 3 | 101.0 |
| Step 4 | 41.4 |
| Step 5 | 45.5 |

| Mass Balance at CSS (Total millimole per cycle) | | | |
|---|---|---|---|
| Feed flow | 3906.2 | Evacuation flow | 3574.2 |
| Product flow | 200.2 | Mass Balance Error (%) | 3.4 |

| Key Performance Parameters | | | |
|---|---|---|---|
| Oxygen Recovery (%) | 22.8 | BSF (kg/TPDc) | 847.1 |
| Power: (kW/TPDc) | 16.0 | Oxygen Purity (%): | 94.6 |

| End of Step CSS Temperature Profile (°C) | | | | | |
|---|---|---|---|---|---|
| z (m) | Step 1 | Step 2 | Step 3 | Step 4 | Step 5 |
| 0 | 12.3 | 11.9 | 11 | 11.9 | 11 |
| 0.1 | 9.2 | 9.3 | 8.7 | 8.8 | 7.9 |
| 0.2 | 0.8 | 1.3 | 0.5 | -0.3 | -0.6 |
| 0.3 | -3.5 | -3 | -3.5 | -5.7 | -6.8 |
| 0.4 | 2 | 3.1 | 1.8 | -2.9 | -4.3 |
| 0.5 | 8.5 | 9.8 | 9.2 | 3.7 | 3.1 |
| 0.6 | 11.7 | 12.9 | 12.8 | 7.5 | 6.9 |
| 0.7 | 14.5 | 16.6 | 16.3 | 10.3 | 9 |
| 0.8 | 16.9 | 19 | 18.5 | 11.9 | 10.8 |
| 0.9 | 17.5 | 20.5 | 20.3 | 14 | 12.7 |
| 1 | 18.2 | 20.7 | 20.6 | 15 | 13.8 |
| 1.1 | 20.2 | 24.8 | 24.6 | 18 | 16.4 |
| 1.2 | 21.3 | 26.8 | 26.9 | 20 | 18.6 |
| 1.3 | 20 | 26.4 | 26.5 | 19.9 | 18.5 |
| 1.4 | 20.6 | 24 | 24 | 20.3 | 19.8 |
| 1.5 | 20 | 22.6 | 22.9 | 19.3 | 18.8 |
| 1.6 | 19.7 | 21 | 21 | 19.1 | 18.8 |
| 1.7 | 17.7 | 18.9 | 19 | 17.4 | 17.1 |
| 1.75 | 18.3 | 19.5 | 19.5 | 17.8 | 17.5 |
| 1.8 | 18.3 | 19.2 | 19.2 | 17.8 | 17.5 |

# Run Number AA300LSX9

**Description of Experiment**

One bed with 300 mm prelayer of activated alumina, main layer LiLSX, PVC bed
No purge step, 50 second cycle

| Sieve Arrangement and Bed | |
|---|---|
| Type of Prelayer | AA |
| Type of Main Layer | LiLSX |
| Bed | PVC |
| Mass of Prelayer: | 2.06 kg |
| Mass of Main layer: | 7.92 kg |
| Height of Prelayer: | 300 mm |
| Height of Main layer: | 1550 mm |

| End of Step Pressures at CSS (kPa) | |
|---|---|
| Step 1 | 134.4 |
| Step 2 | 137.8 |
| Step 3 | 101.2 |
| Step 4 | 44.6 |

| Mass Balance at CSS (Total millimole per cycle) | | | |
|---|---|---|---|
| Feed flow | 3098.2 | Evacuation flow | 2881.9 |
| Product flow | 162.0 | Mass Balance Error (%) | 1.8 |

| Key Performance Parameters | | | |
|---|---|---|---|
| Oxygen Recovery (%) | 12.1 | BSF (kg/TPDc) | 1981.9 |
| Power: (kW/TPDc) | 26.9 | Oxygen Purity (%): | 50.0 |

| End of Step CSS Temperature Profile (°C) | | | | | |
|---|---|---|---|---|---|
| z (m) | Step 1 | Step 2 | Step 3 | Step 4 | Step 5 |
| 0 | 11.7 | 12.7 | 12.2 | 11.4 | 11.1 |
| 0.1 | 10.5 | 11.1 | 10.9 | 10.5 | 10.3 |
| 0.2 | 7.3 | 7.8 | 7.6 | 6.8 | 6.8 |
| 0.3 | 5.4 | 5.8 | 5.6 | 4.5 | 4.5 |
| 0.4 | 9.6 | 11 | 10.4 | 4.4 | 4.4 |
| 0.5 | 12 | 12.9 | 12.4 | 7.3 | 7.3 |
| 0.6 | 13 | 14 | 13.8 | 8.8 | 8.8 |
| 0.7 | 14.1 | 15.4 | 15.2 | 9.7 | 9.7 |
| 0.8 | 15.2 | 16.4 | 15.8 | 10.2 | 10.2 |
| 0.9 | 14.5 | 15.9 | 15.7 | 10.4 | 10.4 |
| 1 | 14.5 | 15.7 | 15.7 | 11.1 | 11.1 |
| 1.1 | 14.6 | 16.2 | 16.2 | 11.3 | 11.3 |
| 1.2 | 14.9 | 16.3 | 16 | 11.9 | 11.9 |
| 1.3 | 14.2 | 15.4 | 15.4 | 11.6 | 11.6 |
| 1.4 | 14.4 | 14.7 | 14.6 | 13 | 13 |
| 1.5 | 14.6 | 15 | 15 | 12.5 | 12.5 |
| 1.6 | 15.2 | 15.6 | 15.4 | 13 | 13 |
| 1.7 | 13.3 | 14.1 | 14.1 | 11.2 | 11.2 |
| 1.75 | 14 | 14.9 | 14.9 | 11.7 | 11.7 |
| 1.8 | 14.5 | 15.3 | 15.3 | 12.1 | 12.1 |

# Run Number AA300LSX10

**Description of Experiment**

One bed with 300 mm prelayer of activated alumina, main layer LiLSX, PVC bed
No purge step, 50 second cycle

| Sieve Arrangement and Bed | |
|---|---|
| Type of Prelayer | AA |
| Type of Main Layer | LiLSX |
| Bed | PVC |
| Mass of Prelayer: | 2.06 kg |
| Mass of Main layer: | 7.92 kg |
| Height of Prelayer: | 300 mm |
| Height of Main layer: | 1550 mm |

| End of Step Pressures at CSS (kPa) | |
|---|---|
| Step 1 | 133.1 |
| Step 2 | 137.6 |
| Step 3 | 100.9 |
| Step 4 | 43.9 |

| Mass Balance at CSS (Total millimole per cycle) | | | |
|---|---|---|---|
| Feed flow | 3271.4 | Evacuation flow | 2909.2 |
| Product flow | 332.6 | Mass Balance Error (%) | 0.9 |

| Key Performance Parameters | | | |
|---|---|---|---|
| Oxygen Recovery (%) | 21.3 | BSF (kg/TPDc) | 1054.3 |
| Power: (kW/TPDc) | 10.3 | Oxygen Purity (%): | 45.7 |

| End of Step CSS Temperature Profile (°C) | | | | | |
|---|---|---|---|---|---|
| z (m) | Step 1 | Step 2 | Step 3 | Step 4 | Step 5 |
| 0 | 14.4 | 14.2 | 14.1 | 13.1 | 13.1 |
| 0.1 | 13.9 | 13.9 | 13.9 | 13.2 | 13.2 |
| 0.2 | 11.1 | 11.3 | 11.1 | 10.5 | 10.5 |
| 0.3 | 9 | 9 | 8.9 | 7.6 | 7.6 |
| 0.4 | 10.9 | 12.2 | 11.4 | 6 | 6 |
| 0.5 | 13.4 | 14.2 | 13.7 | 9.3 | 9 |
| 0.6 | 15.7 | 16.6 | 15.9 | 11.8 | 11.8 |
| 0.7 | 17.7 | 19.3 | 18.5 | 13.4 | 13.4 |
| 0.8 | 18.9 | 20.4 | 19.8 | 14.3 | 14.3 |
| 0.9 | 18.5 | 20 | 19.7 | 15 | 15 |
| 1 | 18.4 | 19.7 | 19 | 15.3 | 15.3 |
| 1.1 | 18.6 | 20.6 | 20 | 15.3 | 15.3 |
| 1.2 | 18.3 | 20 | 19.7 | 15.5 | 15.5 |
| 1.3 | 17.4 | 18.8 | 18.8 | 14.8 | 14.8 |
| 1.4 | 17 | 17.5 | 17.4 | 15.7 | 15.7 |
| 1.5 | 17.1 | 17.7 | 17.6 | 14.9 | 14.9 |
| 1.6 | 17.5 | 17.9 | 17.8 | 15.3 | 15.2 |
| 1.7 | 15.7 | 16.6 | 16.6 | 13.6 | 13.5 |
| 1.75 | 16.5 | 17.5 | 17.4 | 14.2 | 14.2 |
| 1.8 | 17.3 | 18.2 | 18.2 | 14.9 | 14.9 |

# Run Number AA300LSX11

**Description of Experiment**

One bed with 300 mm prelayer of activated alumina, main layer LiLSX, PVC bed
No Purge Step, 50 second cycle

| Sieve Arrangement and Bed | |
|---|---|
| Type of Prelayer | AA |
| Type of Main Layer | LiLSX |
| Bed | PVC |
| Mass of Prelayer: | 2.06 kg |
| Mass of Main layer: | 7.92 kg |
| Height of Prelayer: | 300 mm |
| Height of Main layer: | 1550 mm |

| End of Step Pressures at CSS (kPa) | |
|---|---|
| Step 1 | 136.4 |
| Step 2 | 121.8 |
| Step 3 | 100.3 |
| Step 4 | 44.1 |

| Mass Balance at CSS (Total millimole per cycle) | | | |
|---|---|---|---|
| Feed flow | 2957.7 | Evacuation flow | 2641.5 |
| Product flow | 282.3 | Mass Balance Error (%) | 1.1 |

| Key Performance Parameters | | | |
|---|---|---|---|
| Oxygen Recovery (%) | 20.2 | BSF (kg/TPDc) | 1234.1 |
| Power: (kW/TPDc) | 10.9 | Oxygen Purity (%): | 46.0 |

| End of Step CSS Temperature Profile (°C) | | | | | |
|---|---|---|---|---|---|
| z (m) | Step 1 | Step 2 | Step 3 | Step 4 | Step 5 |
| 0 | 12.8 | 12.7 | 12.6 | 11.6 | 11.6 |
| 0.1 | 12.6 | 12.8 | 12.7 | 12.2 | 12.2 |
| 0.2 | 11 | 11.1 | 11 | 10.3 | 10.3 |
| 0.3 | 8.8 | 8.9 | 8.8 | 7.6 | 7.6 |
| 0.4 | 11.5 | 11.6 | 11.3 | 5.7 | 5.7 |
| 0.5 | 12.2 | 12.2 | 12.1 | 7.4 | 7.4 |
| 0.6 | 12.9 | 13.1 | 12.9 | 8.7 | 8.7 |
| 0.7 | 14.1 | 14.9 | 14.5 | 9.6 | 9.6 |
| 0.8 | 15.4 | 15.8 | 15.4 | 10.4 | 10.4 |
| 0.9 | 14.7 | 15.3 | 15.4 | 10.6 | 10.6 |
| 1 | 14.9 | 15.5 | 15.4 | 11.5 | 11.5 |
| 1.1 | 15.3 | 16.6 | 16.2 | 12 | 12 |
| 1.2 | 15.9 | 16.8 | 16.6 | 12.8 | 12.9 |
| 1.3 | 15.5 | 16.3 | 16.1 | 12.6 | 12.6 |
| 1.4 | 15.5 | 15.7 | 15.5 | 14 | 14 |
| 1.5 | 16.4 | 16.4 | 16.3 | 14 | 14 |
| 1.6 | 17.2 | 17.2 | 17 | 14.8 | 14.7 |
| 1.7 | 15.9 | 16.4 | 16.3 | 13.6 | 13.6 |
| 1.75 | 16.5 | 17.2 | 17 | 14.1 | 14.1 |
| 1.8 | 17.3 | 17.8 | 17.8 | 14.9 | 14.9 |

# Run Number AA300LSXEXT

**Description of Experiment**

One bed with 300 mm prelayer of activated alumina, main layer LiLSX, PVC bed, 56 second cycle, total external reflux

| Sieve Arrangement and Bed | |
|---|---|
| Type of Prelayer | AA |
| Type of Main Layer | LiLSX |
| Bed | PVC |
| Mass of Prelayer: | 2.06 kg |
| Mass of Main layer: | 7.92 kg |
| Height of Prelayer: | 300 mm |
| Height of Main layer: | 1550 mm |

| End of Step Pressures at CSS (kPa) | |
|---|---|
| Step 1 | 135.3 |
| Step 2 | 141.1 |
| Step 3 | 101.4 |
| Step 4 | 41.1 |
| Step 5 | 45.6 |

| Mass Balance at CSS (Total millimole per cycle) | | | |
|---|---|---|---|
| Feed flow | 3708.2 | Evacuation flow | 3695.8 |
| Product flow | 0.0 | Mass Balance Error (%) | 0.3 |

| Key Performance Parameters | | | |
|---|---|---|---|
| Oxygen Recovery (%) | 0.0 | BSF (kg/TPDc) | |
| Power: (kW/TPDc) | 0.0 | Oxygen Purity (%): | |

| End of Step CSS Temperature Profile (°C) | | | | | |
|---|---|---|---|---|---|
| z (m) | Step 1 | Step 2 | Step 3 | Step 4 | Step 5 |
| 0 | 13.7 | 13.7 | 13 | 13.1 | 13 |
| 0.1 | 9 | 9.5 | 8.9 | 7.7 | 8.1 |
| 0.2 | -0.8 | -0.3 | -1 | -1.7 | -1.9 |
| 0.3 | -2.7 | -2.2 | -2.4 | -4.9 | -5.1 |
| 0.4 | 12.2 | 13.2 | 12.7 | 6.9 | 6.1 |
| 0.5 | 19.6 | 21 | 20.6 | 14.5 | 13.5 |
| 0.6 | 20.6 | 22.2 | 21.5 | 15.5 | 14.7 |
| 0.7 | 23.5 | 26 | 25.4 | 18.8 | 17.2 |
| 0.8 | 25.8 | 28 | 27.7 | 20.1 | 18.6 |
| 0.9 | 26.9 | 30.1 | 29.9 | 23 | 21.7 |
| 1 | 26.2 | 29.6 | 28.9 | 22.7 | 21.6 |
| 1.1 | 30.1 | 36.2 | 35.9 | 28.3 | 26.6 |
| 1.2 | 28.4 | 36.6 | 36.5 | 28.2 | 26.8 |
| 1.3 | 20.8 | 25.5 | 26.5 | 20.2 | 19.6 |
| 1.4 | 17.5 | 17.9 | 17.8 | 17.1 | 17 |
| 1.5 | 16.8 | 17.2 | 17.1 | 16 | 15.9 |
| 1.6 | 17.5 | 18 | 17.9 | 16.8 | 16.7 |
| 1.7 | 15.9 | 16.7 | 16.6 | 15.4 | 15.2 |
| 1.75 | 16.6 | 17.5 | 17.4 | 16 | 15.9 |
| 1.8 | 16.9 | 17.9 | 17.9 | 16.3 | 16.2 |

# Run Number AA300LSXINT

**Description of Experiment**

One bed with 300 mm prelayer of activated alumina, main layer LiLSX, PVC bed
No Purge Step, 50 second cycle, Total Internal Reflux

| Sieve Arrangement and Bed | |
|---|---|
| Type of Prelayer | AA |
| Type of Main Layer | LiLSX |
| Bed | PVC |
| Mass of Prelayer: | 2.06 kg |
| Mass of Main layer: | 7.92 kg |
| Height of Prelayer: | 300 mm |
| Height of Main layer: | 1550 mm |

| End of Step Pressures at CSS (kPa) | |
|---|---|
| Step 1 | 101.6 |
| Step 2 | 136.7 |
| Step 3 | 101.0 |
| Step 4 | 44.8 |
| Step 5 | |

| Mass Balance at CSS (Total millimole per cycle) | | | |
|---|---|---|---|
| Feed flow | 2743.0 | Evacuation flow | 2741.1 |
| Product flow | 0.0 | Mass Balance Error (%) | 0.1 |

| Key Performance Parameters | | | |
|---|---|---|---|
| Oxygen Recovery (%) | 0.0 | BSF (kg/TPDc) | |
| Power: (kW/TPDc) | 0.0 | Oxygen Purity (%): | |

| End of Step CSS Temperature Profile (°C) | | | | | |
|---|---|---|---|---|---|
| z (m) | Step 1 | Step 2 | Step 3 | Step 4 | Step 5 |
| 0 | 13.1 | 12.7 | 12.2 | 12.7 | 12.7 |
| 0.1 | 11.4 | 11.1 | 11 | 11.4 | 11.4 |
| 0.2 | 8.4 | 8.6 | 8.2 | 8.1 | 8.1 |
| 0.3 | 7 | 7.1 | 7.1 | 6.8 | 6.8 |
| 0.4 | 13.4 | 15.7 | 15.3 | 10.7 | 10.7 |
| 0.5 | 15.3 | 17.6 | 17.6 | 12.7 | 12.7 |
| 0.6 | 15.6 | 17.8 | 17.5 | 12.9 | 12.9 |
| 0.7 | 16 | 19.1 | 18.7 | 13.5 | 13.5 |
| 0.8 | 16.4 | 19.7 | 19.3 | 13.5 | 13.5 |
| 0.9 | 15.2 | 18.3 | 18.4 | 13.4 | 13.4 |
| 1 | 14.5 | 17.5 | 17.2 | 13.2 | 13.2 |
| 1.1 | 13.6 | 17.6 | 17.4 | 12.6 | 12.6 |
| 1.2 | 13.6 | 16.5 | 16.6 | 12.3 | 12.3 |
| 1.3 | 12.8 | 15 | 15 | 11.9 | 11.9 |
| 1.4 | 13.6 | 14.4 | 14.4 | 13 | 13 |
| 1.5 | 14 | 15.2 | 15.2 | 13 | 13 |
| 1.6 | 14.8 | 15.9 | 15.9 | 13.8 | 13.8 |
| 1.7 | 12.7 | 14.2 | 14.3 | 12.1 | 12.1 |
| 1.75 | 13.2 | 15 | 15.1 | 12.6 | 12.6 |
| 1.8 | 13.1 | 14.9 | 14.9 | 12.4 | 12.5 |

# Run Number AA115LSX1

**Description of Experiment**

One bed with 115 mm prelayer of activated alumina, main layer LiLSX, PVC bed 56 second cycle

| Sieve Arrangement and Bed | |
|---|---|
| Type of Prelayer | AA |
| Type of Main Layer | LiLSX |
| Bed | PVC |
| Mass of Prelayer: | 0.756 kg |
| Mass of Main layer: | 7.91 kg |
| Height of Prelayer: | 115 mm |
| Height of Main layer: | 1550 mm |

| End of Step Pressures at CSS (kPa) | |
|---|---|
| Step 1 | 133.8 |
| Step 2 | 140.5 |
| Step 3 | 101.0 |
| Step 4 | 31.6 |
| Step 5 | 34.8 |

| Mass Balance at CSS (Total millimole per cycle) | | | |
|---|---|---|---|
| Feed flow | 4684.4 | Evacuation flow | 4256.2 |
| Product flow | 440.2 | Mass Balance Error (%) | -0.3 |

| Key Performance Parameters | | | |
|---|---|---|---|
| Oxygen Recovery (%) | 38.4 | BSF (kg/TPDc) | 403.1 |
| Power: (kW/TPDc) | 10.0 | Oxygen Purity (%): | 90.2 |

| End of Step CSS Temperature Profile (°C) | | | | | |
|---|---|---|---|---|---|
| z (m) | Step 1 | Step 2 | Step 3 | Step 4 | Step 5 |
| 0 | 11.2 | 10 | 9.7 | 10.5 | 9.5 |
| 0.025 | 8.8 | 9.2 | 8.8 | 7.3 | 7.3 |
| 0.05 | 5.4 | 6 | 5.5 | 3.8 | 3.4 |
| 0.1 | 3.5 | 3.8 | 3.2 | 1.5 | 0.7 |
| 0.2 | -1.9 | 0.1 | -0.4 | -7 | -8.5 |
| 0.3 | 4 | 5.7 | 5.3 | -1.9 | -3 |
| 0.4 | 8.8 | 10.2 | 9.7 | 3.1 | 1.5 |
| 0.5 | 10.8 | 12.7 | 12.5 | 5.7 | 4.9 |
| 0.6 | 12.6 | 14.8 | 14.5 | 8.5 | 7.4 |
| 0.7 | 14.3 | 17.8 | 17.2 | 10.4 | 8.8 |
| 0.8 | 16.4 | 19.9 | 19.3 | 11.4 | 10 |
| 0.9 | 16.1 | 20 | 20 | 13.2 | 11.8 |
| 1 | 16.8 | 21.2 | 21 | 14.7 | 13.2 |
| 1.1 | 18.3 | 24.5 | 24.3 | 17.6 | 16.1 |
| 1.2 | 19.9 | 26.6 | 26.5 | 19.6 | 18.1 |
| 1.3 | 19.1 | 25.4 | 25.6 | 18.9 | 17.6 |
| 1.4 | 19.9 | 23.5 | 23.7 | 19.2 | 18.7 |
| 1.5 | 20.4 | 22.5 | 22.7 | 19.8 | 19.1 |
| 1.6 | 20.6 | 22.6 | 22.6 | 20.5 | 19.8 |
| 1.7 | 18.6 | 19.4 | 19.4 | 18.2 | 18 |
| 1.75 | 19.6 | 20.1 | 19.9 | 18.5 | 18.5 |
| 1.8 | 20.1 | 20 | 19.7 | 17.7 | 17.6 |

# Run Number AA25LSX1

**Description of Experiment**

One bed with 25 mm prelayer of activated alumina, main layer LiLSX, PVC bed, 56 second cycle

| Sieve Arrangement and Bed | |
|---|---|
| Type of Prelayer | AA |
| Type of Main Layer | LiLSX |
| Bed | PVC |
| Mass of Prelayer: | 0.192 kg |
| Mass of Main layer: | 7.91 kg |
| Height of Prelayer: | 25 mm |
| Height of Main layer: | 1550 mm |

| End of Step Pressures at CSS (kPa) | |
|---|---|
| Step 1 | 135.1 |
| Step 2 | 140.4 |
| Step 3 | 101.1 |
| Step 4 | 31.6 |
| Step 5 | 35.1 |

| Mass Balance at CSS (Total millimole per cycle) | | | |
|---|---|---|---|
| Feed flow | 4612.6 | Evacuation flow | 4203.2 |
| Product flow | 436.8 | Mass Balance Error (%) | -0.6 |

| Key Performance Parameters | | | |
|---|---|---|---|
| Oxygen Recovery (%) | 38.5 | BSF (kg/TPDc) | 407.7 |
| Power: (kW/TPDc) | 9.7 | Oxygen Purity (%): | 90.0 |

| End of Step CSS Temperature Profile (°C) | | | | | |
|---|---|---|---|---|---|
| z (m) | Step 1 | Step 2 | Step 3 | Step 4 | Step 5 |
| 0 | 12.1 | 11.6 | 11.3 | 12.1 | 11.4 |
| 0.025 | 8.1 | 9.4 | 9.1 | 4.4 | 3.2 |
| 0.05 | 4.3 | 6.2 | 5.9 | -1.5 | -2.8 |
| 0.075 | 5.3 | 7.3 | 6.7 | -0.5 | -1.9 |
| 0.1 | 7.3 | 8.7 | 8.1 | 2.4 | 1.2 |
| 0.2 | 12.6 | 14.7 | 14.5 | 8.1 | 6.6 |
| 0.3 | 16.3 | 18.5 | 17.9 | 11 | 9.8 |
| 0.4 | 19.4 | 21.3 | 21.2 | 14.5 | 12.8 |
| 0.5 | 20.3 | 22.4 | 22 | 15.3 | 14.3 |
| 0.6 | 21.3 | 23.5 | 22.7 | 16.6 | 15.8 |
| 0.7 | 22.6 | 26.2 | 25.7 | 18.8 | 18 |
| 0.8 | 24.2 | 27.8 | 27.4 | 20 | 18.7 |
| 0.9 | 22.9 | 27.2 | 27.3 | 20.9 | 19.4 |
| 1 | 21.9 | 27.3 | 27.6 | 20.9 | 19.4 |
| 1.1 | 24.4 | 31 | 31.1 | 24.7 | 23 |
| 1.2 | 25.6 | 32.4 | 32.4 | 25.5 | 23.9 |
| 1.3 | 24.1 | 30.3 | 30.7 | 24.2 | 23 |
| 1.4 | 23.8 | 26.4 | 26.7 | 23.5 | 22.9 |
| 1.5 | 24 | 26.1 | 26.2 | 23.7 | 23 |
| 1.6 | 23.8 | 26 | 26 | 23.7 | 23.1 |
| 1.7 | 21.1 | 22.3 | 22.3 | 21 | 20.6 |
| 1.75 | 20 | 20.8 | 20.6 | 17.2 | 17.6 |
| 1.8 | 22.1 | 22 | 21.7 | 19 | 19.1 |

# Run Number AA115LSXCu

**Description of Experiment**

One bed with 115 mm prelayer of activated alumina, main layer LiLSX, PVC bed 56 second cycle, Copper Thermal Diluent Added

| Sieve Arrangement and Bed | |
|---|---|
| Type of Prelayer | AA |
| Type of Main Layer | LiLSX + Cu |
| Bed | PVC |
| Mass of Prelayer: | 0.756 kg |
| Mass of Main LSX: | 7.91 kg |
| Mass of Main Cu: | 4 kg |
| Height of Prelayer: | 115 mm |
| Height of Main layer: | 1550 mm |

| End of Step Pressures at CSS (kPa) | |
|---|---|
| Step 1 | 135.0 |
| Step 2 | 140.5 |
| Step 3 | 101.3 |
| Step 4 | 31.4 |
| Step 5 | 35.4 |

| Mass Balance at CSS (Total millimole per cycle) | | | |
|---|---|---|---|
| Feed flow | 4731.1 | Evacuation flow | 4304.2 |
| Product flow | 455.2 | Mass Balance Error (%) | -0.6 |

| Key Performance Parameters | | | |
|---|---|---|---|
| Oxygen Recovery (%) | 39.1 | BSF (kg/TPDc) | 391.4 |
| Power: (kW/TPDc) | 9.8 | Oxygen Purity (%): | 89.9 |

| End of Step CSS Temperature Profile (°C) | | | | | |
|---|---|---|---|---|---|
| z (m) | Step 1 | Step 2 | Step 3 | Step 4 | Step 5 |
| 0 | 14.2 | 14.6 | 14.2 | 12.8 | 13.1 |
| 0.1 | 6.2 | 7.6 | 6.9 | 3.8 | 3.5 |
| 0.2 | 3.9 | 5.9 | 5.4 | -2 | -2.8 |
| 0.3 | 9.6 | 10.9 | 10.5 | 3.5 | 2.7 |
| 0.4 | 12.3 | 14.7 | 14.2 | 6.2 | 5.4 |
| 0.5 | 16.3 | 18.6 | 18.2 | 12.2 | 11.2 |
| 0.6 | 17.7 | 20.4 | 20.5 | 13.2 | 12.2 |
| 0.7 | 20 | 22.7 | 22.4 | 14.7 | 13.6 |
| 0.8 | 19 | 19.9 | 19.5 | 16.6 | 16.2 |
| 0.9 | 19.9 | 23.4 | 23.2 | 17.4 | 16.2 |
| 1 | 20.8 | 24.2 | 24.4 | 18.2 | 17.2 |
| 1.1 | 22.9 | 25.2 | 25.2 | 20.6 | 20 |
| 1.2 | 22.4 | 28.8 | 28.6 | 21.6 | 20.3 |
| 1.3 | 21.9 | 28.1 | 28.3 | 21.6 | 20.4 |
| 1.4 | 22.7 | 27.3 | 27.3 | 22.1 | 21.6 |
| 1.5 | 23.7 | 26.3 | 27.3 | 23 | 22.6 |
| 1.6 | 23.7 | 25.4 | 25.4 | 23.2 | 22.7 |
| 1.7 | 22 | 24 | 24.1 | 22.5 | 21.7 |
| 1.75 | 22.9 | 25.2 | 25.3 | 23.4 | 22.7 |
| 1.8 | 21 | 23.6 | 23.7 | 20.9 | 20.3 |

# Run Number LSX1

**Description of Experiment**
One bed, no prelayer, main layer LiLSX, PVC bed, 56 second cycle

| Sieve Arrangement and Bed | |
|---|---|
| Type of Prelayer | No Prelayer |
| Type of Main Layer | LiLSX |
| Bed | PVC |
| Mass of Prelayer: | 0 kg |
| Mass of Main layer: | 9.59 kg |
| Height of Prelayer: | 0 mm |
| Height of Main layer: | 1850 mm |

| End of Step Pressures at CSS (kPa) | |
|---|---|
| Step 1 | 128.9 |
| Step 2 | 141.1 |
| Step 3 | 101.2 |
| Step 4 | 28.6 |
| Step 5 | 29.4 |

| Mass Balance at CSS (Total millimole per cycle) | | | |
|---|---|---|---|
| Feed flow | 5027.9 | Evacuation flow | 4354.1 |
| Product flow | 484.2 | Mass Balance Error (%) | 3.8 |

| Key Performance Parameters | | | |
|---|---|---|---|
| Oxygen Recovery (%) | 42.0 | BSF (kg/TPDc) | 442.8 |
| Power: (kW/TPDc) | 9.3 | Oxygen Purity (%): | 90.6 |

| End of Step CSS Temperature Profile (°C) | | | | | |
|---|---|---|---|---|---|
| z (m) | Step 1 | Step 2 | Step 3 | Step 4 | Step 5 |
| 0 | 9.8 | 9.3 | 9.1 | 6.9 | 5.5 |
| 0.1 | 12 | 13.9 | 13.3 | 6.1 | 4.2 |
| 0.2 | 17.1 | 19.4 | 19.1 | 11.9 | 10.3 |
| 0.3 | 19.8 | 22.1 | 21.9 | 14.3 | 12.7 |
| 0.4 | 22.3 | 24.2 | 24.1 | 16.3 | 14.8 |
| 0.5 | 21.4 | 24.2 | 23.9 | 16.5 | 15.4 |
| 0.6 | 21.9 | 24.3 | 24.4 | 17.8 | 16.2 |
| 0.7 | 24.2 | 27.7 | 27.5 | 20.2 | 19 |
| 0.8 | 25.8 | 29.3 | 28.9 | 21 | 20 |
| 0.9 | 23.2 | 27.6 | 27.6 | 20.8 | 19.5 |
| 1 | 22.8 | 27.4 | 27.5 | 20.5 | 19.7 |
| 1.1 | 24.6 | 31.1 | 31.2 | 23.8 | 22.7 |
| 1.2 | 25.3 | 32.3 | 32.5 | 24.8 | 23.5 |
| 1.3 | 24.7 | 31.6 | 32 | 24.4 | 23.3 |
| 1.4 | 23.1 | 27.4 | 27.4 | 22.5 | 22.1 |
| 1.5 | 23.5 | 26.7 | 27.7 | 22.5 | 22.1 |
| 1.6 | 23.7 | 25.4 | 25.3 | 22.9 | 22.5 |
| 1.7 | 22 | 24 | 24.2 | 21.9 | 21.4 |
| 1.75 | 22.8 | 25 | 25.2 | 22.8 | 22.2 |
| 1.8 | 22.4 | 24.7 | 24.8 | 22.5 | 21.9 |

# Run Number LSX2

**Description of Experiment**

One bed, no prelayer of activated alumina, main layer LiLSX, PVC, 53 second cycle (10 sec Feed Repress, 10 sec Feed, 2 sec Blowdown, 25 sec Evacuation, 6 sec Purge)

| Sieve Arrangement and Bed | |
|---|---|
| Type of Prelayer | No Prelayer |
| Type of Main Layer | LiLSX |
| Bed | PVC |
| Mass of Prelayer: | 0 kg |
| Mass of Main layer: | 9.59 kg |
| Height of Prelayer: | 0 mm |
| Height of Main layer: | 1850 mm |

| End of Step Pressures at CSS (kPa) | |
|---|---|
| Step 1 | 129.5 |
| Step 2 | 139.8 |
| Step 3 | 101.3 |
| Step 4 | 28.6 |
| Step 5 | 38.6 |

| Mass Balance at CSS (Total millimole per cycle) | | | |
|---|---|---|---|
| Feed flow | 5118.1 | Evacuation flow | 4507.5 |
| Product flow | 521.5 | Mass Balance Error (%) | 1.7 |

| Key Performance Parameters | | | |
|---|---|---|---|
| Oxygen Recovery (%) | 42.0 | BSF (kg/TPDc) | 431.9 |
| Power: (kW/TPDc) | 10.7 | Oxygen Purity (%): | 86.3 |

| End of Step CSS Temperature Profile (°C) | | | | | |
|---|---|---|---|---|---|
| z (m) | Step 1 | Step 2 | Step 3 | Step 4 | Step 5 |
| 0 | 11 | 11.1 | 10.4 | 7.6 | 7.7 |
| 0.1 | 12 | 14.2 | 13.7 | 5.6 | 4.8 |
| 0.2 | 16.5 | 19 | 18.7 | 11.4 | 10.4 |
| 0.3 | 18.7 | 21.3 | 21 | 13.2 | 12.3 |
| 0.4 | 20.6 | 23.2 | 22.8 | 14.9 | 14.2 |
| 0.5 | 20.6 | 23 | 22.7 | 15.5 | 14.7 |
| 0.6 | 21.4 | 23.6 | 23.6 | 16.9 | 16.1 |
| 0.7 | 22.9 | 26.2 | 26.4 | 19 | 17.6 |
| 0.8 | 24.6 | 27.9 | 27.7 | 19.9 | 18.8 |
| 0.9 | 22.5 | 26.5 | 26.4 | 19.7 | 18.5 |
| 1 | 22.4 | 26.4 | 26.6 | 19.9 | 18.6 |
| 1.1 | 23.6 | 29.4 | 29.8 | 22.7 | 21.1 |
| 1.2 | 24.1 | 30.6 | 30.7 | 23.3 | 22.1 |
| 1.3 | 23.7 | 30.2 | 30.4 | 23.2 | 22.1 |
| 1.4 | 22.7 | 26.4 | 26.6 | 22 | 21.5 |
| 1.5 | 23.2 | 26.6 | 27.5 | 22.1 | 21.6 |
| 1.6 | 23.6 | 25.2 | 25.3 | 22.6 | 22.2 |
| 1.7 | 21.7 | 23.9 | 24.1 | 21.6 | 20.9 |
| 1.75 | 22.5 | 24.9 | 25 | 22.3 | 21.6 |
| 1.8 | 22.2 | 24.7 | 24.9 | 22.3 | 21.4 |

# Run Number LSX3

**Description of Experiment**

One bed no prelayer of activated alumina, main layer LiLSX, PVC, 53 second cycle (10 sec Feed Repress, 10 sec Feed, 2 sec Blowdown, 25 sec Evacuation, 6 sec Purge)

| Sieve Arrangement and Bed | |
|---|---|
| Type of Prelayer | No Prelayer |
| Type of Main Layer | LiLSX |
| Bed | PVC |
| Mass of Prelayer: | 0 kg |
| Mass of Main layer: | 9.59 kg |
| Height of Prelayer: | 0 mm |
| Height of Main layer: | 1850 mm |

| End of Step Pressures at CSS (kPa) | |
|---|---|
| Step 1 | 129.3 |
| Step 2 | 139.4 |
| Step 3 | 100.4 |
| Step 4 | 30.1 |
| Step 5 | 30.8 |

| Mass Balance at CSS (Total millimole per cycle) | | | |
|---|---|---|---|
| Feed flow | 4594.4 | Evacuation flow | 4034.0 |
| Product flow | 340.0 | Mass Balance Error (%) | 4.8 |

| Key Performance Parameters | | | |
|---|---|---|---|
| Oxygen Recovery (%) | 31.7 | BSF (kg/TPDc) | 572.0 |
| Power: (kW/TPDc) | 11.2 | Oxygen Purity (%): | 93.9 |

| End of Step CSS Temperature Profile (°C) | | | | | |
|---|---|---|---|---|---|
| z (m) | Step 1 | Step 2 | Step 3 | Step 4 | Step 5 |
| 0 | 12.7 | 11.9 | 11.2 | 8.7 | 8.4 |
| 0.1 | 15.6 | 16.8 | 16.3 | 9 | 7.9 |
| 0.2 | 21.5 | 23.7 | 23.6 | 16.6 | 15.4 |
| 0.3 | 22.2 | 23.2 | 22.9 | 18.2 | 17.6 |
| 0.4 | 26.4 | 28.3 | 28.2 | 20.2 | 19.2 |
| 0.5 | 25.8 | 28.1 | 27.8 | 20.5 | 19.7 |
| 0.6 | 25.7 | 28.3 | 27.6 | 21.3 | 20.3 |
| 0.7 | 27.6 | 31.7 | 31 | 23.7 | 22.5 |
| 0.8 | 29.7 | 32.9 | 32.6 | 25 | 23.7 |
| 0.9 | 27.1 | 30.9 | 30.9 | 24.3 | 23.1 |
| 1 | 26.3 | 30.6 | 30.3 | 24.1 | 23.2 |
| 1.1 | 28.2 | 34.8 | 34.5 | 27.4 | 26 |
| 1.2 | 29 | 35.8 | 36 | 28.5 | 27.2 |
| 1.3 | 28.5 | 34.9 | 35.6 | 28.3 | 27.2 |
| 1.4 | 26.1 | 28.7 | 29.6 | 25.5 | 25.2 |
| 1.5 | 25.5 | 27.2 | 27.2 | 24.8 | 24.4 |
| 1.6 | 25.4 | 26.6 | 26.6 | 24.7 | 24.5 |
| 1.7 | 23.7 | 25.1 | 25.2 | 23.5 | 23.1 |
| 1.75 | 24.3 | 25.8 | 25.9 | 24.1 | 23.7 |
| 1.8 | 23.9 | 25.4 | 25.4 | 23.7 | 23.3 |

# Run Number NaX300LSX1

**Description of Experiment**

One bed with 300 mm prelayer of NaX, main layer LiLSX, PVC bed, 56 second cycle

| Sieve Arrangement and Bed | |
|---|---|
| Type of Prelayer | NaX |
| Type of Main Layer | LiLSX |
| Bed | PVC |
| Mass of Prelayer: | 1.54 kg |
| Mass of Main layer: | 7.88 kg |
| Height of Prelayer: | 300 mm |
| Height of Main layer: | 1550 mm |

| End of Step Pressures at CSS (kPa) | |
|---|---|
| Step 1 | 135.8 |
| Step 2 | 140.7 |
| Step 3 | 101.3 |
| Step 4 | 41.0 |
| Step 5 | 45.4 |

| Mass Balance at CSS (Total millimole per cycle) | | | |
|---|---|---|---|
| Feed flow | 4232.8 | Evacuation flow | 3764.8 |
| Product flow | 336.4 | Mass Balance Error (%) | 3.1 |

| Key Performance Parameters | | | |
|---|---|---|---|
| Oxygen Recovery (%) | 33.0 | BSF (kg/TPDc) | 536.0 |
| Power: (kW/TPDc) | 10.2 | Oxygen Purity (%): | 88.5 |

| End of Step CSS Temperature Profile (°C) | | | | | |
|---|---|---|---|---|---|
| z (m) | Step 1 | Step 2 | Step 3 | Step 4 | Step 5 |
| 0 | 10.1 | 9.7 | 9.5 | 9.5 | 9.7 |
| 0.1 | 12.7 | 13.6 | 13.1 | 9.7 | 9.9 |
| 0.2 | 12.1 | 13.6 | 13.3 | 9.6 | 8.9 |
| 0.3 | 9.4 | 10.9 | 10.3 | 4.6 | 4.2 |
| 0.4 | 12.5 | 14 | 13.4 | 8.1 | 7 |
| 0.5 | 13.9 | 15.6 | 15.1 | 9.8 | 8.8 |
| 0.6 | 15.4 | 16.9 | 16.9 | 11.6 | 10.6 |
| 0.7 | 16.3 | 19 | 19.1 | 13.1 | 12.2 |
| 0.8 | 17.8 | 20.5 | 20.2 | 13.9 | 13.1 |
| 0.9 | 17.7 | 20.6 | 20.5 | 15.2 | 13.9 |
| 1 | 17.2 | 20.2 | 20.4 | 14.8 | 13.9 |
| 1.1 | 18.3 | 22.3 | 22.5 | 16.9 | 16 |
| 1.2 | 19.2 | 23.4 | 23.3 | 17.9 | 16.9 |
| 1.3 | 18.4 | 22.2 | 22.3 | 17.6 | 16.6 |
| 1.4 | 18.4 | 21 | 21 | 17.6 | 17.1 |
| 1.5 | 19 | 21.7 | 22 | 18.1 | 17.3 |
| 1.6 | 19.5 | 21.7 | 21.8 | 18.8 | 18.1 |
| 1.7 | 18.1 | 20.7 | 20.9 | 18.6 | 17.6 |
| 1.75 | 18.6 | 21.2 | 21.4 | 19 | 18.1 |
| 1.8 | 19.2 | 22.2 | 22.5 | 20.5 | 19.1 |

# Run Number NaX300LSX2

**Description of Experiment**

One bed with 300 mm prelayer of NaX, main layer LiLSX, PVC bed
56 second cycle

| Sieve Arrangement and Bed | |
|---|---|
| Type of Prelayer | NaX |
| Type of Main Layer | LiLSX |
| Bed | PVC |
| Mass of Prelayer: | 1.54 kg |
| Mass of Main layer: | 7.88 kg |
| Height of Prelayer: | 300 mm |
| Height of Main layer: | 1550 mm |

| End of Step Pressures at CSS (kPa) | |
|---|---|
| Step 1 | 136.1 |
| Step 2 | 140.8 |
| Step 3 | 101.3 |
| Step 4 | 29.3 |
| Step 5 | 33.6 |

| Mass Balance at CSS (Total millimole per cycle) | | | |
|---|---|---|---|
| Feed flow | 4803.6 | Evacuation flow | 4378.4 |
| Product flow | 441.4 | Mass Balance Error (%) | -0.3 |

| Key Performance Parameters | | | |
|---|---|---|---|
| Oxygen Recovery (%) | 38.1 | BSF (kg/TPDc) | 395.2 |
| Power: (kW/TPDc) | 10.4 | Oxygen Purity (%): | 91.5 |

| End of Step CSS Temperature Profile (°C) | | | | | |
|---|---|---|---|---|---|
| z (m) | Step 1 | Step 2 | Step 3 | Step 4 | Step 5 |
| 0 | 12.7 | 12.8 | 12.2 | 11.9 | 11.6 |
| 0.1 | 15.9 | 17.3 | 16.9 | 12.8 | 12.3 |
| 0.2 | 15 | 16.7 | 16.5 | 11.6 | 10.9 |
| 0.3 | 10.8 | 13 | 12.4 | 5.1 | 4 |
| 0.4 | 14.9 | 17 | 16.5 | 9.6 | 8.1 |
| 0.5 | 17.3 | 19 | 18.9 | 11.8 | 11 |
| 0.6 | 19 | 20.8 | 20.8 | 14.3 | 13.3 |
| 0.7 | 20.8 | 23.9 | 23.7 | 16.8 | 15.4 |
| 0.8 | 22.8 | 25.7 | 25.2 | 18.1 | 16.8 |
| 0.9 | 22.7 | 25.9 | 25.9 | 19.4 | 18.4 |
| 1 | 22 | 26 | 25.7 | 19 | 18.5 |
| 1.1 | 23.8 | 28.9 | 29 | 22.3 | 21.2 |
| 1.2 | 24.4 | 30.2 | 30.4 | 23.7 | 22.6 |
| 1.3 | 23.4 | 28.6 | 28.7 | 23.3 | 22.1 |
| 1.4 | 23.4 | 27.3 | 27.2 | 23 | 22.3 |
| 1.5 | 24.3 | 28.6 | 29 | 23.5 | 22.9 |
| 1.6 | 24.6 | 26.8 | 27.2 | 24 | 23.5 |
| 1.7 | 23.3 | 25.4 | 25.5 | 23.5 | 22.7 |
| 1.75 | 23.7 | 26.1 | 26.2 | 23.9 | 23.2 |
| 1.8 | 24.4 | 26.5 | 26.7 | 25 | 24 |

# Run Number NaX300LSX3

**Description of Experiment**

One bed with 300 mm prelayer of NaX, main layer LiLSX, PVC bed

56 second cycle

| Sieve Arrangement and Bed | |
|---|---|
| Type of Prelayer | NaX |
| Type of Main Layer | LiLSX |
| Bed | PVC |
| Mass of Prelayer: | 1.54 kg |
| Mass of Main layer: | 7.88 kg |
| Height of Prelayer: | 300 mm |
| Height of Main layer: | 1550 mm |

| End of Step Pressures at CSS (kPa) | |
|---|---|
| Step 1 | 135.5 |
| Step 2 | 139.7 |
| Step 3 | 101.4 |
| Step 4 | 32.4 |
| Step 5 | 37.8 |

| Mass Balance at CSS (Total millimole per cycle) | | | |
|---|---|---|---|
| Feed flow | 4738.6 | Evacuation flow | 4314.5 |
| Product flow | 406.6 | Mass Balance Error (%) | 0.4 |

| Key Performance Parameters | | | |
|---|---|---|---|
| Oxygen Recovery (%) | 36.3 | BSF (kg/TPDc) | 423.5 |
| Power: (kW/TPDc) | 10.3 | Oxygen Purity (%): | 92.7 |

| End of Step CSS Temperature Profile (°C) | | | | | |
|---|---|---|---|---|---|
| z (m) | Step 1 | Step 2 | Step 3 | Step 4 | Step 5 |
| 0 | 12.5 | 11.9 | 11.2 | 11 | 10.7 |
| 0.025 | 13.8 | 14.8 | 14.4 | 10.2 | 9.6 |
| 0.05 | 14.7 | 15.4 | 15 | 11 | 10.3 |
| 0.075 | 14.8 | 16 | 15.4 | 11.5 | 10.9 |
| 0.1 | 14.8 | 15.9 | 15 | 11.3 | 10.6 |
| 0.2 | 12.6 | 14.2 | 13.8 | 9.2 | 8.3 |
| 0.3 | 8.5 | 10.6 | 9.7 | 3.1 | 2.1 |
| 0.4 | 12.7 | 14.2 | 13.7 | 7.1 | 5.9 |
| 0.5 | 14.9 | 16.7 | 16.5 | 10.1 | 9.1 |
| 0.6 | 16.9 | 18.8 | 18.5 | 12.8 | 12 |
| 0.7 | 18.7 | 21.7 | 21.1 | 14.4 | 13.2 |
| 0.8 | 20.4 | 23 | 22.9 | 15.7 | 14.6 |
| 0.9 | 20.1 | 23.7 | 23.6 | 17.5 | 15.9 |
| 1 | 19.9 | 23.9 | 23.6 | 17.5 | 16.1 |
| 1.1 | 21.4 | 26.7 | 26.7 | 20.9 | 19.1 |
| 1.2 | 22.5 | 28.4 | 28.5 | 22.3 | 20.9 |
| 1.3 | 21.8 | 27.3 | 27.4 | 22 | 20.7 |
| 1.4 | 22.1 | 26.4 | 26.3 | 22 | 21.2 |
| 1.5 | 22.8 | 27.3 | 28 | 22.5 | 21.8 |
| 1.6 | 23.1 | 25 | 25 | 22.7 | 22.2 |
| 1.7 | 21.7 | 23.5 | 23.5 | 21.8 | 21.3 |
| 1.75 | 22.1 | 24.1 | 24.1 | 22.3 | 21.8 |
| 1.8 | 22.5 | 24.2 | 24.3 | 22.8 | 22.2 |

# Run Number NaX300LSX4

**Description of Experiment**
One bed with 300 mm prelayer of activated alumina, main layer LiLSX, PVC, 56 second cycle

| Sieve Arrangement and Bed | |
|---|---|
| Type of Prelayer | NaX |
| Type of Main Layer | LiLSX |
| Bed | PVC |
| Mass of Prelayer: | 1.54 kg |
| Mass of Main layer: | 7.88 kg |
| Height of Prelayer: | 300 mm |
| Height of Main layer: | 1550 mm |

| End of Step Pressures at CSS (kPa) | |
|---|---|
| Step 1 | 135.6 |
| Step 2 | 140.2 |
| Step 3 | 101.3 |
| Step 4 | 41.0 |
| Step 5 | 45.4 |

| Mass Balance at CSS (Total millimole per cycle) | | | |
|---|---|---|---|
| Feed flow | 4197.1 | Evacuation flow | 3806.6 |
| Product flow | 323.7 | Mass Balance Error (%) | 1.6 |

| Key Performance Parameters | | | |
|---|---|---|---|
| Oxygen Recovery (%) | 31.3 | BSF (kg/TPDc) | 561.6 |
| Power: (kW/TPDc) | 10.1 | Oxygen Purity (%): | 87.8 |

| End of Step CSS Temperature Profile (°C) | | | | | |
|---|---|---|---|---|---|
| z (m) | Step 1 | Step 2 | Step 3 | Step 4 | Step 5 |
| 0 | 12.5 | 11.9 | 11.2 | 11 | 10.7 |
| 0.025 | 13.8 | 14.8 | 14.4 | 10.2 | 9.6 |
| 0.05 | 14.7 | 15.4 | 15 | 11 | 10.3 |
| 0.075 | 14.8 | 16 | 15.4 | 11.5 | 10.9 |
| 0.1 | 14.8 | 15.9 | 15 | 11.3 | 10.6 |
| 0.2 | 12.6 | 14.2 | 13.8 | 9.2 | 8.3 |
| 0.3 | 8.5 | 10.6 | 9.7 | 3.1 | 2.1 |
| 0.4 | 12.7 | 14.2 | 13.7 | 7.1 | 5.9 |
| 0.5 | 14.9 | 16.7 | 16.5 | 10.1 | 9.1 |
| 0.6 | 16.9 | 18.8 | 18.5 | 12.8 | 12 |
| 0.7 | 18.7 | 21.7 | 21.1 | 14.4 | 13.2 |
| 0.8 | 20.4 | 23 | 22.9 | 15.7 | 14.6 |
| 0.9 | 20.1 | 23.7 | 23.6 | 17.5 | 15.9 |
| 1 | 19.9 | 23.9 | 23.6 | 17.5 | 16.1 |
| 1.1 | 21.4 | 26.7 | 26.7 | 20.9 | 19.1 |
| 1.2 | 22.5 | 28.4 | 28.5 | 22.3 | 20.9 |
| 1.3 | 21.8 | 27.3 | 27.4 | 22 | 20.7 |
| 1.4 | 22.1 | 26.4 | 26.3 | 22 | 21.2 |
| 1.5 | 22.8 | 27.3 | 28 | 22.5 | 21.8 |
| 1.6 | 23.1 | 25 | 25 | 22.7 | 22.2 |
| 1.7 | 21.7 | 23.5 | 23.5 | 21.8 | 21.3 |
| 1.75 | 22.1 | 24.1 | 24.1 | 22.3 | 21.8 |
| 1.8 | 22.5 | 24.2 | 24.3 | 22.8 | 22.2 |

# Run Number NaX300LSX5

**Description of Experiment**

One bed with 300 mm prelayer of NaX, main layer LiLSX, PVC bed, 56 second cycle

| Sieve Arrangement and Bed | |
|---|---|
| Type of Prelayer | NaX |
| Type of Main Layer | LiLSX |
| Bed | PVC |
| Mass of Prelayer: | 1.54 kg |
| Mass of Main layer: | 7.88 kg |
| Height of Prelayer: | 300 mm |
| Height of Main layer: | 1550 mm |

| End of Step Pressures at CSS (kPa) | |
|---|---|
| Step 1 | 135.1 |
| Step 2 | 140.8 |
| Step 3 | 101.2 |
| Step 4 | 40.6 |
| Step 5 | 44.2 |

| Mass Balance at CSS (Total millimole per cycle) | | | |
|---|---|---|---|
| Feed flow | 4357.0 | Evacuation flow | 3797.7 |
| Product flow | 623.9 | Mass Balance Error (%) | -1.5 |

| Key Performance Parameters | | | |
|---|---|---|---|
| Oxygen Recovery (%) | 38.8 | BSF (kg/TPDc) | 422.9 |
| Power: (kW/TPDc) | 7.5 | Oxygen Purity (%): | 60.5 |

| End of Step CSS Temperature Profile (°C) | | | | | |
|---|---|---|---|---|---|
| z (m) | Step 1 | Step 2 | Step 3 | Step 4 | Step 5 |
| 0 | 12.5 | 12.4 | 12.1 | 10.5 | 11.1 |
| 0.025 | 12.7 | 13.9 | 13.4 | 9.9 | 9.4 |
| 0.05 | 13.4 | 15 | 14.1 | 10.3 | 10.3 |
| 0.075 | 14 | 15.2 | 14.9 | 11.3 | 10.8 |
| 0.1 | 14.6 | 15.6 | 14.6 | 11 | 11.3 |
| 0.2 | 14.8 | 16.2 | 15.9 | 12.1 | 11.7 |
| 0.3 | 12.6 | 14.2 | 13.5 | 7.9 | 7.4 |
| 0.4 | 14.8 | 16.4 | 15.9 | 9.5 | 9.3 |
| 0.5 | 14.6 | 16.3 | 16.1 | 10.7 | 10.2 |
| 0.6 | 15.4 | 17.1 | 17 | 12.3 | 11.6 |
| 0.7 | 16.1 | 19 | 18.7 | 13.2 | 12.2 |
| 0.8 | 17.4 | 20.2 | 19.6 | 13.7 | 13.2 |
| 0.9 | 16.7 | 19.5 | 19.5 | 14.4 | 13.7 |
| 1 | 16.7 | 19.4 | 19.4 | 14.6 | 13.8 |
| 1.1 | 17.2 | 20.9 | 20.7 | 15.6 | 15.1 |
| 1.2 | 18.2 | 21.6 | 21.4 | 16.3 | 15.8 |
| 1.3 | 17.5 | 20.5 | 20.5 | 16 | 15.5 |
| 1.4 | 17.8 | 19.6 | 19.4 | 16.4 | 16.1 |
| 1.5 | 18.3 | 20.5 | 20.4 | 16.7 | 16 |
| 1.6 | 19 | 21 | 21 | 17.7 | 16.9 |
| 1.7 | 16.8 | 20.2 | 20.3 | 17.3 | 15.9 |
| 1.75 | 17.3 | 21 | 21 | 17.9 | 16.6 |
| 1.8 | 17.7 | 22.4 | 22.4 | 19.4 | 17.5 |

# Run Number LSX300NaX1

**Description of Experiment**
One bed with 300 mm prelayer of LiLSX, main layer NaX, PVC bed
56 second cycle

| Sieve Arrangement and Bed | |
|---|---|
| Type of Prelayer | LiLSX |
| Type of Main Layer | NaX |
| Bed | PVC |
| Mass of Prelayer: | 1.526 kg |
| Mass of Main layer: | 8.6 kg |
| Height of Prelayer: | 300 mm |
| Height of Main layer: | 1550 mm |

| End of Step Pressures at CSS (kPa) | |
|---|---|
| Step 1 | 138.7 |
| Step 2 | 141.4 |
| Step 3 | 101.2 |
| Step 4 | 38.1 |
| Step 5 | 44.3 |

| Mass Balance at CSS (Total millimole per cycle) | | | |
|---|---|---|---|
| Feed flow | 3754.0 | Evacuation flow | 3453.7 |
| Product flow | 208.0 | Mass Balance Error (%) | 2.5 |

| Key Performance Parameters | | | |
|---|---|---|---|
| Oxygen Recovery (%) | 23.2 | BSF (kg/TPDc) | 932.8 |
| Power: (kW/TPDc) | 16.1 | Oxygen Purity (%): | 89.8 |

| End of Step CSS Temperature Profile (°C) | | | | | |
|---|---|---|---|---|---|
| z (m) | Step 1 | Step 2 | Step 3 | Step 4 | Step 5 |
| 0 | 11.9 | 11.9 | 11.5 | 11.1 | 11.3 |
| 0.025 | 13.4 | 15.1 | 14.5 | 8.6 | 7.7 |
| 0.05 | 14.9 | 16.6 | 16.1 | 10.4 | 9.5 |
| 0.1 | 16.2 | 17.6 | 16.8 | 11.8 | 11.1 |
| 0.2 | 20.6 | 22.4 | 22.1 | 16.8 | 16 |
| 0.3 | 25.9 | 27.2 | 26.4 | 21.9 | 21.4 |
| 0.4 | 26.6 | 27.4 | 27 | 23.1 | 22.9 |
| 0.5 | 23.7 | 24.4 | 24 | 20.6 | 20.2 |
| 0.6 | 22.2 | 22.8 | 22.9 | 19.8 | 19.4 |
| 0.7 | 21.8 | 23.2 | 23 | 20.1 | 19.6 |
| 0.8 | 21.9 | 22.8 | 22.5 | 19.7 | 19.3 |
| 0.9 | 19.3 | 20.9 | 21.1 | 17.6 | 17 |
| 1 | 19.3 | 20.6 | 20.6 | 17.3 | 16.8 |
| 1.1 | 19 | 21 | 20.8 | 17.7 | 17 |
| 1.2 | 19.1 | 21.3 | 21.2 | 17.8 | 17.1 |
| 1.3 | 18.1 | 20.5 | 20.5 | 17.2 | 16.6 |
| 1.4 | 17.5 | 19.2 | 19.1 | 16.6 | 16.3 |
| 1.5 | 17.9 | 19.9 | 19.8 | 17.1 | 16.7 |
| 1.6 | 17.6 | 19.9 | 20.1 | 17.5 | 16.8 |
| 1.7 | 16.1 | 17.8 | 17.9 | 16.2 | 15.6 |
| 1.75 | 16.8 | 18.8 | 18.9 | 16.9 | 16.3 |
| 1.8 | 17.3 | 19.1 | 19.1 | 17.4 | 16.8 |
| 1.8 | 17.7 | 22.4 | 22.4 | 19.4 | 17.5 |

# Run Number LSX300NaX2

**Description of Experiment**

One bed with 300 mm prelayer of LiLSX, main layer NaX, PVC bed
56 second cycle

| Sieve Arrangement and Bed | |
|---|---|
| Type of Prelayer | LiLSX |
| Type of Main Layer | NaX |
| Bed | PVC |
| Mass of Prelayer: | 1.526 kg |
| Mass of Main layer: | 8.6 kg |
| Height of Prelayer: | 300 mm |
| Height of Main layer: | 1550 mm |

| End of Step Pressures at CSS (kPa) | |
|---|---|
| Step 1 | 137.3 |
| Step 2 | 140.1 |
| Step 3 | 101.3 |
| Step 4 | 39.5 |
| Step 5 | 45.5 |

| Mass Balance at CSS (Total millimole per cycle) | | | |
|---|---|---|---|
| Feed flow | 3589.0 | Evacuation flow | 3345.5 |
| Product flow | 203 0 | Mass Balance Error (%) | 1.1 |

| Key Performance Parameters | | | |
|---|---|---|---|
| Oxygen Recovery (%) | 23.2 | BSF (kg/TPDc) | 961.1 |
| Power: (kW/TPDc) | 14.5 | Oxygen Purity (%): | 89.3 |

| End of Step CSS Temperature Profile (°C) | | | | | |
|---|---|---|---|---|---|
| z (m) | Step 1 | Step 2 | Step 3 | Step 4 | Step 5 |
| 0 | 13.2 | 13.8 | 13.4 | 13.1 | 13.1 |
| 0.025 | 15.1 | 16.8 | 15.9 | 10.3 | 9.6 |
| 0.05 | 16.5 | 18.6 | 17.5 | 12.1 | 11.3 |
| 0.075 | 17.3 | 19.5 | 18.8 | 13 | 12.3 |
| 0.1 | 18 | 19.3 | 18.9 | 13.5 | 13.1 |
| 0.2 | 21.4 | 23.5 | 23.2 | 18.3 | 17.4 |
| 0.3 | 27.1 | 28.1 | 27.8 | 23 | 22.9 |
| 0.4 | 27.2 | 28.4 | 28.2 | 24.5 | 24 |
| 0.5 | 24.8 | 25.5 | 25.4 | 22 | 21.8 |
| 0.6 | 23.3 | 24.2 | 24.5 | 21 | 20.9 |
| 0.7 | 23.2 | 24.4 | 24.5 | 21 | 20.5 |
| 0.8 | 22.7 | 23.8 | 23.5 | 20.7 | 20.5 |
| 0.9 | 20.2 | 21.9 | 21.9 | 18.7 | 18.1 |
| 1 | 20.3 | 21.5 | 21.5 | 18.5 | 18 |
| 1.1 | 20 | 21.8 | 21.7 | 18.6 | 18.1 |
| 1.2 | 20 | 22.2 | 22 | 18.6 | 18.2 |
| 1.3 | 19.2 | 21.4 | 21.5 | 18.4 | 17.8 |
| 1.4 | 18.9 | 20.4 | 20.4 | 18 | 17.7 |
| 1.5 | 19.3 | 21.1 | 21.2 | 18.6 | 18.2 |
| 1.6 | 19.1 | 21.2 | 21.5 | 19 | 18.4 |
| 1.7 | 17.6 | 19.2 | 19.4 | 17.6 | 17.1 |
| 1.75 | 18.3 | 20.1 | 20.3 | 18.4 | 17.8 |
| 1.8 | 18.8 | 20.5 | 20.6 | 18.9 | 18.3 |

# Run Number LSX300NaX3

**Description of Experiment**

One bed with 300 mm prelayer of LiLSX, main layer NaX, PVC bed

56 second cycle

| Sieve Arrangement and Bed | |
|---|---|
| Type of Prelayer | LiLSX |
| Type of Main Layer | NaX |
| Bed | PVC |
| Mass of Prelayer: | 1.526 kg |
| Mass of Main layer: | 8.6 kg |
| Height of Prelayer: | 300 mm |
| Height of Main layer: | 1550 mm |

| End of Step Pressures at CSS (kPa) | |
|---|---|
| Step 1 | 134.9 |
| Step 2 | 140.5 |
| Step 3 | 101.0 |
| Step 4 | 30.5 |
| Step 5 | 33.6 |

| Mass Balance at CSS (Total millimole per cycle) | | | |
|---|---|---|---|
| Feed flow | 4004.2 | Evacuation flow | 3741.5 |
| Product flow | 318.3 | Mass Balance Error (%) | -1.4 |

| Key Performance Parameters | | | |
|---|---|---|---|
| Oxygen Recovery (%) | 28.5 | BSF (kg/TPDc) | 683.2 |
| Power: (kW/TPDc) | 12.8 | Oxygen Purity (%): | 80.1 |

| End of Step CSS Temperature Profile (°C) | | | | | |
|---|---|---|---|---|---|
| z (m) | Step 1 | Step 2 | Step 3 | Step 4 | Step 5 |
| 0 | 11 | 10.7 | 10.5 | 9.6 | 9.2 |
| 0.1 | 15.5 | 16.7 | 16.2 | 9.5 | 8.5 |
| 0.2 | 18.8 | 20.8 | 20.7 | 14.7 | 13.5 |
| 0.3 | 24.7 | 25.9 | 25.5 | 19.9 | 19.3 |
| 0.4 | 26.3 | 27.1 | 26.9 | 22.9 | 22.1 |
| 0.5 | 23.6 | 24.8 | 24.4 | 20.7 | 20.4 |
| 0.6 | 22.7 | 23.8 | 23.7 | 20.4 | 20 |
| 0.7 | 23.1 | 24.2 | 24.5 | 20.9 | 20.4 |
| 0.8 | 23.2 | 23.9 | 23.9 | 20.8 | 20.7 |
| 0.9 | 21 | 22.8 | 22.6 | 19.1 | 18.7 |
| 1 | 21 | 22.5 | 22.4 | 19 | 18.4 |
| 1.1 | 21.1 | 23.2 | 22.9 | 19.2 | 18.8 |
| 1.2 | 21 | 23.5 | 23.4 | 19.7 | 19.2 |
| 1.3 | 19.9 | 22.2 | 22.3 | 18.9 | 18.3 |
| 1.4 | 18.8 | 20.5 | 20.4 | 17.8 | 17.3 |
| 1.5 | 19.1 | 21.1 | 21 | 18.4 | 17.9 |
| 1.6 | 19.1 | 21.8 | 21.9 | 19.1 | 18.2 |
| 1.7 | 17.7 | 20.1 | 20.3 | 18 | 17.1 |
| 1.75 | 18.7 | 21.2 | 21.4 | 18.9 | 18.1 |
| 1.8 | 19.4 | 21.9 | 22 | 19.7 | 18.8 |
| 1.7 | 17.6 | 19.2 | 19.4 | 17.6 | 17.1 |
| 1.75 | 18.3 | 20.1 | 20.3 | 18.4 | 17.8 |
| 1.8 | 18.8 | 20.5 | 20.6 | 18.9 | 18.3 |

# Run Number PL100LSX1

**Description of Experiment**

One bed with 100 mm prelayer of plastic, main layer LiLSX, PVC bed
56 second cycle

| Sieve Arrangement and Bed | |
|---|---|
| Type of Prelayer | Plastic |
| Type of Main Layer | LiLSX |
| Bed | PVC |
| Mass of Prelayer: | 0.2 kg |
| Mass of Main layer: | 7.9 kg |
| Height of Prelayer: | 100 mm |
| Height of Main layer: | 1550 mm |

| End of Step Pressures at CSS (kPa) | |
|---|---|
| Step 1 | 136.1 |
| Step 2 | 140.0 |
| Step 3 | 101.2 |
| Step 4 | 31.4 |
| Step 5 | 34.6 |

| Mass Balance at CSS (Total millimole per cycle) | | | |
|---|---|---|---|
| Feed flow | 4614.7 | Evacuation flow | 4201.3 |
| Product flow | 434.1 | Mass Balance Error (%) | -0.4 |

| Key Performance Parameters | | | |
|---|---|---|---|
| Oxygen Recovery (%) | 38.0 | BSF (kg/TPDc) | 413.2 |
| Power: (kW/TPDc) | 9.9 | Oxygen Purity (%): | 89.2 |

| End of Step CSS Temperature Profile (°C) | | | | | |
|---|---|---|---|---|---|
| z (m) | Step 1 | Step 2 | Step 3 | Step 4 | Step 5 |
| 0 | 12.4 | 12.7 | 12.4 | 10.8 | 11.3 |
| 0.025 | 12.3 | 12.8 | 12.1 | 8.8 | 8.2 |
| 0.05 | 12 | 13.4 | 12.3 | 7.5 | 7 |
| 0.075 | 10.5 | 12 | 11.6 | 7.4 | 6.7 |
| 0.1 | 12.5 | 13.3 | 12.7 | 7 | 6.5 |
| 0.2 | 12.7 | 15.4 | 15 | 8.2 | 7.1 |
| 0.3 | 16.6 | 18.4 | 17.8 | 10.5 | 9.6 |
| 0.4 | 19.2 | 21.5 | 21 | 13.4 | 12.5 |
| 0.5 | 19.6 | 21.5 | 20.9 | 14.6 | 13.4 |
| 0.6 | 20.1 | 22.3 | 21.8 | 15.6 | 14.5 |
| 0.7 | 21.3 | 24.5 | 24.6 | 17.4 | 16.1 |
| 0.8 | 23.4 | 26.5 | 26.1 | 19.2 | 18.1 |
| 0.9 | 22.3 | 25.9 | 26.1 | 20 | 18.8 |
| 1 | 21.9 | 26.3 | 26.5 | 20.2 | 18.9 |
| 1.1 | 23.1 | 29.3 | 29.3 | 23.1 | 21.6 |
| 1.2 | 24.1 | 30.4 | 30.4 | 23.9 | 22.4 |
| 1.3 | 23.6 | 29.5 | 29.6 | 23.5 | 22.3 |
| 1.4 | 23 | 26.5 | 26.8 | 22.4 | 22 |
| 1.5 | 23.1 | 24.9 | 24.9 | 22.7 | 22 |
| 1.6 | 22.4 | 24.5 | 24.6 | 22.2 | 21.6 |
| 1.7 | 21.9 | 20.7 | 20.5 | 17.4 | 18.6 |
| 1.75 | 22.8 | 22.1 | 21.8 | 18.4 | 19.3 |
| 1.8 | 27.5 | 24.6 | 24.3 | 22.7 | 22.9 |

# Run Number AA300LSXPU1

**Description of Experiment**

One bed with 300 mm prelayer of activated alumina, main layer LiLSX, Polyurethane Bed
56 second cycle

| Sieve Arrangement and Bed | |
|---|---|
| Type of Prelayer | AA |
| Type of Main Layer | LiLSX |
| Bed | PU |
| Mass of Prelayer: | 1.69 kg |
| Mass of Main layer: | 6.87 kg |
| Height of Prelayer: | 300 mm |
| Height of Main layer: | 1500 mm |

| End of Step Pressures at CSS (kPa) | |
|---|---|
| Step 1 | 120.5 |
| Step 2 | 124.3 |
| Step 3 | 100.5 |
| Step 4 | 40.0 |
| Step 5 | 44.2 |

| Mass Balance at CSS (Total millimole per cycle) | | | |
|---|---|---|---|
| Feed flow | 3217.7 | Evacuation flow | 3042.7 |
| Product flow | 174.0 | Mass Balance Error (%) | 0.0 |

| Key Performance Parameters | | | |
|---|---|---|---|
| Oxygen Recovery (%) | 23.0 | BSF (kg/TPDc) | 856.2 |
| Power: (kW/TPDc) | 15.7 | Oxygen Purity (%): | 93.4 |

| End of Step CSS Temperature Profile (°C) | | | | | |
|---|---|---|---|---|---|
| z (m) | Step 1 | Step 2 | Step 3 | Step 4 | Step 5 |
| 0 | 13 | 12.7 | 12.9 | 12.7 | 12.6 |
| 0.245 | -8.1 | -7.2 | -7.7 | -10.2 | -10.8 |
| 0.395 | -2 | -0.4 | -0.4 | -5.7 | -6.9 |
| 0.545 | 8.1 | 9.4 | 9.6 | 4.5 | 3.4 |
| 0.945 | 19.6 | 19.6 | 19.7 | 19.6 | 19.5 |
| 1.345 | 25 | 27.6 | 28.1 | 24.9 | 24.2 |
| 1.8 | 18.3 | 18.8 | 18.6 | 16.8 | 16.6 |

# Run Number AA300LSXPU2

**Description of Experiment**

One bed with 300 mm prelayer of activated alumina, main layer LiLSX, Polyurethane Bed
56 second cycle

| Sieve Arrangement and Bed | |
|---|---|
| Type of Prelayer | AA |
| Type of Main Layer | LiLSX |
| Bed | PU |
| Mass of Prelayer: | 1.69 kg |
| Mass of Main layer: | 6.87 kg |
| Height of Prelayer: | 300 mm |
| Height of Main layer: | 1500 mm |

| End of Step Pressures at CSS (kPa) | |
|---|---|
| Step 1 | 119.4 |
| Step 2 | 124.3 |
| Step 3 | 100.6 |
| Step 4 | 41.0 |
| Step 5 | 51.5 |

| Mass Balance at CSS (Total millimole per cycle) | | | |
|---|---|---|---|
| Feed flow | 3159.5 | Evacuation flow | 3117.6 |
| Product flow | 87.19 | Mass Balance Error (%) | -1.4 |

| Key Performance Parameters | | | |
|---|---|---|---|
| Oxygen Recovery (%) | 11.5 | BSF (kg/TPDc) | 1717.0 |
| Power: (kW/TPDc) | 15.7 | Oxygen Purity (%): | 93.0 |

| End of Step CSS Temperature Profile (°C) | | | | | |
|---|---|---|---|---|---|
| z (m) | Step 1 | Step 2 | Step 3 | Step 4 | Step 5 |
| 0 | 13.7 | 13.7 | 13.4 | 12.9 | 13.4 |
| 0.245 | -5.6 | -4.8 | -5.3 | -7.6 | -8.1 |
| 0.395 | 7.7 | 9 | 9.1 | 4 | 3 |
| 0.545 | 17.6 | 19.4 | 19.4 | 14.6 | 13.5 |
| 1.345 | 9.7 | 11.4 | 11.7 | 9.4 | 9.6 |
| 1.8 | 15.4 | 15.8 | 15.7 | 13.7 | 14 |

# Run Number AA300LSXPU3

**Description of Experiment**

One bed with 300 mm prelayer of activated alumina, main layer LiLSX, Polyurethane Bed
56 second cycle

| Sieve Arrangement and Bed | |
|---|---|
| Type of Prelayer | AA |
| Type of Main Layer | LiLSX |
| Bed | PU |
| Mass of Prelayer: | 1.69 kg |
| Mass of Main layer: | 6.87 kg |
| Height of Prelayer: | 300 mm |
| Height of Main layer: | 1500 mm |

| End of Step Pressures at CSS (kPa) | |
|---|---|
| Step 1 | 134.8 |
| Step 2 | 140.0 |
| Step 3 | 101.1 |
| Step 4 | 40.9 |
| Step 5 | 43.3 |

| Mass Balance at CSS (Total millimole per cycle) | | | |
|---|---|---|---|
| Feed flow | 3902.1 | Evacuation flow | 3520.4 |
| Product flow | 315.6 | Mass Balance Error (%) | 1.7 |

| Key Performance Parameters | | | |
|---|---|---|---|
| Oxygen Recovery (%) | 32.4 | BSF (kg/TPDc) | 509.1 |
| Power: (kW/TPDc) | 9.1 | Oxygen Purity (%): | 86.6 |

| End of Step CSS Temperature Profile (°C) | | | | | |
|---|---|---|---|---|---|
| z (m) | Step 1 | Step 2 | Step 3 | Step 4 | Step 5 |
| 0 | 13.9 | 14.3 | 14.4 | 13.7 | 14.3 |
| 0.245 | -2.9 | -1.8 | -2.8 | -5.5 | -6.2 |
| 0.395 | 0.7 | 1.1 | 0.3 | -5 | -6.2 |
| 0.545 | 6.3 | 7.8 | 7.2 | 2.5 | 1.7 |
| 1.345 | 24.4 | 29.8 | 30.1 | 24.3 | 23 |
| 1.8 | 23.3 | 24.4 | 24.3 | 21.6 | 21.3 |

# Run Number AA300LSXPU4

**Description of Experiment**

One bed with 300 mm prelayer of activated alumina, main layer LiLSX, Polyurethane Bed
56 second cycle

| Sieve Arrangement and Bed | |
|---|---|
| Type of Prelayer | AA |
| Type of Main Layer | LiLSX |
| Bed | PU |
| Mass of Prelayer: | 1.69 kg |
| Mass of Main layer: | 6.87 kg |
| Height of Prelayer: | 300 mm |
| Height of Main layer: | 1500 mm |

| End of Step Pressures at CSS (kPa) | |
|---|---|
| Step 1 | 134.2 |
| Step 2 | 139.2 |
| Step 3 | 100.9 |
| Step 4 | 30.1 |
| Step 5 | 34.0 |

| Mass Balance at CSS (Total millimole per cycle) | | | |
|---|---|---|---|
| Feed flow | 4364.7 | Evacuation flow | 4017.8 |
| Product flow | 413.5 | Mass Balance Error (%) | -1.5 |

| Key Performance Parameters | | | |
|---|---|---|---|
| Oxygen Recovery (%) | 38.7 | BSF (kg/TPDc) | 369.0 |
| Power: (kW/TPDc) | 10.4 | Oxygen Purity (%): | 91.2 |

| End of Step CSS Temperature Profile (°C) | | | | | |
|---|---|---|---|---|---|
| z (m) | Step 1 | Step 2 | Step 3 | Step 4 | Step 5 |
| 0 | 12.8 | 12.9 | 12.7 | 13.1 | 13.3 |
| 0.245 | -7.4 | -6.3 | -7 | -10.3 | -10.7 |
| 0.395 | -5.8 | -3.7 | -4.4 | -11.8 | -12.6 |
| 0.545 | 2.8 | 4.7 | 4.5 | -2.4 | -3.4 |
| 1.345 | 26.9 | 34 | 34.5 | 27.5 | 25.9 |
| 1.8 | 24.3 | 25.6 | 25.5 | 21.8 | 21.2 |

## Run Number NaXDLP

**Description of Experiment**
Two bed with a single layer of NaX, PVC, 60 second cycle, Dry Air Feed

| Sieve Arrangement and Bed | | |
|---|---|---|
| Type of Prelayer | None | None |
| Type of Main Layer | NaX | NaX |
| Bed | PVC | PVC |
| | **Bed 1** | **Bed 2** |
| Mass of Main layer(kg) | 10.4 | 10.3 |
| Height of Main layer(mm) | 1850 | 1850 |

| End of Step Press. at CSS (kPa) | Bed 1 | Bed 2 |
|---|---|---|
| Step 1 | 126.6 | 54.6 |
| Step 2 | 136.6 | 37.7 |
| Step 3 | 105.6 | 51.4 |
| Step 4 | 95.6 | 66.6 |
| Step 5 | 53.4 | 127.1 |
| Step 6 | 36.7 | 137.8 |
| Step 7 | 51.8 | 106.6 |
| Step 8 | 65.6 | 96.8 |

| Mass Balance at CSS (Total millimole per cycle) | | | |
|---|---|---|---|
| Feed flow | 4485.3 | Evacuation flow | 3873.3 |
| Product flow | 622.8 | Mass Balance Error (%) | -0.2 |

| Key Performance Parameters | | | |
|---|---|---|---|
| Oxygen Recovery (%) | 50.6 | BSF (kg/TPDc) | 900.8 |
| Oxygen Purity (%): | 80.1 | | |

| End of Step CSS Temperature Profile (°C) | | | | | | | | |
|---|---|---|---|---|---|---|---|---|
| z (m) | Step 1 | Step 2 | Step 3 | Step 4 | Step 5 | Step 6 | Step 7 | Step 8 |
| 0 | 19.1 | 19.7 | 18.6 | 17.7 | 17.1 | 17.8 | 18.3 | 18.7 |
| 0.025 | 19 | 20.3 | 19.8 | 19.5 | 17.5 | 16.3 | 16.3 | 16.3 |
| 0.05 | 19.3 | 20.5 | 20.2 | 20.3 | 18.2 | 16.9 | 16.6 | 16.9 |
| 0.075 | 19.6 | 20.8 | 20.8 | 20.4 | 18.7 | 17.4 | 16.9 | 17.3 |
| 0.1 | 20 | 21.3 | 21.4 | 21.1 | 18.2 | 17.2 | 17.4 | 17.4 |
| 0.2 | 21.2 | 22.6 | 22.6 | 22.3 | 20.4 | 19.5 | 19.3 | 19.4 |
| 0.3 | 21.7 | 23 | 23.5 | 21.7 | 20.5 | 19.9 | 20 | 20.4 |
| 0.4 | 23 | 24.5 | 24.1 | 23.7 | 21.6 | 20.7 | 20.8 | 20.7 |
| 0.5 | 22.8 | 23.8 | 23.3 | 23.2 | 21.6 | 20.4 | 20.5 | 20.6 |
| 0.6 | 23.1 | 24 | 23.9 | 23.6 | 22.1 | 21 | 21.4 | 20.9 |
| 0.7 | 23.6 | 24.9 | 25.2 | 25 | 23 | 22 | 21.9 | 21.4 |
| 0.8 | 24.5 | 25.7 | 25.7 | 25.4 | 23.7 | 22.7 | 22.4 | 22.4 |
| 0.9 | 23.7 | 25.8 | 25.9 | 25.4 | 23.2 | 22.1 | 22.1 | 21.9 |
| 1 | 23.9 | 26 | 26.1 | 25.2 | 23.9 | 22.8 | 23.1 | 22.8 |
| 1.1 | 24.6 | 26.9 | 27 | 26.8 | 25.1 | 24.2 | 23.9 | 23.7 |
| 1.2 | 25.5 | 27.5 | 27.7 | 27.5 | 26 | 25 | 24.6 | 24.3 |
| 1.3 | 25.1 | 26.7 | 27.2 | 27.2 | 25.9 | 25 | 24.5 | 24.1 |
| 1.4 | 25.6 | 27.1 | 27.9 | 27.9 | 26.8 | 26 | 25.4 | 25.1 |
| 1.5 | 25.6 | 26.3 | 27.4 | 27.4 | 26.3 | 25.7 | 25.2 | 25 |
| 1.7 | 25.4 | 25.8 | 26.5 | 27.2 | 26.9 | 26.3 | 25.5 | 25.2 |
| 1.75 | 26.1 | 26.5 | 27.2 | 28 | 27.6 | 27 | 26.2 | 25.9 |
| 1.8 | 26.8 | 27.1 | 27.6 | 28.4 | 28.1 | 27.5 | 26.7 | 26.5 |

## Run Number NaXDLP2

**Description of Experiment**
Two bed with a single layer of NaX, PVC, 60 second cycle, Dry Air Feed

| Sieve Arrangement and Bed | | |
|---|---|---|
| Type of Prelayer | None | None |
| Type of Main Layer | NaX | NaX |
| Bed | PVC | PVC |
| | **Bed 1** | **Bed 2** |
| Mass of Main layer(kg) | 10.4 | 10.3 |
| Height of Main layer(mm) | 1850 | 1850 |

| End of Step Press. at CSS (kPa) | Bed 1 | Bed 2 |
|---|---|---|
| Step 1 | 126.6 | 52.8 |
| Step 2 | 136.8 | 35.9 |
| Step 3 | 107.8 | 48.9 |
| Step 4 | 96.1 | 64.4 |
| Step 5 | 52.4 | 127.5 |
| Step 6 | 35.6 | 137.8 |
| Step 7 | 49.3 | 106.7 |
| Step 8 | 64.8 | 96.1 |

| Mass Balance at CSS (Total millimole per cycle) | | | |
|---|---|---|---|
| Feed flow | 4754.4 | Evacuation flow | 4257.9 |
| Product flow | 622.8 | Mass Balance Error (%) | -2.7 |

| Key Performance Parameters | | | |
|---|---|---|---|
| Oxygen Recovery (%) | 48.8 | BSF (kg/TPDc) | 880.3 |
| Oxygen Purity (%): | 82.1 | | |

| End of Step CSS Temperature Profile (°C) | | | | | | | | |
|---|---|---|---|---|---|---|---|---|
| z (m) | Step 1 | Step 2 | Step 3 | Step 4 | Step 5 | Step 6 | Step 7 | Step 8 |
| 0 | 18 | 17.7 | 15.7 | 14.5 | 15.1 | 15 | 15.8 | 18 |
| 0.025 | 18 | 19.2 | 19 | 18.9 | 16.6 | 15.2 | 14.9 | 15 |
| 0.05 | 18.3 | 19.5 | 19.3 | 19.1 | 16.6 | 15.2 | 15.3 | 15.5 |
| 0.075 | 18.9 | 20.1 | 19.7 | 19.4 | 16.9 | 15.8 | 15.5 | 16 |
| 0.1 | 18.6 | 19.7 | 19 | 19.3 | 17 | 15.9 | 15.7 | 16.5 |
| 0.2 | 19.7 | 21 | 20.6 | 20.6 | 18.7 | 17.5 | 17.2 | 17.7 |
| 0.3 | 20.5 | 21 | 20.7 | 20.5 | 19 | 18.5 | 18.6 | 19 |
| 0.4 | 21.4 | 22.6 | 22.3 | 22.2 | 19.7 | 18.9 | 18.6 | 19 |
| 0.5 | 20.9 | 22.1 | 21.7 | 21.3 | 19.7 | 18.7 | 18.4 | 18.8 |
| 0.6 | 21.3 | 22.4 | 22.8 | 22 | 20.4 | 19.6 | 18.9 | 19.2 |
| 0.7 | 21.8 | 22.3 | 22.4 | 22.1 | 20.1 | 19.5 | 19.3 | 19.2 |
| 0.8 | 22.6 | 23.9 | 23.6 | 23.3 | 21.5 | 20.3 | 20.3 | 20.2 |
| 0.9 | 21.6 | 23 | 23.2 | 23 | 21.5 | 20.5 | 19.9 | 19.9 |
| 1 | 22.1 | 23.5 | 23.6 | 23.4 | 21.7 | 21.2 | 20.7 | 20.6 |
| 1.1 | 22.9 | 24.8 | 25 | 24.8 | 23.1 | 22.3 | 21.9 | 21.6 |
| 1.2 | 23.7 | 25.4 | 25.7 | 25.5 | 24.2 | 23.3 | 22.8 | 22.6 |
| 1.3 | 22.9 | 24.4 | 25.3 | 25.2 | 23.9 | 23 | 22.4 | 22.1 |
| 1.4 | 22.8 | 23.6 | 24.4 | 24.3 | 23.4 | 22.9 | 22.6 | 22.3 |
| 1.5 | 23.6 | 24.4 | 25.4 | 25.6 | 24.4 | 23.7 | 23.2 | 22.9 |
| 1.6 | 24.4 | 25 | 25.9 | 26.3 | 25.3 | 24.6 | 24.1 | 23.9 |
| 1.75 | 24.1 | 24.5 | 25 | 25.7 | 25.7 | 24.9 | 24.1 | 23.8 |
| 1.8 | 24.4 | 24.7 | 25 | 25.6 | 25.7 | 25 | 24.2 | 23.9 |

## Run Number NaXDHP

**Description of Experiment**
Two bed with a single layer of NaX, PVC, 60 second cycle, Dry Air Feed

| Sieve Arrangement and Bed | | |
|---|---|---|
| Type of Prelayer | None | None |
| Type of Main Layer | NaX | NaX |
| Bed | PVC | PVC |
| | **Bed 1** | **Bed 2** |
| Mass of Main layer(kg) | 10.4 | 10.3 |
| Height of Main layer(mm) | 1850 | 1850 |

| End of Step Press. at CSS (kPa) | Bed 1 | Bed 2 |
|---|---|---|
| Step 1 | 132.8 | 52.1 |
| Step 2 | 141.6 | 35.2 |
| Step 3 | 109.4 | 50.2 |
| Step 4 | 93.6 | 68.8 |
| Step 5 | 51.4 | 133.4 |
| Step 6 | 34.2 | 142.6 |
| Step 7 | 50.8 | 109.1 |
| Step 8 | 68.3 | 94.0 |

| Mass Balance at CSS (Total millimole per cycle) | | | |
|---|---|---|---|
| Feed flow | 3978.4 | Evacuation flow | 3632.34 |
| Product flow | 234.4 | Mass Balance Error (%) | 2.8 |

| Key Performance Parameters | | | |
|---|---|---|---|
| Oxygen Recovery (%) | 25.4 | BSF (kg/TPDc) | 1920.1 |
| Oxygen Purity (%): | 94.9 | | |

| End of Step CSS Temperature Profile (°C) | | | | | | | | |
|---|---|---|---|---|---|---|---|---|
| z (m) | Step 1 | Step 2 | Step 3 | Step 4 | Step 5 | Step 6 | Step 7 | Step 8 |
| 0 | 24.5 | 23.5 | 23.4 | 22.1 | 22.8 | 21.9 | 22.5 | 22.7 |
| 0.025 | 24.4 | 25.2 | 25.2 | 24.8 | 22.9 | 22 | 21.5 | 21.5 |
| 0.05 | 25.3 | 26.4 | 26.3 | 25.8 | 23.9 | 22.8 | 22.3 | 22.2 |
| 0.075 | 25.8 | 27 | 26.8 | 26.2 | 24.9 | 23.5 | 22.9 | 23 |
| 0.1 | 27.2 | 27.5 | 27.7 | 27.2 | 25.4 | 23.5 | 23.7 | 23.4 |
| 0.2 | 28.1 | 28.8 | 29 | 28.6 | 27.3 | 26 | 25.7 | 25.6 |
| 0.4 | 29.9 | 30.2 | 30.3 | 29.6 | 28.3 | 27 | 27 | 26.6 |
| 0.5 | 29.3 | 30.4 | 30.1 | 30 | 28.7 | 27.3 | 27 | 26.8 |
| 0.7 | 29.4 | 31.3 | 31.8 | 31.4 | 30 | 29 | 28.2 | 28.3 |
| 0.8 | 30.3 | 32.6 | 32.8 | 32.6 | 31.3 | 30 | 29.4 | 29.3 |
| 0.9 | 29.8 | 30.4 | 31.8 | 31.8 | 30.4 | 29.8 | 29.3 | 29.3 |
| 1 | 30 | 30.5 | 31.2 | 31.7 | 30.8 | 30.1 | 29.6 | 29.4 |
| 1.1 | 30.2 | 30.8 | 31.3 | 32.4 | 31.6 | 30.3 | 29.8 | 30.1 |
| 1.2 | 29.7 | 30.1 | 30 | 30.8 | 30.1 | 29.3 | 29.1 | 29.1 |
| 1.3 | 27.9 | 28.2 | 28.2 | 28.1 | 27.7 | 27.3 | 27.2 | 27.2 |
| 1.4 | 27.4 | 27.8 | 27.7 | 27.6 | 27.2 | 26.9 | 26.8 | 26.8 |
| 1.5 | 27.1 | 27.2 | 27.2 | 27 | 26.8 | 26.6 | 26.6 | 26.5 |
| 1.6 | 27.7 | 28 | 27.9 | 27.8 | 27.3 | 27.1 | 27 | 27 |
| 1.75 | 26.6 | 26.9 | 26.9 | 26.6 | 26.2 | 26.1 | 26 | 26 |
| 1.8 | 27.2 | 27.5 | 27.4 | 27.2 | 26.9 | 26.6 | 26.5 | 26.6 |

## Run Number NaXDHP2

**Description of Experiment**
Two bed with a single layer of NaX, PVC, 60 second cycle, Dry Air Feed

| Sieve Arrangement and Bed | | |
|---|---|---|
| Type of Prelayer | None | None |
| Type of Main Layer | NaX | NaX |
| Bed | PVC | PVC |
| | **Bed 1** | **Bed 2** |
| Mass of Main layer(kg) | 10.4 | 10.3 |
| Height of Main layer(mm) | 1850 | 1850 |

| End of Step Press. at CSS (kPa) | Bed 1 | Bed 2 |
|---|---|---|
| Step 1 | 129.8 | 50.0 |
| Step 2 | 140.3 | 33.3 |
| Step 3 | 107.5 | 48.9 |
| Step 4 | 92.8 | 66.6 |
| Step 5 | 50.0 | 131.4 |
| Step 6 | 33.1 | 141.6 |
| Step 7 | 48.9 | 106.4 |
| Step 8 | 66.4 | 92.3 |

| Mass Balance at CSS (Total millimole per cycle) | | | |
|---|---|---|---|
| Feed flow | 4527.2 | Evacuation flow | 4274.0 |
| Product flow | 230.9 | Mass Balance Error (%) | 0.5 |

| Key Performance Parameters | | | |
|---|---|---|---|
| Oxygen Recovery (%) | 22.5 | BSF (kg/TPDc) | 1917.5 |
| Oxygen Purity (%): | 95.8 | | |

| End of Step CSS Temperature Profile (°C) | | | | | | | | |
|---|---|---|---|---|---|---|---|---|
| z (m) | Step 1 | Step 2 | Step 3 | Step 4 | Step 5 | Step 6 | Step 7 | Step 8 |
| 0 | 19.4 | 19 | 16.8 | 15.2 | 17.3 | 16.1 | 17.5 | 18.4 |
| 0.025 | 19.8 | 20.8 | 20.7 | 20.2 | 18.5 | 16.8 | 16.4 | 16.5 |
| 0.05 | 20.5 | 21.7 | 21.4 | 21 | 19.3 | 18 | 17.7 | 17.6 |
| 0.075 | 21.1 | 22.2 | 22.1 | 22 | 19.9 | 18.8 | 18.3 | 18.2 |
| 0.1 | 21.3 | 22.6 | 22.1 | 21.4 | 20.2 | 18.4 | 18.2 | 18 |
| 0.2 | 23.3 | 24.4 | 24.3 | 23.9 | 22.5 | 21 | 20.7 | 20.6 |
| 0.3 | 23.4 | 24 | 23.6 | 23.6 | 22.4 | 21.3 | 21.1 | 21.1 |
| 0.4 | 24.8 | 25.9 | 25.3 | 25.1 | 23.6 | 22 | 21.8 | 21.5 |
| 0.5 | 24.3 | 25.2 | 25.1 | 24.7 | 23.2 | 21.9 | 21.6 | 21.2 |
| 0.6 | 24.6 | 26.8 | 27.1 | 26.8 | 25.2 | 23.4 | 23.3 | 22.9 |
| 0.7 | 24.7 | 25.5 | 25.8 | 25.6 | 23.9 | 22.5 | 22.2 | 22.4 |
| 0.8 | 25.5 | 28.3 | 28.5 | 28.3 | 26.4 | 25.1 | 24.5 | 24.3 |
| 0.9 | 25.6 | 27.5 | 28.3 | 28.1 | 27.1 | 25.8 | 25.3 | 25 |
| 1 | 26.1 | 26.2 | 27.9 | 28.2 | 27 | 25.8 | 25.4 | 25.7 |
| 1.1 | 26.3 | 26.6 | 27.5 | 28.8 | 27.8 | 26.2 | 26.2 | 26.2 |
| 1.2 | 25.7 | 25.9 | 26.2 | 27.2 | 26.2 | 25.2 | 25.2 | 25.1 |
| 1.3 | 23.7 | 24.1 | 24.2 | 24.2 | 23.7 | 23.2 | 23 | 23.1 |
| 1.4 | 22.4 | 22.6 | 22.6 | 22.5 | 22.1 | 22 | 22 | 22.1 |
| 1.5 | 22.1 | 22.4 | 22.4 | 22.2 | 21.8 | 21.6 | 21.5 | 21.6 |
| 1.6 | 22.4 | 22.5 | 22.5 | 22.3 | 21.9 | 21.7 | 21.8 | 21.9 |
| 1.7 | 20.7 | 20.8 | 20.9 | 20.7 | 20.6 | 20.4 | 20.4 | 20.4 |
| 1.75 | 21.1 | 21 5 | 21.5 | 21.3 | 20.7 | 20.4 | 20.4 | 20.5 |
| 1.8 | 22 | 22.4 | 22.3 | 22.1 | 21.6 | 21.3 | 21.2 | 21.3 |

## Run Number NaXWLP

**Description of Experiment**
Two bed with a single layer of NaX, PVC, 60 second cycle, Wet Air Feed

| Sieve Arrangement and Bed | | |
|---|---|---|
| Type of Prelayer | None | None |
| Type of Main Layer | NaX | NaX |
| Bed | PVC | PVC |
| | **Bed 1** | **Bed 2** |
| Mass of Main layer(kg) | 10.4 | 10.3 |
| Height of Main layer(mm) | 1850 | 1850 |

| End of Step Press. at CSS (kPa) | Bed 1 | Bed 2 |
|---|---|---|
| Step 1 | 127.7 | 52.4 |
| Step 2 | 137.4 | 35.6 |
| Step 3 | 106.6 | 49.7 |
| Step 4 | 95.1 | 65.1 |
| Step 5 | 51.8 | 128.4 |
| Step 6 | 35.2 | 138.1 |
| Step 7 | 49.8 | 105.7 |
| Step 8 | 65.3 | 95.1 |

| Mass Balance at CSS (Total millimole per cycle) | | | |
|---|---|---|---|
| Feed flow | 4799.4 | Evacuation flow | 4249.7 |
| Product flow | 627.2 | Mass Balance Error (%) | -1.6 |

| Key Performance Parameters | | | |
|---|---|---|---|
| Oxygen Recovery (%) | 48.5 | BSF (kg/TPDc) | 877.3 |
| Oxygen Purity (%): | 82.4 | | |

| End of Step CSS Temperature Profile (°C) | | | | | | | | |
|---|---|---|---|---|---|---|---|---|
| z (m) | Step 1 | Step 2 | Step 3 | Step 4 | Step 5 | Step 6 | Step 7 | Step 8 |
| 0 | 20.6 | 19.5 | 18.2 | 16.8 | 18.2 | 17.5 | 18.1 | 19.2 |
| 0.025 | 13.2 | 14.6 | 14.8 | 14.6 | 13 | 11.8 | 10.9 | 11 |
| 0.05 | 8.2 | 8.9 | 9 | 8.6 | 6.4 | 5.1 | 4.5 | 4.9 |
| 0.075 | 9 | 9.9 | 10.1 | 9.9 | 7.5 | 6 | 5.6 | 5.7 |
| 0.1 | 11.5 | 11.7 | 11.8 | 11.8 | 9.5 | 8.4 | 7.8 | 8.2 |
| 0.2 | 15.2 | 15.9 | 16.1 | 15.8 | 13.8 | 12.5 | 12.2 | 12.4 |
| 0.3 | 18.4 | 18.7 | 18.7 | 18.4 | 17.1 | 16.6 | 16.1 | 16.4 |
| 0.4 | 20.4 | 21 | 21.1 | 20.6 | 18.8 | 17.3 | 17.3 | 17.5 |
| 0.5 | 20.5 | 21.4 | 21.3 | 20.9 | 19.3 | 18.4 | 18.2 | 18.1 |
| 0.6 | 21.6 | 22.4 | 22.4 | 21.7 | 20.5 | 19.5 | 19 | 19.3 |
| 0.7 | 21.8 | 23.3 | 23.1 | 22.4 | 21 | 19.8 | 19.3 | 19.7 |
| 0.8 | 22.9 | 24.3 | 23.9 | 23.7 | 21.9 | 20.8 | 20.6 | 20.7 |
| 0.9 | 22.5 | 23.7 | 23.9 | 23.7 | 22.2 | 21.3 | 20.8 | 20.6 |
| 1 | 23.2 | 24.4 | 24.5 | 24 | 23.1 | 22.2 | 21.7 | 21.9 |
| 1.1 | 23.5 | 25.6 | 25.7 | 25.6 | 24 | 23 | 22.4 | 22.3 |
| 1.2 | 24.4 | 26.3 | 26.5 | 26.3 | 25 | 24.2 | 23.7 | 23.4 |
| 1.3 | 23.7 | 25.3 | 26.1 | 26.1 | 25 | 23.9 | 23.4 | 23.1 |
| 1.4 | 24.4 | 25.1 | 25.9 | 25.9 | 25 | 24.4 | 24.1 | 23.8 |
| 1.5 | 25.1 | 25.8 | 26.8 | 26.9 | 25.9 | 25.2 | 24.8 | 24.5 |
| 1.6 | 25.9 | 26.4 | 27.3 | 27.8 | 26.8 | 26.1 | 25.6 | 25.4 |
| 1.7 | 24.7 | 25.1 | 25.5 | 26.3 | 26.3 | 25.5 | 24.9 | 24.5 |
| 1.75 | 25.4 | 25.8 | 26.2 | 26.9 | 26.9 | 26.1 | 25.4 | 25.1 |
| 1.8 | 25.8 | 26.1 | 26.3 | 27 | 27.2 | 26.4 | 25.6 | 25.4 |

## Run Number NaXWHP

**Description of Experiment**
Two bed with a single layer of NaX, PVC, 60 second cycle, Wet Air Feed

| Sieve Arrangement and Bed | | |
|---|---|---|
| Type of Prelayer | None | None |
| Type of Main Layer | NaX | NaX |
| Bed | PVC | PVC |
| | **Bed 1** | **Bed 2** |
| Mass of Main layer(kg) | 10.4 | 10.3 |
| Height of Main layer(mm) | 1850 | 1850 |

| End of Step Press. at CSS (kPa) | Bed 1 | Bed 2 |
|---|---|---|
| Step 1 | 128.4 | 50.5 |
| Step 2 | 137.5 | 33.8 |
| Step 3 | 105.8 | 49.2 |
| Step 4 | 93.1 | 64.4 |
| Step 5 | 50.7 | 129.6 |
| Step 6 | 33.6 | 138.8 |
| Step 7 | 49.1 | 104.6 |
| Step 8 | 64.5 | 92.1 |

| Mass Balance at CSS (Total millimole per cycle) | | | |
|---|---|---|---|
| Feed flow | 4340.8 | Evacuation flow | 4109.8 |
| Product flow | 242.7 | Mass Balance Error (%) | -0.3 |

| Key Performance Parameters | | | |
|---|---|---|---|
| Oxygen Recovery (%) | 23.6 | BSF (kg/TPDc) | 1918.4 |
| Oxygen Purity (%): | 96.2 | | |

| End of Step CSS Temperature Profile (°C) | | | | | | | | |
|---|---|---|---|---|---|---|---|---|
| z (m) | Step 1 | Step 2 | Step 3 | Step 4 | Step 5 | Step 6 | Step 7 | Step 8 |
| 0 | 19.1 | 19 | 17.5 | 16.1 | 16.4 | 16.2 | 17.1 | 17.9 |
| 0.025 | 10.8 | 11.8 | 12.2 | 12.2 | 10.6 | 9.1 | 8.4 | 8.3 |
| 0.05 | 11.3 | 11.9 | 11.9 | 11.7 | 9.6 | 8.4 | 7.9 | 7.8 |
| 0.075 | 13.6 | 14.6 | 14.2 | 14.1 | 12.2 | 10.8 | 10 | 10.3 |
| 0.1 | 14.9 | 15.8 | 15.8 | 15.6 | 13.3 | 12.1 | 11.9 | 12.1 |
| 0.2 | 21.7 | 22.9 | 22.9 | 22.6 | 20.7 | 19.6 | 19.2 | 19 |
| 0.3 | 22.9 | 23.3 | 23.2 | 22.9 | 21.6 | 20.9 | 20.7 | 20.8 |
| 0.4 | 24.7 | 25.9 | 25.7 | 25.3 | 23.1 | 22.1 | 21.4 | 21.3 |
| 0.5 | 24.3 | 25.3 | 25.2 | 24.7 | 23.2 | 21.9 | 21.7 | 21.3 |
| 0.6 | 24.7 | 25.6 | 25.3 | 24.9 | 23.6 | 22.1 | 21.9 | 21.6 |
| 0.7 | 25.4 | 27 | 27.1 | 27.1 | 25.4 | 24.1 | 23.3 | 23.1 |
| 0.8 | 26 | 28.5 | 28.6 | 28.3 | 26.5 | 25.3 | 24.5 | 24.3 |
| 0.9 | 25.7 | 27.9 | 28.6 | 28.5 | 27.2 | 26 | 25.5 | 25.3 |
| 1 | 26.4 | 26.4 | 28 | 28.4 | 27.2 | 26.4 | 25.9 | 25.9 |
| 1.1 | 27.1 | 27.4 | 28.1 | 29.2 | 28.1 | 27 | 26.5 | 26.4 |
| 1.2 | 26.2 | 26.6 | 26.6 | 27.6 | 26.4 | 25.6 | 25.5 | 25.5 |
| 1.3 | 24 | 24.5 | 24.5 | 24.7 | 24.1 | 23.6 | 23.5 | 23.6 |
| 1.4 | 23 | 23.2 | 23.1 | 23.2 | 22.8 | 22.7 | 22.6 | 22.6 |
| 1.5 | 23 | 23.2 | 23.1 | 23.1 | 22.6 | 22.3 | 22.3 | 22.4 |
| 1.6 | 23.1 | 23.4 | 23.2 | 23.1 | 22.7 | 22.5 | 22.5 | 22.7 |
| 1.7 | 21.2 | 21.3 | 21.3 | 21.2 | 21 | 20.8 | 20.8 | 20.9 |
| 1.75 | 21.9 | 22.3 | 22.2 | 22.1 | 21.6 | 21.2 | 21.2 | 21.3 |
| 1.8 | 22.4 | 22.9 | 22.7 | 22.6 | 22.1 | 21.8 | 21.8 | 21.9 |

# Run Number NaXWHP2

**Description of Experiment**
Two bed with a single layer of NaX, PVC, 60 second cycle, Wet Air Feed

| Sieve Arrangement and Bed | | |
|---|---|---|
| Type of Prelayer | None | None |
| Type of Main Layer | NaX | NaX |
| Bed | PVC | PVC |
| | **Bed 1** | **Bed 2** |
| Mass of Main layer(kg) | 10.4 | 10.3 |
| Height of Main layer(mm) | 1850 | 1850 |

| End of Step Press. at CSS (kPa) | Bed 1 | Bed 2 |
|---|---|---|
| Step 1 | 128.7 | 50.9 |
| Step 2 | 137.8 | 34.4 |
| Step 3 | 106.1 | 49.5 |
| Step 4 | 93.6 | 64.6 |
| Step 5 | 51.1 | 129.3 |
| Step 6 | 34.1 | 138.7 |
| Step 7 | 49.4 | 104.8 |
| Step 8 | 64.6 | 92.6 |

| Mass Balance at CSS (Total millimole per cycle) | | | |
|---|---|---|---|
| Feed flow | 4344.6 | Evacuation flow | 4135.9 |
| Product flow | 234.2 | Mass Balance Error (%) | -0.6 |

| Key Performance Parameters | | | |
|---|---|---|---|
| Oxygen Recovery (%) | 23.5 | BSF (kg/TPDc) | 1917.3 |
| Oxygen Purity (%): | 95.8 | | |

| End of Step CSS Temperature Profile (°C) | | | | | | | | |
|---|---|---|---|---|---|---|---|---|
| z (m) | Step 1 | Step 2 | Step 3 | Step 4 | Step 5 | Step 6 | Step 7 | Step 8 |
| 0 | 19 | 18.6 | 16.9 | 15.2 | 17.1 | 16.8 | 17.9 | 18.1 |
| 0.025 | 10.9 | 12.3 | 12.1 | 12.4 | 10.7 | 9.3 | 8.7 | 8.5 |
| 0.05 | 6.4 | 7.3 | 6.8 | 6.4 | 4.6 | 3 | 2.9 | 3.2 |
| 0.075 | 9.4 | 10.6 | 10.2 | 9.7 | 8.2 | 6.4 | 6.3 | 6.5 |
| 0.1 | 11.7 | 12.4 | 12.3 | 11.9 | 10.2 | 9.2 | 9.1 | 8.9 |
| 0.2 | 20.6 | 21.7 | 21.6 | 21.2 | 19.8 | 18.5 | 18.3 | 17.9 |
| 0.3 | 22.5 | 22.6 | 22.4 | 22.2 | 21.2 | 20.5 | 20.2 | 20.2 |
| 0.4 | 24.3 | 25.3 | 25.3 | 24.5 | 23.2 | 21.7 | 21.4 | 21.2 |
| 0.5 | 24.3 | 25.1 | 25 | 24.7 | 23.1 | 21.7 | 21.5 | 21.2 |
| 0.6 | 24.2 | 25.5 | 25.5 | 25 | 23.5 | 22.4 | 22 | 21.5 |
| 0.7 | 25.2 | 27.4 | 27.3 | 26.8 | 25.3 | 24.4 | 23.4 | 23.1 |
| 0.8 | 26.1 | 28.7 | 28.6 | 28.3 | 26.7 | 25.3 | 24.6 | 24.5 |
| 0.9 | 25.5 | 27.8 | 28.5 | 28.4 | 27.2 | 25.8 | 25.5 | 25.1 |
| 1 | 26.1 | 26.6 | 28.1 | 28.1 | 26.9 | 26.1 | 25.9 | 25.9 |
| 1.1 | 26.8 | 27.3 | 28 | 29.2 | 27.7 | 26.9 | 26.3 | 26.3 |
| 1.2 | 25.8 | 26.2 | 26.2 | 27.3 | 26.2 | 25.3 | 25.2 | 25.2 |
| 1.3 | 23.8 | 24.2 | 24.2 | 24.3 | 23.8 | 23.3 | 23.2 | 23.2 |
| 1.4 | 22.9 | 23.1 | 23 | 22.9 | 22.6 | 22.4 | 22.4 | 22.4 |
| 1.5 | 22.8 | 23.1 | 22.9 | 22.9 | 22.4 | 22.2 | 22.1 | 22.3 |
| 1.6 | 23 | 23.3 | 23.1 | 23 | 22.6 | 22.4 | 22.4 | 22.4 |
| 1.7 | 21.2 | 21.7 | 21.6 | 21.5 | 21 | 20.6 | 20.6 | 20.7 |
| 1.75 | 21.8 | 22.2 | 22.1 | 21.9 | 21.5 | 21.1 | 21 | 21.2 |
| 1.8 | 22.3 | 22.5 | 22.4 | 22.4 | 22.2 | 22.1 | 21.9 | 22.1 |

## Run Number AA38NaXLP

**Description of Experiment**

Two bed with a 38 mm prelayer of AA and main layer of NaX, PVC beds
60 sec cycle,. Dry Air Feed

| Sieve Arrangement and Bed | | |
|---|---|---|
| Type of Prelayer | AA | AA |
| Type of Main Layer | NaX | NaX |
| Bed | PVC | PVC |
| | **Bed 1** | **Bed 2** |
| Mass of Prelayer (kg) | 0.299 | 0.3059 |
| Mass of Main layer(kg) | 9.826 | 10.153 |
| Height of Prelayer (mm) | 38 | 38 |
| Height of Main layer(mm) | 1812 | 1812 |

| End of Step Press. at CSS (kPa) | Bed 1 | Bed 2 |
|---|---|---|
| Step 1 | 129.8 | 53.5 |
| Step 2 | 137.8 | 36.0 |
| Step 3 | 106.6 | 49.5 |
| Step 4 | 98.4 | 62.6 |
| Step 5 | 52.5 | 129.6 |
| Step 6 | 34.8 | 138.6 |
| Step 7 | 50.8 | 107.2 |
| Step 8 | 62.4 | 99.1 |

| Mass Balance at CSS (Total millimole per cycle) | | | |
|---|---|---|---|
| Feed flow | 4618.7 | Evacuation flow | 3991.5 |
| Product flow | 622.6 | Mass Balance Error (%) | 0.1 |

| Key Performance Parameters | | | |
|---|---|---|---|
| Oxygen Recovery (%) | 49.3 | BSF (kg/TPDc) | 865.6 |
| Oxygen Purity (%): | 80.5 | | |

| End of Step CSS Temperature Profile (°C) | | | | | | | | |
|---|---|---|---|---|---|---|---|---|
| z (m) | Step 1 | Step 2 | Step 3 | Step 4 | Step 5 | Step 6 | Step 7 | Step 8 |
| 0 | 23.2 | 23 | 20.1 | 19 | 20.9 | 20.2 | 21.7 | 22.5 |
| 0.025 | 19.2 | 19.5 | 19.5 | 19.4 | 18.6 | 18.2 | 17.7 | 17.9 |
| 0.05 | 16.7 | 17.4 | 17.1 | 17 | 15.2 | 14.1 | 13.6 | 13.8 |
| 0.075 | 16.7 | 18.2 | 17.9 | 17.8 | 15.8 | 14.1 | 14.1 | 14.3 |
| 0.1 | 18.2 | 19.1 | 18.2 | 18 | 16.1 | 15.1 | 15.5 | 15.5 |
| 0.2 | 20.1 | 21.3 | 21.1 | 20.8 | 19.2 | 17.9 | 17.7 | 17.7 |
| 0.3 | 22.7 | 22.9 | 22.7 | 22.4 | 21.1 | 20.6 | 20.8 | 20.9 |
| 0.4 | 24 | 24.6 | 24 | 23.7 | 23 | 22.2 | 22.4 | 22.1 |
| 0.5 | 23.7 | 24.9 | 24.7 | 24.2 | 22.6 | 21.9 | 21.6 | 21.7 |
| 0.6 | 24.7 | 25.5 | 25.3 | 24.9 | 23.6 | 23 | 22.5 | 22.9 |
| 0.7 | 25.5 | 26.3 | 26.2 | 26.2 | 24.9 | 23.5 | 23.4 | 23.2 |
| 0.8 | 26.6 | 27.5 | 27.4 | 27.2 | 25.7 | 24.4 | 24.2 | 24.1 |
| 0.9 | 25.6 | 27.1 | 27.1 | 26.6 | 25.3 | 24.5 | 24 | 23.9 |
| 1 | 26.2 | 27.4 | 27.3 | 27.1 | 25.9 | 25.2 | 24.9 | 24.9 |
| 1.1 | 27 | 28.3 | 28.4 | 28.5 | 27.2 | 25.9 | 25.7 | 25.4 |
| 1.2 | 27.6 | 29.4 | 29.5 | 29.3 | 28.2 | 27 | 26.6 | 26.2 |
| 1.3 | 27.2 | 29 | 29.4 | 29.3 | 28.1 | 27.2 | 26.6 | 26.4 |
| 1.4 | 27.9 | 29.3 | 30 | 30 | 29 | 28.1 | 27.5 | 27.3 |
| 1.5 | 28.2 | 29 | 30 | 30 | 28.9 | 28.3 | 27.9 | 27.6 |
| 1.6 | 29.6 | 30.4 | 31.5 | 31.8 | 31.2 | 30.3 | 29.7 | 29.3 |
| 1.7 | 28.3 | 28.7 | 29.3 | 29.8 | 29.7 | 28.9 | 28.2 | 28 |
| 1.75 | 29 | 29.4 | 29.9 | 30.5 | 30.3 | 29.5 | 28.9 | 28.7 |
| 1.8 | 29.3 | 29.5 | 29.8 | 30.5 | 30.3 | 29.5 | 28.8 | 28.7 |

## Run Number AA38NaXDHP

**Description of Experiment**
Two bed with a 38 mm prelayer of AA and main layer of NaX, PVC beds
60 sec cycle, Dry Air Feed

| Sieve Arrangement and Bed | | |
|---|---|---|
| Type of Prelayer | AA | AA |
| Type of Main Layer | NaX | NaX |
| Bed | PVC | PVC |
| | **Bed 1** | **Bed 2** |
| Mass of Prelayer (kg) | 0.299 | 0.3059 |
| Mass of Main layer(kg) | 9.826 | 10.153 |
| Height of Prelayer (mm) | 38 | 38 |
| Height of Main layer(mm) | 1812 | 1812 |

| End of Step Press. at CSS (kPa) | Bed 1 | Bed 2 |
|---|---|---|
| Step 1 | 126.6 | 51.4 |
| Step 2 | 140.3 | 34.0 |
| Step 3 | 105.4 | 50.3 |
| Step 4 | 96.3 | 62.6 |
| Step 5 | 51.1 | 126.1 |
| Step 6 | 32.7 | 140.8 |
| Step 7 | 50.7 | 105.1 |
| Step 8 | 62.1 | 95.6 |

| Mass Balance at CSS (Total millimole per cycle) | | | |
|---|---|---|---|
| Feed flow | 4085.4 | Evacuation flow | 3842.2 |
| Product flow | 234.3 | Mass Balance Error (%) | 0.2 |

| Key Performance Parameters | | | |
|---|---|---|---|
| Oxygen Recovery (%) | 24.8 | BSF (kg/TPDc) | 1850.4 |
| Oxygen Purity (%): | 95.3 | | |

| End of Step CSS Temperature Profile (°C) | | | | | | | | |
|---|---|---|---|---|---|---|---|---|
| z (m) | Step 1 | Step 2 | Step 3 | Step 4 | Step 5 | Step 6 | Step 7 | Step 8 |
| 0 | 24.9 | 24.5 | 22.4 | 20.4 | 22 | 21.9 | 23.1 | 24.3 |
| 0.025 | 19.9 | 20.5 | 20.3 | 20.5 | 19.5 | 19.1 | 18.6 | 18.6 |
| 0.05 | 17.8 | 18.6 | 18.7 | 18.1 | 16.8 | 15.5 | 15.1 | 15 |
| 0.075 | 20.1 | 20.9 | 21.2 | 20.5 | 19 | 17.4 | 17.1 | 17.3 |
| 0.1 | 20.8 | 21.3 | 20.9 | 20.3 | 18.8 | 17.5 | 17.6 | 18.2 |
| 0.2 | 26.4 | 27.4 | 27.4 | 27.1 | 25.5 | 24.2 | 23.8 | 23.9 |
| 0.3 | 27.4 | 27.7 | 27.[illegible] | 27.5 | 26.2 | 25.7 | 25.4 | 25.7 |
| 0.4 | 28.7 | 29.3 | 29 | 28.7 | 27.7 | 27 | 26.7 | 27 |
| 0.5 | 28.5 | 29.4 | 29.3 | 29.1 | 27.7 | 26.5 | 26.1 | 26 |
| 0.6 | 28.9 | 30.1 | 29.8 | 29.4 | 28.1 | 27.1 | 26.6 | 26.5 |
| 0.7 | 29.9 | 31.9 | 31.9 | 31.6 | 29.9 | 28.9 | 28.1 | 27.9 |
| 0.8 | 31.2 | 32.9 | 32.9 | 32.4 | 31.1 | 29.9 | 29.3 | 29.1 |
| 0.9 | 29.9 | 32.1 | 32.5 | 32.5 | 31.3 | 30.1 | 29.5 | 29.5 |
| 1 | 30.6 | 31.5 | 32.8 | 32.9 | 31.5 | 30.6 | 30.1 | 30.3 |
| 1.1 | 31.7 | 31.8 | 33.9 | 33.8 | 32.8 | 31.8 | 31.3 | 31.3 |
| 1.2 | 31.4 | 31.5 | 32.9 | 33.3 | 32.1 | 31 | 30.9 | 30.7 |
| 1.3 | 29.3 | 29.8 | 30 | 31 | 29.9 | 29.1 | 28.9 | 28.8 |
| 1.4 | 28.2 | 28.6 | 28.7 | 28.7 | 28.2 | 27.7 | 27.7 | 27.6 |
| 1.5 | 27.6 | 27.8 | 27.8 | 27.6 | 27.2 | 27 | 27.1 | 27 |
| 1.6 | 27.8 | 28.2 | 28.2 | 28.1 | 27.6 | 27.2 | 27.2 | 27.2 |
| 1.7 | 26 | 26.4 | 26.4 | 26.2 | 25.8 | 25.5 | 25.5 | 25.5 |
| 1.75 | 26.6 | 27.1 | 27.1 | 26.9 | 26.5 | 26.2 | 26.2 | 26.2 |
| 1.8 | 27.3 | 27.8 | 27.8 | 27.6 | 27.2 | 26.9 | 26.9 | 26.8 |

## Run Number AA300NaXDLP

**Description of Experiment**
Two bed with a 300 mm prelayer of AA and main layer of NaX, PVC beds
60 sec cycle, Dry Air Feed

| Sieve Arrangement and Bed | | |
|---|---|---|
| Type of Prelayer | AA | AA |
| Type of Main Layer | NaX | NaX |
| Bed | PVC | PVC |
| | **Bed 1** | **Bed 2** |
| Mass of Prelayer (kg) | 1.88 | 1.86 |
| Mass of Main layer(kg) | 8.49 | 8.58 |
| Height of Prelayer (mm) | 300 | 300 |
| Height of Main layer(mm) | 1550 | 1550 |

| End of Step Press. at CSS (kPa) | Bed 1 | Bed 2 |
|---|---|---|
| Step 1 | 129.7 | 53.2 |
| Step 2 | 133.9 | 36.0 |
| Step 3 | 104.1 | 49.9 |
| Step 4 | 96.1 | 61.1 |
| Step 5 | 52.1 | 130.2 |
| Step 6 | 34.8 | 134.9 |
| Step 7 | 50.2 | 104.8 |
| Step 8 | 61.1 | 97.0 |

| Mass Balance at CSS (Total millimole per cycle) | | | |
|---|---|---|---|
| Feed flow | 4802.6 | Evacuation flow | 4119.3 |
| Product flow | 624.1 | Mass Balance Error (%) | 1.2 |

| Key Performance Parameters | | | |
|---|---|---|---|
| Oxygen Recovery (%) | 46.3 | BSF (kg/TPDc) | 756.6 |
| Oxygen Purity (%): | 78.5 | | |

| End of Step CSS Temperature Profile (°C) | | | | | | | | |
|---|---|---|---|---|---|---|---|---|
| z (m) | Step 1 | Step 2 | Step 3 | Step 4 | Step 5 | Step 6 | Step 7 | Step 8 |
| 0 | 19.3 | 18.6 | 16.5 | 15.7 | 16.8 | 17.6 | 18.6 | 20.1 |
| 0.025 | 18.9 | 19 | 18.9 | 18.9 | 18.9 | 18.6 | 18.6 | 18.7 |
| 0.05 | 18.3 | 18.7 | 18.2 | 18.7 | 18.3 | 17.9 | 18.2 | 18 |
| 0.075 | 18.2 | 18.4 | 18 | 18.6 | 17.9 | 17.7 | 18.1 | 17.6 |
| 0.1 | 17.4 | 17.4 | 17.4 | 17.7 | 17.1 | 17.5 | 17.3 | 17.6 |
| 0.2 | 14 | 14.2 | 13.8 | 13.8 | 13.2 | 13 | 12.7 | 12.7 |
| 0.3 | 4.8 | 5.3 | 4.8 | 5 | 3.5 | 2 | 1.4 | 1.9 |
| 0.4 | 9 | 10.1 | 9.3 | 8.8 | 6.7 | 5.3 | 4.7 | 5 |
| 0.5 | 12.2 | 13 | 12.5 | 12.2 | 9.7 | 8.5 | 8.3 | 8.5 |
| 0.6 | 15 | 15.6 | 14.9 | 14.7 | 12.8 | 11.8 | 11.9 | 12.1 |
| 0.7 | 16.3 | 17.2 | 17.3 | 16.5 | 14.9 | 13.6 | 13.4 | 13.4 |
| 0.8 | 20.1 | 20.7 | 20.5 | 20.3 | 18.4 | 17.5 | 17.3 | 17.2 |
| 0.9 | 19.3 | 20.4 | 20.3 | 20.1 | 18.7 | 17.4 | 17 | 16.8 |
| 1 | 20.3 | 21.9 | 21.4 | 21.1 | 19.8 | 18.8 | 18.3 | 18.1 |
| 1.1 | 21.4 | 23 | 22.7 | 22.5 | 21.1 | 20.3 | 19.9 | 19.6 |
| 1.2 | 22.6 | 24 | 24.1 | 23.9 | 22.4 | 21.4 | 20.9 | 20.7 |
| .. | 21.9 | 23.6 | 23.8 | 23.7 | 22.4 | 21.3 | 20.7 | 20.5 |
| 1.4 | 22.1 | 23 | 23.4 | 23.3 | 22.5 | 22 | 21.6 | 21.5 |
| 1.5 | 23.1 | 23.9 | 24.9 | 24.9 | 23.8 | 23.1 | 22.6 | 22.4 |
| 1.75 | 24 | 24.4 | 25.1 | 25.8 | 25.6 | 24.7 | 23.9 | 23.6 |
| 1.8 | 24.5 | 24.7 | 25 | 25.8 | 25.7 | 24.7 | 23.9 | 23.8 |

## Run Number AA300NaXDHP

**Description of Experiment**

Two bed with a 300 mm prelayer of AA and main layer of NaX, PVC beds
60 sec cycle, Dry Air Feed

| Sieve Arrangement and Bed | | |
|---|---|---|
| Type of Prelayer | AA | AA |
| Type of Main Layer | NaX | NaX |
| Bed | PVC | PVC |
| | **Bed 1** | **Bed 2** |
| Mass of Prelayer (kg) | 1.88 | 1.86 |
| Mass of Main layer(kg) | 8.49 | 8.58 |
| Height of Prelayer (mm) | 300 | 300 |
| Height of Main layer(mm) | 1550 | 1550 |

| End of Step Press. at CSS (kPa) | Bed 1 | Bed 2 |
|---|---|---|
| Step 1 | 134.6 | 51.8 |
| Step 2 | 140.5 | 34.4 |
| Step 3 | 106.4 | 51.0 |
| Step 4 | 96.3 | 62.9 |
| Step 5 | 51.2 | 135.3 |
| Step 6 | 33.0 | 141.6 |
| Step 7 | 50.3 | 106.3 |
| Step 8 | 62.2 | 95.8 |

| Mass Balance at CSS (Total millimole per cycle) | | | |
|---|---|---|---|
| Feed flow | 4441.8 | Evacuation flow | 4010.2 |
| Product flow. | 234.2 | Mass Balance Error (%) | 4.4 |

| Key Performance Parameters | | | |
|---|---|---|---|
| Oxygen Recovery (%) | 22.9 | BSF (kg/TPDc) | 1581.5 |
| Oxygen Purity (%): | 95.6 | | |

| End of Step CSS Temperature Profile (°C) | | | | | | | | |
|---|---|---|---|---|---|---|---|---|
| z (m) | Step 1 | Step 2 | Step 3 | Step 4 | Step 5 | Step 6 | Step 7 | Step 8 |
| 0 | 21.7 | 21.6 | 19.3 | 18.5 | 19.9 | 19.9 | 20.6 | 21.5 |
| 0.1 | 18.7 | 19.1 | 18.6 | 19 | 19.4 | 19.6 | 19.1 | 19.4 |
| 0.2 | 10.4 | 10.1 | 9.9 | 10.1 | 11.5 | 11.4 | 11.3 | 11.2 |
| 0.3 | 0.3 | -0.5 | -0.9 | -0.7 | 2 | 2.7 | 2.3 | 2.2 |
| 0.4 | 12.6 | 11.7 | 10.9 | 11.2 | 15.3 | 15.9 | 15.3 | 14.9 |
| 0.5 | 18.1 | 16.7 | 16.2 | 16.2 | 20.3 | 21.1 | 20.8 | 20.4 |
| 0.6 | 21.1 | 19.7 | 19.6 | 19.3 | 23.2 | 23.9 | 23.3 | 23.1 |
| 0.7 | 23.6 | 21.9 | 21.7 | 21.4 | 25.1 | 25.5 | 25.3 | 25.2 |
| 0.8 | 25.1 | 23.7 | 23.2 | 23.1 | 26.2 | 27.2 | 27 | 26.7 |
| 0.9 | 25.6 | 24.6 | 23.6 | 23.4 | 26.4 | 27.6 | 27.7 | 27.5 |
| 1 | 27.3 | 26 | 25.3 | 24.9 | 26.9 | 28.6 | 29.1 | 29 |
| 1.1 | 28.5 | 27.1 | 26.2 | 26.3 | 27.2 | 28.8 | 30.3 | 30.1 |
| 1.2 | 28.6 | 27.5 | 27.2 | 27.1 | 27.7 | 28.1 | 29.3 | 29.6 |
| 1.3 | 28.7 | 27.5 | 27.1 | 27 | 27.6 | 28 | 28.8 | 29.5 |
| 1.6 | 25.7 | 26 | 26 | 25.9 | 25.4 | 25 | 25 | 25 |
| 1.75 | 23.6 | 23.2 | 23.2 | 23.2 | 23.9 | 24.2 | 24.1 | 24 |

## Run Number AA300NaXWLP

**Description of Experiment**
Two bed with a 300 mm prelayer of AA and main layer of NaX, PVC beds
60 sec cycle, Wet Air Feed

| Sieve Arrangement and Bed | | |
|---|---|---|
| Type of Prelayer | AA | AA |
| Type of Main Layer | NaX | NaX |
| Bed | PVC | PVC |
| | **Bed 1** | **Bed 2** |
| Mass of Prelayer (kg) | 1.88 | 1.86 |
| Mass of Main layer(kg) | 8.49 | 8.53 |
| Height of Prelayer (mm) | 300 | 300 |
| Height of Main layer(mm) | 1550 | 1550 |

| End of Step Press. at CSS (kPa) | Bed 1 | Bed 2 |
|---|---|---|
| Step 1 | 127.4 | 52.4 |
| Step 2 | 135.3 | 35.2 |
| Step 3 | 105.9 | 48.1 |
| Step 4 | 96.8 | 60.5 |
| Step 5 | 51.4 | 127.2 |
| Step 6 | 34.3 | 136.0 |
| Step 7 | 48.4 | 105.9 |
| Step 8 | 60.8 | 97.1 |

| Mass Balance at CSS (Total millimole per cycle) | | | |
|---|---|---|---|
| Feed flow | 4698.1 | Evacuation flow | 4234.27 |
| Product flow | 622.96 | Mass Balance Error (%) | -3.4 |

| Key Performance Parameters | | | |
|---|---|---|---|
| Oxygen Recovery (%) | 48.21 | BSF (kg/TPDc) | 743.453 |
| Oxygen Purity (%): | 79.98 | | |

| End of Step CSS Temperature Profile (°C) | | | | | | | | |
|---|---|---|---|---|---|---|---|---|
| z (m) | Step 1 | Step 2 | Step 3 | Step 4 | Step 5 | Step 6 | Step 7 | Step 8 |
| 0 | 19.3 | 19.1 | 16.8 | 15.9 | 18.1 | 17.4 | 18.2 | 19.5 |
| 0.025 | 19.5 | 20.1 | 20.1 | 20 | 19.4 | 19.1 | 19 | 18.7 |
| 0.05 | 19 | 19.7 | 19.5 | 19.4 | 19.2 | 18.8 | 18.6 | 18.4 |
| 0.075 | 18.8 | 19.2 | 19.1 | 19.3 | 19.2 | 18.5 | 18.4 | 18.8 |
| 0.1 | 18.3 | 19.1 | 18.6 | 18.8 | 18.8 | 18.2 | 17.7 | 18.1 |
| 0.2 | 15.1 | 15.1 | 14.9 | 15 | 14.2 | 14 | 13.7 | 13.8 |
| 0.3 | 6.1 | 6.7 | 6.4 | 6.2 | 4.1 | 3.4 | 2.7 | 3 |
| 0.4 | 9.9 | 10.8 | 10.3 | 10.2 | 7.5 | 6 | 5.6 | 6.1 |
| 0.5 | 12.9 | 13.8 | 13.7 | 13.3 | 10.7 | 9.5 | 9.2 | 9.3 |
| 0.6 | 15.9 | 16.4 | 16.1 | 15.9 | 14 | 12.7 | 12.8 | 12.7 |
| 0.7 | 17.1 | 18.1 | 18.1 | 17.4 | 15.4 | 13.9 | 14.1 | 14.2 |
| 0.8 | 20.9 | 21.7 | 21.6 | 21.3 | 19.7 | 18.5 | 18.3 | 18 |
| 0.9 | 20.2 | 21.6 | 21.4 | 21 | 19.4 | 18.3 | 18.1 | 18.1 |
| 1 | 21 | 22.7 | 22.4 | 22.3 | 20.6 | 19.3 | 19.3 | 19 |
| 1.1 | 21.9 | 23.4 | 23.6 | 23.6 | 22.1 | 20.8 | 20.6 | 19.9 |
| 1.2 | 22.9 | 24.7 | 24.9 | 24.7 | 23.2 | 22.1 | 21.5 | 21.3 |
| 1.3 | 22.6 | 24.6 | 24.9 | 24.8 | 23.4 | 22.3 | 21.8 | 21.5 |
| 1.4 | 23.4 | 24.2 | 24.8 | 24.6 | 23.7 | 23.3 | 22.9 | 22.7 |
| 1.5 | 24.2 | 25 | 26.1 | 26.1 | 25 | 24.3 | 23.8 | 23.5 |
| 1.6 | 25.2 | 25.8 | 26.8 | 27.1 | 26.1 | 25.4 | 24.9 | 24.7 |
| 1.7 | 24.1 | 24.5 | 25.2 | 25.9 | 25.7 | 24.9 | 24 | 23.8 |
| 1.75 | 25 | 25.3 | 25.9 | 26.6 | 26.5 | 25.7 | 24.8 | 24.6 |
| 1.8 | 25.3 | 25.6 | 25.9 | 26.7 | 26.6 | 25.7 | 24.9 | 24.8 |

## Run Number AA300NaXWHP

**Description of Experiment**

Two bed with a 300 mm prelayer of AA and main layer of NaX, PVC beds
60 sec cycle, Wet Air Feed

| Sieve Arrangement and Bed | | |
|---|---|---|
| Type of Prelayer | AA | AA |
| Type of Main Layer | NaX | NaX |
| Bed | PVC | PVC |
| | **Bed 1** | **Bed 2** |
| Mass of Prelayer (kg) | 1.88 | 1.86 |
| Mass of Main layer(kg) | 8.49 | 8.58 |
| Height of Prelayer (mm) | 300 | 300 |
| Height of Main layer(mm) | 1550 | 1550 |

| End of Step Press. at CSS (kPa) | Bed 1 | Bed 2 |
|---|---|---|
| Step 1 | 128.4 | 50.9 |
| Step 2 | 141.2 | 33.7 |
| Step 3 | 105.5 | 50.8 |
| Step 4 | 94.8 | 63.3 |
| Step 5 | 50.3 | 128.6 |
| Step 6 | 32.6 | 142.2 |
| Step 7 | 50.4 | 105.5 |
| Step 8 | 63.0 | 94.4 |

| Mass Balance at CSS (Total millimole per cycle) | | | |
|---|---|---|---|
| Feed flow | 4252.1 | Evacuation flow | 4095.19 |
| Product flow | 234.44 | Mass Balance Error (%) | -1.8 |

| Key Performance Parameters | | | |
|---|---|---|---|
| Oxygen Recovery (%) | 23.77 | BSF (kg/TPDc) | 1580.17 |
| Oxygen Purity (%): | 94.85 | | |

| End of Step CSS Temperature Profile (°C) | | | | | | | | |
|---|---|---|---|---|---|---|---|---|
| z (m) | Step 1 | Step 2 | Step 3 | Step 4 | Step 5 | Step 6 | Step 7 | Step 8 |
| 0 | 17.5 | 16.6 | 17.5 | 18.8 | 18.9 | 19.2 | 17.1 | 15.9 |
| 0.1 | 15.5 | 14.8 | 14.3 | 14.8 | 15.2 | 15.5 | 15.8 | 15.8 |
| 0.2 | 8.1 | 8.1 | 8 | 8 | 6.9 | 6.7 | 6.6 | 6.6 |
| 0.3 | -1.8 | -1.1 | -1.3 | -1.6 | -3.8 | -5 | -5.2 | -5.3 |
| 0.4 | 13.4 | 14.4 | 13.8 | 13.3 | 10.9 | 9.8 | 9.5 | 9.4 |
| 0.5 | 18.7 | 19.7 | 19.4 | 18.8 | 16.8 | 15.5 | 14.9 | 14.6 |
| 0.6 | 21.8 | 22.2 | 22.1 | 21.7 | 19.8 | 18.6 | 18.2 | 17.9 |
| 0.7 | 23.5 | 24.6 | 24.6 | 24.1 | 22 | 20.6 | 20.2 | 20.1 |
| 0.8 | 25.3 | 26.5 | 26.4 | 26.1 | 24.3 | 23.2 | 22.5 | 22.2 |
| 0.9 | 24.2 | 26.3 | 26.3 | 26.1 | 24.7 | 23.3 | 22.8 | 22.3 |
| 1 | 24.3 | 27.1 | 27.4 | 27.5 | 25.9 | 24.5 | 23.9 | 23.7 |
| 1.1 | 26.8 | 27.8 | 29.3 | 29.8 | 28.2 | 27.1 | 26.2 | 26.4 |
| 1.2 | 27 | 27.2 | 29.1 | 29.5 | 28.3 | 27.1 | 26.4 | 26.3 |
| 1.3 | 25.6 | 26.1 | 26.9 | 27.9 | 26.7 | 25.6 | 25.2 | 25.2 |
| 1.4 | 23.6 | 23.7 | 23.7 | 24 | 23.5 | 23.3 | 23.3 | 23.2 |
| 1.5 | 23.2 | 23.5 | 23.4 | 23.3 | 22.8 | 22.5 | 22.6 | 22.6 |
| 1.6 | 23.1 | 23.4 | 23.2 | 23.1 | 22.6 | 22.4 | 22.5 | 22.5 |
| 1.7 | 21.1 | 21.6 | 21.5 | 21.4 | 20.8 | 20.5 | 20.5 | 20.5 |
| 1.75 | 21.7 | 22.1 | 22 | 21.9 | 21.3 | 20.9 | 20.9 | 21 |
| 1.8 | 22.1 | 22.5 | 22.4 | 22.3 | 21.8 | 21.4 | 21.4 | 21.5 |

# Run Number MAACaX1

**Description of Experiment**

Two bed with 200 mm prelayer of activated alumina, main layer CaX, PVC bed
60 second cycle

| Sieve Arrangement and Bed | | |
|---|---|---|
| Type of Prelayer | AA | AA |
| Type of Main Layer | VSA2 | VSA2 |
| Bed | Metal | Metal |
| | **Bed 1** | **Bed 2** |
| Mass of Prelayer (kg) | 1.3 | 1.3 |
| Mass of Main layer(kg) | 10 | 10 |
| Height of Prelayer (mm) | 200 | 200 |
| Height of Main layer(mm) | 1750 | 1750 |

| End of Step Press. at CSS (kPa) | Bed 1 | Bed 2 |
|---|---|---|
| Step 1 | 126.9 | 58.0 |
| Step 2 | 131.9 | 46.9 |
| Step 3 | 106.6 | 55.6 |
| Step 4 | 86.8 | 72.9 |
| Step 5 | 54.3 | 125.0 |
| Step 6 | 43.6 | 131.6 |
| Step 7 | 53.6 | 108.0 |
| Step 8 | 72.6 | 90.5 |

| Mass Balance at CSS (Total millimole per cycle) | | | |
|---|---|---|---|
| Feed flow | 3990.1 | Evacuation flow | 3624.6 |
| Product flow | 401.2 | Mass Balance Error (%) | -0.9 |

| Key Performance Parameters | | | |
|---|---|---|---|
| Oxygen Recovery (%) | 38.9 | BSF (kg/TPDc) | 1233.9 |
| Power: (kW/TPDc) | 15.3 | Oxygen Purity (%): | 89.8 |

| T/C | Axial Position | Min Temp | Max Temp |
|---|---|---|---|
| Temp9 | 0 | 12.8 | 13.5 |
| Temp10 | 0.1 | 9.9 | 10.8 |
| Temp11 | 0.26 | 4.5 | 7.6 |
| Temp12 | 0.42 | 11.4 | 13.5 |
| Temp13 | 0.97 | 12.9 | 16.4 |
| Temp14 | 1.37 | 14.7 | 16.8 |
| Temp17 | 1.81 | 13.7 | 17.1 |

# Run Number MAACaX2

**Description of Experiment**

Two bed with 200 mm prelayer of activated alumina, main layer CaX, PVC bed
60 second cycle

| Sieve Arrangement and Bed | | |
|---|---|---|
| Type of Prelayer | AA | AA |
| Type of Main Layer | VSA2 | VSA2 |
| Bed | Metal | Metal |
| | **Bed 1** | **Bed 2** |
| Mass of Prelayer (kg) | 1.3 | 1.3 |
| Mass of Main layer(kg) | 10 | 10 |
| Height of Prelayer (mm) | 200 | 200 |
| Height of Main layer(mm) | 1750 | 1750 |

| End of Step Press. at CSS (kPa) | Bed 1 | Bed 2 |
|---|---|---|
| Step 1 | 134.3 | 65.6 |
| Step 2 | 140.3 | 53.1 |
| Step 3 | 118.6 | 62.7 |
| Step 4 | 101.0 | 80.8 |
| Step 5 | 68.5 | 136.7 |
| Step 6 | 56.4 | 140.8 |
| Step 7 | 64.7 | 116.3 |
| Step 8 | 80.7 | 99.2 |

| Mass Balance at CSS (Total millimole per cycle) | | | |
|---|---|---|---|
| Feed flow | 3773.8 | Evacuation flow | 3109.2 |
| Product flow | 458.3 | Mass Balance Error (%) | 5.5 |

| Key Performance Parameters | | | |
|---|---|---|---|
| Oxygen Recovery (%) | 36.1 | BSF (kg/TPDc) | 1428.6 |
| Power: (kW/TPDc) | 10.1 | Oxygen Purity (%): | 65.3 |

| T/C | Axial Position | Min Temp | Max Temp |
|---|---|---|---|
| Temp9 | 0 | 14 | 15.2 |
| Temp10 | 0.1 | 10 | 11.5 |
| Temp11 | 0.26 | 10.5 | 12.5 |
| Temp12 | 0.42 | 12.4 | 14.7 |
| Temp13 | 0.97 | 13.9 | 15.9 |
| Temp14 | 1.37 | 14.5 | 16.2 |
| Temp17 | 1.81 | 16.1 | 18.6 |

# Run Number MAACaX3

**Description of Experiment**

Two bed with 200 mm prelayer of activated alumina, main layer CaX, PVC bed
60 second cycle

| Sieve Arrangement and Bed | | |
|---|---|---|
| Type of Prelayer | AA | AA |
| Type of Main Layer | VSA2 | VSA2 |
| Bed | Metal | Metal |
| | **Bed 1** | **Bed 2** |
| Mass of Prelayer (kg) | 1.3 | 1.3 |
| Mass of Main layer(kg) | 10 | 10 |
| Height of Prelayer (mm) | 200 | 200 |
| Height of Main layer(mm) | 1750 | 1750 |

| End of Step Press. at CSS (kPa) | Bed 1 | Bed 2 |
|---|---|---|
| Step 1 | 129.4 | 57 |
| Step 2 | 129.3 | 46.3 |
| Step 3 | 105.6 | 55.4 |
| Step 4 | 88.1 | 72.2 |
| Step 5 | 57.0 | 129.6 |
| Step 6 | 46.5 | 129.4 |
| Step 7 | 55.9 | 105.5 |
| Step 8 | 72.7 | 88.6 |

| Mass Balance at CSS (Total millimole per cycle) | | | |
|---|---|---|---|
| Feed flow | 4057.6 | Evacuation flow | 3663.9 |
| Product flow | 389.1 | Mass Balance Error (%) | 0.1 |

| Key Performance Parameters | | | |
|---|---|---|---|
| Oxygen Recovery (%) | 40.60 | BSF (kg/TPDc) | 1197.00 |
| Power: (kW/TPDc) | 14.55 | Oxygen Purity (%): | 93.20 |

| T/C | Axial Position | Min Temp | Max Temp |
|---|---|---|---|
| Temp9 | 0 | 14.1 | 15.6 |
| Temp10 | 0.1 | 11 | 12.5 |
| Temp11 | 0.26 | 7.5 | 9.6 |
| Temp12 | 0.42 | 13.4 | 15.2 |
| Temp13 | 0.97 | 15.5 | 18 |
| Temp14 | 1.37 | 16.9 | 18.6 |
| Temp17 | 1.81 | 14.8 | 16.7 |

# Run Number 1BAA300NaX1

**Description of Experiment**

One bed with 300 mm prelayer of activated alumina, main layer NaX (APG), 56 second cycle, PVC Bed

| Sieve Arrangement and Bed | |
|---|---|
| Type of Prelayer | AA |
| Type of Main Layer | NaX(APG) |
| Bed | PVC |
| Mass of Prelayer: | 2.04 kg |
| Mass of Main layer: | 8.3 kg |
| Height of Prelayer: | 300 mm |
| Height of Main layer: | 1550 mm |

| End of Step Pressures at CSS (kPa) | |
|---|---|
| Step 1 | 133.7 |
| Step 2 | 138.4 |
| Step 3 | 101 |
| Step 4 | 30.5 |
| Step 5 | 34.5 |

| Mass Balance at CSS (Total millimole per cycle) | | | |
|---|---|---|---|
| Feed flow | 3505.6 | Evacuation flow | 3121.4 |
| Product flow | 228.7 | Mass Balance Error (%) | 4 |

| Key Performance Parameters | | | |
|---|---|---|---|
| Oxygen Recovery (%) | 26.5 | BSF (kg/TPDc) | 822.1 |
| Power: (kW/TPDc) | 16.7 | Oxygen Purity (%): | 89.4 |

| End of Step CSS Temperature Profile (°C) | | | | | |
|---|---|---|---|---|---|
| z (m) | Step 1 | Step 2 | Step 3 | Step 4 | Step 5 |
| 0 | 19.2 | 19.1 | 19.1 | 19.1 | 19.6 |
| 0.1 | 16.4 | 16.4 | 15.8 | 15.6 | 15.7 |
| 0.2 | 12.1 | 12.3 | 12.1 | 11.6 | 11.6 |
| 0.3 | 8.4 | 8.5 | 7.9 | 7.5 | 7.3 |
| 0.4 | 10.6 | 11.9 | 11.7 | 7.2 | 6.9 |
| 0.5 | 14.7 | 16 | 15.7 | 11.2 | 11 |
| 0.6 | 17.5 | 18.8 | 18.3 | 14.7 | 14.7 |
| 0.7 | 19.3 | 20.7 | 20 | 16.4 | 16.2 |
| 0.8 | 21 | 22.4 | 22.1 | 18.6 | 18.1 |
| 0.9 | 21.3 | 22.9 | 22.7 | 18.9 | 18.5 |
| 1 | 22.2 | 23.9 | 23.5 | 19.8 | 19.5 |
| 1.1 | 23.2 | 24.9 | 24.4 | 20.8 | 20.5 |
| 1.2 | 23.4 | 25.2 | 25 | 22.1 | 21.5 |
| 1.3 | 23.3 | 25.4 | 25.4 | 22.2 | 21.6 |
| 1.4 | 23.4 | 25.2 | 25.2 | 22.7 | 22.2 |
| 1.5 | 24.8 | 27.3 | 27.3 | 24.1 | 23.3 |
| 1.6 | 25.5 | 28 | 28.1 | 25.3 | 24.7 |
| 1.7 | 23.8 | 25.9 | 26 | 23.8 | 23.2 |
| 1.75 | 24.4 | 26.4 | 26.5 | 24.5 | 24 |
| 1.8 | 25.5 | 27.2 | 27.3 | 25.6 | 25.1 |

# Run Number 1BAA300NaX2

**Description of Experiment**
One bed with 300 mm prelayer of activated alumina, main layer NaX (APG), 56 second cycle, PVC Bed

| Sieve Arrangement and Bed | |
|---|---|
| Type of Prelayer | AA |
| Type of Main Layer | NaX(APG) |
| Bed | PVC |
| Mass of Prelayer: | 2.04 kg |
| Mass of Main layer: | 8.3 kg |
| Height of Prelayer: | 300 mm |
| Height of Main layer: | 1550 mm |

| End of Step Pressures at CSS (kPa) | |
|---|---|
| Step 1 | 135 |
| Step 2 | 140 |
| Step 3 | 101 |
| Step 4 | 30.8 |
| Step 5 | 34.4 |

| Mass Balance at CSS (Total millimole per cycle) | | | |
|---|---|---|---|
| Feed flow | 3709.4 | Evacuation flow | 3096.8 |
| Product flow | 491.8 | Mass Balance Error (%) | 3 |

| Key Performance Parameters | | | |
|---|---|---|---|
| Oxygen Recovery (%) | 37.4 | BSF (kg/TPDc) | 550.5 |
| Power: (kW/TPDc) | 11.6 | Oxygen Purity (%): | 62.1 |

| End of Step CSS Temperature Profile (°C) | | | | | |
|---|---|---|---|---|---|
| z (m) | Step 1 | Step 2 | Step 3 | Step 4 | Step 5 |
| 0 | 23.6 | 23.5 | 23.5 | 23.2 | 23.8 |
| 0.1 | 21.2 | 20.9 | 21.1 | 20.3 | 20.7 |
| 0.2 | 18.5 | 18.6 | 18.4 | 18 | 18.1 |
| 0.3 | 15.4 | 15.2 | 15.4 | 14.2 | 14.2 |
| 0.4 | 13.7 | 15.2 | 14.8 | 10.1 | 9.9 |
| 0.5 | 15.9 | 17.1 | 16.5 | 12.3 | 11.7 |
| 0.6 | 17.9 | 18.8 | 18.5 | 14.8 | 14.5 |
| 0.7 | 18.5 | 19.9 | 19.6 | 15.8 | 15.2 |
| 0.8 | 19.5 | 21 | 20.7 | 17.1 | 16.6 |
| 0.9 | 19.9 | 21.4 | 21 | 17.2 | 16.7 |
| 1 | 20.8 | 22.2 | 22.1 | 18.4 | 17.8 |
| 1.1 | 21.5 | 23.3 | 23.2 | 19.5 | 18.9 |
| 1.2 | 22.9 | 24.5 | 24.3 | 21.2 | 20.9 |
| 1.3 | 22.4 | 24.3 | 24.3 | 21.2 | 20.6 |
| 1.4 | 23.9 | 25.3 | 25.2 | 23 | 22.6 |
| 1.5 | 24.5 | 26.6 | 26.6 | 23.4 | 22.7 |
| 1.6 | 25.3 | 27.4 | 27.3 | 24.7 | 24 |
| 1.7 | 24.1 | 26.1 | 26.1 | 24.1 | 23.4 |
| 1.75 | 24.9 | 27.2 | 27.2 | 25 | 24.1 |
| 1.8 | 25.6 | 27.9 | 28 | 26 | 25.1 |

# Run Number 1BAA300NaX3

**Description of Experiment**
One bed with 300 mm prelayer of activated alumina, main layer NaX (APG), 56 second cycle, PVC Bed

| Sieve Arrangement and Bed | |
|---|---|
| Type of Prelayer | AA |
| Type of Main Layer | NaX(APG) |
| Bed | PVC |
| Mass of Prelayer: | 2.04 kg |
| Mass of Main layer: | 8.3 kg |
| Height of Prelayer: | 300 mm |
| Height of Main layer: | 1550 mm |

| End of Step Pressures at CSS (kPa) | |
|---|---|
| Step 1 | 133.4 |
| Step 2 | 138.2 |
| Step 3 | 101.0 |
| Step 4 | 33.1 |
| Step 5 | 36.4 |

| Mass Balance at CSS (Total millimole per cycle) | | | |
|---|---|---|---|
| Feed flow | 3321.7 | Evacuation flow | 2960.6 |
| Product flow | 251.2 | Mass Balance Error (%) | 3 |

| Key Performance Parameters | | | |
|---|---|---|---|
| Oxygen Recovery (%) | 28.5 | BSF (kg/TPDc) | 806.7 |
| Power: (kW/TPDc) | 14.8 | Oxygen Purity (%): | 86.8 |

| End of Step CSS Temperature Profile (°C) | | | | | |
|---|---|---|---|---|---|
| z (m) | Step 1 | Step 2 | Step 3 | Step 4 | Step 5 |
| 0 | 22.3 | 22.4 | 22.5 | 22.2 | 22.7 |
| 0.1 | 19.8 | 19.8 | 20.1 | 19.3 | 19.7 |
| 0.2 | 17.2 | 17.4 | 17.2 | 16.6 | 16.7 |
| 0.3 | 13.5 | 13.7 | 13.9 | 12.8 | 12.8 |
| 0.4 | 14.3 | 15.7 | 15.6 | 11.3 | 11.1 |
| 0.5 | 17.9 | 19 | 18.5 | 14.5 | 14.2 |
| 0.6 | 20.1 | 20.9 | 20.6 | 17.5 | 17.1 |
| 0.7 | 20.9 | 22.1 | 22 | 18.7 | 18.3 |
| 0.8 | 22.3 | 23.6 | 23.6 | 20.1 | 19.8 |
| 0.9 | 22.6 | 24 | 23.7 | 20.3 | 19.9 |
| 1 | 23.1 | 24.5 | 24.3 | 20.8 | 20.6 |
| 1.1 | 23.6 | 25 | 25 | 21.5 | 21 |
| 1.2 | 24.2 | 25.4 | 25.5 | 22.7 | 22.1 |
| 1.3 | 23.8 | 25.5 | 25.6 | 22.6 | 22.1 |
| 1.4 | 24.3 | 25.8 | 25.8 | 23.5 | 23.1 |
| 1.5 | 25.1 | 27.1 | 27.2 | 24.1 | 23.5 |
| 1.6 | 25.8 | 27.7 | 27.8 | 25.2 | 24.6 |
| 1.7 | 24.4 | 26.2 | 26.2 | 24.4 | 23.8 |
| 1.75 | 25.1 | 27.1 | 27.2 | 25.3 | 24.6 |
| 1.8 | 26 | 27.9 | 28.1 | 26.3 | 25.6 |

# Run Number 1BAA300NaX4

**Description of Experiment**

One bed with 300 mm prelayer of activated alumina, main layer NaX (APG), 56 second cycle, PVC Bed

| Sieve Arrangement and Bed | |
|---|---|
| Type of Prelayer | AA |
| Type of Main Layer | NaX(APG) |
| Bed | PVC |
| Mass of Prelayer: | 2.04 kg |
| Mass of Main layer: | 8.3 kg |
| Height of Prelayer: | 300 mm |
| Height of Main layer: | 1550 mm |

| End of Step Pressures at CSS (kPa) | |
|---|---|
| Step 1 | 135.1 |
| Step 2 | 140.2 |
| Step 3 | 101.0 |
| Step 4 | 30.6 |
| Step 5 | 35.4 |

| Mass Balance at CSS (Total millimole per cycle) | | | |
|---|---|---|---|
| Feed flow | 3527.6 | Evacuation flow | 3057.736 |
| Product flow | 367.6 | Mass Balance Error (%) | 3 |

| Key Performance Parameters | | | |
|---|---|---|---|
| Oxygen Recovery (%) | 35.3 | BSF (kg/TPDc) | 613.5 |
| Power: (kW/TPDc) | 12.4 | Oxygen Purity (%): | 74.6 |

| End of Step CSS Temperature Profile (°C) | | | | | |
|---|---|---|---|---|---|
| z (m) | Step 1 | Step 2 | Step 3 | Step 4 | Step 5 |
| 0 | 24.2 | 23.7 | 24.7 | 23.8 | 24.5 |
| 0.1 | 21.6 | 21.1 | 21.7 | 20.8 | 21.1 |
| 0.2 | 19 | 19 | 19 | 18.4 | 18.5 |
| 0.3 | 15.6 | 15.4 | 15.4 | 14.4 | 14.2 |
| 0.4 | 14.8 | 15.9 | 15.9 | 11.1 | 11 |
| 0.5 | 17.6 | 18.7 | 18.5 | 14.2 | 13.8 |
| 0.6 | 19.9 | 20.9 | 20.8 | 16.9 | 16.8 |
| 0.7 | 21 | 22.4 | 22 | 18 | 17.7 |
| 0.8 | 22.2 | 23.6 | 23.3 | 19.8 | 19.3 |
| 0.9 | 22.5 | 24.1 | 23.7 | 20.1 | 19.8 |
| 1 | 23 | 24.8 | 24.5 | 20.8 | 20.6 |
| 1.1 | 23.7 | 25.3 | 25.4 | 21.7 | 21.2 |
| 1.2 | 24.7 | 26.2 | 26.2 | 23.1 | 22.6 |
| 1.3 | 24.5 | 26.2 | 26.3 | 23.2 | 22.7 |
| 1.4 | 25.2 | 26.8 | 26.8 | 24.3 | 23.8 |
| 1.5 | 26 | 28.2 | 28.2 | 25 | 24.2 |
| 1.6 | 26.6 | 28.8 | 28.8 | 26.1 | 25.4 |
| 1.7 | 25.4 | 27.4 | 27.4 | 25.4 | 24.8 |
| 1.75 | 26.1 | 28.4 | 28.5 | 26.2 | 25.5 |
| 1.8 | 27 | 29.2 | 29.3 | 27.4 | 26.6 |

# Run Number 1BAA300NaX5

**Description of Experiment**

One bed with 300 mm prelayer of activated alumina, main layer NaX (APG), 56 second cycle, PVC Bed

| Sieve Arrangement and Bed | |
|---|---|
| Type of Prelayer | AA |
| Type of Main Layer | NaX(APG) |
| Bed | PVC |
| Mass of Prelayer: | 2.04 kg |
| Mass of Main layer: | 8.3 kg |
| Height of Prelayer: | 300 mm |
| Height of Main layer: | 1550 mm |

| End of Step Pressures at CSS (kPa) | |
|---|---|
| Step 1 | 135.3 |
| Step 2 | 140.2 |
| Step 3 | 101.0 |
| Step 4 | 30.2 |
| Step 5 | 35.6 |

| Mass Balance at CSS (Total millimole per cycle) | | | |
|---|---|---|---|
| Feed flow | 3341.5 | Evacuation flow | 3039.2 |
| Product flow | 189.4 | Mass Balance Error (%) | 3 |

| Key Performance Parameters | | | |
|---|---|---|---|
| Oxygen Recovery (%) | 24.2 | BSF (kg/TPDc) | 944.4 |
| Power: (kW/TPDc) | 18.5 | Oxygen Purity (%): | 94 |

| End of Step CSS Temperature Profile (°C) | | | | | |
|---|---|---|---|---|---|
| z (m) | Step 1 | Step 2 | Step 3 | Step 4 | Step 5 |
| 0 | 25.6 | 26.3 | 25.8 | 26.3 | 25.6 |
| 0.1 | 21.6 | 22.1 | 21.8 | 21.6 | 20.8 |
| 0.2 | 18.4 | 18.7 | 18.4 | 18 | 17.7 |
| 0.3 | 14.5 | 14.7 | 14.6 | 14.1 | 13.4 |
| 0.4 | 17 | 18.4 | 17.8 | 13.8 | 13.2 |
| 0.5 | 20.7 | 21.9 | 21.4 | 17.2 | 16.9 |
| 0.6 | 22.7 | 23.7 | 23.5 | 19.9 | 19.4 |
| 0.7 | 23.7 | 24.8 | 24.8 | 20.8 | 20.2 |
| 0.8 | 24.8 | 26.1 | 25.8 | 22.3 | 21.6 |
| 0.9 | 24.7 | 26.2 | 25.9 | 22 | 21.6 |
| 1 | 25.2 | 26.7 | 26.7 | 22.8 | 22.2 |
| 1.1 | 25.8 | 27.8 | 27.4 | 23.8 | 23 |
| 1.2 | 26.8 | 28.6 | 28.6 | 25.5 | 24.8 |
| 1.3 | 26.6 | 28.9 | 28.9 | 25.6 | 25.1 |
| 1.4 | 27 | 29.4 | 29.3 | 26.8 | 26.4 |
| 1.5 | 27.5 | 30.8 | 30.9 | 27.3 | 26.7 |
| 1.6 | 28 | 30.5 | 30.7 | 27.7 | 27.5 |
| 1.7 | 25.8 | 26.5 | 26.5 | 25.3 | 25.3 |
| 1.75 | 26.4 | 27.1 | 27 | 26 | 25.9 |
| 1.8 | 26.8 | 27.4 | 27.4 | 26.4 | 26.3 |

# Run Number 1BAA300NaX6

**Description of Experiment**
One bed with 300 mm prelayer of activated alumina, main layer NaX (APG), 56 second cycle, PVC Bed

| Sieve Arrangement and Bed | |
|---|---|
| Type of Prelayer | AA |
| Type of Main Layer | NaX(APG) |
| Bed | PVC |
| Mass of Prelayer: | 2.04 kg |
| Mass of Main layer: | 8.3 kg |
| Height of Prelayer: | 300 mm |
| Height of Main layer: | 1550 mm |

| End of Step Pressures at CSS (kPa) | |
|---|---|
| Step 1 | 136.6 |
| Step 2 | 141.0 |
| Step 3 | 101.0 |
| Step 4 | 28.9 |
| Step 5 | 34.4 |

| Mass Balance at CSS (Total millimole per cycle) | | | |
|---|---|---|---|
| Feed flow | 3337.0 | Evacuation flow | 3028.3 |
| Product flow | 170.9 | Mass Balance Error (%) | 4 |

| Key Performance Parameters | | | |
|---|---|---|---|
| Oxygen Recovery (%) | 22 | BSF (kg/TPDc) | 1041.6 |
| Power: (kW/TPDc) | 20.6 | Oxygen Purity (%): | 94.45 |

| End of Step CSS Temperature Profile (°C) | | | | | |
|---|---|---|---|---|---|
| z (m) | Step 1 | Step 2 | Step 3 | Step 4 | Step 5 |
| 0 | 22.6 | 23.1 | 22.8 | 23 | 22.7 |
| 0.1 | 21.2 | 21 | 21.3 | 20.7 | 21 |
| 0.2 | 18.2 | 18.5 | 18.3 | 17.8 | 17.8 |
| 0.3 | 14.7 | 14.7 | 14.7 | 13.7 | 13.9 |
| 0.4 | 17.4 | 18.9 | 18.3 | 14.4 | 13.9 |
| 0.5 | 21.5 | 22.6 | 22.2 | 18.2 | 17.8 |
| 0.6 | 23.9 | 24.7 | 24.6 | 21.2 | 20.9 |
| 0.7 | 25.7 | 26.5 | 26.5 | 22.8 | 22.6 |
| 0.8 | 27 | 28.2 | 28.1 | 24.5 | 24.1 |
| 0.9 | 27 | 28.3 | 28.1 | 24.5 | 23.9 |
| 1 | 27.5 | 28.8 | 28.8 | 25.4 | 24.7 |
| 1.1 | 28.3 | 29.6 | 29.7 | 25.9 | 25.5 |
| 1.2 | 28.3 | 30.2 | 30.1 | 26.9 | 26.5 |
| 1.3 | 28.3 | 30.5 | 30.5 | 27.3 | 26.7 |
| 1.4 | 28.1 | 30.4 | 30.3 | 27.7 | 27.3 |
| 1.5 | 29.5 | 32.8 | 32.8 | 29.3 | 28.8 |
| 1.6 | 30.4 | 33 | 33.1 | 30.1 | 29.8 |
| 1.7 | 27.8 | 28.6 | 28.7 | 27.4 | 27.3 |
| 1.75 | 27.8 | 28.5 | 28.5 | 27.4 | 27.3 |
| 1.8 | 28.4 | 29.1 | 29.2 | 28 | 27.9 |

# Run Number 1BAA300NaX7

**Description of Experiment**
One bed with 300 mm prelayer of activated alumina, main layer NaX (APG);
56 second cycle, PVC Bed

| Sieve Arrangement and Bed | |
|---|---|
| Type of Prelayer | AA |
| Type of Main Layer | NaX(APG) |
| Bed | PVC |
| Mass of Prelayer: | 2.04 kg |
| Mass of Main layer: | 8.3 kg |
| Height of Prelayer: | 300 mm |
| Height of Main layer: | 1550 mm |

| End of Step Pressures at CSS (kPa) | |
|---|---|
| Step 1 | 124.0 |
| Step 2 | 125.6 |
| Step 3 | 101.0 |
| Step 4 | 31.3 |
| Step 5 | 36.5 |

| Mass Balance at CSS (Total millimole per cycle) | | | |
|---|---|---|---|
| Feed flow | 2923.6 | Evacuation flow | 2801.588 |
| Product flow | 221.6 | Mass Balance Error (%) | -3 |

| Key Performance Parameters | | | |
|---|---|---|---|
| Oxygen Recovery (%) | 31.2 | BSF (kg/TPDc) | 837.6 |
| Power: (kW/TPDc) | 14.9 | Oxygen Purity (%): | 90.5 |

| End of Step CSS Temperature Profile (°C) | | | | | |
|---|---|---|---|---|---|
| z (m) | Step 1 | Step 2 | Step 3 | Step 4 | Step 5 |
| 0 | 25.1 | 24.5 | 24.7 | 24.1 | 24.7 |
| 0.1 | 22.5 | 22.4 | 22.7 | 22 | 22.4 |
| 0.2 | 20 | 20 | 20 | 19.4 | 19.4 |
| 0.3 | 16.4 | 16.4 | 16.6 | 15.9 | 15.7 |
| 0.4 | 17.5 | 18.3 | 18 | 14.3 | 14.2 |
| 0.5 | 20.6 | 21.5 | 21.2 | 17.7 | 17.3 |
| 0.6 | 23 | 23.7 | 23.4 | 20.3 | 20.5 |
| 0.7 | 24.2 | 25 | 24.8 | 21.6 | 21.6 |
| 0.8 | 25.4 | 26.4 | 26.4 | 23.5 | 23.1 |
| 0.9 | 25.6 | 26.7 | 26.8 | 23.6 | 23.2 |
| 1 | 26 | 27.5 | 27.6 | 24.1 | 24.1 |
| 1.1 | 26.7 | 28.3 | 28.3 | 24.9 | 24.8 |
| 1.2 | 27.4 | 28.7 | 28.7 | 26.2 | 25.7 |
| 1.3 | 27.2 | 29 | 29 | 26.4 | 25.9 |
| 1.4 | 27.5 | 29.2 | 29.2 | 27.1 | 26.7 |
| 1.5 | 28.6 | 31 | 31 | 28.3 | 27.6 |
| 1.6 | 29.4 | 31.7 | 31.7 | 29.4 | 28.9 |
| 1.7 | 28 | 29.6 | 29.7 | 28 | 27.6 |
| 1.75 | 28.4 | 30 | 30.1 | 28.5 | 28.1 |
| 1.8 | 29.2 | 30.3 | 30.5 | 29.3 | 28.9 |

# Run Number PuAA400NaX1

**Description of Experiment**
Two bed with 400 mm prelayer of activated alumina, main layer NaX, Polyurethane Bed, 60 second cycle, Cycle 1 (No Pressure Equalisation Step)

| Sieve Arrangement and Bed | | |
|---|---|---|
| Type of Prelayer | AA | AA |
| Type of Main Layer | NaX | NaX |
| Bed | PU | PU |
| | **Bed 1** | **Bed 2** |
| Mass of Prelayer (kg) | 2.418 | 2.424 |
| Mass of Main layer(kg) | 7.363 | 7.406 |
| Height of Prelayer (mm) | 400 | 400 |
| Height of Main layer(mm) | 1410 | 1410 |

| End of Step Press. at CSS (kPa) | Bed 1 | Bed 2 |
|---|---|---|
| Step 1 | 112.6 | 101.0 |
| Step 2 | 129.0 | 55.8 |
| Step 3 | 117.6 | 67.5 |
| Step 4 | 101.2 | 114.2 |
| Step 5 | 55.7 | 129.1 |
| Step 6 | 66.8 | 117.5 |

| Mass Balance at CSS (Total millimole per cycle) | | | |
|---|---|---|---|
| Feed flow | 3500.0 | Evacuation flow | 3216.0 |
| Product flow | 240.0 | Mass Balance Error (%) | 1.3 |

| Key Performance Parameters | | | |
|---|---|---|---|
| Oxygen Recovery (%) | 27.9 | BSF (kg/TPDc) | 1367.8 |
| Power: (kW/TPDc) | | Oxygen Purity (%): | 89.5 |

| End of Step CSS Temperature Profile (°C) | | |
|---|---|---|
| z (m) | Thigh | Tlow |
| 0 | 14.594 | 13.813 |
| 0.245 | 5.3125 | 4.6875 |
| 0.395 | -0.2 | -4.3 |
| 1.345 | 20.406 | 17.313 |
| 1.8 | 17.313 | 16.688 |

# Run Number PuAA400NaX2

**Description of Experiment**

Two bed with 400 mm prelayer of activated alumina, main layer NaX, Polyurethane Bed, 55 second cycle, Cycle 1 (No Pressure Equalisation Step)

| Sieve Arrangement and Bed | | |
|---|---|---|
| Type of Prelayer | AA | AA |
| Type of Main Layer | NaX | NaX |
| Bed | PU | PU |
| | **Bed 1** | **Bed 2** |
| Mass of Prelayer (kg) | 2.418 | 2.424 |
| Mass of Main layer(kg) | 7.363 | 7.406 |
| Height of Prelayer (mm) | 400 | 400 |
| Height of Main layer(mm) | 1410 | 1410 |

| End of Step Press. at CSS (kPa) | Bed 1 | Bed 2 |
|---|---|---|
| Step 1 | 107.0 | 86.0 |
| Step 2 | 132.0 | 60.0 |
| Step 3 | 100.0 | 76.0 |
| Step 4 | 85.0 | 108.0 |
| Step 5 | 59.0 | 132.0 |
| Step 6 | 73.0 | 101.0 |

| Mass Balance at CSS (Total millimole per cycle) | | | |
|---|---|---|---|
| Feed flow | 2858.6 | Evacuation flow | 2641.8 |
| Product flow | 245.4 | Mass Balance Error (%) | -1.0 |

| Key Performance Parameters | | | |
|---|---|---|---|
| Oxygen Recovery (%) | 35.5 | BSF (kg/TPDc) | 1315.0 |
| Power: (kW/TPDc) | | Oxygen Purity (%): | 91.0 |

| End of Step CSS Temperature Profile (°C) | | | | | | |
|---|---|---|---|---|---|---|
| z (m) | Step 1 | Step 2 | Step 3 | Step 4 | Step 5 | Step 6 |
| 0 | 19.0 | 19.1 | 18.6 | 19.0 | 19.0 | 19.2 |
| 289 | 9.1 | 9.1 | 9.3 | 9.0 | 8.8 | 8.9 |
| 414 | 0.9 | 3.0 | 2.3 | 1.6 | -0.2 | -0.3 |
| 1364 | 20.2 | 20.9 | 21.4 | 21.2 | 20.6 | 20.1 |
| 1810 | 22.3 | 22.5 | 22.5 | 22.1 | 22.6 | 22.3 |

# Run Number PuAA400NaX3

**Description of Experiment**

Two bed with 400 mm prelayer of activated alumina, main layer NaX, Polyurethane Bed, 55 second cycle, Cycle 1 (No Pressure Equalisation Step)

| Sieve Arrangement and Bed | | |
|---|---|---|
| Type of Prelayer | AA | AA |
| Type of Main Layer | NaX | NaX |
| Bed | PU | PU |
| | **Bed 1** | **Bed 2** |
| Mass of Prelayer (kg) | 2.418 | 2.424 |
| Mass of Main layer(kg) | 7.363 | 7.406 |
| Height of Prelayer (mm) | 400 | 400 |
| Height of Main layer(mm) | 1410 | 1410 |

| End of Step Press. at CSS (kPa) | Bed 1 | Bed 2 |
|---|---|---|
| Step 1 | 101.8 | 69.8 |
| Step 2 | 130.2 | 44.6 |
| Step 3 | 94.1 | 55.8 |
| Step 4 | 69.6 | 103.0 |
| Step 5 | 44.6 | 130.4 |
| Step 6 | 55.4 | 94.1 |

| Mass Balance at CSS (Total millimole per cycle) | | | |
|---|---|---|---|
| Feed flow | 3814.0 | Evacuation flow | 3427.55 |
| Product flow | 301.1 | Mass Balance Error (%) | 2.2 |

| Key Performance Parameters | | | |
|---|---|---|---|
| Oxygen Recovery (%) | 32.8 | BSF (kg/TPDc) | 1068.7 |
| Power: (kW/TPDc) | | Oxygen Purity (%): | 91.3 |

| End of Step CSS Temperature Profile (°C) | | |
|---|---|---|
| z (m) | Thigh | Tlow |
| 0 | 15.5 | 14.5 |
| 0.245 | 6.0938 | 4.8125 |
| 0.295 | 5.5 | 4.6875 |
| 0.395 | -2.4 | -7.6 |
| 1.345 | 24.688 | 21.813 |
| 1.8 | 20.188 | 19.188 |

## Run Number PuAANaXVSA69

**Description of Experiment**

Two bed with 180 mm prelayer of AA and NaX, main layer NaX, Polyurethane Bed, 70 second cycle, Cycle 2

| Sieve Arrangement and Bed | | |
|---|---|---|
| Type of Prelayer 1 | AA | AA |
| Type of Prelayer 2 | NaX | NaX |
| Type of Main Layer | VSA6 | VSA6 |
| Bed | PU | PU |
| | **Bed 1** | **Bed 2** |
| Mass of Prelayer AA (kg) | 1.577 | 1.577 |
| Mass of Prelayer NaX (kg) | 0.886 | 0.881 |
| Mass of Main layer(kg) | 7.3329 | 7.518 |
| Height of Prelayer AA (mm) | 260 | 240 |
| Height of Prelayer NaX(mm) | 180 | 180 |
| Height of Main layer(mm) | 1375 | 1400 |

| End of Step Press. at CSS (kPa) | Bed 1 | Bed 2 |
|---|---|---|
| Step 1 | 127.8 | 49.2 |
| Step 2 | 137.5 | 36.0 |
| Step 3 | 111.2 | 47.4 |
| Step 4 | 81.8 | 77.7 |
| Step 5 | 51.4 | 131.4 |
| Step 6 | 38.7 | 138.5 |
| Step 7 | 53.2 | 104.7 |
| Step 8 | 76.1 | 80.2 |

| Mass Balance at CSS (Total millimole per cycle) | |
|---|---|
| Feed flow | 4081.1 |
| Product flow | 491.9 |

| Key Performance Parameters | | | |
|---|---|---|---|
| Oxygen Recovery (%) | 48.6 | BSF (kg/TPDc) | 961.6 |
| Power: (kW/TPDc) | | Oxygen Purity (%): | 88.7 |

| End of Step CSS Temperature Profile (°C) | | |
|---|---|---|
| z (m) | Thigh | Tlow |
| 0 | 12.188 | 11.8125 |
| 0.215 | -13 | -17.799 |
| 0.245 | -13.6 | -20.499 |
| 0.295 | -5.901 | -12.201 |
| 0.395 | 6.0034 | 1.64656 |
| 0.545 | 12.094 | 8.6875 |
| 0.945 | 18.188 | 14.4063 |
| 1.8 | 15.906 | 14.1875 |

# Run Number PuAANaXVSA610

**Description of Experiment**

Two bed with 180 mm prelayer of AA and NaX, main layer NaX, Polyurethane Bed, 70 second cycle, Cycle 2

| Sieve Arrangement and Bed | | |
|---|---|---|
| Type of Prelayer 1 | AA | AA |
| Type of Prelayer 2 | NaX | NaX |
| Type of Main Layer | VSA6 | VSA6 |
| Bed | PU | PU |
| | **Bed 1** | **Bed 2** |
| Mass of Prelayer AA (kg) | 1.577 | 1.577 |
| Mass of Prelayer NaX (kg) | 0.886 | 0.881 |
| Mass of Main layer(kg) | 7.3329 | 7.518 |
| Height of Prelayer AA (mm) | 260 | 240 |
| Height of Prelayer NaX(mm) | 180 | 180 |
| Height of Main layer(mm) | 1375 | 1400 |

| End of Step Press. at CSS (kPa) | Bed 1 | Bed 2 |
|---|---|---|
| Step 1 | 120.0 | 56.3 |
| Step 2 | 134.7 | 43.7 |
| Step 3 | 108.3 | 56.4 |
| Step 4 | 83.5 | 81.9 |
| Step 5 | 58.5 | 123.7 |
| Step 6 | 43.4 | 136.3 |
| Step 7 | 62.0 | 102.9 |
| Step 8 | 81.0 | 82.3 |

| Mass Balance at CSS (Total millimole per cycle) | | | |
|---|---|---|---|
| Feed flow | 3740.0 | Evacuation flow | 3360 |
| Product flow | 420.0 | Mass Balance Error (%) | -1.1 |

| Key Performance Parameters | | | |
|---|---|---|---|
| Oxygen Recovery (%) | 45.4 | BSF (kg/TPDc) | 1125.6 |
| Power: (kW/TPDc) | | Oxygen Purity (%): | 89.0 |

| End of Step CSS Temperature Profile (°C) | | |
|---|---|---|
| z (m) | Thigh | Tlow |
| 0 | 13.188 | 12.1875 |
| 0.215 | -9.3 | -12.699 |
| 0.245 | -10.5 | -15.999 |
| 0.295 | -2.4 | -7.2994 |
| 0.395 | 8.5003 | 5.05032 |
| 0.545 | 14.313 | 11.5 |
| 0.945 | 19.906 | 16.5 |
| 1.345 | 19.406 | 15.3125 |
| 1.8 | 17.094 | 15.5 |

# Run Number PuAANaXVSA611

**Description of Experiment**

Two bed with 180 mm prelayer of AA and NaX, main layer NaX, Polyurethane Bed, 70 second cycle, Cycle 2

| Sieve Arrangement and Bed | | |
|---|---|---|
| Type of Prelayer 1 | AA | AA |
| Type of Prelayer 2 | NaX | NaX |
| Type of Main Layer | VSA6 | VSA6 |
| Bed | PU | PU |
| | **Bed 1** | **Bed 2** |
| Mass of Prelayer AA (kg) | 1.577 | 1.577 |
| Mass of Prelayer NaX (kg) | 0.886 | 0.881 |
| Mass of Main layer(kg) | 7.3329 | 7.518 |
| Height of Prelayer AA (mm) | 260 | 240 |
| Height of Prelayer NaX(mm) | 180 | 180 |
| Height of Main layer(mm) | 1375 | 1400 |

| End of Step Press. at CSS (kPa) | Bed 1 | Bed 2 |
|---|---|---|
| Step 1 | 123.0 | 56.9 |
| Step 2 | 134.4 | 43.7 |
| Step 3 | 109.0 | 53.7 |
| Step 4 | 85.0 | 79.3 |
| Step 5 | 58.5 | 125.9 |
| Step 6 | 45.9 | 136.8 |
| Step 7 | 58.6 | 104.3 |
| Step 8 | 70.5 | 84.5 |

| Mass Balance at CSS (Total millimole per cycle) | | | |
|---|---|---|---|
| Feed flow | 4260.0 | Evacuation flow | 3300 |
| Product flow | 840.0 | Mass Balance Error (%) | 2.8 |

| Key Performance Parameters | | | |
|---|---|---|---|
| Oxygen Recovery (%) | 49.3 | BSF (kg/TPDc) | 910.7 |
| Power: (kW/TPDc) | | Oxygen Purity (%): | 55.0 |

| End of Step CSS Temperature Profile (°C) | | |
|---|---|---|
| z (m) | Thigh | Tlow |
| 0 | 14.156 | 13.5938 |
| 0.215 | 2.91 | 2.39625 |
| 0.245 | -0.743 | -1.9688 |
| 0.295 | 2.6644 | 1.48125 |
| 0.395 | 7.14 | 1.455 |
| 0.545 | 12.688 | 10.4063 |
| 0.945 | 15.656 | 14.9375 |
| 1.8 | 18.344 | 17.4688 |

# Run Number PuAANaXVSA612

**Description of Experiment**

Two bed with 180 mm prelayer of AA and NaX, main layer NaX, Polyurethane Bed, 70 second cycle, Cycle 2

| Sieve Arrangement and Bed | | |
|---|---|---|
| Type of Prelayer 1 | AA | AA |
| Type of Prelayer 2 | NaX | NaX |
| Type of Main Layer | VSA6 | VSA6 |
| Bed | PU | PU |
| | **Bed 1** | **Bed 2** |
| Mass of Prelayer AA (kg) | 1.577 | 1.577 |
| Mass of Prelayer NaX (kg) | 0.886 | 0.881 |
| Mass of Main layer(kg) | 7.3329 | 7.518 |
| Height of Prelayer AA (mm) | 260 | 240 |
| Height of Prelayer NaX(mm) | 180 | 180 |
| Height of Main layer(mm) | 1375 | 1400 |

| End of Step Press. at CSS (kPa) | Bed 1 | Bed 2 |
|---|---|---|
| Step 1 | 123.8 | 57.5 |
| Step 2 | 134.7 | 44.5 |
| Step 3 | 108.8 | 55.0 |
| Step 4 | 84.3 | 80.6 |
| Step 5 | 59.1 | 125.1 |
| Step 6 | 46.8 | 136.3 |
| Step 7 | 60.6 | 104.3 |
| Step 8 | 84.5 | 84.5 |

| Mass Balance at CSS (Total millimole per cycle) | | | |
|---|---|---|---|
| Feed flow | 4104.0 | Evacuation flow | 3258.29 |
| Product flow | 620.0 | Mass Balance Error (%) | 5.5 |

| Key Performance Parameters | | | |
|---|---|---|---|
| Oxygen Recovery (%) | 46.2 | BSF (kg/TPDc) | 1008.3 |
| Power: (kW/TPDc) | | Oxygen Purity (%): | 67.3 |

| End of Step CSS Temperature Profile (°C) | | |
|---|---|---|
| z (m) | Thigh | Tlow |
| 0 | 14.406 | 13.6875 |
| 0.215 | -1.701 | -5.3006 |
| 0.245 | -3.699 | -9 |
| 0.295 | 1.2 | -3.8006 |
| 0.395 | 8.5034 | 5.00281 |
| 0.545 | 13.813 | 11.1875 |
| 0.945 | 16.5 | 13.5 |
| 1.8 | 17.5 | 16 |

# Run Number PuAANaXVSA613

**Description of Experiment**
Two bed with 180 mm prelayer of AA and NaX, main layer NaX, Polyurethane Bed, 70 second cycle, Cycle 2

| Sieve Arrangement and Bed | | |
|---|---|---|
| Type of Prelayer 1 | AA | AA |
| Type of Prelayer 2 | NaX | NaX |
| Type of Main Layer | VSA6 | VSA6 |
| Bed | PU | PU |
| | **Bed 1** | **Bed 2** |
| Mass of Prelayer AA (kg) | 1.577 | 1.577 |
| Mass of Prelayer NaX (kg) | 0.886 | 0.881 |
| Mass of Main layer(kg) | 7.3329 | 7.518 |
| Height of Prelayer AA (mm) | 260 | 240 |
| Height of Prelayer NaX(mm) | 180 | 180 |
| Height of Main layer(mm) | 1375 | 1400 |

| End of Step Press. at CSS (kPa) | Bed 1 | Bed 2 |
|---|---|---|
| Step 1 | 122.0 | 56.4 |
| Step 2 | 135.0 | 44.0 |
| Step 3 | 107.9 | 55.9 |
| Step 4 | 82.5 | 80.9 |
| Step 5 | 59.5 | 123.4 |
| Step 6 | 47.7 | 136.9 |
| Step 7 | 61.6 | 103.7 |
| Step 8 | 80.8 | 82.1 |

| Mass Balance at CSS (Total millimole per cycle) | | | |
|---|---|---|---|
| Feed flow | 3580.12 | Evacuation flow | 3353.4 |
| Product flow | 250.9 | Mass Balance Error (%) | -0.7 |

| Key Performance Parameters | | | |
|---|---|---|---|
| Oxygen Recovery (%) | 29.6 | BSF (kg/TPDc) | 1803.1 |
| Power: (kW/TPDc) | | Oxygen Purity (%): | 93.0 |

| End of Step CSS Temperature Profile (°C) | | |
|---|---|---|
| z (m) | Thigh | Tlow |
| 0 | 13.3 | 12.6 |
| 0.215 | -12.8 | -16.9 |
| 0.245 | -9.7 | -14.9 |
| 0.295 | 1.0 | -3.8 |
| 0.395 | 11.8 | 8.0 |
| 0.545 | 15.4 | 12.6 |
| 0.945 | 20.5 | 17.0 |
| 1.8 | 16.4 | 15.4 |

## Run Number PuNaXVSA6

**Description of Experiment**

Two bed with 310 mm prelayer of NaX, main layer VSA6, Polyurethane Bed, 70 second cycle, Cycle 2

| Sieve Arrangement and Bed | | |
|---|---|---|
| Type of Prelayer | NaX | NaX |
| Type of Main Layer | VSA6 | VSA6 |
| Bed | PU | PU |
| | **Bed 1** | **Bed 2** |
| Mass of Prelayer (kg) | 1.803 | 1.805 |
| Mass of Main layer(kg) | 7.58 | 7.64 |
| Height of Prelayer (mm) | 310 | 310 |
| Height of Main layer(mm) | 1500 | 1505 |

| End of Step Press. at CSS (kPa) | Bed 1 | Bed 2 |
|---|---|---|
| Step 1 | 124.0 | 52.0 |
| Step 2 | 128.0 | 40.0 |
| Step 3 | 107.0 | 48.0 |
| Step 4 | 79.0 | 74.0 |
| Step 5 | 52.0 | 124.0 |
| Step 6 | 40.0 | 128.0 |
| Step 7 | 50.0 | 105.0 |
| Step 8 | 75.0 | 79.0 |

| Mass Balance at CSS (Total millimole per cycle) | |
|---|---|
| Feed flow | 4000.0 |
| Product flow | 488.0 |

| Key Performance Parameters | | | |
|---|---|---|---|
| Oxygen Recovery (%) | 49.5 | BSF (kg/TPDc) | 857.6 |
| Power: (kW/TPDc) | | Oxygen Purity (%): | 89.3 |

| End of Step CSS Temperature Profile (°C) | | |
|---|---|---|
| z (m) | Thigh | Tlow |
| 0 | 15.594 | 14.688 |
| 0.245 | 15.813 | 11.688 |
| 0.395 | 14.594 | 10 |
| 0.545 | 16.906 | 13.188 |
| 0.945 | 20.813 | 16 |
| 1.345 | 22.313 | 17.688 |
| 1.8 | 17.594 | 16.406 |

# Appendix 10 - Power and VSA Performance Formula

Detailed below are the governing equations utilised in the PLC program to calculate the power and other performance measures that characterise oxygen VSA.

**Power:**

The feed and vacuum blower power requirements can be estimated using the equation for adiabatic compression of air. The instantaneous power requirement can be integrated over a cycle to determine the specific power of the oxygen VSA unit. In the PLC, this integration is performed each scan, with a time interval of 25 msec.

In addition, some assumptions are required concerning the power requirements of the blowers. It is assumed that when the flow is zero, the blower is idling, the power requirement is zero. The power is also assumed to be zero under conditions where the differential pressure across the blower is negative. This condition may occur at the start of a feed repressurisation step when the adsorption bed is below atmospheric pressure. It is also assumed that the typical efficiency of a Rootes type blower is 0.7 ($\eta$=0.7). These assumptions are reasonable to apply in the absence of machine specific data.

**Instantaneous Feed Blower Power:** $$W_{fi} = 2.78\text{x}10^{-4}\,\frac{k}{k-1}\,\frac{Q_f P_f}{\eta_f}\left[\left(\frac{P_f}{P_{atm}}\right)^{\frac{k-1}{k}} - 1\right] \quad \text{(kW)}$$

where

$\eta_f$ = 0.7 (Blower efficiency)

k = 1.395 (Ratio of heat capacities for air)

$Q_f$ = Instantaneous feed flow after compression (actual $m^3/hr$)

$P_f$ = Instantaneous feed pressure (kPa)

$P_{atm}$ = Atmospheric pressure (101.325 kPa)

This instantaneous power can be integrated over a cycle.

**Feed Blower Power per Cycle:** $$W_{fc} = \int_0^{\tau_c} w_{fi}\,dt \approx \sum_{i=0}^{Ns} w_{fi}\,\Delta s \quad \text{(kJ)}$$

Where $\tau_c$ is the cycle time, $\Delta s$ is the PLC scan time, and Ns is the number of scan per cycle.

The analogous equations can be written for the vacuum blower.

**Instantaneous Vacuum Blower Power:** $$W_{vi} = 2.78x10^{-4} \frac{k}{k-1} \frac{Q_v P_v}{\eta_v} \left[ \left( \frac{P_{atm}}{P_v} \right)^{\frac{k-1}{k}} - 1 \right] \quad (kW)$$

where:
$Q_V$ = Instantaneous vacuum flow before compression (m3/hr)

$P_V$ = Vacuum pressure (before compression) (kPa)

**Vacuum Blower Power per Cycle:** $$W_{vc} = \int_0^{\tau_c} w_{vi} dt \approx \sum_{i=0}^{Ns} w_{vi} \Delta s \quad (kJ)$$

These equations can be combined to enable the calculation of the specific total power per tonne of oxygen per day (TPDc). This is a general measure of the power efficiency of the cycle VSA.

Specific Total Power/TPDc, $$W_T = \frac{\left[ \frac{W_{fc} + W_{vc}}{\tau_c} \right]}{TPDc} \quad (kW/TPDc)$$

**Oxygen VSA Performance**

In addition to specific total power, oxygen VSA performance is further characterised by two additional parameters – oxygen recovery and Bed Sizing Factor (BSF). Oxygen recovery is the ratio of the quantity of oxygen in the product stream to the oxygen fed to the VSA unit. This is typically stated as a percentage. The other critical performance parameter is the Bed Sizing Factor (BSF), which is the mass of adsorbent required to produce one TPDc.

**Oxygen Recovery**

$$\text{Oxygen Recovery (\%)}\quad Rec = \frac{N_{po}}{N_{fo}}\frac{100}{1}$$

where: $N_{po}$ = mols of oxygen in the product stream over a cycle (mol)

$N_{fo}$ = mols of oxygen in the feed stream over a cycle (mol)

In the PLC this can be calculated as:

$$Rec(\%) = 100 * \frac{\sum_{i=0}^{Ns} \frac{y_{O2,pr} P_{pr} Q_{pr}}{RT_{pr}} \Delta s}{\sum_{i=0}^{Ns} \frac{y_{O2,f} P_f Q_f}{RT_f} \Delta s} = \frac{N_{po}}{N_{fo}}\frac{100}{1}$$

where

$P_{pr}$ = Instantaneous product pressure (Pa)

$Q_{pr}$ = Instantaneous actual product flow ($m^3$/sec)

$T_{pr}$ = Instantaneous product temperature (K)

$y_{O2,pr}$ = Instantaneous product mol oxygen mol fraction

$P_f$ = Instantaneous feed pressure (Pa)

$Q_f$ = Instantaneous actual feed flow ($m^3$/sec)

$T_f$ = Instantaneous feed temperature (K)

$y_{O2,f}$ = Instantaneous feed mol oxygen mol fraction

Recovery can also be expressed on a two component basis by including argon and oxygen as a single component. This is required to enable comparison with MINSA which is a two component simulator. The purity of the product stream can be cited on a two component basis as follows:

$$(\%O2 + \%Ar)_{pr} = \frac{(\%O2_f + \%Ar_f)}{\%O2_f} \%O2_{pr} = (23/22) * \%O2_{pr}$$

where the percentage oxygen in the feed after the PSA air dryer is 22%, and the percentage argon in the feed after the PSA air dryer is 1%.

This product purity and feed purity can be used to calculate the recovery on a two component basis.

**Bed Sizing Factor (BSF)**

$$\text{Bed Sizing Factor, } BSF = \frac{\text{Total.Mass.of.Adsorbent}}{\frac{864(N_{po}Mw_{O2})}{\tau_c}} \text{ (kg/TPDc)}$$

where $Mw_{O2}$ = molecular weight of oxygen.

BSF can be readily calculated in the PLC based on the calculation of $N_{po}$ detailed above. BSF can also be determined on a two component basis by treating oxygen and argon as a single component. The reciprocal of BSF (1/BSF) is a measure of the adsorbent productivity.

## Bibliography


Ackley, M., Stewart, A., Henzler, G., Leavitt, F., Notaro, F., and Kane, M., "PSA Apparatus and Process Using Adsorbent Mixtures", U.S. Patent 6,027,548, February 2000

Armond, J., "Pressure Swing Adsorption Plants", U.S. Patent 5,624,477, April 19, 1997

Basmadjian D., The Little Adsorption Book, CRC Press, Florida, 1997

Beh, C., Wilson, S., Webley, P., and He, J., "The Control of the Vacuum Swing Adsorption Process for Air Separation", Proceedings of the Second Pacific Basin Conference on Adsorption Science and Technology, Brisbane, Australia, May 14-18 2000, (World Scientific, Singapore, 2000)

Bird, B., Stewart, W., and Lightfoot, E., Transport Phenomena, Wiley, New York, 1960

Bossy, A., and Tondeur, D., "A Non-Linear Equilibrium Analysis of Blowdown Policy in Pressure-Swing-Adsorption Separation", The Chem. Eng. Journal, 1992, 48, 173

Calis, H., Gerritsen, A., and Van Den Bekkum, H., "Zeolites Grown on Wire Gauze: A New Structured Catalyst Packing for Dustproof, Low Pressure Drop DeNOx Processes", The Can. Journal of Chem. Eng., 1995, 73, 120

Campbell, M., Lagree, D., and Smolarek, J., "Advances in Oxygen Production by Pressure Swing Adsorption", AIChE Symposium Series, 1993, 89, 293, 104

Carter, J., "Isothermal and Adiabatic Adsorption Fixed Beds", Transactions of the Institution of Chemical Engineers, 1968, 46, 213

Cheng, H., and Hill F., "Separation of Helium–Methane Mixtures by Pressure Swing Adsorption", AIChE Journal, 1985, 31, 95.

Chiang, A., "An Analytical Solution to Equilibrium PSA Cycles". Chem. Eng. Sci. 1996, 51, 207.

Chiang, A., "Arithmetic of PSA Process Scheduling", AIChE Journal, 1988, 34, 11

Chou, C., and Huang, W., "Simulation of a Four–Bed Pressure Swing Adsorption Process for Oxygen Enrichment", Ind. Eng. Chem. Res., 1994, 33, 1250

C[illegible] C., and Huang, W., "A Moving Finite Element Simulation of a Pressure Swing Adsorption Process", Compt. Chem. Eng., 1997, 21, 301.

Chou, C., Ju, D., and Chang, S., "Simulation of a Fractionated Vacuum Swing Adsorption Process for Air Separation", Separation Science and Technology, 1998, 33(13), 2059

Choudray, N., Jasra, R., and Bhat, S., "Process for the Preparation of a Molecular Sieve Adsorbent for Selectively Adsorbing Oxygen from a Gaseous Mixture", U.S. Patent 6,087,289, 11 July 2000

Collins, J., "Air Separation by Adsorption", U.S. Patent 3,973,931, Aug. 1976

Collins, J., "Air Separation by Adsorption", U.S. Patent 4,026, 680, May 1977

Davis, M., and LeVan, D., "Equilibrium Theory for Complete Adiabatic Adsorption Cycles", AIChE Journal, March 1987, 33, 3, 470

Dixon, A., "Thermal Resistance Models of Packed-Bed Effective Heat Transfer Parameters", AIChE Journal, May 1985, 31, 5, 826

Dixon, A., and Cresswell, D., "Theoretical Prediction of Effective Heat Transfer Parameters in Packed Beds", AIChE Journal, July 1979, 25, 4, 663

Doshi, K., Katira, C., and Stewart, H., "Optimization of a Pressure Swing Adsorption Cycle" AIChE Symposium Series, 1971, 67, 117, 90

Ergun, S., "Fluid flow through Packed Columns", Chem. Eng. Prog., 1952, 48, 49

Farooq, S., and Ruthven, D., "Heat Effects in Adsorption Column Dynamics 1. Comparison of One and Two Dimensional Models", Ind. Eng. Chem. Res., 1990, 29, 1076

Farooq, S., Hassan, M., and Ruthven, D., "Heat Effects in Pressure Swing Adsorption Systems", Chem. Eng. Sci., 1988, 43, 5, 1017

Farooq, S., Ruthven D., and Boniface, H., "A. Numerical Simulation of a Pressure Swing Adsorption Oxygen Unit", Chem. Eng. Sci., 1989, 44, 2809

Fernandez, G., and Kenney C. N. "Modeling of the Pressure Swing Air Separation Process", Chem. Eng. Sci., 1983, 38, 827

Friday, D., and LeVan, M, "Hot Purge Gas Regeneration of Adsorption Beds with Solute Condensation: Experimental Studies", AIChE Journal, 1985, 31, 1322

Fuderer, A., "Activated carbon adsorbent with increased heat capacity and the production thereof", US Patent 4,499,208, 12th February 1985

Gaffney T., Kirner J., Kumar R., and Maliszewskyj, R. , "Adsorptive Separation Using Diluted Adsorptive Phase", U.S Patent 5,258,060, 2nd November, 1993

Gluceckauf, E., "Theory of Chromatography, Part 10: Formula for Diffusion into Spheres and Their Applications to Chromotography", Trans. Faraday Society, 1955, 51, 1540

Glueckauf, E, and Coates, J., "Theory of Chromatography. Part 4 - The Influence of Incomplete Equilibrium on the Front Boundary of Chromatograms and on the Effectiveness of Separation", J. Chem. Soc., 1947, 1315.

Haefner, D., and Thodos, G., "Transient Sorption of Water Vapor from Air flowing through Beds of Zeolite 13X.", Ind.Eng.Chem.Fund., 1986, 25(4), 498.

Harriott, G., and Tsirukis, A., Convective Approximation of Adsorption Processes, Unpublished

Harriott, G., "Direct Finite Element Computation of Periodic Adsorption Processes", Comp. Fluid Dyn., 1996, 7, 201.

He, J., Webley, P., and Wilson, S., "Optimisation of PSA Systems - Comparison of Equilibrium and Non-Equilibrium Models", Chemeca 98 , Port Douglas

Hofmann, U., Loehr, M., and Straub, M., "Sensitivity Analysis of PSA Processes Supported by Numerical Simulation", AIChE Annual Meeting, Dallas, Texas, October 31-November 5, 1999

Holmes, M., Introduction to Perturbation Methods, New York, Springer-Verlag, 1995.

Huntley, I., and Johnson, R., Linear and Non-Linear Differential Equations, New York, Halsted Press, 1983

Hutson, N., Zajic, S., and Yang, R., "Influence of Residual Water on the Adsorption of Atmospheric Gases in Li-X Zeolite: Experiment and Simulation", Ind. Eng. Chem. Res., 2000, 39,1775

Ishida, M., and Takeuchi, K., "Development of a Compiler-Type Simulator for Pressure Swing Adsorption and its Application to Oxygen Enrichment in Air", Journal of Chemical Engineering of Japan, 1987, 20, 2

Izumi, J., "High Efficiency Oxygen Separation with the Low Temperature and Pressure PSA", A.I.Ch.E Annual Meeting, Nov 1989, San Fransico, California

Jasra, R, Choudray, N., and Bhat, S., "Correlation of Sorption Behaviour of Nitrogen, Oxygen and Argon with Cation Locations in Zeolite X", Ind. Eng. Chem. Res., 1996, 35, 4221

Kaguei, S, Yu, Q., and Wakao, N., Thermal Waves in Adsorption Column, Parameter Estimation, Chem. Eng. Sci., 1985, 40, 1069

Kandybin, A., Anderson, R., and Reichley; D., "System for Separation of Oxygen from Argon/Oxygen Mixture" , U.S. Patent 5,470,378, 28th November 1998

Karsten-Bar, N., Balcom, B., and Ruthven, D., "Direct Measurement of Transient Concentration Profiles in Molecular Sieve Particles and Columns by MRI", Proceeds of the Second Pacific Basin Conference on Adsorption Science and Technology, Editor. Duong Do, 14-18 May 2000 (World Scientific, Singapore, 2000)

Kapoor, A., and Yang, R., Optimization of a Pressure Swing Adsorption Cycle, Ind. Eng. Chem. Res., 1988, 27, 204

Karger, J., and Ruthven, D., Diffusion in Zeolites, John Wiley and Sons, 1992

Karwat, E., "Selective Adsorption of Gas at Low Temperature", U.S Patent 3,355,859, 5th December 1967

Kayser, J., and Knaebel, K., Pressure Swing Adsorption: Experimental Study of an Equilibrium Theory, Chem. Eng. Sci., 1986, 41, 11, 2931

Keefer; B., and McLean, C., "High Frequency Rotary Pressure Swing Adsorption Apparatus", U.S. Patent 6,056,804, 2nd May, 2000

Kikkinides, E., Sikavitsas, V., and Yang, R., "Natural Gas Desulfurization by Adsorption: Feasibility and Multiplicity of Cyclic Steady States", Ind. Eng. Chem. Res., 1995, 34, 255

Knaebel, K., and Matz, M., "Pressure Swing Adsorption: Effects of Incomplete Purge", AIChE Journal, 1988, 34, 1486.

Knaebel, K., and Hill, F., "Pressure Swing Adsorption: Development of an Equilibrium Theory for Gas Separations", Chem. Eng. Sci. 1985, 40, 2351.

Koroa, W., and Mahajan, R., "Pushing the Limits on Possibilities for Large Scale Gas Separation: Which Strategies" , Journal of Membrane Science, 2001, 181, 141

Kumar, R., and Sircar, S., "Adiabatic Sorption of Bulk Single Adsorbate from an Inert Gas - Effects of Gas-Solid Mass and Heat Transfer Co-efficients", Chem. Eng. Comm., 1986, 26, 319

Kumar, R., et.al., "A Versatile Process Simulator for Adsorptive Separations", Chem. Eng. Sci., 1994, 49, 18, 3115

Kumar, R., Vacuum Swing Adsorption Process for Oxygen Production - A Historical Perspective, Separation Science and Technology, 31(7), pp. 877-893, 1996

Kumar, R. and Sircar, S., "Adiabatic Sorption of Bulk Single Adsorbate from an Inert Gas - Effect of Gas-Solid Mass and Heat Transfer Coefficients", Chem.Eng.Comm., 1986, 26, 319.

Leavitt, F., "Low Temperature Pressure Swing Adsorption with Refrigeration", U.S. Patent 5,1169,413, 1992

Lee, W. , Hwang, K., and Jun, J., "Fixed-Bed Adsorption for Bulk Component System. Non-equilibrium, Non-isothermal and Non-adiabatic Model", Chem. Eng. Sci.,1995, 50, 813.

LeVan, D., et.al., "Fixed-Bed Adsorption of Gases: Effect of Velocity Variations on Transition Types", AIChE Journal., 1988, 34, 6, 996

LeVan, M., and Davis, M., "Equilibrium Theory for Complete Adiabatic Adsorption Cycles", AIChE Journal, 1987, 33, 470

LeVan, M., and Croft, D., "Determination of periodic states of pressure swing adsorption cycles", Gas.Sep.Purif., 1995, 9, 1, 13

Li,and Finlayson, "Heat Transfer in Packed Beds – a Re-evaluation", Chem.Eng.Sci., 1977, 32, 1055, 1977.

Li., Y., Perara, S., and Crittenden, B., "Zeolite Monoliths for Air Separation Part 2: Oxygen Enrichment, Pressure Drop and Pressurisation", Transactions of the Institution of Chemical Engineers, 1998, 76, Part A, 931

Lin, W., Farooq, S., and Tien, C., "Estimation of Overall Effective Coefficient of Heat Transfer for Non-isothermal Fixed-Bed Adsorption", Chem. Eng. Sci, 1999, 54, 4031

Liu. Y., and Ritter, J., "Periodic State Heat Effects in Pressure Swing Adsorption-Solvent Vapor Recovery," Adsorption, 4, 1998a, 159

Liu, Y., Holland, C., and Ritter, J., "Solvent vapor Recovery by Pressure Swing Adsorption II – Experimental Periodic Performance of the Butane-Activated Carbon System", Separation Science and Technology, 1998b, 33, 16, 2431

Lou, H., Kodama, A., Goto, M., and Hirose, T, "Temperature Profile and Separation Efficiency in Adiabatic Pressure Swing Adsorption Process", Fundamentals of Adsorption 6, Paris, 24-28 May 1998

Lou, H., Miyajima, H., Dong, F., Kodama, A., Goto, M., and Hirose, T., "Experimental Study of Thermal Phenomenon in PSA Air Dehumidification", Separation and Purification Technology, 1999b, 17, 65

Mahle, J., Friday, D., and LeVan, D., "Pressure Swing Adsorption for Air Purification 1. Temperature Cycling and Role of Weakly Adsorbed Carrier Gas", Ind. Eng.Chem.Res., 1996, 35, 2342

Mahle, J., Tevault, D., and Le Van, D., "Non-isothermal Effects of PSA for Air Purification", Fundamentals of Adsorption 5, Kluwer Academic Publishers, Boston, 1996

Marcussen, L., and Vinding, C., "Experimental Breakthrough Curves Determined Under Carefully Controlled Conditions for the Adsorption of Water Vapour on Alumina in Adiabatic Fixed Beds", Chem. Eng. Sci., 1982, 37, 2, 311

Matros, Y., Catalytic Processes Under Unsteady-State Conditions, Elsevier, Amsterdam, 1989

Michael, K., "Industrial Gas: Surveying Onsite Supplying Options", Chemical Engineering, January 1997, 72

Miller,G. "Adsorption of Nitrogen, Oxygen, Argon, and Ternary Mixtures of these gases in 13X Molecular Sieve", AIChE Symp.Ser., 1973, 83, 259

Murray, J., "Air Separation by Rapid Pressure Swing Adsorption", PhD Thesis, University of Cambridge, 1996

Nilchan, S., "The Optimisation of Periodic Adsorption Processes", PhD Thesis, Univesity of London, 1997

Nilchan, S., and Pantelides, C., "On the Optimization of Periodic Adsorption Processes", Adsorption, 1998, 4, 113.

Notaro, F., Mullhaupt, T., Leavitt, F., and Ackley, M., "Adsorptive Process and System Using Multilayer Adsorbent Beds", U.S. Patent 5,674,311, October 1997

Ozil, P., and Bonnetain, L., "Theoretical Prediction of Temperature Profiles in an Adsorption Fixed-Bed", Chem. Eng. Sci., 1978, 33, 1233

Park, J., Kim, J., Chi, S., Kim, J., and Yang, R., "Adsorber Dynamics and Optimal Design of Layered Beds for Multicomponent Gas Adsorption", Chem.Eng. Sci., 1998, 53, 3951

Perry, R., ed., Perry's Chemical Engineers' Handbook Sixth Edition, McGraw-Hill, New York, 1984

Petzold L., "Automatic Selection of Methods for Solving Stiff and Nonstiff Systems of Ordinary Differential Equations", SIAM J. Sci. Stat. Comput., 1983, 4, 136

Pigorini, G., and Le Van, D., "Equilibrium Theory for Pressure Swing Adsorption 2. Purification and Enrichment in Layered Beds", Ind. Eng. Chem. Res., 1997, 36, 2296

Poteau, M., et.al. "Adsorber Compromising Annular Superposed Beds of Adsorbent Materials", U.S. Patent 5,232,479, 1993

Psaras, D., and Leach, G., and LaCava, A., "Experimental Study of Transient Thermal Effects on a Model Pressure Swing Adsorption Process", AIChE Symp. Ser., 1988, 264, 133

Ramprasad, D., Pez, G., Pearlstein, R., and Meier, I., "Reversible Oxygen Sorbent Compositions", U.S. Patent 5,208,335, May 1993

Rege, S., and Yang, R., "Limits for Air Separation by Adsorption with LiX Zeolites", Ind. Eng., Chem. Res., 1997, 36, 5358

Rota, R., and Wankat, P., "Intensification of Pressure Swing Adsorption Processes", AIChE Journal, 1990, 36, 1299

Rousar, I., and Ditl, P., "Optimization of Pressure Swing Adsorption Equipment Part I", Chem. Eng. Comm., 1988, 70, 67

Rousar, I., and Ditl, P., "Optimization of Pressure Swing Adsorption Equipment Part II", Chem. Eng. Comm., 1988, 70, 93

Ruthven D., Farooq, S., and Knaebel, K., Pressure Swing Adsorption, VCH Publishers, New York, 1994

Ruthven, D., Raghavan, N., and Hassan, M., "Air Separation by Pressure Swing Adsorption on a Carbon Molecular Sieve", Chem. Eng. Sci., 1986, 41, 1333

Ruthven, D., and Raghavan, N., "Pressure Swing Adsorption. Part III: Numerical Simulation of a Kinetically Controlled Bulk Gas Separation", AIChE Journal, 1985, 31, 2017

Ruthven, D., and Xu, Z., "Diffusion of Oxygen and Nitrogen in 5A Zeolite Crystals and Commercial 5A Pellets", Chemical Engineering Science, 1993, 48, 18, 3307

Ruthven, D., Principles of Adsorption and Adsorption Processes, John Wiley and Sons, New York, 1984

Ruthven, D., "Past Progress and Future Challenges in Adsorption Research", Ind. Eng. Chem. Res., 2000, 39, 2127

Schmidt, F., and Wilmott, A., Thermal Energy Storage and Regeneration, Hemisphere Publishing Corporation, New York, 1981

Seo, B., Jang, J., Lee, C., Baek, K., Ko, S., "Effect of Temperature Variation on Breakthrough Curve in $H_2$/CO System", Journal of the Korean Institute of Chemical Engineering, October, 1998, 36, 5

Sherwood, T.; Pigford, R., and Wilke,C., Mass Transfer; McGraw-Hill: New York, 1975.

Sircar, S., "Excess Properties and Thermodynamics of Multicomponent Gas Adsorption", J. Chem. Soc. Faraday Trans. I., 1985, 81, 1527

Sircar, S., "Adsorption Technology: A Versatile Separation Tool", in Garside, J., Separation Technology, IChemE, London, 1996

Sircar,S.; and Kumar,R. "Adiabatic Adsorption of Bulk Binary Gas Mixtures: Analysis by Constant Pattern Model", Ind. Eng. Chem. Res. , 1983, 22, 271.

Skarstrom, C., "Oxygen Concentration Process", U.S. Patent 3,237,377, 1st March, 1966

Smith, O., and Westerberg, A., "Acceleration of Cyclic Steady State Convergence for Pressure Swing Adsorption Models", Ind. Eng. Chem. Res. , 1992, 31, 1569.

Smith, O., and Westerberg, A., "Mixed-Integer Programming for Pressure Swing Adsorption Cycle Scheduling", Chem. Eng. Sci., 1990, 45, 9, 2833

Smith, O., and Westerberg, A., The Optimal Design of Pressure Swing Adsorption, Chem. Eng. Sci., 1991, 46., 12, 2967

Sotirchos, S., and Serbezov, A., "Multicomponent Transport Effects in Sorbent Particles under Pressure Swing Conditions", Ind. Eng.Chem.Res., 1997a, 36, 3002

Sotirchos, S.V., and Serbezov, A.,"Mathematical Modellling of the Adsorptive Separation of Multicomponent Gaseous Mixtures", Chem. Eng. Sci., 1997b, 52, 79

Stegmaier, M., "Temperatureffekte beim Zusammenspeil zwischen Lufttrocknung und Lufttennung bei technischen Druckwechseladsorptionsprozen", July 1996, University of Stuttgart, Unpublished

Subramanian, D., and Ritter, J., "Equilibrium Theory for Binary Solvent Vapor Recovery by PSA: Conceptual Process Design for Separation of the Lighter Component", Chem. Eng. Sci., 1998, 53, 6, 1295

Suzuki, M., Adsorption Engineering, Elseveir, Tokyo, 1990

Suzuki, M., and Chihara, K., "Simulation of Non-Isothermal Pressure Swing Adsorption", J.Chem.Eng. Japan, 1983, 16, 53

Todd, R., He, J., Webley, P., Wilson, S., and Beh, C., "Fast finite volume method for PSA/VSA Cycle Simulation- Analytic and Experimental Validation", Submitted to Ind. Eng. Chem. Res., 2000b

Todd, R., "Mass Transfer Kinetics within Rapid Pressure swing Adsorption Systems", Transfer Report, Monash University, 2000a, Unpublished

Todd, R., Beh. C., Wilson, S., and Webley, P., "Simplified Modelling of Pressure Drive Flow in Pressure Swing Adsorption" , Melbourne Graduate Fluids Conference 2001, Monash University, Melbourne, Australia

Todd, R., "Heat and Mass Transfer in Adiabatic, Bulk Adsorption Systems", Minor Thesis, Monash University, 1998, Unpublished

Wakao, N, "Particle-to_Fluid Transfer Co-efficients and Fluid Diffusivities at Low Flow Rate in Packed Beds", 1976, Chem. Eng. Sci., 31, 115

Wakao, N., and Kaguei, S., Heat and Mass Transfer in Packed Beds, Gordon and Breach Science Publishers, New York, 1982

Wakao, N., Kaguei, S., and Yu, Q. "Thermal Waves in an Adsorption Column: Parameter Estimation", Chem. Eng. Sci., 1985, 40, 1069

Walter, K., Adsorberbehaelter, German Patent P4,443,191, June 1996

Wankat, P., Rate Controlled Separations, Elsevier Science Pub., New York, 1990

Wang X., Lu E., Lin W., Liu T., Shi Z., Tang R., and Wang C. "Heat Storage Performance of the Binary Systems of Neopentyl Glycol Pentaerythritol and Neopentyl Glycol Trihydroxymethyl – Aminomethane as Solid Phase Change Materials", Energy Conservation and Management, 2000, 41, 129

Watson, C., Whitley, R., and Meyer, M., "Multiple Zeolite Adsorbent Layers in Oxygen Separation", U.S. Patent, 5,529,610, 1996

Webley, P., and He, J., "Criteria for Establishing Cyclic Steady State for Non-Isothermal Cyclic Adsorption Systems", Accepted for publication in Compt.Chem.Eng. 2000b.

Webley, P., and He, J., "Fast Solution-Adaptive Finite Volume Method for PSA/VSA Cycle Simulation. 1. Single Step Simulation", Compt.Chem.Eng. 2000a, 23,1701.

Webley, P., Beh., C., He, J, Wilson, S., and Todd, S., "Numerical Simulation and Experimental Validation of Multiple Layer Non-Isothermal, Bulk Gas Separation", Proceedings of the Second Pacific Basin Conference on Adsorption Science and Technology, Brisbane, Australia, May 14-18, 2000c(World Scientific, Singapore, 2000c)

Webley, P., He, J., Wilson, S., and Hu, E., "Optimization of PSA Systems for Air Separation", Fundamentals of Adsorption 6, 24-28 May 1998, Elsevier

Wilson, S., and Webley, P., and He, J.,, "Thermal Effects in Oxygen Vacuum Swing Adsorption", Chemeca 98, Port Douglas

Wilson, S., and Webley, P., "A Technique for Accelerated Convergence of Cyclic Steady State in Oxygen VSA Simulations", AIChE Annual Meeting 1999, Dallas, Texas, 1999c

Wilson, S., and Webley, P., "Thermal Effects in Oxygen Vacuum Swing Adsorption - An Accelerated Approximate Solution", Chemeca 99, Newcastle, 1999a

Wilson, S., and Webley, P., "Laboratory Scale Oxygen VSA and Thermal Behaviour: How Close to Industrial Scale?", AIChE Annual Meeting 1999, Dallas, Texas, 1999b

Wilson, S., Beh, C., Webley, P., Todd, R., "The Effects of a Readily Adsorbed Trace Component (Water) in A Bulk Separation PSA Process: The Case of Oxygen VSA" (Accepted Ind. Eng.Chem. Res., 2000)

Yanagi, H., and Qiu, J., "Oxygen Generator Using Low Temperature Vacuum Swing Adsorption", Fundamentals of Adsorption 6, Paris 24-28 May 1998

Yang R., and Doong, S., "Gas Separation by Pressure Swing Adsorption: A Pore-Diffusion Model for Bulk Separation", AIChE Journal, 1985, 31, 1, 1829

Yang, R., and Cen, P. "Improved Pressure Swing Adsorption Process for Gas Separation by Heat Exchange between Adsorbers and by High-Heat Capacity Inert Additives", Ind. Eng. Chem. Process Des. Dev., 1986, 25, 54

Yang, R., and Cen, P., "Bulk Gas Separation by Pressure Swing Adsorption", Ind. Eng. Chem. Fundam. 1986, 25, 758.

Yang, R., Gas Separation by Adsorption Processes, Butterworths, MA, 1987